UC Santa Barbara

UC Santa Barbara Electronic Theses and Dissertations

Title

Construction of Functional and Sustainable Materials Using Well-Defined Diels—Alder Cyclopentadiene Monomers

Permalink

https://escholarship.org/uc/item/5cr447md

Author

Tran, Thi

Publication Date

2024

Supplemental Material

https://escholarship.org/uc/item/5cr447md#supplemental

Peer reviewed|Thesis/dissertation

eScholarship.org Powered by the California Digital Library
University of California

UNIVERSITY OF CALIFORNIA

Santa Barbara

Construction of Functional and Sustainable Materials Using Well-Defined Diels–Alder Cyclopentadiene Monomers

A dissertation submitted in partial satisfaction of the

requirements for the degree Doctor of Philosophy

in Chemistry

by

Thi M. Tran

Committee in charge:

Professor Javier Read de Alaniz, Chair

Professor Yang Yang

Professor Craig Hawker

Professor Alison Butler

June 2024

The dissertation of Thi M. Tran is approved.

Alison Butler

Craig Hawker

Yang Yang

Javier Read de Alaniz, Committee Chair

June 2024

Construction of Functional and Sustainable Materials Using Well-Defined Diels–Alder Cyclopentadiene Monomers

Copyright © 2024

by

Thi M. Tran

This dissertation is dedicated to my mom, Đoàn Thị Nguyên Dung, and my dad, Trần Hữu Phước. I am forever grateful and fortunate to receive your unconditional support, love, self-sacrifice, and wisdom.

ACKNOWLEDGEMENTS

First and foremost, I would like to thank Javier for being the most supportive, incredible, and patient advisor. I could not ask for a better mentor to build me up during my Ph.D. studies. You have guided and let me explore research in a way that I would never thought I could, by backing me up regardless of my most random or almost impossible ideas to conduct. Your professional advice is outstanding, which aided me a lot when I was not sure what would be next. You have also been a great supporter and patient teacher when I was struggling (i.e., writing and practicing for presentations). Overall, I have learned so much from you in every aspect, including research, writing, presenting, mentoring, leadership, professional development or just being a wholesome person. You have really raised my confidence and even inspired me to follow your path. I am truly grateful to be able to work with and learn from you.

I would also like to thank my undergraduate advisors, Dr. Borguet and Dr. Andrade. I am fortunate to enjoy my first research experience with Dr. Borguet. Thank you for letting me work in your lab even though I was just a freshman. If I had not joined and known about the positive learning environment, I would probably have not chosen a research career. You have encouraged me to go to conferences, join a wide range of collaborative projects, and treated me as an independent researcher. Your emphasis on following my real research interest has pushed me to find my way to organic synthesis. Even when I am not your student anymore, you are still available to help me with my career development or just to update about each other. I am also thankful to meet Dr. Andrade during the "Lunch and Learn" at Temple University and later join the "A team." Your excitement in research was truly amazing, which motivated me to switch my field from analytical chemistry to organic total synthesis. Your

wisdom about hard working and “no pain no gain,” also guided me through so many difficult times during graduate school.

I am appreciative of the constructive environment that UCSB has fostered. I appreciate the guidance and ideas suggestion from my committee members, Craig, Yang, and Alison, during my candidacy exam. Thank you, Craig, for the beneficial presentation class. I have gained so many insights when I begin to care about my “messages and delivery.” I’d also like to acknowledge my wonderful collaborators and mentors when I began my graduate works at UCSB – Andrei, Jamie and Sophia. Thank you, Andrei and Jamie, for showing me how to screen reactions, handling multiple projects, or just chatting about random things. “Sophiaaaa,” you are such a remarkable researcher, mentor, friend, and labmate. Thank you for guiding me with everything and being one of the best fumehood neighbors in lab. Also, thanks, Julie, Ronnie, Fritz, Livius, Mike, and Lindsay for your assistance and advice that really pushed my projects forward and enhanced my presentation skills. Julie, you are such a fun buddy. I miss chatting and doing bonfire with you. And Ronnie, thanks for being great at keeping in touch even during Covid time. People I have met through conferences and across campus – Alisha, Hiba, Kaitlin, Parker, Pat, Marvin and the UCSB staff, Eleni and Rachel – thanks for the fun chat and pleasant conversation that really make a lot of my days. I am also thankful for all the funded events inside and outside of academia at UCSB, such as the department seminars, local conferences, bagel hours, BBQs, and ice skating that really make a cohesive community here at UCSB.

To my undergraduate mentors, Manish, Alex, and Sam (even though you are not my “official” mentor), you guys have taught me so much about being patient in research, building my working skills, crafting my applications to graduate schools, or just having fun inside and

outside of lab. I am also grateful to the Temple University Scholarship Board members in 2015 for giving me the full tuition remission. I could not ask for a better undergraduate institute to provide me the supportive learning environment both financially and emotionally. Everyone I have met and become friend at Temple, I really appreciate you – Gia Gia, Julie, Truc, Thao, Thao Quach, Hoang, Linh, Thinh, Thanh, Mai, Viya, Olivia, Yukino, and Liz.

Graduate school experiences would not be complete without the people who have gone through ups and downs with me. Angelique, you have become my closest friend in graduate school and in life. I miss hanging out with you every other week until you graduated. Thank you for always checking, confiding in me and being the sweetest as you naturally are. Main lab people – Guillen, Cassidy, Komal, Kseniia, Takashi, and ex-member, Sophia, you guys are so diverse, sometimes chaotic but the most wonderful and enjoyable co-workers and friends. Each of you is so unique and I like how lab can become messy, but our bond stays strong. Guillen and Cassidy, thanks for being my second family members, with me being the youngest of course :) Komal, I really appreciate our matcha and grocery runs. Thank you for being patient with me as a graduate mentee. I am learning as much as you are. I am also thankful for the hard works from my undergraduate mentees, Ashley and Kaitlyn. I have enjoyed working with you for the past two years, Ashley. You are amazing not only in lab but also in extracurricular activities. Thanks for working hard in lab and inviting me to your acapella concerts. Also, thank you, Kaylaa, for being a great office mate even though we are not in the same lab. I will miss our Costco trips and little activities. I really appreciate my housemate and friend, Lucy. You are just like my little sister, and I miss having you around.

Being a part of the Viet community is also a wonderful distraction from academia. I am grateful for all the fun events and delicious food we had throughout the years. Linh and My,

thanks for all the cooking hangouts, fun activities, and adventures. My middle and high school classmates and friends, Phuong Thao, Hoa, Xuan, Quyen, Trieu, Chi, Nhi, Uyen, Quoc Thi, Hang, Trang, Han, and more – you guys are adorable and so fun to be around.

I am truly grateful for the encouragement from my extended family since I was young. My maternal grandpa, Tien Quyet Doan, who emphasized the importance of education and motivated me to follow a learning path. Even though your health is not in a great condition, you still ask and wonder about me. My maternal grandma, Thom Nguyen, always gives me the most nostalgic and delicious food and ponders if I am doing okay. I really appreciate my uncle, Thu Doan, and his family for always being there and so helpful throughout my time at UCSB, especially during Covid. And to my other uncles and aunts, I am thankful for all of your care and attention. Finally, I would like to give a special thanks to my mom, Thi Nguyen Dung Doan, and my dad, Huu Phuoc Tran. You both have raised me up and taught me so many things, not only through words but also by your loving actions. I am grateful that you are my parents, best friends, supporters, and cheerleaders with your unconditional support, self-sacrifice and crucial advice.

VITA OF THI M. TRAN
May 2024

EDUCATION
Bachelor of Science in Chemistry with ACS certificate and Bachelor of Arts in Biology, Temple University, May 2019 (*Magna cum laude*)
Doctor of Philosophy in Chemistry, University of California, Santa Barbara, June 2024 (Expected)

RESEARCH EXPERIENCE
Research advisor: Javier Read de Alaniz
Department of Chemistry and Biochemistry, University of California, Santa Barbara, CA
"Cyclopentadiene Derivatives to Construct Diels–Alder Materials with Advanced Properties" (2019 – 2024)

- Developed methodologies and designed advanced functional polymers using highly reactive cyclopentadiene derivatives
- Monitored reactions and characterized materials via Fourier Transform Infrared spectroscopy (FTIR), Differential Scanning Calorimetry (DSC), Dynamic Mechanical Analyzer (DMA), Texture Analyzer (TA), Thermogravimetric Analyzer (TGA), Gel Permeation or Size-Exclusion Chromatography (GPC/SEC), GPC with Multi-Angle Light Scattering Detection (MALS), and Viscometer
- Generated computational models of different Diels–Alder isomers for spatial assessment

Research advisor: Rodrigo Andrade
Department of Chemistry, Temple University, Philadelphia, PA
"Semi-Synthesis of (–)-Melodinine K, a Potent Compound for Diabetes and Cancer Treatment" (2017 – 2019)

- Isolated and synthesized intermediates via chemical and biological routes (i.e., yeast oxidation) to target a natural product, (–)-melodinine K, potent drug for cancer and diabetes treatment

Research advisor: Eric Borguet
Department of Chemistry, Temple University, Philadelphia, PA
"Optical Properties of Layered and Two-Dimensional Materials" (2016 – 2017)

- Characterized a transition metal dichalcogenides, specifically molybdenum disulfide (MoS_2), via UV-Visible spectroscopy (UV-Vis), fluorimeter, and Raman microscope
- Exfoliated MoS_2 from sapphire substrate into different solvents to analyze environmental effects and utilize as a catalyst for oxidation-reduction experiments
- Tuned properties of MoS_2 with porphyrin (Pc) and tetracyanoquinodimethane (TCNQ) to optimize the sensing and emitting efficiency

TEACHING AND MENTORING

Womxn in STEM (WiSE) Mentor, *University of California, Santa Barbara* (Winter and Spring 2024)

Research Mentor for Future Leaders in Advanced Materials (FLAM) program, *NSF Materials Research Science and Engineering Center (MRSEC), University of California, Santa Barbara* (Summer of 2022)

Teaching Assistant (TA), *Chemistry and Biochemistry department, University of California, Santa Barbara* (2019 – 2021)

- Led laboratory sections of organic chemistry – Beginning and advanced courses (Chem 6AL and 6CL)

Student Success Center (SSC) Tutor, *Temple University* (2018 – 2019)

- Tutored in Calculus, General Chemistry, Organic Chemistry, Biochemistry, and Biology

LEADERSHIP AND OUTREACH ACTIVITIES

MAPS Project Leader, *BioPACIFIC MIP, Campus: University of California, Santa Barbara* (2022 – 2024)

- Designed and provided synthetic insights for digital screening of potential natural product polymers
- Assisted in organizing workshops to collect data for artificial intelligence (AI) implementation

SciTrek Elementary Outreach Volunteer, *University of California, Santa Barbara* (Spring of 2022)

Temple University Chemical Society, *Chapter of American Chemical Society*

- Volunteer for Educational Outreach at secondary schools (2016 – 2019)
- Committee in Planning Community Services (Spring of 2017 and Spring of 2018)
- General Body Meeting Coordinator (2018 – 2019)

PUBLICATIONS

1. Attanayake, N. H.; Thenuwara, A. C.; Patra, A.; Aulin, Y. V.; **Tran, T. M.**; Chakraborty, H.; Borguet, E.; Klein, M. L.; Perdew, J. P.; Strongin, D. R. Effect of Intercalated Metals on the Electrocatalytic Activity of 1T-MoS_2 for the Hydrogen Evolution Reaction. *ACS Energy Lett.* **2018**, *3*, 7–13.
2. Walia, M.; Teijaro, C. N.; Gardner, A.; **Tran, T.**; Kang, J.; Zhao, S.; O'Connor, S. E.; Courdavault, V.; Andrade, R. B. Synthesis of (−)-Melodinine K: A Case Study of Efficiency in Natural Product Synthesis. *J. Nat. Prod.* **2020**, *83*, 2425–2433.
3. Oh, S.; Nikolaev, A.; Tagami, K.; **Tran, T.**; Lee, D.; Mukherjee, S.; Segalman, R. A.; Han, S.; Read de Alaniz, J.; Chabinyc, M. L. Redox-Active Polymeric Ionic Liquids with Pendant N-Substituted Phenothiazine. *ACS Appl. Mater. Interfaces* **2021**, *13*, 5319–5326.
4. **Tran, T. M.**; Read de Alaniz, J. Controlled Synthesis of a Homopolymer Network Using a Well-Defined Single-Component Diels–Alder Cyclopentadiene Monomer. *J. Am. Chem. Soc.* **2023**, *145*, 3462–3469.
5. Oh, S.; Nguyen, P. H.; **Tran, T. M.**; DeStefano, A. J.; Tagami, K.; Yuan, D.; Nikolaev, A.; Condarcure, M.; Han, S.; Read De Alaniz, J.; Chabinyc, M. L.

Interfacial Doping of Semiconducting Polymers with Phenothiazine-Based Polymeric Ionic Liquids. *J. Mater. Chem. C* **2023**, *11*, 15435–15442.

6. **Tran, T. M.**; Read de Alaniz, J. Synthesis and Thermal Recycling of Diels–Alder Cyclopentadiene Thermoplastics, *under review*.
7. **Tran, T. M.**; Nowzari, A.; Talamantez, K.; Sahid Hossain, M.; Bates, C.; Read de Alaniz, J. A Re-Mendable and Degradable Thermoset Using Thermally Reversible Diels–Alder Cyclopentadiene-Maleimide Adducts, *in preparation*.
8. **Tran, T. M.**; Kaneko, T.; Neris, N.; Read de Alaniz, J. A Perspective on Synthetic Strategies and Material Designs Utilizing Diels–Alder Cyclopentadiene Components. *Review article*, *in preparation*.
9. **Tran, T. M.**; Muff, L.; Nowzari, A.; K.; Read de Alaniz, J. Controlled Degradation of Thermoplastic Polyurethanes through the Incorporation of Diels–Alder Cyclopentadiene Dimers, *in progress*.

TALKS

1. **Tran, T.**, Aulin, Y.V., Borguet, E. Functionalization of MoS_2 with Organic Molecules. Temple Undergraduate Research Forum and Creative Works Symposium (TURF-CreWS), 2017.
2. **Tran, T.**, Walia, M., Teijaro, C., Andrade, R. Chemical Synthesis of (–)-Melodinine K. TURF-CreWS, 2018.
3. **Tran, T.**, Walia, M., Gardner, A., Teijaro, C., Andrade, R. Semi-Synthesis of (–)-Melodinine K via Chemical and Biological Routes. TURF-CreWS, 2019.
4. **Tran, T.**, Walia, M., Gardner, A., Teijaro, C., Andrade, R. Semi-Synthesis of (–)-Melodinine K via Chemical and Biological Routes**.** American Chemical Society (ACS) annual meeting, 2019.
5. **Tran, T.**, Read de Alaniz, J. Cyclopentadiene derivative as a single component, catalyst-free to form a flexible polymer network. ACS annual meeting, 2022.
6. **Tran, T.**, Read de Alaniz, J. Synthesis of a well-defined network homopolymer using a single-component Diels-Alder monomer. ACS Division of Organic Chemistry (DOC) Graduate Research Symposium, 2022.
7. **Tran, T.**, Read de Alaniz, J. Controlled Synthesis of Degradable Diels–Alder Polymers Using Single-Component Cyclopentadiene Derivatives. Center for Polymers and Organic Solid (CPOS) Seminar, 2023.
8. **Tran, T.**, Read de Alaniz, J. Controlled Synthesis of a Degradable Diels–Alder Network Using a Single-Component Cyclopentadiene Monomer. Polymers Gordon Research Seminar (GRS), 2023.

AWARDS AND HONORS

Temple University Honors Scholar (2015 – 2019)

Temple University Presidential Scholar with full tuition remission (2015 – 2019)

Temple University Science Scholar (2017 – 2019)

Temple University Robert A. Figlin Family Research Award for outstanding research (2019)

Temple University Herbert M. Winegard Memorial Award for highest GPA in chemistry (2019)

Temple University CARAS Travel Grant (2019)

Philadelphia Section of the American Chemical Society Award (2019)

UCSB International Doctoral Recruitment Fellowship (2019 – 2021)

Chair's Fellowship (2022)

UCSB Summer Support Stipend (2022)

BioPACIFIC MIP Speed Pitch Competition Finalist (2022)

BioPACIFIC MIP Travel Grant (2023)

BioPACIFIC MIP Fellow and Associate (2020 – 2023)

CPOS Workshop Poster Award (2023)

FIELDS OF STUDY

Major Field: Organic Chemistry and Polymer Methodology with Prof. Javier Read de Alaniz

Studies in Organic Synthesis with Prof. Rodrigo Andrade

Studies in Analytical Chemistry and Raman Microscopy Characterization with Prof. Eric Borguet

ABSTRACT

Construction of Functional and Sustainable Materials Using Well-Defined Diels–Alder Cyclopentadiene Monomers

by

Thi M. Tran

Integrating sustainability into high-performance polymers is at the forefront of research efforts to reduce the environmental adverse impact of plastics. Recent approaches have benefited from the reversible chemistry to recycle and degrade materials. Among the promising strategies, Diels–Alder (DA) cycloaddition offers exceptional features, including synthetic ease, absence of catalysts, and the thermally-activated retro-DA (rDA) reaction. The implementation of accessible DA building blocks (e.g., furan and maleimide as the diene-dienophile pair) has provided the synthetic toolbox to fabricate self-healing and degradable thermosets. However, when used as reversible step-growth polymerization, the traditional diene-dienophile or two-component systems generally suffer from the inherent mismatch in stoichiometry, solubility, and/or low rDA temperature (i.e., ~100 °C for furan-maleimide adduct). In comparison, cyclopentadiene (Cp) can serve as a dual role via self-dimerization and thus, holds potential as a solvent-free and single-component platform. Furthermore, combined with the high rDA temperature of the Cp dimer (i.e., 150–180 °C) or Cp-maleimide adduct (i.e., ~150 °C), the application of Cp analogs in polymerization is promising to

fabricate advanced functional polymers with enhanced sustainability. Despite its compelling chemistry, Cp is highly reactive with the propensity to isomerize, dimerize and oligomerize, making the monomer synthesis and polymerization notoriously challenging. In fact, Cp polymerization has remained uncontrolled since the first attempt by Staudinger in 1926.

Herein, the successful stories of obtaining well-defined Cp polymer building blocks and controlling the Cp polymerization will be demonstrated, followed by the construction of complex and reversible materials based on the developed methodologies. The first part of the dissertation explores the efficient access to a well-defined tetra-functional Cp monomer under mild conditions via the optimized deprotection of a norbornadiene precursor using a tetrazine reagent. The controlled synthesis of a tough and degradable homopolymer network is subsequently showcased. The second part builds upon the deprotection platform to synthesize and study di-functional Cp derivatives with varied substituent effects. The goal is to understand and suppress uncontrolled cross-linking for the formation of reversible high-MW DA homopolymers. The utilization of a radical inhibitor, butylated hydroxytoluene, was discovered to prevent cross-linking, leading to the first general Cp homopolymerization. Notably, a Cp thermoplastic with the backbone derived from hydrogenated polybutadiene can be thermally recycled (i.e., M_n = 68 to 23 kDa and back to 68 kDa) three times without solvents and additional purification steps. The last three stories were developed by utilizing the well-defined Cp derivatives to fabricate degradable thermoplastic polyurethanes, a Cp-maleimide self-healing thermoset, and the stereo-chemical homopolymer networks. Through the development of controlled Cp polymerization, the expansion of DA chemical toolbox can be realized to fabricate a variety of promising materials with optimized mechanical performance and sustainability.

TABLE OF CONTENTS

1. Chapter 1: *Introduction*.....1

1.1 Architectures of Thermoplastics and Thermosets Determine Their End-of-Life Fates 1

1.2 Industrial Strategies to Recycle Thermoplastics and Thermosets 4

1.3 Classic Diels–Alder as the Modern Chemical Tool to Fabricate Re-mendable and Degradable Thermosets 6

1.4 Efforts towards the Synthesis of Recyclable Diels–Alder Thermoplastics 10

1.5 Discovery of Cyclopentadiene and its Unique Dimerization 11

1.6 Strategies to Utilize Cyclopentadiene for Material Synthesis 14

1.7 Thesis Scope 17

1.8 References.....20

2. Chapter 2: *Controlled Synthesis of a Homopolymer Network Using a Well-Defined Single-Component Cyclopentadiene Monomer* 30

2.1 Overview.....30

2.2 Abstract.....32

2.3 Introduction.....33

2.4 Results and Discussion 40

2.5 Conclusion 52

2.6 Acknowledgements.....54

2.7 Supporting Information 54

2.8 References.....103

3. Chapter 3: *Synthesis and Thermal Recycling of Cyclopentadiene Thermoplastics* 110

3.1 Overview 110

3.2 Abstract 111

3.3 Introduction 112

3.4 Results and Discussion 120

3.5 Conclusion 138

3.6 Acknowledgements 139

3.7 Supporting Information 139

3.8 References 298

4. Chapter 4: *Controlled Degradation of Spandex Thermoplastic Polyurethanes through the Incorporation of Diels–Alder Cyclopentadiene Dimers* 307

4.1 Overview 307

4.2 Abstract 308

4.3 Introduction 309

4.4 Results and Discussion 316

4.5 Conclusion 328

4.6 Acknowledgements 329

4.7 Supporting Information 330

4.8 References 342

5. Chapter 5: *A Re-mendable and Degradable Thermoset Using Thermally Reversible Diels–Alder Cyclopentadiene-Maleimide Adducts* 344

5.1 Overview 344

5.2 Abstract 345

5.3 Introduction....346
5.4 Experimental Section....351
5.5 Results and Discussion....356
5.6 Conclusion....365
5.7 Supporting Information....366
5.8 Acknowledgements....370
5.9 References....370
6. Chapter 6: *The Synthesis and Studies of Stereo- and Regio- Diels–Alder Homopolymer Networks Based on a Class of Azetidine-Cyclopentadiene Derivatives*....373
6.1 Overview....373
6.2 Abstract....374
6.3 Introduction....375
6.4 Results and Discussion....382
6.5 Conclusion....392
6.6 Acknowledgements....392
6.7 Supporting Information....393
6.8 References....412
7. Chapter 7: *Future Directions and Outlook*....415
7.1 Concluding Remarks....418
7.2 References....419
8. Appendix....421

1. Chapter 1: *Introduction*

Sections of this chapter were previously published in Journal of American Chemical Society (JACS). The contents and figures are reprinted with permission from *J. Am. Chem. Soc.* **2023**, *145*, 3462–3469. DOI: 10.1021/jacs.2c11416. Copyright 2023 American Chemical Society.

1.1 Architectures of Thermoplastics and Thermosets Determine Their End-of-Life Fates

The recognition of covalent bonding in "macromolecules" by Staudinger has led to the discovery of polymers and sparked the industrial fabrication of a wide range of plastics, ranging from the robust, high-performance to re-processable and broadly used materials.[1–4] However, the chemical connections that provide the favorable mechanical properties also make these macromolecules persist in the environment at the end of their lifecycles.[4–7] In fact, most plastics take hundreds of years to break down into smaller fragments after they are disposed of.[6–8] The combination of the fast-growing production and never-ending lifetime of plastics leads to the waste buildup and thus, adversely impacting the environment.[6–8] This factor has urged a vast amount of research efforts to investigate and improve the plastic degradation and recycling.[9–11] Closer look at the polymer architectures can assist in understanding the recycling and degrading capabilities of traditional plastics, which also correlates with their mechanical properties.[12–15] Polymers are generally divided into two main categories, including thermoplastics and thermosets.[12–15]

Thermoplastics are composed of linear high-molecular-weight (high-MW) polymers (**Figure 1.1**). The physical entanglement and the interactions among the long-chain polymers

(e.g., non-covalent bonding, degree of crystallinity) equip these materials with a wide range of mechanical properties.[12–14] These loosely packed polymer chains also lead to the solubility of thermoplastics in organic solvents and their recycling ability, mainly involving melting and hardening through heating and cooling conditions.[12] Certain types of thermoplastics can be reprocessed after their first use by this melting-and-remolding to form recycled products, which typically have lower mechanical properties compared to the virgin materials.[13,14,16] The versatile mechanical performance along with the re-processability in thermoplastics are suitable for commodity applications, especially in packaging and textile fibers.[12] Hence, thermoplastics contribute to about 80% of the overall consumed plastics. About 50% of them are single-use materials.[12] The prime examples of thermoplastics are polyethylene terephthalate (PET), polyethylene (PE), and polystyrene (PS), and polycarbonate (PC).[12]

Thermosets, in contrast, are chemically cross-linked polymers (**Figure 1.1**), which results in the rigid three-dimensional architectures and high-performance properties.[12,13,15] The affixation of the chemical bonding provides these materials with excellent chemical and thermal resistance.[12] Common thermosets encompass vulcanized rubber, epoxy resins, and polyurethane foam.[12] They are typically used in the durable settings, such as composites for wind-turbine blades, aeronautical and automotive parts, or structural components.[12] Thermosets comprise about 20% of manufactured polymeric materials, and typically last longer than thermoplastics due to their mechanical robustness.[12] However, once damage, these materials cannot be melted and re-processed in the same conditions that are applicable for thermoplastics and thus, mostly end up in a landfill or become incinerated (i.e., energy recovery).[12,15]

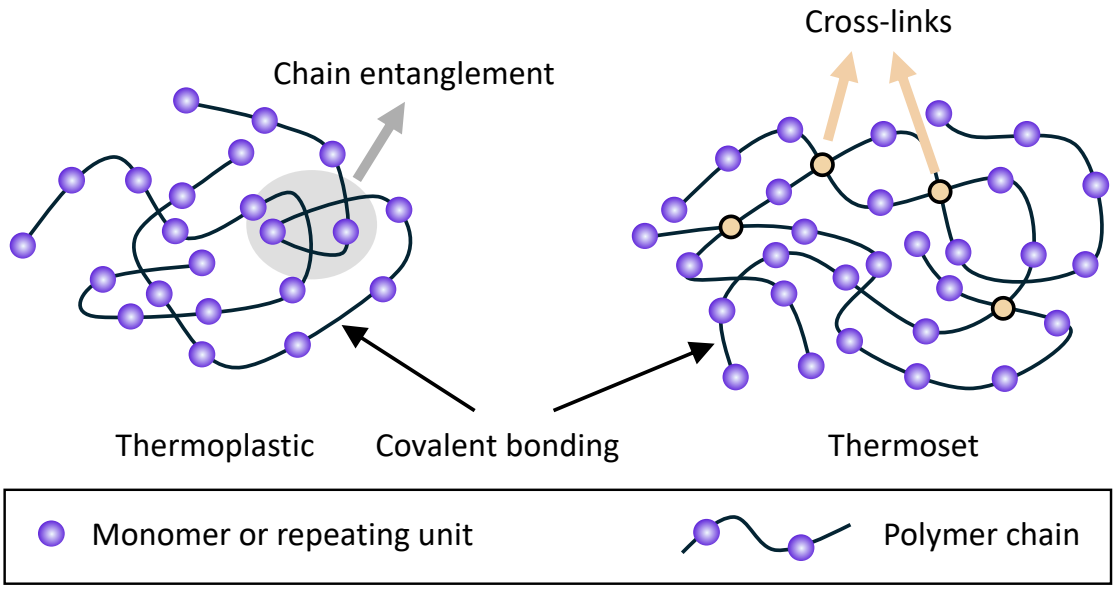


Figure 1.1. The schemes of thermoplastics (left) versus thermosets (right) to highlight the difference in the architectures of these materials that correlates to their varied mechanical performance, degradability, and recyclability.

The ability of the polymer chains in thermoplastics to flow under high temperatures provides these materials with their mechanically recycling, compared to the fixed chemical connections in thermosets.[12] However, the irreversible covalent bonding (**Figure 1.1**) between the small molecules that constitute most thermoplastics renders them resistant to degradation and hydrolytic cleavage into the smaller fragments.[12] Therefore, even though thermoplastics can be reused compared to thermosets, majority are discarded and remain in the environment after their last use.[17,18] In other words, reprocessing thermoplastics solely delays their time to eventually become waste.[17,18] As a result, most types of conventional polymers, including thermoplastics and thermosets, though fundamentally different in architectures, proposes comparable level of pressing environmental concern with their intrinsic non-degradability at the end of their lifecycles.[12,18] The following chapters will cover the industrial recycling of thermoplastics and thermosets and the adaptation of a classic chemistry that holds potential to expand the design and construction of advanced functional and sustainable materials.

1.2 Industrial Strategies to Recycle Thermoplastics and Thermosets

Even though it remains a grand challenge to mitigate the aftermaths of thermoplastics, there are strategies that have been employed in industry to contribute to decreasing the plastic waste. Chemical closed-loop recycling methods can be applied for certain types of polymers, mostly limited to a subset of thermoplastics.[12] These strategies target labile bonds in the high-molecular-weight (high-MW) polymers and convert them into smaller fragments or intermediates, which are ideally subjected to re-polymerization to form the virgin-like or similarly functional materials.[12,19–22] This method holds potential to preserve the macromolecular properties, maximize the monomer resources and thus, reduce the adverse environmental impacts of plastics.[12,19,20]

One of the most recyclable materials is a class of step-growth polycondensation thermoplastics (i.e., PET, PC).[12,20] With the high content of ester, carbonate, or labile linkages, known chain-breaking conditions can enable the chain degradation in these materials.[12,20] Glycolysis is the most favorable, especially for PET deconstruction, because of its efficiency and mild conditions.[12,20,23] In this process, ester bonds are broken through transesterification with a diol to form the de-polymerized hydroxylated derivatives.[12,20,23] Glycolysis is typically sluggish. Therefore, metal-based catalysts (mostly titanium-based) are often used to speed up the de-polymerization, which unfortunately, are difficult to remove and harmful to the environment.[12,24] There are other pathways include hydrolysis, methanolysis, alcoholysis, and aminolysis.[12] The categories depend on the chemical reagents, conditions and catalysts that are used for the decomposition. For example, hydrolysis is conducted under either basic, acidic, or neutral aqueous conditions.[25] The first two processes respectively employ strong basic and acidic solvents while the latter recruits hot water or steam in high-pressure

autoclaves at temperature ranging 200–300 °C and pressure 1–4 MPa.[12,26] Other types of decomposition methodology (i.e., methanolysis, alcoholysis, and aminolysis) also require high temperature, pressure and sometimes, metal-based catalysts.[12] For long-chain hydrocarbon polymers such as polyethylene, pyrolysis is the major method for the decomposition pathway.[12,27] The process includes the heating (in the range of 300–450 °C) and pressurizing the high-MW polymers in the absence of oxygen to produce smaller fragments in the form of liquid oil or wax that are valuable in other industrial applications such as fuel production and refineries.[16,27,28] Recycling of other classes of thermoplastics, such as PS, polypropylene (PP), and polyvinylchloride (PVC), remain limited or challenging.[12]

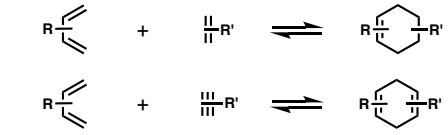
Thermosetting polymers, as aforementioned in the previous section, are not chemically recyclable under practical conditions in most cases compared to thermoplastics.[12,15] The main recycling strategies in industry are restricted to mechanical processing of these materials under high shearing, elevated temperature, and pressure (e.g., polyurethane foams[29–33] or vulcanized rubber[34–38]).[12] Some methods are proposed to improve the degradation process such as glycolysis,[39] hydrolysis with supercritical water,[40] pyrolysis,[41] microwave treatment,[42] and microbial degradation.[43] However, extreme conditions and limited recycling or decomposition are generally encountered in these processes.

In general, industrial recycling of polymers is possible and mostly restricted to certain types of thermoplastics (i.e., polycondensate polymers). The process generally involves harsh conditions (e.g., strong bases, acids, high temperature, pressure), and sometimes, with harmful catalysts. Thermosets, on the contrary, are largely not recyclable.

1.3 Classic Diels–Alder as the Modern Chemical Tool to Fabricate Re-mendable and Degradable Thermosets

The discovery of Diels–Alder (DA) in 1928 has expanded the chemical toolbox in organic synthesis to construct a variety of complex natural products with cyclic moieties that are formed through the stereo-controlled cycloaddition between the conjugated dienes and alkenes (or dienophiles) (**Scheme 1.1**).[44–48] Overtime, the original purpose of classic DA reactions has evolved and especially, been adapted for the burgeoning polymer field.[48–50] These cycloaddition reactions have created a profound impact on the fabrication of increasingly intricate polymers (e.g., block, star, and graft copolymers) due to their attractive "click-like" features.[50] First, the formation of the C–C linkages is thermally driven and thus, generally absent of metal-based catalysts, photochemical stimulus, or chemical reagents (e.g., bases, acids, or reducing reagents).[49,50] No by-products are generated when the two chemical building blocks are put together. Furthermore, the reactivity and functionality of the DA partners (e.g., dienes and dienophiles) can be broaden through the substituent modification, creating a generous space for improvement of the polymerization platforms and structure-property relationship investigation.

Scheme 1.1. Diels–Alder reaction scheme shows the reaction between an unsaturated diene and a dienophile to form a cyclic DA adduct.

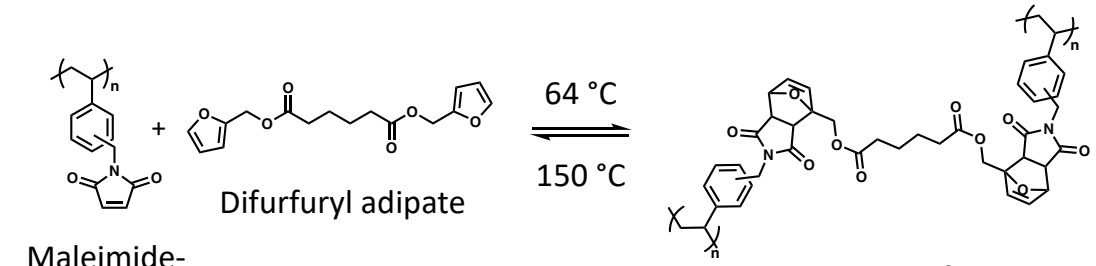


Diene Dienophile DA adducts

R = Electron-donating groups
R' = Electron-withdrawing groups

Notably, during the past half-century, the thermoreversible feature of DA has captured the attention of the polymer science and expanded the construction of environmental-friendly materials.[48,49,51,52] The earliest synthesis of thermally reversible cross-linked polymers using furan-maleimide adduct was described in the patent from Craven in 1969.[53] Upon heating the cross-linked polymers at the retro-DA temperature, the reverse reaction is enabled and thus, the materials begin to thermally de-cross-link into soluble mixtures.[53–56] This report sparked several research efforts to integrate reversible furan-maleimide adducts, mostly as pendant groups, into the cross-linked polymers.[54–56] The prime example is the synthesis of a thermoreversible cross-linked polystyrene between the maleimide-functionalized polystyrene with a difurfuryl adipate from Canary and Stevens (**Scheme 1.2**).[56] Despite an early interest, the application of rDA reaction to the synthesis of a re-mendable thermoset was not introduced until 2002 by Wudl and coworkers (**Figure 1.2**).[57] Incorporation of the furan-maleimide DA adducts into the polymer backbones or as cross-linkers facilitates the bond rearrangement upon heating.[57] When damaged (e.g., crack propagation), the material integrity can be restored through the breakage and re-formation of the reversible linkages at the rDA temperature range.[57] Applying this approach, re-mendable polymers can be re-used multiple times after damage. By increasing their service times or lifecycles, the environmental adverse impact of thermosets can be mitigated.[48,51,52,54,55] The rapid adoption of this concept has advanced the development of a wide range of self-healing and degradable DA polymer networks (e.g., DA-adduct-functionalized epoxy resins, polyamides, polyesters, and polymethacrylates).[48,54–62]

Scheme 1.2. The synthesis of a cross-linked furan-maleimide polystyrene between the maleimide-functionalized polystyrene and difurfuryl adipate, reported from Canary and Stevens.[56]



Maleimide-functionalized polystyrene

Cross-linked furan-maleimide polystyrene

The fruitful fabrication of re-mendable thermosets generally requires relevant rDA temperatures of the DA adducts, the accessible synthesis of the diene-dienophile building blocks, and the efficient curing based on the reactivity of these starting materials.[51–57] Furan as the diene and maleimide as the dienophile have been extensively exploited due to their stability at ambient atmosphere and synthetic accessibility. The reactivity of furan and maleimide is slow but efficient enough for the curing of the highly cross-linked polymers. The furan-maleimide materials can be useful for certain applications (e.g., self-mending electronic packaging) despite its low rDA temperature (i.e., in the range of 100–110 °C). The field has also expanded to utilize other diene-dienophile pairs, such as anthracene and maleimide, and cyclopentadiene-cyanothioester.[48,51,52] Anthracene-maleimide adduct possesses a high rDA temperature range of 200–250 °C and thus, is more thermally stable than the furan-maleimide analog.[48,51,52] Using anthracene and maleimide, several re-mendable thermosets that can withstand harsh environment were fabricated. However, the mending temperatures are near the thermal decomposition of the most polymer chains and organic materials, leading to the complicated de-cross-linking mechanism and challenging self-healing.[63–65] Hetero-DA reaction between cyclopentadiene and cyanothioester was also developed by Barner-Kowollik

to synthesize a fast self-healing cross-linked polymer. No catalyst is required in this system and repetitive cyclability of polymerizing/de-polymerizing in the range of 40–120 °C was demonstrated.[66] Of note, most of the described works are based on two components (i.e., diene and dienophile) to form the DA adducts. There is another unique chemistry where a single component (i.e., cyclopentadiene) is employed to construct the re-mendable DA polymers, which will be discussed in the sections 1.5 and 1.6.

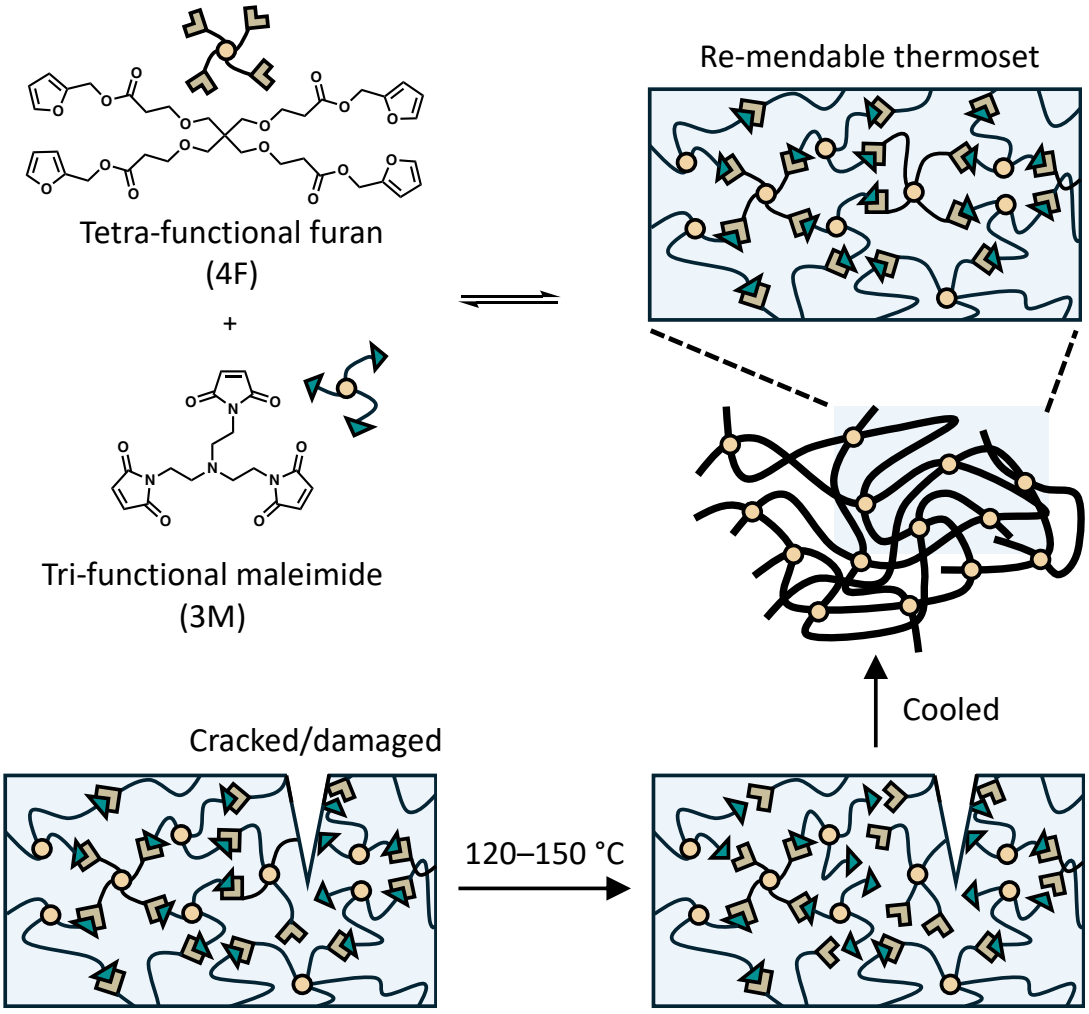
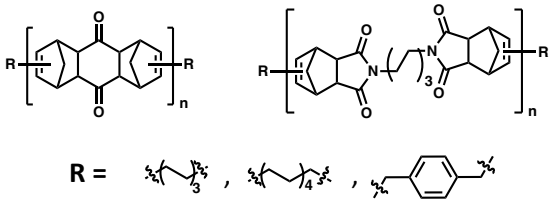


Figure 1.2. The fabrication of a re-mendable thermoset, using a tetra-functional furan and tri-functional maleimide. Upon damage (i.e., cracked), the material is heated at 120–150 °C to facilitate bond rearrangement through the reversible linkages (DA bonds). After the material is cooled down, the damaged surface can be re-mended, and the thermoset can be reused.[57]

1.4 Efforts towards the Synthesis of Recyclable Diels–Alder Thermoplastics

The unique rDA feature has been rigorously investigated in re-mendable and degradable cross-linked polymers. However, the construction of high-MW linear materials using DA chemistry to leverage the reversibility of DA bonds remains challenging.[48,52,55,62,67–69] This section will focus on the prime examples as the synthetic efforts towards the fabrication of thermoplastics using DA chemistry.

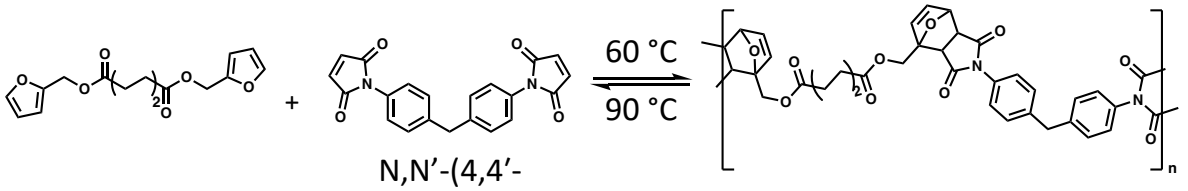
Scheme 1.3. The A_2B_2-type polymerization between Cp derivatives and *p*-benzoquinone or *N,N′*-hexmethylenebismaleimide.[70]



The interest in the formation of linear Diels–Alder polymers was initiated by Stille in 1961 via an A_2B_2-type process using cyclopentadiene (Cp) units as the diene and *p*-benzoquinone or *N,N′*-hexmethylenebismaleimide as the dienophile.[70] More than two decades later, Kennedy and Carlson reported a tenfold chain extension of their functionalized polyisobutylene with terminal silylcyclopentadiene and *N,N′*-hexamethylenebismaleimide.[71] Despite the successful demonstration of these A_2B_2-type syntheses, there was no follow-up study on this subject, presumably due to the synthetic challenges associated with preparing bis-cyclopentadiene monomers.[54,72–74] The focus, instead, has been shifted to furan and maleimide materials after Tesoro and Sastri prepared a bis-furan-functionalized siloxane and initiated polyaddition using a bis-maleimide.[75] Functionalization of a polymer by furan and maleimide units to obtain the corresponding A_2 and B_2 macromonomers is straightforward and synthetically accessible to a range of polymer backbones.[54,55,62,67–69,76] Unfortunately, the materials generally suffer from poor solubility, slow chain-growth reactivity, and low

molecular weights (MWs). [54,55,62,67–69,76] Therefore, even though the thermal reversibility of linear furan-maleimide polymers was recognized early by Kuramoto and the coworkers in 1994,[77] there still lacks reports about the chemical recycling of DA thermoplastics.

Scheme 1.4. Thermoreversible furan-maleimide linear polymer, first proposed by Kuramoto and coworkers in 1994.[77]



Difurfuryl adipate

N,N′-(4,4′-diphenylmethane bismaleimide)

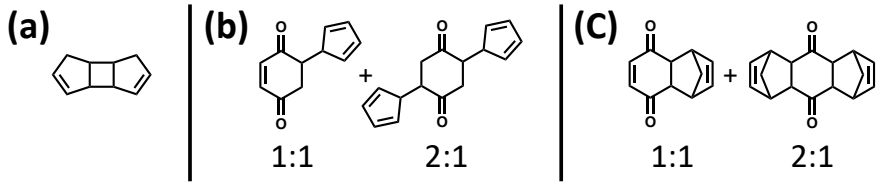
Absence of catalysts and chemical reagents to form and deconstruct DA polymers is highly advantageous to improve recycling efficiency, compared to the available methods in industry. Nonetheless, the current building blocks, which largely comprise of furan and maleimide, have not provided the field with a successful platform to recycle thermoplastics.

1.5 Discovery of Cyclopentadiene and its Unique Dimerization

Cyclopentadiene is one of the most reactive dienes in the DA reaction.[73,74,83] It can also serve as both diene and dienophile and thus, readily dimerizes under ambient atmosphere to form dicyclopentadiene (diCp).[73,74,83] The diCp mixture was believed to be present in the distillation of coal tars as early as the 1870s–1880s.[84,85] As a matter of fact, in 1866, Roscoe first identified a dimeric compound with a molecular formula of $C_{10}H_{12}$ from the products of phenol pyrolysis.[85] He correctly rationalized its interconversion to a volatile monomeric compound, disapproving a previous assumption about the possible oxidation.[85] The same phenomenon was observed in the condensation products of oil gas by Etard and Lambert.[86] Later in 1896, Kraemer and Spilker described the initial structures of cyclopentadiene (C_5H_6)

and its dimer ($C_{10}H_{12}$), which were not correct but the dimerization of Cp was confirmed (**Scheme 1.5a**).[87] Albrecht reported the 1:2 and 2:1 adducts between Cp and 1,4-benzoquinone as if Cp reacts with an α,β-unsaturated ketone via a Michael addition.[74,88] The mischaracterized structures of the Cp-benzoquinone products are shown in **Scheme 1.5b**. The reaction mechanism and structures of the products were later corrected in the seminal report in 1928 by Diels and his student, Alder (**Scheme 1.5c**).[44]

Scheme 1.5. Mischaracterized structures of dicyclopentadiene from Kraemer and Spilker[87] (a), and of cyclopentadiene-benzoquinone adducts from Albrecht[88] (b), versus the correct structures of the cyclopentadiene-benzoquinone adducts from Diels and Alder.[44]

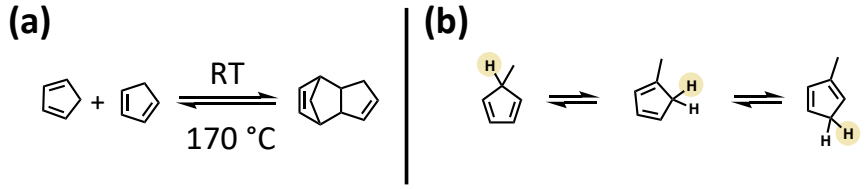


The formation of Cp dimer was recognized even before the discovery of Diels–Alder reaction and has initiated a plethora of research to understand Cp reactivity.[74,93,94] The typical frontier molecular orbital theory does not fully support the high reactivity of Cp as the diene.[74] As established in DA reactions, the reaction rate is influenced by the interaction between the highest occupied molecular orbital (HOMO) of one reactant (i.e., diene) and the lowest unoccupied molecular orbital (LUMO) of the other reactant (i.e., dienophile).[78,89–92] Lower separation of LUMO–HOMO decreases the transition-state energy of the reaction. Therefore, the reaction is accelerated when the HOMO is raised and the LUMO is lowered.[89–92] This effect is normally achieved by adding the electron donating groups to the diene and electron withdrawing substituents to the dienophile.[89–92] However, Cp possesses a fast reaction rate even without any substituents.[74,93,94] This rapid reactivity of Cp majorly stems from its unique geometry.[74,93,94] The cyclic structure of Cp "locked" the diene in the *s-cis*-form, which is the more favorable configuration for the DA reaction compared to the *s-trans*-form.[78,89–92]

Furthermore, as analyzed by Levandowski and Houk, the 5-carbon ring structure of Cp leads to its minimal distortion requirement to achieve the envelope-like geometry that is adopted in the transition state of the DA reaction. Less distortion is observed for Cp to react due to its rigid geometry compared to other cyclic dienes (i.e., cyclohexadiene, cycloheptadiene) and thus, leading to its faster reaction rate.[74,93,94]

The high reactivity of Cp without substituents also assists its dual role as both diene and dienophile. Dimerization is readily observed for the neat monomer at room temperature (**Scheme 1.6a**). In fact, the rate constant of the dimerization of Cp to the *endo*-dicyclopentadiene at 25 °C is reported as $8.3 \times 10^{-7}\ M^{-1}s^{-1}$.[95,96] Cp is thermodynamically unstable at room temperature with the half-life of neat Cp at 25 °C is ~28 h.[74] Fortuitously, Cp dimerization is reversible and thus, the source of Cp is normally derived from the distillation or cracking of diCp at 150–170 °C (the rDA temperature).[74,97,98] Apart from the high reactivity as the diene and its dimerization ability, Cp also undergoes a fast 1,5-hydride (1,5-H) sigmatropic shift to form different isomers at ambient atmosphere.[74] For instance, methylcyclopentadiene, a mono-substituted Cp derivative, typically exists in 3 different isomers, 5-methyl, 1-methyl, and 2-methyl (**Scheme 1.6b**).[99] The developed Cp analysis demonstrates that the increased number of substituents can slow down the 1,5-H shift.[74,100–104] The addition of alkyl groups across the double bonds in Cp can decrease the rate of the 1,5-H shift. A 1,5-substituted methyl Cp has a rate constant of $5.5 \times 10^{-5}\ s^{-1}$ in 1,5-H migration compared to a 5-methyl Cp with a value of $6.2 \times 10^{-4}\ s^{-1}$ (reported at 30 °C).[74,105] Pentamethylcyclopentadiene is known to not dimerize readily at room temperature with the 1,5-H migration rate constant of $2.4 \times 10^{-7}\ s^{-1}$.[105,106]

Scheme 1.6. (a) Cp readily dimerizes at room temperature to form diCp; the cracking of diCp at 170 °C provides the source of Cp.[74,95,96] (b) 1,5-H shift is observed in 5-methylcyclopentadienes. All the isomers are observed at room temperature.[74,99]



Cp is unique and holds great potential as a single-component platform in reversible step-growth polymerization. Furthermore, combined with the high retro-DA reaction of the Cp-dimer (i.e., 150–180 °C), Cp is promising to expand the range of applications in polymeric materials. However, as delineated, Cp is highly reactive with the propensity to isomerize and dimerize. Constant investigation and methodology development are necessary to control Cp and allow for its promising utilization in polymerization.

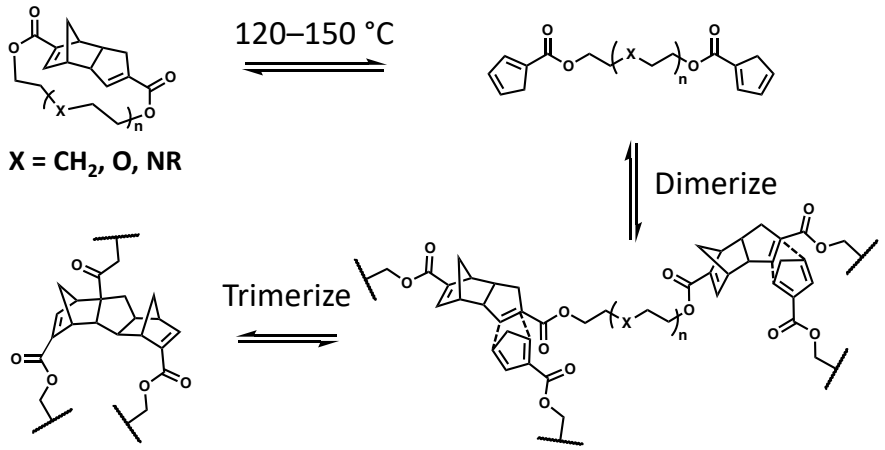
1.6 Strategies to Utilize Cyclopentadiene for Material Synthesis

Regardless of the mischaracterized and puzzling reactivity when it was first discovered, Cp was sufficiently employed to construct intriguing macromolecules. In 1924, Staudinger alongside Rheiner,[107] and later with Bruson[108] attempted to synthesize Cp macromolecules by heating the dimer at 170–180 °C, followed by thorough purification to isolate five different polymerization products.[107,108] Although pioneering, the uncontrolled nature of Cp oligomerization (i.e., trimers, tetramers, octamers, etc.) resulted in a material with a high decomposition temperature, and poor processability.[83,108,109] As recognized early, Cp oligomerization did not lead to a fruitful type of material. Controlled incorporation of Cp monomeric units into better-defined polymer architectures is promising to reveal the formation of useful polymeric materials. In this section, the synthetic efforts of utilizing Cp moiety to construct cross-linked and linear polymers will be discussed.

The construction of linear Cp polymer is divided into two main pathways, including the single-component (i.e., A_2A_2 type) and the two-component (i.e., A_2B_2 type) systems. The first linear Cp homopolymerization (i.e., A_2A_2 type) was described by Stille in 1961,[70] almost three decades after Staundinger's phenomenal work. Bis(cyclopentadienyl)alkane derivative was explored as a telechelic monomer (the structures are shown in **Scheme 1.3**). However, due to the high reactivity of Cp as aforementioned – at room temperature, Cp readily dimerizes and undergoes fast 1,5-H shift – the monomer could not be purified prior to polymerization.[70] Despite the impure mixture of Cp monomers, the homopolymerization was still conducted at high temperature (i.e., 80–110 °C) with different solvents (i.e., benzene, toluene).[70] Either an uncontrolled cross-linking process was observed, or low-MW materials was attained.[70] Bulk polymerization of these telechelic Cp monomers in the presence of radical inhibitors was not successful to prevent the cross-linking even though it was presumably attributed to a random vinyl radical polymerization.[70] Since then, no other works have been reported about this single-component or A_2A_2 type of polymerization utilizing telechelic Cp monomers. In his same report in 1961, Stille reacted the telechelic Cp monomer as the diene with *p*-benzoquinone (**Scheme 1.3**) to form a soluble linear polymer.[70] Kennedy and Carlson synthesized a polyisobutylene with nonfluxional terminal silylcyclopentadiene units that refrain from self-dimerization.[71] Coupling this derivative with bis-dienophiles created tenfold chain extension of their functionalized polyisobutylene.[71] However, no reversibility test was described.[71] The most recent attempt was proposed by Deck group to fabricate thermally reversible polymers using sterically hindered bis-alkylcyclopentadienes and bis-maleimides.[72] In general, the utility of di-functional Cp monomers remains challenging to execute in the construction of linear polymers.

Fabrication of Cp cross-linked polymer also displays complication and several limitations. Most strategies generate Cp groups *in-situ* via post-functionalization or pair it with a highly reactive dienophile such as cyanodithioester (CDTE).[66,110] For example, Kennedy and Castner reported the incorporation of pendant Cp units by cyclopentadienylation with chlorinated butyl rubber polymers.[110] *In-situ* dimerization of Cp lead to the formation of reversible networks.[110] Barner-Kowollik and co-workers exploited the fast hetero-DA reaction between Cp and CDTE to prepare a highly efficient self-healing polymer network with repetitive recyclability.[66] The most recent effort to control Cp polymerization was proposed by Wudl in 2008 (**Scheme 1.7**).[73] The synthesis of well-defined cyclic diCp derivatives as a single component was achieved to form DA-based thermally re-mendable polymer materials.[73] The basis of this approach lies in the thermally reversible DA cycloaddition. Upon heating to 120–150 °C, the cyclic Cp dimer undergoes the retro-DA (rDA) reaction to reveal telechelic Cp monomers that subsequently underwent DA polyaddition to form self-healable cross-linked polymer networks.[73] By providing access to a well-defined monomer using the rDA reaction, Wudl demonstrated that the cross-linking occurred via an uncontrolled trimer formation between the alkene on the polymer backbone from the Cp-dimer and another reactive Cp (**Scheme 1.7**).[73] This approach realized the feasible processability of Cp-based homopolymers, subsequently enabling characterization studies and post-damage (i.e., re-mendable) repair strategies.[73] Despite a remarkable realization in controlling Cp polymerization through the synthesis of well-defined Cp monomers, the practice of utilizing Cp units to prepare tailored advanced materials remains in infancy.[83]

Scheme 1.7. The protected cyclic diCp monomers developed by Wudl and coworkers. The isolation of well-defined monomers leads to the polymerization at high temperatures (i.e., 120–150 °C). The diCp monomers undergo rDA reaction and form linear polymers that are cross-linked through the trimerization of Cp *in-situ*.[83]



1.7 Thesis Scope

Given the challenges to recycle thermoplastics and degrade thermosets with conventional DA strategies (e.g., two-component furan-maleimide), the ability to control cyclopentadiene in the single-component step-growth polymerization will propose a promising platform for efficient construction of selectively degradable and recyclable materials. In Chapter 2, the importance will be emphasized on accessing a well-defined tetra-functional Cp (TCp) monomer under mild conditions that leads to the controlled synthesis of a reversible homopolymer network. The isolation of TCp was realized through the optimization of the previously developed deprotection of a norbornadiene precursor using a tetrazine reagent. Different curing conditions (i.e., varied temperatures) of the TCp monomer were performed to analyze the polymerization behaviors, which reveals the uncontrolled cross-linking at 130 °C or higher. A better-defined homopolymer network was fabricated under the optimal

curing condition (i.e., 110 °C for 3 h). Upon characterization, the polymer is tough and elastic, compared to the brittleness observed in prior works by Wudl and Staudinger.[73,108,109] The network also possesses a shape-memory effect and can be selectively degraded via a retro-Diels–Alder reaction with a "capping" and N15-labeled reagent, ^{15}N-phenyl maleimide. Furthermore, this work also introduces a general platform to isolate and synthesize varied well-defined Cp monomers that unfolds the following investigation in the dissertation.

Chapter 3 builds upon the recognition of the limitations in the DA linear polymerization utilizing the current building blocks (e.g., furan-maleimide). As discussed in Section 1.4, low-MW and challenging recyclability in DA polymers are typically encountered. Cp is promising as a single component in the step-growth polymerization. In addition, the high rDA temperature of the Cp-dimer hypothetically expands the utility of Cp materials. However, the uncontrolled cross-linking in these materials has limited its potential. Chapter 3 begins with the synthesis and investigation of di-functional Cp derivatives with varied substituent effects. The goal is to understand and suppress uncontrolled cross-linking for the formation of reversible high-MW DA homopolymers. The utilization of a radical inhibitor, butylated hydroxytoluene, was discovered to prevent cross-linking, leading to the first successful Cp homopolymerization. To demonstrate the generality of the methodology, six Cp homopolymers were synthesized and characterized with backbones derived from common thermoplastics, such as polydimethylsiloxane, hydrogenated polybutadiene, and ethylene phthalate. Remarkably, the hydrogenated polybutadiene-Cp analog can be chemically recycled (M_n = 68 to 23 kDa, and back to 68 kDa) three times with high consistency. No additional purification and solvents are required throughout the process.

Chapter 4 were initiated by a mutual interest in recycling a class of thermoplastic polyurethanes (TPUs). TPUs are typically used as the addictive in several applications, such as Elastane or Spandex in the textile industry, structural and automobile components. We are specifically intrigued by the utility of TPUs in Spandex, which provides the elasticity in our clothes. Despite a small percentage of Spandex (5–30%) in clothing, it has created a pressing environmental concern because it is not recyclable. Furthermore, the lack of separation between Spandex and other recyclable polymers in the elastane fibers increases the difficulty and cost to the industrial recycling of textile products. By utilizing a Cp-dimer diol derivative as an addictive during the polyurethane synthesis, a new class of degradable thermoplastic polyurethanes has become accessible. Chapter 5 draws back to the implementation of the re-mendable DA cross-linked polymer. A re-mendable thermoset was synthesized and characterized based on the reaction of Cp as the diene and maleimide as the dienophile. Due to the high rDA temperature of Cp-maleimide (i.e., ~150 °C), the repairing is only activated upon damage at high temperature to preserve the mechanical performance. Therefore, the material is supposedly more thermally stable and can withstand harsh conditions compared to the furan-maleimide analog. Furthermore, the fast reaction between Cp and maleimide hypothetically facilitates the bond rearrangement at the rDA reaction. This increased dynamic bond exchange at high temperature potentially improves the self-healing property compared to other high-performance materials (e.g., Cp homopolymer network, anthracene-maleimide cross-linked polymer). Chapter 6 is developed through a long-standing interest in the synthesis of stereo-chemical polymer networks. Even though stereochemistry is known to impact the properties of linear polymers, the effect of stereochemistry to the mechanical performance of cross-linked materials remains limited. In fact, the three-dimensional effect is omitted in most

of the structure-property relationship studies in polymer networks. One of the challenges is the lack of a methodology that provides a consistent curing condition. To provide the field with a new promising chemical toolbox, in this chapter, a new class of azetidine-Cp homopolymer networks will be explored, each was synthesized from a different stereo- or regioisomer of the azetidine-Cp cross-linker. Finally, Chapter 7 will summarize the developed reversible step-growth polymerization using well-defined Cp monomers and prepare an outlook to apply Cp into a variety of highly complex polymer architectures. Appendix can be found at the of the dissertation that will include interesting data to reveal new directions for Cp materials.

1.8 References

(1) Staudinger, H. Über Polymerisation. *Ber. dtsch. Chem. Ges. A/B* **1920**, *53*, 1073–1085. DOI: 10.1002/cber.19200530627.

(2) Mülhaupt, R. Hermann Staudinger and the Origin of Macromolecular Chemistry. *Angew. Chem. Int. Ed.* **2004**, *43*, 1054–1063. DOI: 10.1002/anie.200330070.

(3) Frey, H.; Johann, T. Celebrating 100 Years of "Polymer Science": Hermann Staudinger's 1920 Manifesto. *Polym. Chem.* **2020**, *11*, 8–14. DOI: 10.1039/C9PY90161B.

(4) Fagnani, D. E.; Tami, J. L.; Copley, G.; Clemons, M. N.; Getzler, Y. D. Y. L.; McNeil, A. J. 100th Anniversary of Macromolecular Science Viewpoint: Redefining Sustainable Polymers. *ACS Macro Lett.* **2021**, *10*, 41–53. DOI: 10.1021/acsmacrolett.0c00789.

(5) Billiet, S.; Trenor, S. R. 100th Anniversary of Macromolecular Science Viewpoint: Needs for Plastics Packaging Circularity. *ACS Macro Lett.* **2020**, *9*, 1376–1390. DOI: 10.1021/acsmacrolett.0c00437.

(6) Geyer, R.; Jambeck, J. R.; Law, K. L. Production, Use, and Fate of All Plastics Ever Made. *Sci. Adv.* **2017**, *3*, e1700782. DOI: 10.1126/sciadv.1700782.

(7) Oladele, I. O.; Okoro, C. J.; Taiwo, A. S.; Onuh, L. N.; Agbeboh, N. I.; Balogun, O. P.; Olubambi, P. A.; Lephuthing, S. S. Modern Trends in Recycling Waste Thermoplastics and Their Prospective Applications: A Review. *J. Compos. Sci.* **2023**, *7*, 198. DOI: 10.3390/jcs7050198.

(8) Chamas, A.; Moon, H.; Zheng, J.; Qiu, Y.; Tabassum, T.; Jang, J. H.; Abu-Omar, M.; Scott, S. L.; Suh, S. Degradation Rates of Plastics in the Environment. *ACS Sustain. Chem. Eng.* **2020**, *8*, 3494–3511. DOI: 10.1021/acssuschemeng.9b06635.

(9) Hopewell, J.; Dvorak, R.; Kosior, E. Plastics Recycling: Challenges and Opportunities. *Phil. Trans. R. Soc. B* **2009**, *364*, 2115–2126. DOI: 10.1098/rstb.2008.0311.

(10) Shen, L.; Worrell, E. Plastic Recycling. In *Handbook of Recycling*; Elsevier, 2024; pp 497–510. DOI: 10.1016/B978-0-323-85514-3.00014-2.

(11) Garcia, J. M.; Robertson, M. L. The Future of Plastics Recycling. *Science* **2017**, *358*, 870–872. DOI: 10.1126/science.aaq0324.

(12) Kazemi, M.; Faisal Kabir, S.; Fini, E. H. State of the Art in Recycling Waste Thermoplastics and Thermosets and Their Applications in Construction. *Resour. Conserv. Recycl.* **2021**, *174*, 105776. DOI: 10.1016/j.resconrec.2021.105776.

(13) Bîrcă, A.; Gherasim, O.; Grumezescu, V.; Grumezescu, A. M. Introduction in Thermoplastic and Thermosetting Polymers. In *Materials for Biomedical Engineering*; Elsevier, 2019; pp 1–28. DOI: 10.1016/B978-0-12-816874-5.00001-3.

(14) Grigore, M. Methods of Recycling, Properties and Applications of Recycled Thermoplastic Polymers. *Recycling* **2017**, *2*, 24. DOI: 10.3390/recycling2040024.

(15) Post, W.; Susa, A.; Blaauw, R.; Molenveld, K.; Knoop, R. J. I. A Review on the Potential and Limitations of Recyclable Thermosets for Structural Applications. *Polym. Rev.* **2020**, *60*, 359–388. DOI: 10.1080/15583724.2019.1673406.

(16) Rahimi, A.; García, J. M. Chemical Recycling of Waste Plastics for New Materials Production. *Nat. Rev. Chem*. **2017**, *1*, 0046. DOI: 10.1038/s41570-017-0046.

(17) Worm, B.; Lotze, H. K.; Jubinville, I.; Wilcox, C.; Jambeck, J. Plastic as a Persistent Marine Pollutant. *Annu. Rev. Environ. Resour.* **2017**, *42*, 1–26. DOI: 10.1146/annurev-environ-102016-060700.

(18) Lai, P.-H.; Hall, S. L.; Lan, Y.-C.; Ai, J.-R.; Jaberi, A.; Sheikhi, A.; Shi, R.; Vogt, B. D.; Gomez, E. D. Upcycling Plastic Waste into Fully Recyclable Composites through Cold Sintering. *Mater. Horiz.* **2024**, *Advanced Article*. DOI: 10.1039/D3MH01976D.

(19) Clark, R. A.; Shaver, M. P. Depolymerization within a Circular Plastics System. *Chem. Rev.* **2024**, *124*, 2617–2650. DOI: 10.1021/acs.chemrev.3c00739.

(20) Thiyagarajan, S.; Maaskant-Reilink, E.; Ewing, T. A.; Julsing, M. K.; Van Haveren, J. Back-to-Monomer Recycling of Polycondensation Polymers: Opportunities for Chemicals and Enzymes. *RSC Adv.* **2022**, *12*, 947–970. DOI: 10.1039/D1RA08217E.

(21) Chen, Z.; Sun, H.; Kong, W.; Chen, L.; Zuo, W. Closed-Loop Utilization of Polyester in the Textile Industry. *Green Chem.* **2023**, *25*, 4429–4437. DOI: 10.1039/D3GC00407D.

(22) Yang, W.; Liu, R.; Li, C.; Song, Y.; Hu, C. Hydrolysis of Waste Polyethylene Terephthalate Catalyzed by Easily Recyclable Terephthalic Acid. *Waste Manag.* **2021**, *135*, 267–274. DOI: 10.1016/j.wasman.2021.09.009.

(23) López-Fonseca, R.; Duque-Ingunza, I.; De Rivas, B.; Arnaiz, S.; Gutiérrez-Ortiz, J. I. Chemical Recycling of Post-Consumer PET Wastes by Glycolysis in the Presence of Metal Salts. *Polym. Degrad. and Stab.* **2010**, *95*, 1022–1028. DOI: 10.1016/j.polymdegradstab.2010.03.007.

(24) Troev, K.; Grancharov, G.; Tsevi, R.; Gitsov, I. A Novel Catalyst for the Glycolysis of Poly(Ethylene Terephthalate). *J. Appl. Polym. Sci.* **2003**, *90*, 1148–1152. DOI: 10.1002/app.12711.

(25) Beltrán, F. R.; Lorenzo, V.; De La Orden, M. U.; Martínez-Urreaga, J. Effect of Different Mechanical Recycling Processes on the Hydrolytic Degradation of Poly(l-Lactic Acid). *Polym. Degrad. and Stab.* **2016**, *133*, 339–348. DOI: 10.1016/j.polymdegradstab.2016.09.018.

(26) Achilias, D. S.; Karayannidis, G. P. The Chemical Recycling of PET in the Framework of Sustainable Development. *Water Air Soil Pollut. Focus* **2004**, *4*, 385–396. DOI: 10.1023/B:WAFO.0000044812.47185.0f.

(27) Das, P.; Tiwari, P. Valorization of Packaging Plastic Waste by Slow Pyrolysis. *Resour. Conserv. and Recycl.* **2018**, *128*, 69–77. DOI: 10.1016/j.resconrec.2017.09.025.

(28) *Feedstock Recycling and Pyrolysis of Waste Plastics: Converting Waste Plastics into Diesel and Other Fuels*; Scheirs, J., Kaminsky, W., Eds.; Wiley series in polymer science; J. Wiley & Sons: Chichester, UK; Hoboken, NJ, 2006.

(29) Yang, W.; Dong, Q.; Liu, S.; Xie, H.; Liu, L.; Li, J. Recycling and Disposal Methods for Polyurethane Foam Wastes. *Procedia Environ. Sci.* **2012**, *16*, 167–175. DOI: 10.1016/j.proenv.2012.10.023.

(30) Cao, M.; Cao, X. Recycling and Disposing Methods for Rigid Polyurethane Foamed Plastic Wastes. *Plastics* **2005**, *34*, 14–18.

(31) Zia, K. M.; Bhatti, H. N.; Ahmad Bhatti, I. Methods for Polyurethane and Polyurethane Composites, Recycling and Recovery: A Review. *React. Funct. Polym.* **2007**, *67*, 675–692. DOI: 10.1016/j.reactfunctpolym.2007.05.004.

(32) Hulme, A. J.; Goodhead, T. C. Cost Effective Reprocessing of Polyurethane by Hot Compression Moulding. *J. Mater. Process. Technol.* **2003**, *139*, 322–326. DOI: 10.1016/S0924-0136(03)00548-X.

(33) Quadrini, F.; Bellisario, D.; Santo, L. Recycling of Thermoset Polyurethane Foams. *Polym. Eng. Sci.* **2013**, *53*, 1357–1363. DOI: 10.1002/pen.23393.

(34) Asaro, L.; Gratton, M.; Seghar, S.; Aït Hocine, N. Recycling of Rubber Wastes by Devulcanization. *Resour. Conserv. Recycl.* **2018**, *133*, 250–262. DOI: 10.1016/j.resconrec.2018.02.016.

(35) Seghar, S.; Asaro, L.; Rolland-Monnet, M.; Aït Hocine, N. Thermo-Mechanical Devulcanization and Recycling of Rubber Industry Waste. *Resour. Conserv. and Recycl.* **2019**, *144*, 180–186. DOI: 10.1016/j.resconrec.2019.01.047.

(36) Tang, Y., American Rubber Technologies Inc, **2003**. *Recycled rubber processing and performance enhancement*. U.S. Patent 6,590,042.

(37) Brown, C., Watson Brown HSM Ltd Great Britain, **2008**. *Mixer and method of mixing*. U.S. Patent 7,461,970.

(38) Diaz, R.; Colomines, G.; Peuvrel-Disdier, E.; Deterre, R. Thermo-Mechanical Recycling of Rubber: Relationship between Material Properties and Specific Mechanical Energy. *J. Mater. Process. Technol.* **2018**, *252*, 454–468. DOI: 10.1016/j.jmatprotec.2017.10.014.

(39) Wu, C.-H.; Chang, C.-Y.; Li, J.-K. Glycolysis of Rigid Polyurethane from Waste Refrigerators. *Polym. Degrad. and Stab.* **2002**, *75*, 413–421. DOI: 10.1016/S0141-3910(01)00237-3.

(40) Liu, M.; Wang, Y.; Wu, Y.; Wan, H. Hydrolysis and Recycling of Urea Formaldehyde Resin Residues. *J. Hazard. Mater.* **2018**, *355*, 96–103. DOI: 10.1016/j.jhazmat.2018.05.019.

(41) Yao, Z.; Yu, S.; Su, W.; Wu, W.; Tang, J.; Qi, W. Comparative Study on the Pyrolysis Kinetics of Polyurethane Foam from Waste Refrigerators. *Waste Manag. Res.* **2020**, *38*, 271–278. DOI: 10.1177/0734242X19877682.

(42) Simon, D. Á.; Pirityi, D.; Tamás-Bényei, P.; Bárány, T. Microwave Devulcanization of Ground Tire Rubber and Applicability in SBR Compounds. *J. Appl. Polym. Sci.* **2020**, *137*, 48351. DOI: 10.1002/app.48351.

(43) Sarkar, B.; Mandal, S. Microbial Degradation of Natural and Synthetic Rubbers. In *Microbial Bioremediation & Biodegradation*; Shah, M. P., Ed.; Springer Singapore: Singapore, 2020; pp 527–550. DOI: 10.1007/978-981-15-1812-6_21.

(44) Diels, O.; Alder, K. Synthesen in Der Hydroaromatischen Reihe. *Justus Liebigs Ann. Chem.* **1928**, *460*, 98–122. DOI: 10.1002/jlac.19284600106.

(45) Fringuelli, F.; Taticchi, A. *The Diels Alder Reaction: Selected Practical Methods*; Wiley: Chichester; New York, **2002**.

(46) Nicolaou, K. C.; Snyder, S. A.; Montagnon, T.; Vassilikogiannakis, G. The Diels-Alder Reaction in Total Synthesis. *Angew. Chem. Int. Ed.* **2002**, *41*, 1668–1698. DOI: 10.1002/1521-3773(20020517)41:10<1668::AID-ANIE1668>3.0.CO;2-Z.

(47) Chaudhary, M.; Shaik, S.; Magan, M.; Hudda, S.; Gupta, M.; Singh, G.; Wadhwa, P. A Brief Review on Recent Developments in Diels-Alder Reactions. *COS* **2024**, *21*. DOI: 10.2174/0115701794262102231214074336.

(48) Yoshie, N. Diels–Alder Polymers. In *Encyclopedia of Polymer Science and Technology*; Mark, H. F., Ed.; Wiley, **2013**. DOI: 10.1002/0471440264.pst607.

(49) Briou, B.; Améduri, B.; Boutevin, B. Trends in the Diels–Alder Reaction in Polymer Chemistry. *Chem. Soc. Rev.* **2021**, *50*, 11055–11097. DOI: 10.1039/D0CS01382J.

(50) Tasdelen, M. A. Diels–Alder "Click" Reactions: Recent Applications in Polymer and Material Science. *Polym. Chem.* **2011**, *2*, 2133. DOI: 10.1039/c1py00041a.

(51) Ratwani, C. R.; Kamali, A. R.; Abdelkader, A. M. Self-Healing by Diels-Alder Cycloaddition in Advanced Functional Polymers: A Review. *Prog. Mater. Sci.* **2023**, *131*, 101001. DOI: 10.1016/j.pmatsci.2022.101001.

(52) Liu, Y.-L.; Chuo, T.-W. Self-Healing Polymers Based on Thermally Reversible Diels–Alder Chemistry. *Polym. Chem.* **2013**, *4*, 2194. DOI: 10.1039/c2py20957h.

(53) J. M. Craven, *US Pat.*, 3,435,003, **1969**.

(54) Engle, L. P.; Wagener, K. B. A Review of Thermally Controlled Covalent Bond Formation in Polymer Chemistry. *J. Macromol. Sci., Part C: Polym. Rev.* **1993**, *33*, 239–257. DOI: 10.1080/15321799308021436.

(55) Bergman, S. D.; Wudl, F. Mendable Polymers. *J. Mater. Chem.* **2008**, *18*, 41–62. DOI: 10.1039/B713953P.

(56) Canary, S. A.; Stevens, M. P., Thermally Reversible Crosslinking of Polystyrene via the Furan-Maleimide Diels-Alder Reaction. *J. Polym. Sci., Part A: Polym. Chem.* **1992**, *30*, 1755-1760. DOI: 10.1002/pola.1992.080300829.

(57) Chen, X.; Dam, M. A.; Ono, K.; Mal, A.; Shen, H.; Nutt, S. R.; Sheran, K.; Wudl, F. A Thermally Re-Mendable Cross-Linked Polymeric Material. *Science* **2002**, *295*, 1698–1702. DOI: 10.1126/science.1065879.

(58) Watanabe, M.; Yoshie, N. Synthesis and Properties of Readily Recyclable Polymers from Bisfuranic Terminated Poly(Ethylene Adipate) and Multi-Maleimide Linkers. *Polymer* **2006**, *47*, 4946–4952. DOI: 10.1016/j.polymer.2006.05.036.

(59) Bednarek, M.; Kubisa, P. Reversible Networks of Degradable Polyesters Containing Weak Covalent Bonds. *Polym. Chem.* **2019**, *10*, 1848–1872. DOI: 10.1039/C8PY01731J.

(60) Polgar, L. M.; Van Duin, M.; Broekhuis, A. A.; Picchioni, F. Use of Diels–Alder Chemistry for Thermoreversible Cross-Linking of Rubbers: The Next Step toward Recycling of Rubber Products? *Macromolecules* **2015**, *48*, 7096–7105. DOI: 10.1021/acs.macromol.5b01422.

(61) Lorero, I.; Rodríguez, A.; Campo, M.; Prolongo, S. G. Thermally Remendable, Weldable, and Recyclable Epoxy Network Crosslinked with Reversible Diels-Alder Bonds. *Polymer* **2022**, *259*, 125334. DOI: 10.1016/j.polymer.2022.125334.

(62) Gandini, A. The Furan/Maleimide Diels–Alder Reaction: A Versatile Click–Unclick Tool in Macromolecular Synthesis. *Prog. Polym. Sci.* **2013**, *38*, 1–29. DOI: 10.1016/j.progpolymsci.2012.04.002.

(63) Jones, J. R.; Liotta, C. L.; Collard, D. M.; Schiraldi, D. A. Cross-Linking and Modification of Poly(Ethylene Terephthalate- *Co* -2,6-Anthracenedicarboxylate) by Diels−Alder Reactions with Maleimides. *Macromolecules* **1999**, *32*, 5786–5792. DOI: 10.1021/ma990638z.

(64) Syrett, J. A.; Mantovani, G.; Barton, W. R. S.; Price, D.; Haddleton, D. M. Self-Healing Polymers Prepared via Living Radical Polymerisation. *Polym. Chem.* **2010**, *1*, 102. DOI: 10.1039/b9py00316a.

(65) Yoshie, N.; Saito, S.; Oya, N. A Thermally-Stable Self-Mending Polymer Networked by Diels–Alder Cycloaddition. *Polymer* **2011**, *52*, 6074–6079. DOI: 10.1016/j.polymer.2011.11.007.

(66) Oehlenschlaeger, K. K.; Mueller, J. O.; Brandt, J.; Hilf, S.; Lederer, A.; Wilhelm, M.; Graf, R.; Coote, M. L.; Schmidt, F. G.; Barner-Kowollik, C. Adaptable Hetero Diels–Alder Networks for Fast Self-Healing under Mild Conditions. *Adv. Mater.* **2014**, *26*, 3561–3566. DOI: 10.1002/adma.201306258.

(67) Lu, X.; Liu, Y.; Zhou, H. Learning Nature: Recyclable Monomers and Polymers. *Chem. Eur. J.* **2018**, *24*, 11255–11266. DOI: 10.1002/chem.201704461.

(68) Gandini, A. The Application of the Diels-Alder Reaction to Polymer Syntheses Based on Furan/Maleimide Reversible Couplings. *Polímeros* **2005**, *15*, 95–101. DOI: 10.1590/S0104-14282005000200007.

(69) Gandini, A.; Coelho, D.; Silvestre, A. J. D. Reversible Click Chemistry at the Service of Macromolecular Materials. Part 1: Kinetics of the Diels–Alder Reaction Applied to Furan–Maleimide Model Compounds and Linear Polymerizations. *Eur. Polym. J.* **2008**, *44*, 4029–4036. DOI: 10.1016/j.eurpolymj.2008.09.026.

(70) Stille, J. K.; Plummer, L. Polymerization by the Diels-Alder Reaction. *J. Org. Chem.* **1961**, *26*, 4026–4029. DOI: 10.1021/jo01068a092.

(71) Kennedy, J. P.; Carlson, G. M. Synthesis, Characterization, and Diels–Alder Extension of Cyclopentadiene Telechelic Polyisobutylene. IV. α,ω-Di(3-cyclopentadienylpropyldimethylsilyl)Polyisobutylene. *J. Polym. Sci. Polym. Chem. Ed.* **1983**, *21*, 3551–3561. DOI: 10.1002/pol.1983.170211013.

(72) Stegall, J. B. Cyclopentadiene-Maleimide Platform for Thermally Reversible Polymers; Virginia Tech: Blacksburg, VA, **2014**.

(73) Murphy, E. B.; Bolanos, E.; Schaffner-Hamann, C.; Wudl, F.; Nutt, S. R.; Auad, M. L. Synthesis and Characterization of a Single-Component Thermally Remendable Polymer Network: Staudinger and Stille Revisited. *Macromolecules* **2008**, *41*, 5203–5209.

(74) Levandowski, B. J.; Raines, R. T. Click Chemistry with Cyclopentadiene. *Chem. Rev.* **2021**, *121*, 6777–6801. DOI: 10.1021/acs.chemrev.0c01055.

(75) Tesoro, G. C.; Sastri, V. R. Synthesis of Siloxane-Containing Bis(Furans) and Polymerization with Bis(Maleimides). *Ind. Eng. Chem. Prod. Res. Dev.* **1986**, *25*, 444–448. DOI: 10.1021/i300023a013.

(76) Brand, T.; Klapper, M. Control of Viscosity through Reversible Addition of Telechelics via Repetitive Diels-Alder Reaction in Bulk. *Des. Monomers Polym.* **1999**, *2*, 287–309. DOI: 10.1163/156855599X00106.

(77) Kuramoto, N.; Hayashi, K.; Nagai, K. Thermoreversible Reaction of Diels—Alder Polymer Composed of Difurufuryladipate with Bismaleimidodiphenylmethane. *J. Polym. Sci., Part A: Polym. Chem.* **1994**, *32*, 2501–2504. DOI: 10.1002/pola.1994.080321312.

(78) Flory, P. J. *Principles of Polymer Chemistry*; Baker lectures 1948; Cornell University Press, **1953**.

(79) Stille, J. K. Step-Growth Polymerization. *J. Chem. Educ.* **1981**, *58*, 862. DOI: 10.1021/ed058p862.

(80) Billmeyer, F. W. *Textbook of Polymer Science*; John Wiley & Sons, 1984.

(81) Lenz, R. W. *Organic Chemistry of Synthetic High Polymers*; Interscience Publishers, **1967**.

(82) Siragusa, F.; Demarteau, J.; Habets, T.; Olazabal, I.; Robeyns, K.; Evano, G.; Mereau, R.; Tassaing, T.; Grignard, B.; Sardon, H.; Detrembleur, C. Unifying Step-Growth Polymerization and On-Demand Cascade Ring-Closure Depolymerization via Polymer

Skeletal Editing. *Macromolecules* **2022**, *55*, 4637–4646. DOI: 10.1021/acs.macromol.2c00696.

(83) Wudl, F. Crosslinking with Hermann Staudinger. In *Hierarchical Macromolecular Structures: 60 Years after the Staudinger Nobel Prize I*; Percec, V., Ed.; Advances in Polymer Science; Springer International Publishing: Cham, **2013**; Vol. 261, pp 211–216.

(84) Wilson, P. J.; Wells, J. H. The Chemistry and Utilization of Cyclopentadiene. *Chem. Reviews* **1944**, *34*, 1–50.

(85) Roscoe, H. E.; F. R. S. Notiz Über Die Freiwillige Polymerisation Flüchtiger Kohlenwasserstoffe Bei Gewöhnlicher Temperatur. *Justus Liebigs Ann. Chem.* **1886**, *232*, 348–352. DOI: 10.1002/jlac.18862320304.

(86) Etard, A.; Lambert, P. Terpene in the Oil from Compressed Gas. *Compt. Rend* **1891**, *112*, 945– 947.

(87) Spilker, A.; Kraemer, G. The Cyclopentadiene of Coal Tar; the Indene of the Aliphatic Series. *Ber. Dtsch. Chem. Ges.* **1896**, *29*, 552– 561. DOI: 10.1002/cber.189602901105.

(88) Albrecht, W. Additionsproducte von Cyklopentadiën Und Chinonen. *Justus Liebigs Annalen der Chemie* **1906**, *348*, 31–49.

(89) Sustmann, R. A Simple Model for Substituent Effects in Cycloaddition Reactions. II. The Diels-Alder Reaction. *Tetrahedron Letters* **1971**, *12*, 2721–2724. DOI: 10.1016/S0040-4039(01)96962-X.

(90) Sauer, J. Diels-Alder Reactions II: The Reaction Mechanism. *Angew. Chem. Int. Ed. Engl.* **1967**, *6*, 16–33. DOI: 10.1002/anie.196700161.

(91) Sauer, J.; Sustmann, R. Mechanistic Aspects of Diels-Alder Reactions: A Critical Survey. *Angew. Chem. Int. Ed. Engl.* **1980**, *19*, 779–807. DOI: 10.1002/anie.198007791.

(92) Houk, K. N.; Liu, F.; Yang, Z.; Seeman, J. I. Evolution of the Diels–Alder Reaction Mechanism since the 1930s: Woodward, Houk with Woodward, and the Influence of Computational Chemistry on Understanding Cycloadditions. *Angew Chem Int Ed* **2021**, *60*, 12660–12681. DOI: 10.1002/anie.202001654.

(93) Levandowski, B. J. Diels−Alder Reactivities of Cyclic Dienes and Dienophiles; UCLA, **2018**.

(94) Levandowski, B. J.; Houk, K. N. Theoretical Analysis of Reactivity Patterns in Diels–Alder Reactions of Cyclopentadiene, Cyclohexadiene, and Cycloheptadiene with Symmetrical and Unsymmetrical Dienophiles. *J. Org. Chem.* **2015**, *80*, 3530–3537. DOI: 10.1021/acs.joc.5b00174.

(95) Raistrick, B.; Sapiro, R. H.; Newitt, D. M. 360. Liquid-Phase Reactions at High Pressures. Part V. The Polymerisation of Cyclo- pentadiene and α-Dicyclopentadiene. *J. Chem. Soc.* **1939**, *0*, 1761− 1769. DOI: 10.1039/JR9390001761.

(96) Turnbull, A. G.; Hull, H. S. A Thermodynamic Study of the Dimerization of Cyclopentadiene. *Aust. J. Chem.* **1968**, *21*, 1789−1797. DOI: 10.1071/CH9681789.

(97) Alder, K.; Stein, G. Zur Polymerisation Cyclischer Kohlenwas- serstoffe. V. Der Abbau Der Polymeren Cyclopentadiene Mit Seleniger Saüre. *Justus Liebigs Ann. Chem.* **1933**, *504*, 205−215.

(98) Krupka, J. Kinetics of Thermal Dimerization of Cyclopentadiene and Methylcyclopentadienes and Their Codimerization. *Pet. Coal* **2010**, *52*, 290−306.

(99) Csicsery, S. M. Methylcyclopentadiene Isomers. J. Org. Chem. **1960**, *25*, 518−521. DOI: 10.1021/jo01074a009.

(99) McLean, S.; Webster, C. J.; Rutherford, R. J. D. Kinetic Isotope Effect for the Thermally-Induced Migration of Hydrogen in Cyclopentadienes. *Can. J. Chem.* **1969**, *47*, 1555–1559. DOI: 10.1139/v69-256.

(100) Spangler, C. W. Thermal [1,j] Sigmatropic Rearrangements. *Chem. Rev.* **1976**, *76*, 187–217. DOI: 10.1021/cr60300a002.

(101) Kahn, S. D.; Hehre, W. J.; Rondan, N. G.; Houk, K. N. Nature of the Migrating Group in 1,5-Sigmatropic Hydrogen Shifts. *J. Am. Chem. Soc.* **1985**, *107*, 8291–8292. DOI: 10.1021/ja00312a096.

(102) Yamabe, S.; Tsuchida, N.; Yamazaki, S. Revisiting Hydrogen [1,5] Shifts in Cyclopentadiene and Cycloheptatriene as Bimolecular Reactions. *J. Chem. Theory Comput.* **2005**, *1*, 944–952. DOI: 10.1021/ct0500646.

(103) Zhang, M.; Liang, G. Understanding the Sigmatropic Shifts of Cyclopenta-2,4-Dien-1-Yltrimethylsilane in Its Diels–Alder Addition. *Org. Biomol. Chem.* **2021**, *19*, 1732–1737. DOI: 10.1039/D0OB02386H.

(104) Froese, R. D. J.; Organ, M. G.; Goddard, J. D.; Stack, T. D. P.; Trost, B. M. Theoretical and Experimental Studies of the Diels-Alder Dimerizations of Substituted Cyclopentadienes. *J. Am. Chem. Soc.* **1995**, *117*, 10931–10938. DOI: 10.1021/ja00149a016.

(105) McLean, S.; Haynes, P. Hydrogen Migration in Cyclopentadienes. Tetrahedron **1965**, *21*, 2329−2342. DOI: 10.1016/S0040-4020(01)93887-6.

(106) St. Amant, A. H.; Lemen, D.; Florinas, S.; Mao, S.; Fazenbaker, C.; Zhong, H.; Wu, H.; Gao, C.; Christie, R. J.; Read de Alaniz, J. Tuning the Diels–Alder Reaction for

Bioconjugation to Maleimide Drug-Linkers. *Bioconjug. Chem.* **2018**, *29*, 2406–2414. DOI: 10.1021/acs.bioconjchem.8b00320.

(107) Staudinger, H.; Rheiner, A. Über Die Konstitution Des Dicyclopentadiens. *Helvetica Chimica Acta* **1924**, *7*, 23–31. DOI: 10.1002/hlca.19240070105.

(108) Bruson, H. A.; Staudinger, H. "Cyclopentadiene Rubber" A. New Cyclic Synthetic Polymerization Product. *Ind. Eng. Chem.* **1926**, *18*, 381–383. DOI: 10.1021/ie50196a013.

(109) Veldman, B.; Kaully, T.; Feller, R. K.; Falcao, E.; Wudl, F. Staudinger's Poly(Cyclopentadiene): Sintering Processing of Poly(Diels−Alder Cyclopentadiene). *Macromolecules* **2009**, *42*, 6848–6850. DOI: 10.1021/ma901123p.

(110) Kennedy, J. P.; Castner, K. F. Thermally Reversible Polymer Systems by Cyclopentadienylation. II. The Synthesis of Cyclopentadiene-containing Polymers. *J. Polym. Sci. Polym. Chem. Ed.* **1979**, *17*, 2055–2070. DOI: 10.1002/pol.1979.170170715.

2. Chapter 2: *Controlled Synthesis of a Homopolymer Network Using a Well-Defined Single-Component Cyclopentadiene Monomer*

2.1 Overview

As aforementioned, cyclopentadiene (Cp) is not stable at room temperature due to its high reactivity and propensity to isomerize, dimerize and oligomerize. Thus, it has remained challenging to synthesize well-defined Cp monomers under mild conditions that allows facile handling and studies of the subsequent polymerization. In fact, the approaches to fabricate Cp polymer networks have been limited to the uncontrolled synthesis of monomer mixtures, and *in-situ* cross-linking or post-functionalization. Therefore, even though Cp dimerization is reversible and attractive for the formation of degradable polymer networks, the scope of high-performance and environmental-friendly Cp materials has not yet to be realized. The goal of the project in this chapter is to investigate the feasibility of isolating a pure Cp monomer under mild conditions (e.g., room temperature, catalyst-free), which potentially provide a general platform to access a variety of Cp materials, investigate the reactivity, and better understand the reversibility of the Cp dimer units. In this work, we design a tetrafunctional Cp (TCp) monomer, which upon dimerization, will provide a highly cross-linked and reversible homopolymer with a definite chain-length between cross-linking points. To isolate TCp monomer in high yield, a deprotection strategy was optimized based on our group's previous publications in JACS, Macromolecule and the initial reaction pathway demonstrated by the

group (Tetrahedron **2015**, *71*, 1966–1970. DOI: 10.1016/j.tet.2015.02.023). A better-defined homopolymer network was fabricated and characterized to compare with the results from prior works by Wudl and Staudinger as well as to expand the insights of the material properties and cross-link density. The network also possesses a shape-memory effect and can be selectively degraded via a retro-Diels–Alder reaction with a "capping" and N15-labeled reagent, ^{15}N-phenyl maleimide. Of note, sections of this chapter were previously published in Journal of American Chemical Society (JACS). The contents and figures are reprinted with permission from *J. Am. Chem. Soc.* **2023**, *145*, 3462–3469. DOI: 10.1021/jacs.2c11416. Copyright 2023 American Chemical Society.

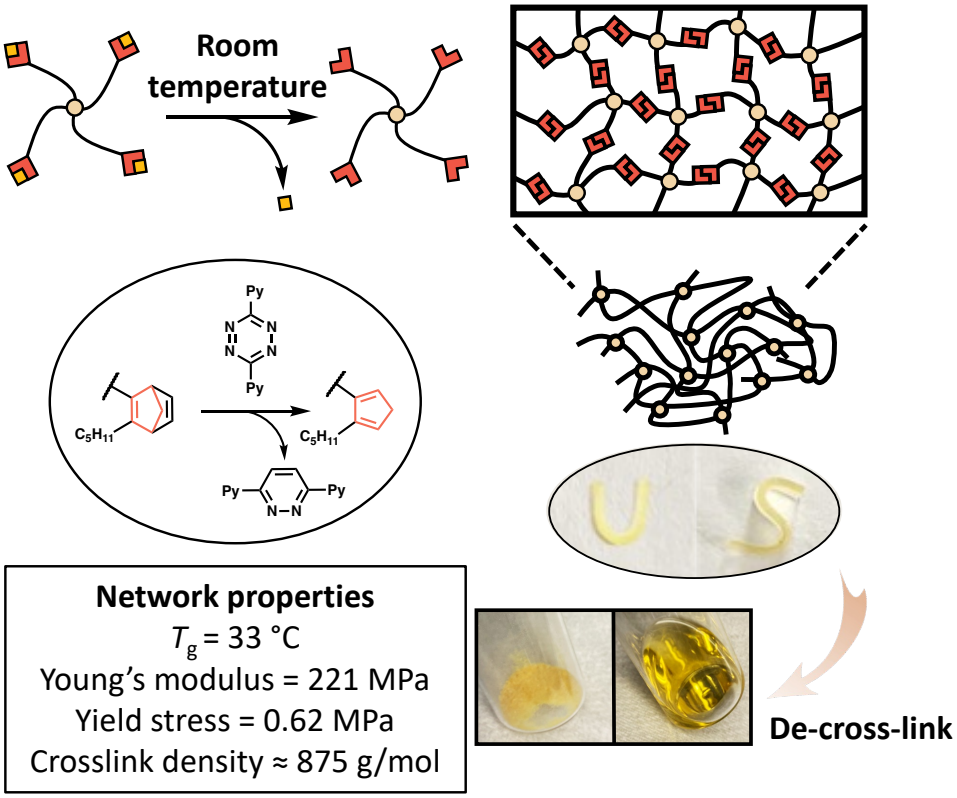


Figure 2.1. Overview of the controlled synthesis of Cp homopolymer network using a well-defined tetra-functional Cp monomer. Deprotection of the norbornadiene (NBD) precursor was utilized to reveal the free Cp. The tough homopolymer network displays shape-memory and de-cross-linking properties.

2.2 Abstract

Despite the long history and compelling chemistry of cyclopentadiene, there are only two reports since the first attempt by Staundinger in 1926. Herein, we develop a method to synthesize, isolate and homopolymerize a well-defined tetracyclopentadiene monomer, that lead to the controlled synthesis of a degradable network homopolymer. Mechanical properties are also investigated, including creep recovery, shape-memory, and tensile behaviors.

Interestingly, the tensile test reflects a tough and elastic material, in contrast to prior Cp-based homopolymer networks. This work provides a versatile platform to access and study new cyclopentadiene-based and better-defined homopolymer networks with potential applications ranging from shape memory polymers to degradable thermosets.

2.3 Introduction

There is a long history in the synthesis of polymer networks dating back to vulcanization of natural rubber in the 19th century.[1] Today, polymer networks are among the most widely studied, broadly used synthetic materials with a range of exceptional properties. While most cross-linked polymer networks are heterogenous and lack controlled structures, recent advances in controlling polymer network topology and studying defective topological structures have enabled access to polymer networks with optimized elasticity, fracture toughness, stimuli responsiveness and minimization of defects.[2,3] Furthermore, these materials facilitate structure-property relationship studies,[2-6] which are essential for tailored designs and optimized functions of advanced materials. One of the most widely adopted strategies to construct well-defined polymer networks (e.g., model or near ideal networks) is "end-linking" where two different multifunctional monomers are linked through a step-growth reaction.[7] The efficient methods include a mixture of precursor telechelic linear polymers (A_2) and multifunctional cross-linkers (B_f with $f > 2$) or multifunctional precursor polymers with controlled chain length (A_f and B_f). A pioneering example is Matsunaga and Sakai's tetrafunctional PEG model network formation using $A_4 + B_4$ that cannot form primary loops,

leading to a material with remarkably high mechanical strength.[8] Johnson and co-workers also reported an elegant strategy through slow addition of B_f to A_2 during network formation which allows for the capping of each B functionality with excess A groups.[9] This approach results in a significant reduction in primary loops defects and improved shear storage moduli compared to networks synthesized by conventional batch mixing.

From a design perspective, there are generally three critical requirements to achieve near ideal or model networks: controlled molecular weights between the two junctions, perfect stoichiometry, and quantitative curing behaviors.[7,10] Among these factors, reaching stoichiometric balance between A and B functions has remained a challenging task.[7,11-15] In this work, we explore an alternative approach to better-defined polymer networks based on a single component dual-role monomer, cyclopentadiene (Cp). Cp has a unique property in that it can serve as both a diene and dienophile in quantitative Diels–Alder (DA) cycloadditions,[16,17] thereby eliminating the internal imbalance/stoichiometry from the two-component multifunctional monomers. While the formation of loop defects and structural diversity of the DA adducts will prevent ideal network formation, the dynamic retro-DA/DA reaction provides a potential pathway to remove defects. The fast, self-reactivity of Cp led to the first single-component network formation in 1926 by Hermann Staudinger,[18] the "father of macromolecular chemistry" (**Figure 2.2**). Although pioneering, the uncontrolled nature of cross-linking resulted in a macromolecule with a high decomposition temperature, and poor polymer processability.[19-21] Expanding upon this work, Stille explored the use of

bis(cyclopentadienyl)alkane derivative as a telechelic monomer, however, due to the high reactivity of Cp – at room temperature, Cp is unstable, readily dimerizes and undergoes fast 1,5-sigmatropic hydride (1,5-H) shift – the monomer could not be purified prior to polymerization. As a result, the formed polymeric materials were contaminated with impurities and the cross-linking process was presumably attributed to random oxidative cross-linking.[22]

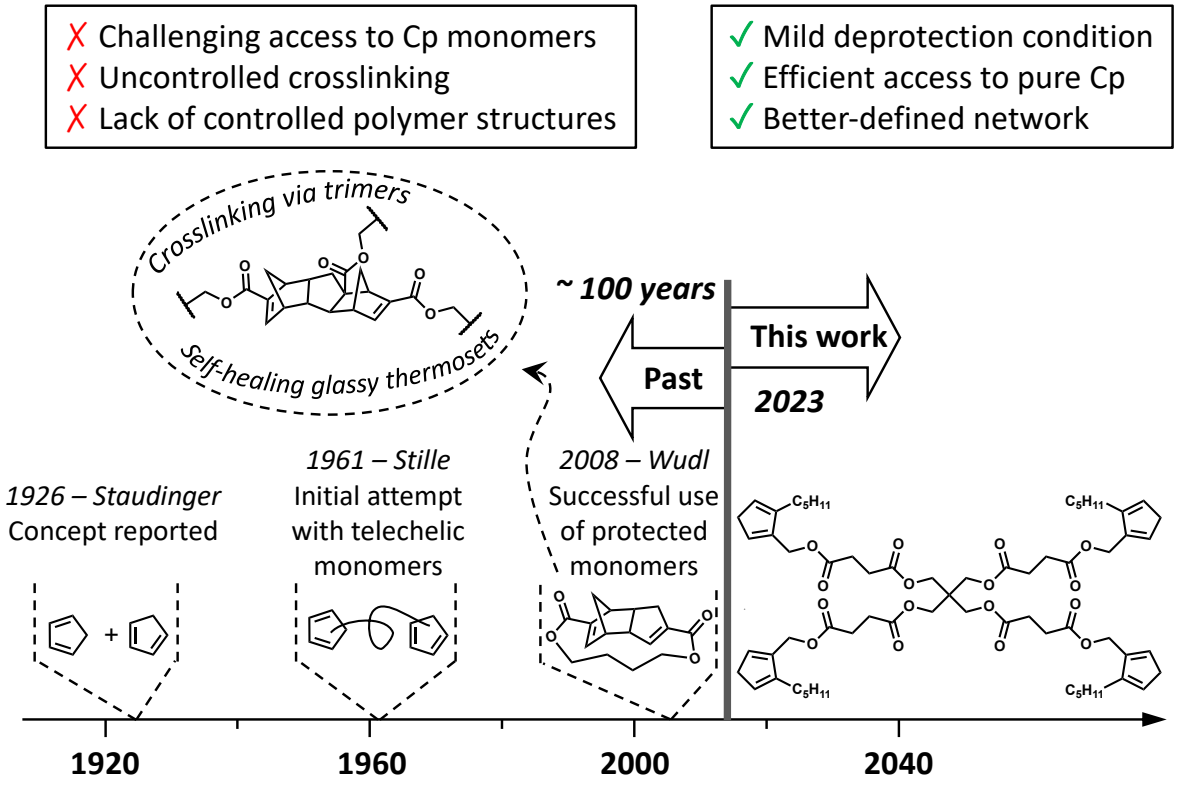


Figure 2.2. Time series of the synthesis of Cp homopolymer (past works remain uncontrolled and challenging). This work targets a mild deprotection condition to reveal free tetra-functional Cp monomer that leads to a better-defined homopolymer network.

Building on the implementation of DA based thermally remendable polymer materials,[23] Wudl developed an innovative strategy using cyclic Cp dimers derived from Thiele's acid as a premonomer[24] (**Figure 2.2**). The basis of this approach lies in the thermally reversible DA cycloaddition. Upon heating to 120–150 °C, the cyclic Cp dimer undergoes the retro-DA (rDA) reaction to reveal telechelic Cp monomers that subsequently underwent DA polyaddition to form self-healable cross-linked polymer networks. By providing access to a

well-defined monomer using the rDA reaction, Wudl elegantly demonstrated that the cross-linking occurred via an uncontrolled trimer formation between the alkene on the polymer backbone from the Cp dimer and another reactive Cp. This approach realized the feasible processability of Cp-based homopolymers, subsequently enabling characterization studies and post-damage (i.e., self-healing) repair strategies. Besides the prominent reports of homopolymer networks, more strategies have been applied to generate Cp groups *in-situ* via post-functionalization[25] or pair it with a highly reactive dienophile such as cyanodithioester (CDTE).[17,26,27] For example, Kennedy and Castner reported the incorporation of pendant Cp units by cyclopentadienylation with chlorinated butyl rubber polymers. *In-situ* dimerization of Cp lead to the formation of reversible networks.[25] More recently, Barner-Kowollik and co-workers exploited the fast hetero-DA reaction between Cp and CDTE to prepare a highly efficient self-healing polymer networks with tunable properties.[26] Despite the pioneering ideas of using Cp derivatives as the sole component to form homopolymer networks or prepare new materials with other dienophiles, the practice of controlling the Cp reactivity to prepare tailored advanced materials remains in infancy.[21,28]

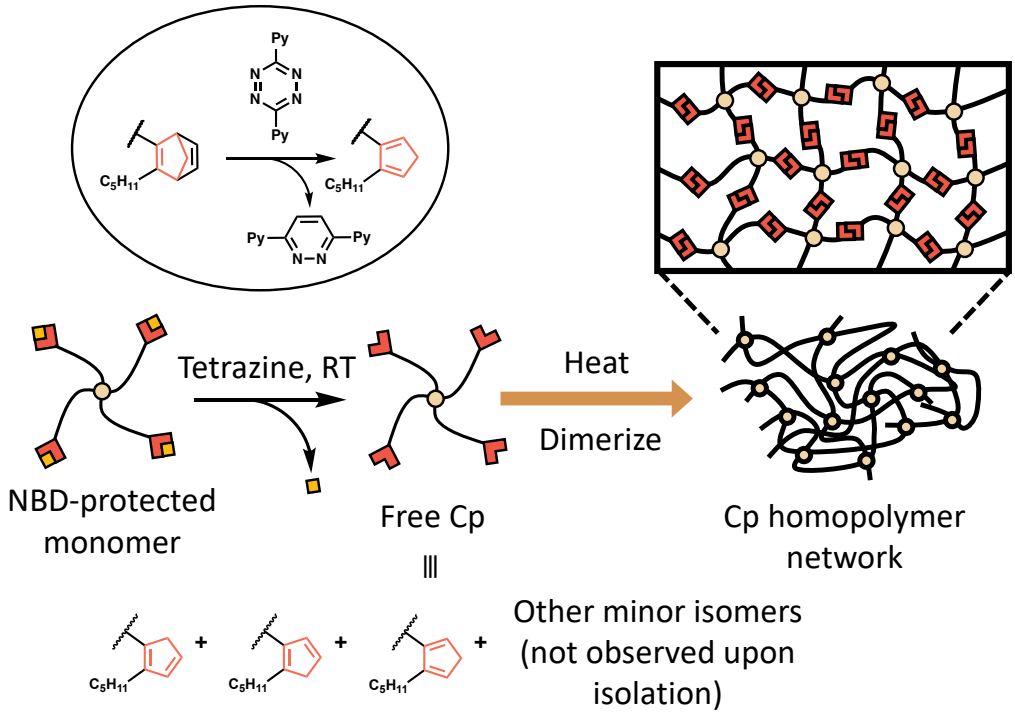


Figure 2.3. Norbornadiene–tetrazine cascade reaction reveals free Cp for dimerization. Efficient access to a 4-arm Cp monomer with minimal trimer leads to the formation of a better-defined network with appealing characteristics. Of note, 1,5-H shift of Cp monomers at RT and formation of *endo/exo* Diels–Alder adducts (not shown) generate a mixture of different diastereomers, leading to topological diversity.

One key synthetic challenge that remains is addressing the high reactivity of Cp and minimizing uncontrolled branch functionality in the polymer network. Given that many properties (e.g., elasticity, shape memory, and fracture toughness) have topology origins, providing controlled access to well-defined Cp-based monomers can result in design of fascinating new polymer networks with tunable advanced properties. Here, we identify three important factors to access better-defined Cp cross-linked homopolymer networks (**Figure 2.3**): (1) efficient and scalable access to a well-defined Cp monomer; (2) modifying the

substitution pattern of the Cp chain-ends to suppress 1,5-sigmatropic hydride (1,5-H) shift and minimize uncontrolled trimer cross-linking; and (3) utilizing a tetra-functional monomer (A_4) to control the end-linked network branch functionality primarily through dimerization rather than uncontrolled trimerization. The realization of these goals, including the isolation of a well-defined pentaerythritol-based Cp monomer, is described. Contrary to previously uncontrolled preparation of Cp-based polymers, the resulting network has a near room-temperature glass transition temperature (T_g), elastomeric tensile behavior, and cold shape-memory effect. Moreover, the material is degradable because it is formed in its entirety by reversible cross-linked covalent bonds. The strategy provides a new general platform, based on step-growth polymerization of A_4 + A_4, to access single-component Cp-based polymer materials with better-defined and tunable properties. Typically, the DA self-reactions of Cp, including its 1,5-H shift isomers, can lead to several diastereomers that increases the number of possible DA cycloadducts at the cross-linking points, each with its own "bite angle" and topological shape. The detailed description and calculation are shown in Supporting Section 2.7 (Supporting Figure S2.1 and Table S.2.1). Furthermore, at high temperatures, an equilibrium between forward and retro-DA reactions provides a pathway to equilibrate the system to the thermodynamically most stable network. Even though these attributes potentially complicate the preparation of ideal networks, they raise new opportunities to study and tune polymer network properties.

2.4 Results and Discussion

Monomer Synthesis and Stability. While exploring the use of norbornadiene (NBD) as a "masked" Cp group,[29,30] we envisioned that access to a pentaerythritol core, substituted with four NBD units (**2**), could serve as an ideal precursor to synthesize and isolate a 4-arm Cp monomer **3**. The NBD adduct can be efficiently prepared on a 10-gram scale and deprotected under mild reaction conditions at room temperature, thus enabling isolation of this notoriously challenging monomer (**Figure 2.3**). The highly efficient deprotection proceeds through an inverse electron demand DA reaction (iEDDA) in the presence of dipyridyl tetrazine (DpTz) to afford a reactive intermediate that subsequently undergoes a rDA reaction that results in the formation of the desired Cp derivative and the corresponding dipyridyl pyridazine (DpPz) byproduct (Supplementary Figure S2.12). Due to the known effects of substitution patterns on the reactivity of Cp derivatives,[31-38] we also postulated that the previously reported utilization of the pentyl substituted Cp derivative,[29,30] could help minimize premature dimerization and 1,5-H shift.

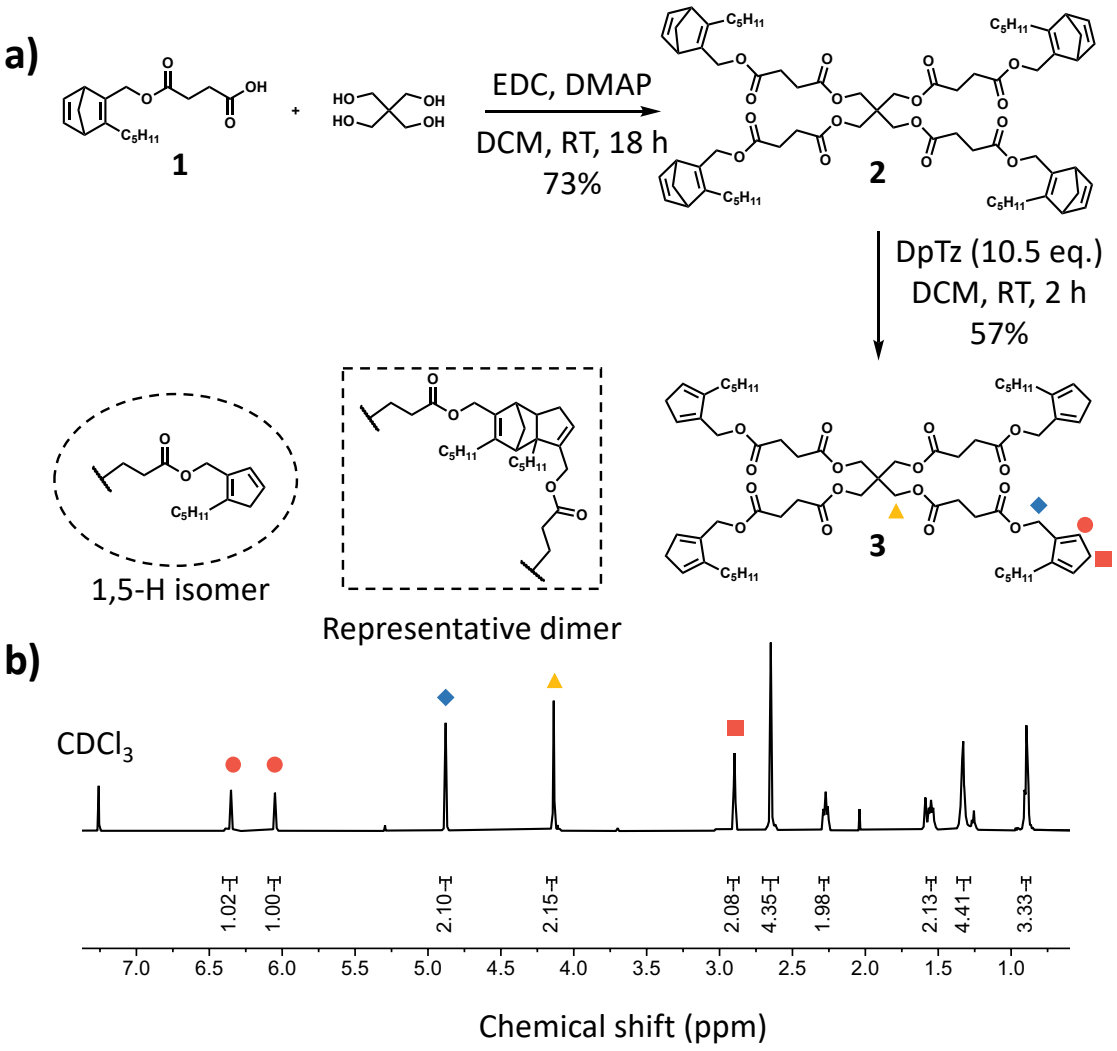


Figure 2.4. (a) Synthetic route to NBD-protected 4-arm monomer, followed by deprotection with tetrazine to reveal the pure, unmasked Cp derivative. (b) ^{1}H NMR shows the clean formation of the free Cp units with negligible appearance of Cp dimers or 1,5-H shift isomers.

Following the straightforward synthetic route in Figure 2a, 4-arm NBD substrate **2** was prepared by reacting the carboxylic NBD derivative **1** with pentaerythritol via carbodiimide EDC coupling. The isolation of tetratelechelic Cp (TCp) monomer **3** was subsequently tested

on a 6-mg scale using our deprotection approach with DpTz.[29] Heating **3** at 50 °C for 18 h in the vacuum oven resulted in a cross-linked polymer as confirmed via its insolubility in dichloromethane. Despite the encouraging preliminary results, we noted a small yellowish by-product during the isolation of compound **3** (~2%). Therefore, optimization of the deprotection conditions, such as concentration, stoichiometry of tetrazine, and reaction time (Supplementary Table S2.2) were necessary to isolate the pure single Cp isomer, as shown by ^{1}H NMR spectroscopy (**Figure 2.4**). We found that treatment of **2** with 10.5 eq. of tetrazine at RT for 2 h, followed by chromatography, afforded **3** in 57% isolated yield on a gram scale. With access to the pure TCp monomer, we next studied the stability of **3** toward 1,5-H shift and dimerization at room temperature. To our gratification, we observed that on short timescales (1-5 h), the dialkylated substitution of the Cp units resulted in minimal dimerization and 1,5-H shift. The isolated Cp chain-ends were monitored at ambient atmosphere via ^{1}H NMR spectroscopy (both neat and in solution) to observe the course of 1,5-H shift and dimer formation. The amount of dimer and constitutional isomer generated within 5 h is negligible (< 10% dimer and 3% isomer), establishing a working timeline for the isolation and polymerization of the TCp monomer. Of note, the dimer forms more readily than the 1,5-H shift isomer; the latter was not observed until after 1 h (Supplementary Figure S2.14). These results demonstrate the ability to isolate a pure single Cp isomer, potentially allowing the construction of a better-defined homopolymer network, polytetracyclopentadiene (PTCp, **4**, **Figure 2.5**). Furthermore, the TCp monomer is stable

when stored in the freezer up to 1.5 months (< 0 °C), thus successful polymerization is not required immediately after isolation. We also tested the possibility of uncontrolled cross-linking, presumably due to trimer formation, by polymerizing a two-arm Cp model compound (Supplementary Figures S2.15 and S2.16). Despite the structural analogy to Wudl's two-arm Cp adduct,[24] the sol-gel test showed minimal gel formation (< ~25%) (Supplementary Figure S16). This suggests that the substitution pattern, including the pentyl side chain, helps suppress uncontrolled trimer formation. There are also other factors that can induce the aforementioned gelation in the model system, such as the possible entanglement of the long linear chains, or radical-mediated cross-linking. We investigated these possible hypotheses and discovered that the addition of a radical inhibitor (5 mol% BHT) to the polymerization of the two-arm Cp model at 90 °C completely inhibits gelation (Supplementary Figure S2.17). We also further confirmed the absence of trimer by analyzing the mass spectrum of a monofunctional Cp model after heating it neat for 25 h at 90 °C (Supplementary Figure S2.18b). Current studies are on-going to evaluate if further modification of the sterics and electronics of the substituents will enable access to high-molecular weight linear polymers.

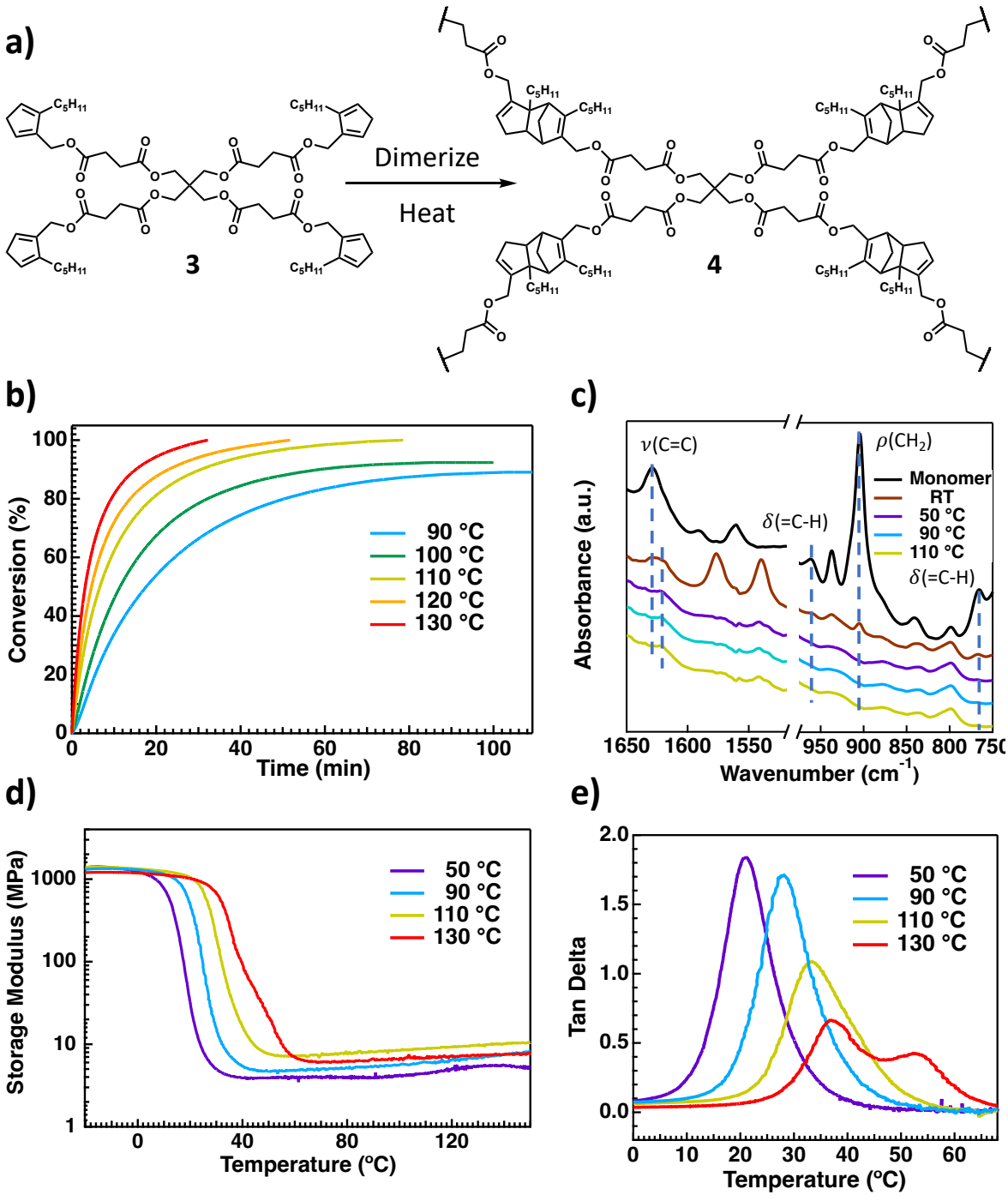

a)
Dimerize
Heat
3
4
b)
Conversion (%)
Time (min)
90 °C
100 °C
110 °C
120 °C
130 °C
c)
Absorbance (a.u.)
Wavenumber (cm-1)
ν(C=C)
δ(=C-H)
ρ(CH2)
δ(=C-H)
Monomer
RT
50 °C
90 °C
110 °C
d)
Storage Modulus (MPa)
Temperature (°C)
50 °C
90 °C
110 °C
130 °C
e)
Tan Delta
Temperature (°C)
50 °C
90 °C
110 °C
130 °C

Figure 2.5. (a) TCp monomer was cured under different conditions: at RT for 9 d, 50 °C for 24 h, 90 °C for 120 min, 110 °C for 100 min, or 130 °C for 80 min. (b) Isothermal conversion plot demonstrates the curing efficiency of TCp monomer at different temperatures. (c) FTIR spectrum shows full consumption of Cp chain-ends for samples cured at high temperatures (> 90 °C). (d) Storage modulus from rubbery plateau region of DMA spectrum is correlated to molecular weight between cross-links (M_c). (e) Comparison of tan delta curves for different samples reveals molecularly heterogeneous cross-linking at high temperatures (e.g., 130 °C).

Polymer Synthesis and Monitoring. With access to the desired TCp monomer, the kinetics of step-growth A_4 polymer network formation was investigated. The homogeneous nature of the monomer enabled the efficient bulk polymerization of **3**, and its behavior was monitored at different curing temperatures via differential scanning calorimetry (DSC) (Supplementary Figure S2.21). As seen by the conversion plot in Figure 3b, after 100 min, the sample heated at 90 °C can reach up to 89% conversion of the Cp chain-ends. The quantitative conversion of chain-ends includes those at 110 °C, 120 °C, and 130 °C with the timescales of 80, 50, and 30 min, respectively. Of note, we refrain from curing at higher than 130 °C due to the increased rate of side reactions at elevated temperature (e.g., radical process) and to avoid accessing a monomer-dimer equilibrium via the dynamic rDA/DA reaction. Based on the conversion plot, Cp monomer was cured at 50 °C, 90 °C, 110 °C and 130 °C and the resulting polymer samples were monitored via Fourier-transform infrared spectroscopy in attenuated total reflectance mode (FTIR-ATR). The intensity of C=C stretching at 1628 cm^{-1} from the monomer was diminished and red-shifted to 1620 cm^{-1} for all samples that are cured at 50 °C or higher. The sample cured at RT for 9 days still shows a broad peak across 1628–1620 cm^{-1}, showing incomplete consumption of Cp chain-ends. The bands at 960, 904, and 765 cm^{-1},

which are characteristics of Cp cyclic C-H and CH_2 bending,[39] completely disappear for samples cured at or higher than 50 °C. Again, the room temperature sample still shows retention of peak intensity, compared to full peak disappearance from other samples (**Figure 2.5**).

Cross-linking Assessment. Dynamic mechanical analysis (DMA) was then utilized to measure the experimental molecular weight between cross-links (M_c) (Supplementary Table S2.3), which were then compared to the theoretically ideal value (Supplementary Figure S2.28). **Figure 2.5** shows that with increasing curing temperatures, the rubber plateau modulus E'_p increases, and correspondingly, M_c decreases. This trend reflects the increasing amount of cross-link density as a function of curing temperatures. The tan delta peak intensity reasonably becomes lower and broader with increasing T_g values. However, the 130 °C cured sample exhibits lower E'_p (or higher M_c) compared to the 110 °C cured sample (Supplementary Table S2.3). The tan delta peak of this sample is also bimodal compared to a single peak from other samples (**Figure 2.6**). This might result from the heterogeneity of cross-link density due to the difference in segmental mobility, thermal lag,[40] or possible competing rDA reaction while curing at 130 °C. From the experiment with the two-arm model system, we postulated that the radical process likely happened at high curing temperature and could contribute to the appearance of the bimodal tan delta curve. Therefore, we repeated the curing of the sample at 130 °C with and without BHT (5 mol%) and observed that the bimodal appearance was completely suppressed (Supplementary Figure S2.29b), which further

supports our hypothesis. Even though higher curing temperatures normally lead to higher cross-link density, other factors can be involved (e.g., vitrification, side reactions, decomposition, etc.).[41,42] Hence, the optimal curing condition for this system was determined to be at 110 °C for 100 min. Under these conditions, the calculated M_c is 875 g/mol, compared to the theoretically ideal value of 558 g/mol (Supplementary Equation S2.3, Table S2.3). Of note, the calculated value is an estimate because it neglects the coefficient of thermal expansion, which is essential to determine the temperature-corrected density. Due to the limited mobility in the gel state, especially with a multi-functional cross-linker, the presence of network imperfections (i.e., loops, chain entanglement and dangling chains)[9,11,43,44] is normal and therefore it is not surprising that the experimental M_c is larger than the theoretically ideal value (Supplementary Figure S2.28). Since the unavoidable network imperfections can possibly influence the property of our material (e.g., T_g values), we further studied the controlled-defect materials by reacting Cp chain-ends with sub-stoichiometric amount of maleimides (5-15 mol%). We attributed these capped chain-ends analogous to dangling chain-ends and to some extent, loop defects. We used *N*-phenyl maleimide (*N*-PhM) as our initial candidate. However, we surprisingly observed a large countereffect of crystallinity in our material. T_g values increased by more than ~10 °C, despite supposedly lower amount of cross-linking in our system (Supplementary Figure S2.30a). We then switched to *N*-methyl maleimide (*N*-MM) and observed that T_g values reasonably decreased with increasing amount of added *N*-MM. However, the variation was insignificant (~5 °C with

15 mol% capped Cp, as shown in Figure S2.30b). As reflected in the control experiments, to a certain degree, we assume that the properties of our materials were not affected significantly by chain-end network defects, but further studies are warranted.

Physical and Mechanical Properties. The homopolymer network **4** is faintly yellow, fully transparent, and flexible with a density of 0.88 ± 0.05 g/cm^3. The sample, cured at 100 °C for 100 min, shows a T_g of 33 °C (from tan delta max) with a storage modulus before glass transition of 1.4 GPa (at T = -15 °C). The storage modulus remains in sufficient value of ~ 9–10 MPa during plateau region up to 160 °C (Supplementary Figure S2.31), which indicates minimal effects from the dynamic rDA/DA reactions at these temperatures and suggests that physical aspects of chain flexibility and mobility also hold significant importance to the thermal stability of the material. Uniaxial tensile tests were also performed, revealing an ultimate tensile strength of 11.8 ± 1.3 MPa, and elongation at break of $101.6 \pm 3.51\%$ (Supplementary Figure S2.33). The Young's modulus was determined as 221.4 ± 23.9 MPa (Supplementary Table S2.4). The tensile behavior reflects a tough and elastic material, which is comparable to rubber and thermoset elastomers[45-48] (**Figure 2.6**). Of note, by controlling the molecular weight between cross-links via structural designs and curing conditions, we were able to lower the T_g to near room temperature. In contrast, previous Cp materials appear as glassy and brittle thermosets with high T_gs, due to the uncontrolled cross-link density, which resulted from the extensive formation of trimers and oligomers.[18-22,24] For example, the only report of a processable Cp cross-linked homopolymer from Wudl has the lowest T_g of

89 °C.[24] These results demonstrate that the viability of controlled cross-linking, via dimerization of a well-defined Cp monomers, enables access to new compelling Cp-based materials.

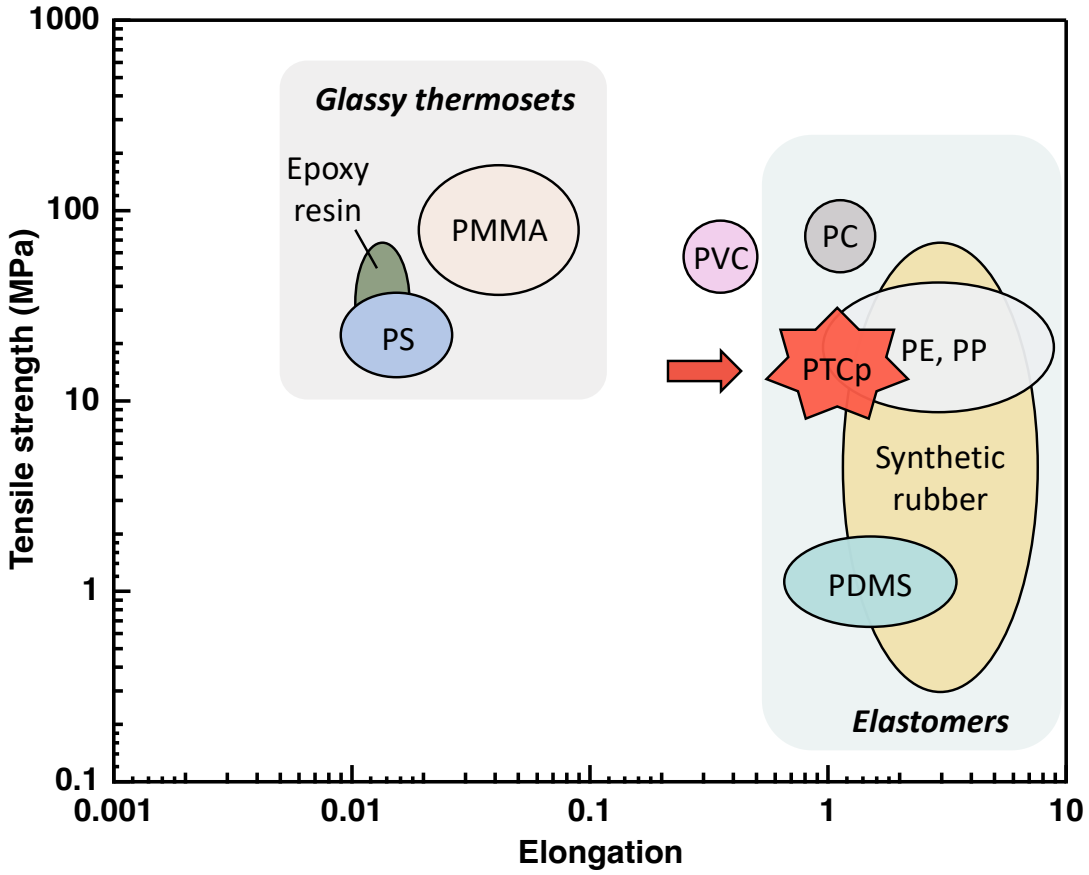


Figure 2.6. Ashby plot of tensile behaviors of common thermoset elastomers versus strong and glassy thermosets. The plot shows that PTCp can be categorized as a thermoset elastomer.

Shape Memory and De-Cross-Linking. After confirming the rubber elasticity of the homopolymerized material, the viscoelastic behavior of **4** was studied by creep-recovery experiments. High elastic recovery was observed below the yield stress of 0.62 MPa at 0.2%

strain (**Figure 2.7**). Based on the shape-recovery ability and sufficient storage modulus difference during glass transition, a cold-programming shape memory behavior was also demonstrated, taking advantage of the T_g in the range of 10–30 °C.[49,50] The desired shapes can be fixed at 0 °C (below T_g) and the original shape can recover at room temperature (or higher than T_g). This process is illustrated in **Figure 2.7b**, where the original rectangular-shaped material can be re-configured into a U- or S-shape at RT. The new shapes were then "locked" by immersing in an ice bath at 0 °C. Upon warming to RT at ambient atmosphere, the material returns to its original shape within 35 seconds, while it takes ~5 seconds in a 30 °C water bath. To further highlight the advanced properties of this material, we sought to demonstrate the ability to convert the highly cross-linked material to small and soluble oligomers. Because **4** is comprised almost entirely from Cp cross-linking dimers, it presents the unique and exciting opportunities for selective degradation upon heating above the rDA temperature (150–180 °C).[25,51] To evaluate this potential feature, the polymer was heated in refluxing xylene (~145 °C) in the presence of *N*-PhM, which served as a DA capping reagent. As expected, the degraded polymer network, yellow solid, was completely soluble in DCM upon treatment to these conditions (**Figure 2.7b**). The soluble material was analyzed by ^{1}H NMR, and ^{13}C NMR spectroscopy to assess de-cross-linking and capping with *N*-PhM by the presence of characteristic Cp-maleimide adduct peaks (Supplementary Figure S2.35). We also repeated the degradation experiment with N15-labeled maleimide (i.e., ^{15}*N*-PhM) and analyzed the crude mixture via Heteronuclear Multiple Bond Correlation (HMBC) NMR spectroscopy

(Supplementary Figure S2.36). The signal at 195 ppm further confirms the capping of Cp chain-ends (Supplementary Figure S2.37). Analysis of the 50 °C cured sample after degradation (24 h in refluxing xylene) by gel permeation chromatography (GPC) indicated an oligomeric mixture of approximately 1-3 repeat units. The GPC curve of the 110 °C cured sample also showed degradation after heating in refluxing xylenes for 48 h. However, a smaller molecular weight than that of the original monomer was observed. One possible explanation is that the polymer might be partially degraded along the backbone upon exposure to the high temperature for an extended period. Heating the cross-linked polymer in refluxing xylene for 24 h without ^{15}N-PhM, resulted in the formation of yellow but insoluble solid in DCM (Supplementary Figure S2.38), presumably due to decomposition. These examples, illustrate that improved network formation of highly cross-linked Cp homopolymer leads to the near-room temperature T_g, as well as elastomeric and shape memory properties. Since polymer **4** is formed entirely from dynamic DA cycloaddition, the self-healing behavior of the material was investigated. Unfortunately, the material became fragile when heated to its rDA temperature (150 °C for a few hours), preventing self-healing studies. As such, current studies are ongoing to improve the material with suitable structural modification to enhance its viscosity (i.e., incorporation of soft-linkers into the core 4-arm structure) to hopefully improve self-healing properties.

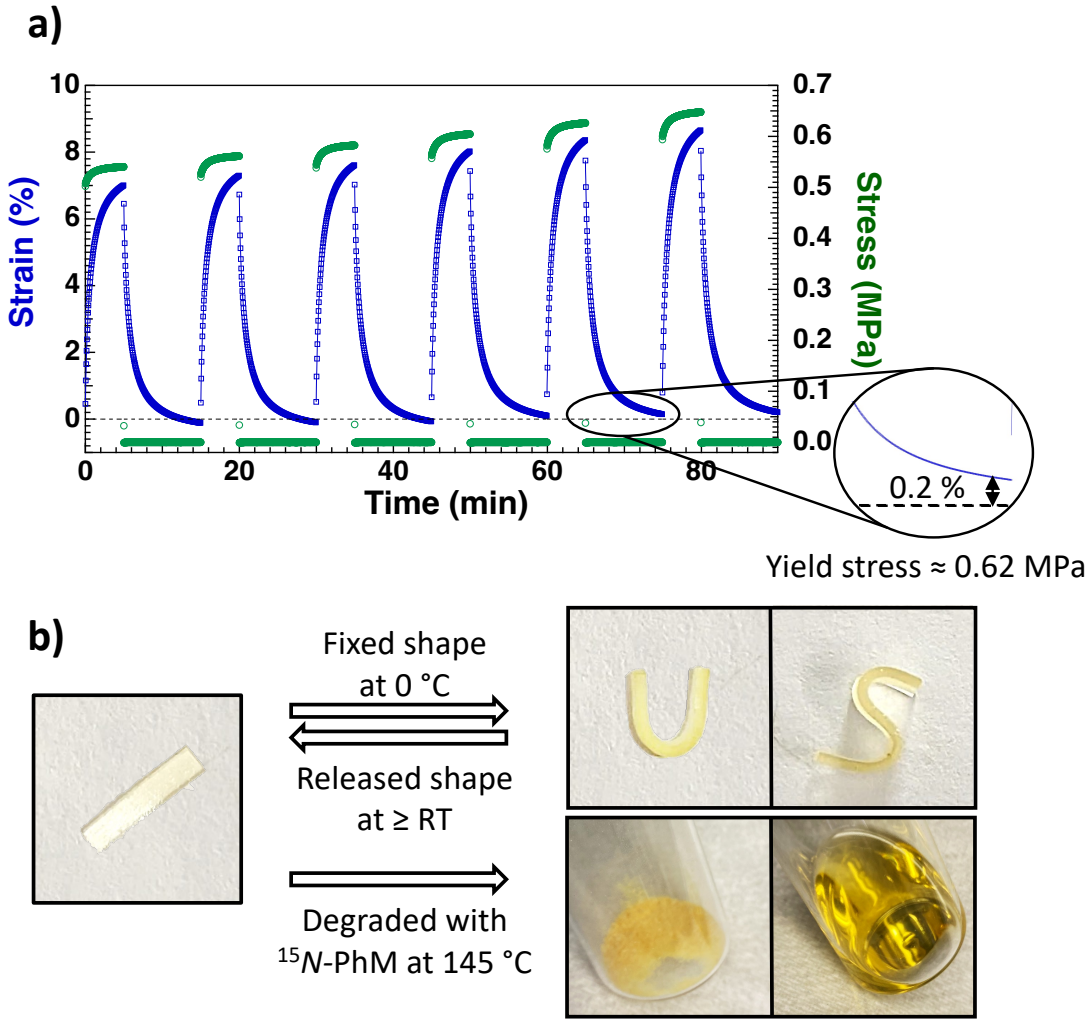


Figure 2.7. (a) Creep–recovery experiments demonstrate high elasticity below the yield stress. (b) Shape memory was cold-programmed due to the near-room-temperature T_g; polymer degradation with ^{15}N-PhM at 145 °C results in a yellow solid (left picture) that is soluble in DCM (right picture).

2.5 Conclusion

We have demonstrated an unprecedented and feasible protocol for the synthesis of a Cp network homopolymer, PTCp. Despite an early interest by Staudinger, the applications of DA

homopolymer networks have remained in a nascent stage over the past century due to the formidably uncontrolled reactivity of Cp. Here, by efficiently accessing a pure Cp monomer, TCp, under mild conditions and through controlling the subsequent homopolymerization, we have discovered intriguing characteristics of the macromolecule, such as a near-room temperature T_g, as well as elastomeric and shape memory properties. We believe the emergent properties and accessible methodology will encourage new syntheses and studies of Cp-based advanced materials that will take advantage of its homogeneous bulk polymerization, better-defined cross-link architecture, compelling shape flexibility and degradability. Though the emergent property of polymer **4** is comparable to elastomeric materials with a compelling T_g and selective de-cross-linking, there are certain limitations as follows and current studies for further improvement are ongoing: (i) the tensile strength and strain of polymer **4** identify a tough material but are not on par with the current state-of-the-art polymers, such as polycarbonate or synthetic rubber; (ii) self-healing of the material was not observed, presumably due to the lack of flexible chain extenders within our structural design. Further investigation will explore the generality of the new single-component homopolymerization of Cp-based monomer, targeting the incorporation of flexible and functional units between the core and terminal Cp-units to enable self-healing materials with enhanced mechanical properties, as well as access to high-molecular weight linear polymers.

2.6 Acknowledgements

The research was supported by National Science Foundation (CHE-2204077). We thank Dr. Julie Peterson for the guidance about the computational calculation. We also thank Dr. Nima Alizadeh for the guidance about the mechanical testing of these materials. This work made use of the NMR instruments, supported by the National Science Foundation under award No. MRI-1920299, and the MRL Shared Experimental Facilities that are supported by the MRSEC Program of the NSF under Award No. DMR 1720256; a member of the NSF-funded Materials Research Facilities Network. The facility for tensile testing was supported by the BioPACIFIC Materials Innovation Platform of the National Science Foundation under Award No. DMR-1933487. This work made use of computational facilities purchased with funds from the National Science Foundation (CNS-1725797) and administered by the Center for Scientific Computing (CSC). The CSC is supported by the California NanoSystems Institute and the Materials Research Science and Engineering Center (MRSEC; NSF DMR 1720256) at UC Santa Barbara.

2.7 Supporting Information

Material and experimental details:

Reactions were conducted using reagent grade solvents. Dichloromethane (DCM) was stored over 3Å molecular sieves. Tetrahydrofuran (THF) was passed over a column of activated alumina. All commercially obtained reagents were bought from Sigma Aldrich,

Fisher Scientific, VWR International and were used as received unless otherwise noted. Compound **1** was synthesized using procedures that are reported in literature.[29,30] ^{15}N-phenyl maleimide was synthesized in one step based on literature procedure[52] with the starting material (N15-labeled aniline) purchased from Cambridge Isotope Laboratories, Inc. Thin-layer chromatography (TLC) was conducted with E. Merck silica gel 60 F254 pre-coated plates (0.25 mm) and visualized by exposure to UV light (254 nm) or stained with p-anisaldehyde. Flash column chromatography was performed using normal phase silica gel (60 Å, 0.040 – 0.063 mm, Geduran).

Characterization methods:

ATR FT-IR spectra were recorded on a Varian 640-IR FT-IR spectrometer equipped with an ATR (attenuated total reflection) accessory or a Thermo Nicolet iS10 FTIR Spectrometer with a Smart Diamond ATR; applied as neat samples or cured thermosets with smooth surfaces and absorbance bands reported as $1/\lambda$ in cm^{-1}. ^{1}H NMR spectra were recorded on Varian and Bruker spectrometers (400, 500, or 600 MHz) and are reported relative to the residual protio-signal in deuterated solvents. Data for ^{1}H NMR spectra are reported as follows: chemical shift (δ ppm), multiplicity, coupling constant (Hz) and integration. ^{13}C NMR spectra were recorded on Varian Spectrometers (500 MHz). Data for ^{13}C NMR spectra are reported in terms of chemical shift (δ ppm). Gel Permeation Chromatography (GPC) eluting with chloroform ($CHCl_3$) and calibrated relative to polystyrene standards was performed on a Waters Alliance HPLC System, 2690 separation module, equipped with Wyatt DAWN

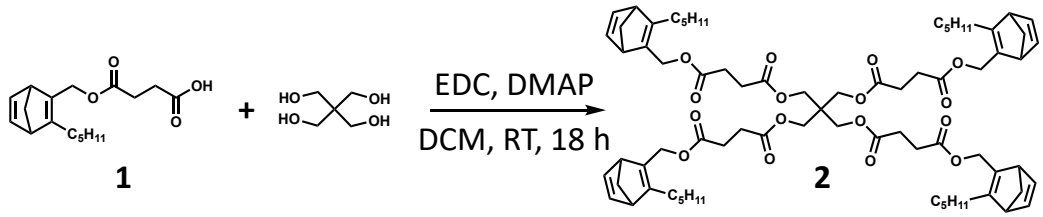
HELEOS-II light scattering and Waters 2410 Differential Refractometer (RI) and Waters 2998 Photodiode Array (PDA) detectors. Mass spectra were obtained using Waters Acquity H-class Ultra High Pressure Liquid Chromatography (UPLC) system coupled with a Waters Xevo G2-XS Time-of-Flight Mass Spectrometer with an ESI or ASAP source. Differential scanning calorimetry (DSC) was performed on a liquid-nitrogen-cooled TA Instruments Q2000 DSC system at a heating rate of 10 °C/min under a nitrogen atmosphere with a sensitivity < 0.2 μW and a baseline drift < 10 μW. The amount of materials in the thermal pans is ~ 5–6 mg. The isothermal experiments were performed by heating the sample at a certain temperature and collect data for typically 100–120 min. Thermo-gravimetric analysis (TGA) was collected on a TA Instruments Discovery 5500 Thermo-Gravimetric Analyzer. The measurements were taken under a nitrogen environment from an initial thermally equilibrated state at 50 °C ramping up to 900 °C at 10 °C per minute. Dynamic mechanical analysis (DMA) data were collected with a Discovery DMA 850. The film clamp geometry was used for the polymer films with dimensions of approximately 8 mm × 2 mm × 0.3 mm. Samples were loaded at room temperature with a 0.01 N preload, cooled to –20 °C, and equilibrated for a minimum of 5 minutes. Data were then collected by ramping temperature from –20 °C to 150 °C at the ramp rate of 3 °C/min to observe the glass transition temperature (at a constant strain of 0.04%, and frequency of 1 Hz). The creep recovery experiment was conducted at room temperature, with a stress ranging from 0.54 to 0.64 MPa to observe the yield stress.

Mechanical tests, videos and pictures:

Tensile testing was performed on a texture analyzer (TA) that combines a linear actuator with a load cell. The model is TA.XT Plus Connect that has a load cell with a maximum force of 50 N and an approximate resolution of ±1 mN and a distance resolution of 1 μm. Displacement is quantified via a stepper motor in conjunction with a known gear ratio. The materials were tested via uniaxial tension mode using mini tensile clamp fixtures. The speed of extension was 1 mm/s and the tests were performed at room temperature and ambient atmosphere. The samples were cut into dumbbell-shaped specimens with active region of 10.0 mm × 1.5 mm × 1 mm. Pictures and videos were captured using iPhone 11 camera.

Synthesis procedures:

Synthesis of 4-arm norbornadiene monomer (**2**):

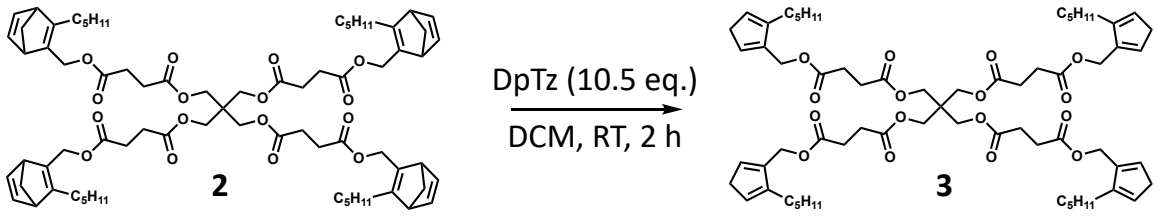


1 **2**

To a dried 250 mL round bottom was added compound **1** (6.1 g, 20.9 mmol, 4.5 eq.), pentaerythritol (637 mg, 4.6 mmol, 1.0 eq.) and 125 mL DCM. To this solution was added EDC (7.7 g, 37.2 mmol, 8.0 eq.) and DMAP (284 mg, 2.3 mmol, 0.5 eq.). Once added, the solution was allowed to stir at room temperature for 18 h. The crude solution was washed with water followed by brine solution until the organic layer became clear. The organic layer was directly passed through a silica plug, eluting with DCM. The clear solution was concentrated

to afford the pure product **2** as a colorless oil (4.5 g, 3.65 mmol, 73 % yield). ^{1}H NMR (500 MHz, $CDCl_3$) δ 6.75 (m, 4H), 6.70 (m, 4H), 4.73 (d, *J* = 12.2 Hz, 4H), 4.57 (d, *J* = 12.2 Hz, 4H), 4.16 (s, 8H), 3.43 (q, *J* = 2.2 Hz, 4H), 3.37 (t, *J* = 2.4 Hz, 4H), 2.67 – 2.58 (m, 16H), 2.22 (m, 4H), 2.13 (m, 4H), 1.94 (dt, *J* = 5.9, 1.7 Hz, 4H), 1.88 (dt, *J* = 5.9, 1.7 Hz, 4H), 1.44 – 1.16 (m, 24H), 0.87 (t, *J* = 7.3 Hz, 12H); ^{13}C NMR (126 MHz, $CDCl_3$) δ 172.11, 171.77, 155.60, 142.92, 141.94, 140.85, 71.32, 62.31, 61.05, 53.79, 52.09, 42.09, 31.40, 28.94, 28.34, 26.87, 22.47, 14.04; IR (ATR) 3064, 2958, 2928, 2859, 1731, 1662, 1556, 1458, 1411, 1381, 1348, 1305, 1289, 1230, 1205, 1141, 1063, 985, 945, 931, 892, 872, 829, 800, 723, 692, 651, 560 cm^{-1}; HRMS TOF MS ES+ exact mass calculated for $C_{73}H_{100}O_{16}Na^{+}$ or $[M+Na]^{+}$: 1255.6909, found: 1255.6914.

Synthesis of 4-arm cyclopentadiene monomer (**3**):



To a dried 250 mL round bottom flask was added 4-arm NBD monomer **2** (1.0 g, 0.81 mmol, 1.0 eq.) in 80 mL DCM. 3,6-Di-2-pyridyl-1,2,4,5-tetrazine (2.0 g, 8.5 mmol, 10.5 eq.) was then added and the solution was stirred rigorously for 2 h (TLC shows product with R_f = 0.67 in 30% EtOAc/Hex). The solution was passed through a plug of silica to remove excess amount of tetrazine (vibrant pink/red solid) and byproduct pyridazine (vibrant yellowish solid). After the silica plug, concentration of the solution afforded the pure product **3** as a

colorless oil (520 mg, 57% yield). ^{1}H NMR (500 MHz, $CDCl_3$) δ 6.35 (m, J = 2.6 Hz, 4H), 6.05 (m, J = 1.9 Hz, 4H), 4.88 (m, J = 1.7 Hz, 8H), 4.14 (s, 8H), 2.90 (m, J = 1.8 Hz, 8H), 2.65 (d, J = 2.9 Hz, 16H), 2.32 – 2.25 (m, 8H), 1.54 (m, 8H), 1.39 – 1.24 (m, 16H), 0.91 – 0.88 (m, 12H) ppm; ^{13}C NMR (126 MHz, $CDCl_3$) δ 171.88, 171.69, 146.20, 141.91, 132.18, 127.38, 62.34, 61.33, 42.06, 39.64, 31.75, 28.96, 28.88, 28.12, 27.90, 22.57, 14.06 ppm; IR (ATR) 3066, 2955, 2927, 2872, 2858, 2740, 1732, 1629, 1561, 1466, 1411, 1379, 1347, 1315, 1260, 1236, 1207, 1144, 1064, 999, 962, 937, 904, 841, 799, 766, 730, 648, 600 cm^{-1}; HRMS TOF MS ES+ exact mass calculated for $C_{65}H_{92}O_{16}Na^{+}$ or $[M+Na]^{+}$: 1151.6283, found: 1151.6281.

Polymer preparation and degradation procedures:

Monomer storage and polymer preparation:

The monomer can be used freshly after deprotection or stored in the freezer (< 0 °C) for up to 1.5 months without significant amount of premature dimerization. The viscous monomer was poured slowly into house-made Teflon molds of various geometries. The dropcasted material was then kept in a vacuum oven under suitable curing conditions (110 °C for ~2 h). After curing, polymers were punched into desired rectangular or dumbbell samples. The authors would like to note that insufficient purification of monomer **3** resulted in vibrant yellowish color in the monomer (from the solid pyridazine product) and the discoloration of the subsequent polymer (can be brown to charcoal depending on the temperature and amount of impurity). Typically, samples used for DMA experiment are 6-8 mm long, 0.4 mm thick, and 2 mm wide. The dumbbell samples have active dimensions of 10 mm × 1.5 mm × 1 mm.

Degradation procedure with N-phenyl maleimide as capping reagent:

Small polymer pieces (93 mg in total) with dimensions of ~2 × 2 × 0.8 mm were added into a solution of 646 mg N-phenyl maleimide in 47 mL of xylene. The mixture was heated to ~150 °C to maintain rigorous boiling for 48 h. The mixture was first filtered to remove any remaining insoluble cross-linked polymer. The soluble materials were precipitated in cold hexane. The obtained solid was then heated in boiling hexane to remove excess maleimide and afford the pure yellow solid as capped Cp oligomer (~420 mg).

Structural diversity of Diels–Alder adducts – Investigation of bite angles among cross-linking points:

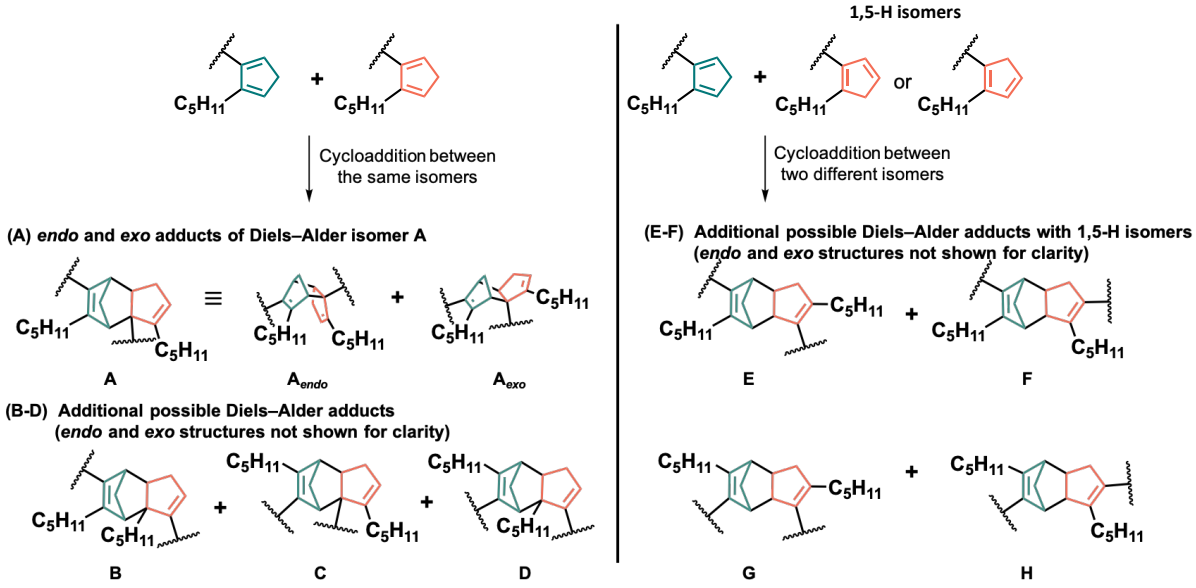


Figure S2.1. General scheme of possible Diels–Alder adducts, resulting from the cycloadditions of either the same or different Cp isomers (diene in blue and dienophile in red). *Endo* and *exo* adducts are only shown for one of the Diels–Alder adducts for clarity. There

are at least 8 unique diastereomers (**A**-**H**), each with different bite angle that must be considered.

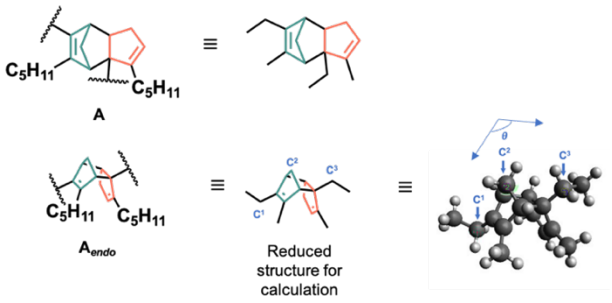


Figure S2.2. Example of the reduced structure for bite angle calculation (*endo* form of structure **A** shown). Three carbons were consistently picked among the structures in **Figure S1** to calculate the bite angles (Table S2.1). C^1 and C^3 are the tethered carbons to the cross-linked network.

Bite angle calculation procedure: Geometries of Diels–Alder adducts were optimized using B3LYP/6-31+G(d,p) in the gas phase using Gaussian 16.[5] Bite angle was calculated by measuring the angle among 3 carbon atoms (C^1, C^2, and C^3). C^1 and C^3 are the tethered carbons to the cross-linked network, C^2 is chosen as shown in Figure S2.2.

Table S2.1. Calculated bite angles with optimized geometries using B3LYP/6-31+G(d,p) in the gas phase via Gaussian 16.[53] Only structure **A** was calculated based on *endo* and *exo* structures. Structures **B**-**H** were calculated based on the *endo* structure (assuming it predominates).

Structure	Calculated bite angles (°)
$\mathbf{A}_{endo}$	115.0
$\mathbf{A}_{exo}$	75.4
$\mathbf{B}_{endo}$	80.5
$\mathbf{C}_{endo}$	91.0
$\mathbf{D}_{endo}$	50.5
$\mathbf{E}_{endo}$	83.8
$\mathbf{F}_{endo}$	59.8
$\mathbf{G}_{endo}$	53.2
$\mathbf{H}_{endo}$	57.9

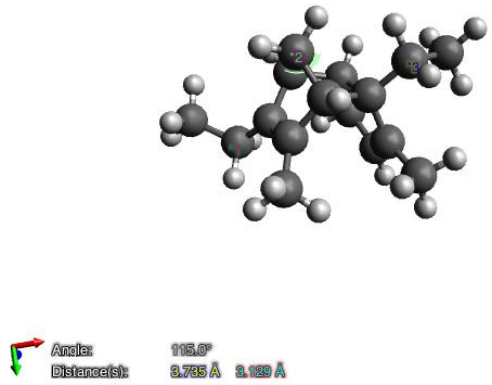


Figure S2.3. Ball and stick display of structure $\mathbf{A}_{endo}$ along with the measured bite angle.

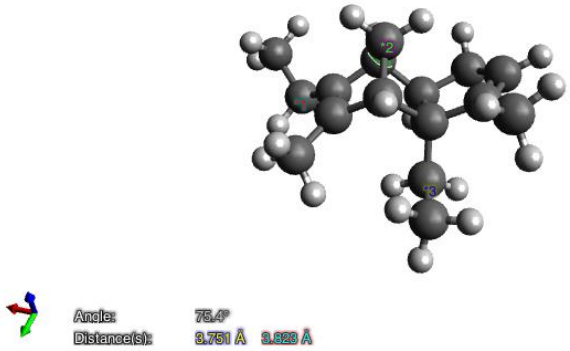


Figure S2.4. Ball and stick display of structure $\mathbf{A}_{exo}$ along with the measured bite angle.

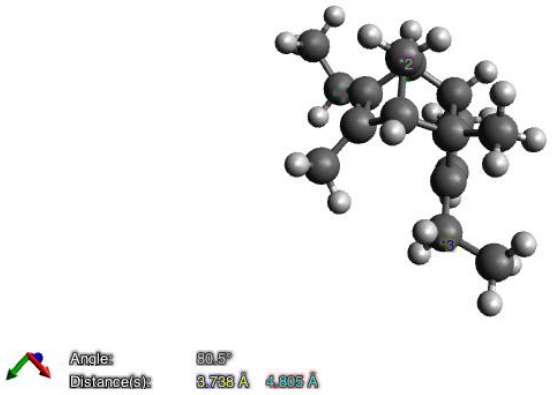


Figure S2.5. Ball and stick display of structure $\mathbf{B}_{endo}$ along with the measured bite angle.

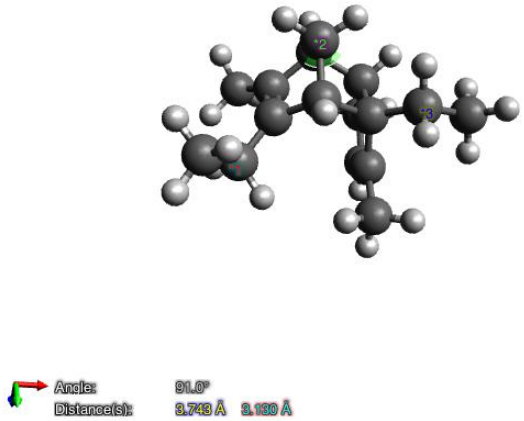


Figure S2.6. Ball and stick display of structure $\mathbf{C}_{endo}$ along with the measured bite angle.

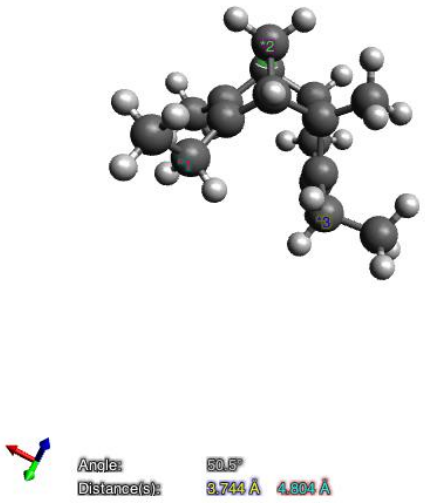


Figure S2.7. Ball and stick display of structure **D***endo* along with the measured bite angle.

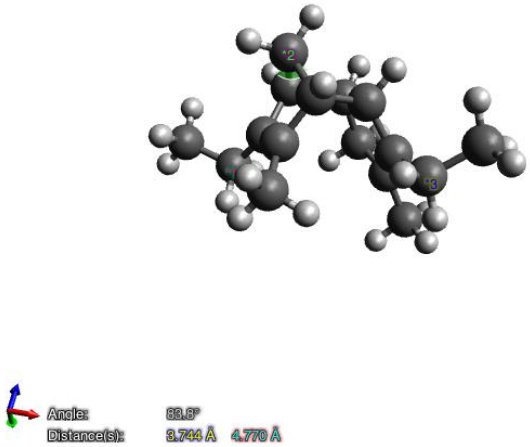


Figure S2.8. Ball and stick display of structure **E***endo* along with the measured bite angle.

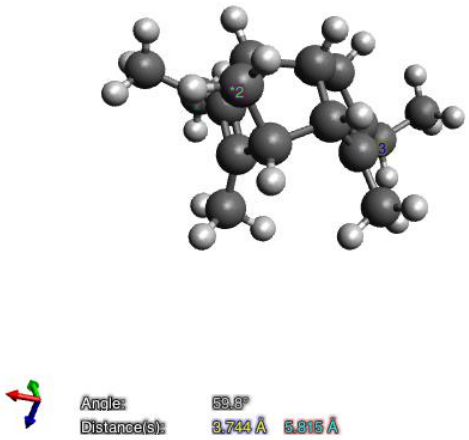


Figure S2.9. Ball and stick display of structure $\mathbf{F}_{endo}$ along with the measured bite angle.

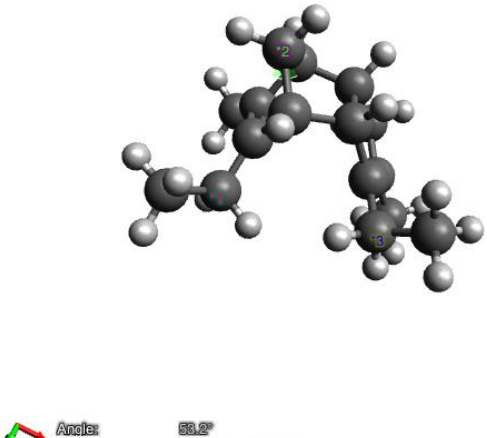


Figure S2.10. Ball and stick display of structure $\mathbf{G}_{endo}$ along with the measured bite angle.

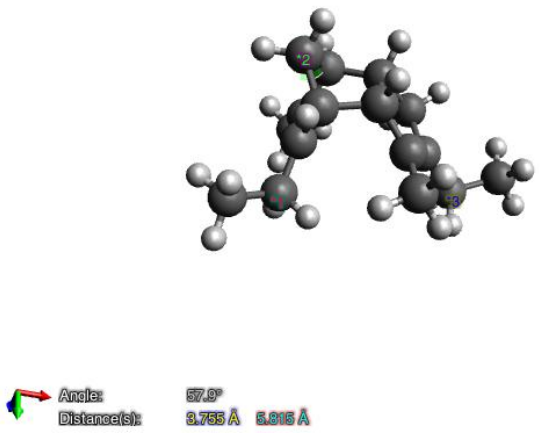


Figure S2.11. Ball and stick display of structure **H***endo* along with the measured bite angle.

Inverse Electron Demands Diels-Alder (IEDDA) deprotection mechanism

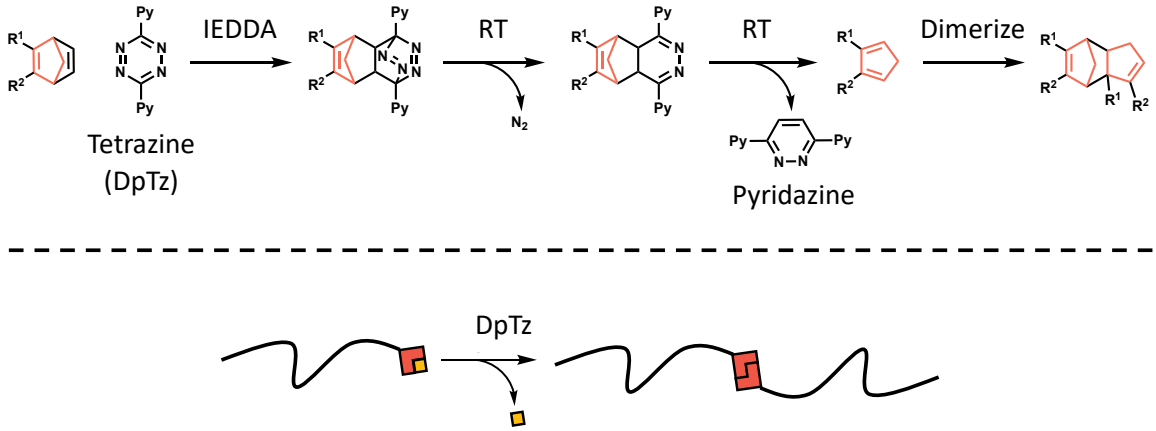


Figure S2.12. Schematic mechanism of the inverse electron demands Diels-Alder reaction.[55]

Screening conditions to obtain the optimized deprotection reaction:

Table S2.2. Different screening conditions to obtain the optimized deprotection reaction with tetrazine cascade. The optimal condition was found in entry 6: 10.5 eq. of tetrazine, in 0.01 M concentration, and 2 h reaction time to afford the optimal yield of 57% on a 1-gram scale.

Entry	Scale (g)	Eq. of DpTz	Concentration (M)	Reaction time (h)	% Isolated yield
1	0.5 and 1.0	10.5	0.04	4	22
2		10.5	0.04	2 – 3	< 20 %
3		8.0	0.08	2 – 4	< 5 %
4		8.0	0.04	2 – 4	< 5 %
5		10.5	0.01	4	< 20 %
6		10.5	0.01	2	40 – 57 %
7		10.5	0.01	1.5	Not full completion
8		10.5	0.01	3	20 – 30 %

1,5-Hydride isomerization and Cp dimerization monitor of the 4-arm Cp monomer via NMR spectroscopy:

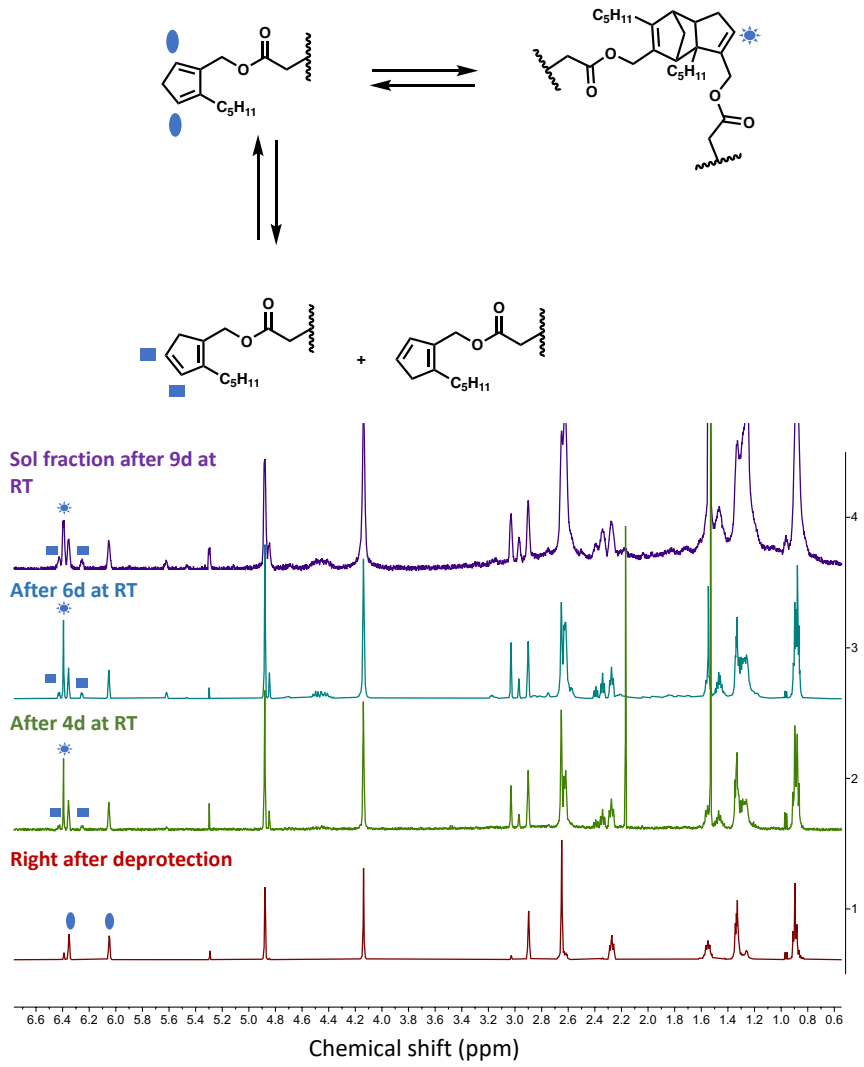
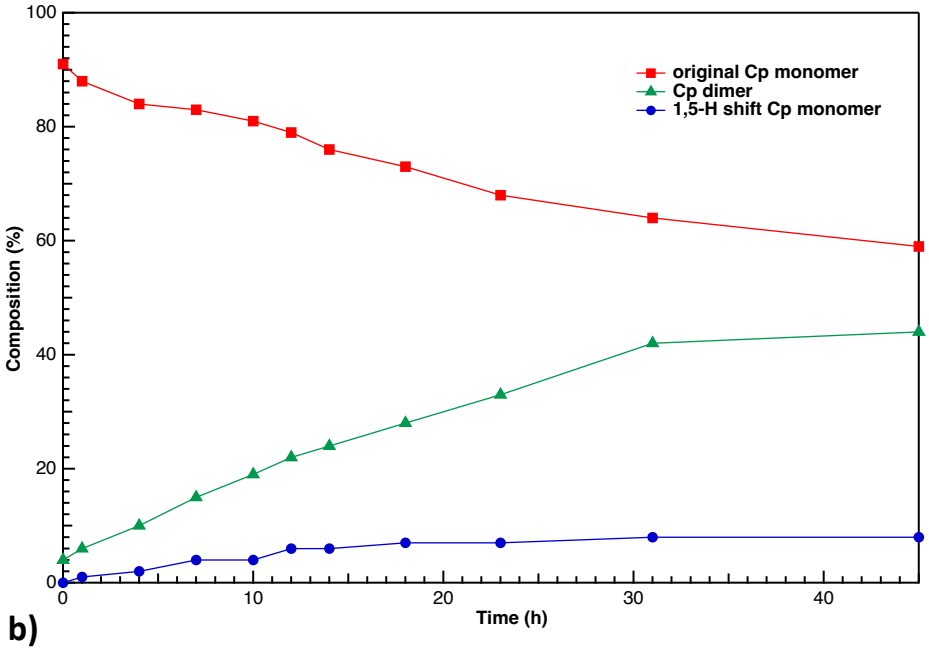


Figure S2.13. ^{1}H NMR monitoring of the neat 4-arm Cp monomer at room temperature until forming a gel after 9 days.

a)


original Cp monomer
Cp dimer
1,5-H shift Cp monomer
Composition (%)
Time (h)
0
20
40
60
80
100
0
10
20
30
40

b)

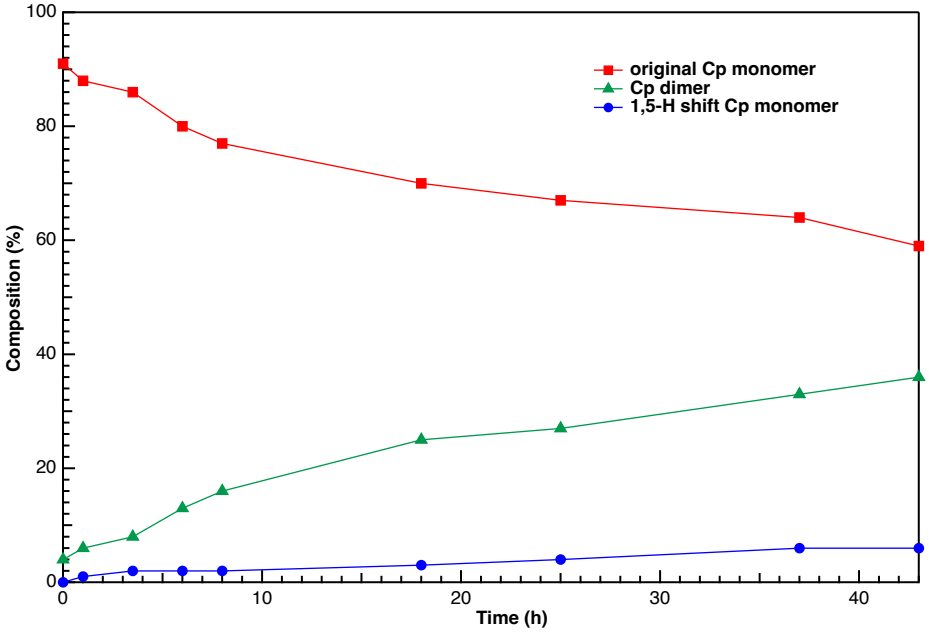

original Cp monomer
Cp dimer
1,5-H shift Cp monomer
Composition (%)
Time (h)
0
20
40
60
80
100
0
10
20
30
40

Figure S2.14. ^{1}H NMR monitoring of 1,5-hydride isomerization and Cp dimerization at room temperature. The monomer was either (a) in deuterated solvent and monitored by ^{1}H NMR or (b) neat, and aliquots were taken, diluted with deuterated solvent.

Polymerization of telechelic Cp monomer model to check trimer formation:

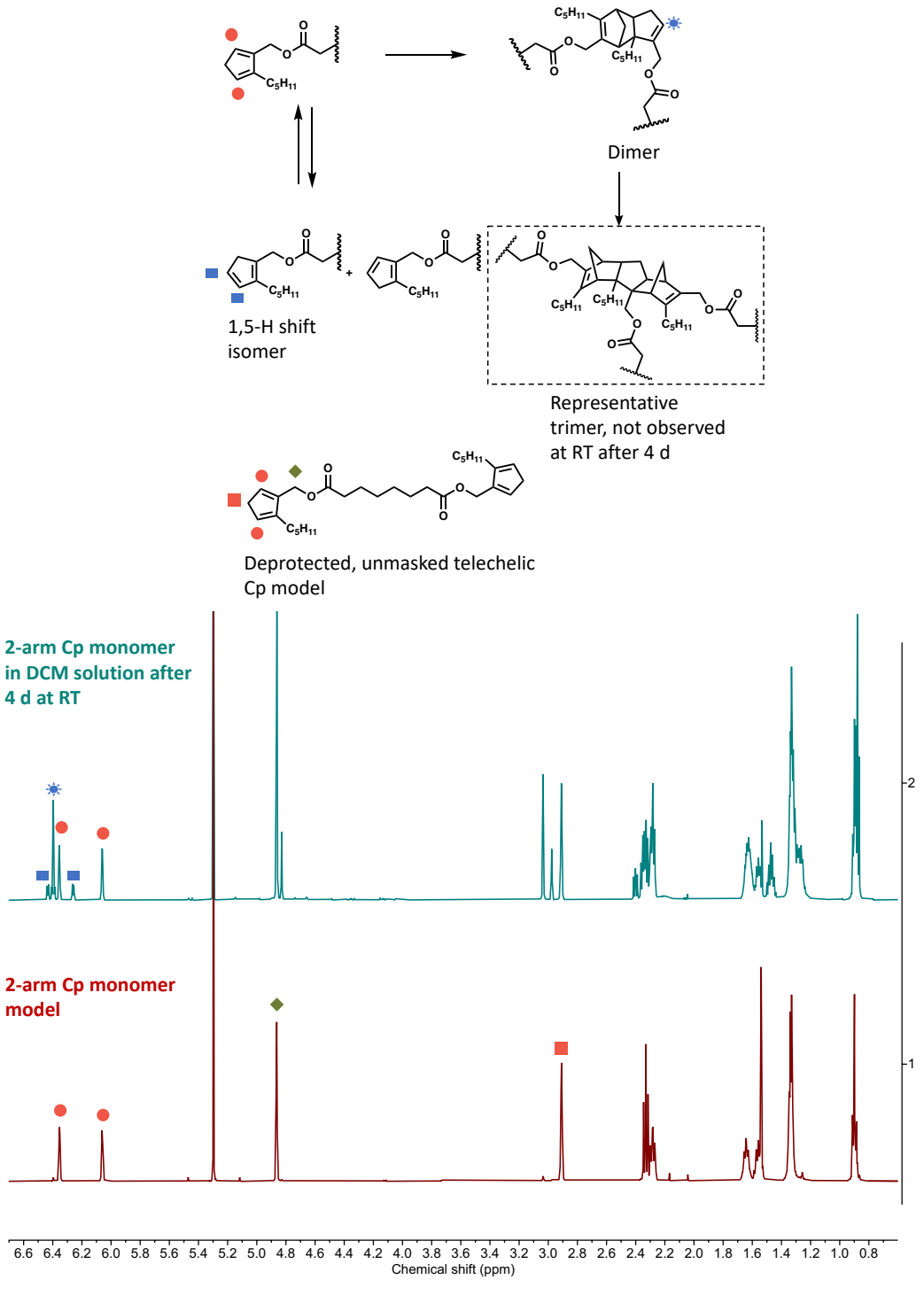

Dimer
1,5-H shift isomer
Representative trimer, not observed at RT after 4 d
Deprotected, unmasked telechelic Cp model
2-arm Cp monomer in DCM solution after 4 d at RT
2-arm Cp monomer model
6.6 6.4 6.2 6.0 5.8 5.6 5.4 5.2 5.0 4.8 4.6 4.4 4.2 4.0 3.8 3.6 3.4 3.2 3.0 2.8 2.6 2.4 2.2 2.0 1.8 1.6 1.4 1.2 1.0 0.8
Chemical shift (ppm)

Figure S2.15. ^{1}H NMR monitoring of the 2-arm model Cp monomer and its bulk polymerization at RT after 4 days.

Sol-gel test procedure: The formed polymer was first immersed in hexane, which was then removed and exchanged for ethyl acetate. The vial that contained the polymer in ethyl acetate was heated to 70 °C for 24 h. The vial was cooled to RT, and the solvent was then removed. The material was washed again with room temperature ethyl acetate and was then deswelled in hexane (x3). Hexane was removed and the polymer was further dried on a rotary evaporator and then high vacuum system for 24 h. The weight of dried polymer was checked before and after the sol-gel test to obtain ~24% gelation.

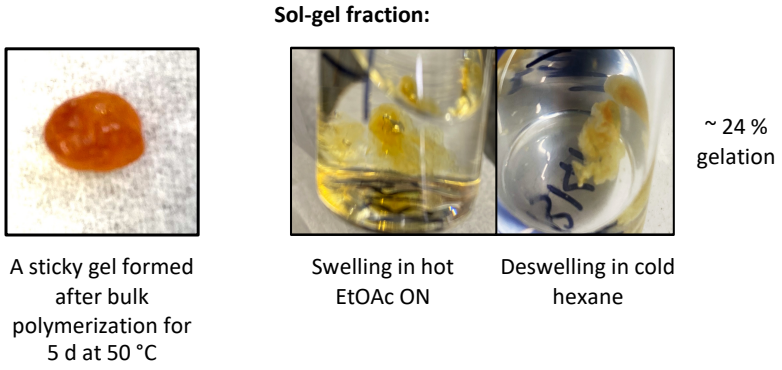
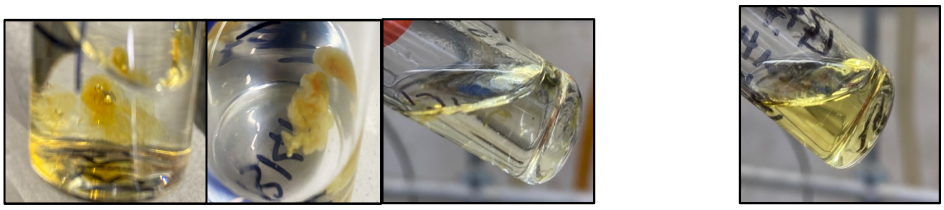


Figure S2.16. Sol-gel test for the model 2-arm Cp monomer after bulk polymerization for 5 d at 50 °C in the vacuum oven. The formed polymer was aged for 3 weeks before the sol-gel test. The test shows ~24 % gel formation.

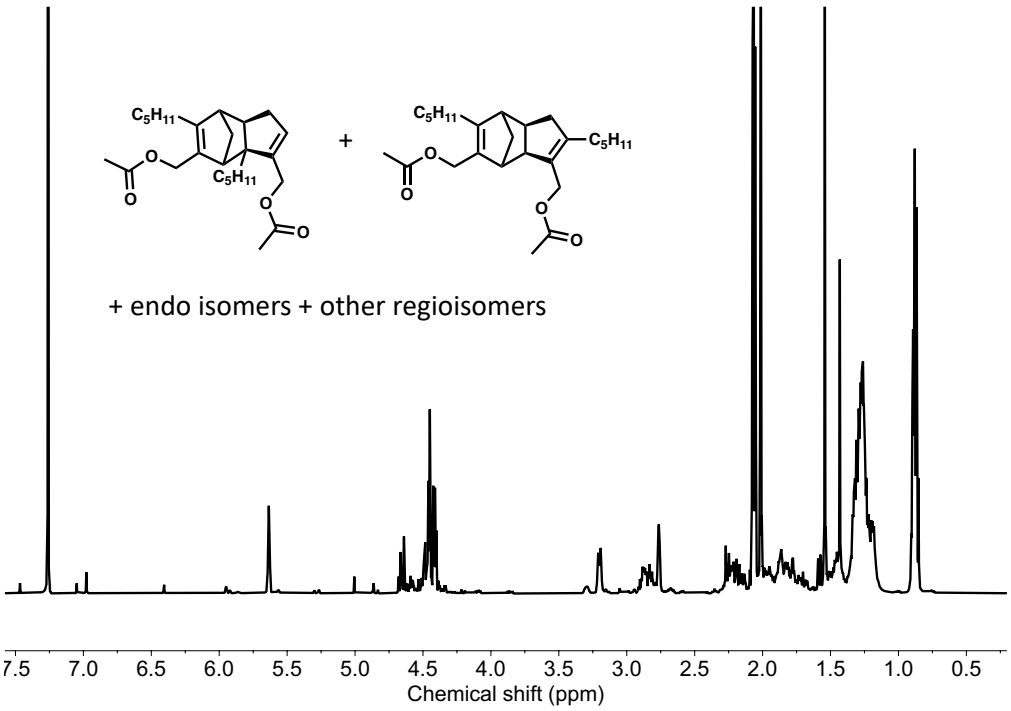


Insoluble gel formation without BHT

Soluble material with 5 mol% BHT

Figure S2.17. A soluble linear polymer was formed by bulk polymerization of the 2-arm model system with the addition of BHT (5 mol%) at 90 °C for 4 days.

a)


C5H11
O
O
C5H11
O
O
+
C5H11
O
O
C5H11
O
O
+ endo isomers + other regioisomers
7.5 7.0 6.5 6.0 5.5 5.0 4.5 4.0 3.5 3.0 2.5 2.0 1.5 1.0 0.5
Chemical shift (ppm)

b)

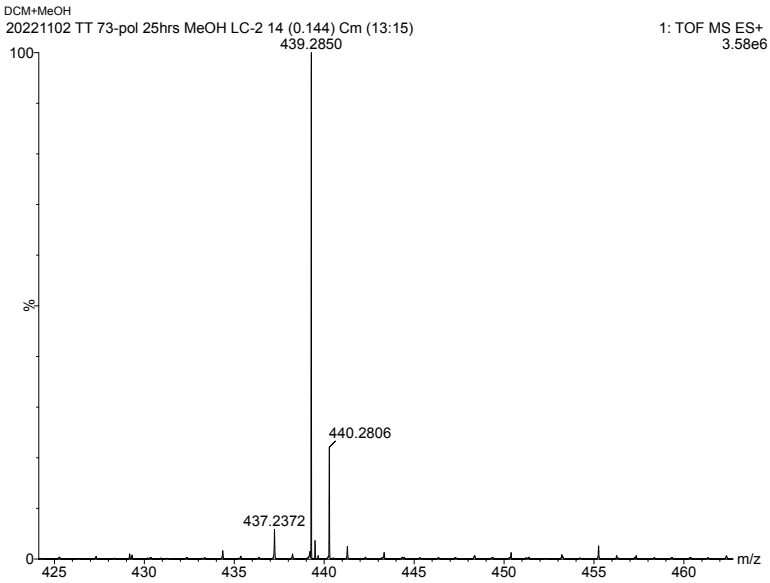

DCM+MeOH
20221102 TT 73-pol 25hrs MeOH LC-2 14 (0.144) Cm (13:15)
1: TOF MS ES+
3.58e6
439.2850
100
%
440.2806
437.2372
0
425 430 435 440 445 450 455 460
m/z

Figure S2.18. (a) ^{1}H NMR and (b) mass spectra of the mixture of different isomers, formed by bulk heating of a small molecule model (monofunctional Cp monomer) at 90 °C for 25 h. The representative structures of the products were shown on the spectrum. Mass spectrum shows only the dimer major product (HRMS TOF MS ES+ exact mass calculated for $C_{26}H_{40}O_4Na^+$ or $[M+Na]^+$: 439.2824, found: 439.2850). No trimer product was found (HRMS TOF MS ES+ exact mass calculated for $C_{39}H_{60}O_6Na^+$ or $[M+Na]^+$: 647.4288).

TGA to measure thermal degradation temperature

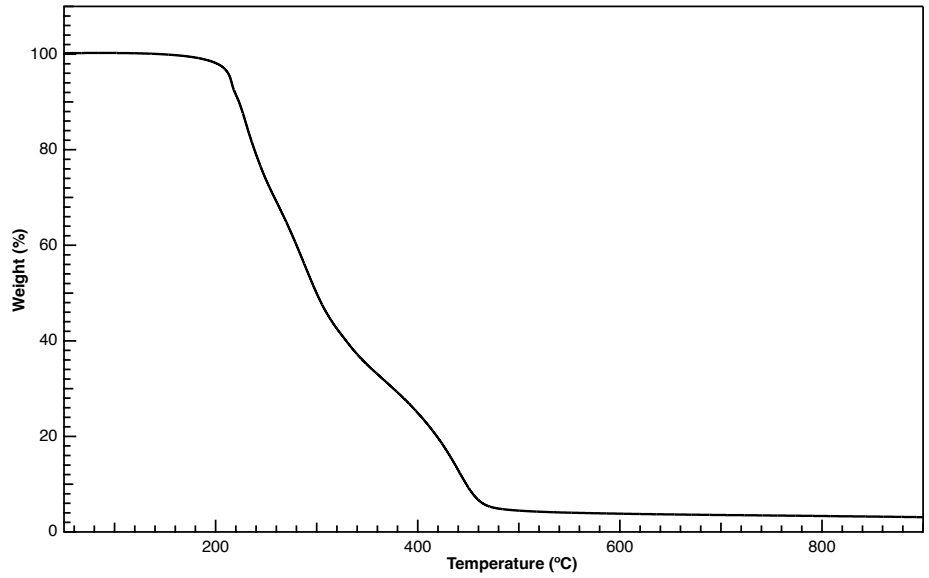


Figure S2.19. TGA shows onset of network degradation at ~220 °C.

Isothermal curing kinetics via DSC:

The monomer was heated at certain temperatures (90, 100, 110, 120, and 130 °C) in the DSC to collect the isothermal curing data. A temperature ramp was also measured for the monomer from -20 °C to 190 °C to obtain the heat of reaction (ΔH_{rxn}). The data were then analyzed using the following formulas:[56-58]

$$\alpha_i = \frac{\sum \Delta H_i}{\Delta H_{rxn}} \quad \text{(S2.1)}$$

$$\left(\frac{d\alpha}{dt}\right)_i = \frac{\left(\frac{dH}{dt}\right)_i}{\Delta H_{rxn}} \quad \text{(S2.2)}$$

Specifically, the ΔH_{rxn} was first calculated by integrating the exothermic curve from 73 °C to 186 °C (Figure S2.20). The baseline heat flow was chosen as -0.277 W/g. The heat flow from each temperature point was subtracted from the baseline. The total sum of the difference was calculated to determine the integral value, which is ΔH_{rxn} equal to 1123 J/mol.

By applying equation (S2.2), the conversion data were calculated. First, the magnitude of each time point was determined by subtracting from the baseline. Then the conversion was calculated at each time point by dividing the magnitude by the ΔH_{rxn}.

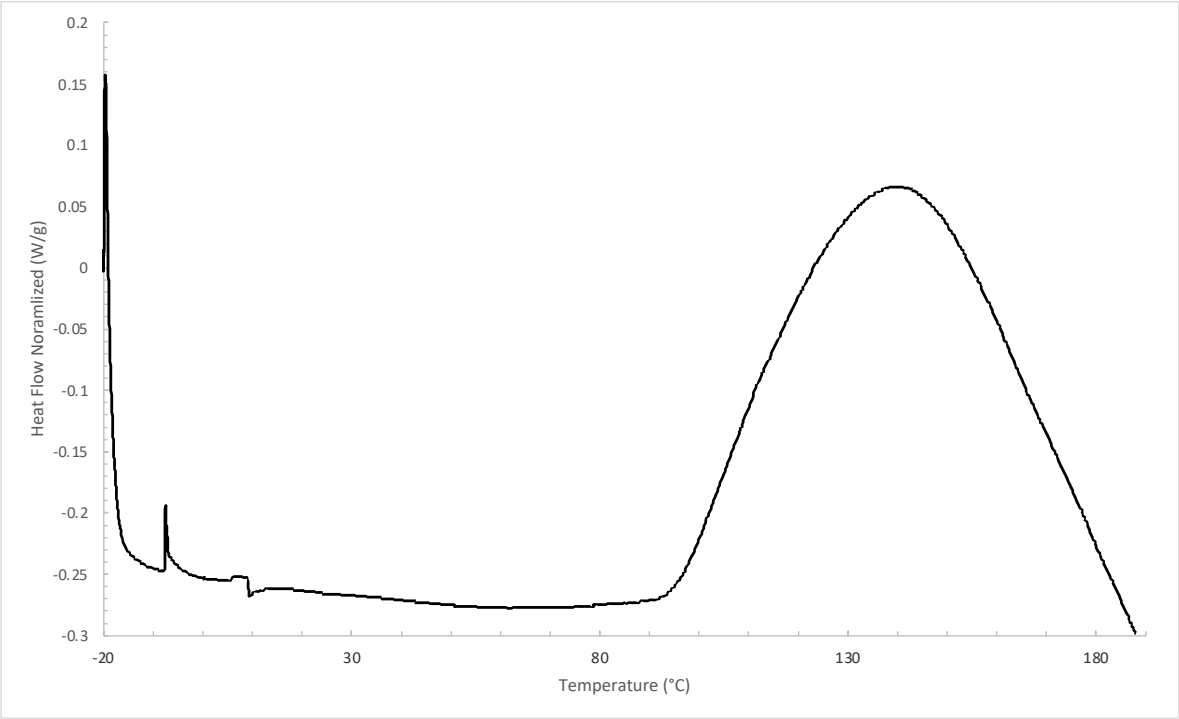


Figure S2.20. DSC thermogram of a temperature ramp of the uncured, freshly prepared, and neat monomer from -20 °C to 190 °C.

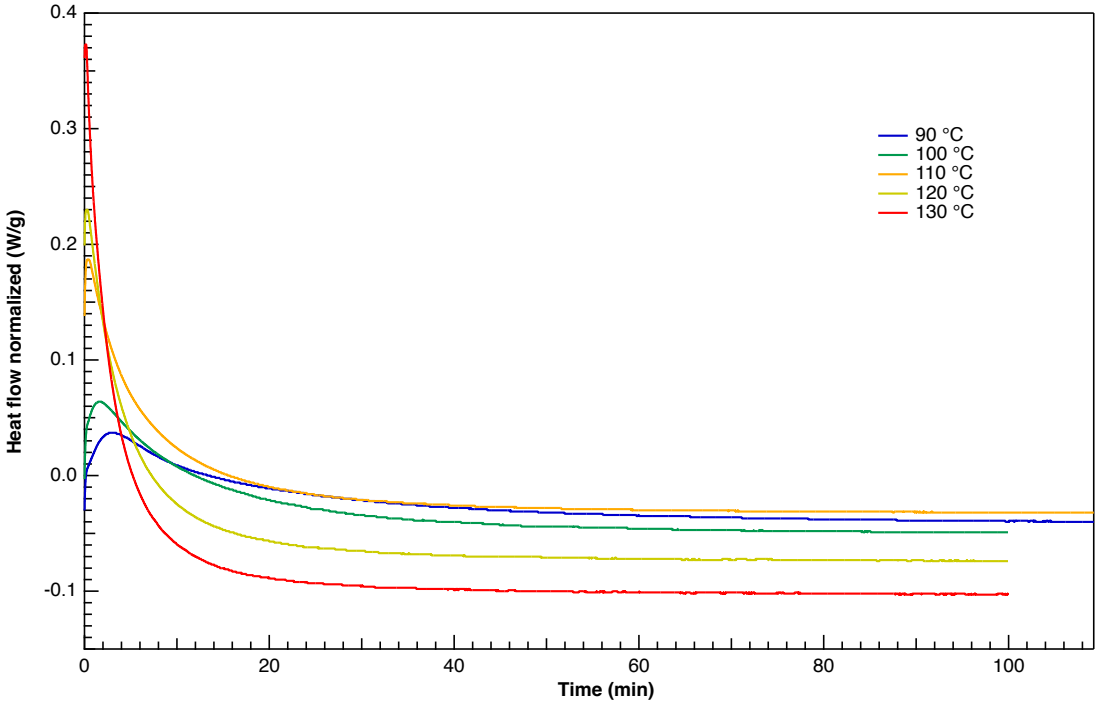


Figure S2.21. Isothermal DSC curves of samples that were hold at different temperatures for approximately 100–120 min.

DSC to monitor post-curing and measure T_gs:

DSC can also be used to monitor whether the sample is completely cured or not by observing the residual heat from the first heating cycle.[59] Figures S2.22 and S2.23 show incomplete curing of samples cured at 50 and 70 °C for 120 min due to the residual heat at 80-150 °C. On the other hand, figure S11 and S12 confirm the complete curing of the samples that were cured at 90 and 110 °C for 120 min. The T_gs measured from DSC are lower (8-12 °C) than those from the DMA when using the tan delta values (22-33 °C).

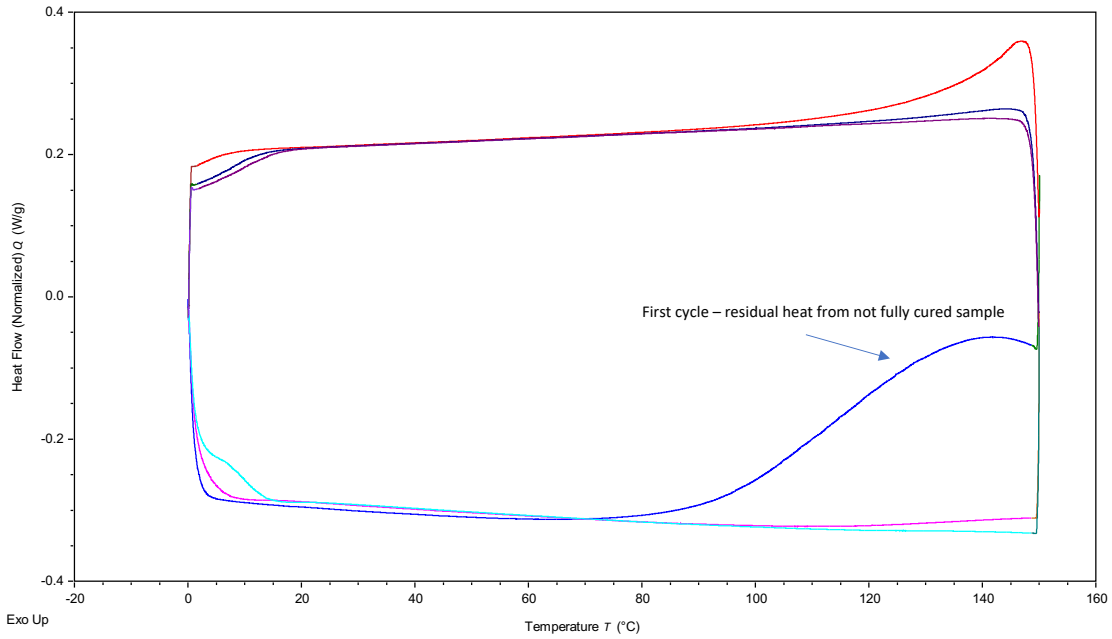


Figure S2.22. DSC thermogram of a polymer sample cured at 50 °C for 120 min (3 heating and cooling cycles).

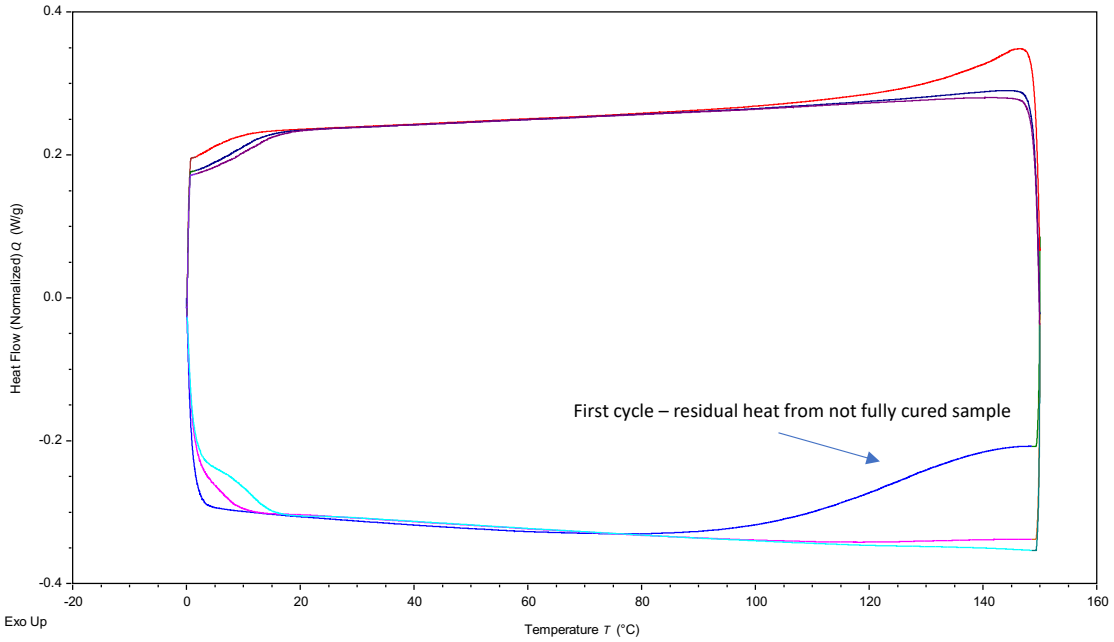


Figure S2.23. DSC of a polymer sample cured at 70 °C for 120 min (3 heating and cooling cycles).

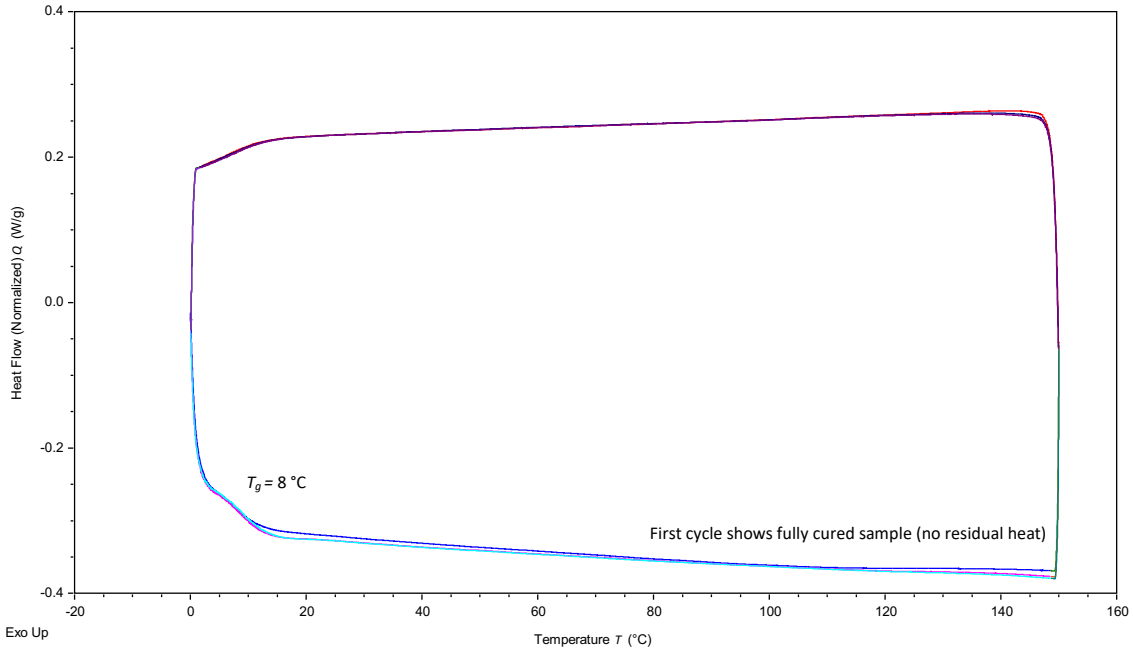


Figure S2.24. DSC of a polymer sample cured at 90 °C for 120 min (3 heating and cooling cycles).

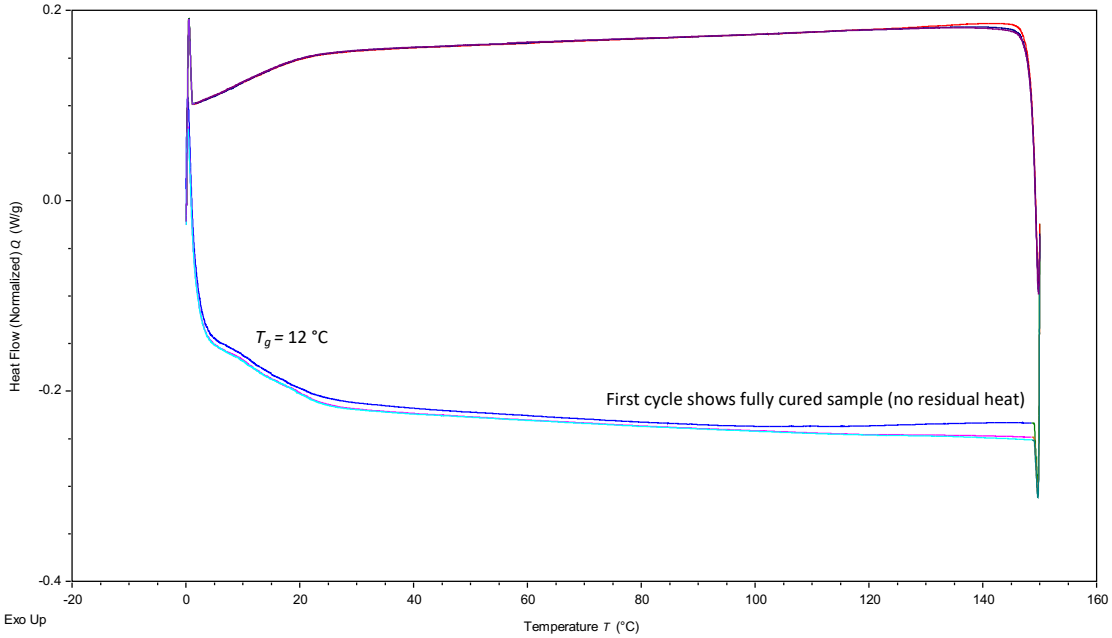


Figure S2.25. DSC of a polymer sample cured at 110 °C for 120 min (3 heating and cooling cycles).

Monitoring consumption of free Cp during network synthesis via FTIR-ATR:

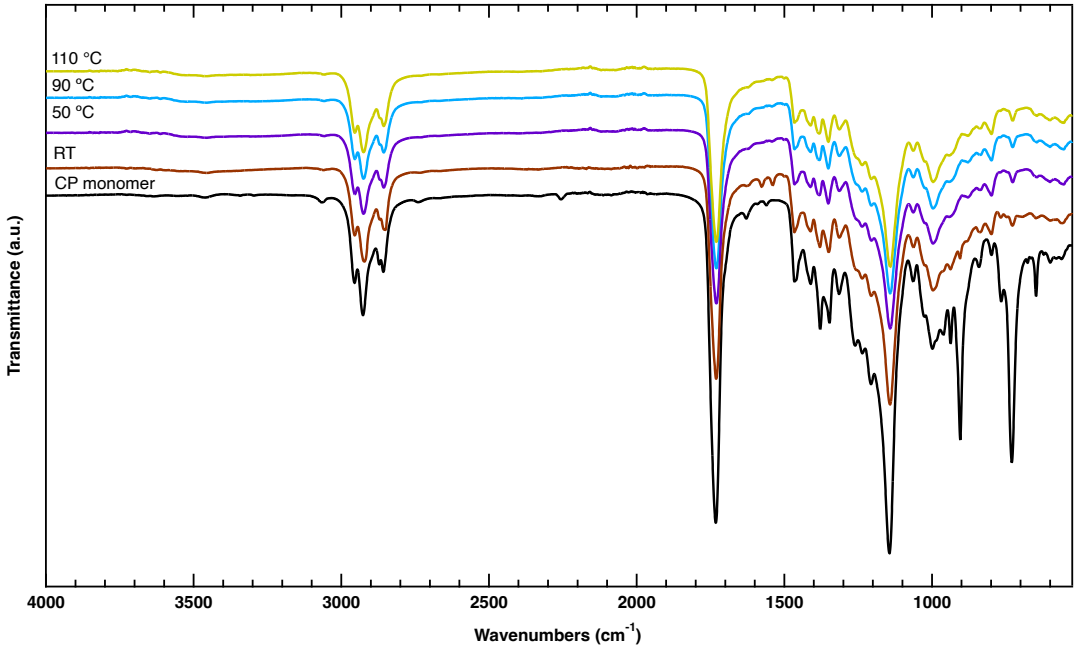


Figure S2.26. FTIR-ATR spectra of samples cured using different conditions.

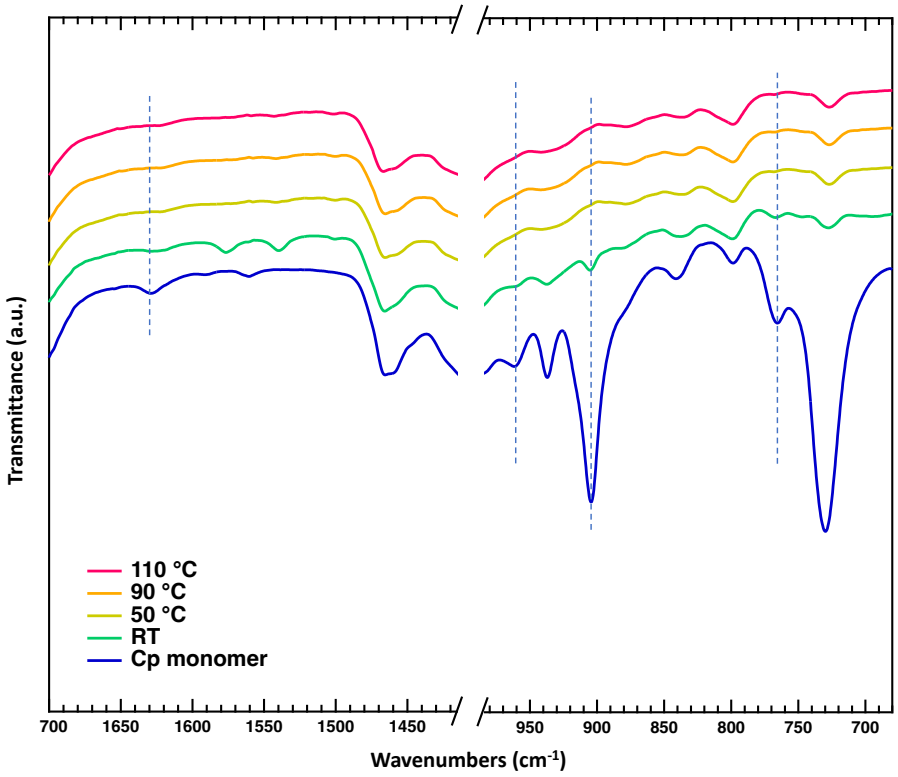


Figure S2.27. Zoomed-in FTIR spectra (% transmittance) for detection of C=C stretching, CH_2 bending and (=C-H) bending.

Molecular weight between cross-links (M_c) via DMA:

Molecular weight between cross-links (M_c) can be calculated based on the following formula:[60-62]

$$M_c = \frac{3RTd}{E'_p} \quad \text{(S2.3)}$$

in which, M_c is molecular weight between cross-linking units, R is gas constant, T is the temperature, E'_p is the storage modulus of the rubbery plateau region at temperature T (beyond glass transition temperature), and d is the polymer density.

The polymer density was measured by dividing the mass of polymer sample by its volume (measured via L×W×H dimensions). Five samples were used, and the density was determined to be 0.88±0.05 g/cm^3. M_c can then be calculated using eq. S2.3 at temperature at ~120–150 °C. An example calculation of sample cured at 50 °C was shown as below:

$$M_c(50\ °C) = \frac{3 \times 8.3145 \frac{J}{mol.K} \times (146+273)K \times 0.88 \frac{g}{cm^3} \times \frac{10^6 \frac{g}{m}^3}{\frac{1\ g}{cm^3}}}{5.31 \times 10^6\ Pa} = 1732 \frac{g}{mol}$$

The experimental values are summarized as in Table S2.3. The theoretical value was determined based on the schematic cross-linking point from the monomer structure or $M_c(ideal\ theoretically) = 558$ g/mol (see schematic in Figure S2.28).

Table S2.3. Summary of the calculated experimental molecular weight between cross-links (M_c) of different samples that were cured at varied temperatures. All E'_p values that were used for the calculation were reported at T = 146 °C.

Curing temperature of sample (°C)	50	90	110	130
E'_p (MPa)	5.31	7.84	10.51	7.66
M_c (g/mol)	1732	1173	875	1201

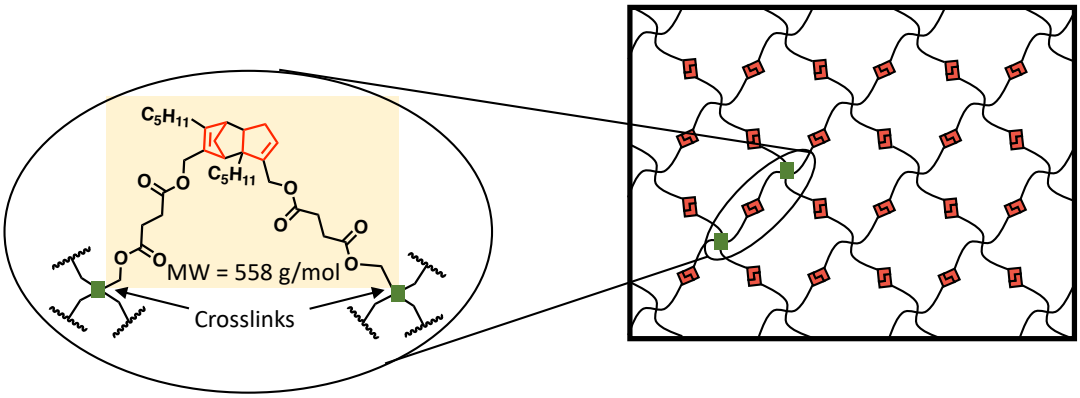


Figure S2.28. Schematic representation of the two cross-linking points for theoretically ideal molecular weight between cross-links.

DMA of samples cured at 130 °C with and without BHT:

Procedure of curing materials with addition of BHT: 5 mol% of BHT was added to the viscous monomer in a minimal amount of DCM. The solution was then evaporated. The viscous material was then dropcast in suitable molds and cured in the vacuum oven based on previously noted conditions.

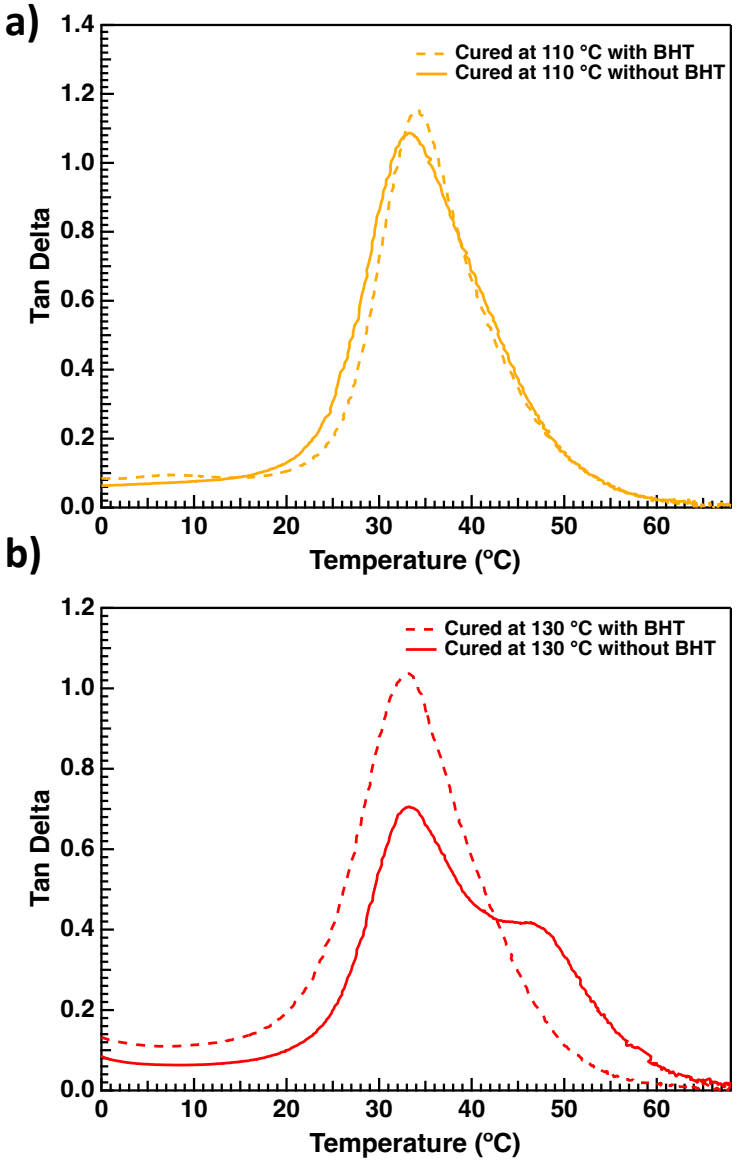


Figure S2.29. Tan delta curves of the samples that were cured (a) at 110 °C and (b) at 130 °C with and without BHT (5 mol%). The addition of BHT resulted in the disappearance of bimodal curve that was observed in the original 130 °C sample, while did not affect the curve of 110 °C sample significantly. Of note, the tan delta curve of the new 130 °C sample without BHT was in the lower temperature range than that of the original sample shown in Figure 3e, which might result from the varied experimental condition during the curing process.

DMA of controlled-defect samples with maleimides:

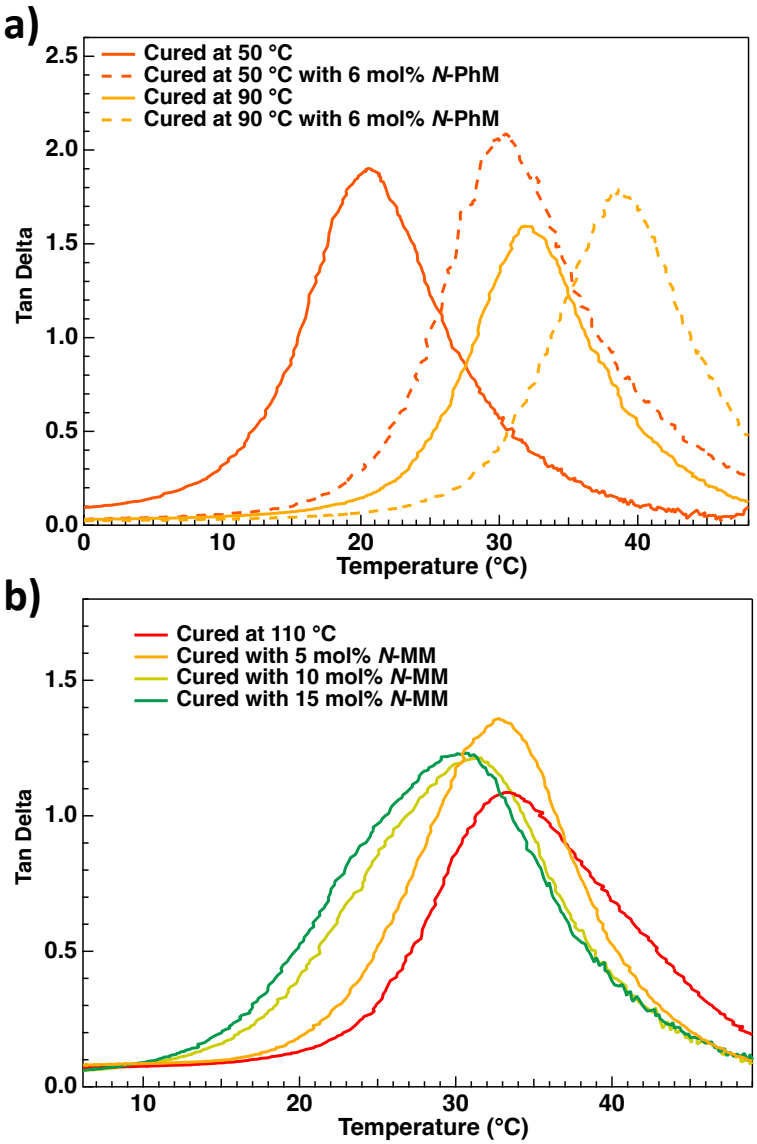


Figure S2.30. Comparison of the tan delta curves of controlled-defect materials versus original samples (a) Effect of 6 mol% of *N*-phenyl maleimide (*N*-PhM) to the samples that were originally cured at 50 °C and 90 °C. Crystallinity of *N*-phenyl maleimide increases T_g values significantly (by ~10 °C) even with 6 mol% of capped Cp chain-ends, which

supposedly would lower T_g. (b) Effect of 5, 10, and 15 mol% of *N*-methyl maleimide (*N*-MM) to the sample that was originally cured at 110 °C. Though T_g values decrease with increasing amount of capped Cp chain-ends, it is considered insignificant (varied by only ~1-2 °C per 5 mol% addition of maleimide).

DMA results to measure storage modulus and T_g:

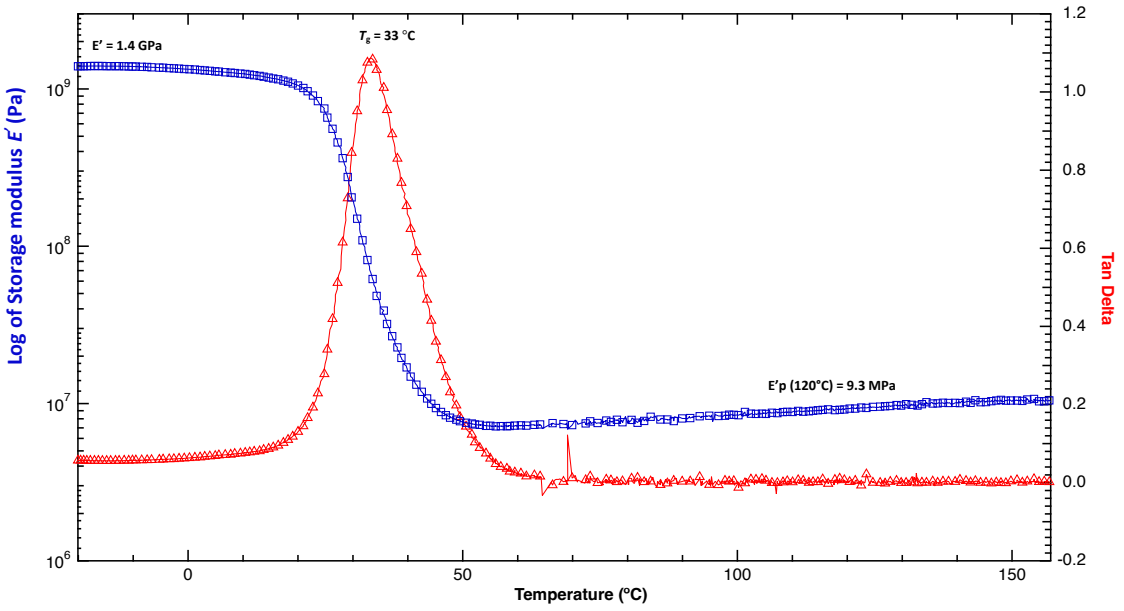


Figure S2.31. DMA temperature ramp shows a T_g of 33 °C (from tandelta max) with a storage modulus before glass transition E' = 1.4 GPa (at T = -15 °C) and storage modulus of the rubbery plateau region beyond glass transition temperature E'_p = 9.3 MPa (at T = 120 °C). The sample was cured at 110 °C for 100 min.

Solid ^{13}C NMR for analysis of cross-linked sample:

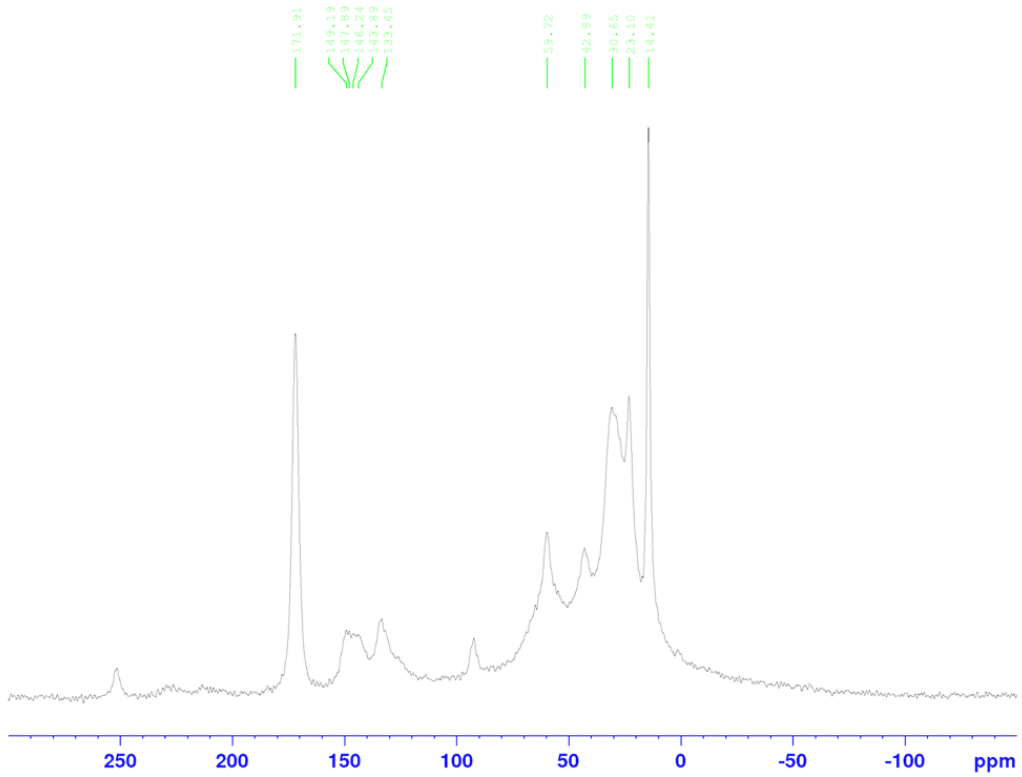


Figure S2.32. Solid ^{13}C NMR spectrum of the cross-linked polymer **4** that was cured at 50 °C. The overlapping of the signals from the free Cp and the dimer renders the spectrum non-informative for further detailed analysis.

Tensile testing and Young's modulus calculation

The Young's modulus was calculated via the slope of the fitting line in the linear elastic region of the tensile curve (Figure S2.33). In this case, the slope of the linear line is 2.55, which can be converted to 255 MPa as the Young's modulus. The tensile tests were done for 3 samples and the results were reported in Table S2.4.

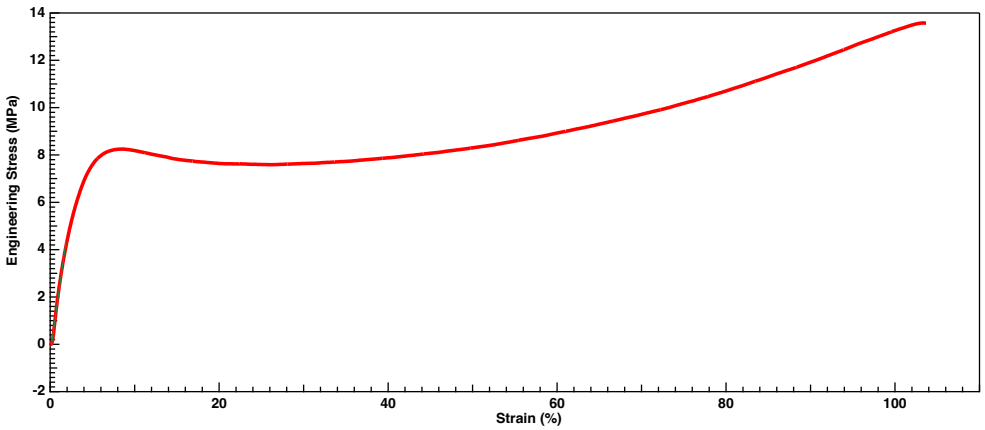


Figure S2.33. Tensile curve of PTCp with a fitted line in the linear elastic region for Young's modulus calculation.

Table S2.4. Young's modulus, ultimate tensile strength, and elongation at break for three different PTCp samples.

Sample #	Young's modulus (MPa)	Ultimate tensile strength (MPa)	Elongation at break (%)
1	254.6	13.6	103.7
2	224.1	12.0	96.3
3	185.5	9.9	104.7

DMA analysis of thermally annealed samples:

Since the cross-linked polymer is formed entirely from DA cycloaddition, which is reversible, the system might reach a more ideal form upon thermal annealing at or higher than the rDA temperature. We used DMA to analyze the materials after thermal annealing at 150 °C for 2 h of samples that were previously cured at 110 °C and 130 °C. We observed that the materials became more rigid and turned more yellowish. The tan delta curves of these materials also became bimodal. It can possibly indicate that the material has reached to a more ideal form with higher cross-link density. However, based on additional control experiments with BHT, we speculate that the bimodal tan delta and higher cross-link density result from radical reactions that presumably occur at high temperature. Figure S2.34a shows a small change in the bimodal peaks with the addition of BHT to the samples during annealing. Presumably, the BHT has little effect because the mobility of the BHT is limited in the highly cross-linked material. On the other hand, Figure S34b shows that the bimodal peak can be suppressed if BHT is added to the viscous monomer in minimal amount of solvent prior to curing (blue trace). In this case, the formation of the bimodal peak is minimized when the material is further annealed at 150 ºC.

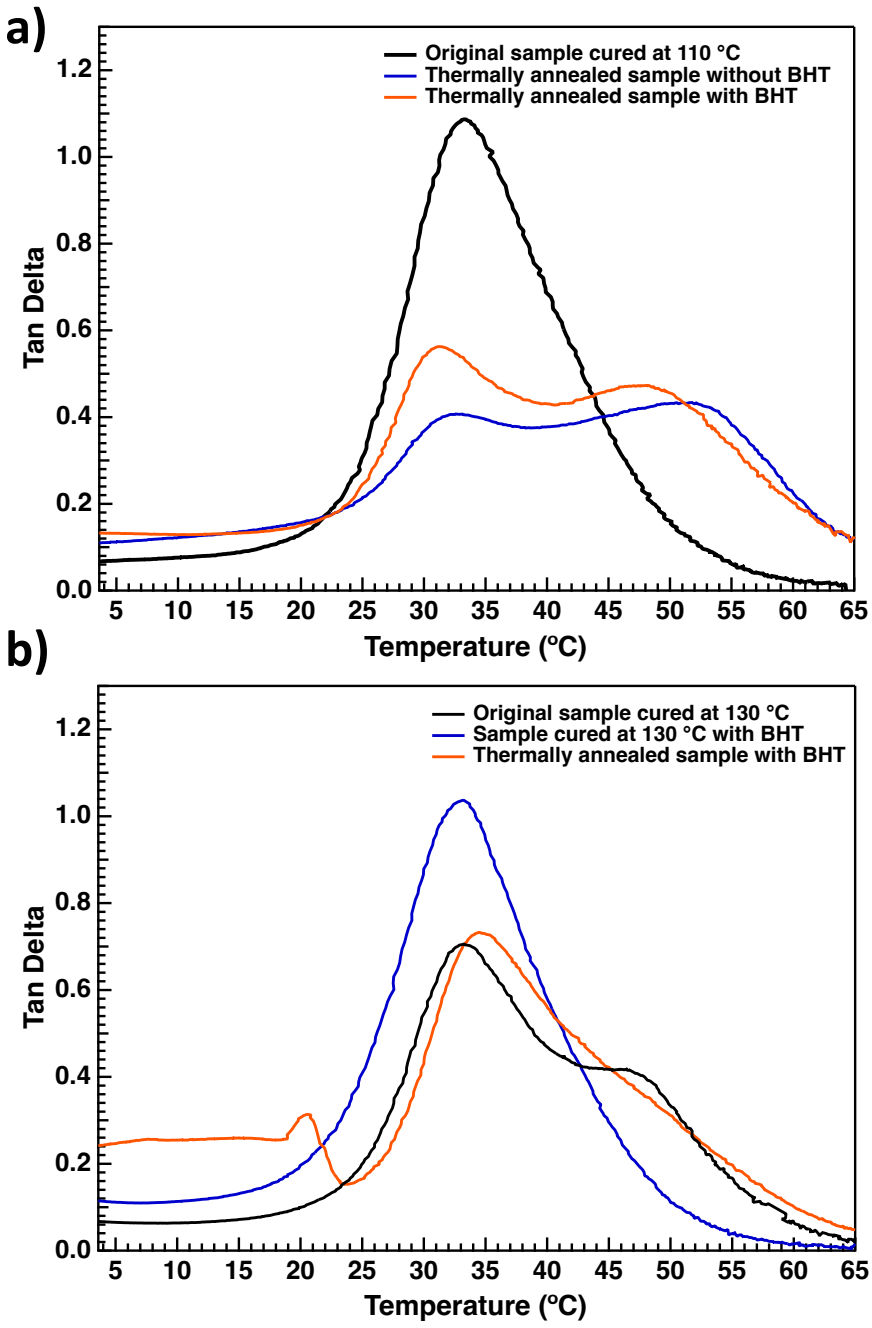


Figure S2.34. Tan delta curves of (a) original sample that was cured at 110 °C and thermal annealing of samples with and without BHT addition (5 mol%); (b) samples that were cured

at 130 °C with and without BHT and thermal annealing of the later sample. All samples were annealed at 150 °C for 2 hours.

Thermal degradation of cross-linked polymer capped with *N*-phenyl maleimide:

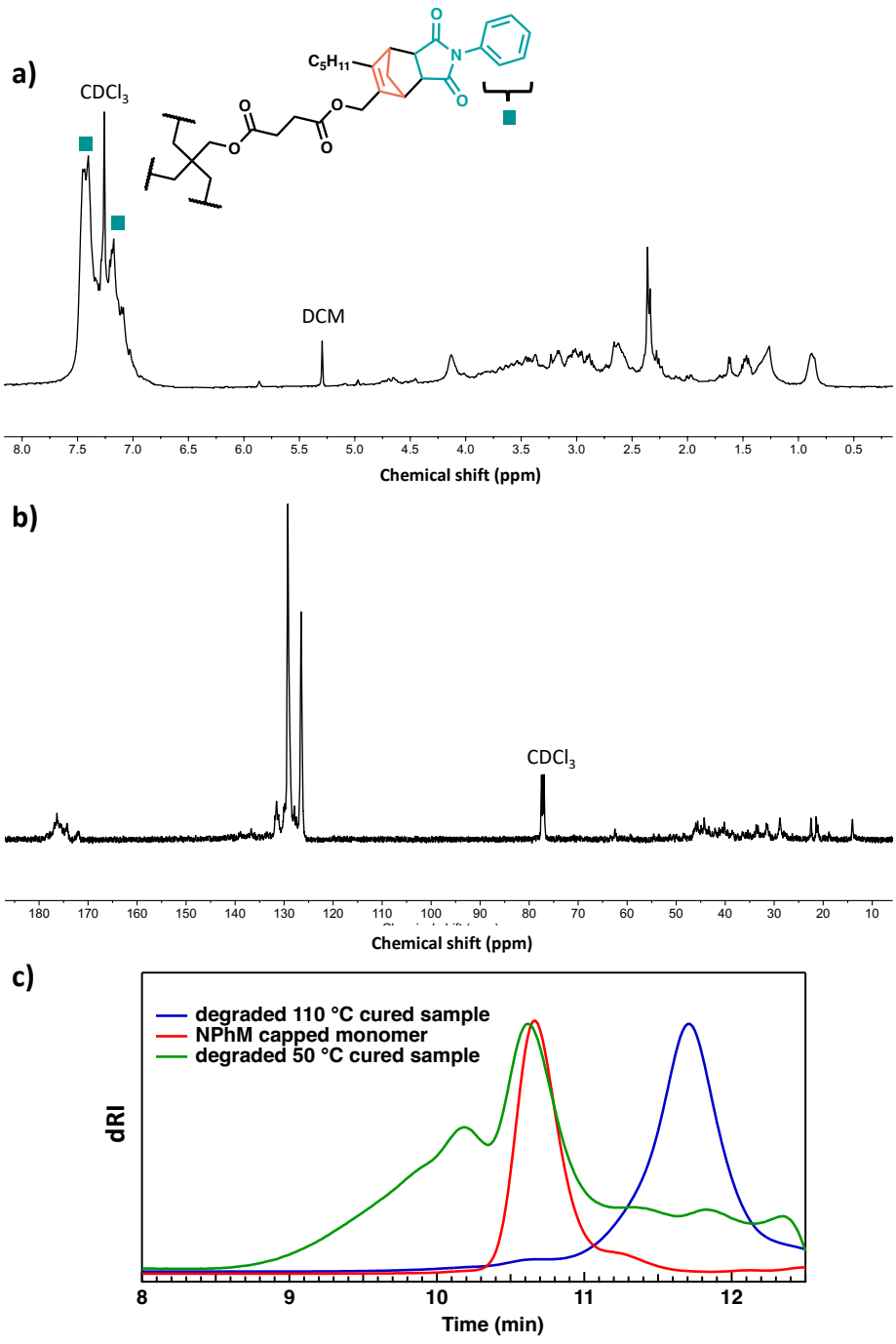

a)
CDCl3
C5H11
O
N
O
O
O
O
O
DCM
8.0 7.5 7.0 6.5 6.0 5.5 5.0 4.5 4.0 3.5 3.0 2.5 2.0 1.5 1.0 0.5
Chemical shift (ppm)
b)
CDCl3
180 170 160 150 140 130 120 110 100 90 80 70 60 50 40 30 20 10
Chemical shift (ppm)
c)
degraded 110 °C cured sample
NPhM capped monomer
degraded 50 °C cured sample
dRI
8 9 10 11 12
Time (min)

Figure S2.35. (a) ^{1}H NMR, (b) ^{13}C NMR of the degraded 110 °C polymer sample. (c) GPC traces of 50 °C and 110 °C polymer samples after degradation.

N15-labeled maleimide to confirm the capping of Cp chain-ends after selective degradation:

Procedure of using N15-labeled maleimide or ^{15}*N*-phenyl maleimide (^{15}*N*-PhM) to degrade the cross-linked polymer and analyzing the Cp-maleimide coupling via two-dimensional (2D) NMR spectroscopy: The selective degradation was repeated as described above but ^{15}*N*-PhM was used instead. The mixture was then analyzed via ^{1}H-^{15}N Heteronuclear Multiple Bond Correlation (HMBC) NMR spectroscopy to enhance the signals for N15-labeled material. The internal projection of the signals was shown on the left vertical axis (Figure S2.36) and was extracted for comparison with that of ^{15}*N*-PhM and the product of ^{15}*N*-PhM with 4-arm Cp monomer (Figure S2.37).

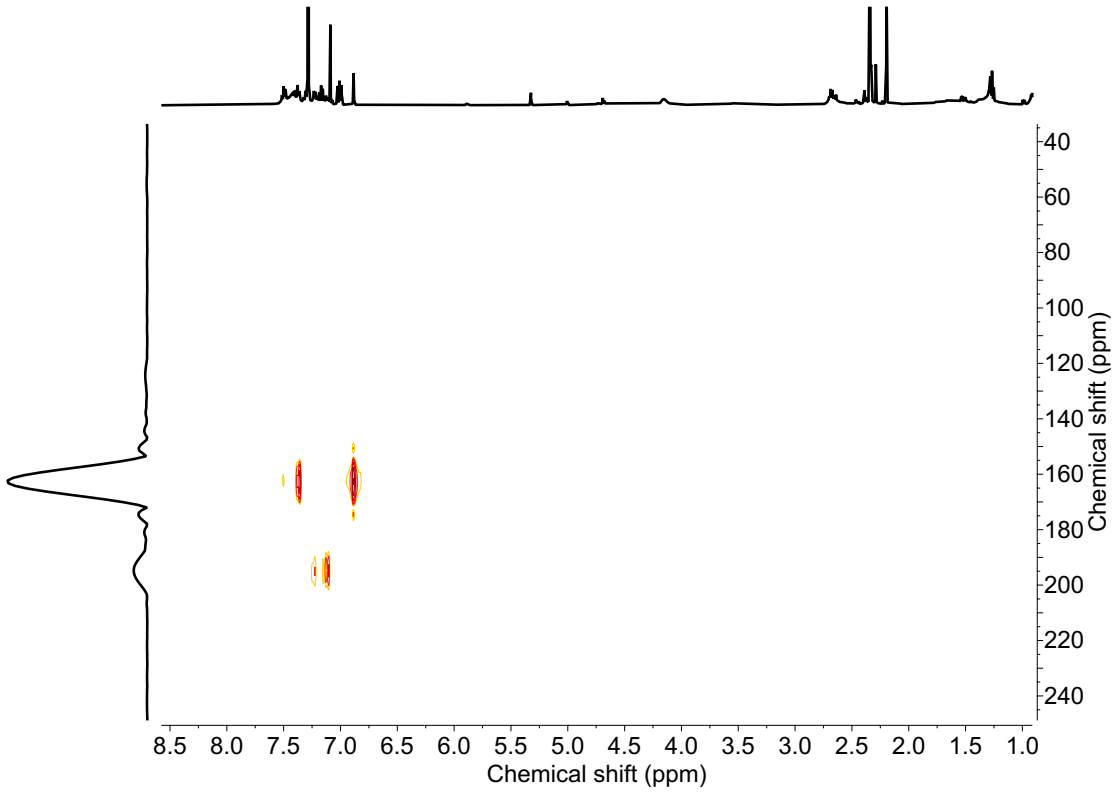


Figure S2.36. ^{1}H-^{15}N HMBC NMR spectrum of the degraded 110 °C polymer sample with ^{15}*N*-PhM. ^{1}H NMR spectrum was shown on top horizontal axis while the internal projection of the signals was shown on the left vertical axis.

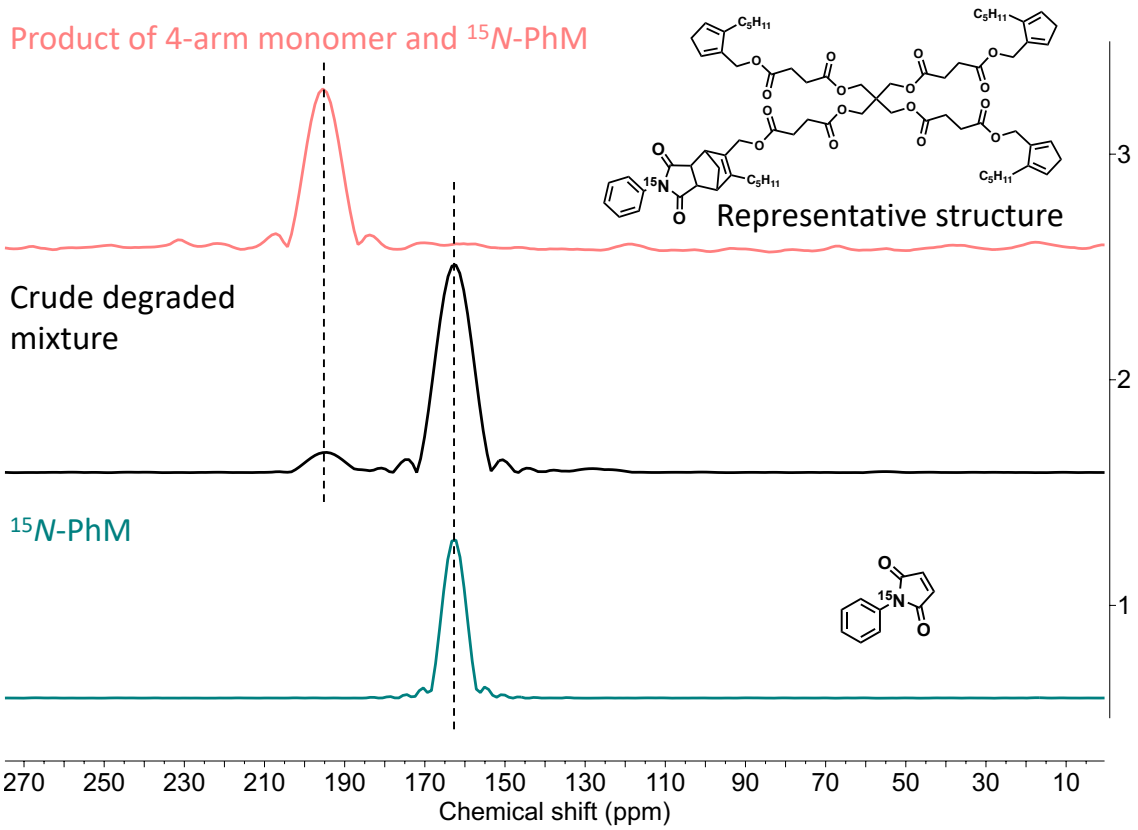


Figure S2.37. Comparison of the internal projection of signals from the crude mixture of the degraded cross-linked polymer, ^{15}N-PhM starting material, and the product of ^{15}N-PhM with 4-arm Cp monomer. The peak at 195 ppm of the crude degraded mixture confirms the presence of the Cp-maleimide chain-ends. Of note, there is still presence of excess ^{15}N-PhM in the crude degraded mixture.

Thermal degradation of the cross-linked polymer without any capping reagent:

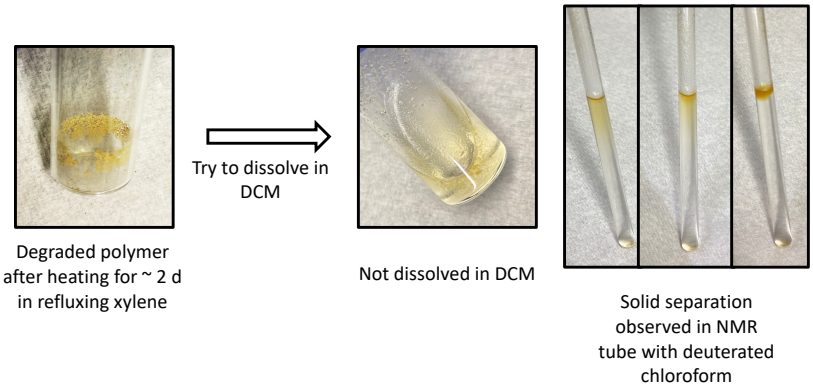


Figure S2.38. Yellow solid was obtained after heating the cross-linked polymer in refluxing xylene for ~2 d without any capping reagent. The solid was insoluble in DCM and thus, separated as floating solid on top of the deuterated chloroform solution in the NMR tube.

NMR spectra:

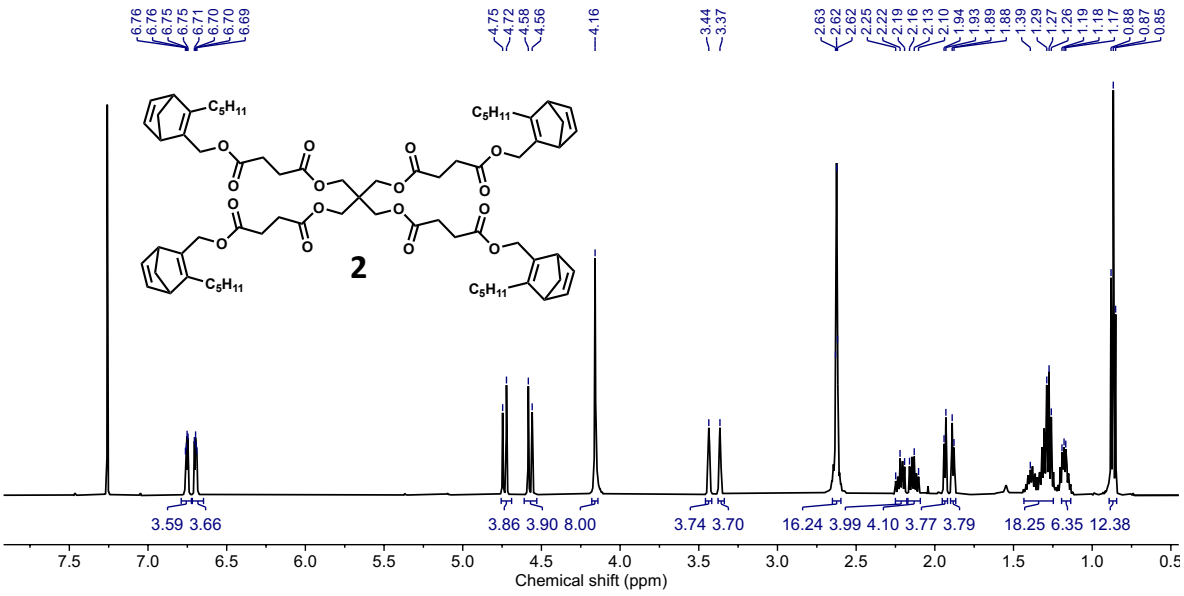


Figure S2.39. ^{1}H NMR spectrum of NBD-protected 4-arm monomer or compound **2**.

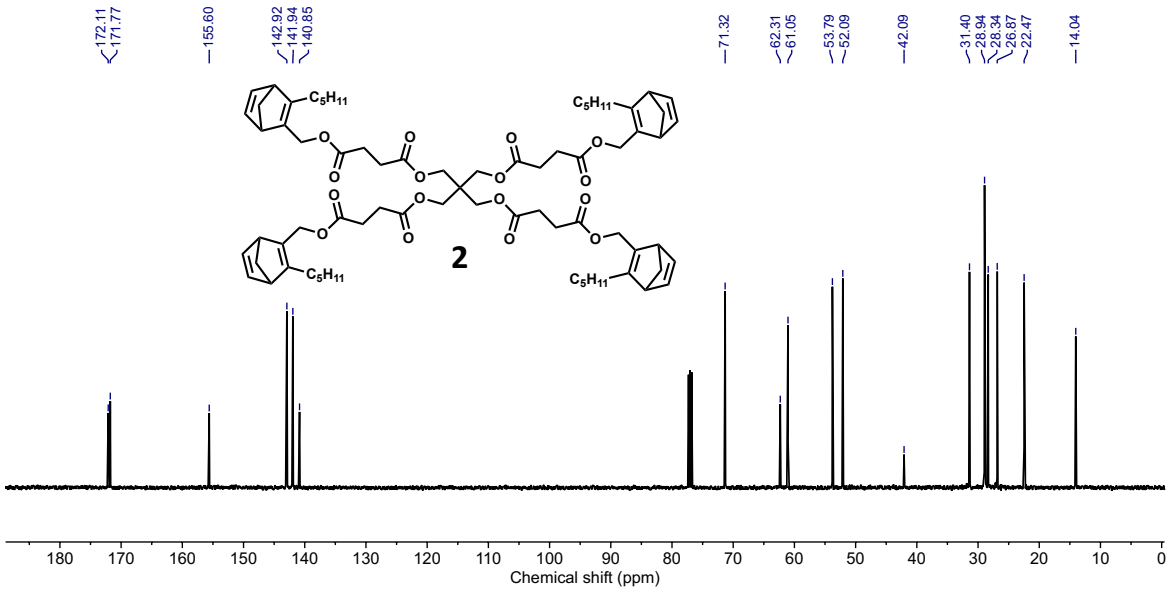


Figure S2.40. ^{13}C NMR spectrum of NBD-protected 4-arm monomer or compound **2**.

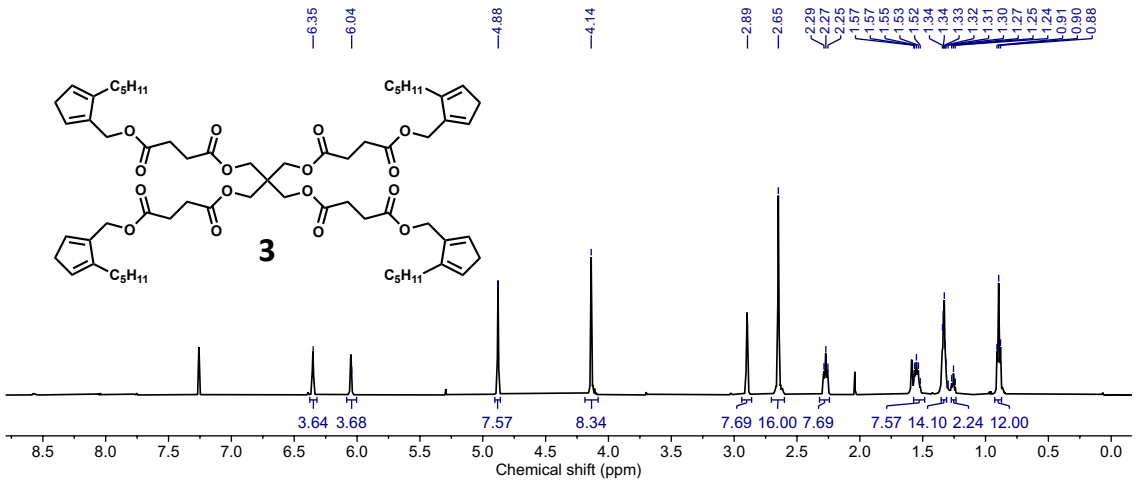


Figure S2.41. ^{1}H NMR spectrum of free Cp monomer or compound **3** in $CDCl_3$.

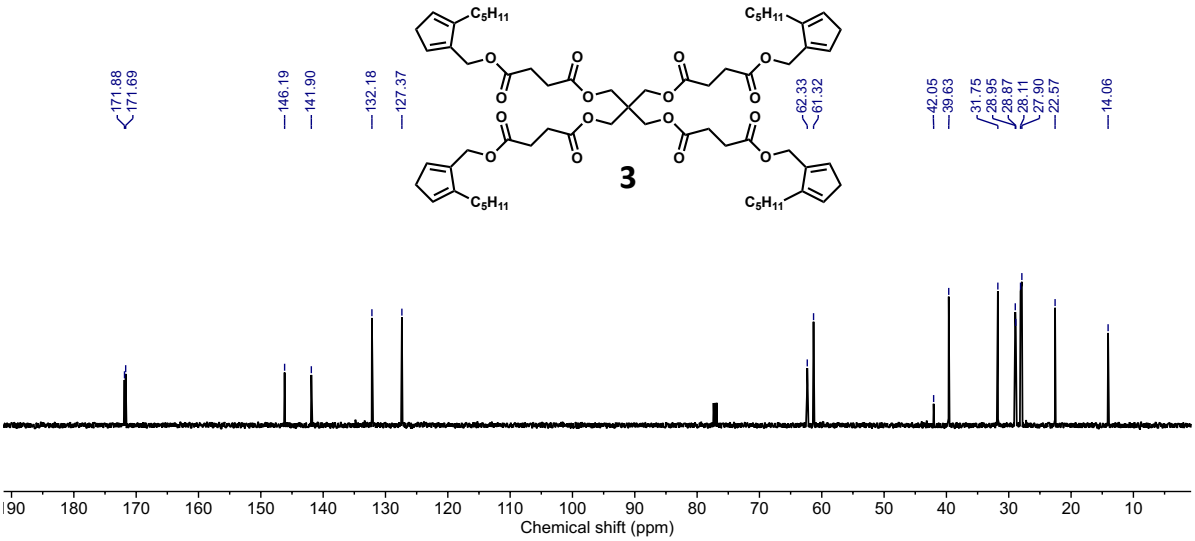


Figure S2.42. ^{13}C NMR spectrum of free Cp monomer or compound **3** in $CDCl_3$.

2.8 References

(1) Varnava, C. K.; Patrickios, C. S. Polymer Networks One Hundred Years after the Macromolecular Hypothesis: A Tutorial Review. *Polymer* **2021**, *215*, 123322. DOI: 10.1016/j.polymer.2020.123322.

(2) Parada, G. A.; Zhao, X. Ideal Reversible Polymer Networks. *Soft Matter* **2018**, *14*, 5186–5196. DOI: 10.1039/C8SM00646F.

(3) Sakai, T.; Akagi, Y.; Kondo, S.; Chung, U. Experimental Verification of Fracture Mechanism for Polymer Gels with Controlled Network Structure. *Soft Matter* **2014**, *10*, 6658–6665. DOI: 10.1039/C4SM00709C.

(4) Akagi, Y.; Katashima, T.; Katsumoto, Y.; Fujii, K.; Matsunaga, T.; Chung, U.; Shibayama, M.; Sakai, T. Examination of the Theories of Rubber Elasticity Using an Ideal Polymer Network. *Macromolecules* **2011**, *44*, 5817–5821. DOI: 10.1021/ma201088r.

(5) Marco-Dufort, B.; Iten, R.; Tibbitt, M. W. Linking Molecular Behavior to Macroscopic Properties in Ideal Dynamic Covalent Networks. *J. Am. Chem. Soc.* **2020,** *142*, 15371–15385. DOI: 10.1021/jacs.0c06192.

(6) Akagi, Y.; Gong, J. P.; Chung, U.; Sakai, T. Transition between Phantom and Affine Network Model Observed in Polymer Gels with Controlled Network Structure. *Macromolecules* **2013**, *46*, 1035–1040. DOI: 10.1021/ma302270a.

(7) Hild, G. Model Networks Based on `endlinking' Processes: Synthesis, Structure and Properties. *Prog. Polym. Sci.* **1998**, *23*, 1019–1149. DOI: 10.1016/S0079-6700(97)00055-5.

(8) Matsunaga, T.; Sakai, T.; Akagi, Y.; Chung, U.; Shibayama, M. Structure Characterization of Tetra-PEG Gel by Small-Angle Neutron Scattering. *Macromolecules* **2009**, *42*, 1344–1351. DOI: 10.1021/ma802280n.

(9) Zhong, M.; Wang, R.; Kawamoto, K.; Olsen, B. D.; Johnson, J. A. Quantifying the Impact of Molecular Defects on Polymer Network Elasticity. *Science* **2016**, *353*, 1264–1268. DOI: 10.1126/science.aag0184.

(10) Rikkou-Kalourkoti, M.; Patrickios, C. S.; Georgiou, T. K. Model Networks and Functional Conetworks. In *Polymer Science: A Comprehensive Reference*; Elsevier, **2012**; pp 293–308.

(11) Richbourg, N. R.; Wancura, M.; Gilchrist, A. E.; Toubbeh, S.; Harley, B. A. C.; Cosgriff-Hernandez, E.; Peppas, N. A. Precise Control of Synthetic Hydrogel Network Structure via Linear, Independent Synthesis-Swelling Relationships. *Sci. Adv.* **2021**, *7*, eabe3245. DOI: 10.1126/sciadv.abe3245.

(12) Chambon, F.; Winter, H. H. Linear Viscoelasticity at the Gel Point of a Cross-linking PDMS with Imbalanced Stoichiometry. *J. Rheol.* **1987**, *31*, 683–697. DOI: 10.1122/1.549955.

(13) Winter, H. H.; Morganelli, P.; Chambon, F. Stoichiometry Effects on Rheology of Model Polyurethanes at the Gel Point. *Macromolecules* **1988**, *21*, 532–535. DOI: 10.1021/ma00180a048.

(14) Winter, H. H.; Chambon, F. Analysis of Linear Viscoelasticity of a Cross-linking Polymer at the Gel Point. *J. Rheol.* **1986**, *30*, 367–382. DOI: 10.1122/1.549853.

(15) Chambon, F.; Petrovic, Z. S.; MacKnight, W. J.; Winter, H. H. Rheology of Model Polyurethanes at the Gel Point. *Macromolecules* **1986**, *19*, 2146–2149. DOI: 10.1021/ma00162a007.

(16) Diels, O.; Alder, K. Synthesen in der hydroaromatischen Reihe. *Justus Liebigs Ann. Chem.* **1928**, *460*, 98–122.

(17) Levandowski, B. J.; Raines, R. T. Click Chemistry with Cyclopentadiene. *Chem. Rev.* **2021**, *121*, 6777–6801. DOI: 10.1021/acs.chemrev.0c01055.

(18) Staudinger, H.; Bruson, H. A. Hochpolymere Verbindungen. 7. Mitteilung. Über das Dicyclopentadien und weitere polymere Cyclopentadiene. *Justus Liebigs Ann. Chem.* **1926**, *447*, 97–110.

(19) Wilson, P. J.; Wells, J. H. The Chemistry and Utilization of Cyclopentadiene. *Chem. Rev.* **1944**, *34*, 1–50.

(20) Veldman, B.; Kaully, T.; Feller, R. K.; Falcao, E.; Wudl, F. Staudinger's Poly(Cyclopentadiene): Sintering Processing of Poly(Diels−Alder Cyclopentadiene). *Macromolecules* **2009**, *42*, 6848–6850. DOI: 10.1021/ma901123p.

(21) Wudl, F. Crosslinking with Hermann Staudinger. In *Hierarchical Macromolecular Structures: 60 Years after the Staudinger Nobel Prize I*; Percec, V., Ed.; Advances in Polymer Science; Springer International Publishing: Cham, **2013**; Vol. 261, pp 211–216.

(22) Stille, J. K.; Plummer, L. Polymerization by the Diels-Alder Reaction *J. Org. Chem.* **1961**, *26*, 4026–4029. DOI: 10.1021/jo01068a092.

(23) Chen, X.; Dam, M. A.; Ono, K.; Mal, A.; Shen, H.; Nutt, S. R.; Sheran, K.; Wudl, F. A Thermally Re-Mendable Cross-Linked Polymeric Material. *Science* **2002**, *295*, 1698–1702. DOI: 10.1126/science.1065879.

(24) Murphy, E. B.; Bolanos, E.; Schaffner-Hamann, C.; Wudl, F.; Nutt, S. R.; Auad, M. L. Synthesis and Characterization of a Single-Component Thermally Remendable Polymer Network: Staudinger and Stille Revisited. *Macromolecules* **2008**, *41*, 5203–5209. DOI: 10.1021/ma800432g.

(25) Kennedy, J. P.; Castner, K. F. Thermally Reversible Polymer Systems by Cyclopentadienylation. II. The Synthesis of Cyclopentadiene-Containing Polymers. *J. Polym. Sci. Polym. Chem. Ed.* **1979**, *17*, 2055–2070. DOI: 10.1002/pol.1979.170170715.

(26) Oehlenschlaeger, K. K.; Mueller, J. O.; Brandt, J.; Hilf, S.; Lederer, A.; Wilhelm, M.; Graf, R.; Coote, M. L.; Schmidt, F. G.; Barner-Kowollik, C. Adaptable Hetero Diels-Alder Networks for Fast Self-Healing under Mild Conditions. *Adv. Mater.* **2014**, *26*, 3561–3566. DOI: 10.1002/adma.201306258.

(27) Ratwani, C. R.; Kamali, A. R.; Abdelkader, A. M. Self-Healing by Diels-Alder Cycloaddition in Advanced Functional Polymers: A Review. *Prog. Mater. Sci.* **2023**, *131*, 101001. DOI: 10.1016/j.pmatsci.2022.101001.

(28) Yoshie, N. Diels-Alder Polymers. In *Encyclopedia of Polymer Science and Technology*; John Wiley & Sons, Inc., Ed.; John Wiley & Sons, Inc.: Hoboken, NJ, USA, **2013**; p pst607.

(29) St. Amant, A. H.; Discekici, E. H.; Bailey, S. J.; Zayas, M. S.; Song, J.-A.; Shankel, S. L.; Nguyen, S. N.; Bates, M. W.; Anastasaki, A.; Hawker, C. J.; Read de Alaniz, J. Norbornadienes: Robust and Scalable Building Blocks for Cascade "Click" Coupling of High Molecular Weight Polymers. *J. Am. Chem. Soc.* **2019**, *141*, 13619–13624. DOI: 10.1021/jacs.9b06328.

(30) Bailey, S. J.; Discekici, E. H.; Barbon, S. M.; Nguyen, S. N.; Hawker, C. J.; Read de Alaniz, J. Norbornadiene Chain-End Functional Polymers as Stable, Readily Available Precursors to Cyclopentadiene Derivatives. *Macromolecules* **2020**, *53*, 4917–4924. DOI: 10.1021/acs.macromol.0c00967.

(31) Turnbull, A.; Hull, H. A Thermodynamic Study of the Dimerization of Cyclopentadiene. *Aust. J. Chem.* **1968**, *21*, 1789. DOI: 10.1071/CH9681789.

(32) McLean, S.; Webster, C. J.; Rutherford, R. J. D. Kinetic Isotope Effect for the Thermally-Induced Migration of Hydrogen in Cyclopentadienes. *Can. J. Chem.* **1969**, *47*, 1555–1559. DOI: 10.1139/v69-256.

(33) Spangler, C. W. Thermal [1,j] Sigmatropic Rearrangements. *Chem. Rev.* **1976**, *76*, 187–217. DOI: 10.1021/cr60300a002.

(34) Kahn, S. D.; Hehre, W. J.; Rondan, N. G.; Houk, K. N. Nature of the Migrating Group in 1,5-Sigmatropic Hydrogen Shifts. *J. Am. Chem. Soc.* **1985**, *107*, 8291–8292. DOI: 10.1021/ja00312a096.

(35) Yamabe, S.; Tsuchida, N.; Yamazaki, S. Revisiting Hydrogen [1,5] Shifts in Cyclopentadiene and Cycloheptatriene as Bimolecular Reactions. *J. Chem. Theory Comput.* **2005**, *1*, 944–952. DOI: 10.1021/ct0500646.

(36) Zhang, M.; Liang, G. Understanding the Sigmatropic Shifts of Cyclopenta-2,4-Dien-1-Yltrimethylsilane in Its Diels–Alder Addition. *Org. Biomol. Chem.* **2021**, *19*, 1732–1737. DOI: 10.1039/D0OB02386H.

(37) Froese, R. D. J.; Organ, M. G.; Goddard, J. D.; Stack, T. D. P.; Trost, B. M. Theoretical and Experimental Studies of the Diels-Alder Dimerizations of Substituted Cyclopentadienes. *J. Am. Chem. Soc.* **1995**, *117*, 10931–10938. DOI: 10.1021/acs.joc.5b00174.

(38) St. Amant, A. H.; Lemen, D.; Florinas, S.; Mao, S.; Fazenbaker, C.; Zhong, H.; Wu, H.; Gao, C.; Christie, R. J.; Read de Alaniz, J. Tuning the Diels–Alder Reaction for Bioconjugation to Maleimide Drug-Linkers. *Bioconjugate Chem.* **2018**, *29*, 2406–2414. DOI: 10.1021/acs.bioconjchem.8b00320.

(39) Gallinella, E.; Fortunato, B.; Mirone, P. Infrared and Raman Spectra and Vibrational Assignment of Cyclopentadiene. *J. Mol. Spectrosc.* **1967**, *24*, 345–362. DOI: 10.1016/0022-2852(67)90097-5.

(40) Cristea, M.; Ionita, D.; Iftime, M. M. Dynamic Mechanical Analysis Investigations of PLA-Based Renewable Materials: How Are They Useful? *Materials* **2020**, *13*, 5302. DOI: 10.3390/ma13225302.

(41) Rubinstein, M.; Colby, R. H.; others. *Polymer Physics*; Oxford university press New York, **2003**; Vol. 23.

(42) Ehrhardt, D.; Mangialetto, J.; Bertouille, J.; Van Durme, K.; Van Mele, B.; Van den Brande, N. Self-Healing in Mobility-Restricted Conditions Maintaining Mechanical Robustness: Furan–Maleimide Diels–Alder Cycloadditions in Polymer Networks for Ambient Applications. *Polymers* **2020**, *12*, 2543. DOI: 10.3390/polym12112543.

(43) Padmavathi, N. Ch.; Chatterji, P. R. Structural Characteristics and Swelling Behavior of Poly(Ethylene Glycol) Diacrylate Hydrogels. *Macromolecules* **1996**, *29*, 1976–1979. DOI: 10.1021/ma950827r.

(44) Charlesby, A. Elastic Modulus Formulae for a Crosslinked Network. *Int. J. Radiat. Appl. Instrum. Part C. Radiat. Phys. Chem.* **1992**, *40*, 117–120. DOI: 10.1016/1359-0197(92)90068-Q.

(45) Huang, N.-J.; Zang, J.; Zhang, G.-D.; Guan, L.-Z.; Li, S.-N.; Zhao, L.; Tang, L.-C. Efficient Interfacial Interaction for Improving Mechanical Properties of Polydimethylsiloxane Nanocomposites Filled with Low Content of Graphene Oxide Nanoribbons. *RSC Adv.* **2017**, *7*, 22045–22053. DOI: 10.1039/C7RA02439H.

(46) Zhang, W.; Deng, Z.; Yuan, H.; Luo, S.; Wen, H.; Liu, T. Preparation and Properties of Silicone Rubber Materials with Foam/Solid Alternating Multilayered Structures. *Polym. J.* **2021**, *53*, 619–631. DOI: 10.1038/s41428-020-00439-x.

(47) Schaefer, R. J. Mechanical Properties of Rubber. Harris' Shock and Vibration Handbook, Sixth edition, A. Piersol, T. Paez (Eds), McGraw-Hill Companies Inc **2010**, 33–1.

(48) Goodman, S. H. Handbook of Thermoset Plastics. Noyes Publications, Mill Rd. at Grand Ave, Park Ridge, New Jersey 07656, USA, 1986. 421 **1986**.

(49) Zhao, Q.; Qi, H. J.; Xie, T. Recent Progress in Shape Memory Polymer: New Behavior, Enabling Materials, and Mechanistic Understanding. *Prog. Polym. Sci.* **2015**, *49–50*, 79–120. DOI: 10.1016/j.progpolymsci.2015.04.001.

(50) Li, G.; Wang, A. Cold, Warm, and Hot Programming of Shape Memory Polymers. *J. Polym. Sci. Part B: Polym. Phys.* **2016**, *54*, 1319–1339. DOI: 10.1002/polb.24041.

(51) Miura, M.; Akutsu, F.; Hirose, S.; Ikeno, Y.; Nagakubo, K. Thermally Dissociative Degradation of Polymers Containing Dicyclopentadiene Ring in Main Chains. *BCSJ* **1977**, *50*, 2682–2685. DOI: 10.1246/bcsj.50.2682.

(52) Liu, Y.; He, M.; Yan, W.; Zhang, D.; Zhao, Q.; Qin, S.; Yu, J. P. (N-phenylmaleimide-alt-styrene) as a Heat-resistant Agent in the Application of Nylon 6. *J. Appl. Polym. Sci.* 2019, *136*, 47689. DOI: 10.1002/app.47689.

(53) Gaussian 16, Revision C.01, Frisch, M. J.; Trucks, G. W.; Schlegel, H. B.; Scuseria, G. E.; Robb, M. A.; Cheeseman, J. R.; Scalmani, G.; Barone, V.; Petersson, G. A.; Nakatsuji, H.; Li, X.; Caricato, M.; Marenich, A. V.; Bloino, J.; Janesko, B. G.; Gomperts, R.; Mennucci, B.; Hratchian, H. P.; Ortiz, J. V.; Izmaylov, A. F.; Sonnenberg, J. L.; Williams-Young, D.; Ding, F.; Lipparini, F.; Egidi, F.; Goings, J.; Peng, B.; Petrone, A.; Henderson, T.; Ranasinghe, D.; Zakrzewski, V. G.; Gao, J.; Rega, N.; Zheng, G.; Liang, W.; Hada, M.; Ehara, M.; Toyota, K.; Fukuda, R.; Hasegawa, J.; Ishida, M.; Nakajima, T.; Honda, Y.; Kitao, O.; Nakai, H.; Vreven, T.; Throssell, K.; Montgomery, J. A., Jr.; Peralta, J. E.; Ogliaro, F.; Bearpark, M. J.; Heyd, J. J.; Brothers, E. N.; Kudin, K. N.; Staroverov, V. N.; Keith, T. A.; Kobayashi, R.; Normand, J.; Raghavachari, K.; Rendell, A. P.; Burant, J. C.; Iyengar, S. S.;

Tomasi, J.; Cossi, M.; Millam, J. M.; Klene, M.; Adamo, C.; Cammi, R.; Ochterski, J. W.; Martin, R. L.; Morokuma, K.; Farkas, O.; Foresman, J. B.; Fox, D. J. Gaussian, Inc., Wallingford CT, 2016.

(54) Dalkılıç, E.; Daştan, A. Synthesis of Cyclopentadiene Derivatives by Retro-Diels–Alder Reaction of Norbornadiene Derivatives. *Tetrahedron* 2015, *71*, 1966–1970. DOI: 10.1016/j.tet.2015.02.023.

(55) Borchardt, H. J.; Daniels, F. The Application of Differential Thermal Analysis to the Study of Reaction Kinetics. *J. Am. Chem. Soc.* 1957, *79*, 41–46. DOI: 10.1021/ja01558a009.

(56) Ozawa, T. Kinetic Analysis of Derivative Curves in Thermal Analysis. *J. Therm. Anal.* 1970, *2*, 301–324. DOI: 10.1007/BF01911411.

(57) Horie, K.; Hiura, H.; Sawada, M.; Mita, I.; Kambe, H. Calorimetric Investigation of Polymerization Reactions. III. Curing Reaction of Epoxides with Amines. *J. Polym. Sci. A-1 Polym. Chem.* 1970, *8*, 1357–1372. DOI: 10.1002/pol.1970.150080605.

(58) Hu, J.; Shan, J.; Zhao, J.; Tong, Z. Isothermal Curing Kinetics of a Flame Retardant Epoxy Resin Containing DOPO Investigated by DSC and Rheology. *Thermochim. Acta* 2016, *632*, 56–63. DOI: 10.1016/j.tca.2016.02.010.

(59) Alizadeh, N.; Thorne, D. P.; Auad, M. L.; Celestine, A. N. Mechanical Performance of Vinyl Ester—Polyurethane Interpenetrating Polymer Network Composites. *J. Appl. Polym. Sci.* 2021, *138*, 50411. DOI: 10.1002/app.50411.

(60) Macosko, C. W. Rheology Principles. *Measurements and Applications* 1994.

(61) Abd-El Salam, F.; Abd-El Salam, M. H.; Mostafa, M. T.; Nagy, M. R.; Mohamed, M. I. Effect of the Vulcanizing System on the Mechanical Properties of Butyl Rubber/Ethylene Propylene Diene Monomer-Carbon Black Blends. *J. Appl. Polym. Sci.* 2003, *90*, 1539–1544. DOI: 10.1002/app.12739.

(62) Barszczewska-Rybarek, I. M.; Korytkowska-Wałach, A.; Kurcok, M.; Chladek, G.; Kasperski, J. DMA Analysis of the Structure of Crosslinked Poly (Methyl Methacrylate)s. *Acta bioeng. biomech.* 2017, *19*.

3. Chapter 3: *Synthesis and Thermal Recycling of Cyclopentadiene Thermoplastics*

3.1 Overview

The efficient isolation of a pure Cp derivative, as described in Chapter 1, has become a powerful tool to study new Cp materials and polymerization strategies. There is one area that has not been fully resolved in the previous work that was described in Chapter 1, the uncontrolled cross-linking, either via the trimerization of the Cp units or other radical processes. In this project, the attention will be focused on achieving linear homopolymerization of telechelic Cp monomers. To understand and subsequently prevent the cross-linking process, different Cp analogs with varied substituents (i.e., different electronic and steric effects) were synthesized. The polymerization behaviors of these derivatives were analyzed, which showed that the cross-linking occurred via a radical process. The addition of a radical inhibitor, butylated hydroxytoluene, during the polymerization completely suppressed the cross-linking. The optimal polymerization condition of the pentyl-substituted Cp derivative displays the highest molecular weight and degree of polymerization. The application of this Cp moiety to the general homopolymerization and chemical recycling of common thermoplastics was also developed. Different Cp thermoplastics were fabricated with the backbones derived from common thermoplastics, allowing for the subsequent investigation in the chemical recycling using Cp chemistry. Sections of this chapter were

submitted, currently are under review, and will potentially be published as Tran, T. M.; Read de Alaniz, J. *Synthesis and Thermal Recycling of Cyclopentadiene Thermoplastics*.

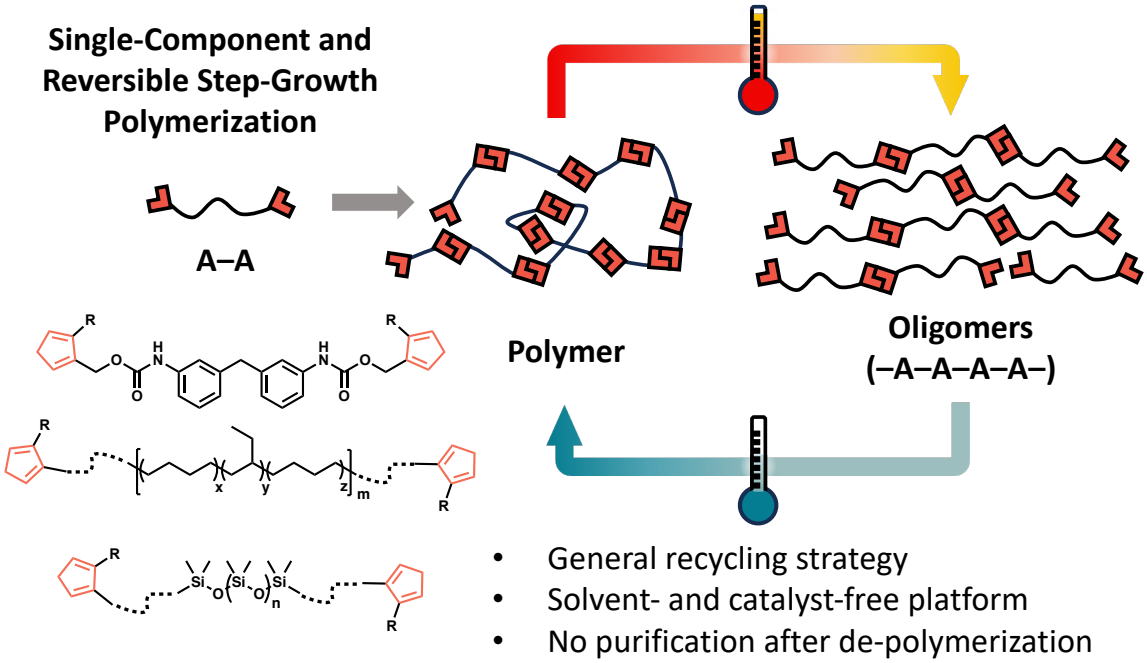


Figure 3.1. Overview of reversible step-growth homopolymerization using a single component, a class of cyclopentadiene monomers. Thermally recyclable thermoplastics can be fabricated through this novel strategy. No solvents, catalysts, or additional purification are required throughout the de- and re-polymerization processes.

3.2 Abstract

Catalyst-free and reversible step-growth Diels–Alder (DA) polymerization has found a wide range of applications in polymer synthesis and especially, is a promising method to fabricate recyclable thermoplastics. The effectiveness of polymerization and de-polymerization relies on the chemical building blocks, often utilizing furan as the diene and maleimide as the dienophile. Compared to the traditional diene–dienophile or two-component

approaches that requires perfect stoichiometry, cyclopentadiene (Cp) can serve a dual role via self-dimerization. This internally balanced platform offers a route to access high-molecular-weight polymers and a dynamic handle for polymer recycling, which remains unexplored. Herein, through the reactivity investigation of different telechelic Cp derivatives, the uncontrolled cross-linking of Cp was addressed, revealing the first successful DA homopolymerization. To demonstrate the generality of our methodology, we synthesized and characterized six Cp homopolymers with backbones derived from common thermoplastics, such as polydimethylsiloxane, hydrogenated polybutadiene, and ethylene phthalate. Among these materials, the hydrogenated polybutadiene-Cp analog can be thermally de-polymerized (M_n = 68 to 23 kDa) and re-polymerized to the parent polymer (M_n = 68 kDa) under solvent- and catalyst-free conditions. This process was repeated over three cycles without intermediate purification, confirming the efficient chemical recyclability. The varied degradable properties of other four Cp-incorporated thermoplastics were also examined. Overall, this work provides a general methodology to access a new class of reversible homopolymers, potentially expanding the designs and construction of sustainable thermoplastics.

3.3 Introduction

The recognition that macromolecules are formed through the covalent bonding of smaller molecules by Staudinger has led to the discovery of polymers and sparked the industrial fabrication of plastics with applications ranging from packaging and adhesives to modern high-performance materials.[1,2] Among these materials, linear polymers or thermoplastics have

become widely produced and consumed due to their synthetic accessibility and mechanical reprocessability.[2] Despite a vast array of research efforts, it remains a grand challenge to efficiently recycle these materials and thus, reduce the environmental adverse impact of plastics.[2–5] One of the most promising strategies to improve polymer sustainability is closed-loop (plastic-to-plastic) chemical recycling.[6,7] The high-molecular-weight (high-MW) polymers are converted into smaller fragments or intermediates, which are ideally subjected to re-polymerization to form the parent polymer or similarly functional materials. This method is promising to preserve the macromolecular properties and maximize monomer resources.

The current state-of-the-art closed-loop chemical recycling relies on the incorporation of labile bonds into the polymer backbone during the polymer fabrication. This can be accomplished with traditional step-growth polycondensation materials (i.e., polyesters, and polyamides) with the high content of ester or amide groups that are predisposed to well-known chain-breaking conditions.[8] For example, hydrolysis and glycolysis (through transesterification) of polyethylene terephthalate (PET) have been applied in closed-loop recycling.[8–10] The field has also expanded to engineer C–C polymer backbones (e.g., polyolefins, polystyrene, etc.) with hetero-atom-containing units. Under acidic, basic, or metal-catalyzed conditions, the labile bonds are selectively broken, converting the otherwise challenging-to-deconstruct polymers into reusable oligomers or small-molecule starting materials.[11–15] A variety of chemical strategies have been introduced and optimized to recycle

these robust polymers, such as the conventional step-growth esterification,[11,12] or the favorable chain-growth ring-opening.[13–15]

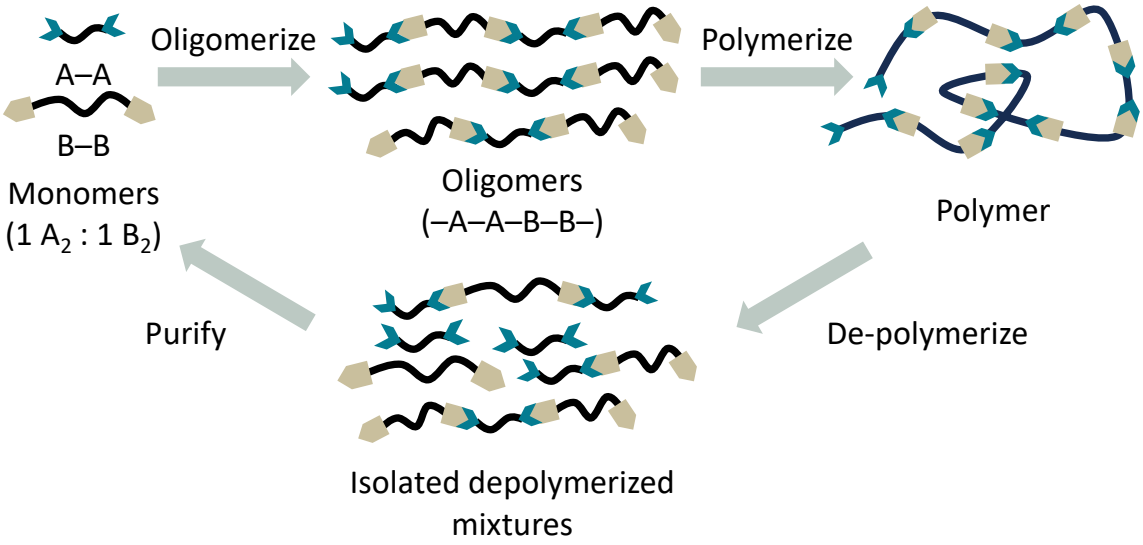


Figure 3.2. General steps that are normally required in a two-component system to chemically recycle step-growth polymers (i.e., A_2 + B_2 monomers); the depolymerization includes the additional purification to achieve high chain-end fidelity of the oligomers/monomers mixture for re-polymerization.

Among the promising closed-loop methodologies, reversible step-growth polymerization (**Figure 3.2**) holds the potential to extend the synthetic accessibility, de-polymerization compatibility and thus, optimizing the recycling process. Monomers with discreet chain-ends (i.e., A–A, or B–B) display advantages in terms of finite distances between the degradable units and synthetic accessibility of the functional chain-end building blocks. Moreover, the incorporation of these well-defined chain-ends into "traditional" polymer backbones (e.g., ester, amide, aliphatic, phenyl, carbonate, siloxane, urethane, etc.) provides a straightforward

method to enable thermoplastic recycling of commonly used plastics.[16–18] However, apart from the well-established esterification between carboxylic acids and amines or alcohols, the scope of reversible step-growth methodology remains underexamined.[18] The prime examples include the ionene formation via a Menshutkin reaction,[19] the nucleophilic ring opening reaction (e.g., 2-oxazolin-5-ones and phenol substrates),[20,21] and the Diels–Alder (DA) [4+2] cycloaddition between furans and maleimides[22–26] (**Figure 3.3a**).

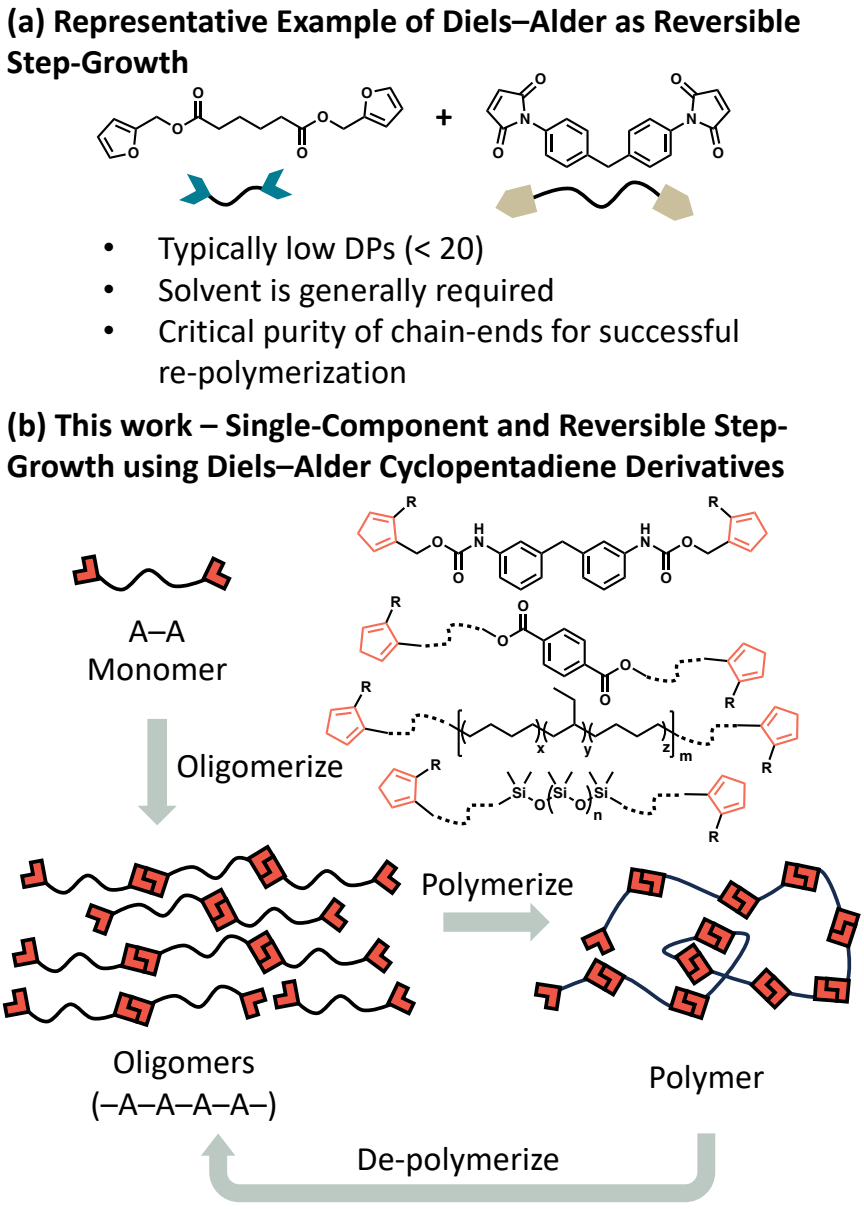


Figure 3.3. (a) The first application of Diels–Alder reaction as reversible step-growth linear polymerization using furan and maleimide materials from Kuramoto and coworkers.[36] There remain limitations of furan-maleimide chemistry, involving low degrees of polymerization,

poor solubility, and the challenging isolation of pure chain-end monomers/oligomers (b) This work – Cp derivatives for applications in reversible and single-component step-growth polymerization. The internally balanced system is absent of solvents, catalysts, chemical reagents and thus, no isolation is required. The platform also accommodates a variety of common polymer backbones, such as ethylene terephthalate ester, urethane, polydimethylsiloxane (PDMS), and hydrogenated polybutadiene.

To achieve high-MW polymers, step-growth reactions necessitate monomer purity, quantitative reactivity, and accurate stoichiometry between the A_2 and B_2 monomers.[27] These factors are normally difficult to achieve and become particularly challenging when coupled with the design of recyclable polymers. Specifically, it requires a chemical building block that allows efficient forward polymerization yet permits the reverse reaction when triggered. Furthermore, the strict stoichiometry demands the precise preservation of the de-polymerized chain-ends to successfully reform the parent polymers. Many current methods also rely on chemical reagents (i.e., acids, bases, and catalysts) for de-polymerization and thus, an additional purification step is generally required to access pure A_2 and B_2 monomers to enable closed-loop recycling (**Figure 3.2** and **3.3a**). This adds increased difficulty and cost to re-polymerization strategies and can limit the number of times that the plastics can be recycled. We hypothesize that Diels–Alder step-growth reactions[26,28] with the prospects of high reactivity and non-chemical stimulus (i.e., heat) for de-polymerization potentially overcomes the challenges associated with additional purification and could increase the number of re-polymerization cycles and generality of closed-loop recycling.

The interest in the formation of linear Diels–Alder polymers was initiated by Stille in 1961 via an A_2B_2-type process using cyclopentadiene (Cp) units as the diene and *p*-benzoquinone

or *N,N′*-hexmethylenebismaleimide as the dienophile.[29] More than two decades later, Kennedy and Carlson reported a tenfold chain extension of their functionalized polyisobutylene with terminal silylcyclopentadiene and a bis-maleimide derivative.[30] Despite the successful demonstration of these A_2B_2-type syntheses, there was no follow-up study on this subject, presumably due to the synthetic challenges associated with preparing bis-cyclopentadiene monomers.[28,31–34] The focus, instead, has been shifted to furan and maleimide materials after Tesoro and Sastri prepared a bis-furan-functionalized siloxane and initiated polyaddition using a bis-maleimide.[35] Functionalization of a polymer by furan and maleimide units to obtain the corresponding A_2 and B_2 macromonomers is straightforward and synthetically accessible to a range of polymer backbones.[22–26,36,37] Unfortunately, the materials generally suffer from poor solubility, slow chain-growth reactivity, and low molecular weights (MWs). Therefore, even though the thermal reversibility of linear furan-maleimide polymers was recognized early by Kuramoto and the coworkers in 1994,[38] there still lacks reports about the closed-loop chemical recycling of DA thermoplastics (**Figure 3.3a**). We hypothesize that overcoming the three main limitations of the current DA tools will provide a pathway to realize the potential of reversible DA step-growth polymerization. First, it is demanding to achieve perfect stoichiometry during both polymerization and recycling process in two-component systems (i.e., A_2B_2 type). Second, the low retro-DA (rDA) temperature (e.g., 110 °C for furan-maleimide adduct) restrains its broad application. Finally, identifying

a solvent compatible with both A_2 and B_2 monomers can become problematic, especially during polymer fabrication with a wide range of backbone architectures.

Herein, we propose a unique strategy, utilizing highly reactive cyclopentadiene monomers as single-component and reversible DA monomer units ($A_2 + A_2$, **Figure 3.3b**). Cp monomers can react with each other due to its high reactivity and dual performance as both diene and dienophile, thereby eliminating the stoichiometry requisite from the two-component or A_2B_2 type process.[39] Moreover, Cp dimer with a high rDA temperature (i.e., 150–180 °C) potentially broaden the utility of these materials and the accessible MW range. While promising, the synthesis of thermoplastics by Cp homopolymerization has yet to be achieved, primarily because of the absence of accessible synthetic pathways for obtaining pure cyclopentadiene monomers and the challenge of uncontrolled cross-linking with current methods. As a result, the homopolymerization of Cp has been restricted to cross-linked polymers.[29,31,33,39] Our group previously developed an approach to isolate a pure tetrafunctional cyclopentadiene derivative under mild conditions, allowing us to further understand the polymerizing behavior of Cp in the context of a degradable homopolymer network.[39] In this study, by investigating different reactivity of bifunctional or telechelic Cp analogs, we have discovered a strategy to enable Cp homopolymerization that leads to high-MW DA linear polymers.

To demonstrate the applicability of our DA recycling platform, we synthesized and characterized a variety of different soluble Cp materials that are integrated with common

thermoplastics backbones, such as ethylene terephthalate, urethane, polydimethylsiloxane, and hydrogenated polybutadiene (**Figure 3.3b**). As planned, the construction and deconstruction of the polymers do not require the presence of catalysts, chemical reagents, and/or solvents. Moreover, as an internally balanced system, no isolation is required to "close the loop." Multiple re-polymerization cycles are also demonstrated for the hydrogenated polybutadiene-Cp analog. The high-MW polymer can be depolymerized to low-MW oligomers and subsequently re-polymerized to the parent material over the three cycles. This demonstration supports the efficiency of our recycling strategy. Overall, the methodology involves a general platform for the construction and recycling of DA thermoplastics, potentially expanding access to advanced sustainable polymers.

3.4 Results and Discussion

Synthesis of Cp Derivatives and the Investigation of Subsequent Homopolymerization Efficiency. As shown in our previous report, the sufficient isolation of a pentyl-substituted cyclopentadiene derivative led to the construction of a better-defined network that exhibits tough and elastic properties, opposite to those of prior polymer networks.[39] To investigate the possible trimer formation, we briefly described the polymerization of a two-arm model Cp monomer. A soluble polymer was formed with the addition of a radical inhibitor, indicating no cross-linking during the step-growth process,[39] and providing a promising pathway to access high-MW DA linear polymers. Based on the preliminary results, we further investigate the reactivity of multiple bulky Cp analogs to

further suppress uncontrolled cross-linking (e.g., trimerization, radical process, etc.), while sustaining the efficient dimerization. The electronic effect of substituents was also explored (i.e., *distal* and *proximal* analogs, based on the relative distance of the carbonyl group to the Cp core). We hypothesized that the realization of these goals will allow us to optimize the synthesis of fully soluble high-MW Cp homopolymers that are potential for efficient chemical recycling (**Figure 3.4**).

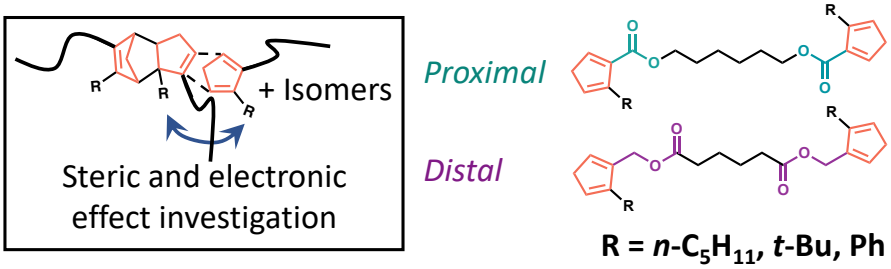
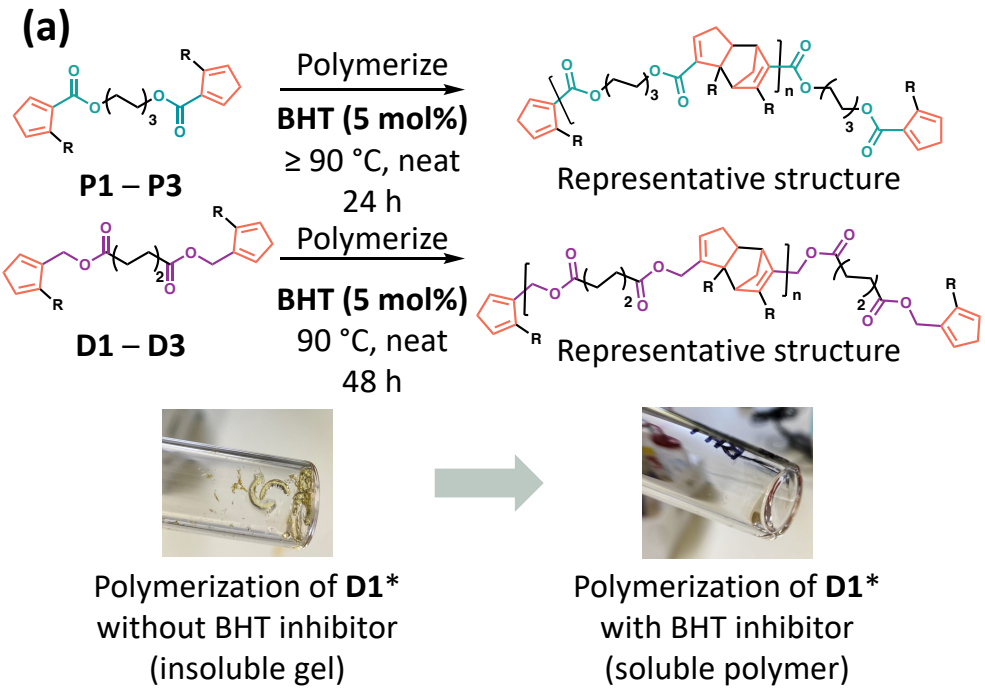


Figure 3.4. Investigation of different Cp analogs, *distal* versus *proximal* (based on the distance of Cp moiety to the carbonyl functional group), with different substituents (i.e., *n*-pentyl, *t*-butyl, and phenyl) will lead to the optimized synthesis of high-MW Cp linear polymer. The uncontrolled cross-linking process was addressed in this work.

We utilized the optimized tetrazine-norbornadiene deprotection to prepare and isolate the *proximal* and *distal* Cp analogs.[39–41] From a diverse source of alkyne starting materials (Supporting Information in Section 3.7), six norbornadiene (NBD) precursors were prepared, each with a different substituent attached to the Cp unit to also evaluate the effects of sterics (e.g., *n*-pentyl, *t*-butyl, or phenyl). The ester NBDs **5**–**7** were prepared on a scale of 5–10 g using alkyne starting materials and dicyclopentadiene (**4**). Analogs **5**–**7** were then reduced to either alcohol (**8**–**10**) or converted to the corresponding carboxylic analogs (**14**–**16**) according

to Scheme S1 in Supporting Information. EDC coupling reaction of alcohols **8**–**10** with adipic acid affords the target *distal* NBD precursors (**11**–**13**), while the synthesis of *proximal* substrates requires an alternative approach. Both Fischer and Steglich esterification of **14**–**16** with the alcohols primarily produced the Alder-ene rearranged by-products (Supporting Figure S3.1, Section 3.7). The same problem occurred with other transesterification methods. Even though Yamaguchi reagents assisted in the formation of the desired product, the conversion was low, and the purification was challenging. Despite these challenges, we discovered that the desired adducts **17**–**19** could be prepared using a solvent-free nucleophilic substitution (S_N2) reaction. Treatment of 1,6-dibromohexane and the corresponding carboxylic acid with triethylamine (TEA) at 90 °C resulted in complete conversion of the desired NBD adducts **17**–**19** (60–70% isolated yield) with minimal amount of the rearranged by-product.[42] Of note, NBD precursors with bulky substituents, **18** and **19** (*t*-butyl and phenyl, respectively) do not undergo rearrangement due to the lack of a hydrogen atom that can participate in the Alder-ene reaction. The synthesized NBD substrates (**11**–**13** and **17**–**19**) were then deprotected with 3,6-di-2-pyridyl-1,2,4,5-tetrazine (DpTz) to afford the respective Cp monomers (**D1**–**D3**, **P1**–**P3**) (Supporting Information in Section 3.7). As expected, based on our previous work, the *distal* substrates **D1**–**D3** were efficiently isolated and only one major isomer was observed by ^{1}H NMR spectroscopy upon isolation. In contrast, accessing pure *proximal* Cp monomers **P1**–**P3** proved more challenging due to the slow tetrazine

deprotection and formation of 1,5-H shift isomeric mixtures. Therefore, *proximal* Cp mixtures were subjected to polymerization without additional purification.



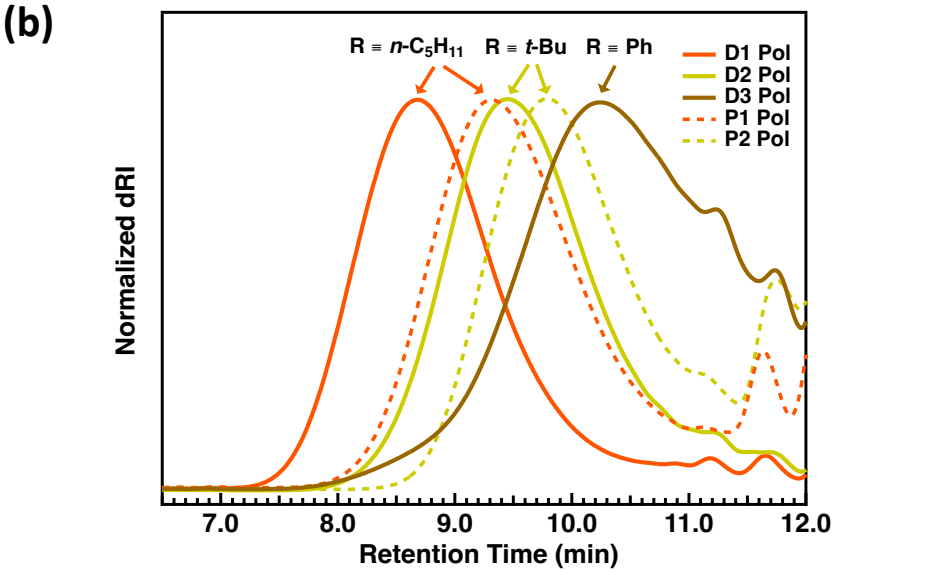
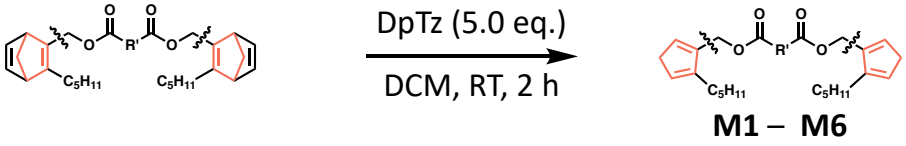


Figure 3.5. (a) The presence of a radical inhibitor, BHT, completely shut down the cross-linking as shown in the bottom pictures. A soluble polymer of **D1** in dichloromethane was observed with the addition of BHT during the polymerization process. *Polymerization conditions: Heating **D1** at 90 °C, neat for 24 h. Thus, the screening polymerization of the *proximal* (**P1**–**P3**) and *distal* (**D1**–**D3**) analogs was performed with the addition of 5 mol% BHT. (b) The polymerization efficiency of each analog was compared. The *n*-pentyl substituted Cp derivative or D1 produces the most promising MW range as observed from the SEC traces of **D1**, **D2**, **D3**, **P1** and **P2** polymers with varied substituents (R = *n*-C_5H_{11}, *t*-Bu, and Ph). The optimized polymerization condition is 90 °C for 48 h (**D1**, **D2**, and **D3**), 125 °C for 22 h (**P1**), and 90 °C for 24 h (**P2**).

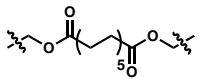
The homopolymerization of each telechelic Cp derivative was performed in different conditions to identify the optimal reaction conditions (Supporting Information in Section 3.7). Initial screening showed gelation of *distal* analogs **D1**–**D3** immediately after heating at high temperatures, while *proximal* substrates **P1**–**P3** remained soluble (Supporting Table S3.1). Contradictory to our hypothesis, the bulkier substituents (*t*-butyl, or phenyl) did not prevent the cross-linking from occurring within the *distal* substrates explored. As for the *proximal* derivatives, despite being soluble, the chain-ends of the formed polymers were not detected by ^{1}H NMR spectroscopy, even with a short polymerization period. Only mixtures of low MW (< 8 kDa) oligomers were obtained, as characterized by the size exclusion chromatography (SEC) with a polystyrene standard in chloroform solvent (Supporting Table S3.1). While performing the screening polymerization, we noticed a residual amount of butylated hydroxytoluene (BHT) from dichloromethane (DCM) solvent that was detected on the ^{1}H NMR spectrum of the **P1** product. Intriguingly, in the presence of BHT, there was a difference in the polymerization behavior of **P1** (Supporting Figure S3.58). In the presence of BHT, the end-groups were observed by the ^{1}H NMR spectroscopy and higher MW was

attained. Guided by this observation, we re-investigated the homopolymerization of both the *distal* and *proximal* substrates in the presence of 5 mol% of BHT (**Figure 3.4a**). Interestingly, despite increase in molecular weights, the polymerization of the *proximal* substrates did not reach the desired range (< 15 kDa), presumably due to the more electron-poor substrates as well as the purification issues as noted above. To our gratification, the radical inhibitor prevented the *distal* analogs from cross-linking, and these adducts reached much higher degree of polymerization. Specifically, after polymerizing **D1** at 90 °C for 24 h, the material is fully soluble in DCM in the presence of BHT, displaying no cross-linking as observed from the pictures in **Figure 3.4a**. Within this series, the original pentyl-substituted Cp (**D1**) monomer showed the highest degree of polymerization (DP_n of 44 and DP_w of 77) among the six analogs (Supporting Table S2 and the SEC spectra from **Figure 3.4b**). The optimal condition was bulk polymerization of **D1** at 90 °C for 48 h, resulting in the highest number-average molecular weight (M_n) of 19.6 kDa and weight-average value (M_w) of 33.9 kDa. In general, the less bulky *distal* Cp derivatives lead to higher-MW polymers. Therefore, we also changed the pentyl group to a less sterically hindered methyl substituent (**22**, Supporting Information 3.7) to determine if reducing the length of the alkyl chain or sterics will further improve the MW range. Polymerization of **22** results in the similar-MW materials with a higher *DP*, yet not significant (Supporting Figure S3.60). Based on the synthetic accessibility and polymerization efficiency, the most promising pentyl-substituted moiety was used to evaluate the generality of the platform with different polymeric backbones.

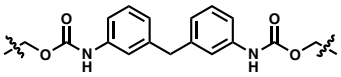
Substrate Scope of Cyclopentadiene Homopolymers and Characterization. To demonstrate the versatility of our Cp linear platform, we focused on monomers that are derived from common thermoplastics, including alkyl chain (**M1**), urethane (**M2**), polydimethylsiloxane or PDMS (**M3**), hydrogenated polybutadiene (**M4**), butylene terephthalate (**M5**), and ethylene terephthalate (**M6**) (**Figure 3.6**). The synthesis of polyimide-Cp polymer was also attempted but only afforded a low-MW polymer ($M_w \approx 8$ kDa) due to the insolubility and hydrolysis-prone issues, as known in literature[43–45] (Supporting Section 1.8 and Table S3.3). After purification, the high-MW polymers (**Pol 1**–**Pol 6**) were characterized by a SEC that is equipped with a triple-detection multi-angle light scattering (MALS) to attain absolute MWs in tetrahydrofuran (THF) solvent (**Figure 3.6** and Supporting Table S3.4). Overall, the six polymers possess M_n values ranging from 12 to 102 kDa with the highest DP_n of 53 (**Pol 5**). The dispersity of 1.1–1.6 was obtained, which is typical for a step-growth polymerization (Supporting Table S3.4).



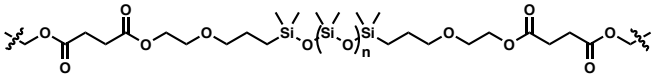
R' =



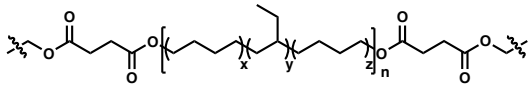
Pol 1, alkyl-Cp
M_n = 24 kDa; DP_n = 46
T_g = -39 °C; [η] = 0.24 dL/g



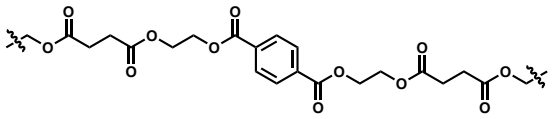
Pol 2, urethane-Cp
M_n = 12 kDa; DP_n = 21
T_g = 88 °C; [η] = 0.16 dL/g



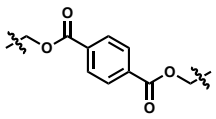
Pol 3, polydimethylsiloxane (PDMS)-Cp
M_n = 102 kDa; DP_n = 13
T_g = -124 °C; [η] = 0.39 dL/g



Pol 4, hydrogenated polybutadiene-Cp
M_n = 72 kDa; DP_n = 16
T_g = -51 °C; [η] = 0.53 dL/g



Pol 5, butylene terephthalate-Cp
M_n = 40 kDa; DP_n = 53
T_g = 3 °C; [η] = 0.18 dL/g



Pol 6, ethylene terephthalate-Cp
M_n = 17 kDa; DP_n = 37
T_g = 49 °C; [η] = 0.17 dL/g

Figure 3.6. The general scheme to access different Cp monomers (**M1**–**M6**) via the tetrazine deprotection of varied NBD starting materials. Of note, the pentyl-substituted Cp moiety was incorporated into the common polymer backbones such as alkyl chain (**M1**), urethane (**M2**), polydimethylsiloxane or PDMS (**M3**), hydrogenated polybutadiene (**M4**), butylene terephthalate (**M5**), and ethylene terephthalate (**M6**). The optimized polymerization conditions include the addition of 5 mol% BHT and heating at 90 °C in the absence of solvents and stirring, at different time durations. **M1**, **M2**, **M5**, and **M6** need 48 h, while **M3** and **M4** require 96 h to reach the optimized MWs, which are dependent on the backbone flexibility and monomer size. After precipitation to remove BHT, and small oligomers, six pure polymers (**Pol 1**–**Pol 6**) were acquired and subsequently characterized via an SEC-MALS to delineate the material properties (i.e., accurate number-average molecular weight M_n, glass transition temperature T_g, and intrinsic viscosity [η]). Of note, PDMS-Cp analog (**Pol 3**) has an iso-refractive effect with the THF solvent from the instrument and thus, the measured numbers might not be exact.

To characterize the intrinsic viscosity, Mark-Houwink-Sakurada (MHS) parameters were used.[46–50] In general, MHS constant a (Supporting Table S3.5) indicates expected flexible chains or random coils in THF ($0.5 \leq a \leq 0.8$).[46–50] The value for PDMS-incorporated Cp polymer (**Pol 3**) was higher than expected (a = 1.34), presumably due to the iso-refractive effect with the THF solvent.[51] The conformation plot (Supporting Figure S3.79) also shows the same phenomenon, where all the polymer chains, apart from **Pol 3**, possess linear configuration, with low to no degree of branching, as shown by the slope reaching 0.58.[52] The Cp adducts do not form trimers under the optimized conditions, evident by mass spectrum analysis[39] and solubility. The intrinsic viscosity and MHS values were analyzed in details for each polymer analog to probe the solution properties. For urethane-Cp polymer or **Pol 2**, the measured MHS constant a (0.69) is near the value of a similar structure that is reported in literature, or 0.78 in THF.[53] **Pol 1** and **Pol 4** have the solution properties similar to the saturated hydrocarbon polymer, especially polyisobutylene.[54] Due to iso-refractive effect of THF with

Pol 3, a viscometer was utilized to measure the polymer behavior in toluene (Supporting Table S3.6 and Figure S3.93). The intrinsic viscosity was determined to be 0.42 dL/g (from both Huggins and Kraemer plots) for $M_w \approx 102$ kDa, matching the literature trend for the same MW range.[55] Both **Pol 5** and **Pol 6** display lower intrinsic viscosity in THF compared to the literature values of commercial polybutylene terephthalate (PBT) and polyethylene terephthalate (PET), respectively, in other solvents (e.g., *m*-cresol, *o*-chlorophenol).[56,57] When solvents are not present in the intrinsic viscosity measurement via the infrared spectroscopy and multivariate calibration method, the value of **Pol 6** is close to that of the post-consumer PET.[58]

We also conducted thermal characterization to probe material properties. Each Cp polymer displays a range of different glass transition temperature (T_g) that was measured via a differential scanning calorimetry (DSC) (**Figure 3.6**). PDMS-Cp polymer (**Pol 3**) exhibits the lowest T_g of -124 °C, while PU-derived analog (**Pol 2**) provides the highest T_g of 88 °C. These results aligned with literature reports.[59] The dodecane ester Cp polymer (**Pol 1**) has a reasonably similar T_g range with its hydrogenated butadiene counterpart (**Pol 4**). The butylene phthalate-Cp polymer (**Pol 5**) has a lower T_g of 3 °C, compared to commercial PBT, which is 27–60 °C.[59] **Pol 6** has a reasonably higher T_g of 49 °C than **Pol 5** due to the shorter alkyl chain. However, it is still lower than the known value. One of the reasons can be related to the lower M_w of **Pol 6** compared with that of the commercial PET ($M_w \geq 30{,}000$ Da).[59] In general,

however, the T_g of the DA-linked thermoplastics were comparable with known commercial analogs.

To extend the property studies of these materials, **Pol 6** was chosen for mechanical evaluation. The glassy nature and ease of melt processing of **Pol 6** made it an accessible candidate for the mechanical analysis. We performed tensile testing on **Pol 6** using both crude and purified materials, which were melted into the dumbbell-shaped samples (more details in Supporting Section 1.13). The ultimate tensile strength is measured to be 18–22 MPa with ~5–7% elongation and the Young's modulus value of ~500 MPa (Supporting Figures S94–95, and Table S7). We also performed the test on a sample derived from crude material using the American Society for Testing and Materials (ASTM) D638-14 standard[60] (Supporting Figures S96 and S97), which has tensile strength of 15 MPa, elongation at break of 2%, and Young's modulus of 1.2 GPa. The performance of **Pol 6** is comparable with the studies of virgin and recycled PET fibers,[61] but lower than that of the commercial PET resin.[59] Of note, melt processing under ambient atmosphere was applied to mold the samples (~90 °C) multiple times before the mechanical characterization. This could potentially affect the original mechanical properties due to the inevitable thermal degradation of PET during the melt processing.[62]

Investigation of Active Chain-Ends and Optimal MW Range. To potentially control and increase the MW range for varied applications, we investigated the Diels–Alder polymerizing behaviors of Cp. First, active chain-ends were probed by reacting **Pol 1** (M_n =

24 kDa) with N15-labeled phenyl maleimide (^{15}*N*-PhMal) at room temperature with DCM as the solvent. To our surprise, no signal was detected for the Cp-maleimide adduct based on the ^{1}H-^{15}N heteronuclear multiple bond correlation (HMBC) NMR spectrum. Factors that could affect the end-group reactivity with maleimide include the formation of cyclic polymers, decomposition of the functional Cp units, and/or the polymers have reached the chemical equilibrium. To inspect chain-end cyclization, we heated **Pol 1** at 150 °C for 2 min in the presence of ^{15}*N*-PhMal "capping" reagent. As known in the field, the physically more compact circular polymers occupy smaller hydrodynamic volumes and thus, exhibit lower-MW reading on the SEC spectra than the linear analogs.[63] We hypothesize that after short thermal de-polymerization, the "hypothetically cyclic" Cp polymer would change to a linear conformation, leading to an SEC trace at higher-MW region. However, due to the incorporation of Cp units across the polymer backbone, **Pol 1** also starts to de-polymerize at 150 °C even during a short amount of time (i.e., 2 min) to smaller fragments and displayed an overall lower-MW reading on the SEC spectrum (Supporting Information in Section 3.7). As such, we were only able to confirm the formation of reactive Cp units after a brief de-polymerization at 150 °C (Supporting Figures S3.98 and S3.101). Given this challenge, we also monitored the polymerization process and tracked the chain-ends via ^{1}H NMR spectroscopy. A predictable step-growth polymerizing mechanism with approximately 95–98% conversion was observed (**Figure 3.7**), based on the consumption of Cp and M_n values (Supporting Table S3.8).

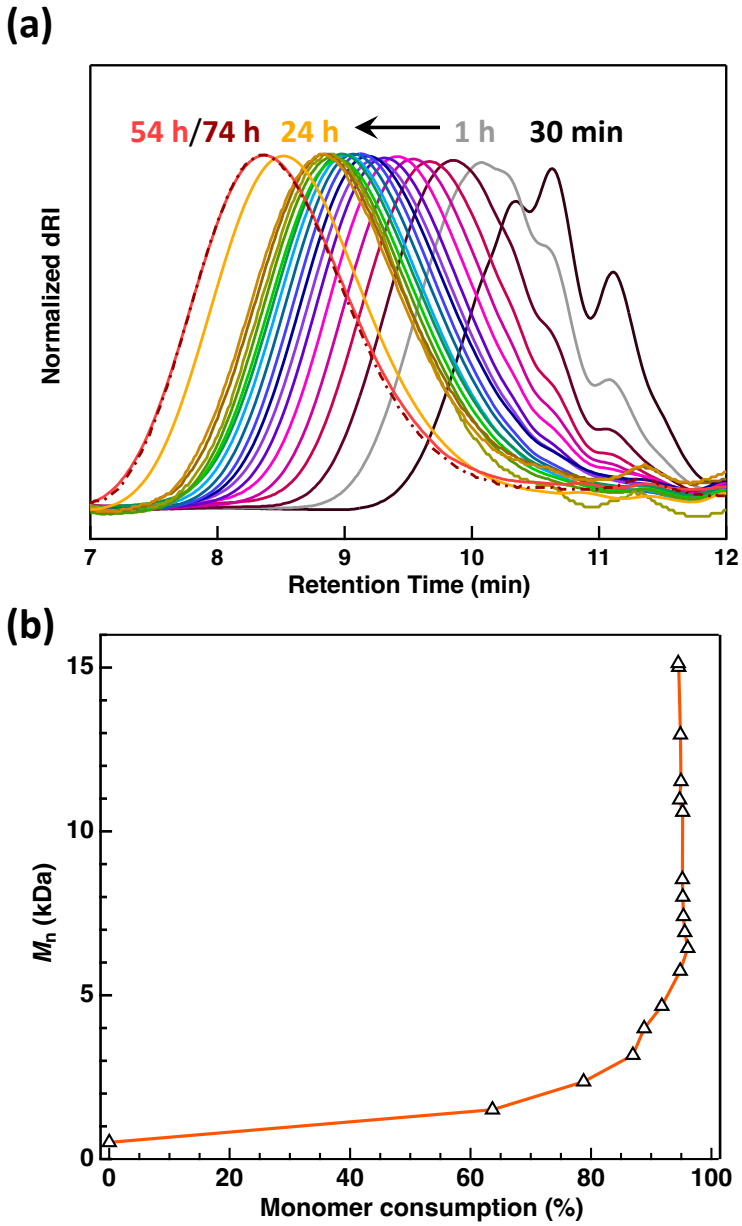


Figure 3.7. (a) The polymerization of M1 (with 5 mol% BHT) at 90 °C was monitored throughout the course of 74 h with the SEC traces recorded at 30-min intervals between 0.5 and 8 h, and then at 24, 54, and 74 h. The highest MW was obtained at 54 h. (b) The monomer consumption from ^{1}H NMR spectra were coupled with M_n values to determine the polymerization kinetics. In the first 30 min, more than 60% monomer was consumed. A step-

growth mechanism is revealed as expected from the Diels–Alder linear polymerization with a conversion of approximately 95–98%.

To investigate the possible decomposition of functional Cp chain-ends, the amount of BHT was increased to 10 mol% but there was no further chain extension, while lowering the amount to less than 1 mol% showed gradual degradation/oxidation of the macromolecule (Supporting Figure S3.103). Different inhibitors (e.g., hydroquinone and mequinol) were also investigated to observe their effect to the polymerization but no improvement was observed (Supporting Figure S3.104). Of the inhibitors examined, BHT was shown to prevent the degradation of Cp materials the most effectively and result in the optimal MW. The polyaddition could also be haunted due to other reasons than decomposition, such as reaching a thermodynamic equilibrium, ceiling temperature,[64] or limitations caused by the bulk polymerization (e.g, diffusion-controlled reaction, improper heat transfer, etc.).[65,66] The kinetics of the step-growth reaction of Cp dimerization could also potentially affects the DP[28,46] and influence the polymerizing behaviors. To test if higher MW could be achieved by increasing the reaction rate of the system, two-component Cp-maleimide polymerization was also attempted (Supporting Figure S3.105). However, this did not result in higher MW despite the faster kinetics of Cp and maleimide as known in literature.[34,40,41,67–70]

Chemical Recycling of Cp Homopolymers. To demonstrate the reversible DA design, selected homopolymers were subjected to chemical recycling experiments by first de-polymerization at 150 °C (the onset of rDA temperature range) and re-polymerization at 90 °C in the same pot without solvent and purification throughout the closed-loop process. All

materials were characterized via the standard chloroform SEC. Specifically, hydrogenated polybutadiene that is integrated with Cp dimers or **Pol 4** (M_n = 68 kDa, DP_n of 11) was heated at 150 °C, neat (in the presence of 1 wt% BHT) and the de-polymerization was monitored at 5, 15, and 30 min (**Figure 3.8**). **Pol 4** reverted to smaller oligomers within 5 min. Heating the material longer, 15 min and 30 min, provided shorter polymer chains (**Figure 3.8**). However, no further change in molecular weight was observed after 30 min of heating (Supporting Figure S3.110). Under these conditions, the de-polymerized material was determined to possess M_n of 23 kDa (DP_n of ~4, contributing to ~70% de-polymerization efficiency). The re-polymerization was achieved by heating the lowest-MW oligomers (23 kDa, dotted-green SEC trace from the graph in **Figure 3.8**) at 90 °C, neat for 96 h, following the original optimal polymerization conditions for **Pol 4**. The MW was fully recovered to that of the parent polymer (dark purple SEC trace). The closed-loop process was repeated over 3 cycles and the near-identical results were observed (**Figures 3.8** and **3.9**).

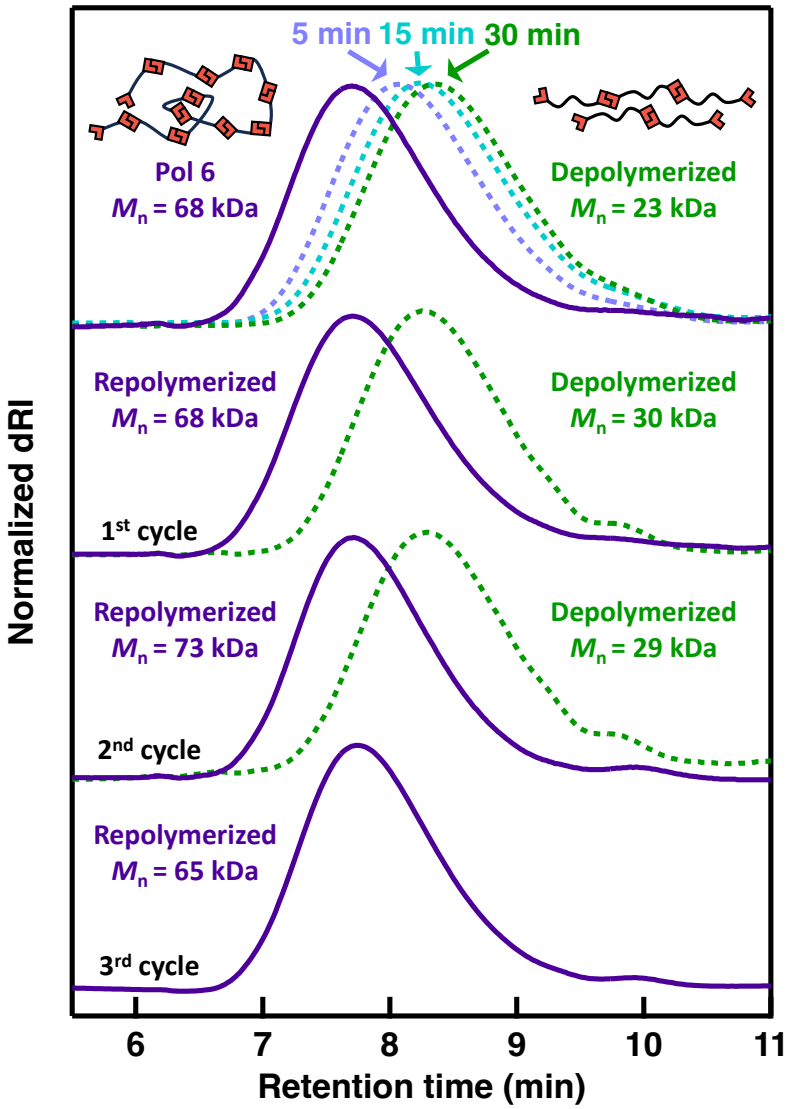


Figure 2.8. The hydrogenated polybutadiene that is integrated with Cp dimers (**Pol 4**) was subjected to 3 cycles of de- and re-polymerization processes with the addition of 1 wt% BHT, in the absence of solvents. The first cycle involves the heating of **Pol 4** (M_n = 68 kDa) at 150 °C for 5, 15, and 30 min (top SEC traces). **Pol 4** was efficiently de-polymerized (M_n = 68 kDa to 23 kDa) after 30 min. No purification was performed as the resulting oligomer (M_n = 23 kDa) was directly subjected to the re-polymerization (i.e., 90 °C for 96 h). A full recovery to the original MW was observed (middle SEC traces). The process was repeated

two more times (middle and bottom SEC traces). The phenomenon persisted with consistent de- and re-polymerization patterns.

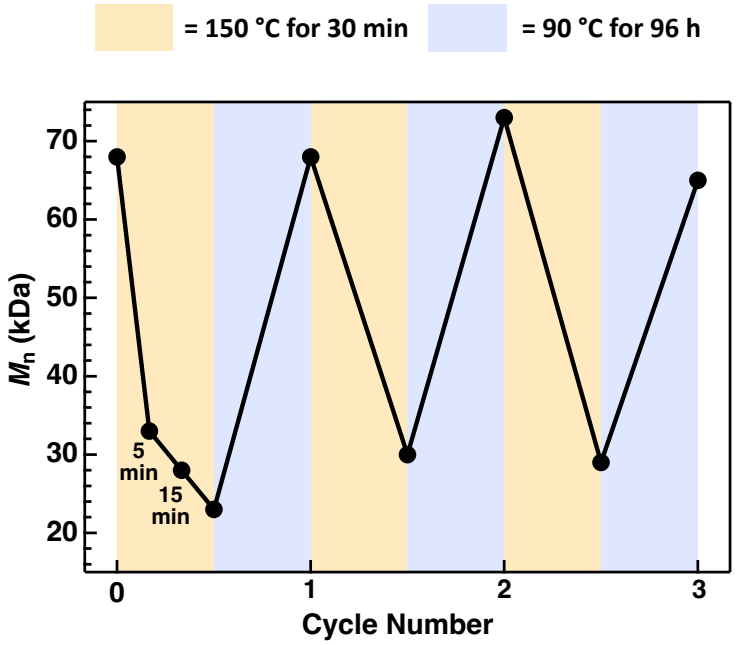


Figure 3.9. Thermal reversibility of **Pol 4** is highly efficient and can be recycled multiple times (i.e., 3 cycles) without additional purification, displaying the potential of single-component step-growth polymerization.

The de- and re-polymerization of **Pol 1**, **Pol 2**, **Pol 3**, and **Pol 6** were also performed with the same conditions as shown for **Pol 4**. Diverse behaviors were attained among the materials (Supporting Information in Section 3.7). Specifically, **Pol 2** was successfully de-polymerized to the oligomers with M_n of 5 kDa, which was subsequently re-polymerized. The recovered material displays a higher-MW range compared to the original polymer (Supporting Information, Figure S3.113). **Pol 1** and **Pol 6** successfully degraded upon heating but unexpectedly did not show efficient re-polymerization behaviors, regardless of the varied de- and re-polymerization conditions (e.g., change in the amount of BHT, purification of de-

polymerized mixtures, re-polymerization with different solvents and temperatures; more details are described in Supporting Information in Section 3.7). Of note, these polymers contain higher concentration of Cp linkages as well as ester linkages, which could contribute to thermal degradation and insufficient re-polymerization.[71] As aforementioned, critical purity of oligomer chain-ends is required to achieve the reformation of the parent polymers. Therefore, minimal degradation of Cp chain-ends or ester linkages can have detrimental effects on the re-polymerization. When **Pol 6** was heated for a shorter amount of time (15 min rather than 30 min), the re-polymerization is improved (Supporting Figure S3.118), supporting our degradation hypothesis. Furthermore, the color of **Pol 6** was changed from transparent to slightly yellowish during the heating process, showing the partial degradation of the polymer (Supporting Figure S3.119). The siloxane-Cp analog, or **Pol 3**, which was polymerized from a macromolecular monomer and thus, contain lower concentration of Cp and ester moieties, displays the closest trait to that of **Pol 4**. The original MW was recovered and close to that of the original polymer (Supporting Information, Figure S3.121). ^{1}H NMR spectra of the de-polymerized materials were also collected for **Pol 1**–**4** and **Pol 6**, which reveal the Cp chain-ends (Supporting Figures S3.112, S3.114, S3.116, S3.120, and S3.122). In this work, only recycling of homopolymer was demonstrated, nevertheless, up-recycling with different functionalized dienophiles is feasible and under ongoing investigation.

3.5 Conclusion

We have demonstrated a new and straightforward methodology to form high-MW recyclable thermoplastics, utilizing single-component cyclopentadiene derivatives and the Diels–Alder polymerization/de-polymerization. In this initial study, we synthesized and characterized six Cp homopolymers that are based on common thermoplastics architectures. All tailored materials possess an excellent range of material properties (e.g., varied glass transition temperatures, flexible backbones, etc.) and show consistent de-polymerization behaviors, except for the substances that contain high amount of Cp and ester linkages. Here, the unavoidable thermal degradation presumably contributed to the complication during the re-polymerization process. Remarkably, the hydrogenated polybutadiene that is modified with Cp units (**Pol 4**) displays the ability to efficiently re-polymerize and de-polymerize over three cycles. Moreover, due to the single-component DA chemistry, no catalysts, or solvents and thus, no purification step is required during the recycling process. Overall, synthesis and characterization of the recyclable Cp homopolymers presents insights into the similar and different properties, compared to the current state-of-the-art thermoplastics, consequently creating a space for further improvement and additional analysis. Specifically, in-dept structure-property relationship studies are important to improve the MW range of the synthesized polymer, to prevent degradation during recycling, or to understand the spatial arrangements of Cp-dimer that affect the material properties. We believe this work could

establish a mild and universal chemical recycling strategy that expands the design and construction of sustainable thermoplastics.

3.6 Acknowledgements

The research was funded by the National Science Foundation (CHE-2204077). We thank Kirk Fields from mechanical engineering workshop at UCSB for the assistance on the mechanical testing. The authors also acknowledge the staff at Wyatt Technology for the helpful guidance on SEC-MALS analysis. We are also thankful for the training on the Carver press from Rachel A. Segalman's laboratory, and the viscometer from Matthew Helgeson's research group. The NMR instruments were supported by the National Science Foundation under award No. MRI-1920299. The facility for tensile testing was provided by the BioPACIFIC Materials Innovation Platform of the National Science Foundation under Award No. DMR-1933487. We used the MRL Shared Experimental Facilities that are supported by the MRSEC Program of the NSF under Award No. DMR 1720256; a member of the NSF-funded Materials Research Facilities Network.

3.7 Supporting Information

Material and experimental details:

Reactions were conducted using reagent grade solvents. Dichloromethane (DCM) was stored over 3Å molecular sieves. Tetrahydrofuran (THF) and toluene were passed over a column of activated alumina. All commercially obtained reagents were bought from Sigma

Aldrich, Fisher Scientific, VWR International and were used as received unless otherwise noted. Compound **2** was synthesized using the procedures that are reported in literature.[72,73] Compound **3** can be synthesized based on the procedure to form **2** or is commercially available. Compounds **5**, **8**, **14**, **20** and **23** were synthesized based on the procedures from the works in our group.[40,41,69] N15-labelled phenyl maleimide was synthesized in one step based on our previous publication[39] with the starting material (N15-labeled aniline) purchased from Cambridge Isotope Laboratories, Inc. Thin-layer chromatography (TLC) was conducted with E. Merck silica gel 60 F254 pre-coated plates (0.25 mm) and visualized by exposure to UV light (254 nm) or stained with p-anisaldehyde. Flash column chromatography was performed using normal phase silica gel (60 Å, 0.040 – 0.063 mm, Geduran).

Characterization methods:

ATR FT-IR spectra were recorded on a Varian 640-IR FT-IR spectrometer equipped with an ATR (attenuated total reflection) accessory or a Thermo Nicolet iS10 FTIR Spectrometer with a Smart Diamond ATR; applied as neat or solid samples with smooth surfaces and absorbance bands reported as $1/\lambda$ in cm^{-1}. ^{1}H NMR spectra were recorded on Varian and Bruker spectrometers (400, 500, or 600 MHz) and are reported relative to the residual protio-signal in deuterated solvents. Data for ^{1}H NMR spectra are reported as follows: chemical shift (δ ppm), multiplicity, coupling constant (Hz) and integration. ^{13}C NMR spectra were recorded on Varian or Bruker Spectrometers (500 MHz). Data for ^{13}C NMR spectra are reported in terms of chemical shift (δ ppm). ^{1}H-^{15}N two-dimensional Heteronuclear Multiple Bond

Correlation (HMBC) NMR was collected on the Bruker spectrometer (500 MHz) to enhance the ^{15}N-labeled signals with the spectrum range is from -400 to 600 ppm.

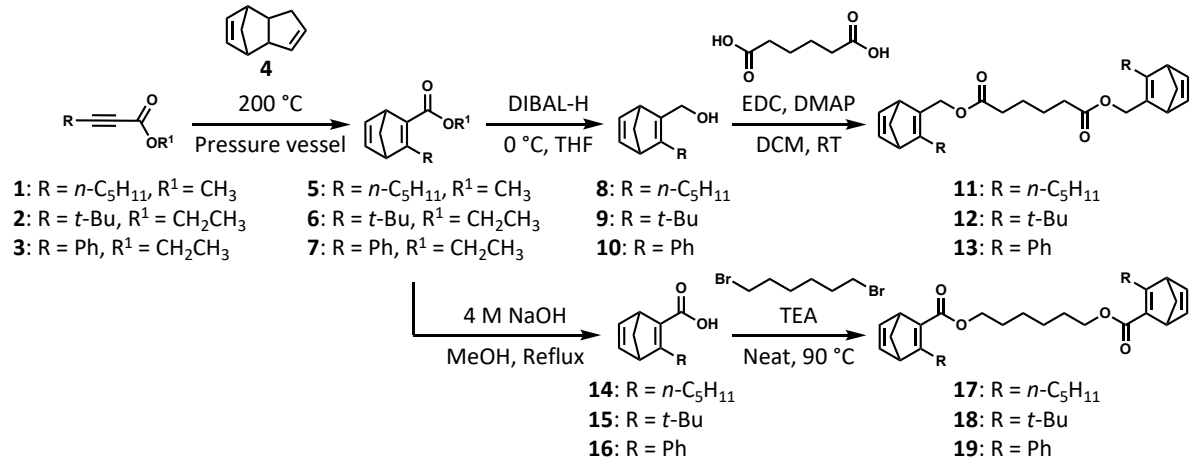
Size Exclusion Chromatography (SEC) eluting with chloroform ($CHCl_3$) and calibrated relative to polystyrene standards was performed on a Waters Alliance HPLC System, 2690 separation module, equipped with Wyatt DAWN HELEOS-II light scattering and Waters 2410 Differential Refractometer (RI) and Waters 2998 Photodiode Array (PDA) detectors. The SEC that is equipped with Multi-Angle Light Scattering Detection (MALS) is used to obtain absolute mass values of the polymer samples. The ViscoStar detector is also connected to measure the specific viscosity, and when coupled with a concentration detector as Optilab rEX, can detect intrinsic viscosity. The intrinsic viscosity leads to the derivation of hydrodynamic radius and shape information of the molecule in solution. The air-cooled Peltier allows temperature control from 4-60 ^{o}C. The measurements are conducted at ambient temperature. In general, the SEC-MALS setup includes a pump (Waters Alliance HPLC System, 2695 Separation Module), SEC columns (2 Agilent PLgel MiniMixed-D bed columns + guard with MW linear range: 200-400,000 g/mol), and detectors (Wyatt DAWN HELEOS-II with laser of 663.1 nm, Wyatt Optilab rEX (RI), Wyatt ViscoStar). The samples with concentration ranging from 3–5 mg/mL were prepared in tetrahydrofuran (THF). 40 μL was injected with a flow rate of 0.375 ml/min. Intrinsic viscosity of the polydimethylsiloxane sample was measured by a viscometer (Anton Paar, Lovis 2000 ME & DMA M). The samples in toluene were injected using capillaries into the instrument via a flow-through method.

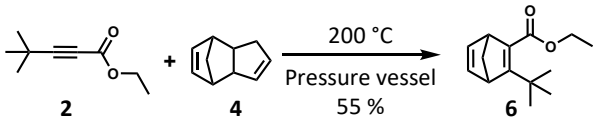
Leveling was performed in between the sample runs and the angle was ensured to be within the reasonable corrected range. Toluene was used as the solvent for the samples and served as the blank.

Mass spectra were obtained using Waters Acquity H-class Ultra High-Pressure Liquid Chromatography (UPLC) system, coupled with a Waters Xevo G2-XS Time-of-Flight Mass Spectrometer with an ESI or ASAP source. Differential scanning calorimetry (DSC) was performed on a liquid-nitrogen-cooled TA Instruments Q2000 DSC system at a heating rate of 10 °C/min under a nitrogen atmosphere with a sensitivity < 0.2 μW and a baseline drift < 10 μW. The amount of material in the thermal pans is ~2–5 mg. Thermo-gravimetric analysis (TGA) was collected on a TA Instruments Discovery 5500 Thermo-Gravimetric Analyzer. The measurements were taken under a nitrogen environment from an initial thermally equilibrated state at 50 °C ramping up to 900 °C at 10 °C per minute.

Synthesis procedures:

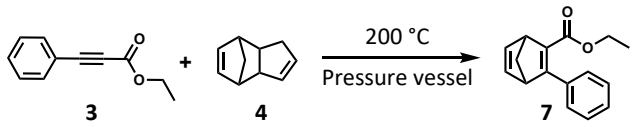
Scheme S3.1. Synthetic routes to access *distal* and *proximal* norbornadiene (NBD) precursors (*distal*: **11**–**13**, *proximal*: **17**–**19**) based on the relative distance between the Cp moieties and the carbonyl functionality. Each category was synthesized with different substituents (e.g., *n*-pentyl, *t*-butyl, and phenyl groups).



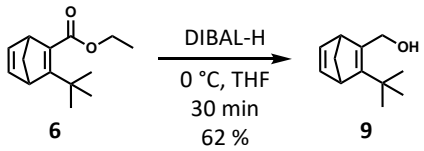


To a pressure vessel were added compound **2** (12.0 g, 77.8 mmol, 1.0 eq.), dicyclopentadiene (6.3 mL, 46.7 mmol, 0.6 eq.) and hydroquinone (197 mg, 2.3 mol%). Once added, the vessel was sealed and heated at 200 °C for 6 h. The crude product was distilled twice (90–150 °C, ~200 mTorr) to afford the pure product **6** as a colorless oil (9.5 g, 43.1 mmol, 55% yield). ^{1}H NMR (500 MHz, $CDCl_3$) δ 6.90 (ddd, *J* = 5.1, 2.4, 1.2 Hz, 1H), 6.73 (ddd, *J* = 5.1, 2.6, 1.4 Hz, 1H), 4.25 – 4.11 (m, 2H), 3.75 – 3.69 (m, 2H), 1.96 (dt, *J* = 6.3, 1.7 Hz, 1H), 1.82 (dt, *J* = 6.3, 1.6 Hz, 1H), 1.30 (t, *J* = 7.1 Hz, 3H), 1.16 (s, 9H) ppm; ^{13}C NMR (126 MHz, $CDCl_3$) δ 171.67, 168.49, 143.65, 141.64, 137.54, 69.92, 60.23, 54.38, 54.19, 34.59, 28.82, 14.37 ppm; IR (ATR) 3069, 2962, 2936, 2905, 2868, 1707, 1596, 1557, 1479, 1462, 1392, 1363, 1311, 1294, 1248, 1226, 1194, 1152, 1085, 1045, 1026, 947, 932,

888, 864, 828, 751, 718, 673, 608 cm^{-1}; HRMS TOF MS ES+ exact mass calculated for $C_{14}H_{20}O_2Na^+$ or $[M+Na]^+$: 243.1361, found: 243.1354.

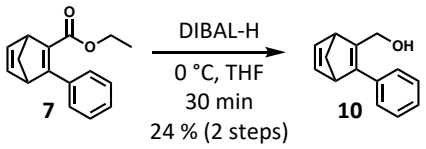


To a pressure vessel were added compound **3** (12.0 g, 77.8 mmol, 1.0 eq.), dicyclopentadiene (6.3 mL, 46.7 mmol, 0.6 eq.) and hydroquinone (197 mg, 2.3 mol%). Once added, the vessel was sealed and heated at 200 °C for 6 h. The crude product was used for the follow-up reactions without further purification. HRMS TOF MS Cl+ exact mass calculated for $C_{16}H_{16}O_2^+$ or $[M]^+$: 240.1150, found: 240.1157.



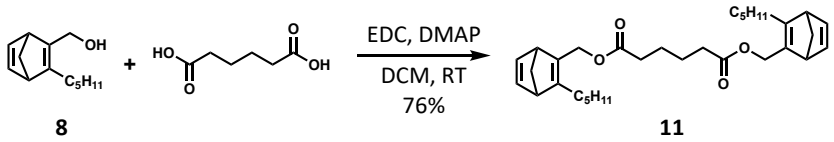
To a flame-dried 500 mL 2-neck round bottom flask was added a solution of alcohol **6** (9.2 g, 1.0 eq., 41.8 mmol) in THF (300 mL). The solution was cooled to 0 °C under a N_2 atmosphere. A solution of diisobutylaluminum hydride (DIBAL) in hexanes (1 M, 120.0 mL, 116.9 mmol, 2.8 eq.) was added dropwise via an addition funnel over 1 h. After that, the solution was stirred at 0 °C for 30 min or until completion as shown on the TLC. The reaction was quenched slowly with 5 mL water, an aqueous solution of sodium hydroxide (NaOH) (1 M, 10 mL), and water (5 mL). The quenched solution was stirred at RT for 30 min. The crude solution was dried with Na_2SO_4, stirred for 10 more min, and then filtered and rinsed

with dichloromethane (DCM). The solution was concentrated, and the residue was subjected to flash column chromatography with hexanes and EtOAc as eluent (hexanes:EtOAc, 6:1) to yield the pure product **9** as a colorless oil (4.6 g, 25.8 mmol, 62% yield). ^{1}H NMR (500 MHz, $CDCl_3$) δ 6.81 (dd, *J* = 5.2, 3.0 Hz, 1H), 6.71 (dd, *J* = 5.3, 3.0 Hz, 1H), 4.44 – 4.32 (m, 2H), 3.56 (dt, *J* = 3.9, 1.9 Hz, 1H), 3.50 (tt, *J* = 2.5, 1.3 Hz, 1H), 1.86 (dt, *J* = 6.0, 1.7 Hz, 1H), 1.78 (dt, *J* = 6.0, 1.7 Hz, 1H), 1.12 (s, 9H) ppm; ^{13}C NMR (126 MHz, $CDCl_3$) δ 159.20, 143.14, 142.91, 142.64, 70.13, 60.19, 54.00, 53.45, 34.88, 29.44 ppm; IR (ATR) 3321 (br), 3121, 3064, 2955, 2932, 2904, 2864, 1639, 1558, 1461, 1390, 1360, 1294, 1252, 1234, 1205, 1129, 1115, 1092, 1051, 998, 973, 934, 887, 875, 830, 809, 775, 756, 738, 704, 663, 631, 607, 587, 568 cm^{-1}; HRMS TOF MS Cl+ exact mass calculated for $C_{12}H_{18}O^+$ or $[M]^+$: 178.1358, found: 178.1361.



Compound **10** was prepared similar to the procedure for compound **9**, with 10 g of crude starting material **7** (1.0 eq., mmol), mL DIBAL in hexanes (1 M, 2.8 eq., mmol) in mL THF. The reaction was quenched with mL water, mL NaOH (1M), and mL water. The crude mixture was subjected to a slow flash column chromatography with EtOAc:Hexanes (1:10) to yield the pure product **10** as slightly yellowish oil (2.0 g, 24% yield in 2 steps). ^{1}H NMR (400 MHz, $CDCl_3$) δ 7.39 – 7.29 (m, 3H), 7.25 – 7.21 (m, 2H), 6.95 (dd, *J* = 5.2, 2.9 Hz, 1H), 6.89 (dd, *J*

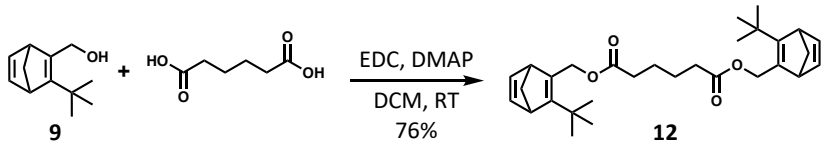
= 5.1, 3.0 Hz, 1H), 4.49 – 4.38 (m, 2H), 3.82 – 3.76 (m, 2H), 2.17 (dt, *J* = 6.2, 1.7 Hz, 1H), 2.03 (dt, *J* = 6.3, 1.7 Hz, 1H), 1.23 (s, 1H) ppm; ^{13}C NMR (126 MHz, $CDCl_3$) δ 151.51, 148.33, 143.08, 142.37, 136.65, 128.49, 127.03, 126.49, 71.21, 59.95, 55.56, 53.43 ppm; IR (ATR) 3338 (br), 3058, 3025, 2972, 2932, 2865, 1952, 1888, 1811, 1705, 1630, 1597, 1556, 1492, 1443, 1398, 1340, 1295, 1226, 1205, 1170, 1116, 1077, 1055, 1017, 983, 940, 926, 909, 867, 820, 790, 761, 723, 696, 660, 625, 591 cm^{-1}; HRMS TOF MS Cl+ exact mass calculated for $C_{14}H_{14}O^+$ or $[M]^+$: 198.1045, found: 198.1042.



8 **11**

To a dried 250 mL round bottom were added compound **8** (300 mg, 1.6 mmol, 2.2 eq.), adipic acid (104 mg, 0.7 mmol, 1.0 eq.) and 12 mL DCM. To this solution were added EDC (816 mg, 4.3 mmol, 6.0 eq.) and DMAP (35 mg, 0.3 mmol, 0.4 eq.). Once added, the solution was allowed to stir at room temperature for 24 h. The crude solution was washed with water followed by brine solution until the organic layer became clear. The organic layer was dried over Na_2SO_4 and concentrated. The crude residue was subjected to flash column chromatography with 1:9 EtOAc:hexanes to afford the pure product **11** as a colorless oil (267 mg, 0.5 mmol, 76% yield). ^{1}H NMR (500 MHz, $CDCl_3$) δ 7.26 (dd, *J* = 5.2, 3.0 Hz, 2H), 7.21 (dd, *J* = 5.2, 3.0 Hz, 2H), 5.22 (d, *J* = 12.2 Hz, 2H), 5.07 (d, *J* = 12.2 Hz, 2H), 3.94 (t, *J* = 2.3 Hz, 2H), 3.87 (t, *J* = 2.4 Hz, 2H), 2.85 – 2.81 (m, 4H), 2.74 (ddd, *J* = 14.3, 8.3, 6.4 Hz, 2H),

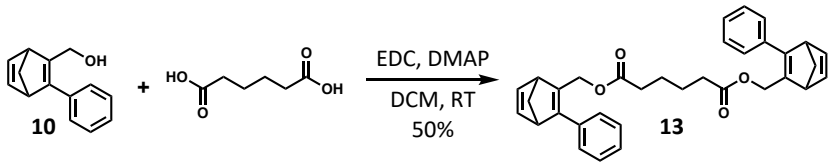
2.65 (ddd, J = 14.0, 8.2, 6.6 Hz, 2H), 2.44 (dt, J = 6.1, 1.7 Hz, 2H), 2.41 – 2.37 (m, 2H), 2.20 – 2.14 (m, J = 3.6, 3.2 Hz, 4H), 1.95 – 1.74 (m, 8H), 1.69 (m, 4H), 1.38 (t, J = 7.3 Hz, 6H) ppm; ^{13}C NMR (126 MHz, $CDCl_3$) δ 173.53, 155.51, 143.02, 142.10, 141.17, 71.48, 60.74, 53.92, 52.29, 34.08, 31.54, 28.48, 27.02, 24.62, 22.62, 14.18 ppm; IR (ATR) 3120, 3065, 2957, 2928, 2860, 1731, 1660, 1556, 1458, 1419, 1378, 1348, 1289, 1229, 1163, 1136, 1074, 1016, 950, 872, 827, 784, 723, 685, 650, 572 cm^{-1}; HRMS TOF MS ES+ exact mass calculated for $C_{32}H_{46}O_4Na^+$ or $[M+Na]^+$: 517.3294, found: 517.3312.



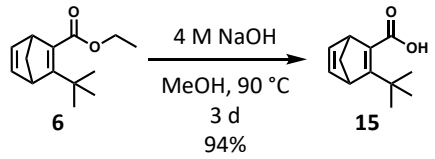
9 **12**

Compound **12** was prepared similar to the procedure for compound **11**, with 300 mg of **9** (1.7 mmol, 2.2 eq.), 112 mg of adipic acid (0.7 mmol, 1.0 eq.), 874 mg of EDC (4.6 mmol, 6.0 eq.), and 37 mg of DMAP (0.3 mmol, 0.4 eq.) in 12 mL DCM. The crude product was subjected to flash column chromatography with EtOAc:Hexanes as eluent (1:9) to afford the pure product **12** as colorless oil (270 mg, 76% yield). ^{1}H NMR (500 MHz, $CDCl_3$) δ 6.74 (dd, J = 5.1, 3.0 Hz, 2H), 6.68 (dd, J = 5.1, 3.1 Hz, 2H), 4.93 (d, J = 12.4 Hz, 2H), 4.76 (d, J = 12.4 Hz, 2H), 3.55 (t, J = 2.7 Hz, 2H), 3.39 (dt, J = 3.0, 1.5 Hz, 2H), 2.34 (h, J = 4.3 Hz, 4H), 1.86 – 1.83 (m, 2H), 1.78 – 1.74 (m, 2H), 1.68 (h, J = 3.4 Hz, 4H), 1.11 (d, J = 1.0 Hz, 18H) ppm; ^{13}C NMR (126 MHz, $CDCl_3$) δ 173.48, 160.99, 142.95, 142.33, 138.64, 69.88, 62.02, 54.00, 53.41, 34.87, 34.12, 29.21, 24.64 ppm; IR (ATR) 3121, 3065, 2956, 2933, 2865, 1731,

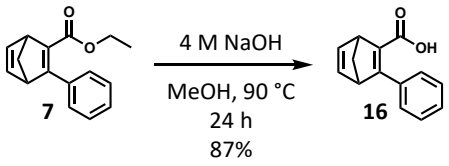
1648, 1595, 1558, 1481, 1461, 1360, 1294, 1234, 1208, 1160, 1135, 1052, 955, 876, 831, 810, 719, 663, 635, 588 cm^{-1}; HRMS TOF MS ES+ exact mass calculated for $C_{30}H_{42}O_4Na^+$ or $[M+Na]^+$: 489.2981, found: 489.2971.



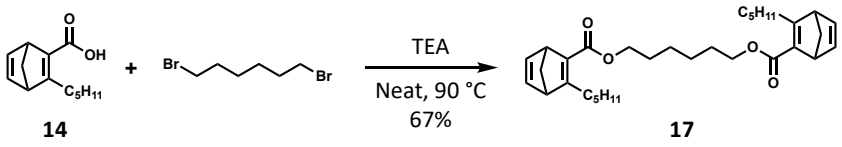
Compound **13** was prepared similar to the procedure for compound **11**, with 300 mg of **10** (1.5 mmol, 2.2 eq.), 100 mg of adipic acid (0.7 mmol, 1.0 eq.), 794 mg of EDC (4.1 mmol, 6.0 eq.), and 34 mg of DMAP (0.3 mmol, 0.4 eq.) in 12 mL DCM. The crude product was subjected to flash column chromatography with EtOAc:Hexanes as eluent (1:9) to afford the pure product **13** as slightly yellowish oil (173 mg, 50% yield). ^1H NMR (500 MHz, $CDCl_3$) δ 7.38 – 7.33 (m, 4H), 7.27 – 7.21 (m, 6H), 6.93 (dd, *J* = 5.1, 3.0 Hz, 2H), 6.85 (dd, *J* = 5.2, 3.0 Hz, 2H), 4.95 (d, *J* = 12.6 Hz, 2H), 4.77 (d, *J* = 12.7 Hz, 2H), 3.83 – 3.77 (m, 2H), 3.67 (t, *J* = 2.3 Hz, 2H), 2.37 (td, *J* = 5.8, 4.5, 2.7 Hz, 4H), 2.17 (dt, *J* = 6.2, 1.7 Hz, 2H), 2.02 (dt, *J* = 6.2, 1.7 Hz, 2H), 1.73 – 1.67 (m, 4H) ppm; ^{13}C NMR (126 MHz, $CDCl_3$) δ 173.43, 153.62, 144.09, 142.94, 142.19, 136.29, 128.55, 127.25, 126.51, 71.15, 61.71, 55.59, 53.69, 34.05, 24.61 ppm; IR (ATR) 3060, 3022, 2935, 2867, 1728, 1636, 1597, 1578, 1557, 1493, 1444, 1416, 1379, 1340, 1295, 1235, 1208, 1159, 1136, 1076, 1021, 908, 849, 821, 727, 697, 660, 647, 591 cm^{-1}; HRMS TOF MS ES+ exact mass calculated for $C_{34}H_{34}O_4Na^+$ or $[M+Na]^+$: 529.2355, found: 529.2332.



Compound **6** (5.0 g, 22.7 mmol) was dissolved in a solution of 150 mL NaOH (4 M) and 50 mL MeOH. The reaction was stirred for 3 d at 90 °C (reflux) or until complete consumption of the ester start material (as shown on the TLC). The solution was cooled to RT before acidifying with an aqueous solution of hydrochloric acid (HCl) (3 M) until the solution became turbid with white solid, then extracting with diethyl ether (3x). The combined organic layers were washed with brine solution, dried over anhydrous Na_2SO_4. The solvent was removed to afford the pure product **15** as a white powder (4.1 g, 21.3 mmol, 94%). ^{1}H NMR (500 MHz, $CDCl_3$) δ 6.92 (dd, *J* = 5.1, 3.0 Hz, 2H), 6.72 (ddd, *J* = 5.1, 3.1, 0.9 Hz, 2H), 3.84 (dq, *J* = 2.6, 1.2 Hz, 2H), 3.79 (m, 2H), 1.97 (dt, *J* = 6.5, 1.8 Hz, 2H), 1.85 (dt, *J* = 6.5, 1.6 Hz, 2H), 1.21 (s, 18H) ppm; ^{13}C NMR (126 MHz, $CDCl_3$) δ 177.55, 173.47, 143.94, 141.29, 137.11, 69.84, 55.24, 54.01, 34.88, 28.97 ppm; IR (ATR) 3073, 3004, 2962, 2931, 2863, 2799, 2706, 2667, 2627, 1423, 1651, 1587, 1555, 1482, 1469, 1448, 1391, 1363, 1290, 1256, 1239, 1216, 1194, 1165, 1093, 1109, 1021, 1005, 943, 889, 871, 832, 816, 796, 735, 718, 678, 619, 570 cm^{-1}; HRMS TOF MS ES+ exact mass calculated for $C_{12}H_{16}O_2Na^+$ or $[M+Na]^+$: 215.1048, found: 215.1037.

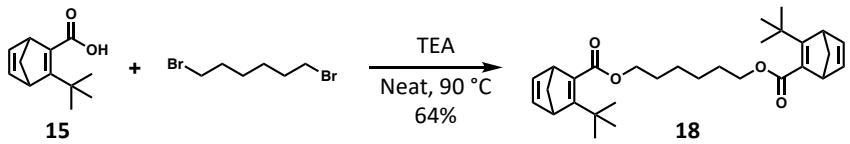


Crude compound **7** (10.0 g, 41.6 mmol) was dissolved in a solution of 300 mL NaOH (4 M) and 100 mL MeOH. The reaction was stirred for 24 h at 90 °C (reflux) or until complete consumption of the ester start material (as shown on the TLC). The solution was cooled to RT before acidifying with an aqueous solution of hydrochloric acid (HCl) (1 M), then extracting with diethyl ether (3x). The combined organic layers were washed with brine solution, dried over Na_2SO_4. The solvent was removed to afford the pure product **16** as dark yellow/brownish oil (7.7 g, 36.3 mmol, 87% yield – 2 steps). ^{1}H NMR (500 MHz, $CDCl_3$) δ 7.57 – 7.52 (m, 2H), 7.40 – 7.32 (m, 3H), 7.02 (dd, *J* = 5.1, 3.0 Hz, 1H), 6.95 – 6.89 (m, 1H), 4.09 (tt, *J* = 2.9, 1.2 Hz, 1H), 3.88 (m, 1H), 2.28 (dt, *J* = 6.7, 1.7 Hz, 1H), 2.09 (dt, *J* = 6.7, 1.6 Hz, 1H) ppm; ^{13}C NMR (126 MHz, $CDCl_3$) δ 171.00, 170.01, 143.97, 140.71, 138.48, 135.51, 128.96, 128.10, 127.93, 70.66, 59.26, 53.00 ppm; IR (ATR) 3050, 3011, 2990, 2974, 2942, 2872, 2738, 2614, 2564, 1644, 1590, 1559, 1491, 1435, 1331, 1312, 1291, 1256, 1247, 1225, 1194, 1157, 1117, 1101, 1079, 1021, 1000, 945, 915, 887, 871, 831, 780, 762, 739, 718, 666, 651, 606 cm^{-1}; HRMS TOF MS ES+ exact mass calculated for $C_{14}H_{12}O_2Na^+$ or $[M+Na]^+$: 235.0735, found: 235.0736.



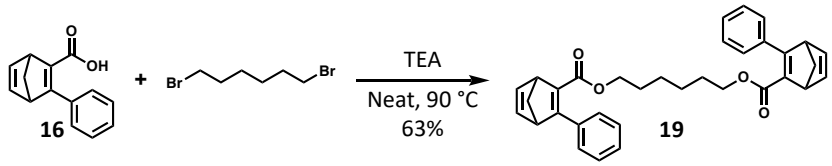
14 **17**

The reaction was based on the procedure that is reported in literature.[42] To a dram vial were added compound **14** (4.4 g, 21.2 mmol, 2.05 eq.) and 1,6-dibromohexane (2.5 g, 10.3 mmol, 1.0 eq.), followed by 8.6 mL triethyl amine (TEA). The reaction was heated to 90 °C for 24 h until completion. The crude product was dissolved in diethyl ether and the triethyl amine hydrobromide salt was filtered via a pad of celite. The solution was concentrated, and the residue was subjected to a flash column chromatography with hexanes and ethyl acetate (EtOAc) as eluent (hexanes:EtOAc, 6:1) to afford a transparent oil as the pure product **17** (3.4 g, 67% yield). ^{1}H NMR (400 MHz, $CDCl_3$) δ 6.87 (dd, *J* = 4.9, 2.8 Hz, 2H), 6.69 (ddd, *J* = 5.1, 3.1, 0.9 Hz, 2H), 4.17 – 4.02 (m, 4H), 3.88 (m, *J* = 2.4, 1.3 Hz, 2H), 3.50 (t, *J* = 2.6 Hz, 2H), 2.76 – 2.58 (m, 4H), 2.02 (dt, *J* = 6.4, 1.7 Hz, 2H), 1.95 (dt, *J* = 6.4, 1.6 Hz, 2H), 1.67 (q, *J* = 6.8 Hz, 4H), 1.56 – 1.18 (m, 16H), 0.88 (t, *J* = 7.1 Hz, 6H) ppm; ^{13}C NMR (126 MHz, $CDCl_3$) δ 173.40, 166.19, 143.96, 140.91, 138.55, 71.13, 63.82, 56.31, 51.22, 31.78, 30.53, 28.85, 26.74, 26.00, 22.59, 14.13 ppm; IR (ATR) 3123, 3067, 2954, 2929, 2858, 1737, 1696, 1624, 1558, 1454, 1386, 1332, 1292, 1230, 1168, 1145, 1097, 1077, 1017, 878, 812, 780, 714, 670, 634, 613 cm^{-1}; HRMS TOF MS Cl+ exact mass calculated for $C_{32}H_{46}O_4^+$ or $[M]^+$: 494.3396, found: 494.3399.



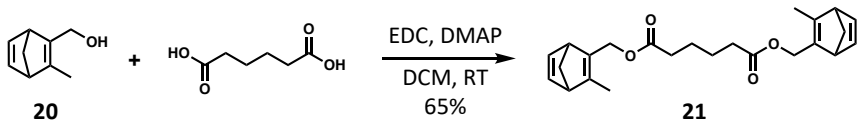
15 18

To a dram vial were added compound **15** (3.5 g, 18.2 mmol, 2.1 eq.) and 1,6-dibromohexane (2.1 g, 8.7 mmol, 1.0 eq.), followed by 7.3 mL triethyl amine (TEA). The reaction was heated to 90 °C for 24 h until completion. The crude product was dissolved in diethyl ether and the triethyl amine hydrobromide salt was filtered via a pad of celite. The solution was concentrated, and the residue was subjected to a flash column chromatography with 6:1 hexanes:EtOAc to afford a transparent oil as the pure product **18** (2.6 g, 64% yield). ^{1}H NMR (500 MHz, $CDCl_3$) δ 6.91 – 6.86 (m, 2H), 6.75 – 6.70 (m, 2H), 4.16 – 4.06 (m, 4H), 3.72 (p, *J* = 1.8 Hz, 4H), 1.96 (dt, *J* = 6.4, 1.7 Hz, 2H), 1.82 (dt, *J* = 6.3, 1.6 Hz, 2H), 1.69 (t, *J* = 6.9 Hz, 4H), 1.43 (dq, *J* = 7.4, 3.4 Hz, 4H), 1.15 (s, 18H) ppm; ^{13}C NMR (126 MHz, $CDCl_3$) δ 172.13, 168.38, 143.65, 141.65, 137.51, 69.89, 64.23, 54.41, 54.18, 34.58, 28.84, 28.69, 25.88 ppm; IR (ATR) 3068, 2952, 2935, 2866, 1705, 1595, 1557, 1461, 1392, 1361, 1310, 1293, 1247, 1225, 1194, 1152, 1085, 1025, 990, 952, 931, 888, 832, 781, 751, 718, 672, 611 cm^{-1}; HRMS TOF MS Cl+ exact mass calculated for $C_{30}H_{42}O_4^+$ or $[M]^+$: 466.3083, found: 466.3085.



16 19

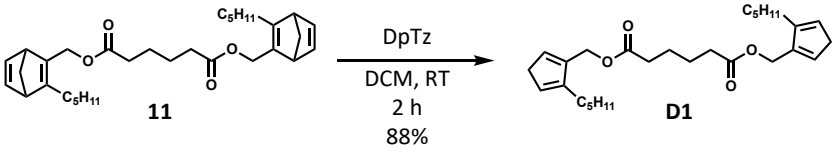
To a dram vial were added compound **16** (5.0 g, 23.6 mmol, 2.2 eq.) and 1,6-dibromohexane (2.6 g, 10.7 mmol, 1.0 eq.), followed by 9.0 mL triethyl amine (TEA). The reaction was heated to 90 °C for 24 h until completion. The crude product was dissolved in diethyl ether and the triethyl amine hydrobromide salt was filtered via a pad of celite. The solution was concentrated, and the residue was subjected to a long flash column chromatography with 10% EtOAc/Hexanes to afford a yellowish oil as the pure product **19** (3.4 g, 6.7 mmol, 63% yield). ^{1}H NMR (500 MHz, $CDCl_3$) δ 7.52 – 7.49 (m, 4H), 7.39 – 7.26 (m, 6H), 7.00 (dd, *J* = 5.1, 3.0 Hz, 2H), 6.96 – 6.90 (m, 2H), 4.06 (ddt, *J* = 10.0, 6.5, 2.8 Hz, 6H), 3.85 (dh, *J* = 2.4, 1.2 Hz, 2H), 2.27 (dt, *J* = 6.6, 1.7 Hz, 2H), 2.07 (dt, *J* = 6.6, 1.6 Hz, 2H), 1.59 – 1.47 (m, 4H), 1.20 (m, 4H) ppm; ^{13}C NMR (126 MHz, $CDCl_3$) δ 166.61, 165.67, 143.83, 140.98, 139.49, 135.98, 128.53, 127.83, 127.77, 70.69, 64.07, 58.70, 53.11, 28.55, 25.80 ppm; IR (ATR) 3067, 2938, 2868, 1687, 1612, 1594, 1573, 1558, 1491, 1444, 1388, 1332, 1294, 1233, 1219, 1179, 1149, 1098, 1080, 1072, 1032, 1023, 992, 906, 811, 760, 727, 716, 648, 600 cm^{-1}; HRMS TOF MS ES+ exact mass calculated for $C_{34}H_{34}O_4Na^+$ or $[M+Na]^+$: 529.2355, found: 529.2345.



20 **21**

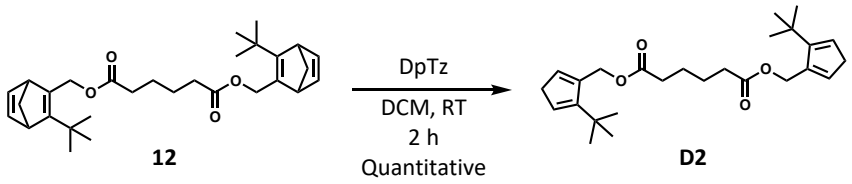
Compound **21** was prepared similar to the procedure for compound **11**, with 200 mg of **20** (0.8 mmol, 2.1 eq.), 59 mg of adipic acid (0.4 mmol, 1.0 eq.), 465 mg of EDC (2.4 mmol, 6.0 eq.), and 20 mg of DMAP (0.2 mmol, 0.4 eq.) in 8 mL DCM. The crude product was subjected

to flash column chromatography with EtOAc:Hexanes as eluent (1:9) to afford the pure product **21** as colorless oil (100 mg, 65% yield). ^{1}H NMR (500 MHz, $CDCl_3$) δ 6.77 (dd, *J* = 5.1, 3.0 Hz, 2H), 6.74 (dd, *J* = 5.1, 3.1 Hz, 2H), 4.71 (d, *J* = 12.3 Hz, 2H), 4.57 (d, *J* = 12.2 Hz, 2H), 3.43 (t, *J* = 2.4 Hz, 2H), 3.28 (t, *J* = 2.4 Hz, 2H), 2.33 (td, *J* = 6.9, 3.4 Hz, 4H), 1.96 (dd, *J* = 6.0, 1.7 Hz, 2H), 1.90 – 1.86 (m, 2H), 1.81 (s, 6H), 1.66 (p, *J* = 3.6 Hz, 4H) ppm; ^{13}C NMR (126 MHz, $CDCl_3$) δ 173.53, 151.64, 143.30, 141.75, 140.82, 71.40, 60.72, 55.86, 52.28, 34.06, 24.61, 14.61 ppm; IR (ATR) 3063, 2963, 2935, 2866, 1728, 1559, 1439, 1418, 1378, 1350, 1291, 1229, 1163, 1136, 1074, 1010, 947, 871, 826, 725, 680, 614, 583 cm^{-1}; HRMS TOF MS ES+ exact mass calculated for $C_{24}H_{30}O_4Na^+$ or $[M+Na]^+$: 405.2042, found: 405.2034.

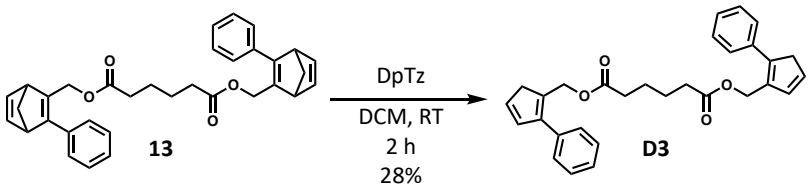


A solution of compound **11** (240 mg, 0.5 mmol, 1.0 eq.) and 3,6-di-2-pyridyl-1,2,4,5-tetrazine (DpTz) (600 mg, 2.5 mmol, 5.5 eq.) in 23 mL DCM was stirred at room temperature for 2 h. The crude solution was passed through a plug of silica with DCM as the eluent to remove excess amount of tetrazine (vibrant pink/red solid) and byproduct pyridazine (vibrant yellowish solid). After the silica plug, concentration of the filtrate afforded the pure product ***distal*-1** (**D1**) as colorless oil (190 mg, 0.4 mmol, 88% yield). ^{1}H NMR (500 MHz, $CDCl_3$) δ 6.35 (s, 2H), 6.06 (d, *J* = 2.8 Hz, 2H), 4.87 (s, 4H), 2.93 – 2.89 (m, 4H), 2.36 (d, *J* = 6.5 Hz,

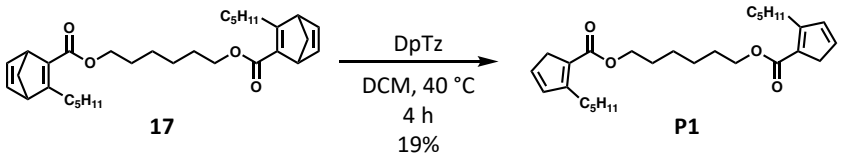
4H), 2.33 – 2.24 (m, 4H), 1.74 – 1.65 (m, 4H), 1.60 – 1.51 (m, 4H), 1.33 (m, 8H), 0.94 – 0.85 (m, 6H) ppm; ^{13}C NMR (126 MHz, $CDCl_3$) δ 173.25, 146.39, 142.24, 132.28, 127.57, 61.11, 39.78, 34.08, 31.92, 28.28, 28.10, 24.57, 22.71, 14.20 ppm; IR (ATR) 3066, 2954, 2926, 2871, 2858, 2740, 1733, 1629, 1560, 1459, 1418, 1377, 1348, 1306, 1260, 1237, 1160, 1138, 1075, 1011, 962, 938, 904, 846, 751, 599 cm^{-1}; HRMS TOF MS ES+ exact mass calculated for $C_{28}H_{42}O_4Na^+$ or $[M+Na]^+$: 465.2981, found: 465.2966.



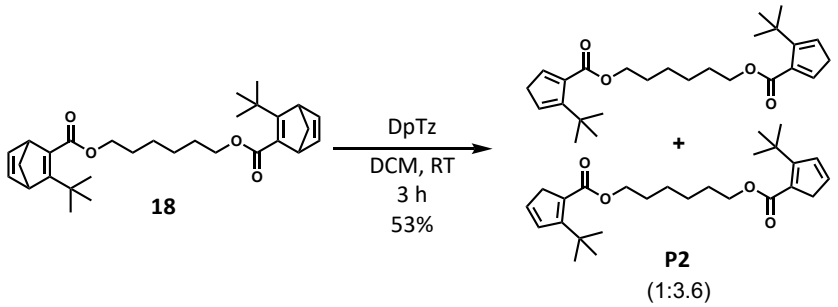
***Distal*-2** (**D2**) was prepared similar to the synthesis of **D1**, with 100 mg of **12** (0.2 mmol, 1.0 eq.) and 280 mg of DpTz (1.2 mmol, 5.5 eq.) in 10 mL DCM. The crude product was subjected to a silica plug with DCM as the eluent. The solution was concentrated to afford the pure product **D2** as colorless oil (quantitative yield). ^{1}H NMR (500 MHz, $CDCl_3$) δ 6.41 (dq, J = 2.8, 1.4 Hz, 2H), 6.09 (q, J = 1.7 Hz, 2H), 5.03 (q, J = 1.7 Hz, 4H), 2.84 (p, J = 1.7 Hz, 4H), 2.40 (m, 4H), 1.76 – 1.67 (m, 4H), 1.22 (s, 18H) ppm; ^{13}C NMR (126 MHz, $CDCl_3$) δ 173.19, 154.73, 142.26, 133.71, 126.55, 62.45, 38.62, 34.15, 32.93, 30.29, 24.55 ppm; IR (ATR) 3073, 2955, 2905, 2870, 2743, 1732, 1461, 1418, 1378, 1362, 1278, 1257, 1235, 1160, 1137, 1076, 1060, 972, 954, 907, 763, 721, 670, 642 cm^{-1}; HRMS TOF MS ES+ exact mass calculated for $C_{26}H_{38}O_4Na^+$ or $[M+Na]^+$: 437.2668, found: 437.2647.



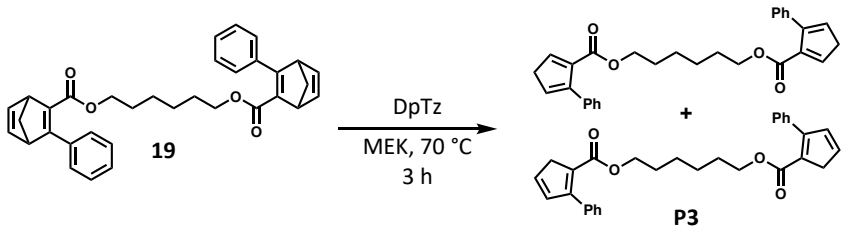
***Distal*-3** (**D3**) was prepared similar to the synthesis of **D1**, with 100 mg of **13** (0.2 mmol, 1.0 eq.) and 256 mg of DpTz (1.1 mmol, 5.5 eq.) in 10 mL DCM. The crude product was subjected to a silica plug with DCM as the eluent. The solution was concentrated to afford the product **D3** as slightly yellowish oil with a small amount of 1,5-H shift isomer (~10%) (25 mg, 0.05 mmol, 28% yield). ^{1}H NMR (500 MHz, $CDCl_3$) δ 7.42 – 7.32 (m, 8H), 7.31 – 7.25 (m, 2H), 6.68 (dt, *J* = 5.4, 1.5 Hz, 0.1H), 6.64 – 6.62 (m, 0.1H), 6.52 (dt, *J* = 2.7, 1.4 Hz, 2H), 6.45 (d, *J* = 2.0 Hz, 2H), 5.03 (s, 0.3H), 5.01 (s, 0.3H), 4.97 (d, *J* = 1.5 Hz, 4H), 4.91 (s, 0.2H), 3.45 (t, *J* = 1.4 Hz, 0.3H), 3.27 (d, *J* = 1.6 Hz, 0.3H), 3.10 (q, *J* = 1.6 Hz, 4H), 2.39 – 2.26 (m, 1H), 2.25 – 2.20 (m, 3H), 1.66 – 1.57 (m, 1H), 1.53 – 1.49 (m, 3H) ppm; ^{13}C NMR (126 MHz, $CDCl_3$) δ 173.05, 146.92, 141.39, 136.53, 133.44, 131.59, 128.49, 127.66, 127.33, 61.15, 40.23, 33.97, 24.42 ppm; IR (ATR) 3056, 3024, 2928, 2870, 1728, 1598, 1572, 1491, 1444, 1416, 1372, 1348, 1312, 1282, 1236, 1156, 1136, 1073, 1031, 959, 911, 886, 835, 758, 697 cm^{-1}; HRMS TOF MS ES+ exact mass calculated for $C_{30}H_{30}O_4Na^+$ or $[M+Na]^+$: 477.2042, found: 477.2053.



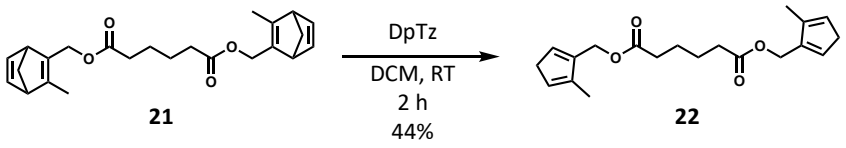
A solution of compound **17** (1.0 g, 2.0 mmol, 1.0 eq.) and DpTz (2.6 g, 11.1 mmol, 5.5 eq.) in 100 mL DCM was stirred at 40 °C for 4 h. The crude solution was passed through a plug of silica with DCM as the eluent to remove excess amount of tetrazine (vibrant pink/red solid) and byproduct pyridazine (vibrant yellowish solid). After the silica plug, concentration of the filtrate afforded the pure product ***proximal*-1** (**P1**) as colorless oil (170 mg, 0.4 mmol, 19% yield). ^{1}H NMR (500 MHz, $CDCl_3$) δ 6.57 (d, *J* = 5.2 Hz, 2H), 6.52 – 6.47 (m, 2H), 4.17 (t, *J* = 6.6 Hz, 4H), 3.32 (m, 4H), 2.85 – 2.78 (m, 4H), 1.71 (t, *J* = 6.9 Hz, 4H), 1.61 – 1.50 (m, 4H), 1.50 – 1.41 (m, 4H), 1.36 – 1.24 (m, 8H), 0.93 – 0.84 (m, 6H) ppm; ^{13}C NMR (126 MHz, $CDCl_3$) δ 165.24, 159.98, 138.21, 136.42, 128.95, 63.68, 43.00, 32.00, 29.19, 28.95, 28.89, 26.07, 22.70, 14.18 ppm; IR (ATR) 3065, 2953, 2926, 2857, 1705, 1636, 1607, 1521, 1433, 1379, 1367, 1309, 1263, 1228, 1211, 1189, 1096, 1038, 961, 926, 896, 840, 785, 752, 728, 683, 616 cm^{-1}; HRMS TOF MS ES+ exact mass calculated for $C_{28}H_{42}O_4Na^+$ or $[M+Na]^+$: 465.2981, found: 465.2966.



A solution of compound **18** (100 mg, 0.2 mmol, 1.0 eq.) and DpTz (278 mg, 1.2 mmol, 5.5 eq.) in 10 mL DCM was stirred at RT for 3 h. The crude solution was passed through a plug of silica with DCM as the eluent. Concentration of the filtrate afforded product ***proximal-2*** (**P2**) as a mixture of 2 major isomers (1:3.6) (47 mg, 0.1 mmol, 53% yield). ^{1}H NMR (500 MHz, $CDCl_3$) δ 7.17 (dd, *J* = 2.6, 1.3 Hz, 0.6H), 6.67 (dd, *J* = 5.4, 1.4 Hz, 2H), 6.50 (dt, *J* = 5.4, 1.3 Hz, 2H), 6.13 – 6.06 (m, 0.6H), 4.20 (td, *J* = 6.7, 1.7 Hz, 2H), 4.15 (t, *J* = 6.6 Hz, 4H), 3.36 (d, *J* = 1.4 Hz, 4H), 2.94 (t, *J* = 1.6 Hz, 1H), 1.71 (m, 8H), 1.49 – 1.39 (m, 7H), 1.35 (s, 18H), 1.28 (s, 8H) ppm; ^{13}C NMR (126 MHz, $CDCl_3$) δ 166.32, 165.59, 164.76, 144.50, 136.62, 135.15, 129.04, 126.53, 64.57, 64.00, 45.34, 39.12, 33.64, 33.09, 29.85, 29.81, 28.82, 28.74, 25.99, 25.82, 23.48, 14.26 ppm; IR (ATR) 2952, 2867, 1706, 1586, 1510, 1463, 1361, 1306, 1265, 1221, 1206, 1156, 1123, 1085, 1036, 986, 893, 813, 791, 753, 728, 690, 650 cm^{-1}; HRMS TOF MS ES+ exact mass calculated for $C_{26}H_{38}O_4Na^+$ or $[M+Na]^+$: 437.2668, found: 437.2647.

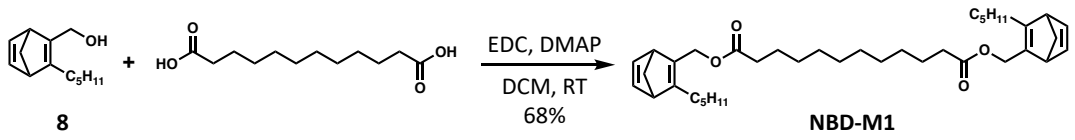


A solution of compound **19** (500 mg, 1.0 mmol, 1.0 eq.) and DpTz (1.3 g, 5.4 mmol, 5.5 eq.) in 50 mL methyl ethyl ketone (MEK) was stirred at 70 °C for 3 h. The crude solution was passed through a plug of silica with DCM. Concentration of the filtrate afforded the crude product mixture of ***proximal*-3** (**P3**), which was subjected to polymerization without further purification.



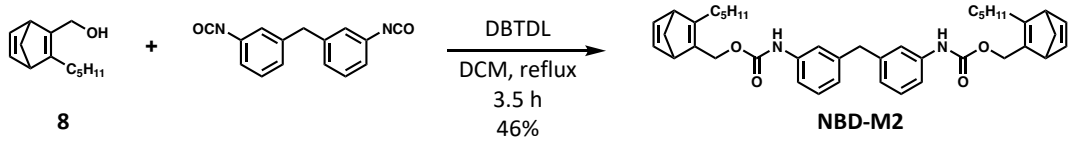
Compound **22** was prepared similar to the synthesis of ***distal*-1**, with 90 mg of **21** (0.2 mmol, 1.0 eq.) and 306 mg of DpTz (1.3 mmol, 5.5 eq.) in 12 mL DCM. The crude product was subjected to a silica plug with DCM as the eluent. The solution was concentrated to afford the pure product **22** as colorless oil (35 mg, 44% yield). ^{1}H NMR (500 MHz, $CDCl_3$) δ 6.35 (s, 2H), 6.08 – 6.05 (m, 2H), 4.87 (d, J = 1.8 Hz, 4H), 2.90 (p, J = 1.7 Hz, 4H), 2.40 – 2.32 (m, 4H), 1.97 (q, J = 1.9 Hz, 6H), 1.74 – 1.66 (m, 4H) ppm; ^{13}C NMR (126 MHz, $CDCl_3$) δ 173.26, 142.36, 141.48, 132.34, 128.92, 61.09, 39.83, 34.07, 24.56, 13.76 ppm; IR (ATR) 3063, 2940, 2875, 1729, 1634, 1564, 1450, 1419, 1378, 1349, 1235, 1160, 1137, 1075, 957,

934, 903, 754, 693, 589 cm^{-1}; HRMS TOF MS ES+ exact mass calculated for $C_{20}H_{26}O_4Na^+$ or $[M+Na]^+$: 353.1729, found: 353.1715.



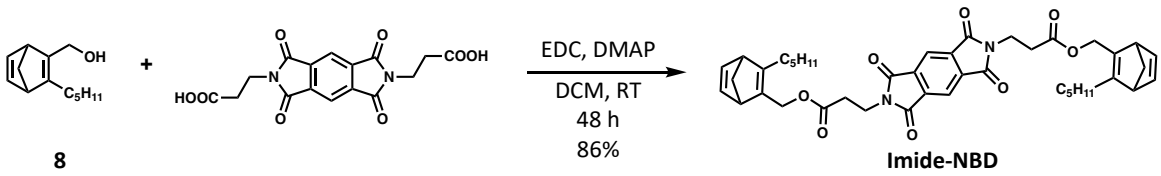
To a dried 250 mL round bottom flask were added compound **8** (918 mg, 4.8 mmol, 2.2 eq.), 1,12-dodecanedioic acid (500 mg, 2.2 mmol, 1.0 eq.) and 40 mL DCM. To this solution were added EDC (2.5 g, 13.0 mmol, 6.0 eq.) and DMAP (80 mg, 0.7 mmol, 0.3 eq.). Once added, the solution was allowed to stir at room temperature for 24 h. The crude solution was washed with water followed by brine solution until the organic layer became clear. The organic layer was dried over Na_2SO_4 and concentrated. The crude residue was subjected to flash column chromatography with 1:6, EtOAc:hexanes to afford the pure product **NBD-M1** as a colorless oil (850 mg, 1.5 mmol, 68% yield). ^{1}H NMR (500 MHz, $CDCl_3$) δ 6.75 (dd, *J* = 5.2, 3.0 Hz, 2H), 6.69 (dd, *J* = 5.1, 3.1 Hz, 2H), 4.71 (d, *J* = 12.3 Hz, 2H), 4.56 (d, *J* = 12.3 Hz, 2H), 3.43 (t, *J* = 2.4 Hz, 2H), 3.36 (t, *J* = 2.3 Hz, 2H), 2.28 (t, *J* = 7.5 Hz, 4H), 2.22 (ddd, *J* = 14.3, 8.2, 6.4 Hz, 2H), 2.14 (dt, *J* = 14.0, 7.4 Hz, 2H), 1.93 (d, *J* = 5.9 Hz, 2H), 1.88 (d, *J* = 6.0 Hz, 2H), 1.61 (dq, *J* = 14.6, 7.2, 6.3 Hz, 4H), 1.43 – 1.23 (m, 20H), 1.17 (m, 4H), 0.86 (t, *J* = 7.3 Hz, 6H) ppm; ^{13}C NMR (126 MHz, $CDCl_3$) δ 174.07, 155.32, 143.03, 142.08, 141.28, 71.45, 60.59, 53.92, 52.31, 34.51, 31.53, 29.55, 29.39, 29.28, 28.47, 27.02, 25.20, 22.62, 14.17 ppm; IR (ATR) 3120, 3064, 2955, 2926, 2855, 1732, 1458, 1378, 1347, 1289,

1229, 1163, 1045, 957, 914, 872, 852, 828, 730, 685, 648, 574 cm^{-1}; HRMS TOF MS ES+ exact mass calculated for $C_{38}H_{58}O_4Na^+$ or $[M+Na]^+$: 601.4233, found: 601.4233.



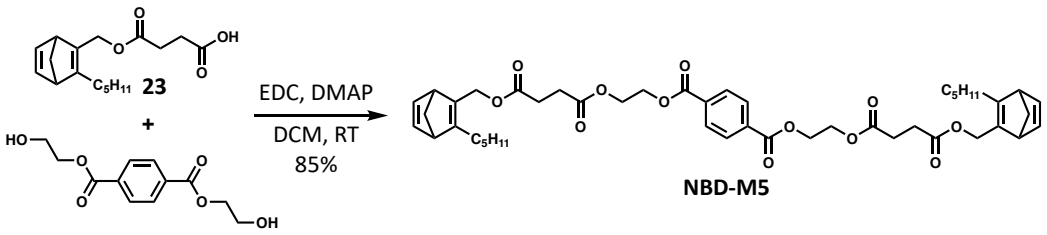
To a flame-dried 100 mL round bottom flask was added methylene diphenyl diisocyanate (MDI) (592 mg, 2.4 mmol, 1.0 eq.) and dibutyltin dilaurate (DBTDL) (30 mg, 0.05 mmol, 2 mol%) in 15 mL DCM. Another solution of alcohol NBD **8** (960 mg, 5.0 mmol, 2.1 eq.) in 15 mL DCM was added dropwise to the flask with MDI and DBTDL. The reaction was then stirred at 60 °C (reflux) for 3.5 h. The reaction was quenched with water and extracted with DCM (x2). The organic solution was washed with brine solution, dried with Na_2SO_4, and concentrated. The crude product was subjected to a column chromatography with 1:6 EtOAc:Hexanes to afford the pure product **NBD-M2** as white solid (695 mg, 1.1 mmol, 46% yield). ^{1}H NMR (500 MHz, $CDCl_3$) δ 7.28 (d, *J* = 8.0 Hz, 4H), 7.13 – 7.06 (m, 4H), 6.79 (dd, *J* = 5.2, 3.0 Hz, 2H), 6.72 (dd, *J* = 5.2, 3.0 Hz, 2H), 6.52 (s, 2H), 4.81 (d, *J* = 12.1 Hz, 2H), 4.64 (d, *J* = 12.1 Hz, 2H), 3.89 (s, 2H), 3.50 (t, *J* = 2.4 Hz, 2H), 3.39 (t, *J* = 2.4 Hz, 2H), 2.25 (ddd, *J* = 14.4, 8.4, 6.4 Hz, 2H), 2.17 (ddd, *J* = 14.1, 8.2, 6.5 Hz, 2H), 1.96 (dt, *J* = 6.0, 1.8 Hz, 2H), 1.91 (dt, *J* = 6.0, 1.7 Hz, 2H), 1.46 – 1.14 (m, 12H), 0.87 (t, *J* = 7.3 Hz, 6H) ppm; ^{13}C NMR (126 MHz, $CDCl_3$) δ 155.87, 153.93, 143.09, 142.12, 141.21, 136.33, 136.19, 129.50, 118.97, 71.55, 61.51, 53.94, 53.54, 52.25, 40.65, 31.52, 28.47, 27.03, 22.59, 14.15

ppm; IR (ATR) 3317, 3120, 3062, 2956, 2927, 2857, 1699, 1596, 1519, 1411, 1378, 1306, 1272, 1214, 1201, 1149, 1120, 1042, 1016, 966, 911, 870, 844, 814, 767, 721, 676, 648, 613, 545 cm^{-1}; HRMS TOF MS ES+ exact mass calculated for $C_{41}H_{50}N_2O_4Na^+$ or $[M+Na]^+$: 657.3668, found: 657.3643.



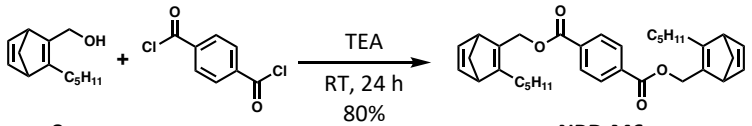
To a dried 150 mL round bottom flask were added compound **8** (1.2 g, 6.1 mmol, 2.2 eq.), *N,N′*-Bis(2-carboxyethyl)pyromellitimide (1.0 g, 2.8 mmol, 1.0 eq.) and 6 mL DCM. To this solution were added EDC (3.2 g, 16.7 mmol, 6.0 eq.) and DMAP (140 mg, 1.1 mmol, 0.4 eq.). Once added, the solution was allowed to stir at room temperature for 48 h. The crude solution was washed with water followed by brine solution until the organic layer became clear. The organic layer was dried over Na_2SO_4 and concentrated. The crude residue was recrystallized in hexanes to afford the pure product **imide-NBD** as a white powder (1.7 g, 2.4 mmol, 86% yield). ^{1}H NMR (500 MHz, $CDCl_3$) δ 8.28 (s, 2H), 6.71 (ddd, *J* = 5.3, 3.0, 0.8 Hz, 2H), 6.66 (ddd, *J* = 5.2, 3.0, 0.9 Hz, 2H), 4.71 (d, *J* = 12.2 Hz, 2H), 4.57 (d, *J* = 12.2 Hz, 2H), 4.05 (t, *J* = 7.1 Hz, 4H), 3.41 (m, 2H), 3.38 – 3.32 (m, 2H), 2.77 (t, *J* = 7.2 Hz, 4H), 2.21 (ddd, *J* = 14.3, 8.3, 6.3 Hz, 2H), 2.12 (ddd, *J* = 13.7, 8.3, 6.6 Hz, 2H), 1.89 (dt, *J* = 5.9, 1.7 Hz, 2H), 1.86 (dt, *J* = 6.0, 1.7 Hz, 2H), 1.44 – 1.23 (m, 8H), 1.22 – 1.11 (m, 4H), 0.86 (t, *J* = 7.3 Hz, 6H) ppm; ^{13}C NMR (126 MHz, $CDCl_3$) δ 170.70, 165.93, 156.20, 142.98, 142.10, 140.69, 137.34,

118.56, 71.49, 61.44, 53.96, 52.26, 34.62, 32.70, 31.55, 28.50, 26.99, 22.61, 14.18 ppm; IR (ATR) 3073, 2970, 2951, 2923, 2869, 2852, 1772, 1725, 1704, 1458, 1446, 1408, 1379, 1338, 1309, 1267, 1249, 1171, 1149, 1113, 1007, 961, 943, 918, 909, 865, 834, 802, 781, 724, 716, 687, 657, 617, 601, 577, 557 cm^{-1}; HRMS TOF MS ESI exact mass calculated for $C_{42}H_{48}N_2O_8Na^+$ or $[M+Na]^+$: 731.3308, found: 731.3292.



To a dried 20 mL vial were added compound **23** (200 mg, 0.7 mmol, 2.1 eq.), bis(2-hydroxyethyl) terephthalate (83 mg, 0.3 mmol, 1.0 eq.) and 6 mL DCM. To this solution were added EDC (345 mg, 1.8 mmol, 6.0 eq.) and DMAP (15 mg, 0.1 mmol, 0.4 eq.). Once added, the solution was allowed to stir at room temperature for 24 h. The crude solution was washed with water followed by brine solution until the organic layer became clear. The organic layer was dried over Na_2SO_4 and concentrated. The crude residue was subjected to a column chromatography with 1:9 EtOAc:Hexanes to afford the pure product **NBD-M5** as colorless oil (204 mg, 85% yield). ^{1}H NMR (500 MHz, $CDCl_3$) δ 8.12 (s, 4H), 6.74 (dd, *J* = 5.2, 3.0 Hz, 2H), 6.69 (dd, *J* = 5.2, 3.0 Hz, 2H), 4.73 (d, *J* = 12.2 Hz, 2H), 4.58 – 4.54 (m, 6H), 4.46 (dd, *J* = 6.0, 3.5 Hz, 4H), 3.42 (t, *J* = 2.4 Hz, 2H), 3.36 (t, *J* = 2.4 Hz, 2H), 2.66 (dq, *J* = 10.6, 5.7 Hz, 8H), 2.21 (m, 2H), 2.16 – 2.07 (m, 2H), 1.93 (dd, *J* = 5.9, 1.6 Hz, 2H), 1.87 (dt, *J* =

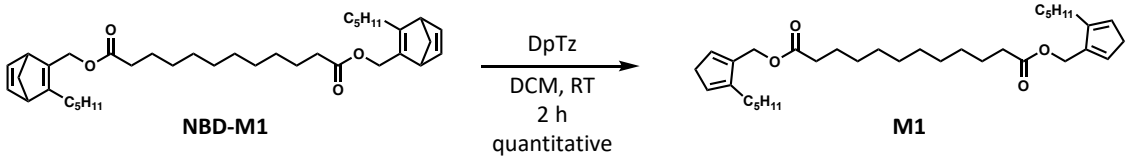
6.0, 1.6 Hz, 2H), 1.43 – 1.35 (m, 2H), 1.28 (m, 6H), 1.16 (m, 4H), 0.86 (t, J = 7.3 Hz, 6H) ppm; ^{13}C NMR (126 MHz, $CDCl_3$) δ 172.33, 172.27, 165.62, 155.79, 143.03, 142.11, 140.95, 133.89, 129.88, 71.47, 63.24, 62.42, 61.19, 53.94, 52.24, 31.53, 29.18, 29.17, 28.48, 27.00, 22.61, 14.17 ppm; IR (ATR) 3064, 2957, 2929, 2859, 1723, 1578, 1556, 1505, 1409, 1377, 1348, 1267, 1208, 1155, 1120, 1101, 1017, 949, 913, 873, 829, 728, 648, 561 cm^{-1}; HRMS TOF MS ES+ exact mass calculated for $C_{46}H_{58}O_{12}Na^+$ or $[M+Na]^+$: 825.3826, found: 825.3862.



8 NBD-M6

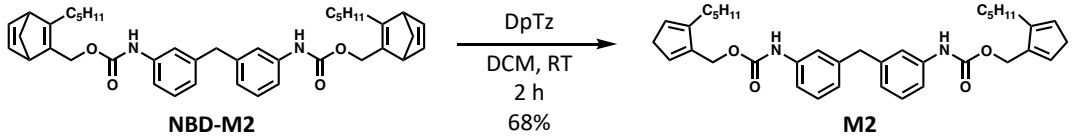
To a flame-dried 100 mL round bottom flask was added the alcohol **8** (7.8 g, 40.6 mmol, 2.0 eq.) and 7.1 mL TEA (50.7 mmol, 2.5 eq.) in 300 mL dried THF. The solution was cooled to 0 °C and stirred. Another solution of terephthaloyl dichloride (4.1 g, 20.3 mmol, 1.0 eq.) in 100 mL THF was then added dropwise. The reaction was continued at RT. After 24 h, the crude mixture was filtered through celite to remove the triethyl amine hydrochloride salt. The THF was then removed and exchanged for diethyl ether. The organic layer was washed with 1M HCl and saturated sodium bicarbonate, followed by brine solution. The organic solution was dried with sodium sulfate, concentrated and the crude product was subjected to a flash column chromatography with EtOAc:hexanes (10%). After purification, 7.5 g of pure product **NBD-M6** was obtained (80% yield). ^{1}H NMR (500 MHz, $CDCl_3$) δ 8.07 (s, 4H), 6.78 (ddd, J

= 5.2, 3.0, 0.8 Hz, 2H), 6.72 (ddd, *J* = 5.2, 3.0, 0.9 Hz, 2H), 4.99 (d, *J* = 12.3 Hz, 2H), 4.85 (d, *J* = 12.2 Hz, 2H), 3.54 (p, *J* = 2.0 Hz, 2H), 3.41 (t, *J* = 2.3 Hz, 2H), 2.29 (ddd, *J* = 14.2, 8.1, 6.3 Hz, 2H), 2.21 (ddd, *J* = 13.8, 8.1, 6.8 Hz, 2H), 2.00 (dt, *J* = 5.9, 1.7 Hz, 2H), 1.92 (dt, *J* = 5.9, 1.7 Hz, 2H), 1.48 – 1.31 (m, 4H), 1.31 – 1.25 (m, 4H), 1.24 – 1.14 (m, 4H), 0.85 (t, *J* = 7.2 Hz, 6H) ppm; ^{13}C NMR (126 MHz, $CDCl_3$) δ 166.00, 156.23, 143.04, 142.15, 140.90, 134.37, 129.63, 71.55, 61.78, 54.05, 52.44, 31.55, 28.60, 27.01, 22.63, 14.17 ppm; IR (ATR) 3120, 3064, 2957, 2928, 2858, 1716, 1662, 1577, 1556, 1504, 1457, 1408, 1368, 1288, 1261, 1244, 1172, 1149, 1096, 1018, 931, 873, 826, 795, 727, 676, 640, 579 cm^{-1}; HRMS TOF MS ES+ exact mass calculated for $C_{34}H_{42}O_4Na^+$ or $[M+Na]^+$: 537.2981, found: 537.2983.



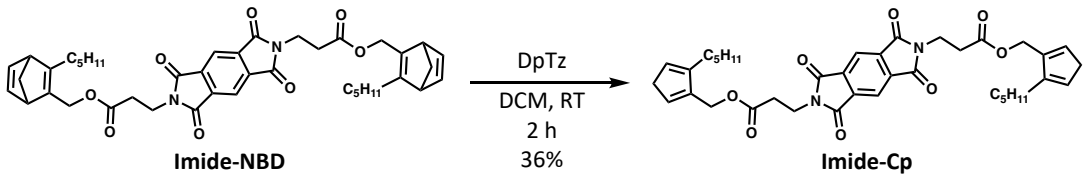
A solution of compound **NBD-M1** (300 mg, 0.5 mmol, 1.0 eq.) and DpTz (690 mg, 2.9 mmol, 5.5 eq.) in 30 mL DCM was stirred at room temperature for 2 h. The crude solution was passed through a plug of silica with DCM as the eluent. After the silica plug, concentration of the filtrate afforded the pure product **M1** as a white waxy solid (270 mg, quantitative yield). ^{1}H NMR (500 MHz, $CDCl_3$) δ 6.36 (s, 2H), 6.06 (d, *J* = 2.5 Hz, 2H), 4.87 (s, 4H), 2.91 (s, 4H), 2.33 (t, *J* = 7.5 Hz, 4H), 2.31 – 2.26 (m, 4H), 1.63 (p, *J* = 7.4 Hz, 4H), 1.56 (p, *J* = 7.2 Hz, 4H), 1.36 – 1.32 (m, 7H), 1.29 – 1.24 (m, 13H), 0.92 – 0.88 (m, 6H) ppm; ^{13}C NMR (126 MHz, $CDCl_3$) δ 173.85, 146.47, 142.35, 132.25, 127.53, 61.00, 39.77, 34.54,

31.95, 29.54, 29.40, 29.31, 28.29, 28.10, 25.15, 22.72, 14.21 ppm; IR (ATR) 3067, 2924, 2854, 2740, 1734, 1629, 1559, 1460, 1418, 1377, 1345, 1259, 1237, 1259, 1237, 1161, 1100, 1053, 962, 939, 904, 845, 749, 731, 648, 599 cm^{-1}; HRMS TOF MS ES+ exact mass calculated for $C_{34}H_{54}O_4Na^+$ or $[M+Na]^+$: 549.3920, found: 549.3929.



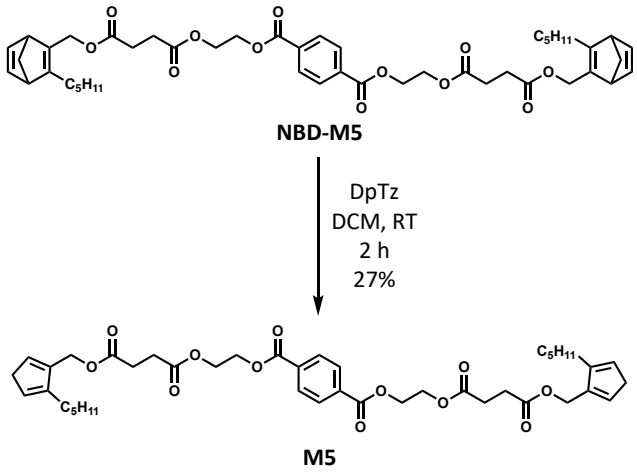
NBD-M2 **M2**

A solution of compound **NBD-M2** (300 mg, 0.5 mmol, 1.0 eq.) and DpTz (614 mg, 2.6 mmol, 5.5 eq.) in 24 mL DCM was stirred at room temperature for 2 h. The crude solution was passed through a plug of silica with DCM as the eluent. After the silica plug, concentration of the filtrate afforded the pure product **M2** as a white powder (185 mg, 0.3 mmol, 68% yield). ^1H NMR (500 MHz, $CDCl_3$) δ 7.29 (d, *J* = 8.1 Hz, 4H), 7.10 (d, *J* = 8.2 Hz, 4H), 6.58 (s, 2H), 6.41 (s, 2H), 6.08 (q, *J* = 1.9 Hz, 2H), 4.96 (s, 4H), 3.89 (s, 2H), 2.93 (t, *J* = 1.8 Hz, 4H), 2.36 – 2.28 (m, 4H), 1.58 (d, *J* = 8.4 Hz, 4H), 1.34 (m, 8H), 0.93 – 0.86 (m, 6H) ppm; ^{13}C NMR (126 MHz, $CDCl_3$) δ 146.41, 142.39, 136.52, 136.05, 132.57, 129.59, 127.61, 119.01, 61.80, 40.69, 39.85, 31.93, 28.31, 28.09, 22.73, 14.21 ppm; IR (ATR) 3367, 3066, 3041, 2961, 2951, 2921, 2871, 2857, 2752, 1704, 1612, 1596, 1533, 1463, 1437, 1415, 1380, 1311, 1288, 1258, 1230, 1212, 1196, 1112, 1099, 1073, 1019, 963, 940, 911, 846, 821, 789, 777, 763, 728, 634, 615 cm^{-1}; HRMS TOF MS ES+ exact mass calculated for $C_{37}H_{46}N_2O_4Na^+$ or $[M+Na]^+$: 605.3355, found: 605.3334.

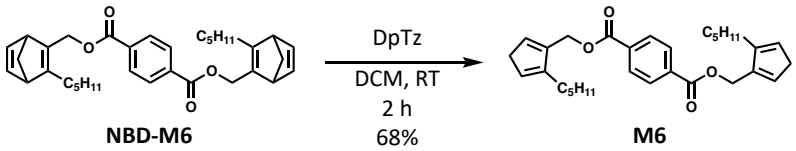


Imide-NBD **Imide-Cp**

A solution of compound **imide-NBD** (300 mg, 0.42 mmol, 1.0 eq.) and DpTz (550 mg, 2.3 mmol, 5.5 eq.) in 24 mL DCM was stirred at room temperature for 2 h. The crude solution was passed through a plug of silica with DCM as the eluent. After the silica plug, concentration of the filtrate afforded the pure product **imide-Cp** as a white powder (100 mg, 36%). ^{1}H NMR (500 MHz, $CDCl_3$) δ 8.25 (s, 2H), 6.34 (s, 2H), 6.02 (d, J = 2.7 Hz, 2H), 4.87 (s, 4H), 4.07 (t, J = 7.1 Hz, 4H), 2.87 (s, 4H), 2.81 (t, J = 7.1 Hz, 4H), 2.28 – 2.20 (m, 4H), 1.52 (t, J = 7.6 Hz, 4H), 1.32 (m, 8H), 0.93 – 0.85 (m, 6H) ppm; ^{13}C NMR (126 MHz, $CDCl_3$) δ 170.49, 165.93, 146.28, 141.74, 137.30, 132.85, 127.58, 118.53, 61.62, 39.82, 34.55, 32.70, 31.89, 28.25, 28.05, 22.71, 14.20 ppm; IR (ATR) 3035, 2953, 2921, 2871, 2857, 1772, 1728, 1702, 1559, 1461, 1444, 1437, 1404, 1382, 1336, 1319, 1290, 1254, 1193, 1156, 1118, 1065, 1008, 969, 953, 940, 914, 832, 805, 779, 723, 598, 560 cm^{-1}; HRMS TOF MS ESI exact mass calculated for $C_{38}H_{44}N_2O_8Na^+$ or $[M+Na]^+$: 679.2996, found: 679.2988.



A solution of compound **NBD-M5** (300 mg, 0.4 mmol, 1.0 eq.) and DpTz (485 mg, 2.1 mmol, 5.5 eq.) in 18 mL DCM was stirred at room temperature for 2 h. The crude solution was passed through a plug of silica with DCM as the eluent to remove the excess DpTz reagent. The yellowish by-product was also collected. The mixture was then concentrated and washed with hexanes to afford the pure product **M5** as white solid (77 mg, 27% yield). ^{1}H NMR (500 MHz, $CDCl_3$) δ 8.11 (d, J = 2.1 Hz, 4H), 6.35 (m, 2H), 6.05 (m, 2H), 4.88 (d, J = 1.6 Hz, 4H), 4.56 – 4.52 (m, 4H), 4.47 – 4.43 (m, 4H), 2.90 (p, J = 1.8 Hz, 4H), 2.69 (s, 8H), 2.30 – 2.23 (m, 4H), 1.55 – 1.50 (m, 4H), 1.33 (m, 8H), 0.95 – 0.81 (m, 6H) ppm. ^{13}C NMR (126 MHz, $CDCl_3$) δ 172.20, 172.12, 165.63, 146.32, 142.01, 133.88, 132.37, 129.88, 127.60, 63.23, 62.45, 61.50, 39.80, 31.90, 29.21, 29.13, 28.27, 28.05, 22.71, 14.21 ppm; IR (ATR) 3065, 2955, 2928, 2872, 2858, 1722, 1505, 1456, 1409, 1377, 1348, 1267, 1248, 1208, 1153, 1120, 1101, 1042, 1017, 961, 938, 905, 875, 728, 648 cm^{-1}; HRMS TOF MS ES+ exact mass calculated for $C_{42}H_{54}O_{12}Na^+$ or $[M+Na]^+$: 773.3513, found: 773.3499.



NBD-M6 **M6**

A solution of compound **NBD-M6** (6.4 g, 12.4 mmol, 1.0 eq.) and DpTz (14.7 g, 62.2 mmol, 5.0 eq.) in 500 mL DCM was stirred at room temperature for 2 h. The crude solution was passed through a plug of silica with DCM as the eluent to remove the excess DpTz reagent and yellowish by-product. The solution was then concentrated to afford the pure product **M6** as white solid (3.9 g, 68% yield). ^{1}H NMR (500 MHz, $CDCl_3$) δ 8.12 (s, 4H), 6.47 (s, 2H), 6.10 (q, J = 1.9 Hz, 2H), 5.15 (d, J = 1.7 Hz, 4H), 2.97 – 2.93 (m, 4H), 2.39 – 2.32 (m, 4H), 1.63 – 1.56 (m, 4H), 1.32 (m, 8H), 0.91 – 0.85 (m, 6H) ppm. ^{13}C NMR (126 MHz, $CDCl_3$) δ 165.78, 146.41, 141.99, 134.24, 132.78, 129.77, 127.73, 62.10, 39.87, 31.92, 28.36, 28.20, 22.70, 14.18 ppm; IR (ATR) 3065, 2961, 2951, 2920, 2870, 2856, 1715, 1504, 1466, 1456, 1405, 1378, 1322, 1273, 1241, 1126, 1106, 1018, 964, 943, 914, 873, 821, 776, 721, 639, 541 cm^{-1}; HRMS TOF MS ES+ exact mass calculated for $C_{30}H_{38}O_4Na^+$ or $[M+Na]^+$: 485.2668, found: 485.2690.

Examples of the Alder-ene rearranged by-products:

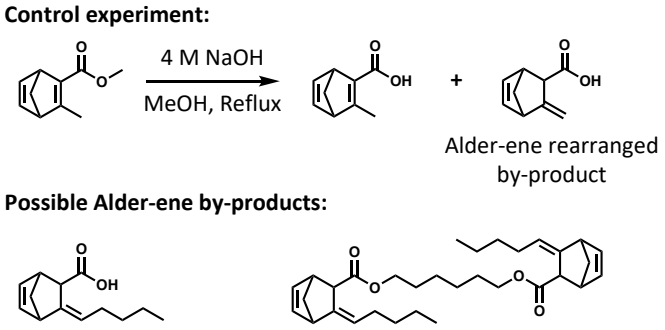


Figure S3.1. Synthesis of the methyl-substituted NBD analog via basic hydrolysis produces the Alder-ene rearranged by-product overtime. The ^{1}H NMR of the *endo*- and *exo*- methyl-substituted by-product was compared to literature[74] and the structure was confirmed. Based on this control experiment, some possible by-products can be produced via the unsuccessful routes (i.e., Fisher and Steglich esterification, transesterification, Yamaguchi reaction, etc.).

^{1}H and ^{13}C NMR spectra:

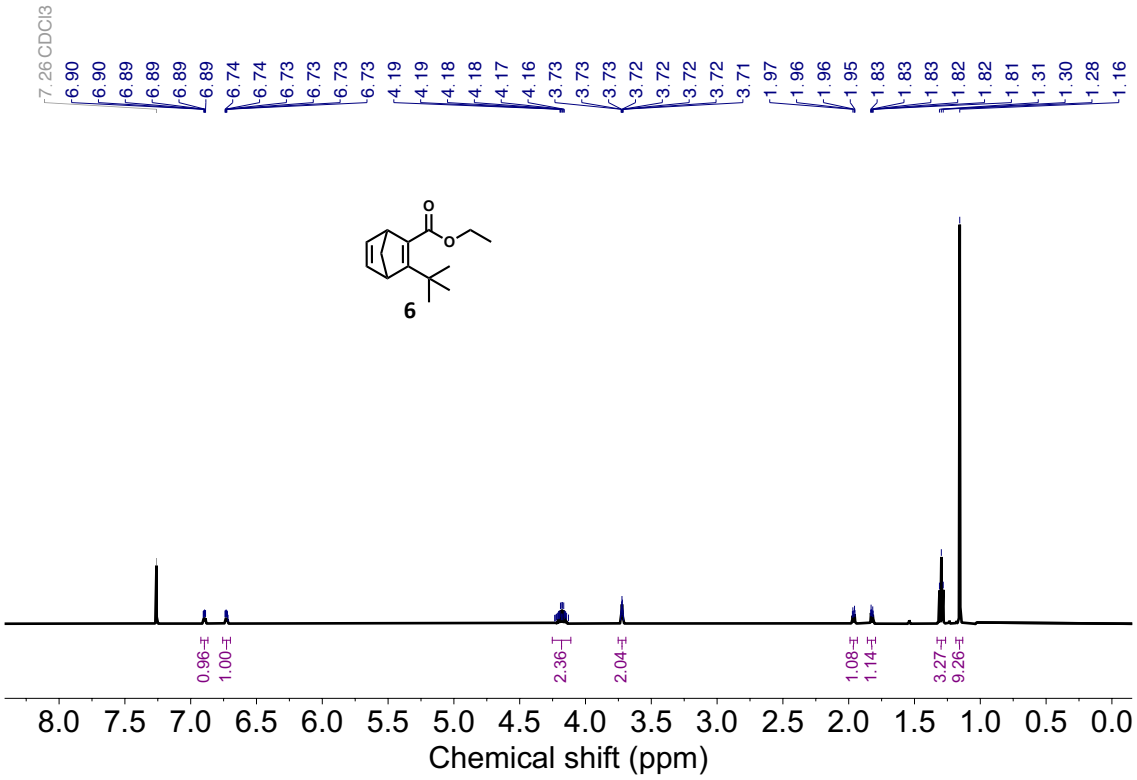


Figure S3.2. ^{1}H NMR spectrum of compound **6** in $CDCl_3$.

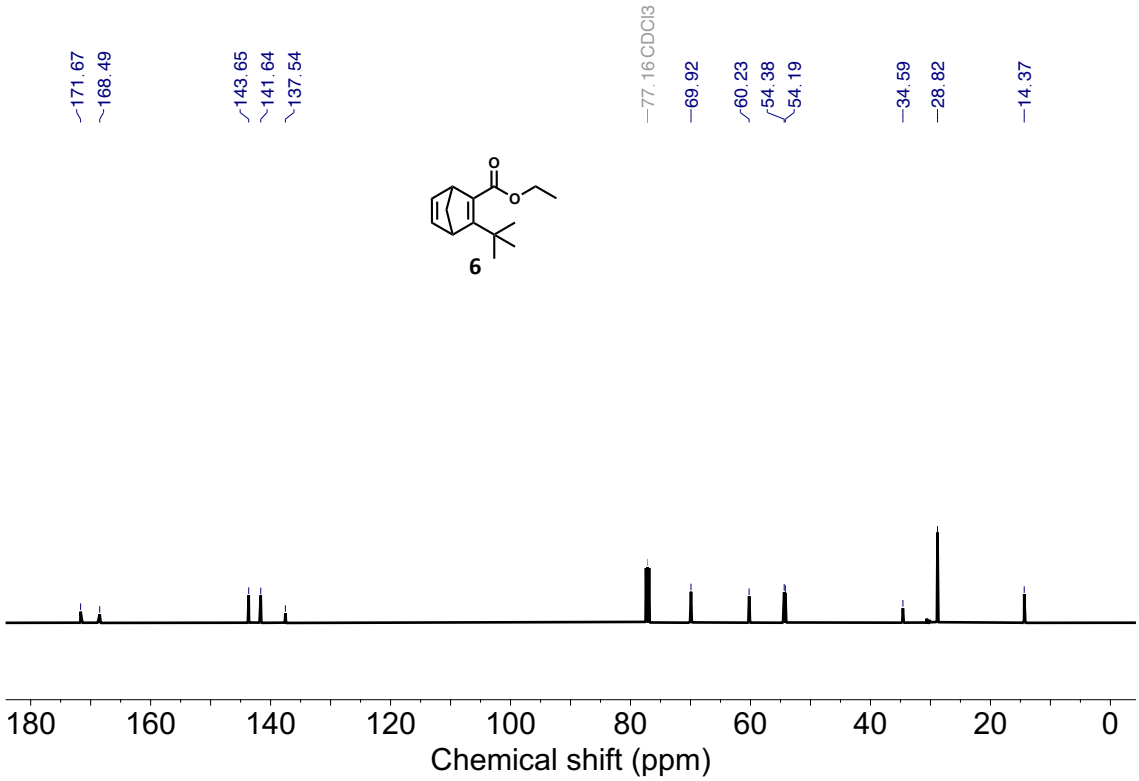


Figure S3.3. ^{13}C NMR spectrum of compound **6** in $CDCl_3$.

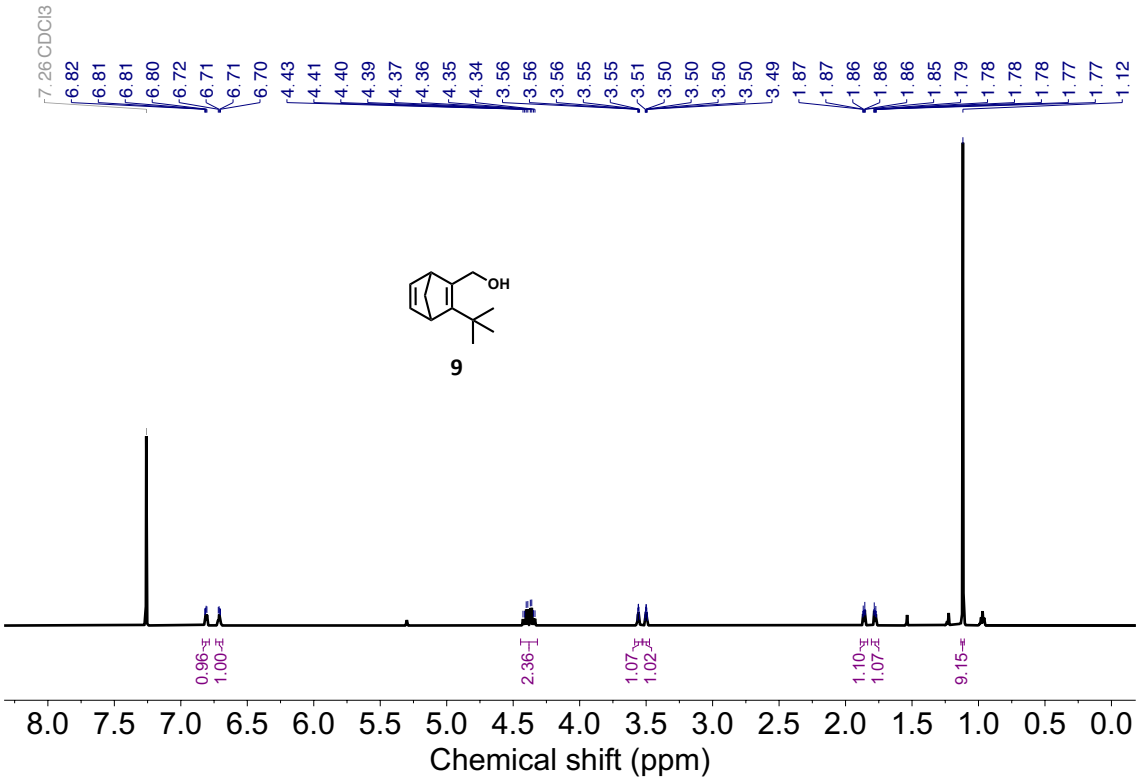


Figure S3.4. ^{1}H NMR spectrum of compound **9** in $CDCl_3$.

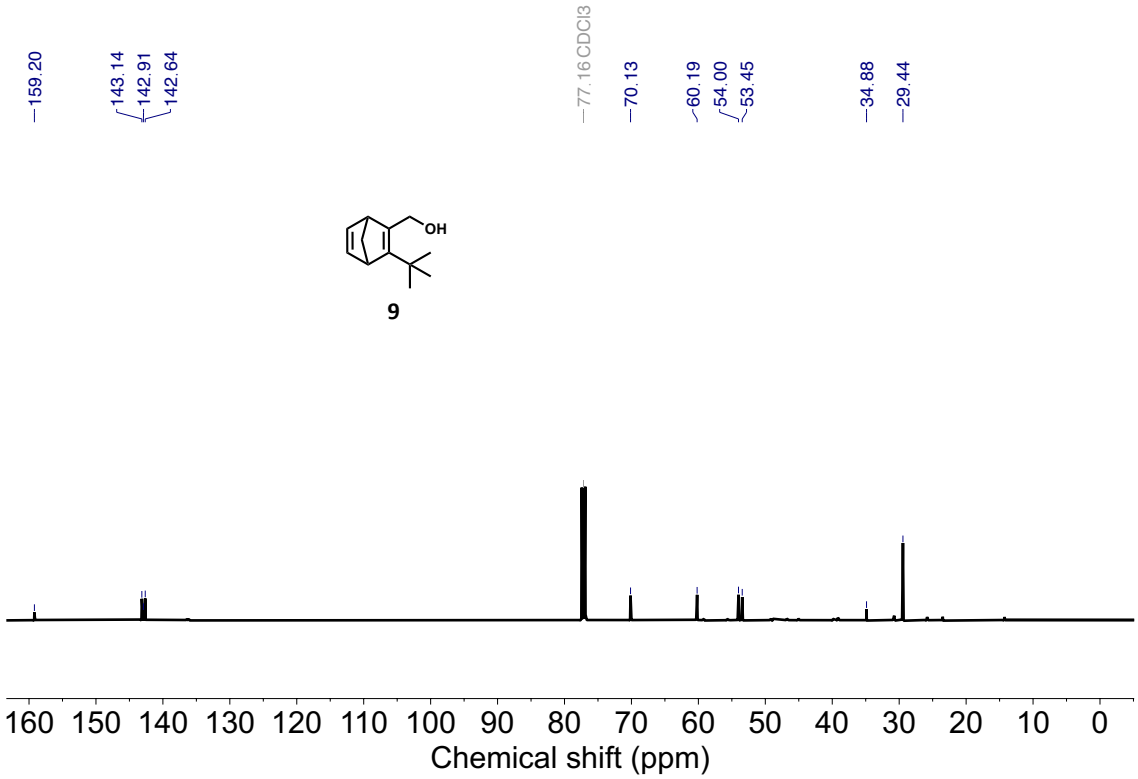


Figure S3.5. ^{13}C NMR spectrum of compound **9** in $CDCl_3$.

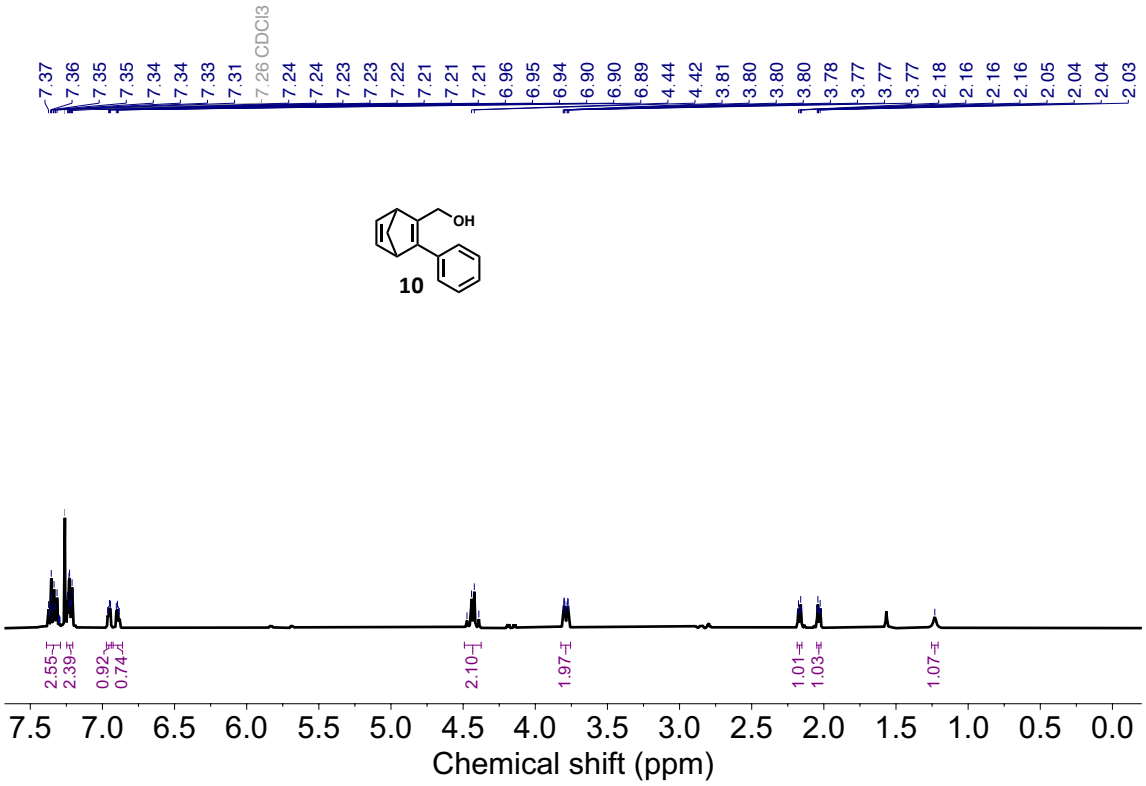


Figure S3.6. ^{1}H NMR spectrum of compound **10** in $CDCl_3$.

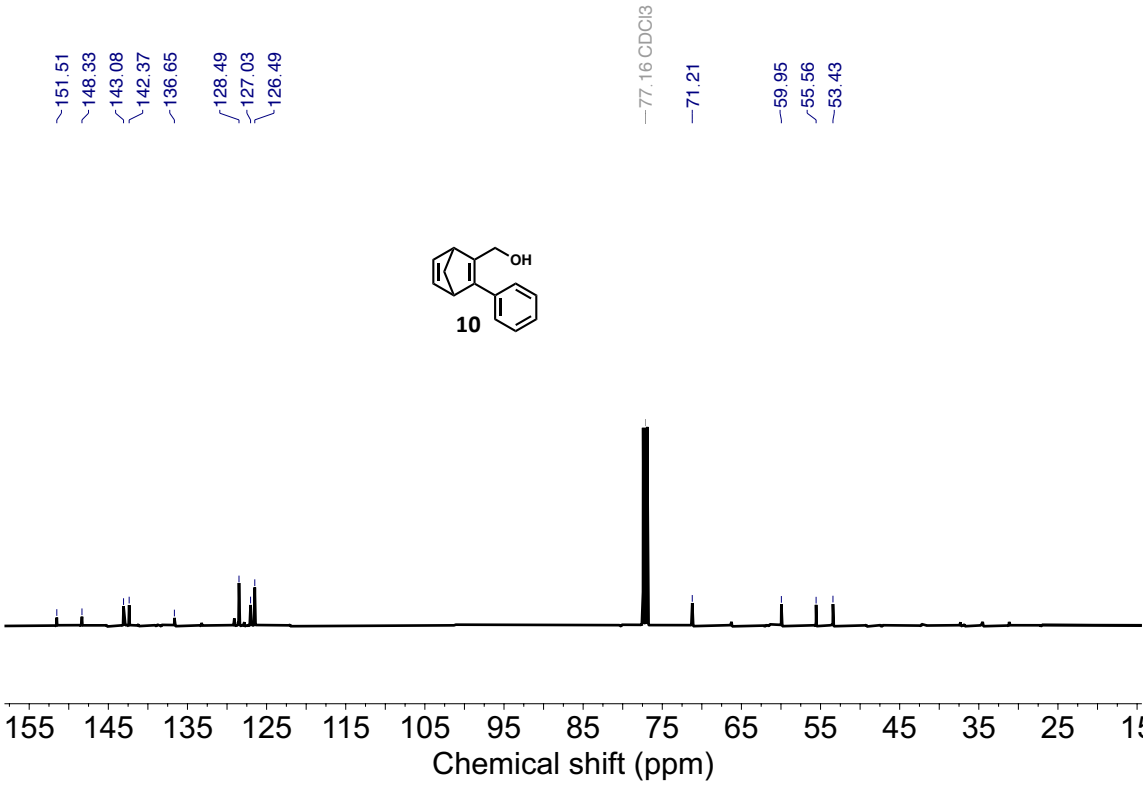


Figure S3.7. ^{13}C NMR spectrum of compound **10** in $CDCl_3$.

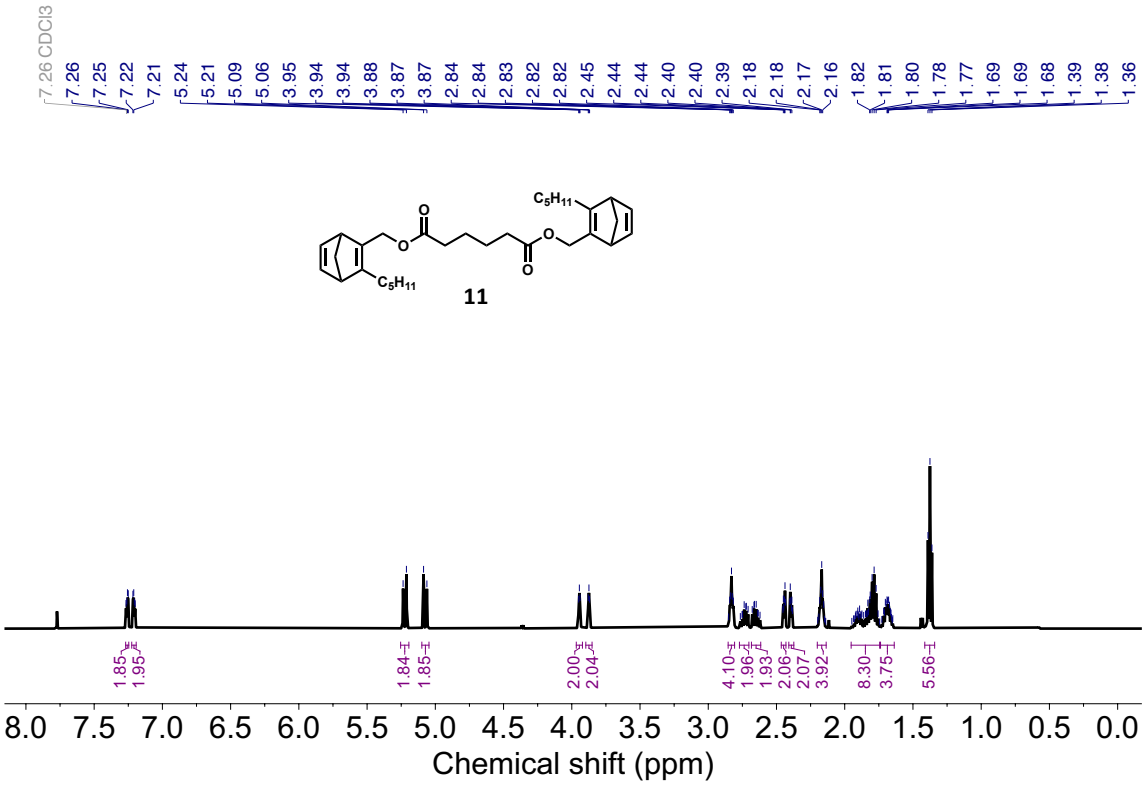


Figure S3.8. ^{1}H NMR spectrum of compound **11** in $CDCl_3$.

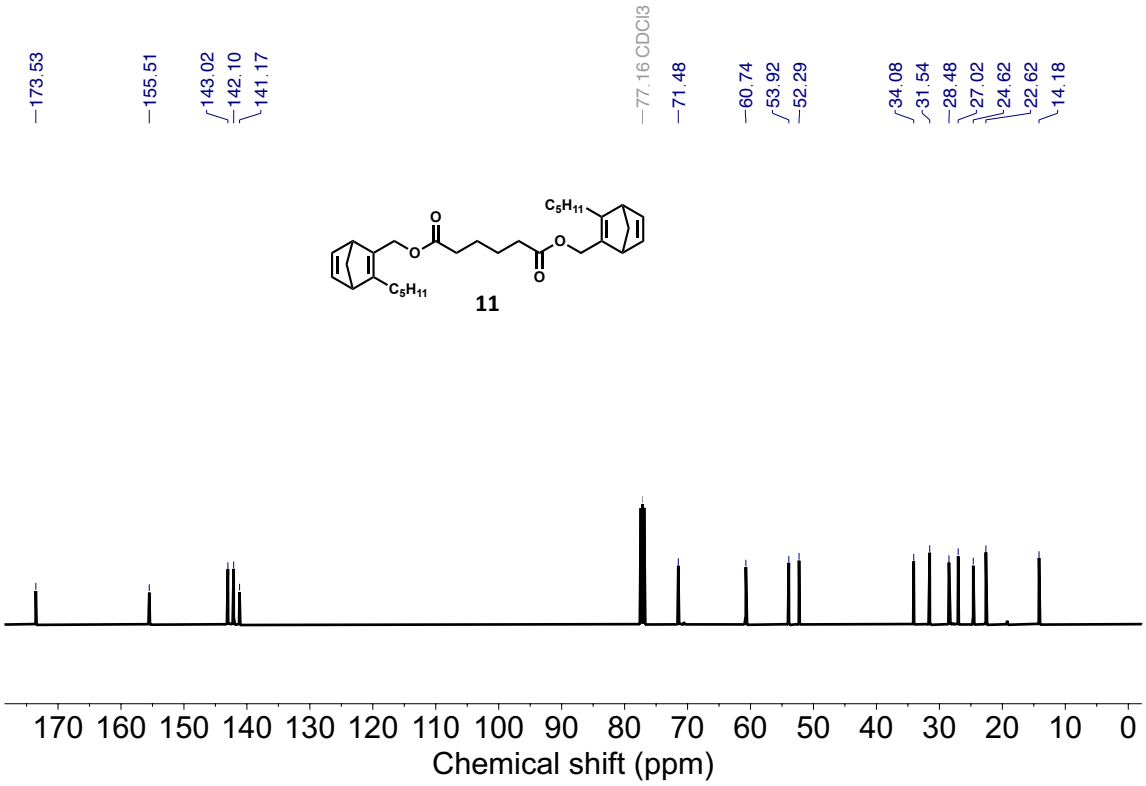


Figure S3.9. ^{13}C NMR spectrum of compound **11** in $CDCl_3$.

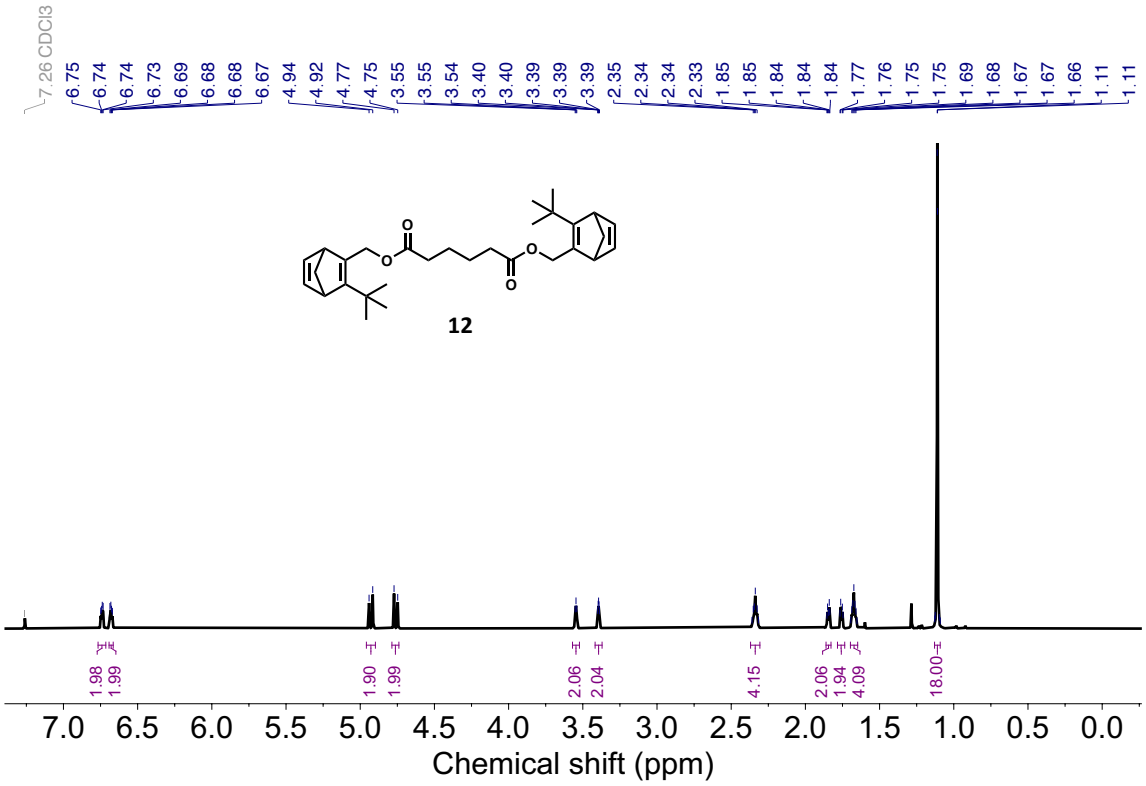


Figure S3.10. ^{1}H NMR spectrum of compound **12** in $CDCl_3$.

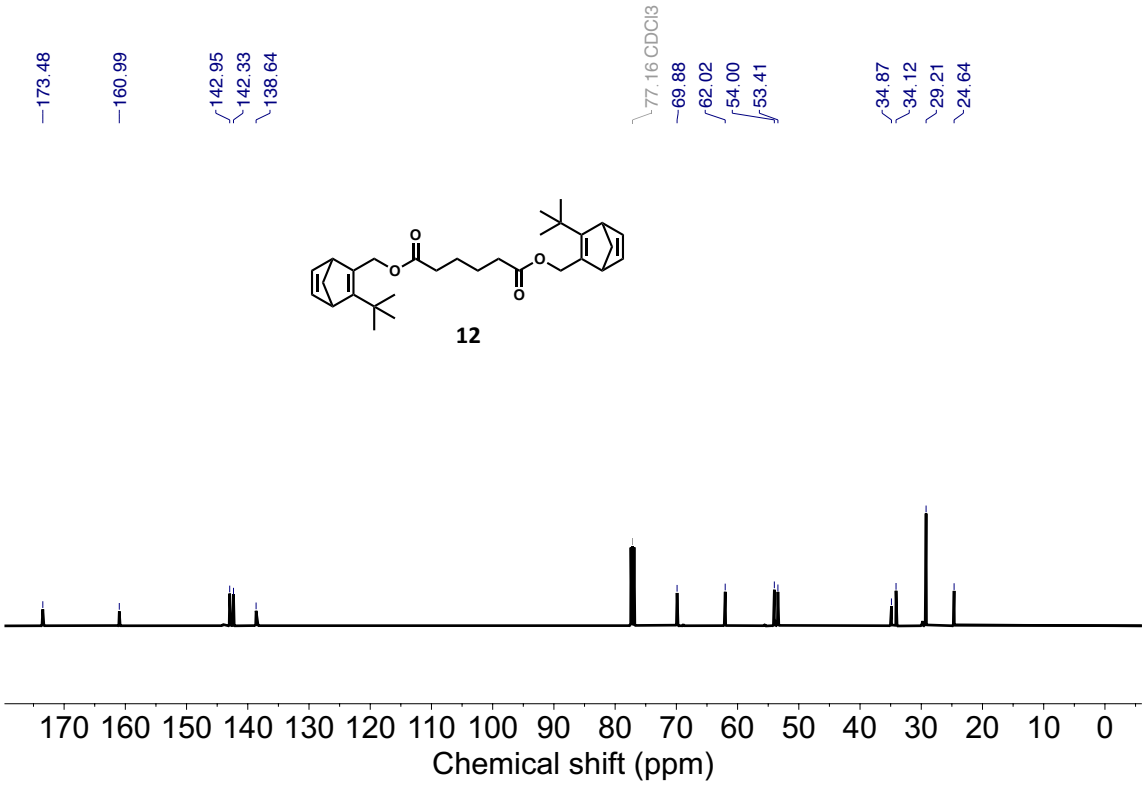


Figure S3.11. ^{13}C NMR spectrum of compound **12** in $CDCl_3$.

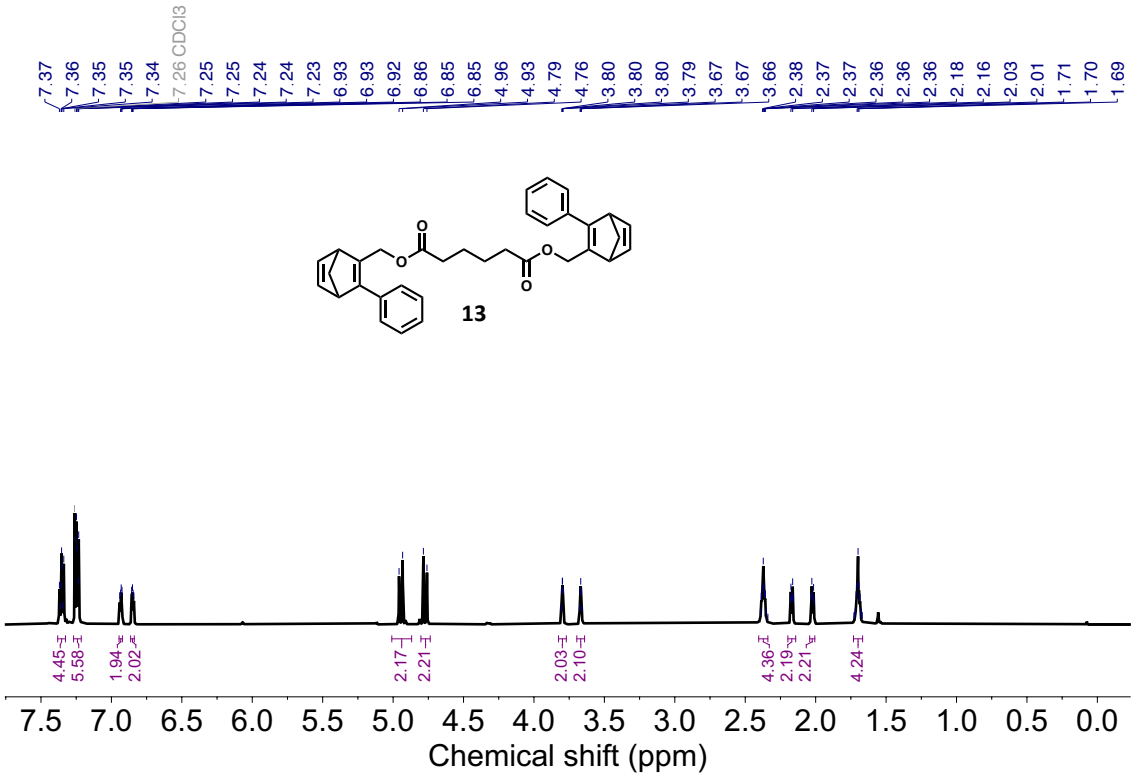


Figure S3.12. ^{1}H NMR spectrum of compound **13** in $CDCl_3$.

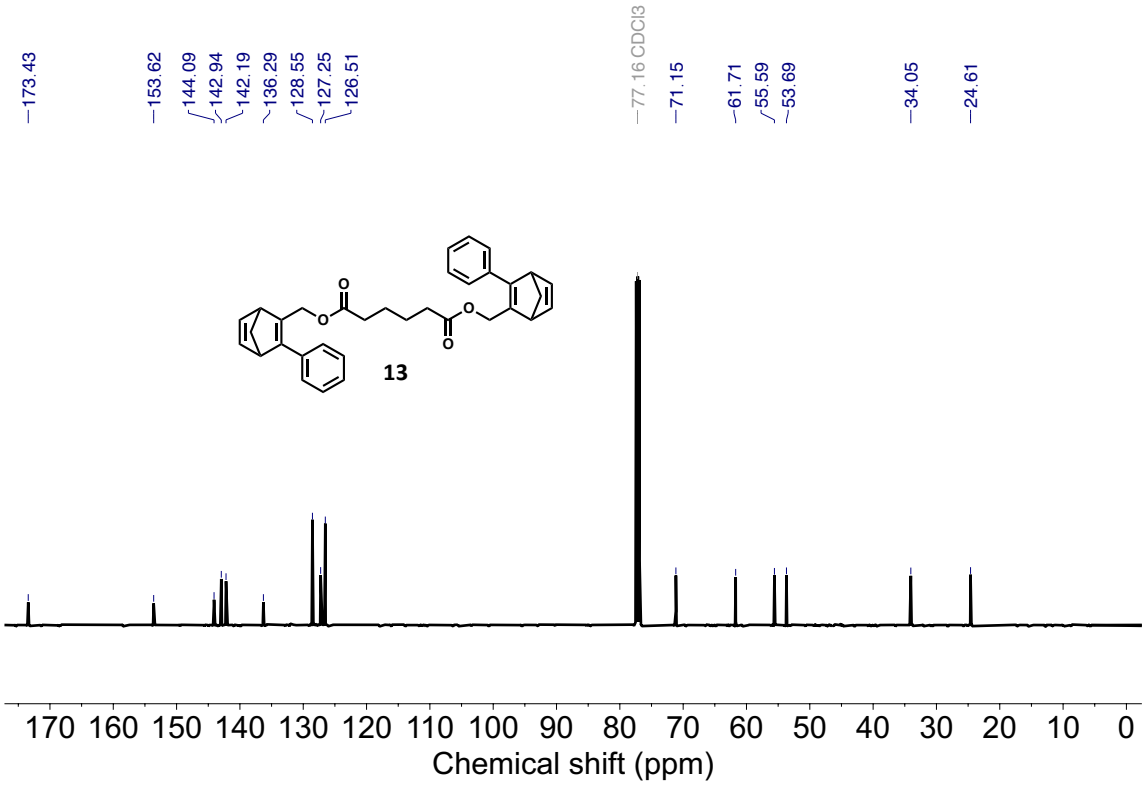


Figure S3.13. ^{13}C NMR spectrum of compound **13** in $CDCl_3$.

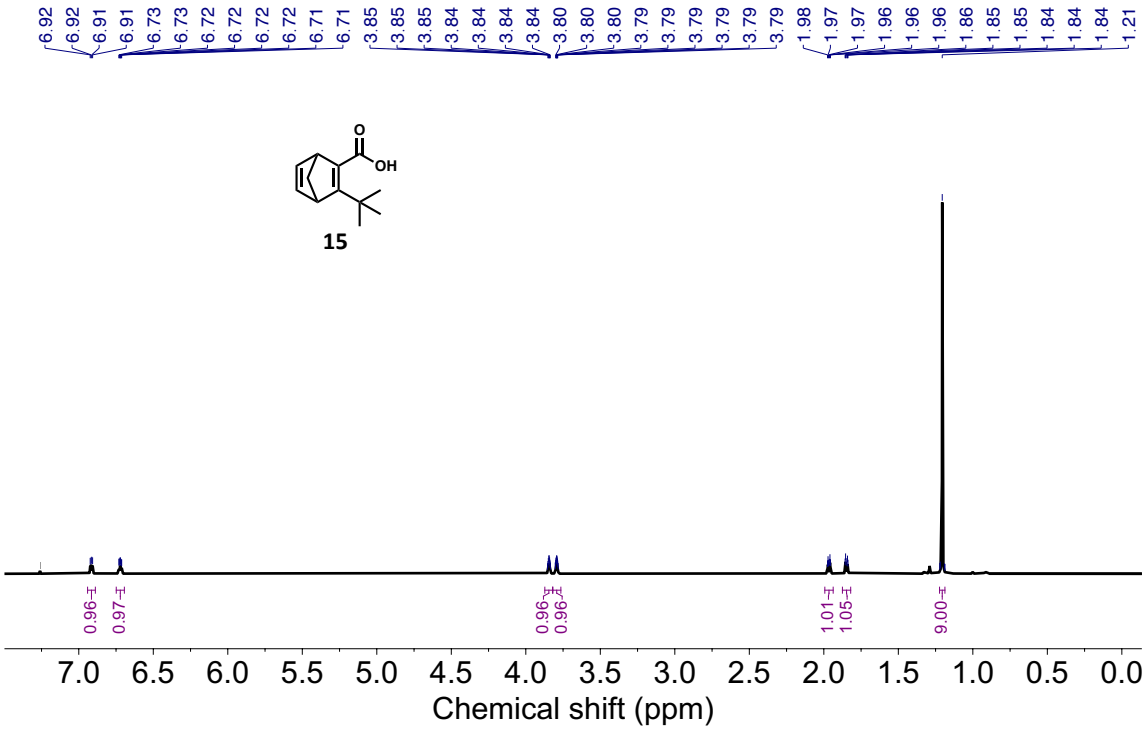


Figure S3.14. ^{1}H NMR spectrum of compound **15** in $CDCl_3$.

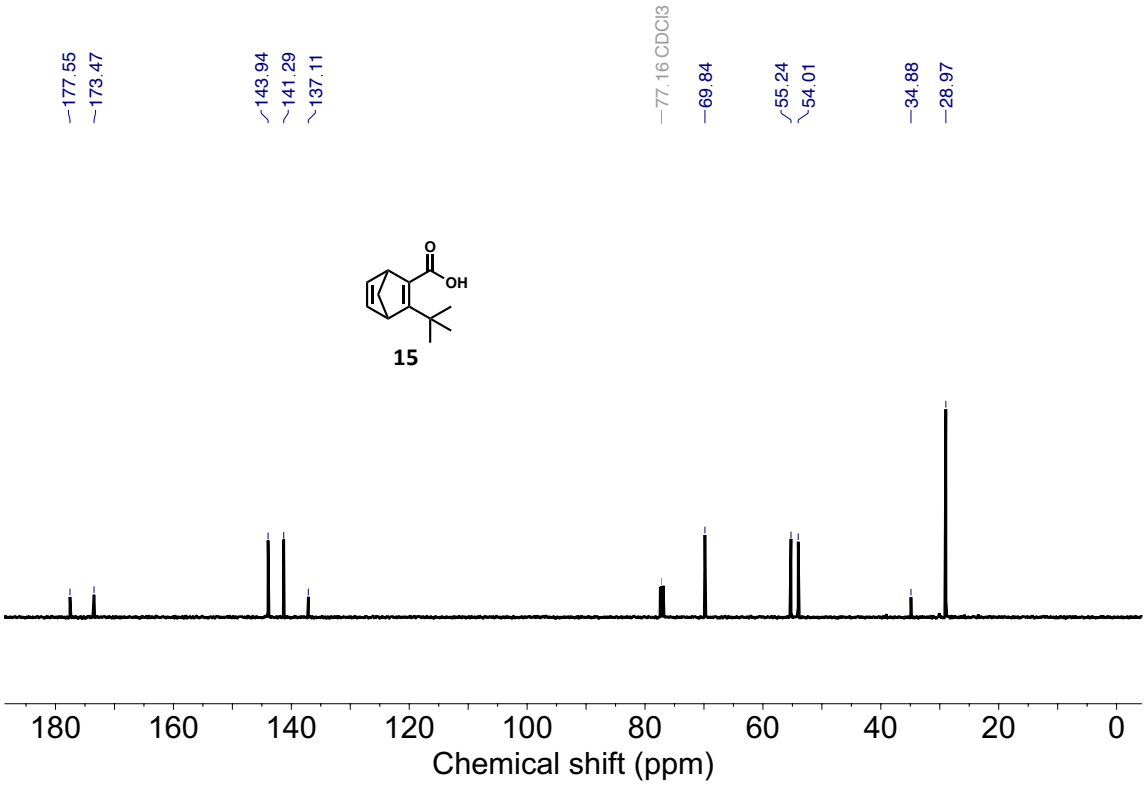


Figure S3.15. ^{13}C NMR spectrum of compound **15** in $CDCl_3$.

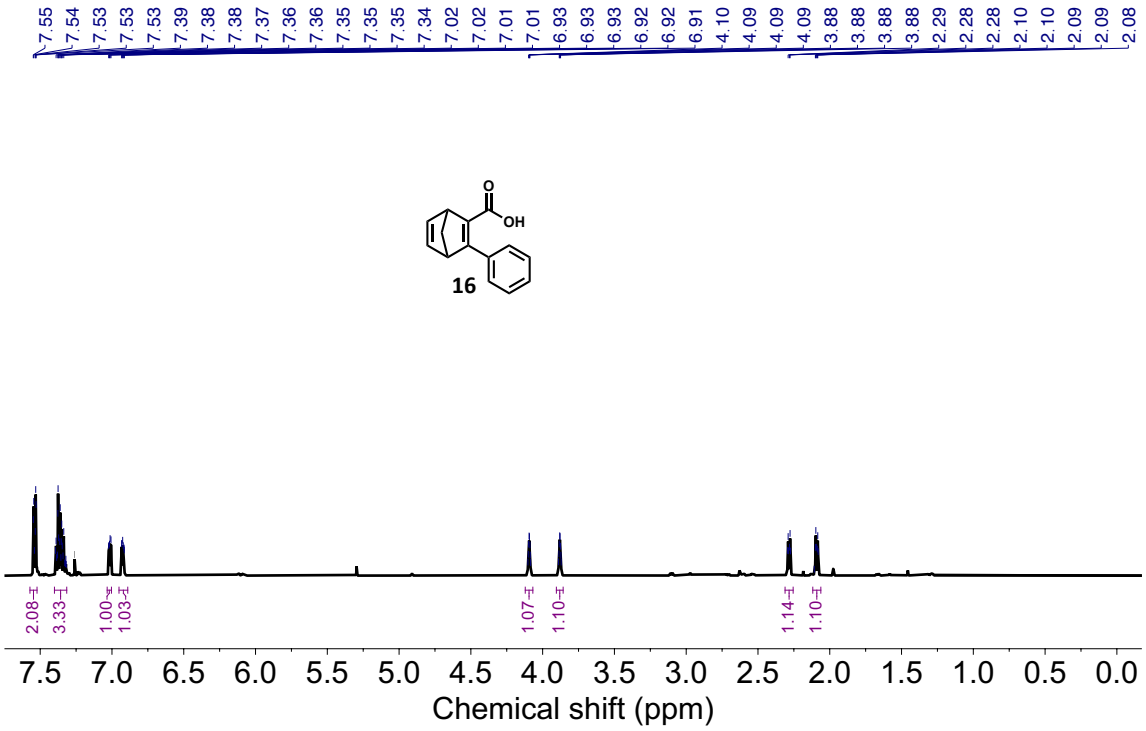


Figure S3.16. ^{1}H NMR spectrum of compound **16** in $CDCl_3$.

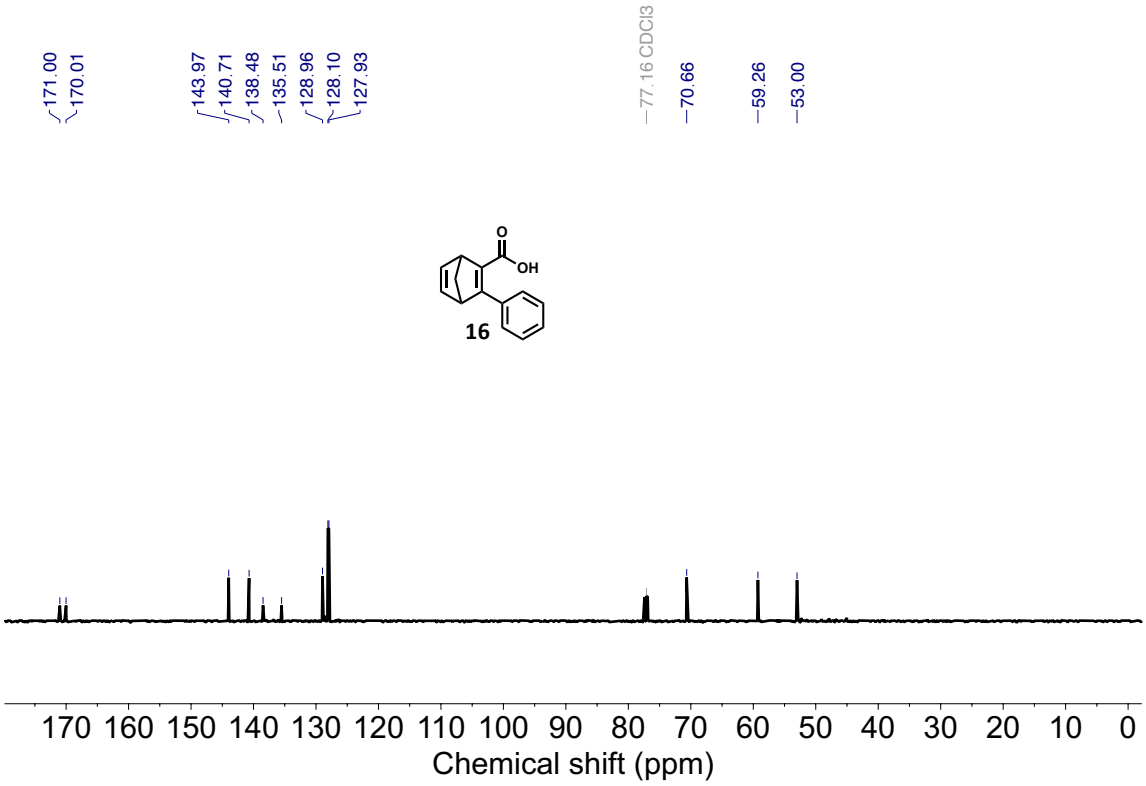


Figure S3.17. ^{13}C NMR spectrum of compound **16** in $CDCl_3$.

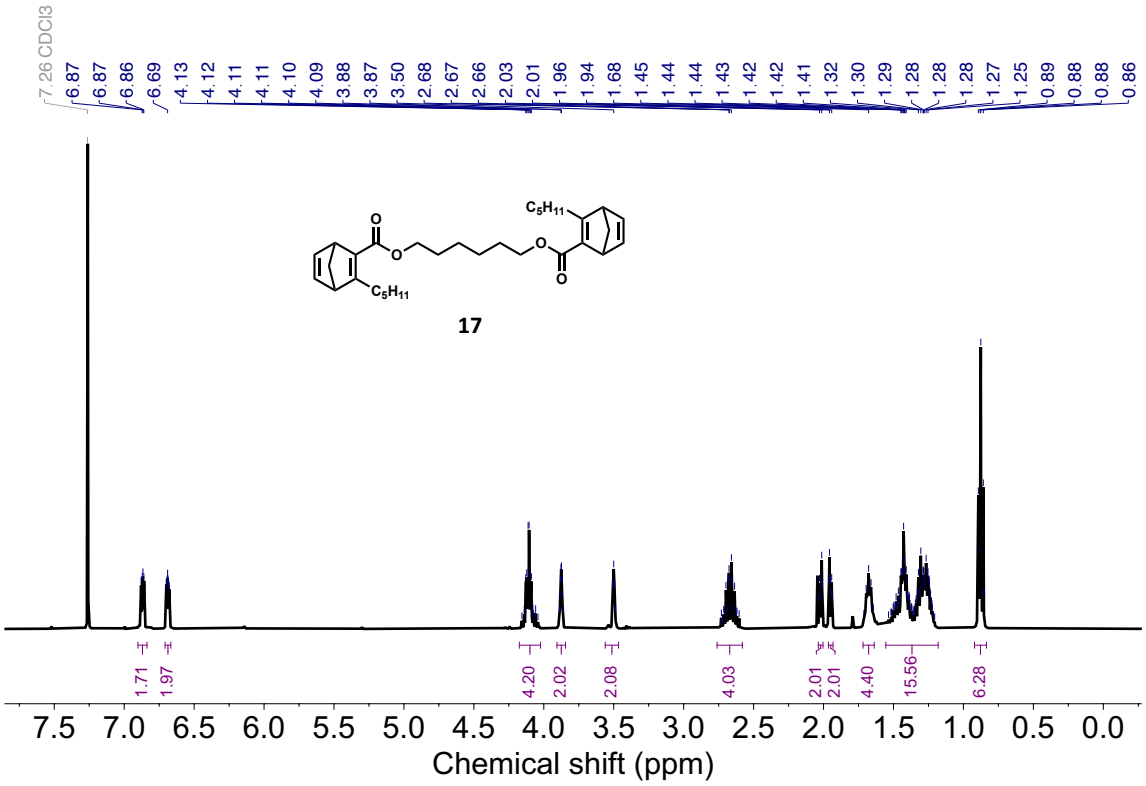


Figure S3.18. ^{1}H NMR spectrum of compound **17** in $CDCl_3$.

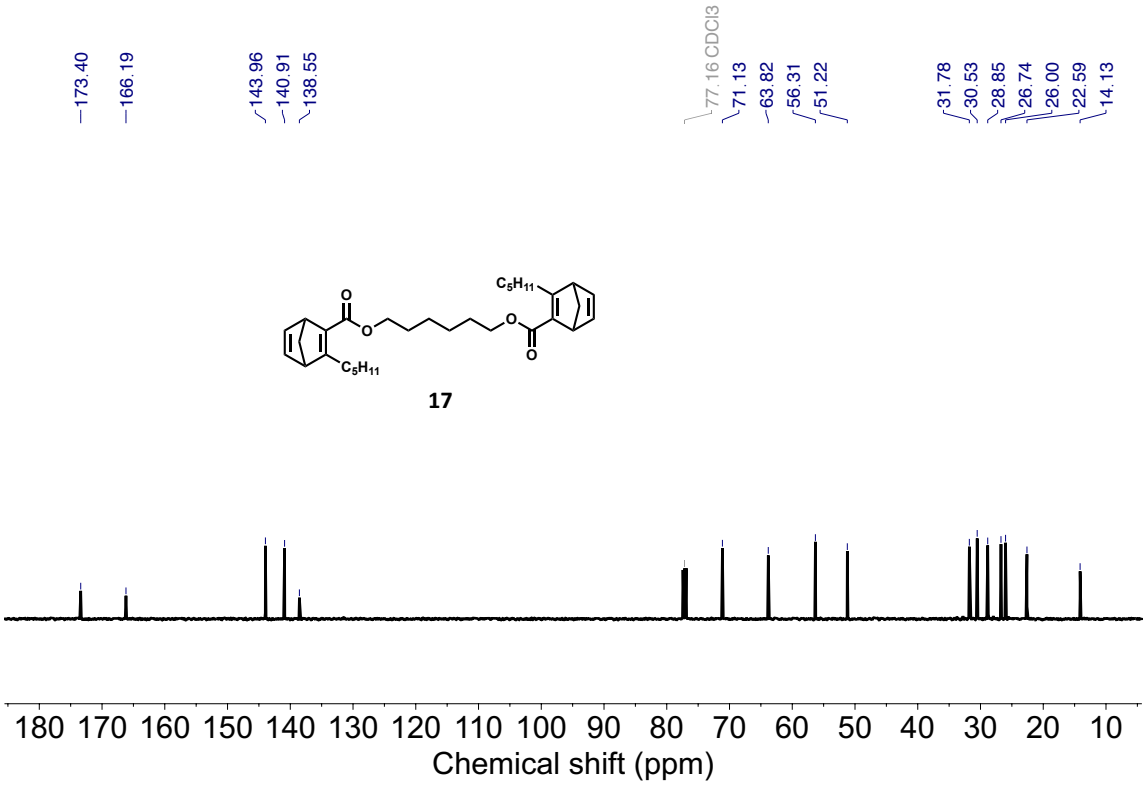


Figure S3.19. ^{13}C NMR spectrum of compound **17** in $CDCl_3$.

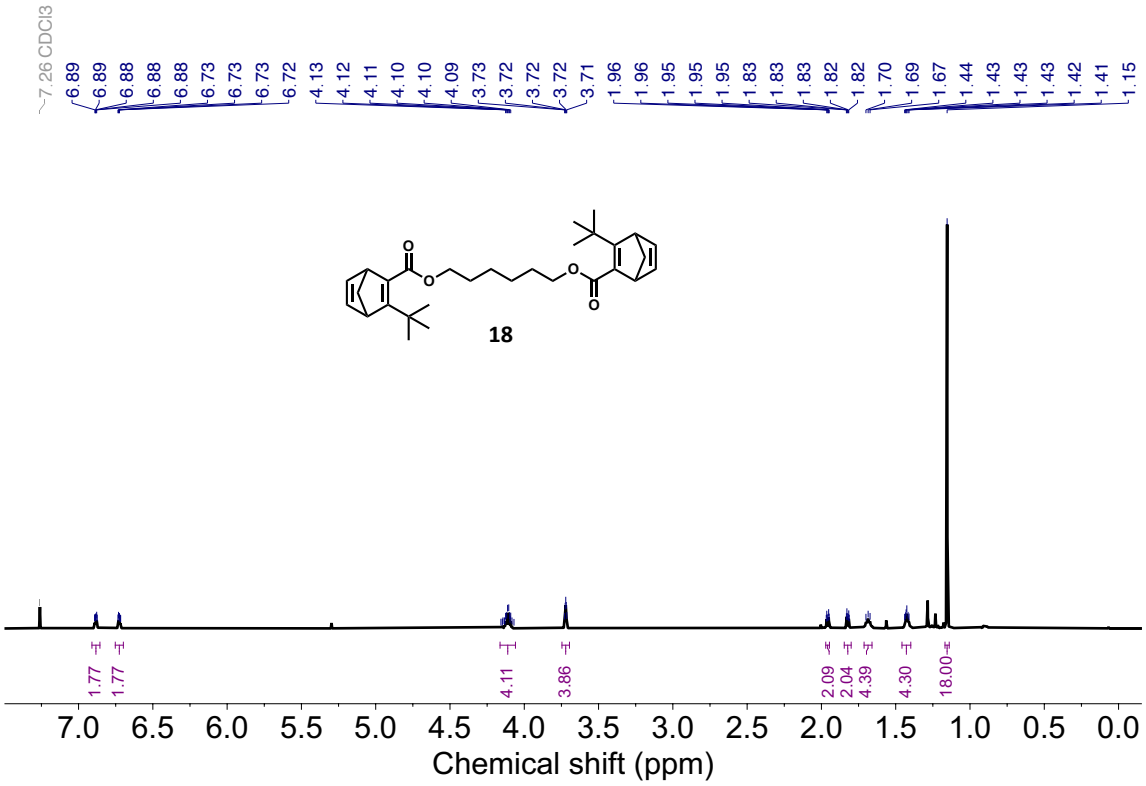


Figure S3.20. ^{1}H NMR spectrum of compound **18** in $CDCl_3$.

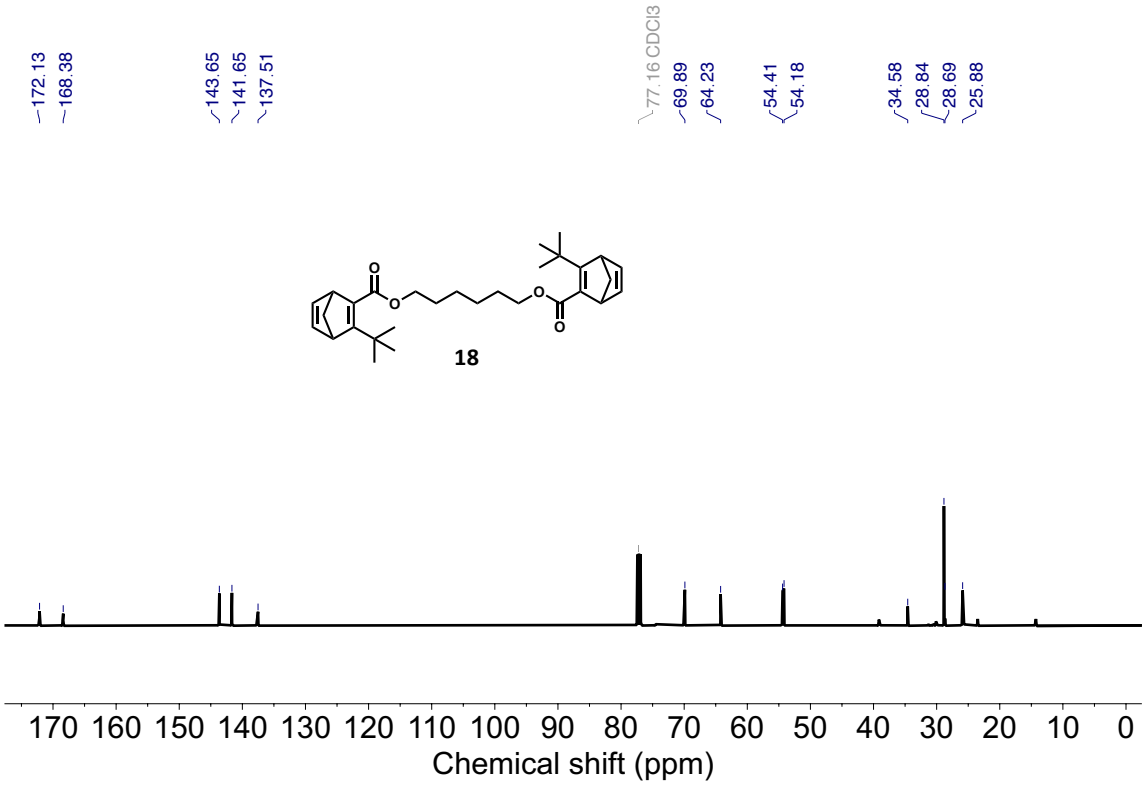


Figure S3.21. ^{13}C NMR spectrum of compound **18** in $CDCl_3$.

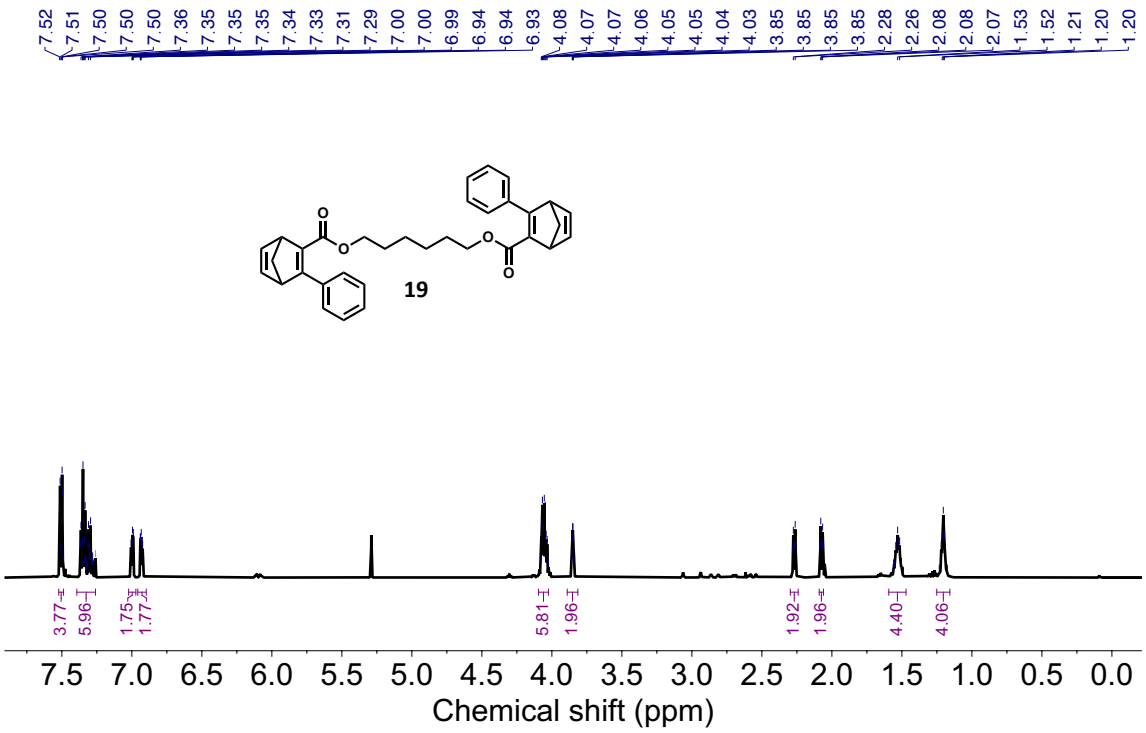


Figure S3.22. ^{1}H NMR spectrum of compound **19** in $CDCl_3$.

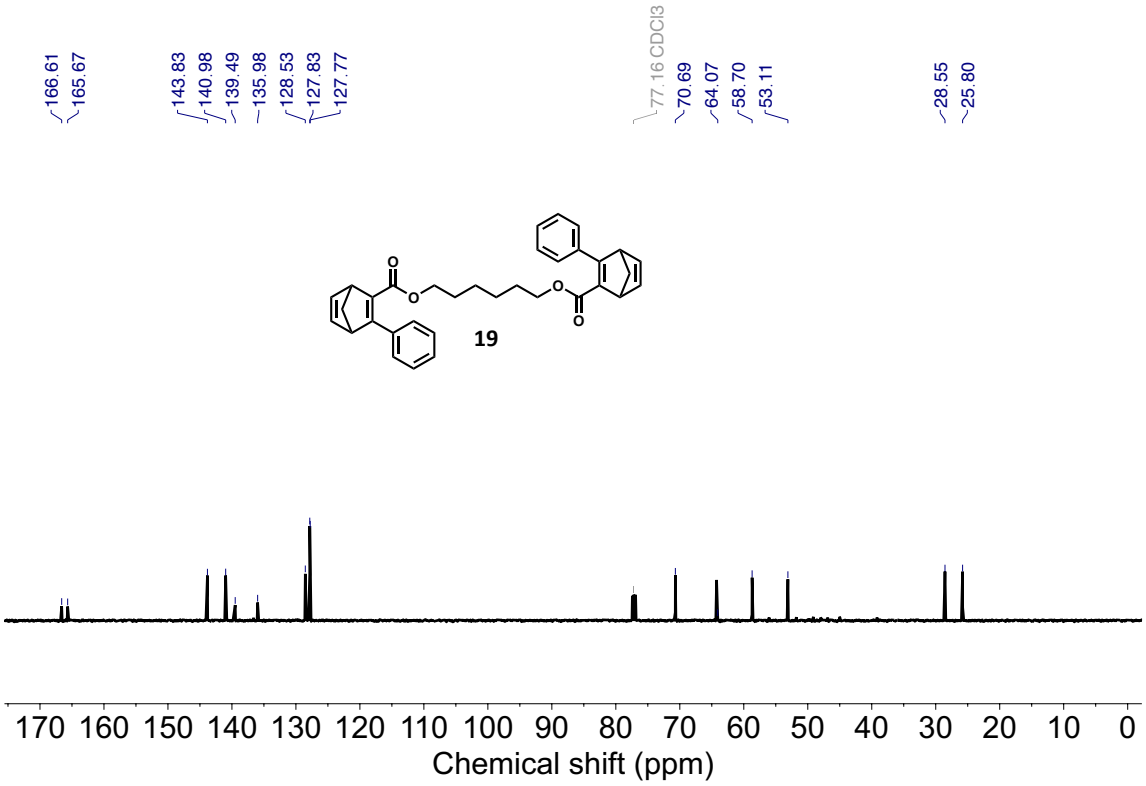


Figure S3.23. ^{13}C NMR spectrum of compound **19** in $CDCl_3$.

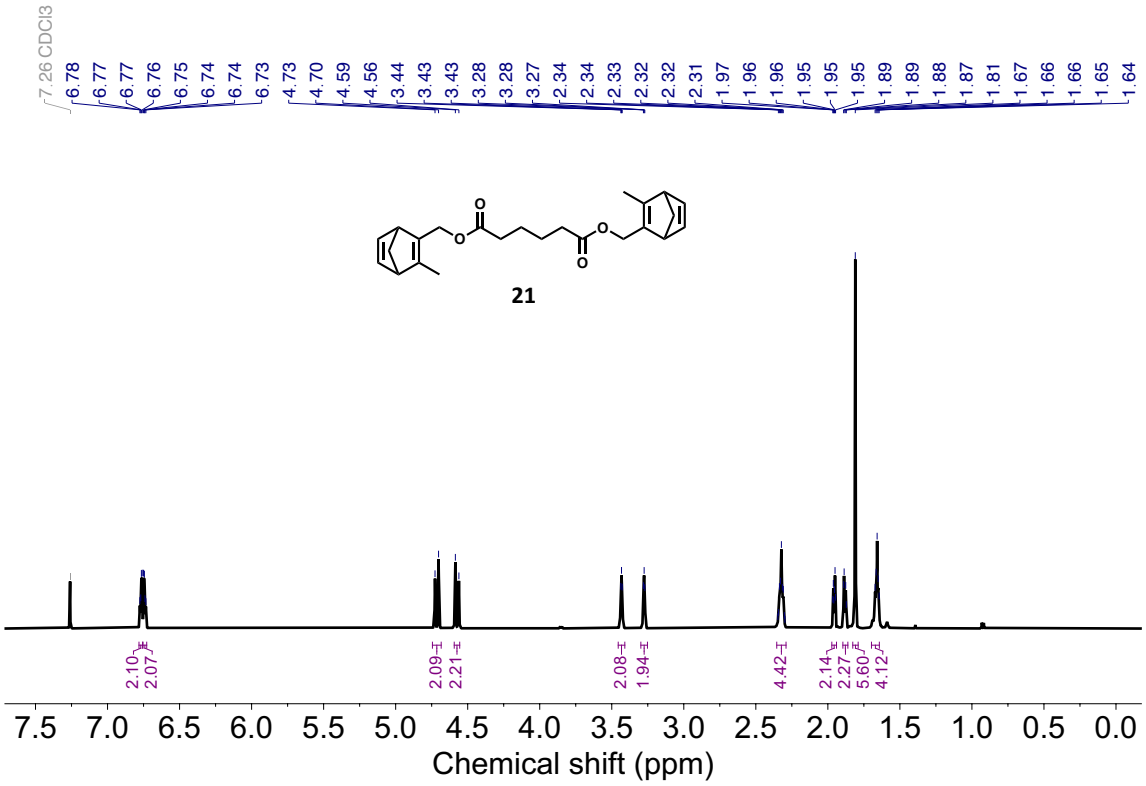


Figure S3.24. ^{1}H NMR spectrum of compound **21** in $CDCl_3$.

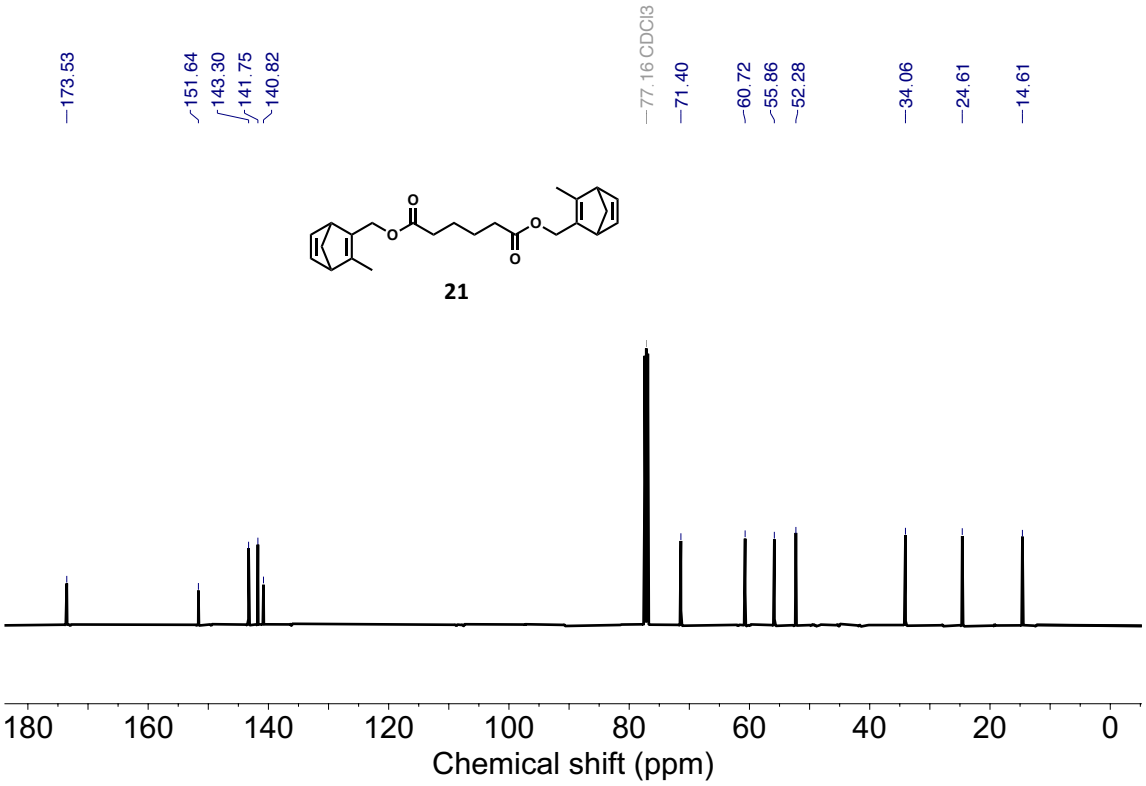


Figure S3.25. ^{13}C NMR spectrum of compound **21** in $CDCl_3$.

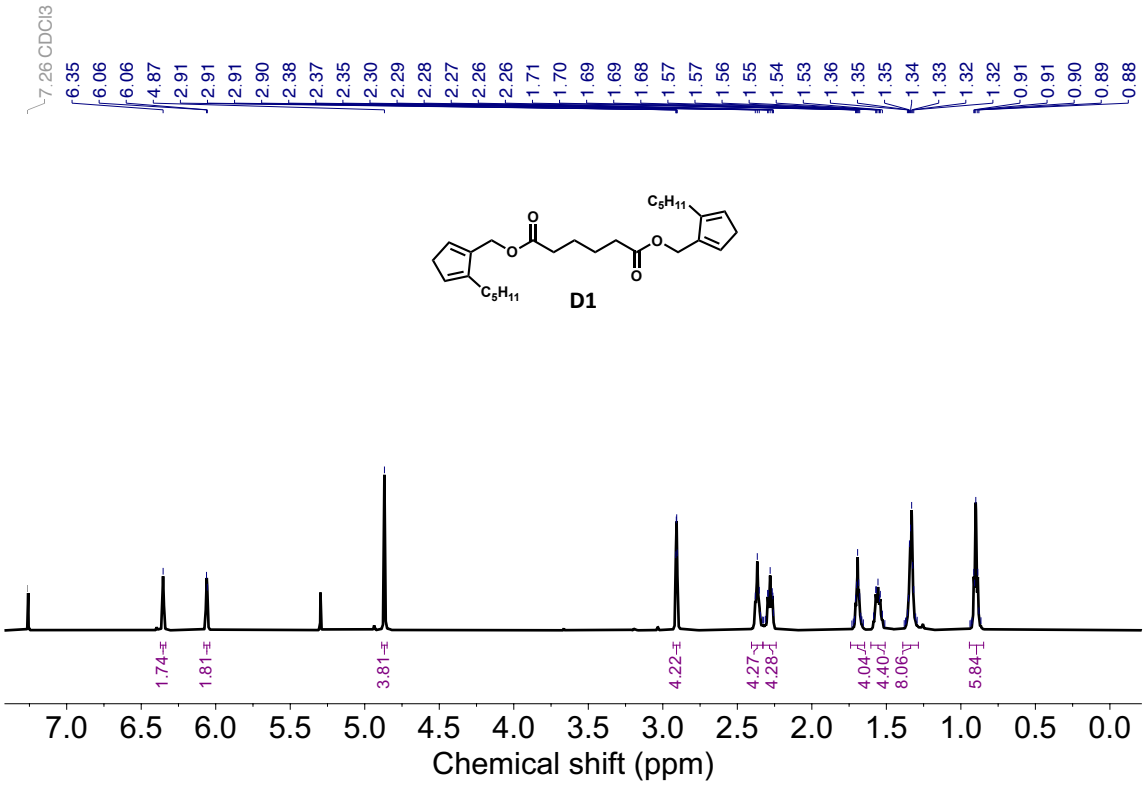


Figure S3.26. ^{1}H NMR spectrum of compound **D1** in $CDCl_3$.

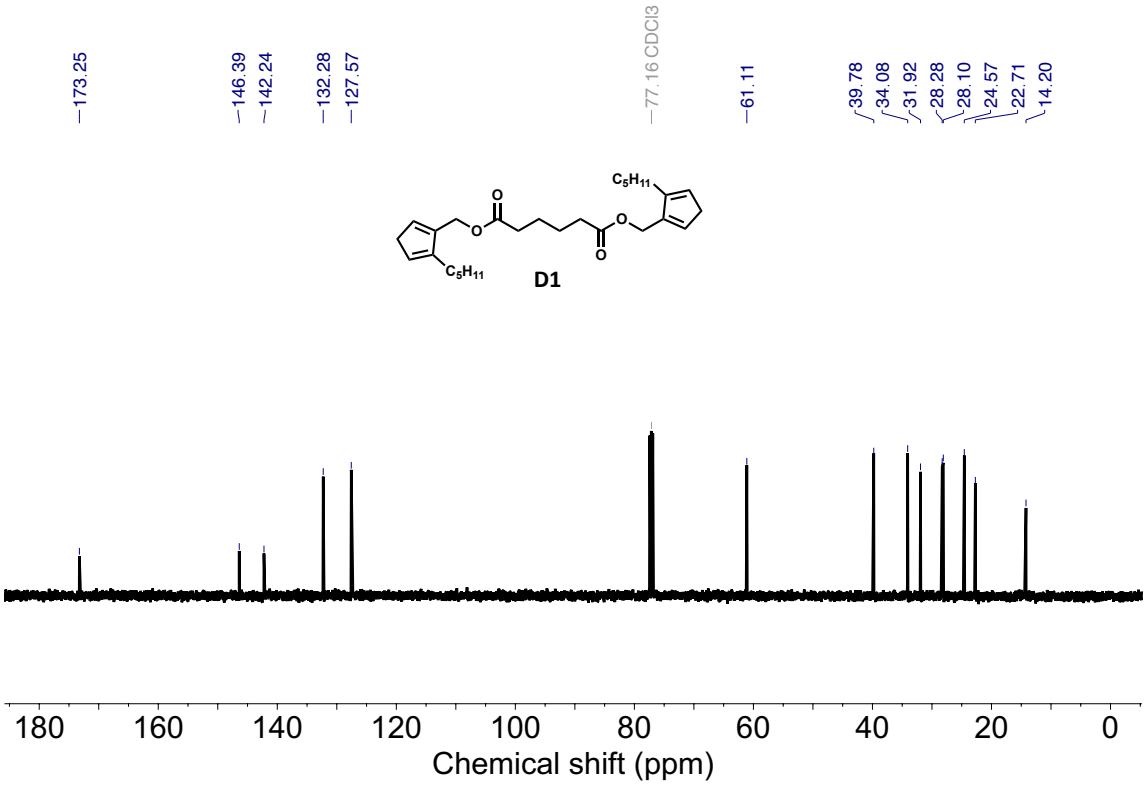


Figure S3.27. ^{13}C NMR spectrum of compound **D1** in $CDCl_3$.

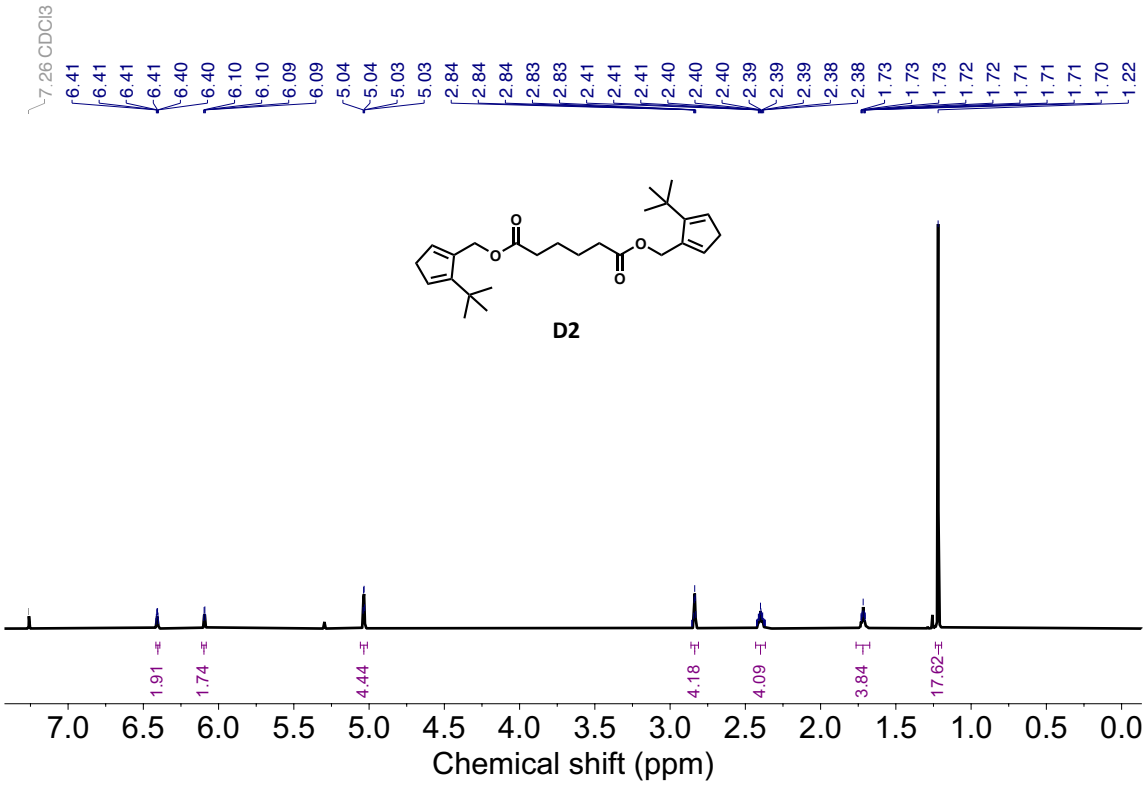


Figure S3.28. ^{1}H NMR spectrum of compound **D2** in $CDCl_3$.

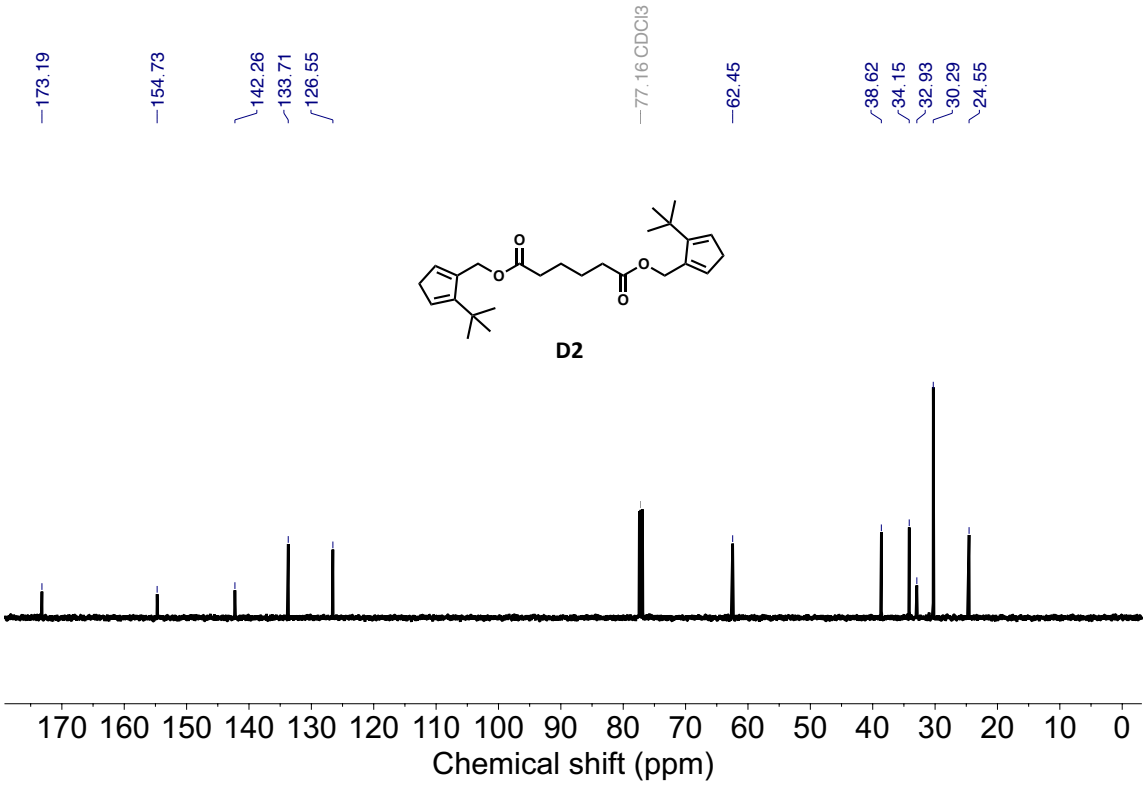


Figure S3.29. ^{13}C NMR spectrum of compound **D2** in $CDCl_3$.

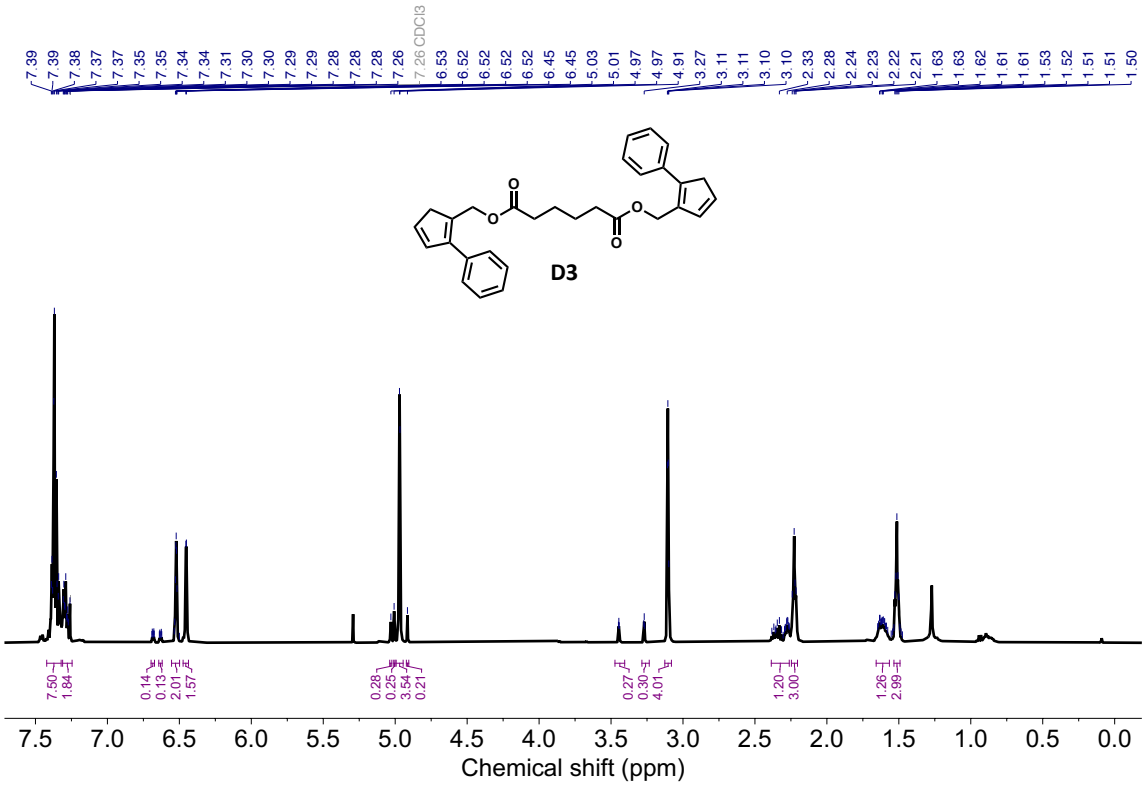


Figure S3.30. ^{1}H NMR spectrum of compound **D3** in $CDCl_3$.

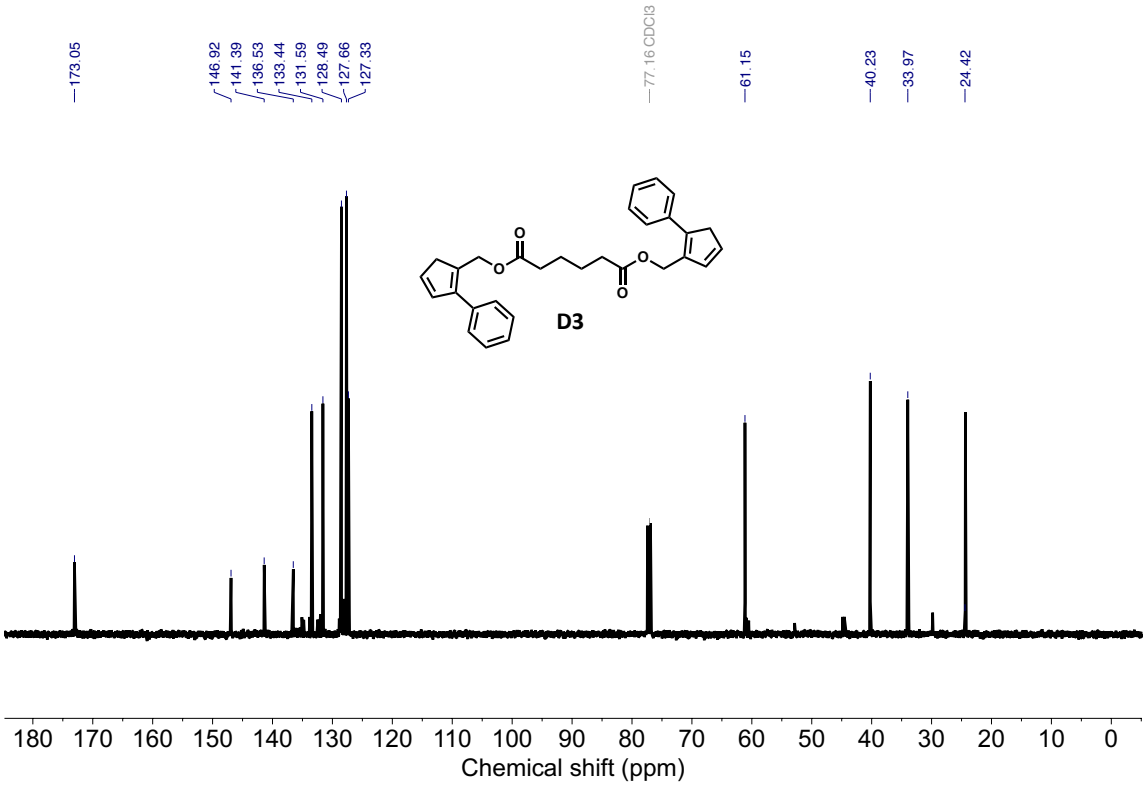


Figure S3.31. ^{13}C NMR spectrum of compound **D3** in $CDCl_3$.

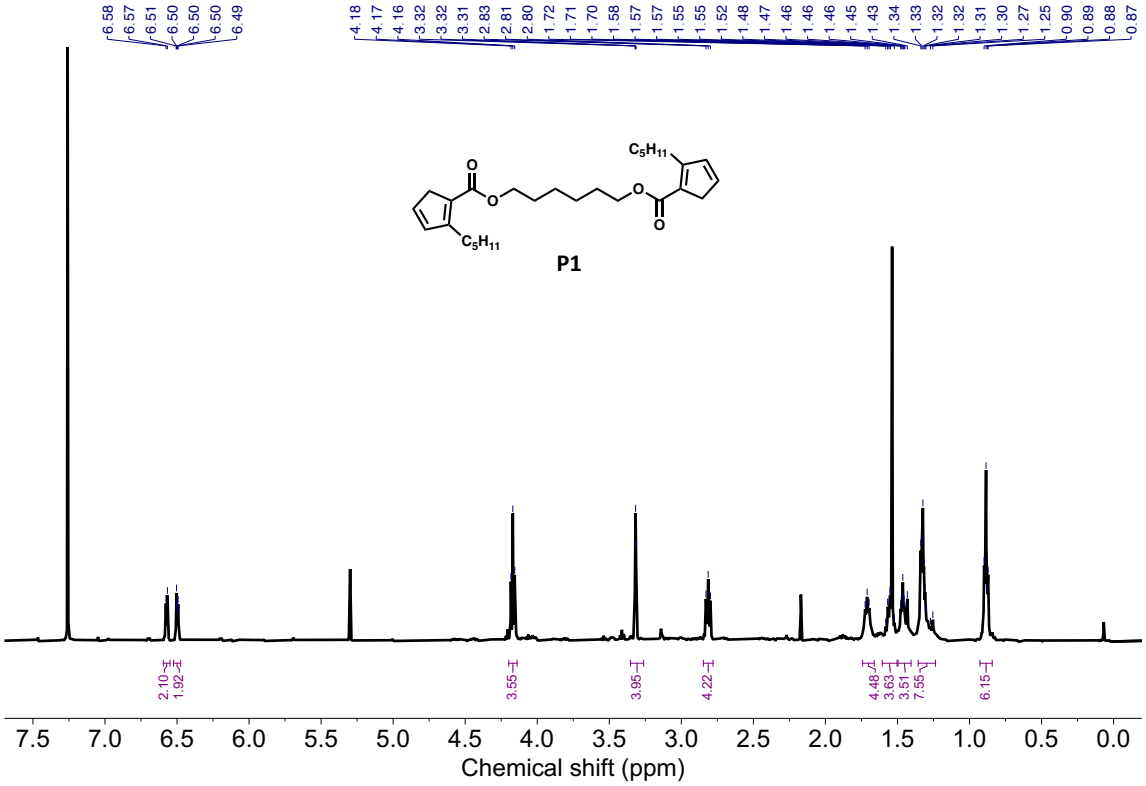


Figure S3.32. ^{1}H NMR spectrum of compound **P1** in $CDCl_3$.

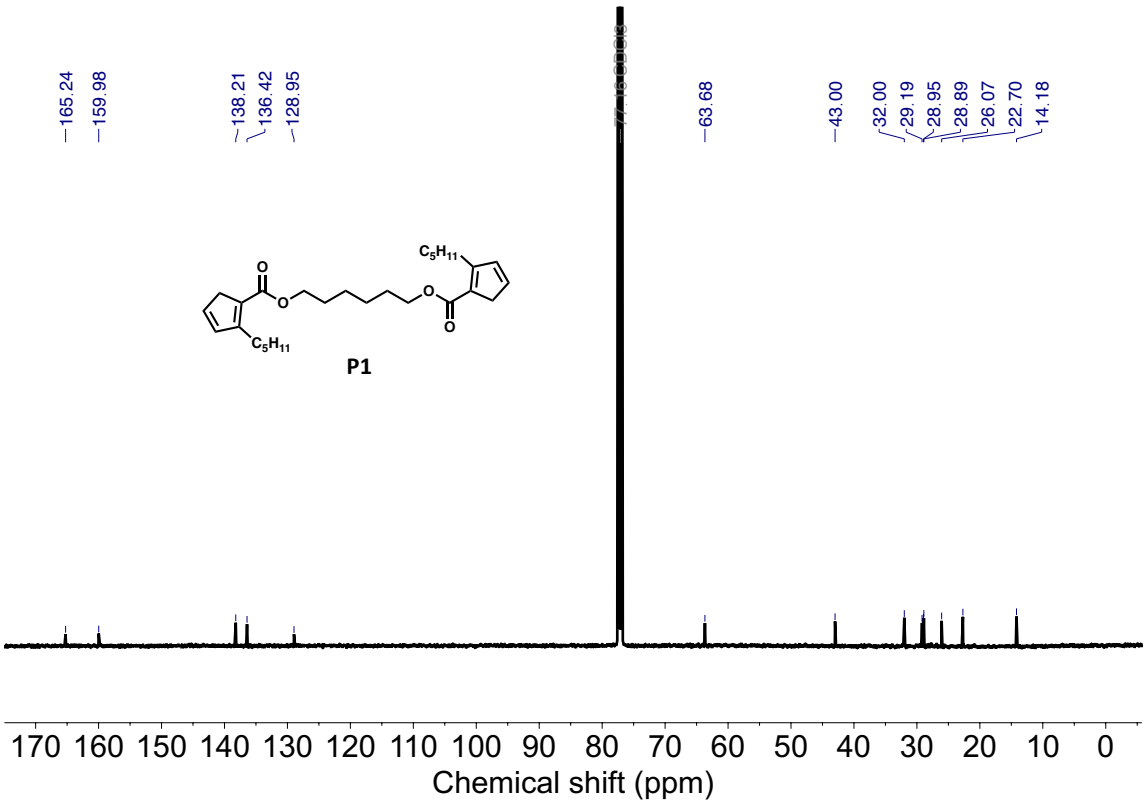


Figure S3.33. ^{13}C NMR spectrum of compound **P1** in $CDCl_3$.

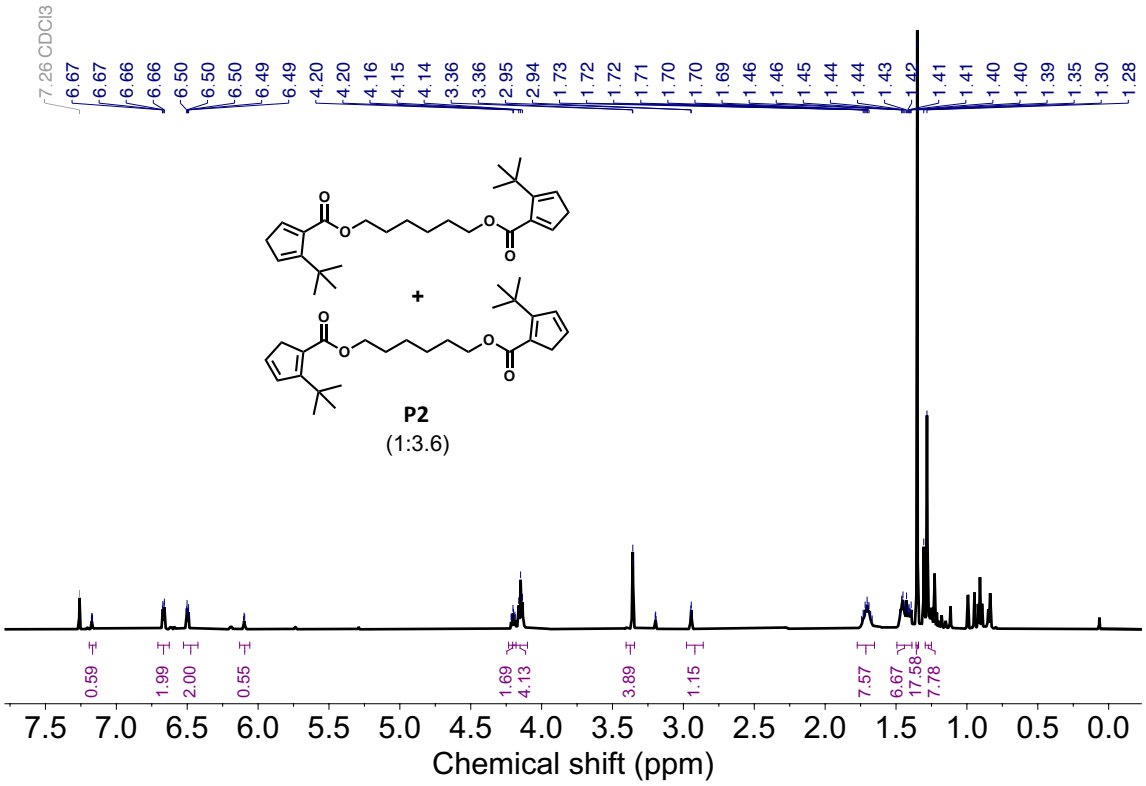


Figure S3.34. ^{1}H NMR spectrum of compound **P2** in $CDCl_3$.

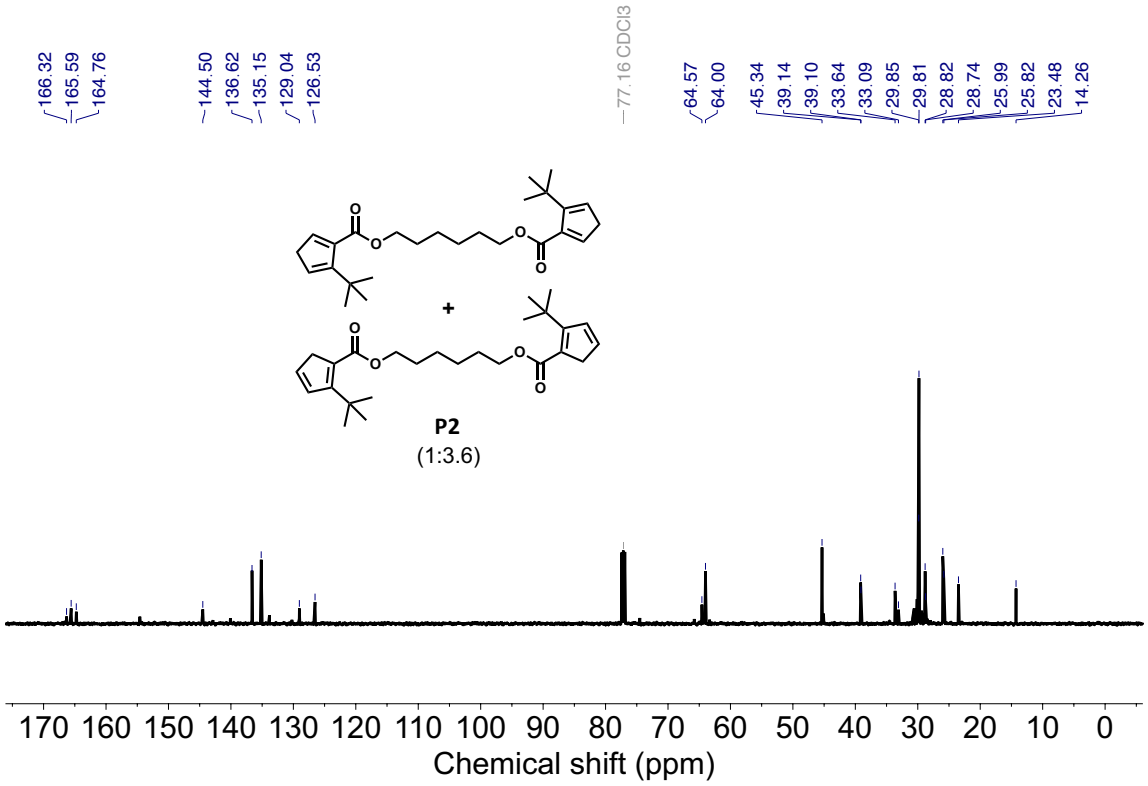


Figure S3.35. ^{13}C NMR spectrum of compound **P2** in $CDCl_3$.

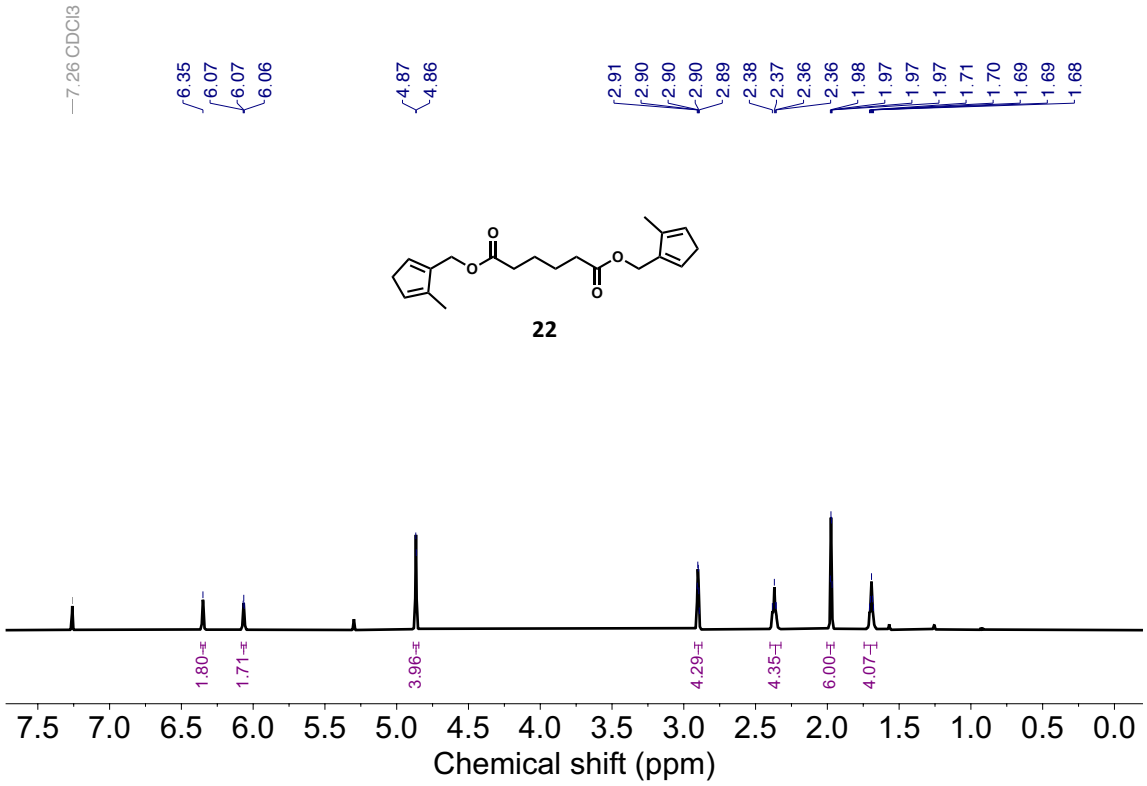


Figure S3.36. ^{1}H NMR spectrum of compound **22** in $CDCl_3$.

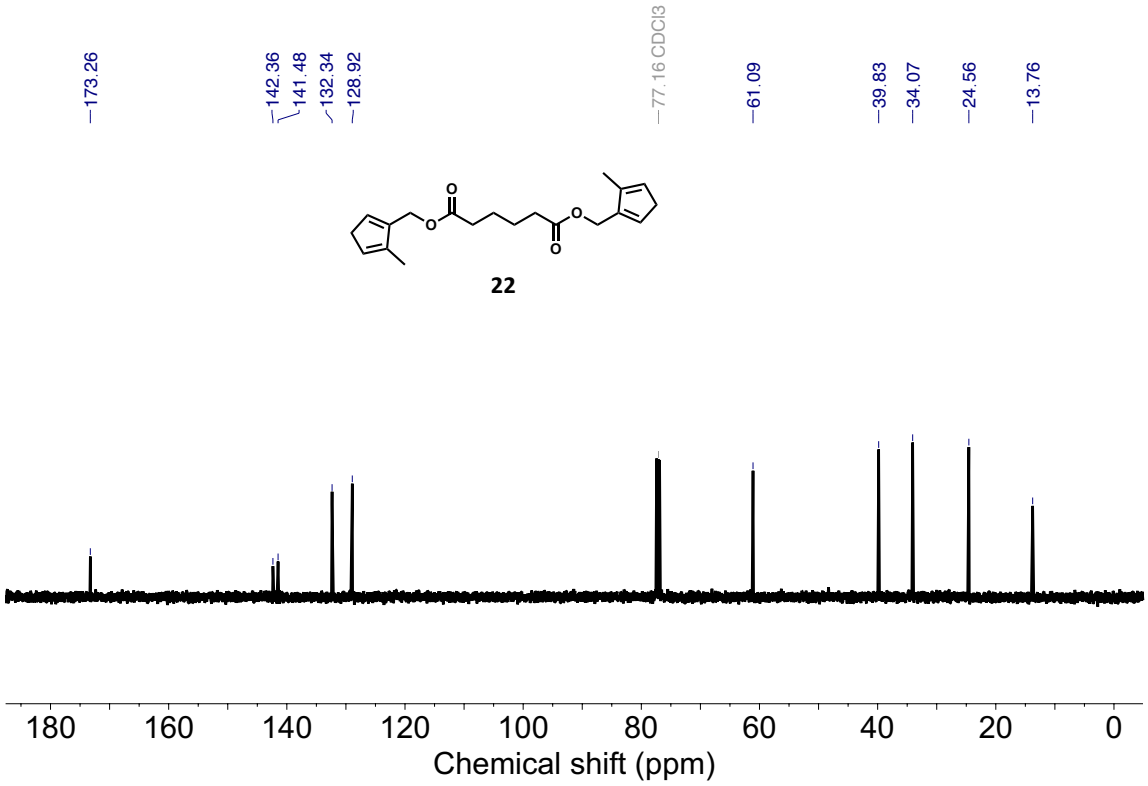


Figure S3.37. ^{13}C NMR spectrum of compound **22** in $CDCl_3$.

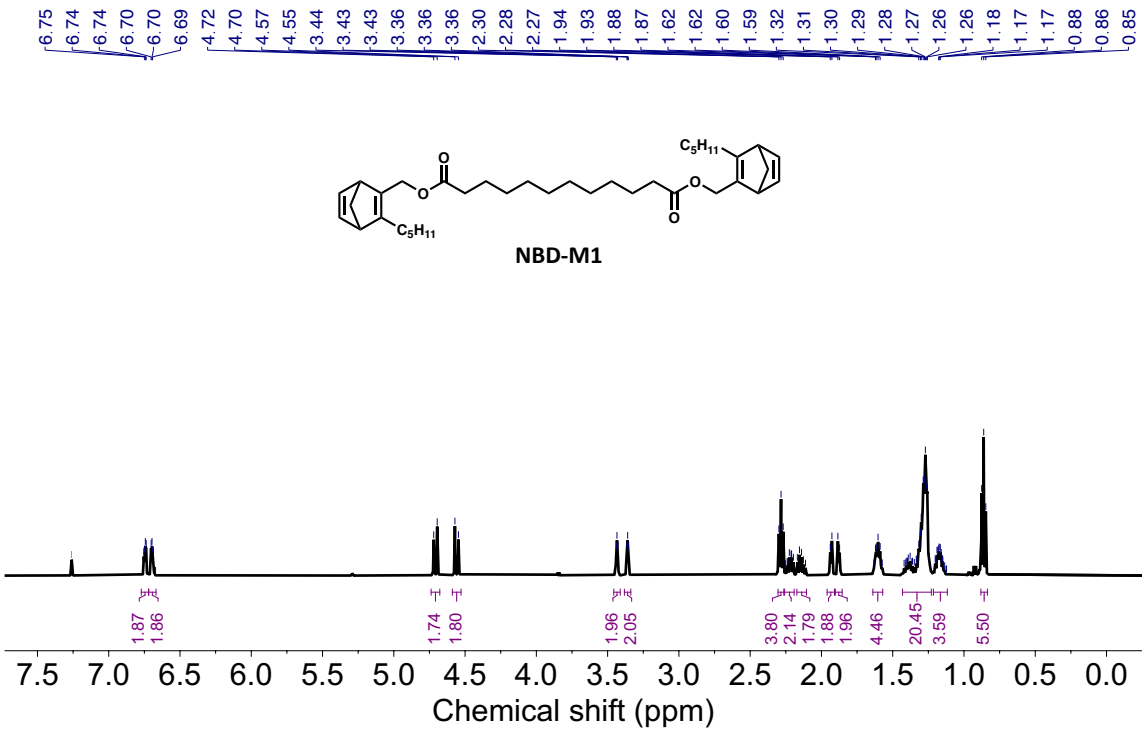


Figure S3.38. ^{1}H NMR spectrum of compound **NBD-M1** in $CDCl_3$.

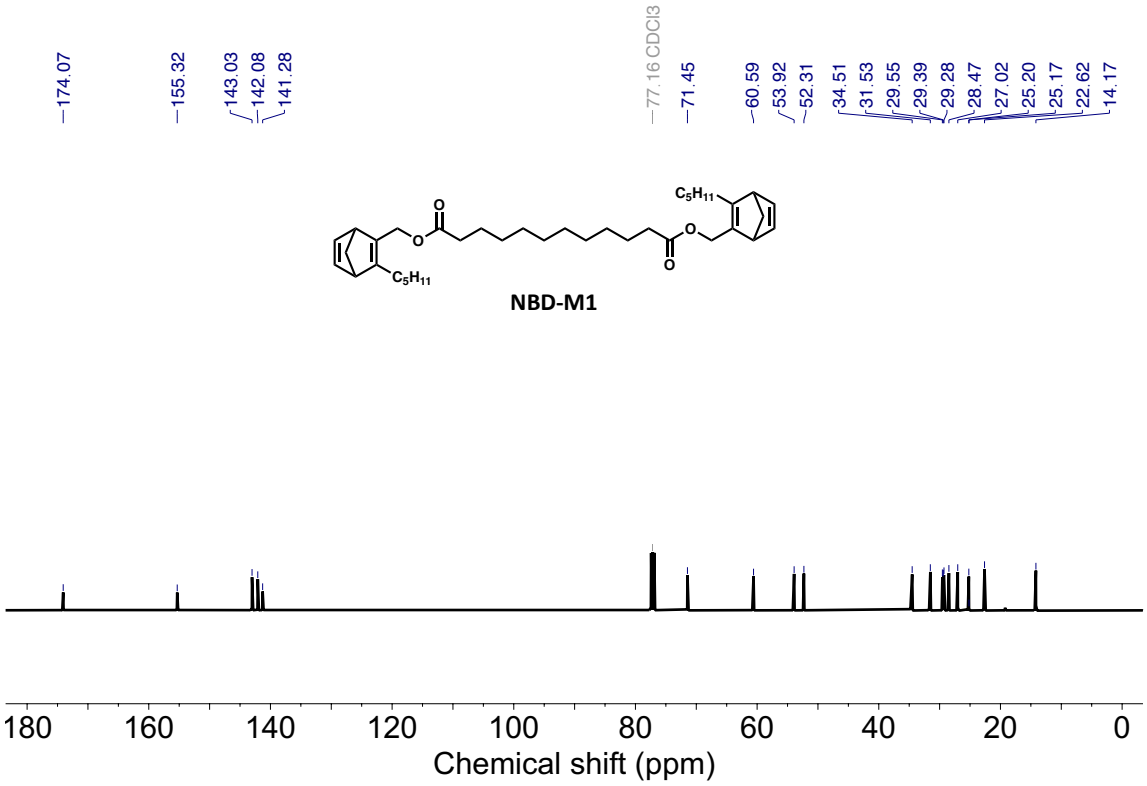


Figure S3.39. ^{13}C NMR spectrum of compound **NBD-M1** in $CDCl_3$.

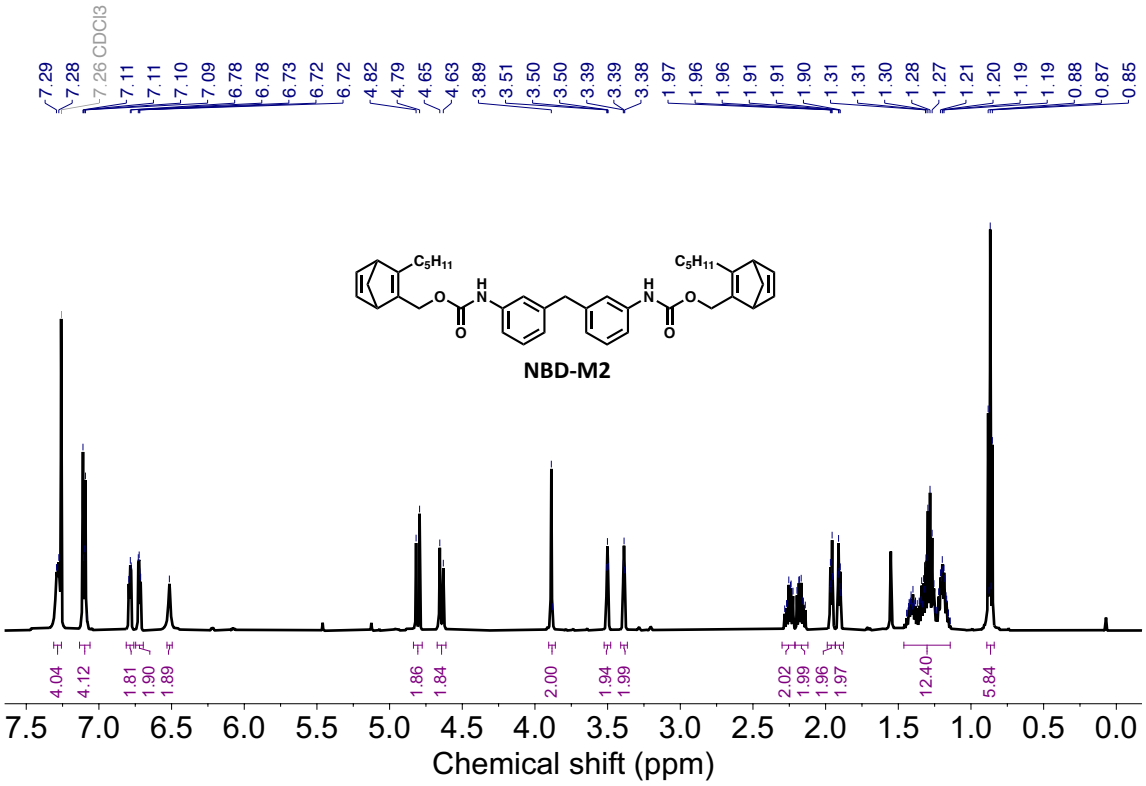


Figure S3.40. ^{1}H NMR spectrum of compound **NBD-M2** in $CDCl_3$.

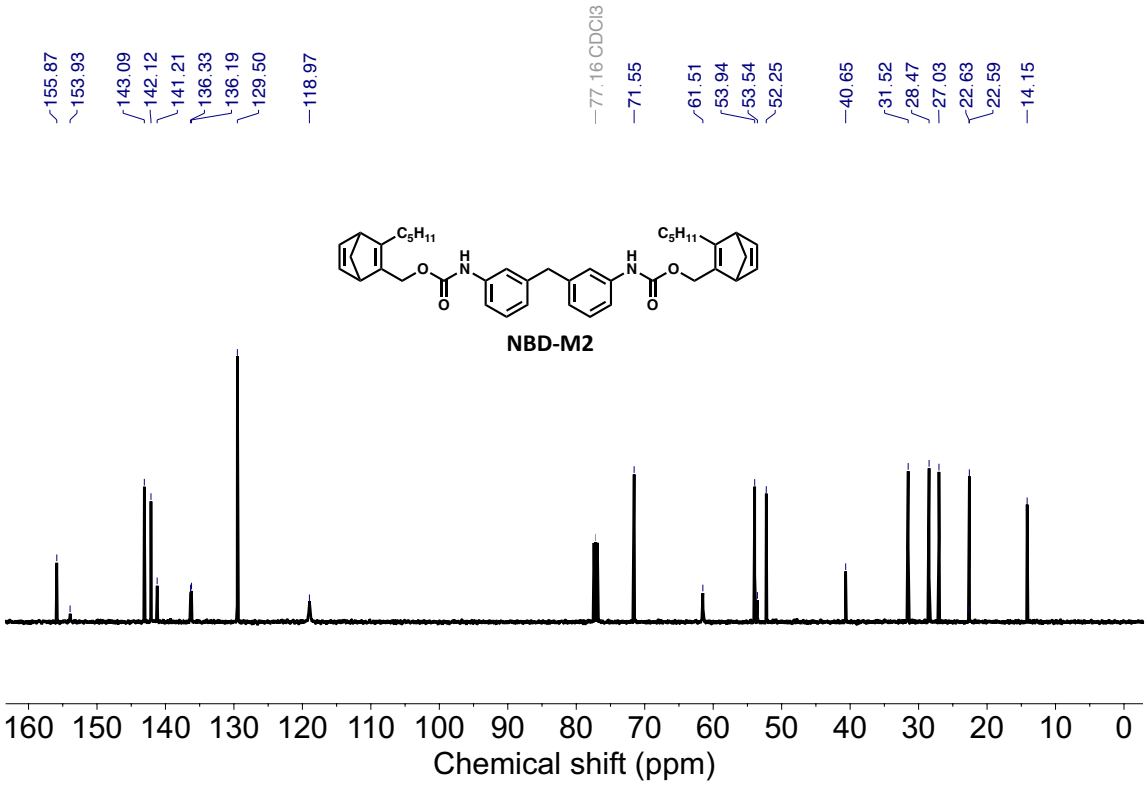


Figure S3.41. ^{13}C NMR spectrum of compound **NBD-M2** in $CDCl_3$.

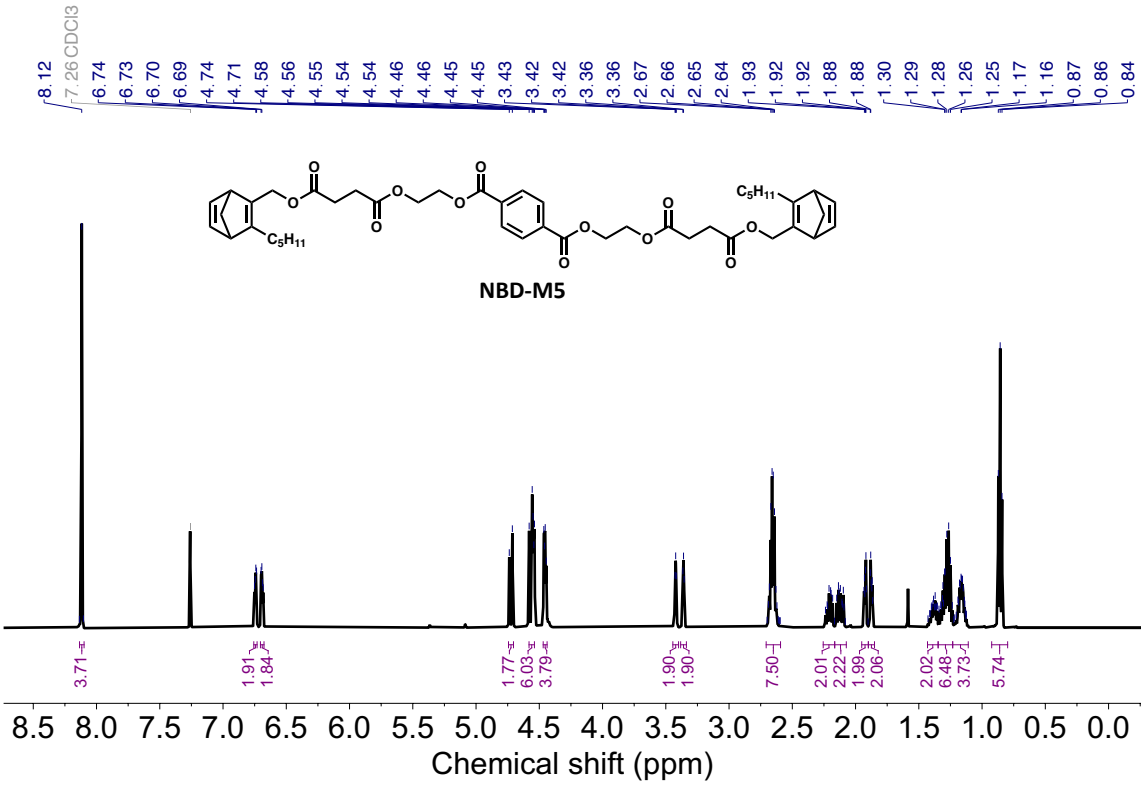


Figure S42. ^{1}H NMR spectrum of compound **NBD-M5** in $CDCl_3$.

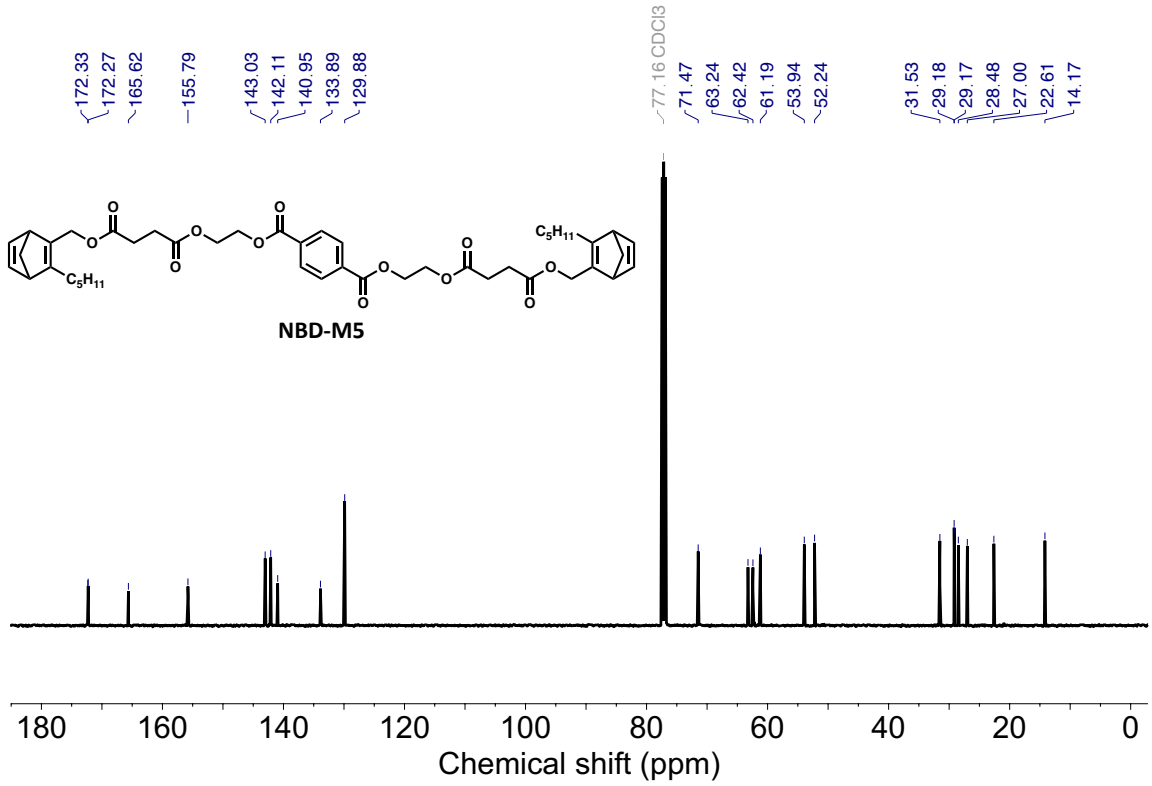


Figure S3.43. ^{13}C NMR spectrum of compound **NBD-M5** in $CDCl_3$.

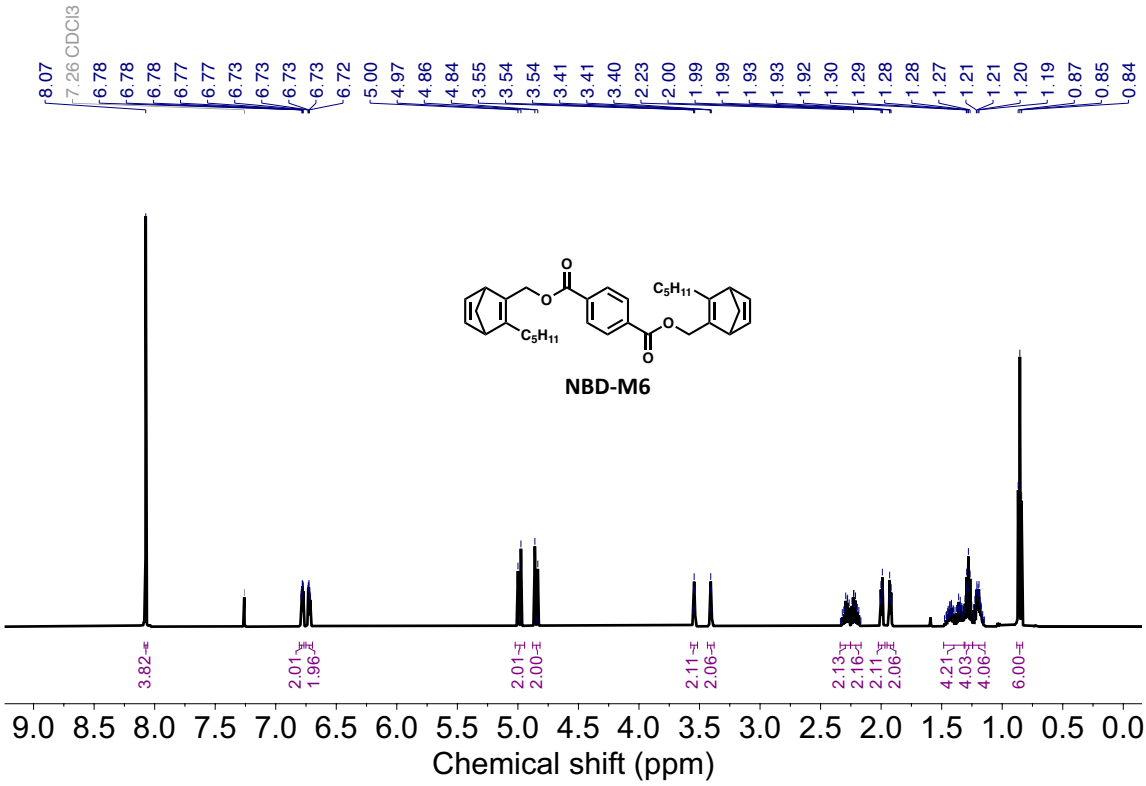


Figure S3.44. ^{1}H NMR spectrum of compound **NBD-M6** in $CDCl_3$.

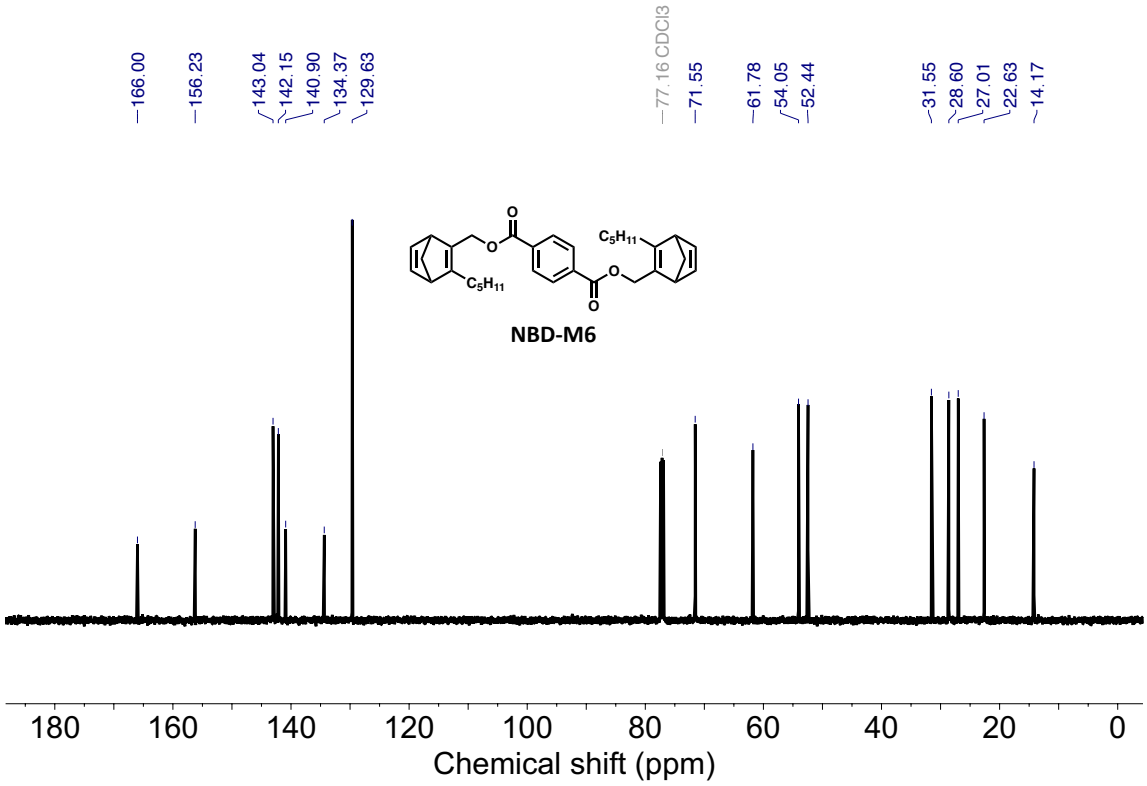


Figure S3.45. ^{13}C NMR spectrum of compound **NBD-M6** in $CDCl_3$.

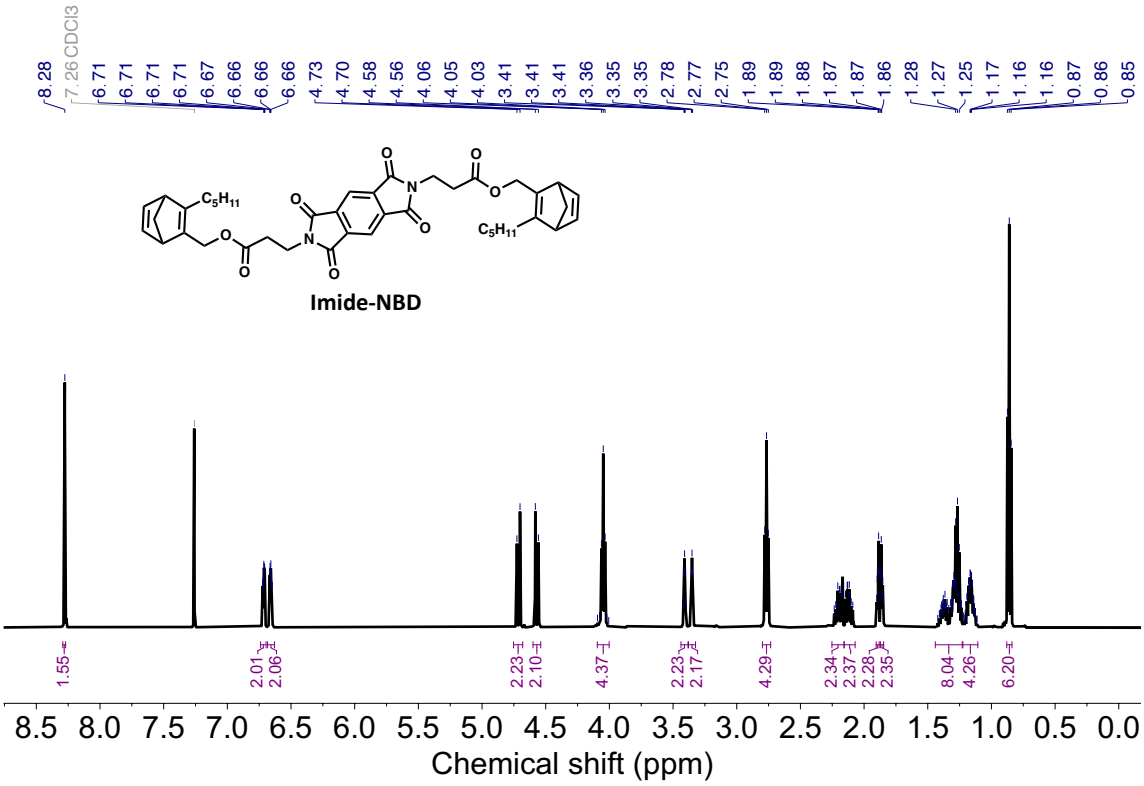


Figure S3.46. ^{1}H NMR spectrum of compound **imide-NBD** in $CDCl_3$.

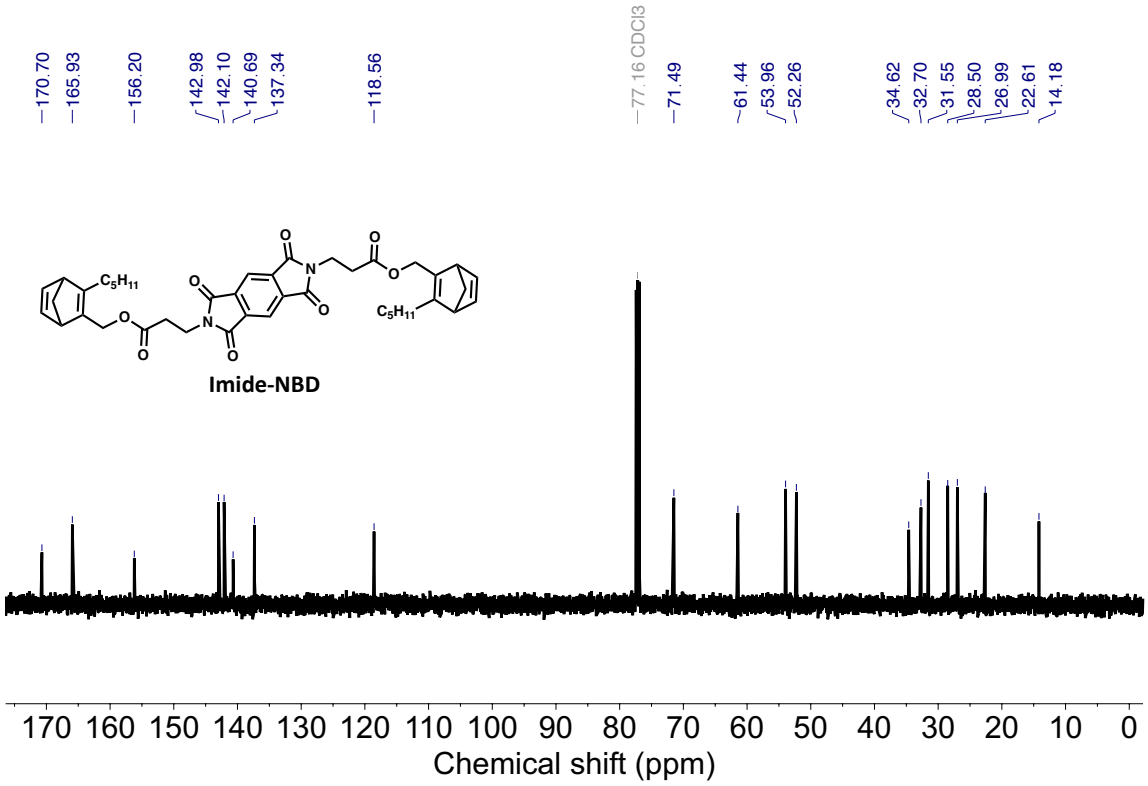


Figure S3.47. ^{13}C NMR spectrum of compound **imide-NBD** in $CDCl_3$.

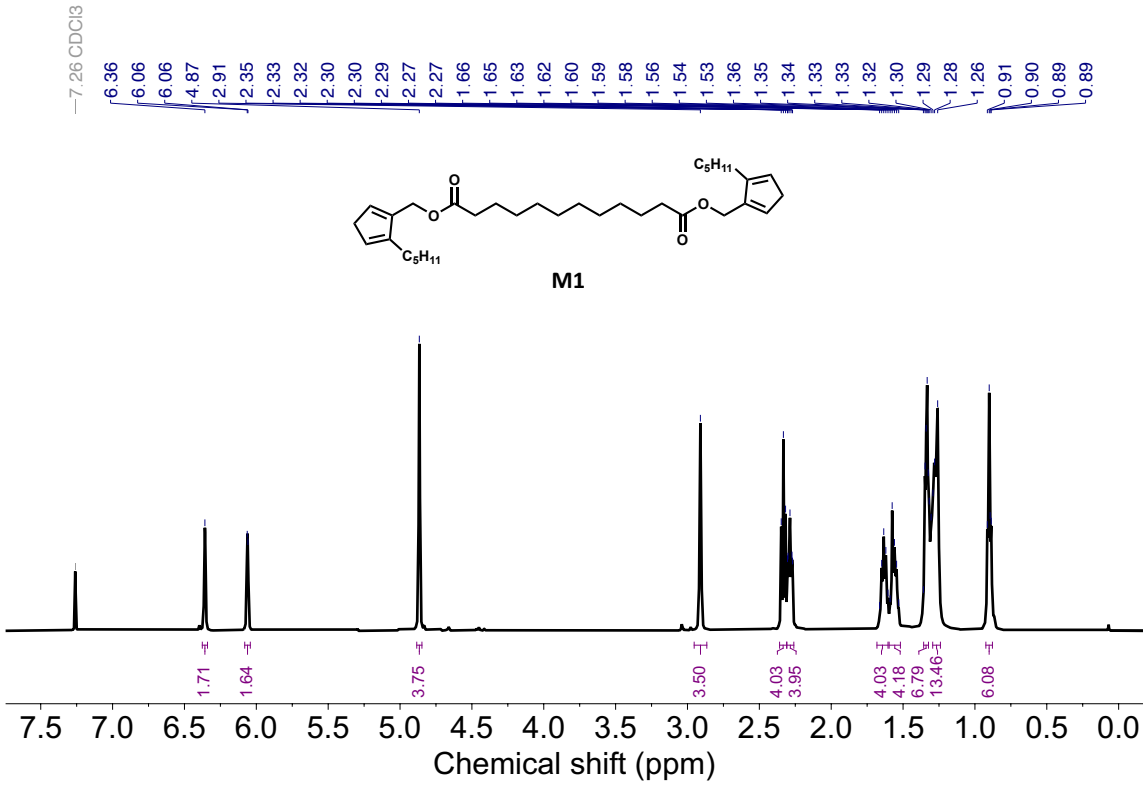


Figure S3.48. ^{1}H NMR spectrum of compound **M1** in $CDCl_3$.

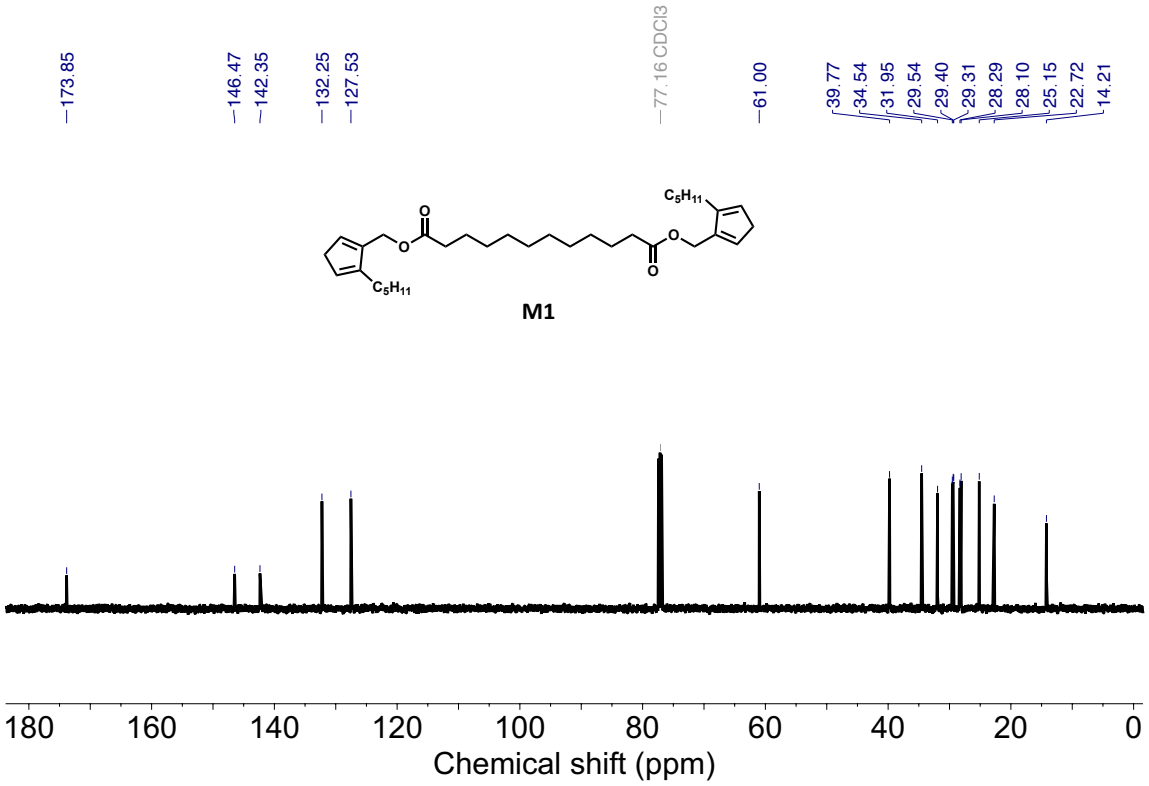


Figure S3.49. ^{13}C NMR spectrum of compound **M1** in $CDCl_3$.

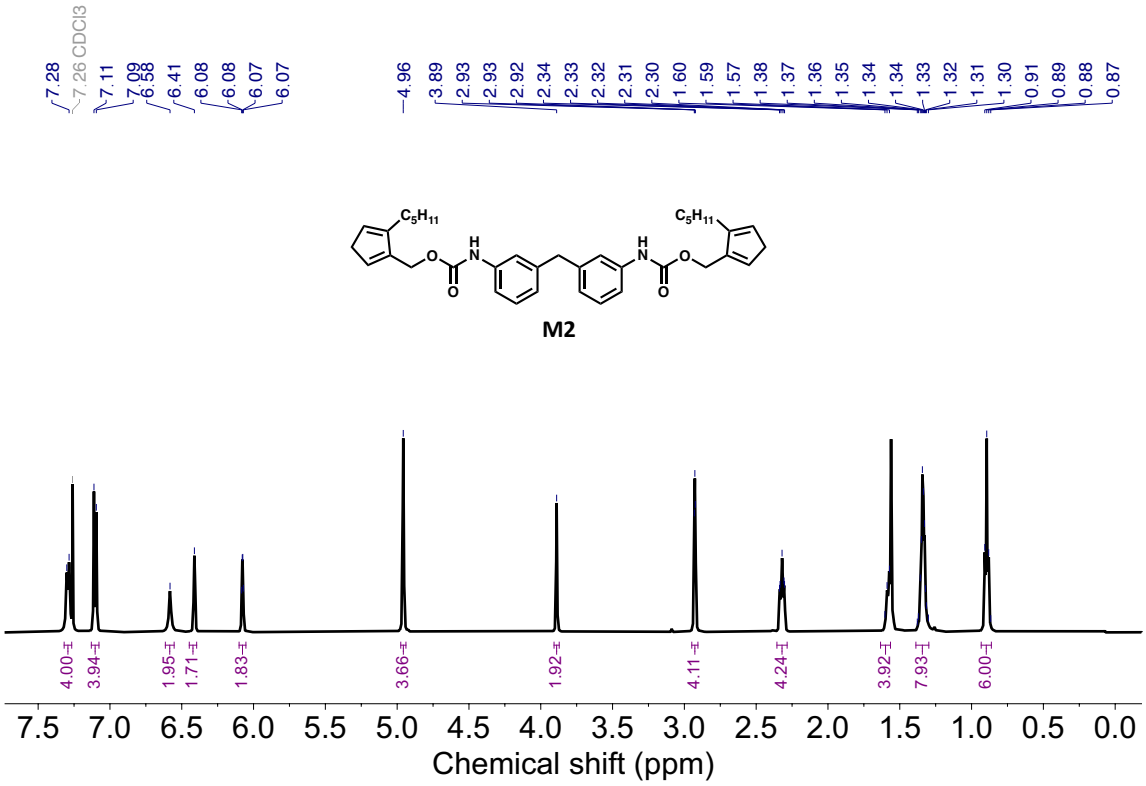


Figure S3.50. ^{1}H NMR spectrum of compound **M2** in $CDCl_3$.

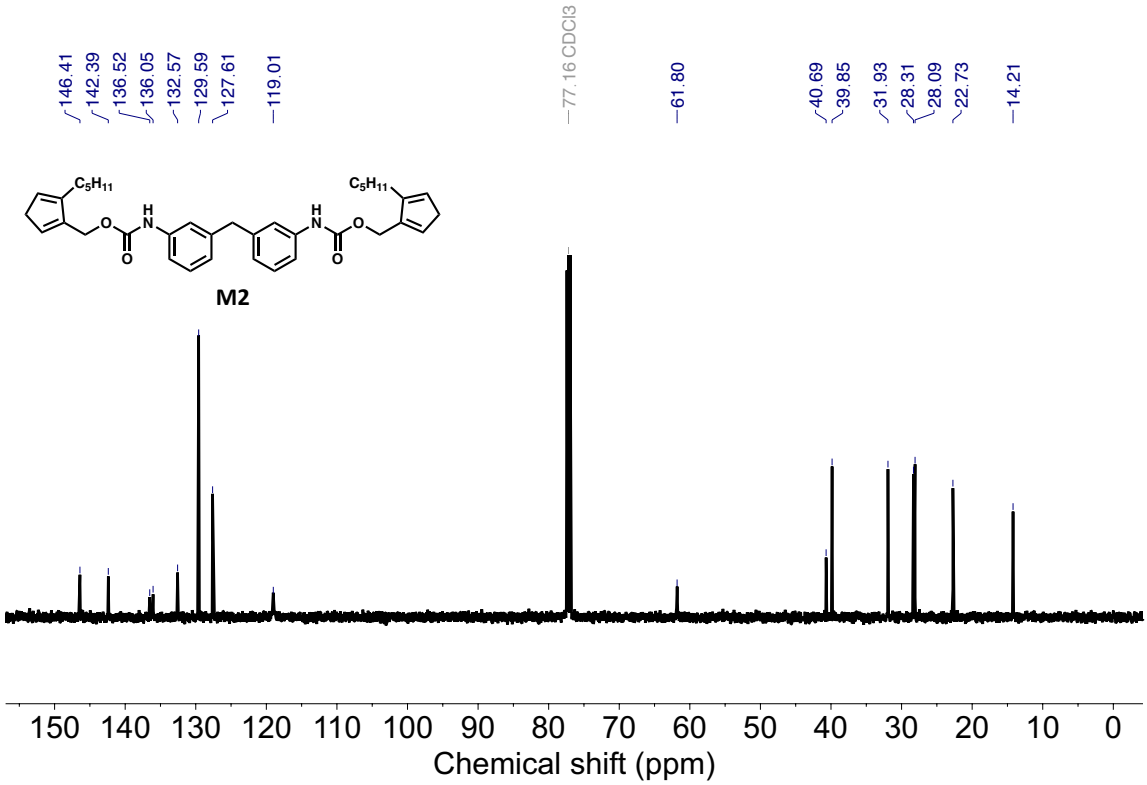


Figure S3.51. ^{13}C NMR spectrum of compound **M2** in $CDCl_3$.

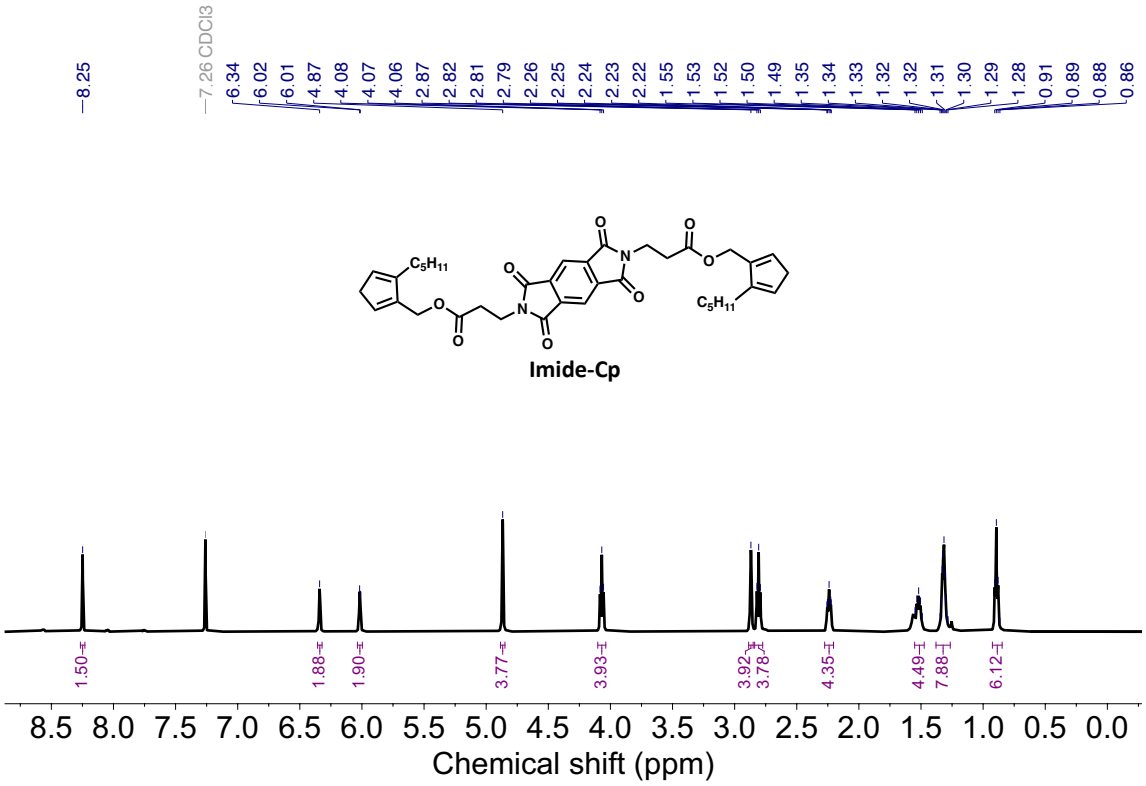


Figure S3.52. ^{1}H NMR spectrum of compound **imide-Cp** in $CDCl_3$.

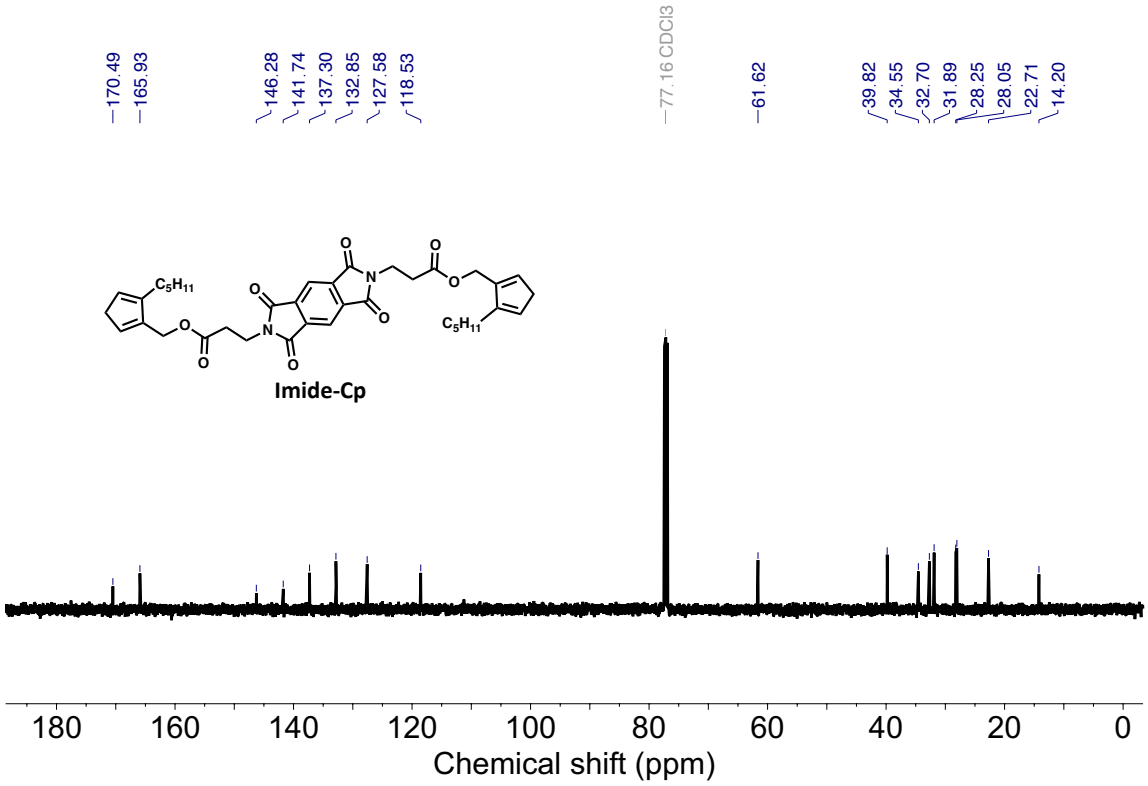


Figure S3.53. ^{13}C NMR spectrum of compound **imide-Cp** in $CDCl_3$.

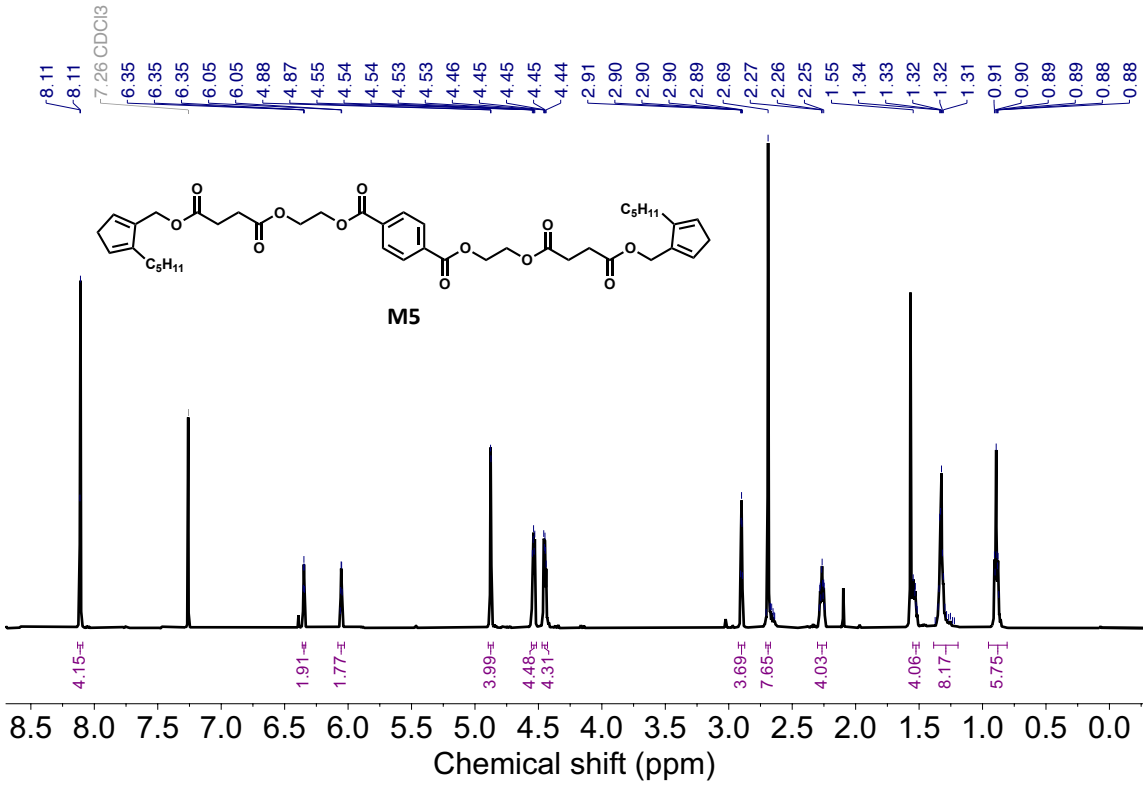


Figure S3.54. ^{1}H NMR spectrum of compound **M5** in $CDCl_3$.

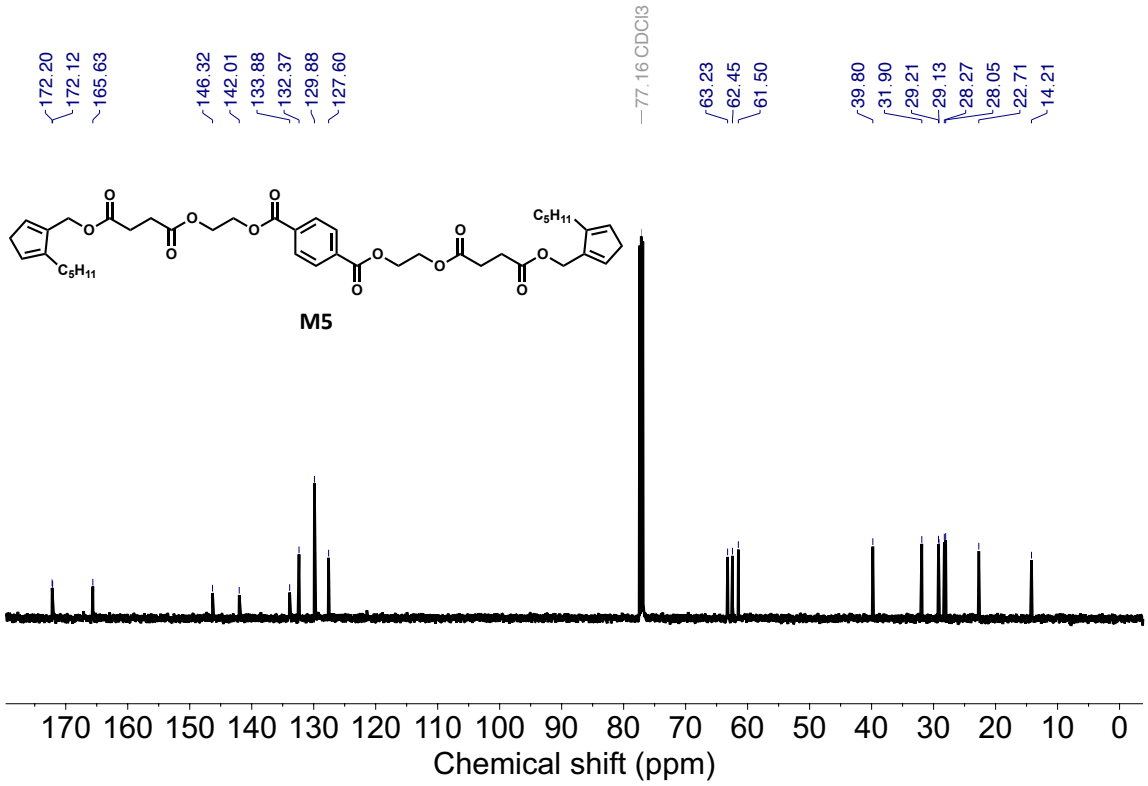


Figure S3.55. ^{13}C NMR spectrum of compound **M5** in $CDCl_3$.

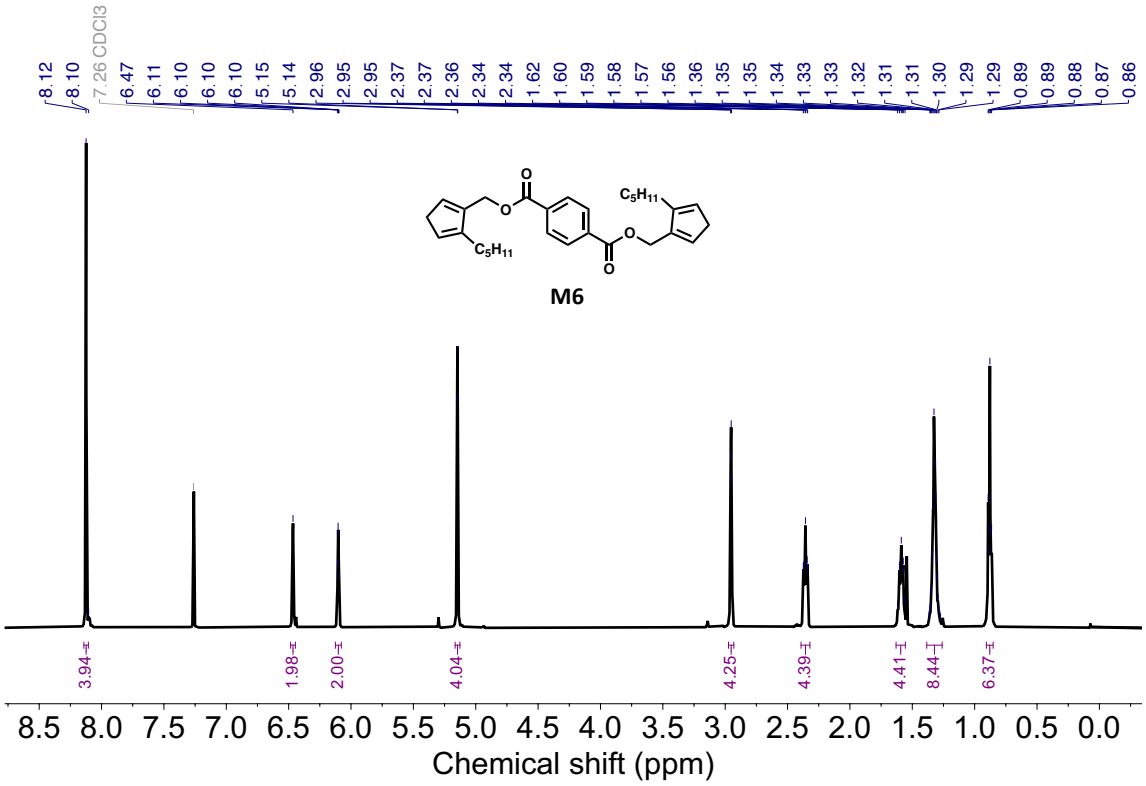


Figure S3.56. ^{1}H NMR spectrum of compound **M6** in $CDCl_3$.

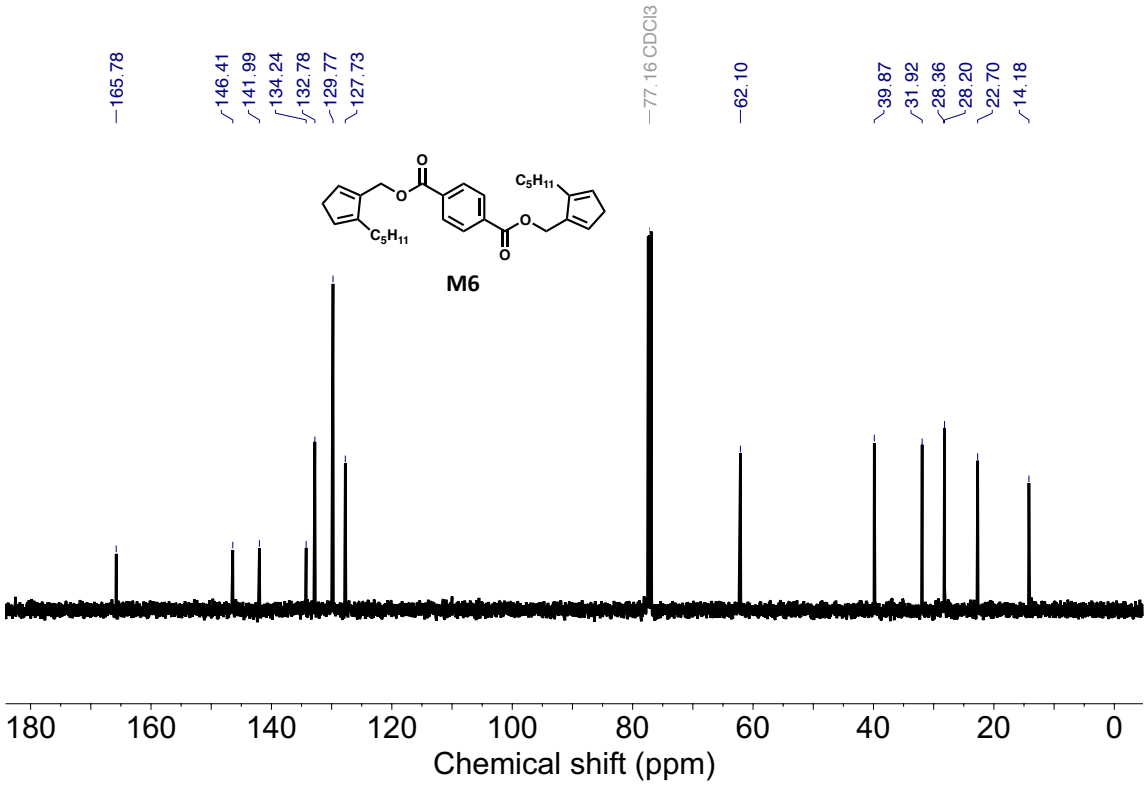


Figure S3.57. ^{13}C NMR spectrum of compound **M6** in $CDCl_3$.

Screening of polymerization conditions:

Since we observed the gelation of a similar analog as **D1** in our previous report,[39] we hypothesized that the bulky substituents such as *t*-butyl and phenyl groups would prevent the potential trimerization or uncontrolled cross-linking. We reported our observations and preliminary results in Table S3.1 with the initial screening conditions of polymerization without the addition of BHT inhibitor. Overall, the *distal* analogs show uncontrolled cross-linking behavior (gelation) upon heating across all conditions. The *proximal* analogs do not gel or cross-link in the same conditions. However, the M_w values do not prove the efficient polymerization as shown in the low range (5-10 kDa). **P3** analog leads to the lowest MW range, presumably due to the phenyl ring substituent effect.

As briefly shown in our precedent publication,[39] the addition of butylated hydroxytoluene (BHT) inhibitor prevents the uncontrolled radical cross-linking in our tetracyclopentadiene polymer. In similar manner, the addition BHT increased the isolation yield and changed the polymerization behavior of **P1** (Figure S3.58). Therefore, we reinvestigated the polymerization of *distal* materials with the addition of BHT. The best polymerization was observed to result from the original pentyl substituent (**D1**) as displayed in Table S2. Upon observation, decreasing bulkiness of the substituents led to the polymers with higher MWs. Subsequently, we tested the polymerization of the methyl substituent **22**, supposedly with smaller group compared to the 5-carbon chain. The DP_n is slightly higher than that of **D1**,

showing the smaller substituent assists the polymerization process, though not significantly (Figure S3.60).

Table S3.1. Initial screening polymerization of the monomer analogs **D1**–**3** and **P1**–**3** without addition of BHT inhibitor.

Monomer	Polymerization solvent	Time (h)	Temperature (°C)	Weight-average molecular weight obtained from SEC or M_w (kDa)	Observation of gelation
D1	Neat	96	50	–	Gelled
D2	Toluene	24–94	110	~ 2	Gelled after 24 h
	Benzene	24–72	80	~ 2 – 3	Gelled after 24 h
D3	Toluene	24	110	–	Gelled
	Benzene	24	80	–	Gelled
P1	Toluene	94	110	3	–
	Neat	48–72	90	~ 7 – 8	–
P2	Toluene	24–96	110	~ 1 – 2	–
	Benzene	24–96	80	~ 1 – 2	–
	Neat	15–48	90	~ 7 – 8	–
P3	Toluene	24–48	110	< 1	–
	Neat	18-60	90	~ 3 – 4	–

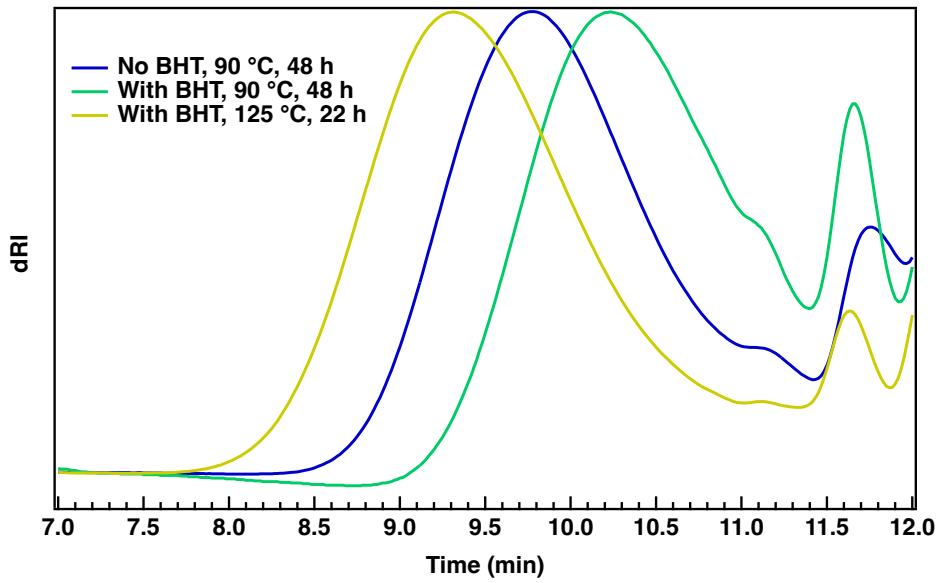


Figure S3.58. Polymerizing behaviors of the **P1** changed with the addition of BHT under ambient conditions. Gelation was observed while polymerizing under ambient atmosphere without addition of BHT at 125 °C. The highest DP_n is 16 ($M_{n(SEC)}$ = 7,000 Da; $M_{w(SEC)}$ = 13,000 Da; $Đ$ = 1.8).

Table S3.2. Polymerization of the monomer analogs **D1**–**D3** with the addition of BHT inhibitor (5 mol%) in neat condition. All the polymers were characterized as crude mixtures, no purification was performed.

	Time (h)	Temperature (°C)	Number-average molecular weight obtained from SEC or M_n (Da)	Weight-average molecular weight obtained from SEC or M_w (Da)	Degree of polymerization from M_n (DP_n)	Degree of polymerization from M_w (DP_w)
D1	24	90	19,000	33,000	43	74
	48		20,000	34,000	44	77
D2	24	90	3,800	8,800	9	21
	48		4,600	11,000	11	28
D3	24	90	1,700	3,000	4	7
	48		1,800	4,400	4	10

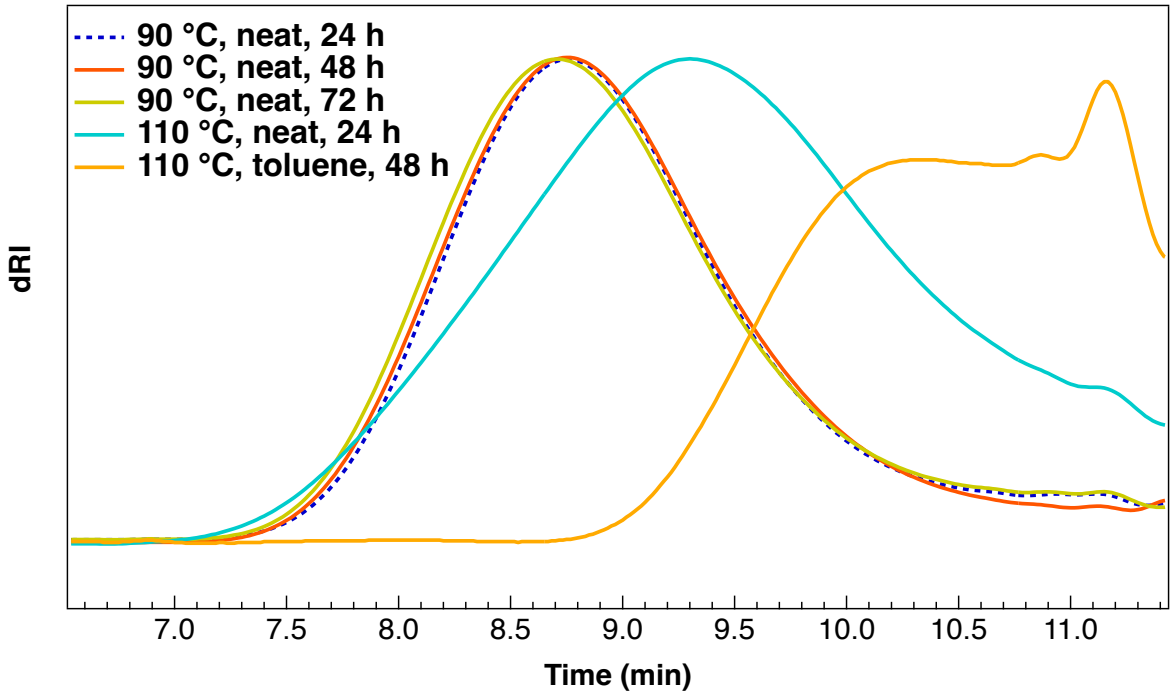


Table S3.59. Screening polymerization of **D1** in various conditions, showing the optimal condition is 90 °C without solvent. Stirring with a stir bar or shaking the monomer mixtures (with no stir bar) at 90 °C did not increase the MW (not shown). Adding solvent (i.e., toluene) to the **D1** mixture at 90 °C lowers the MW range of the polymer. Heating **D1** at 125 °C for 24 h resulted in uncontrolled cross-linked polymer. Of note, all the polymers were characterized as crude mixtures (no purification was performed).

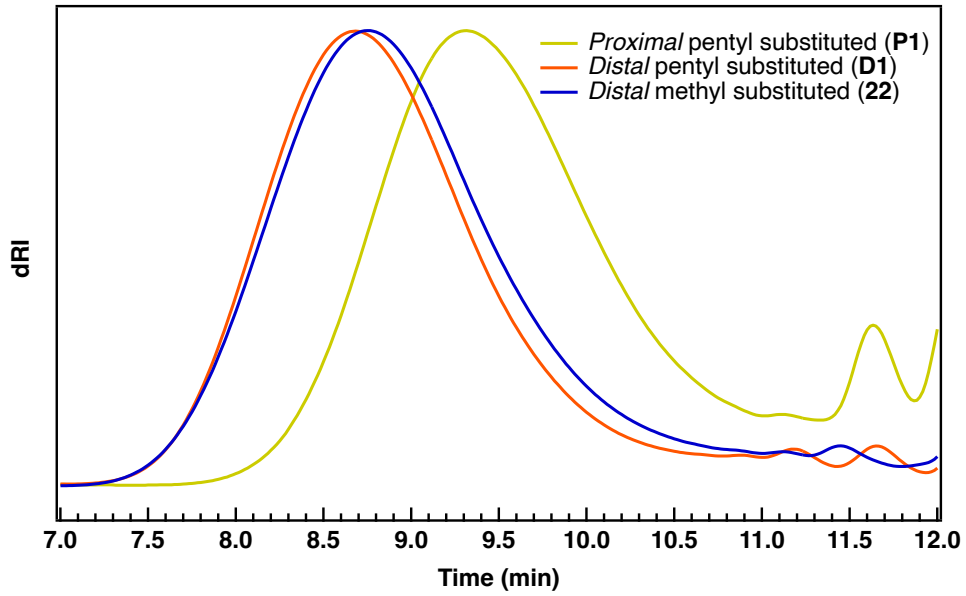
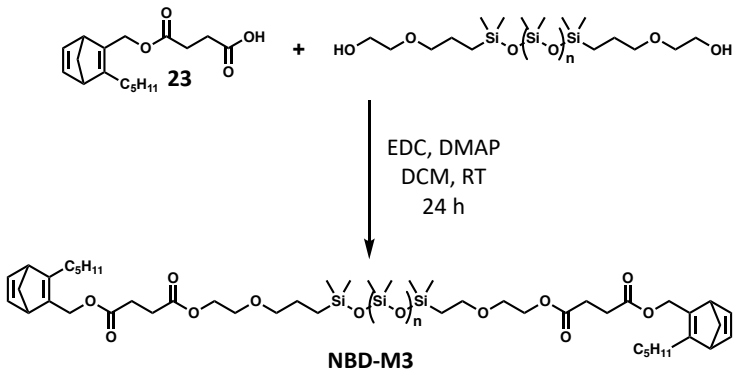


Figure S3.60. Comparison of polymerization among different analogs (**P1**, **D1**, **22**) shows similar MW range between **D1** and **22** analogs. the *distal* methyl substituted substrate displays slightly higher polymerization efficiency ($M_{n(SEC)}$ = 16,000 Da; $M_{w(SEC)}$ = 32,000 Da, DP_n = 49, DP_w = 95). All the polymers were characterized as synthesized (no purification was performed).

Synthesis of the pre-polymers or macromonomers:



To a dried 250 mL round bottom were added compound **23** (360 mg, 1.2 mmol, 2.2 eq.) and the poly(dimethylsiloxane) bis(hydroxyalkyl) terminated or PDMS-bisOH (purchased from Sigma-Aldrich, M_n ~ 5,600 Da, 3.1 g, 0.6 mmol, 1.0 eq.) and 12 mL DCM. To this solution were added EDC (645 mg, 3.4 mmol, 6.0 eq.) and DMAP (27 mg, 0.2 mmol, 0.4 eq.). Once added, the solution was allowed to stir at room temperature for 24 h. The crude solution was washed with water followed by brine solution until the organic layer became clear. The organic layer was dried over Na_2SO_4 and concentrated. The crude residue was subjected to precipitation with cold methanol, which was repeated three times, to afford the pre-polymer **NBD-M3** as a colorless oil (2.8 g). ^{1}H NMR analysis displayed quantitative incorporation of the NBD chain-ends. $M_{n(NMR)}$ = 8,500 Da; $M_{n(SEC)}$ = 9,800 Da; $M_{w(SEC)}$ = 14,000 Da; $Đ$ = 1.4.

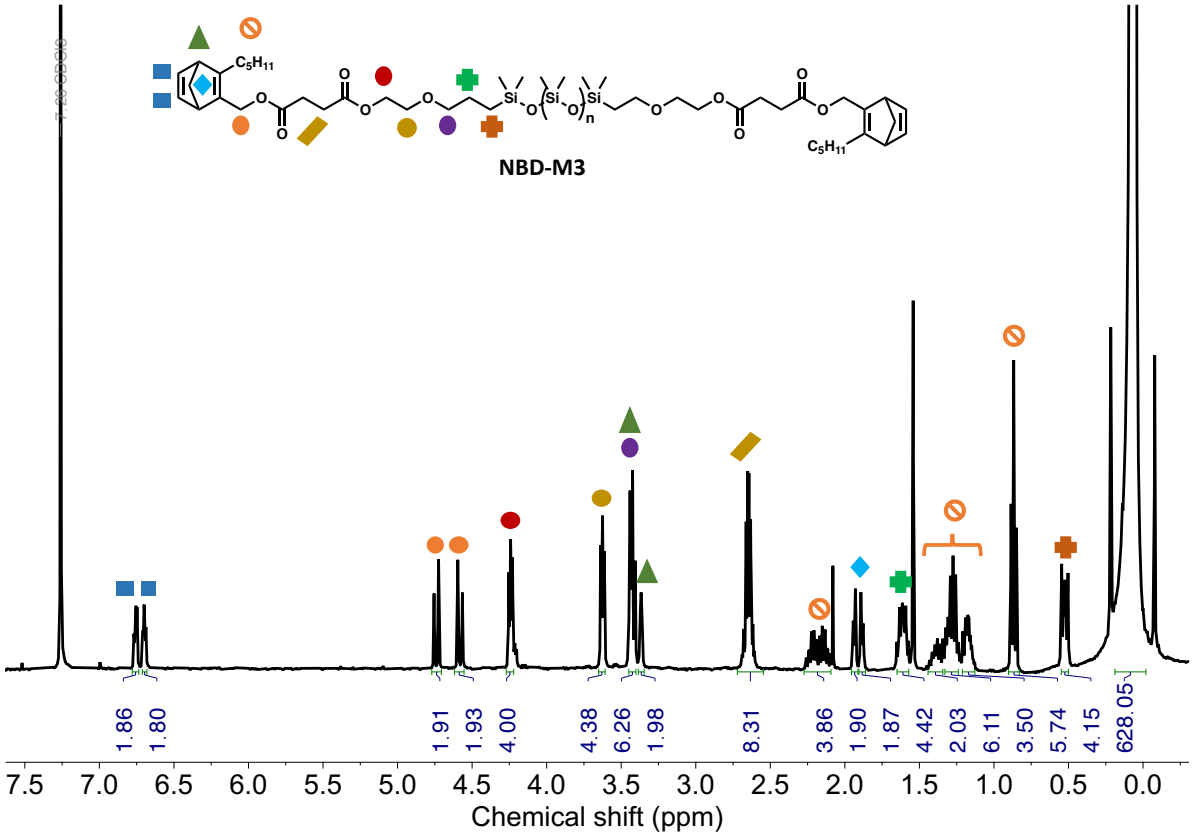
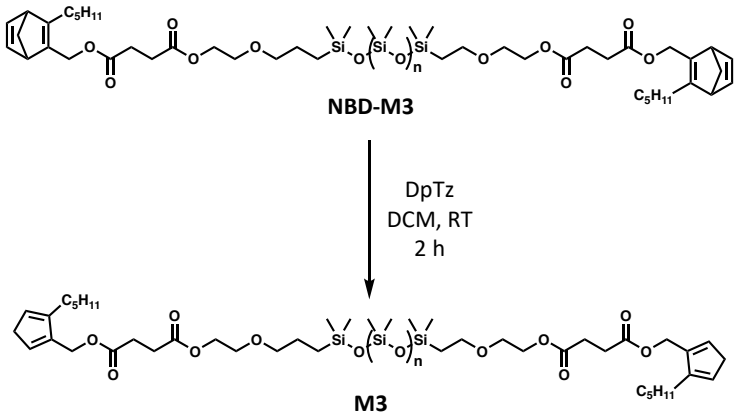


Figure S3.61. ^{1}H NMR spectrum of **NBD-M3** ($M_{n(NMR)}$ = 8,500 Da) in $CDCl_3$ indicates quantitative chain-end incorporation.



A solution of compound **NBD-M3** (2.8 g, 1.0 eq.) and DpTz (600 mg, 5.5 eq.) in 23 mL DCM was stirred at room temperature for 2 h. The crude solution was passed through a plug of silica with DCM as the eluent to remove excess amount of tetrazine (vibrant pink/red solid) and byproduct pyridazine (vibrant yellowish solid). After the silica plug, concentration of the filtrate afforded the pure product **M3** as colorless oil (2.2 g). ^{1}H NMR analysis displayed successful deprotection of the NBD chain-ends to reveal the Cp chain-ends. $M_{n(NMR)}$ = 8,600 Da; $M_{n(SEC)}$ = 11,000 Da; $M_{w(SEC)}$ = 13,000 Da; $Đ$ = 1.3.

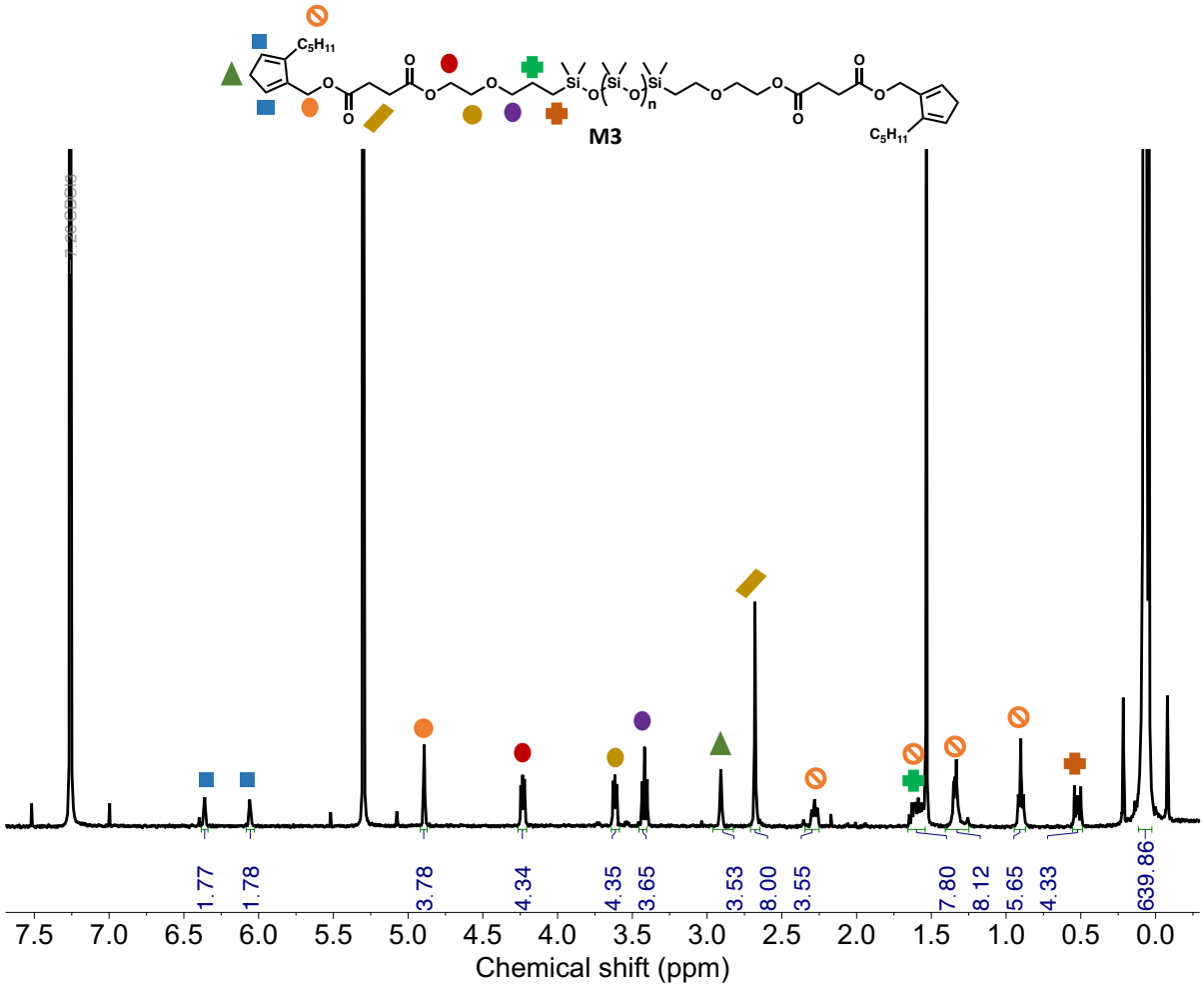


Figure S3.62. ^{1}H NMR spectrum of **M3** ($M_{n(NMR)}$ = 8,600 Da) in $CDCl_3$ to clearly display the quantitative deprotection to reveal Cp chain-ends.

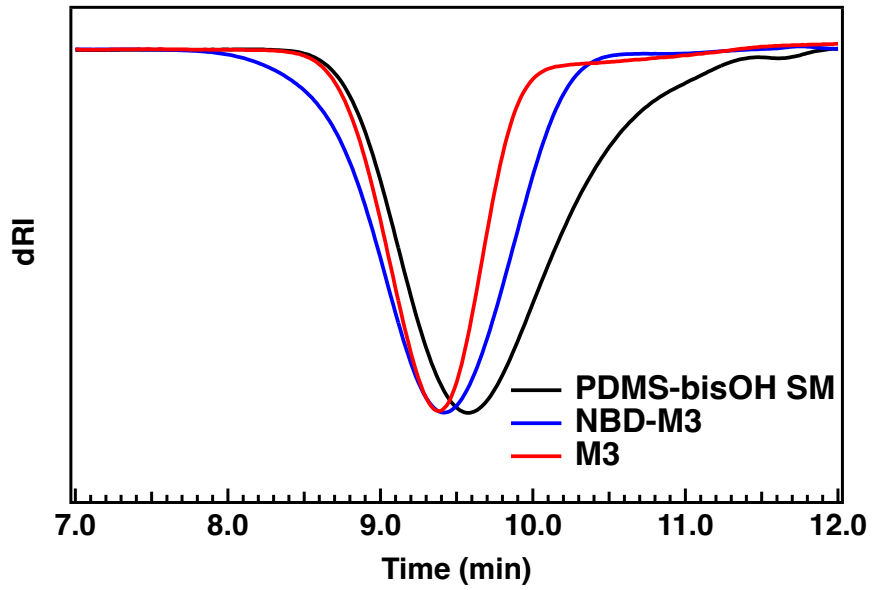
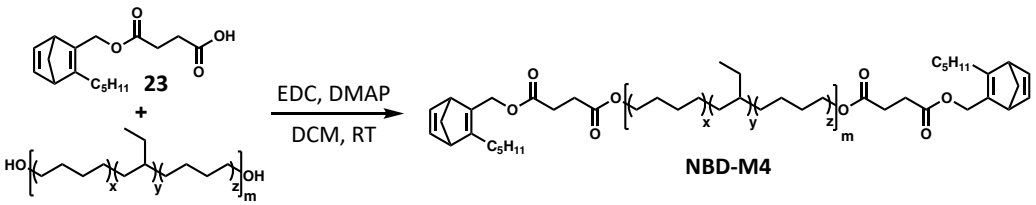


Figure S3.63. Overlay of SEC trace of the starting material **PDMS-bisOH** (M_n = 5,400 Da; M_w = 9,200 Da; $Đ$ = 1.7), **NBD-M3** (M_n = 9,800 Da; M_w = 13,000 Da; $Đ$ = 1.4), and the deprotected product **M3** (M_n = 11,000 Da; M_w = 13,000 Da; $Đ$ = 1.3).



Compound **NBD-M4** was prepared similar to the procedure for compound **NBD-M3**, with 200 mg of **23** (0.7 mmol, 2.2 eq.), 935 mg of hydrogenated hydroxyl-terminated polybutadiene or Krasol (purchased from Cray Valley, M_n = 3,100 Da – reported from the vendor, 0.3 mmol, 1.0 eq.), 360 mg of EDC (1.9 mmol, 6.0 eq.), and 11 mg of DMAP (0.09 mmol, 0.3 eq.) in 8 mL DCM. After concentration, the crude residue was subjected to precipitation with cold ethanol, which was repeated three times, to afford the pre-polymer

NBD-M4 as a colorless oil (680 mg). ^{1}H NMR analysis displayed quantitative incorporation of the NBD chain-ends. $M_{n(SEC)}$ = 6,200 Da; $M_{w(SEC)}$ = 6,900 Da; $Đ$ = 1.1.

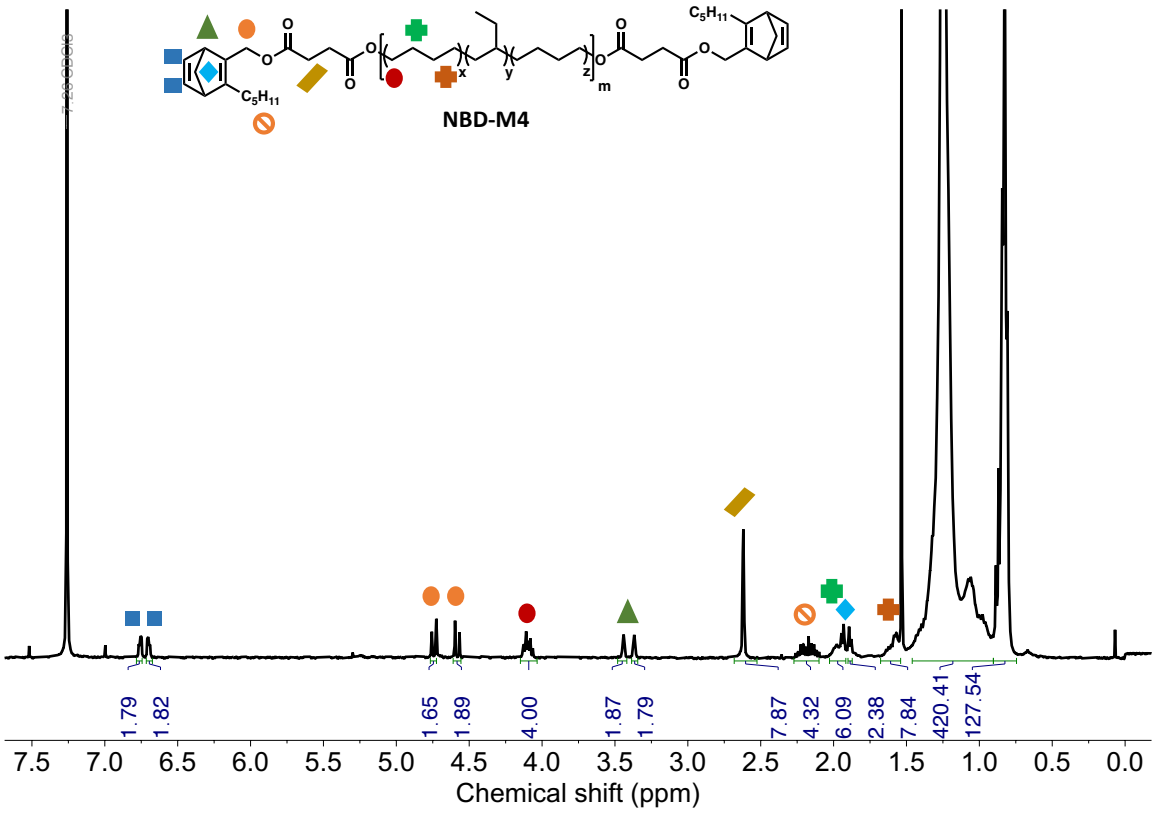
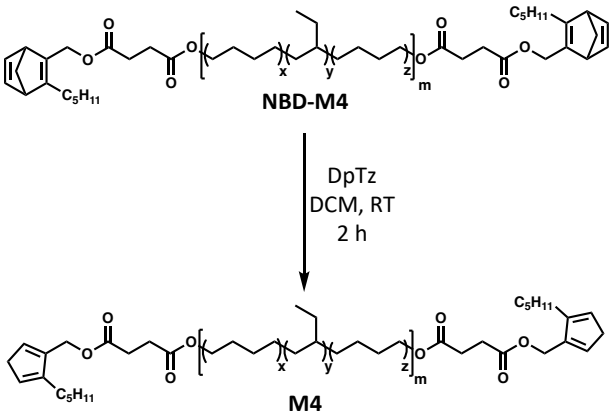


Figure S3.64. ^{1}H NMR spectrum of **NBD-M4** in $CDCl_3$ displays the quantitative incorporation of NBD chain-ends.



Compound **M4** was prepared similar to the synthesis of **M3**, with 680 mg of **NBD-M4** (1.0 eq.) and 250 mg of DpTz (5.5 eq.) in mL DCM. The crude product was subjected to a silica plug with DCM as the eluent. The solution was concentrated to afford the pure product **M4** as colorless oil (611 mg). ^{1}H NMR analysis displayed successful incorporation of the NBD chain-ends. $M_{n(SEC)}$ = 6,200 Da; $M_{w(SEC)}$ = 6,900 Da; $Đ$ = 1.1.

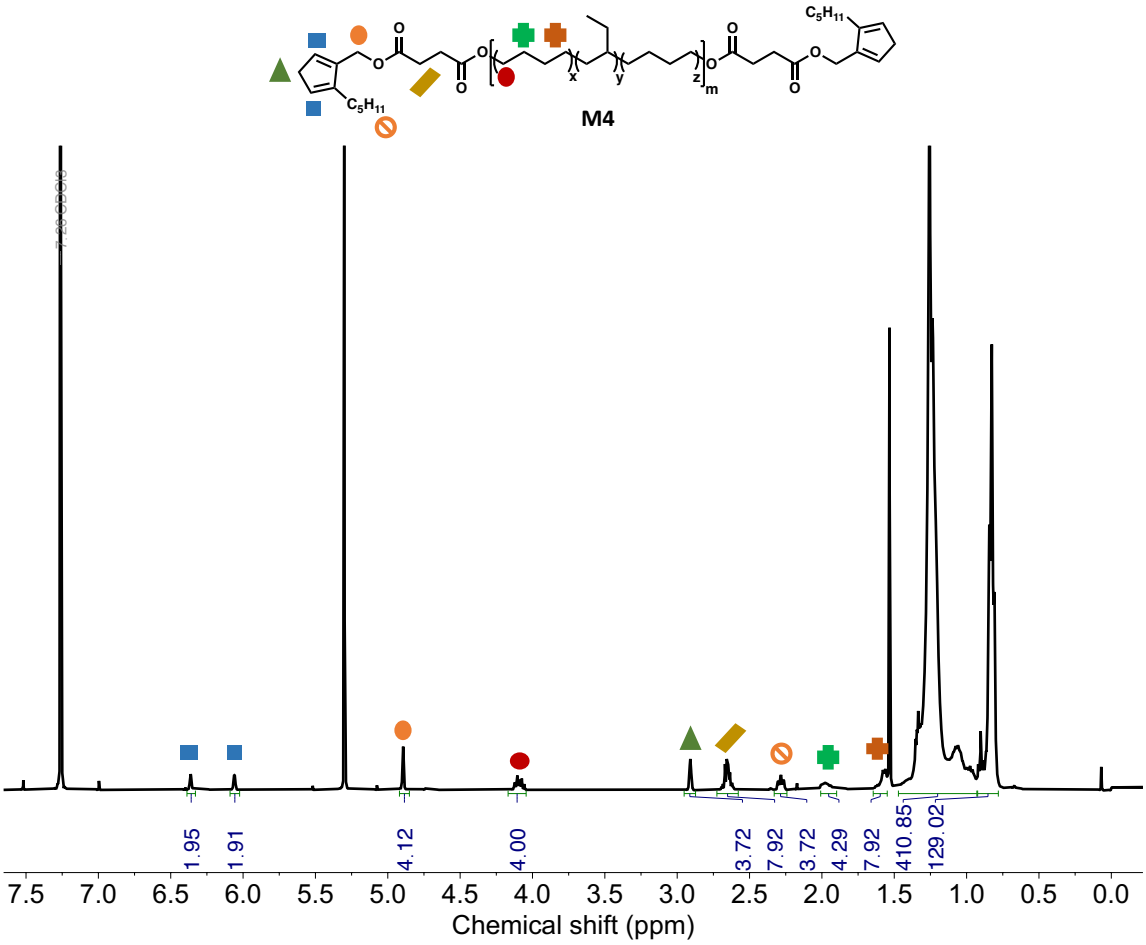


Figure S3.65. ^{1}H NMR spectrum of **M4** in $CDCl_3$ reveals the quantitative deprotection to reveal Cp chain-ends.

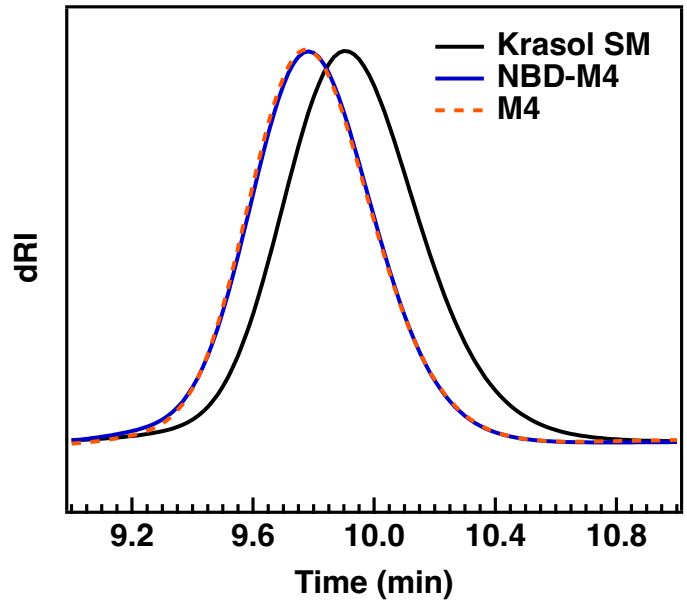


Figure S3.66. Overlay of SEC trace of the Krasol starting material (M_n = 5,000 Da, M_w = 5,700 Da, $Đ$ = 1.1), **NBD-M4** (M_n = 6,200 Da; M_w = 6,900 Da; $Đ$ = 1.1), and the deprotected product **M4** (M_n = 6,200 Da; M_w = 6,900 Da; $Đ$ = 1.1).

Screening polymerization conditions of solid and high T_g polymers

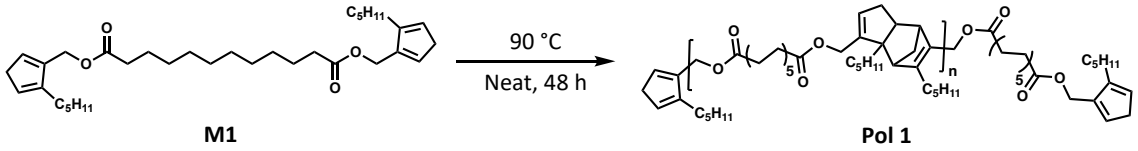
Polymerization conditions of solid Cp monomers, urethane-Cp (**M2**) and **imide-Cp**, were screened. Solubility of the materials is essential to ensure proper polymerization. As observed, prolonged heating increased degradation of the synthesized polymers. As discussed in section 1.6, no solvent and heating at 90 °C was proven to be the optimal polymerization condition. Therefore, with low melting point, **M2** liquefied at 90 °C. Heating the melt material for 48 h provided the polymer with sufficient MW. **Imide-Cp**, on the contrary, did not melt at the screening temperature range (90 – 110 °C), thus did not form high-MW polymer. Nonetheless,

the highly insolubility of polyimide has been studied and the MW range is typically low as reported in literature.[43-45]

Table S3.3. Polymerization of imide and urethane Cp monomers (**imide-Cp** and **M2**, respectively) with 5 mol% BHT to form similar analogs as polyimide and polyurethane, respectively.

Monomer	Solvent	Temperature (°C)	Time (h)	Observation	M_w (kDa)
M2	DCM	50 °C	24	Soluble	1.8
			72		9.5
	DCE	80 °C	48	Soluble	10
			72		2.8
	Chlorobenzene	110 °C	48	Insoluble	–
	Hexachlorobutadiene	110 °C	48	Partially soluble	3.4
	None (neat)	110 °C	5	Melted, polydispersity increased with longer heating	11
			48		8.5
	None (neat)	90 °C	24	Melted	14
			48		14
Imide-Cp	DCE	80 °C	48 – 72	Soluble	1.0
	Chlorobenzene	110 °C	48	Partially soluble	–
	Hexachlorobutadiene	110 °C	48	Soluble, discolored with prolonged heating	2.0
	DMF	110 °C	24	Soluble, discolored with prolonged heating	7.9
	DMF	90 °C	24 – 48	Soluble	0.8

NMR spectra and SEC curves of the synthesized polymers:



M1 Pol 1

To a 20-mL scintillation vial was added **M1** (63 mg, 0.1 mmol, 1 eq.) and butylated hydroxytoluene (BHT, 1.4 mg, 5 mol%). The material was polymerized at 90 °C, neat. No stirring was required for 48 h. The polymer was precipitated in cold ethanol three times to obtain the pure polymer **Pol 1** (45 mg).

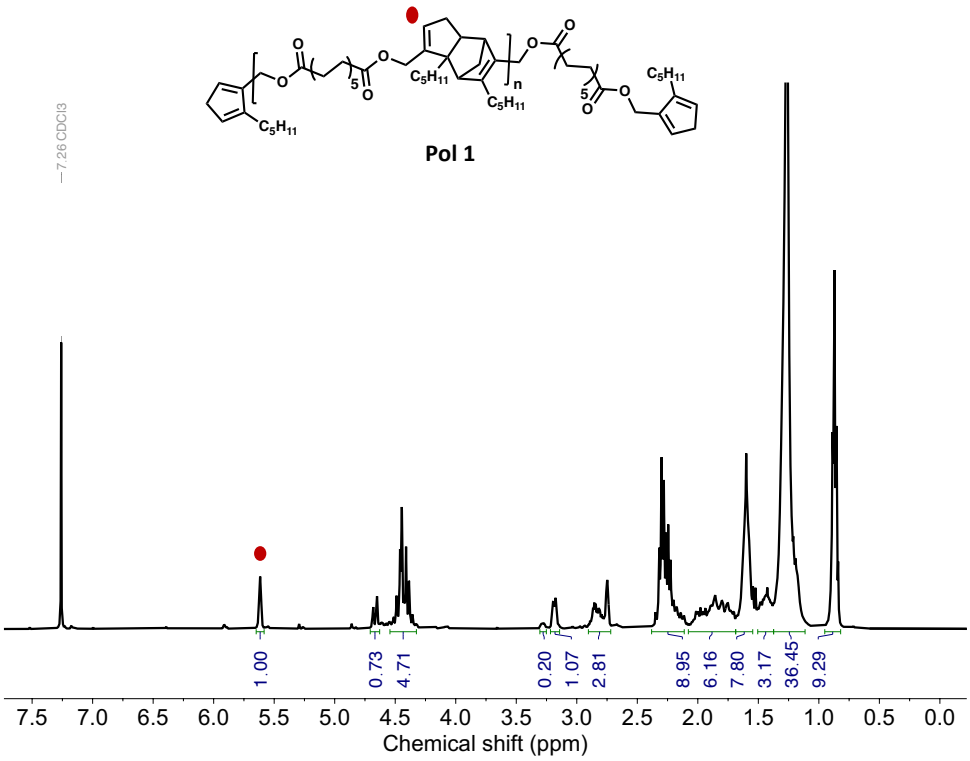


Figure S3.67. ^{1}H NMR spectrum of **Pol 1** in $CDCl_3$. One of the major isomers is shown. Stereo-configuration is not shown but the major *exo* form is expected. Chain-ends are not evident and thus, are not assigned on the spectrum.

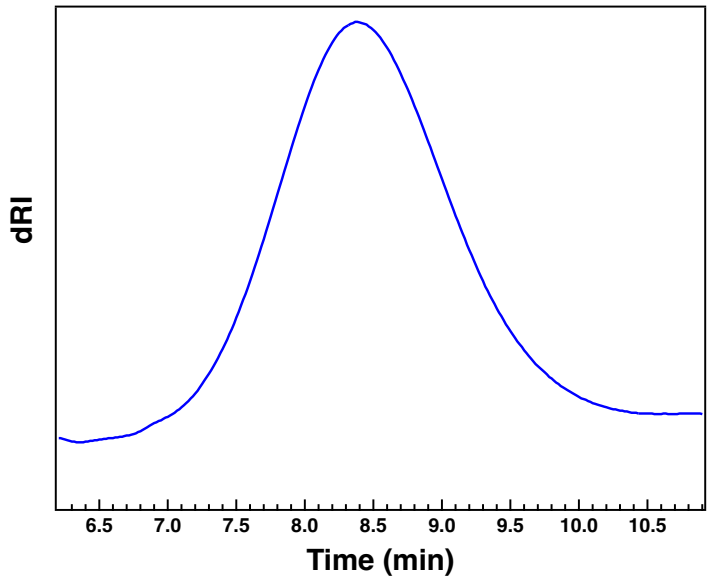
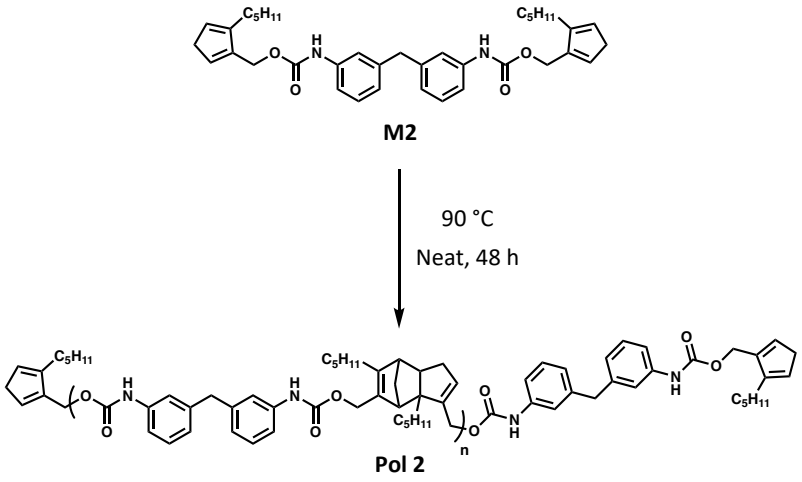


Figure S3.68. The SEC trace of **Pol 1**, showing M_n = 27,000 Da; M_w = 57,000 Da; $Đ$ = 2.1.



To a dram vial was added **M2** (51 mg, 0.09 mmol, 1 eq.) and BHT (1 mg, 5 mol%). The material was polymerized at 90 °C, neat. No stirring was required for 48 h. The polymer was precipitated in cold hexanes three times to obtain the pure polymer **Pol 2** (36 mg).

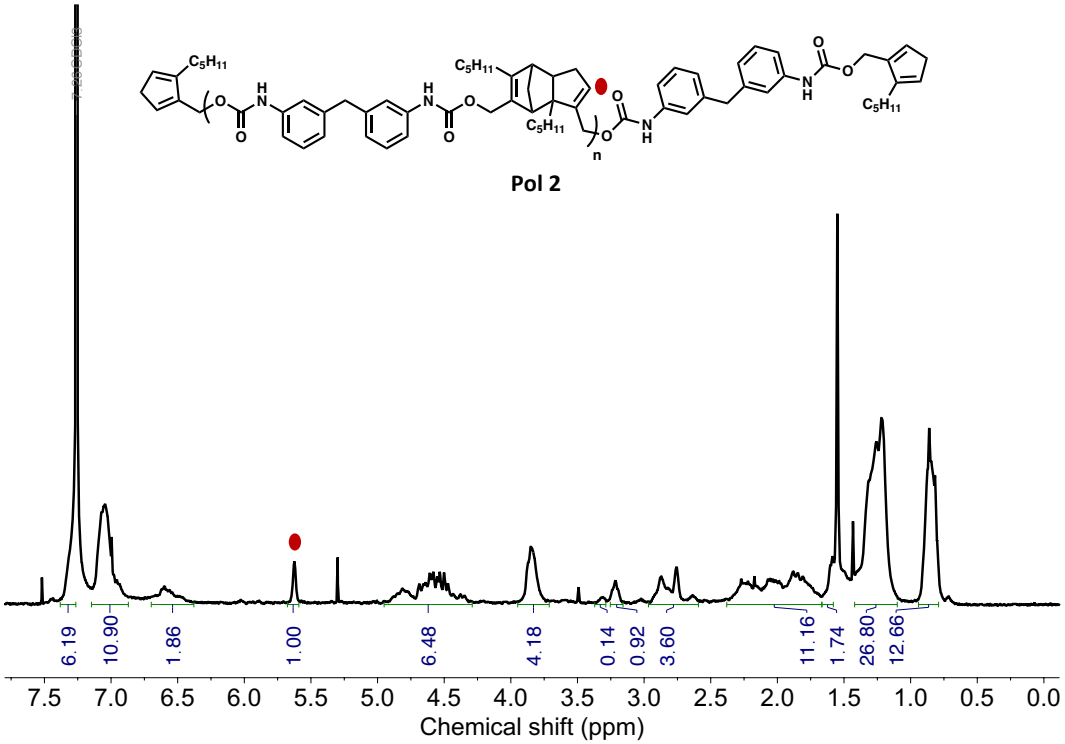


Figure S3.69. ^{1}H NMR spectrum of **Pol 2** in $CDCl_3$. One of the major isomers is shown. Stereo-configuration is not shown but the major *exo* form is expected. Chain-ends are not evident and thus, are not assigned on the spectrum.

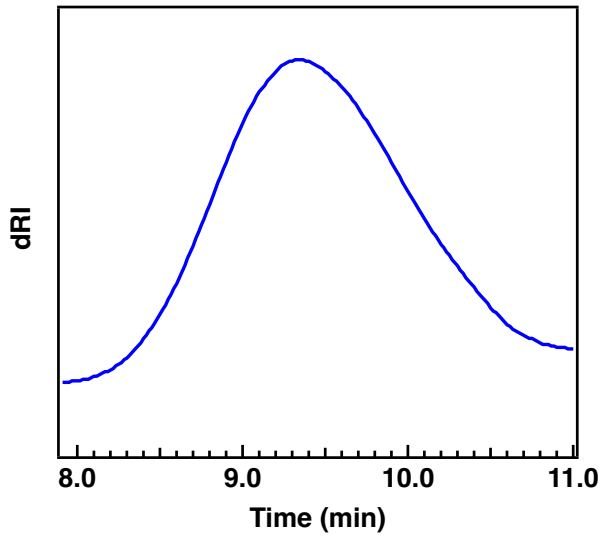
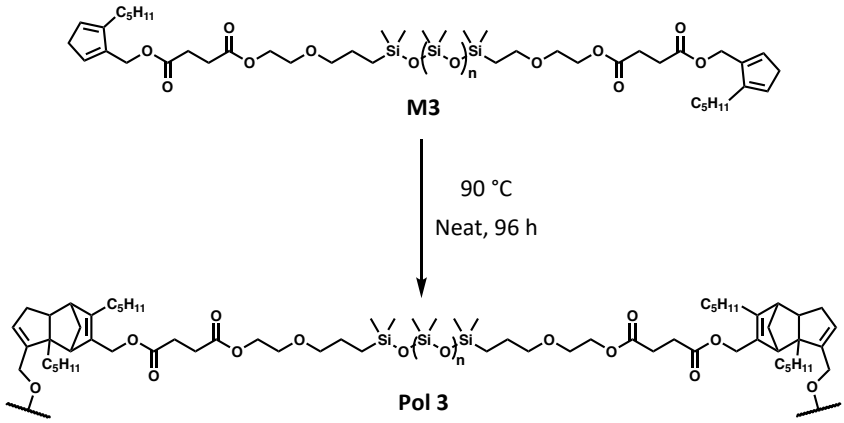


Figure S3.70. The SEC trace of **Pol 2**, showing M_n = 8,800 Da; M_w = 14,000 Da; $Đ$ = 1.6.



To a 20-mL scintillation vial was added **M3** (80 mg, 1 eq.) and BHT (0.2 mg, 5 mol%). The material was polymerized at 90 °C, neat. No stirring was required for 96 h. The polymer was precipitated in cold methanol three times to obtain the pure polymer **Pol 3** (61 mg).

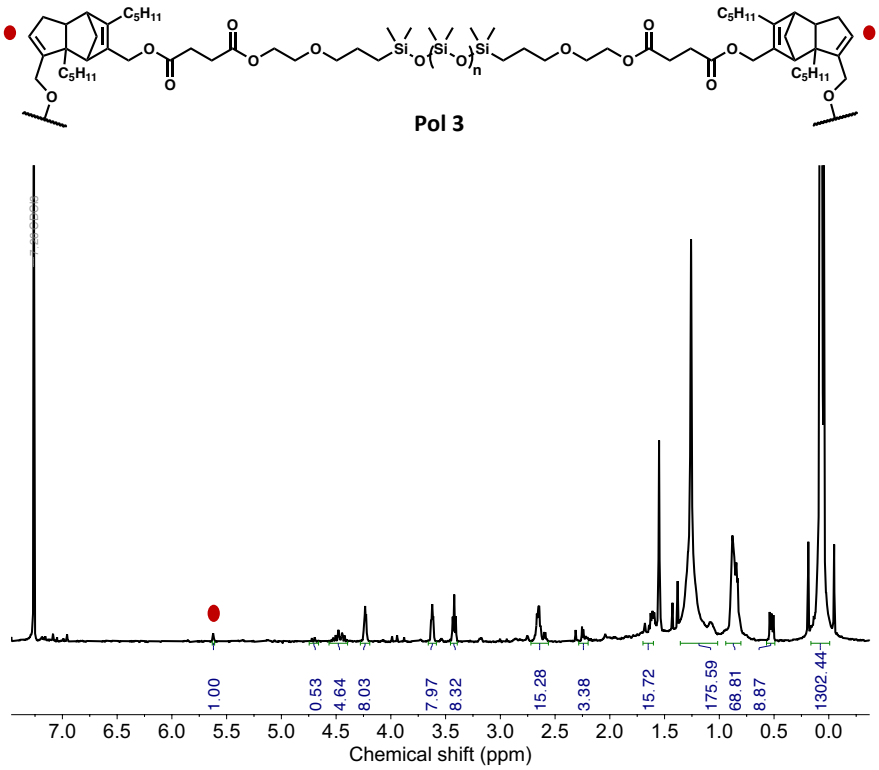


Figure S3.71. ^{1}H NMR spectrum of **Pol 3** in $CDCl_3$. One of the major isomers is shown. Stereo-configuration is not shown but the major *exo* form is expected. Chain-ends are not evident and thus, are not assigned on the spectrum.

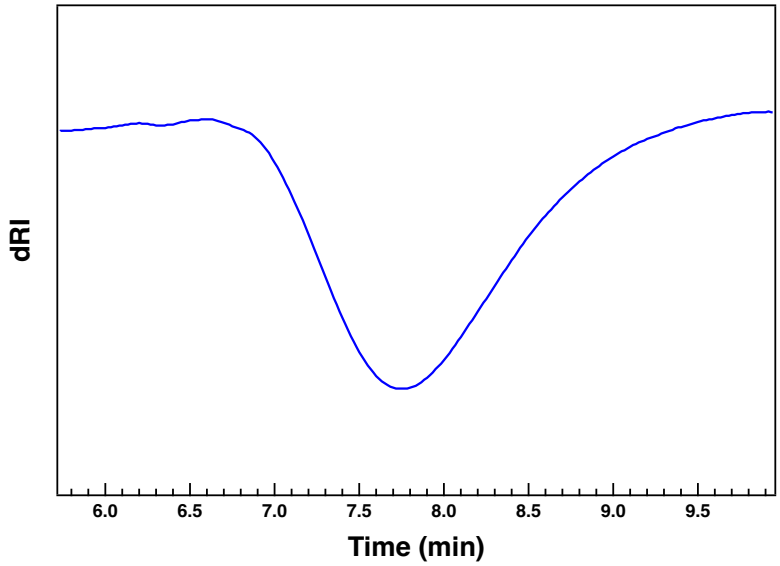
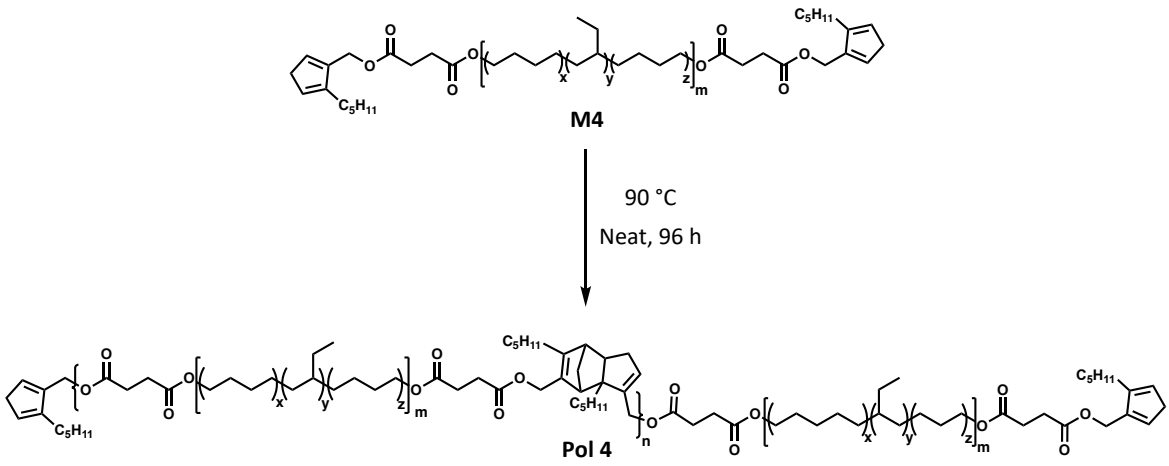


Figure S3.72. The SEC trace of **Pol 3**, showing M_n = 78,000 Da; M_w = 150,000 Da; $Đ$ = 2.0.



To a 20-mL scintillation vial was added **M4** (300 mg, 1 eq.) and BHT (0.4 mg, 5 mol%). The material was polymerized at 90 °C, neat. No stirring was required for 96 h. The polymer was precipitated in cold methanol three times to obtain the pure polymer **Pol 4** (220 mg).

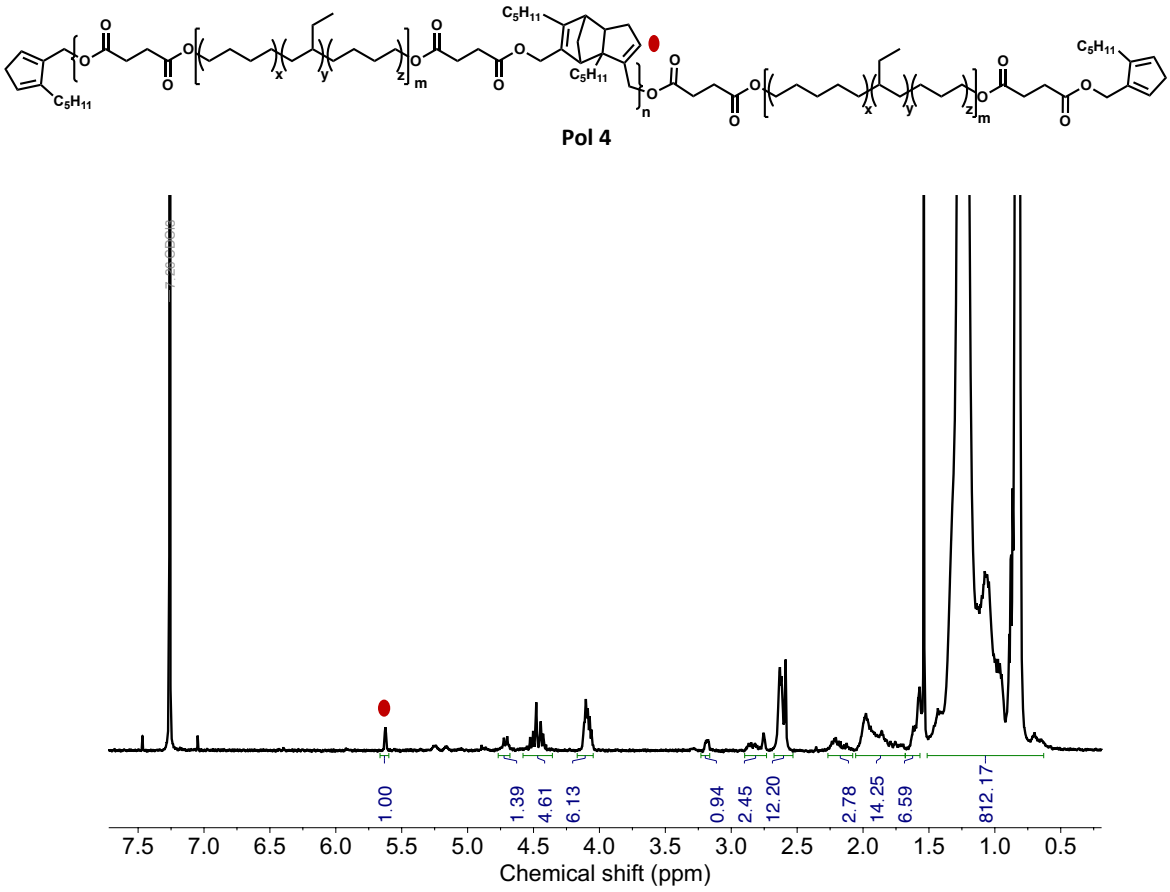


Figure S3.73. ^{1}H NMR spectrum of **Pol 4** in $CDCl_3$. One of the major isomers is shown. Stereo-configuration is not shown but the major *exo* form is expected. Chain-ends are not evident and thus, are not assigned on the spectrum.

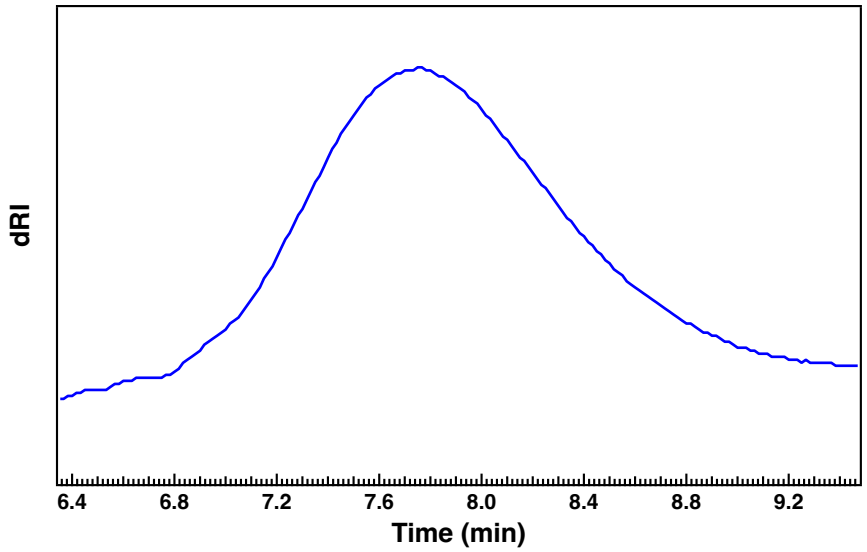
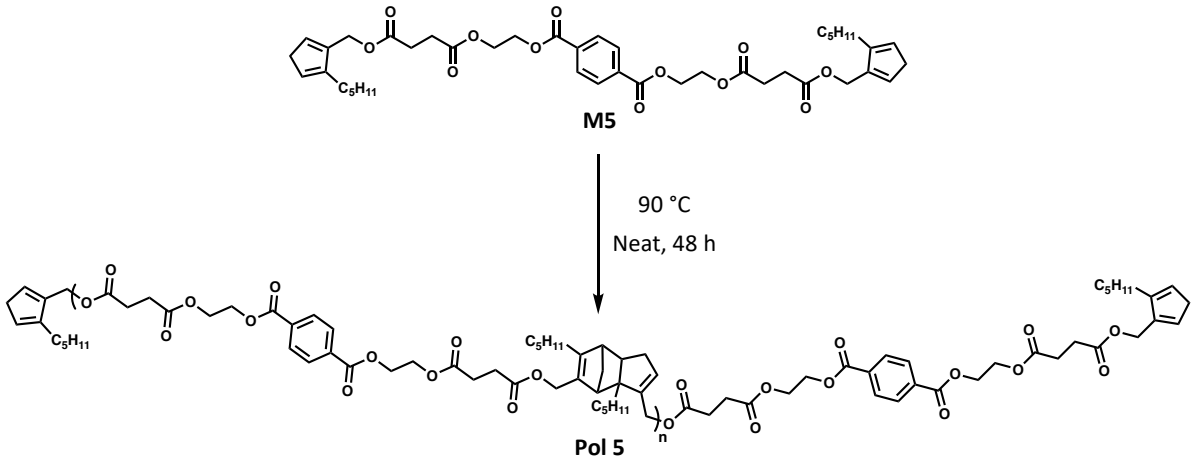


Figure S3.74. The SEC trace of **Pol 4**, showing M_n = 76,000 Da; M_w = 119,000 Da; $Đ$ = 1.6.



To a dram vial was added **M5** (40 mg, 0.05 mmol, 1 eq.) and BHT (0.6 mg, 5 mol%). The material was polymerized at 90 °C, neat. No stirring was required for 48 h. The polymer was precipitated in cold hexanes three times to obtain the pure polymer **Pol 5** (34 mg).

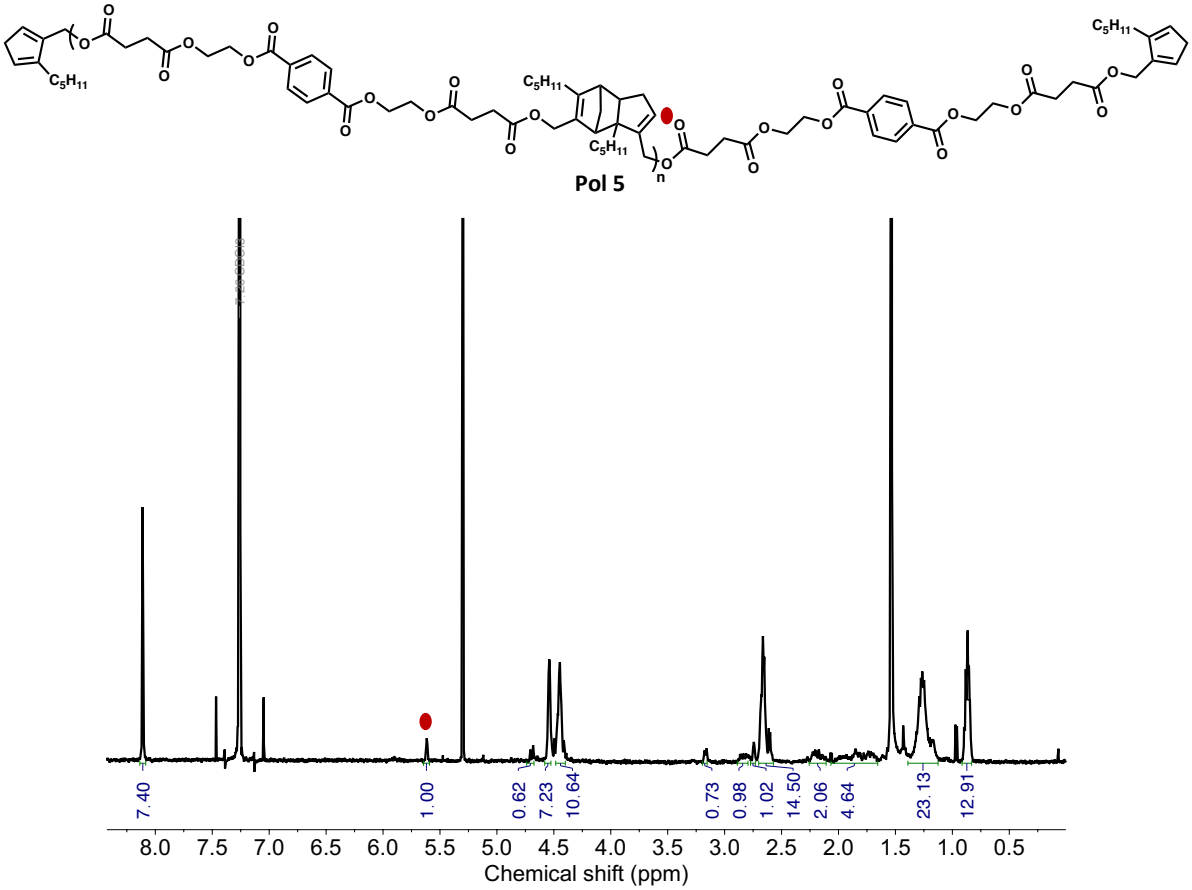


Figure S3.75. ^{1}H NMR spectrum of **Pol 5** in $CDCl_3$. One of the major isomers is shown. Stereo-configuration is not shown but the major *exo* form is expected. Chain-ends are not evident and thus, are not assigned on the spectrum.

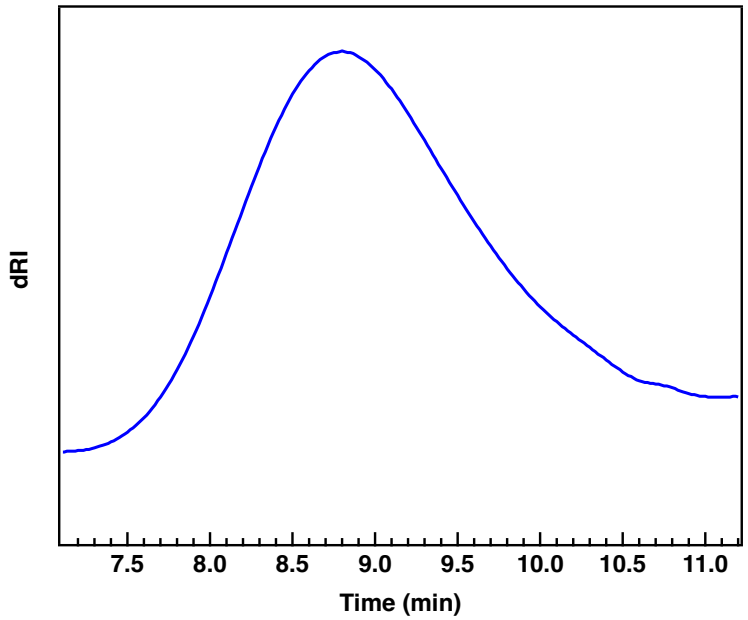
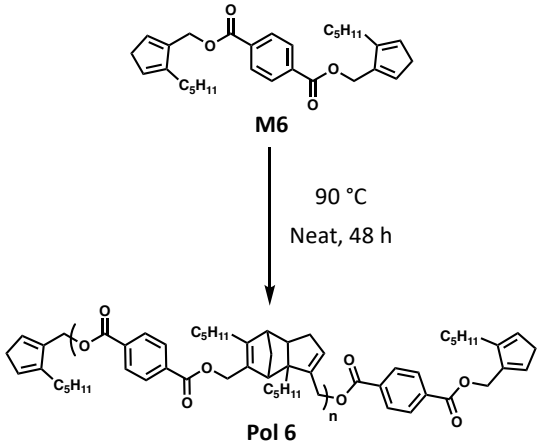


Figure S3.76. The SEC trace of **Pol 5**, showing M_n = 16,000 Da; M_w = 32,000 Da; $Đ$ = 2.0.



To a 20-mL vial was added **M6** (110 mg, 0.2 mmol, 1 eq.) and BHT (2.6 mg, 5 mol%). The material was polymerized at 90 °C, neat. No stirring was required for 48 h. The polymer was precipitated in cold ethanol three times to obtain the pure polymer **Pol 6** (88 mg).

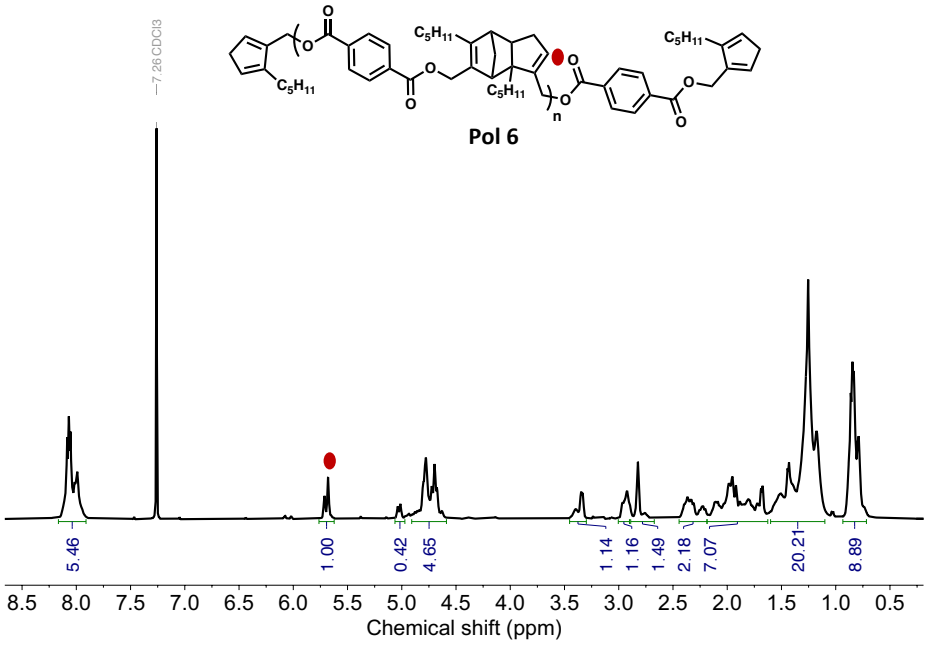


Figure S3.77. ^{1}H NMR spectrum of **Pol 6** in $CDCl_3$. One of the major isomers is shown. Stereo-configuration is not shown but the major *exo* form is expected. Chain-ends are not evident and thus, are not assigned on the spectrum.

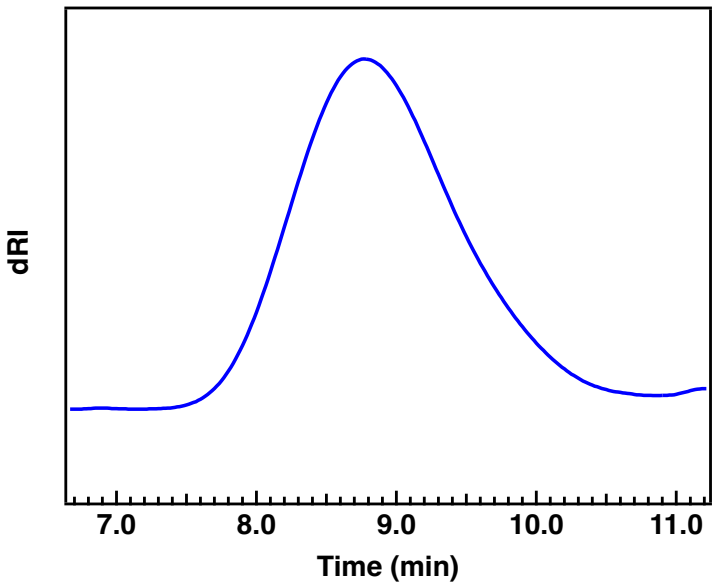


Figure S3.78. The SEC trace of **Pol 6**, showing M_n = 16,000 Da; M_w = 29,000; $Đ$ = 1.7.

SEC with Multi-Angle Light Scattering (MALS) to obtain accurate MW and intrinsic viscosity values:

Table S3.4. A variety of common thermoplastics that are integrated with Cp dimers display different properties (e.g., intrinsic viscosity, glass transition temperature).

Polymer	M_n (Da)[a]	M_w (Da)[a]	$Đ$[a]	DP_n[b]	Intrinsic viscosity (dL/g)[c]	T_g (°C)[d]
Pol 1	24,030	39,610	1.6	46	0.2377	-39
Pol 2	12,150	15,240	1.3	21	0.1620	88
Pol 3	101,800*	110,900*	1.1*	~12*	0.3919*	-124
Pol 4	72,150	95,180	1.3	~12	0.5260	-51
Pol 5	39,620	50,960	1.3	53	0.1805	3
Pol 6	17,250	23,470	1.4	37	0.1736	49

[a]Number (M_n) and weight (M_w) average molecular weight of the synthesized linear polymers and their corresponding polydispersity ($Đ$) were obtained from SEC-MALS in THF. [b]Degree of polymerization (DP_n) was calculated based on the M_n values of the polymers divided by those of the monomer units; For pre-polymers **M3** and **M4**, M_n values of the macromonomers were obtained from the ^{1}H NMR analysis (**Pol 3**) and SEC-chloroform (**Pol 4**). [c]Intrinsic viscosity was calculated based on the MHS equation using M_n values. [d]Glass transition temperature (T_g) was measured from DSC. *Of note, the obtained values might not be absolutely accurate due to the iso-refractive effect between PDMS and THF solvent that is used for the SEC-MALS analysis.

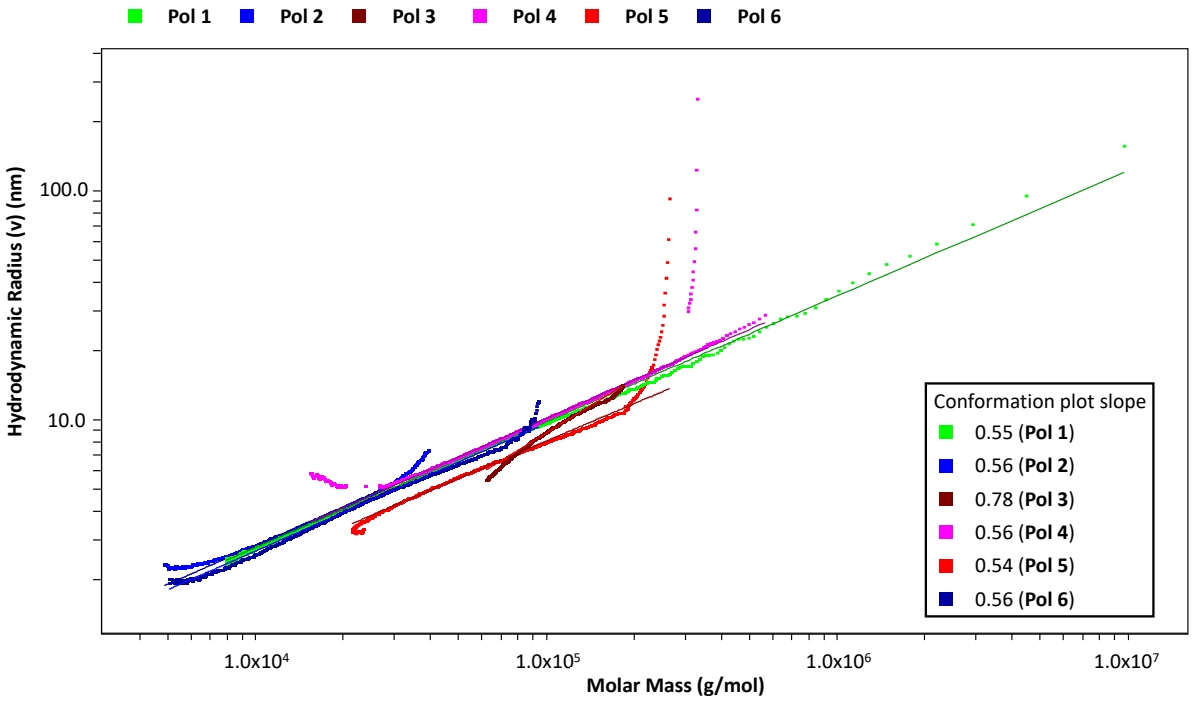


Figure S3.79. Conformation plot shows the linear configuration of the measured polymers with the slope values close to 0.58,[52] except for **Pol 3**. It is an expected trend due to the absence of the branching points in the polymer architectures. **Pol 3**, which is derived from PDMS, is known to be iso-refractive with the THF solvent[51] that is used for the SEC-MALS measurement. Therefore, analysis of **Pol 3** requires the measurement in combination with other methods to confirm the accurate configuration.

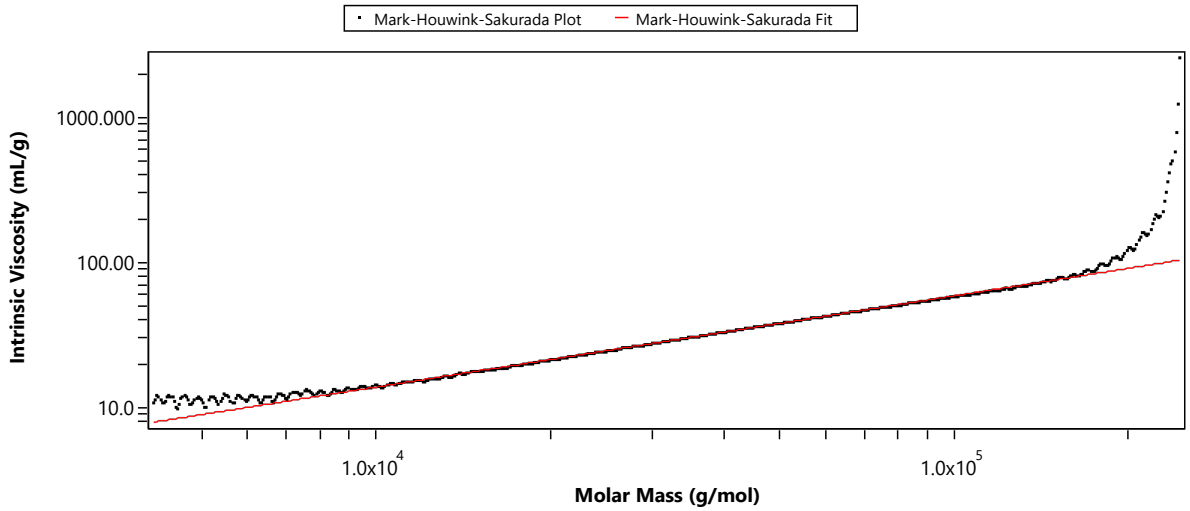


Figure S3.80. Mark-Houwink-Sakurada (MHS) plot of **Pol 1** shows an expected linear correlation between the extrapolated intrinsic viscosity and molar mass values. The obtained values for MHS constants *a* and *K* are 0.630 (±0.038%) and 0.04132 (±0.254%) mL/g, respectively.

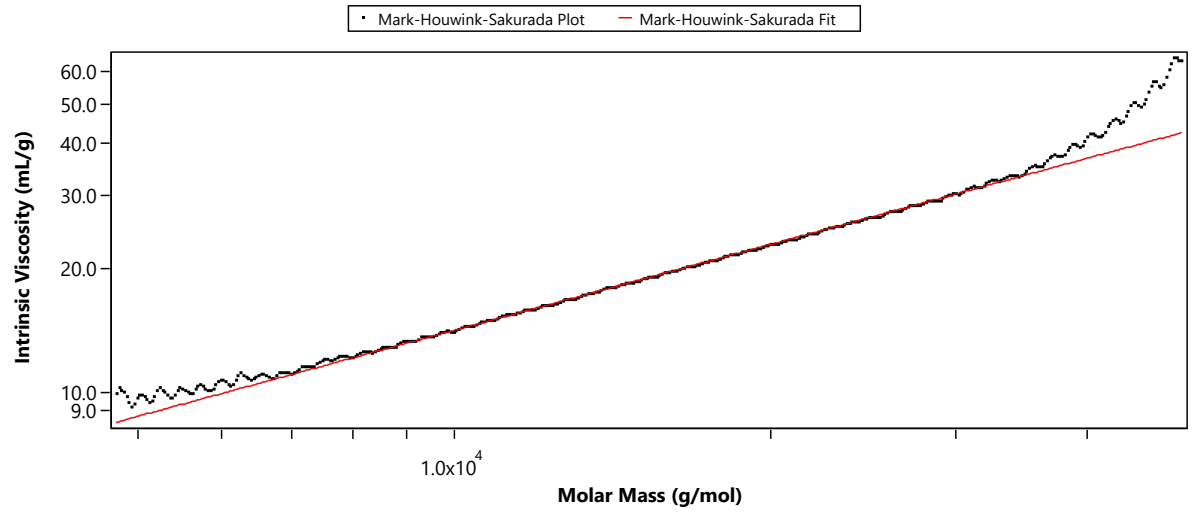


Figure S3.81. MHS plot of **Pol 2** shows an expected linear correlation between the extrapolated intrinsic viscosity and molar mass values. The obtained values for MHS constants *a* and *K* are 0.693 (±0.063%) and 0.02393 (±0.421%) mL/g, respectively.

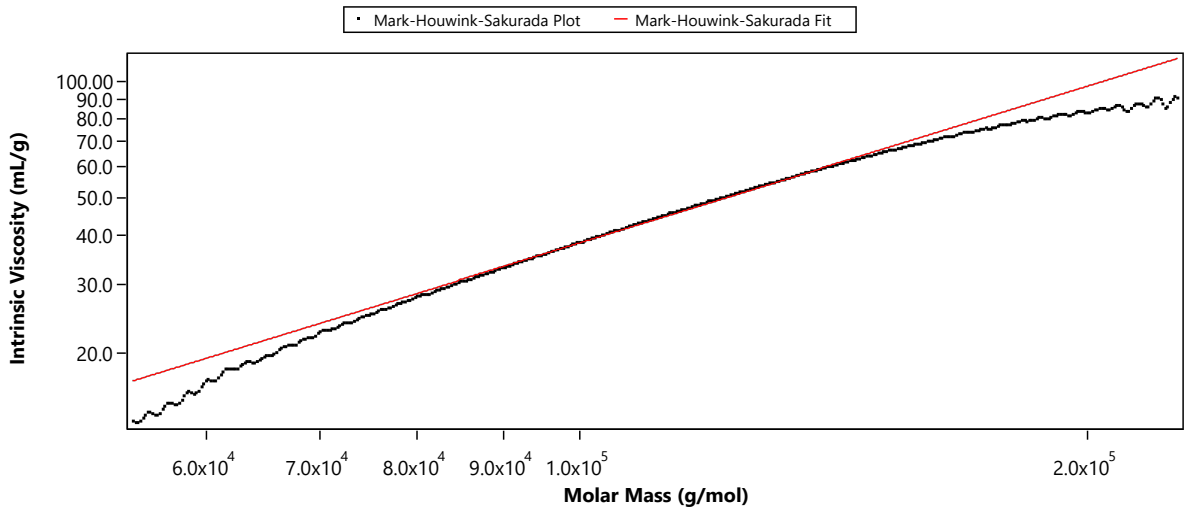


Figure S3.82. MHS plot of **Pol 3** shows an expected linear correlation between the extrapolated intrinsic viscosity and molar mass values. The obtained values for MHS constants *a* and *K* are 1.344 (±0.039%) and 7.291×10^{-6} (±0.610%) mL/g, respectively.

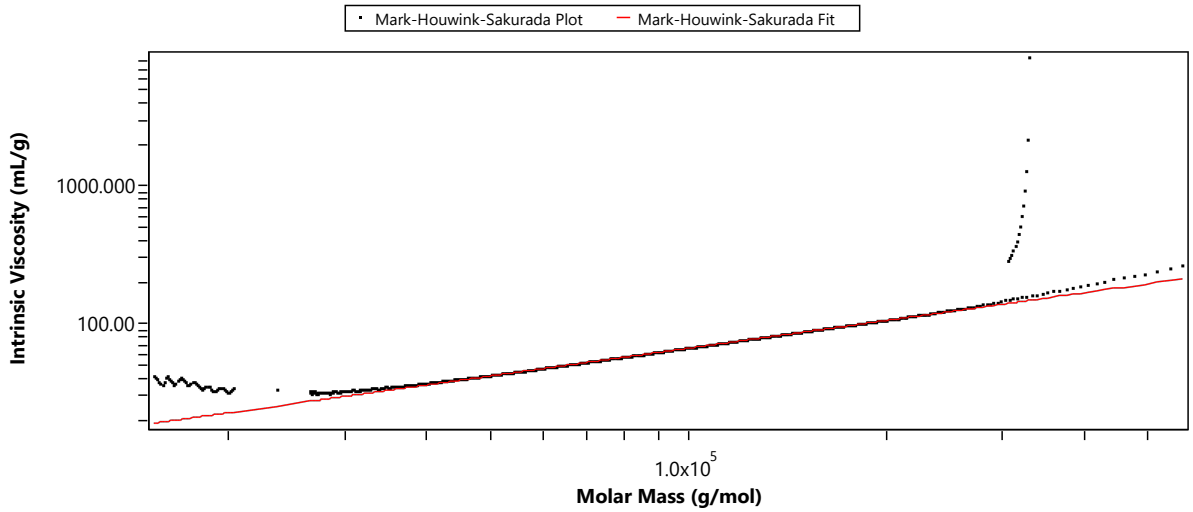


Figure S3.83. MHS plot of **Pol 4** shows an expected linear correlation between the extrapolated intrinsic viscosity and molar mass values. The obtained values for MHS constants *a* and *K* are 0.668 (±0.016%) and 0.02990 (±0.120%) mL/g, respectively.

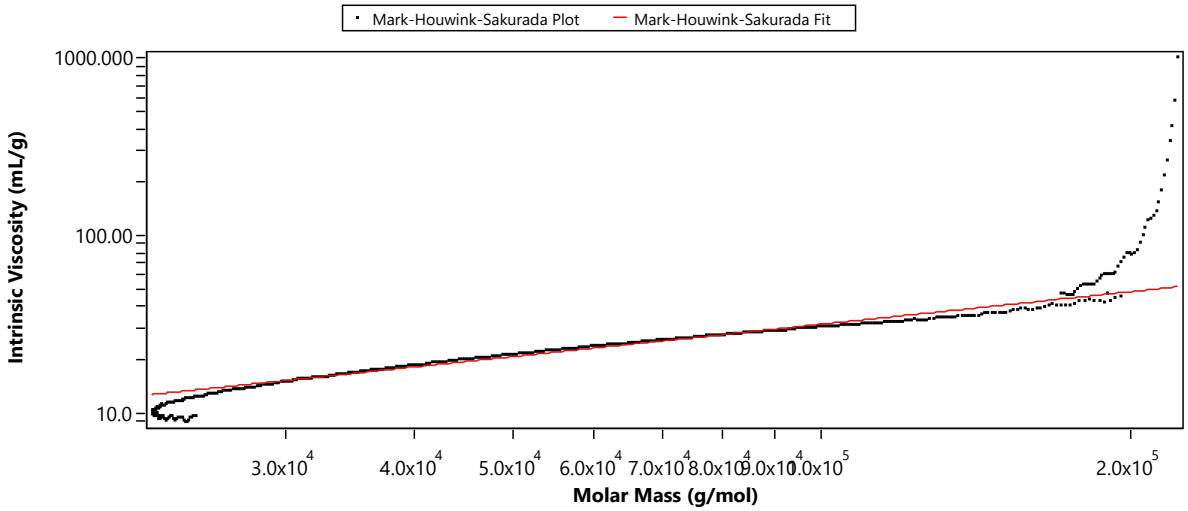


Figure S84. MHS plot of **Pol 5** shows an expected linear correlation between the extrapolated intrinsic viscosity and molar mass values. The obtained values for MHS constants *a* and *K* are 0.609 (±0.062%) and 0.02860 (±0.408%) mL/g, respectively.

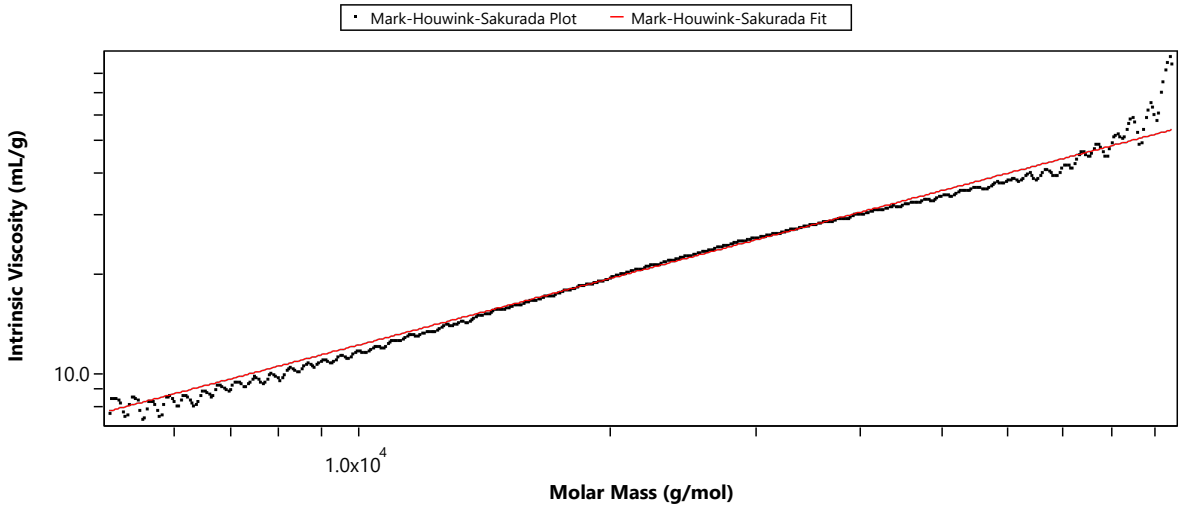


Figure S3.85. MHS plot of **Pol 6** shows an expected linear correlation between the extrapolated intrinsic viscosity and molar mass values. The obtained values for MHS constants a and K are 0.661 (±0.065%) and 0.02748 (±0.437%) mL/g, respectively.

The intrinsic viscosity is calculated based on the MHS equation as below:[46]

$$[\eta] = KM^a \quad \text{(S1)}$$

where $[\eta]$ and M are the intrinsic viscosity (dL/g) and molar mass (g/mol), respectively. K (mL/g) and a are the MHS parameters that were measured in THF using the SEC-MALS instrument.

Table S3.5. Obtained data from the SEC-MALS and the calculated intrinsic viscosity values of the six synthesized polymers in THF solvent.

	Number average molecular weight (M_n, Da)	Weight average molecular weight (M_w, Da)	Poly-dispersity ($Đ$)	MHS constant a	MHS constant K (dL/g)	Intrinsic viscosity (dL/g) based on M_n values	Intrinsic viscosity (dL/g) based on M_w values
Pol 1	2.403×10^4 (±0.486%)	3.961×10^4 (±0.350%)	1.649 (±0.599%)	0.630 (±0.038%)	4.132×10^{-4} (±0.254%)	0.2377	0.3257
Pol 2	1.215×10^4 (±0.602%)	1.524×10^4 (±0.480%)	1.254 (±0.770%)	0.693 (±0.063%)	2.393×10^{-4} (±0.421%)	0.1620	0.1896
Pol 3	1.018×10^5 (±0.325%)	1.109×10^5 (±0.286%)	1.089 (±0.433%)	1.344 (±0.039%)	7.291×10^{-8} (±0.610%)	0.3919	0.4397
Pol 4	7.215×10^4 (±0.425%)	9.518×10^4 (±0.106%)	1.319 (±0.438%)	0.668 (±0.016%)	2.990×10^{-4} (±0.120%)	0.5260	0.6329
Pol 5	3.962×10^4 (±0.318%)	5.096×10^4 (±0.298%)	1.286 (±0.436%)	0.609 (±0.062%)	2.860×10^{-4} (±0.408%)	0.1805	0.2104
Pol 6	1.725×10^4 (±0.180%)	2.347×10^4 (±0.126%)	1.361 (±0.220%)	0.661 (±0.065%)	2.748×10^{-4} (±0.437%)	0.1736	0.2128

TGA and DSC data of the synthesized polymers:

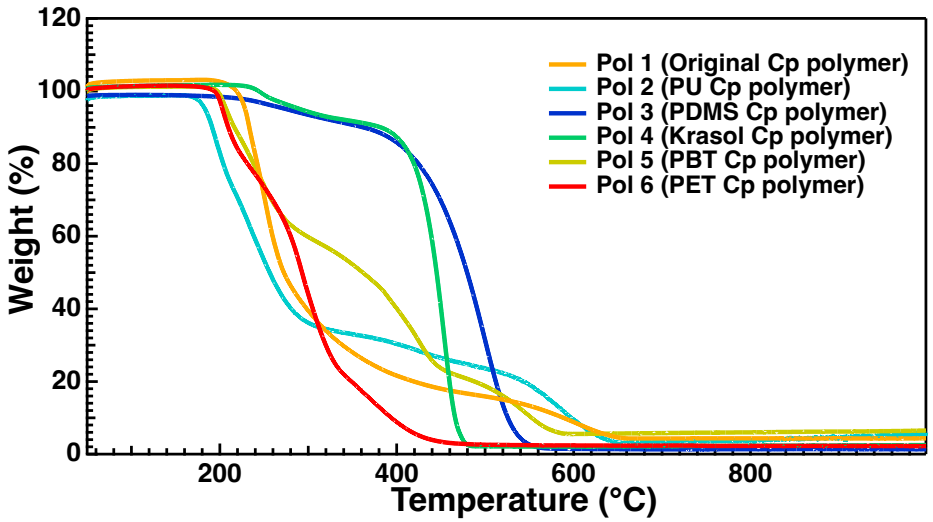


Figure S3.86. The TGA spectra of 6 Cp polymers display an initial degradation process at 200–240 °C. As shown in our previous publication,[5] this phenomenon is observed due to Cp chain-end dissociation. The later-stage degradation is at higher temperature range, depending on the incorporation of different monomers with varied MW range. PDMS and hydrogenated polybutadiene Cp polymers fully degrade at very high temperature (~500 °C), presumably based on the expected range of degradation for higher-MW PDMS and hydrogenated polybutadiene backbones.

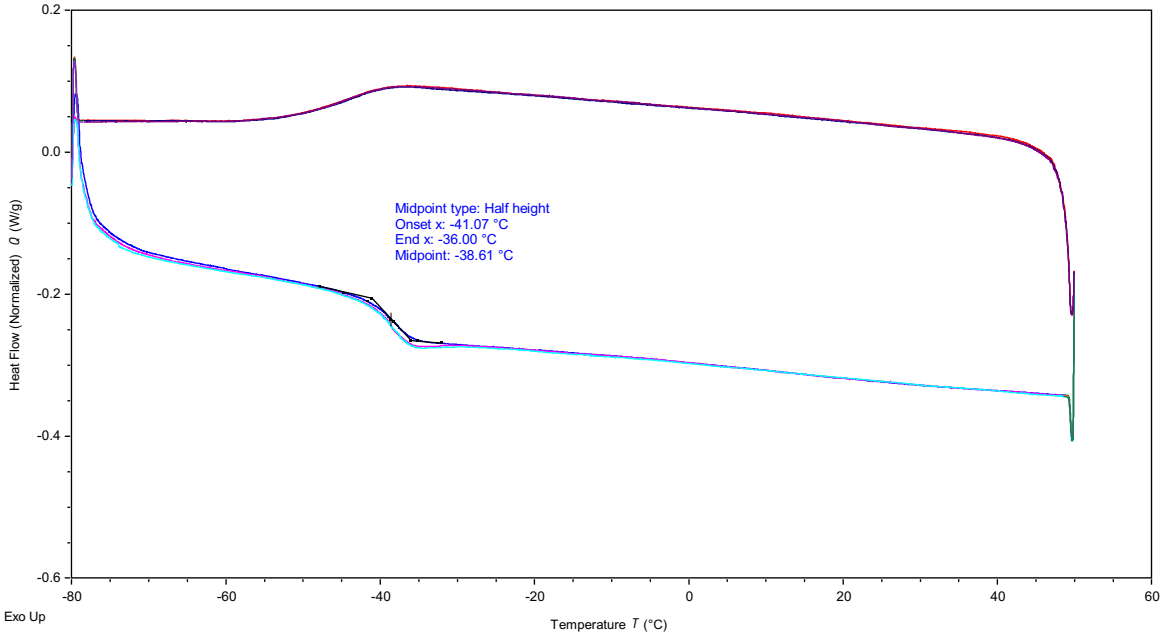


Figure S3.87. DSC spectrum displays three heating and cooling cycles of **Pol 1** (alkyl-Cp polymer), showing the T_g of -39 °C.

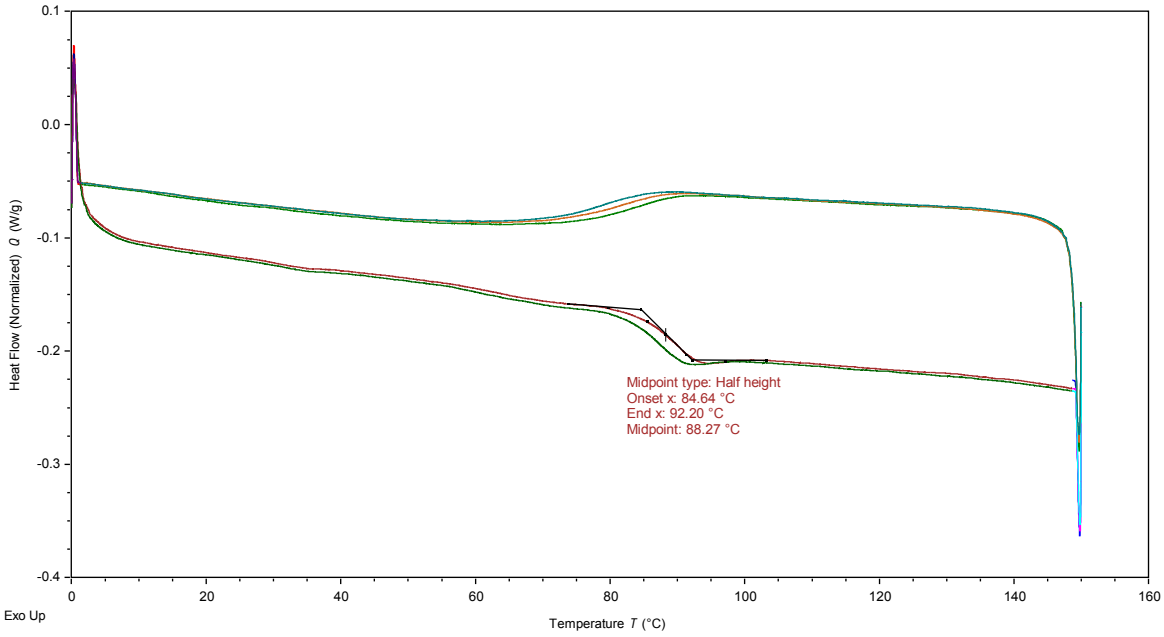


Figure S3.88. DSC spectrum displays three heating and cooling cycles of **Pol 2** (urethane-Cp polymer), showing the T_g of 88 °C.

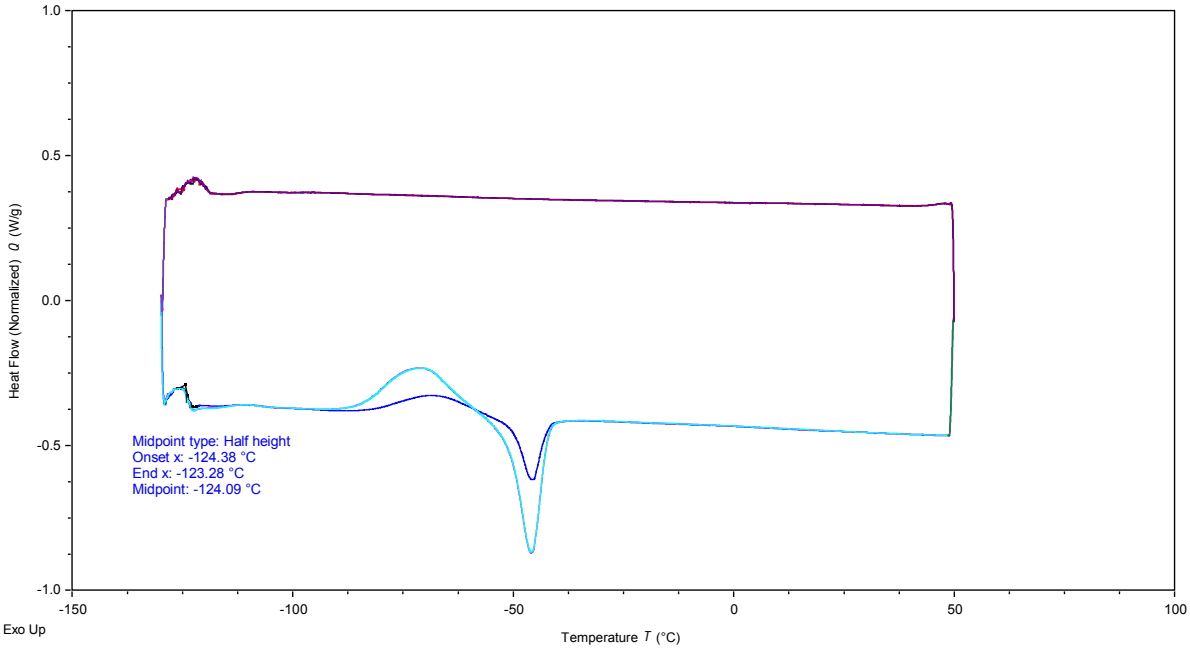


Figure S3.89. DSC spectrum displays three heating and cooling cycles of **Pol 3** (PDMS-Cp polymer), showing the T_g of -124 °C.

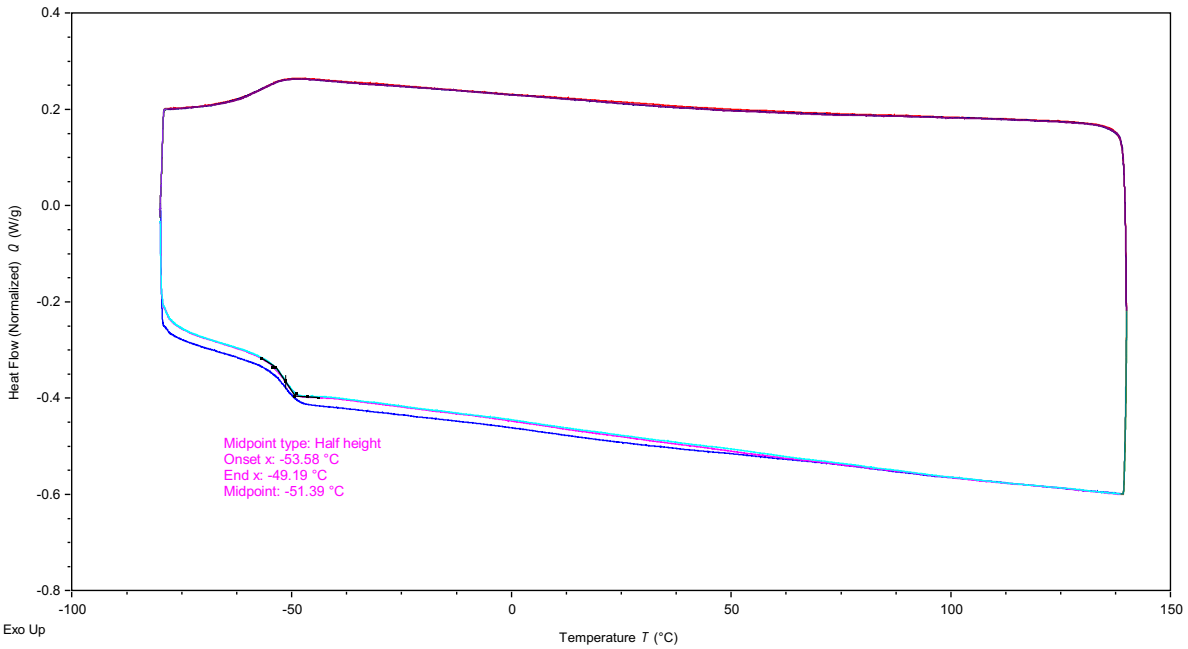


Figure S3.90. DSC spectrum displays three heating and cooling cycles of **Pol 4** (hydrogenated polybutadiene-Cp polymer), showing the T_g of -51 °C.

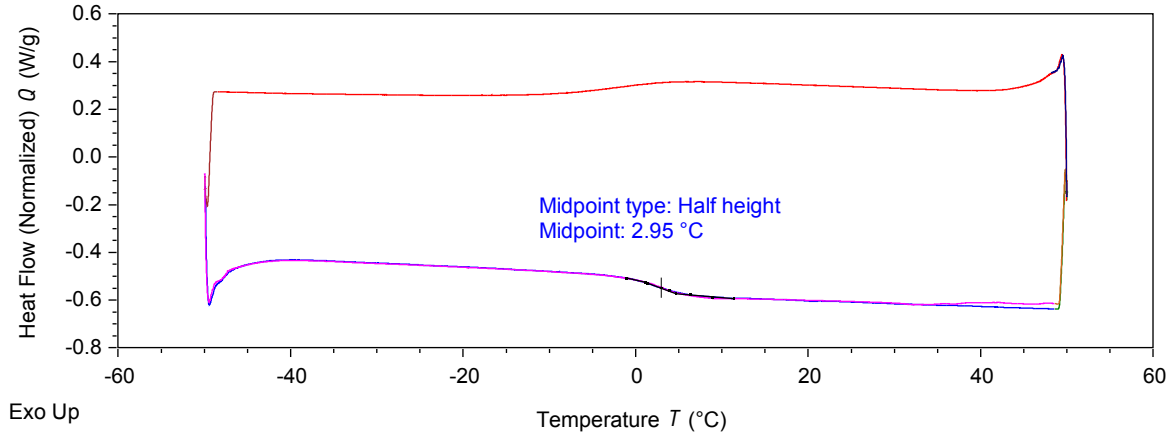


Figure S3.91. DSC spectrum displays two heating and cooling cycles of **Pol 5** (butylene terephathalate-Cp polymer), showing the T_g of 3 °C.

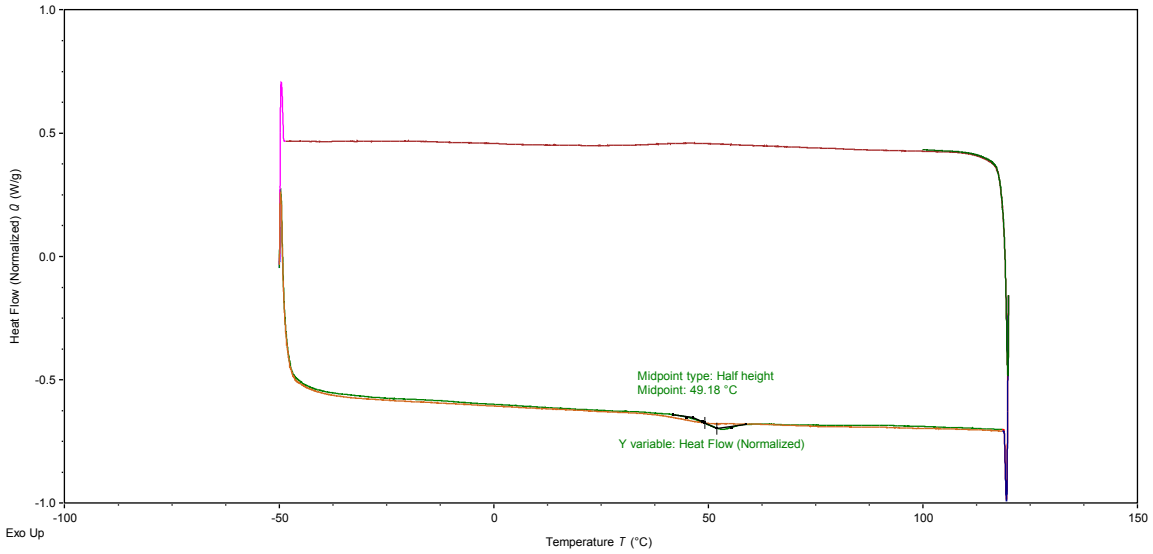


Figure S3.92. DSC spectrum displays two heating and cooling cycles of **Pol 6** (ethylene terephthalate-Cp polymer), showing the T_g of 49 °C.

Calculation of intrinsic viscosity values via Huggins and Kraemer plots:

Table S3.6. Different solutions of **Pol 3** were prepared in toluene with varied concentration. Of note, the minimum concentration is 0.5 g/dL to provide significant contribution to the viscosity values. The dynamic viscosity values were collected using the viscometer (Anton Paar brand). The relative, specific, reduced, and inherent viscosity were calculated to determine intrinsic viscosity based on the equations S2–S5, as shown below.[46,75,76] The calculated values are reported. Of note, to guarantee an exact analysis, the relative viscosities of the polymer solutions should be between 1.2 and 2.5.

Concentration (g/dL)	Dynamic viscosity η (mPa.s)	Relative viscosity η_{rel}	Specific viscosity η_{sp}	Reduced viscosity η_{red} (dL/g)	Inherent viscosity η_{inh} (dL/g)
0.526	0.691	1.24	0.240	0.456	0.409
0.586	0.710	1.27	0.275	0.469	0.414
0.851	0.754	1.35	0.353	0.543	0.465
0.651	0.793	1.42	0.423	0.497	0.414

Most polymer solutions are shear-dependent (i.e., non-Newtonian), but under a range of sufficiently low shear rates, they display Newtonian behaviors. The relative viscosity (dimensionless unit) is thereby obtained by dividing the viscosity of the polymer solution (i.e., dynamic viscosity η) by the viscosity of the pure solvent (η_0). The polymer solutions are prepared in toluene, so the viscosity of pure solvent η_0 = 0.5571 mPa.s, which is measured under ambient temperture (25 °C). Intrinsic viscosity [η] (dL/g) is the slope at infinite dilution based on the Huggins and Kraemer plots.[46,65,76]

Relative viscosity (dimensionless unit) is obtained by the equation as below: [46,65,76]

$$\eta_{rel} = \frac{t}{t_0} = \frac{\eta}{\eta_0} \quad \text{(S3.2)}$$

where *t* denotes the solution flow time and t_0 denotes the solvent flow time, η (mPa.s) is the dynamic viscosity values that were obtained from the viscometer, η_0 is the dynamic viscosity of the solvent (i.e., toluene).

Specific viscosity (dimensionless unit) is calculated based on the equation as below: [46,65,76]

$$\eta_{sp} = \frac{t-t_0}{t_0} = \eta_{rel} - 1 \quad \text{(S3.3)}$$

where η_{rel} is the relative viscosity (dimensionless unit).

Reduced viscosity (dL/g) is calculated based on the equation as below: [46,65,76]

$$\eta_{red} = \frac{t-t_0}{t_0 \times c} = \frac{\eta_{sp}}{c} \quad \text{(S3.4)}$$

where η_{sp} is the specific viscosity (dimensionless unit), and *c* is the concentration of the polymer solution (g/dL).

Inherent viscosity (dL/g) is calculated based on the equation as below: [46,65,76]

$$\eta_{inh} = \frac{\ln \frac{t}{t_0}}{c} = \frac{\ln \eta_{rel}}{c} \quad \text{(S3.5)}$$

where η_{rel} is the relative viscosity (dimensionless unit), and *c* is the concentration of the polymer solution (g/dL).

Intrinsic viscosity $[\eta]$ (dL/g) is obtained based on the equations from Huggins and Kraemer: [46,65,76]

Huggins: $$[\eta] = \frac{\ln (\eta_{red})}{c} \quad \text{(S3.6)}$$

Kraemer: $$[\eta] = \frac{\ln (\eta_{inh})}{c} \quad \text{(S3.7)}$$

where η_{red} and η_{inh} are the reduced viscosity and inherent viscosity, respectively (dL/g), while c is the concentration of the polymer solutions (g/dL).

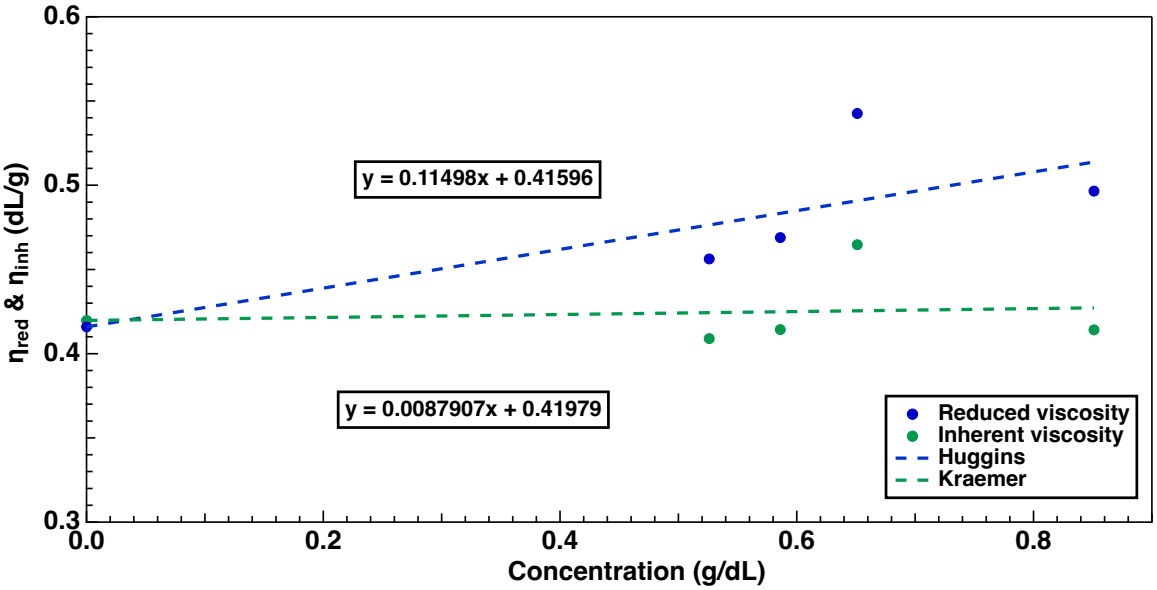


Figure S3.93. Huggins and Kraemer plots of the PDMS-Cp polymer (**Pol 3**) with M_n = 61,780, M_w = 102,404, and $Đ$ = 1.7 (based on SEC trace of the sample in chloroform). The different concentrated samples were prepared in toluene and measured at 25 °C. The linear fitting was applied to represent the Huggins and Kraemer plots. Intrinsic viscosity values, which are the y-intercept of the straight line fit and determined to be 0.416 dL/g (from Huggins) and 0.420 dL/g (from Kraemer).

Mechanical testing of PET-Cp polymer (Pol 6)

Tensile testing was performed on a texture analyzer (TA) that combines a linear actuator with a load cell. The model is TA.XT Plus Connect that has a load cell with a maximum force of 50 N and an approximate resolution of ±1 mN and a distance resolution of 1 µm. Displacement is quantified via a stepper motor in conjunction with a known gear ratio. The materials were tested via uniaxial tension mode using mini tensile clamp fixtures. The speed

of extension was 1.2 mm/min and the tests were performed at room temperature and ambient atmosphere. The samples were melted into dumbbell-shaped specimens with active region of 10.0 mm × 1.5 mm × 1 mm. One crude sample of **Pol 6** was tested based on the ASTM D638-14 standard with the strain rate of 1 mm/min.[60] Pictures were captured using iPhone 11 camera.

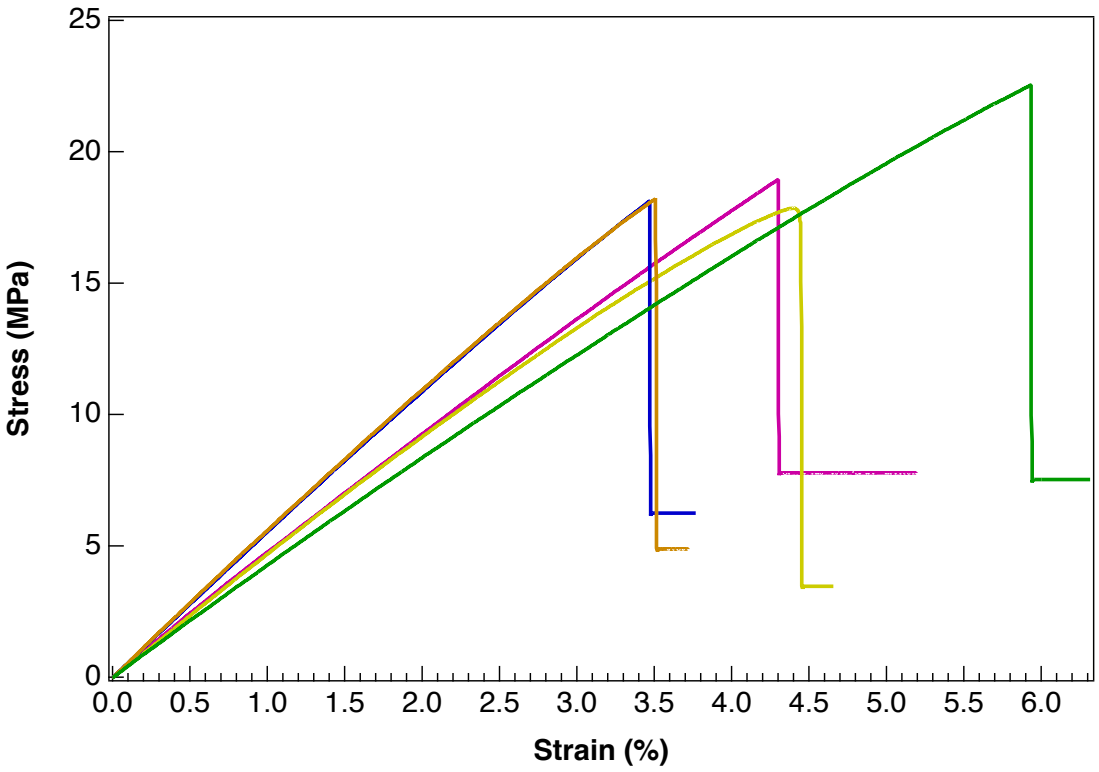


Figure S3.94. Tensile testing of 5 different crude PET-CP polymer (**Pol 6**) samples (used as synthesized without further purification). The pellets of crude **Pol 6** were melted into dumbbell-shaped specimens with active region of 10.0 mm × 1.5 mm × 1 mm. The strain rate is 1.2 mm/min. The Young's modulus was calculated as the slope of the linear fitting of each curve.

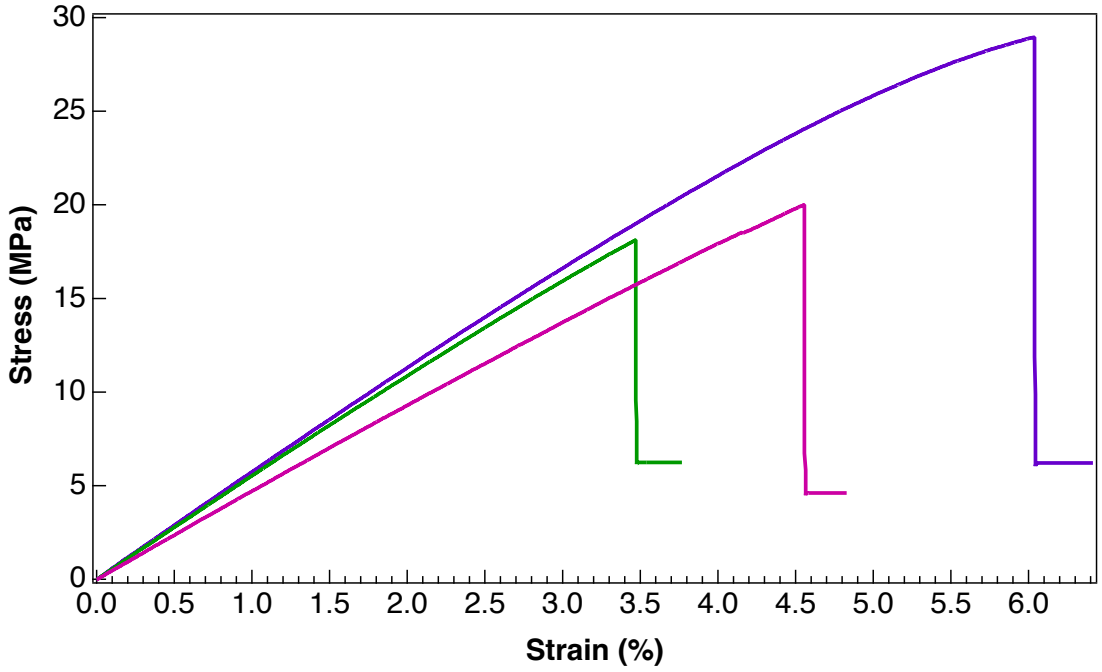


Figure S3.95. Tensile testing of 3 different purified PET-CP polymer (**Pol 6**) samples. After polymerization, the crude polymer mixture was dissolved in DCM and precipitated in cold ethanol to remove BHT inhibitor and low MW oligomers. The purified solid of **Pol 6** was melted into dumbbell-shaped specimens with active region of 10.0 mm × 1.5 mm × 1 mm. The strain rate is 1.2 mm/min. The Young's modulus is calculated as the slope of the linear fitting line of each curve.

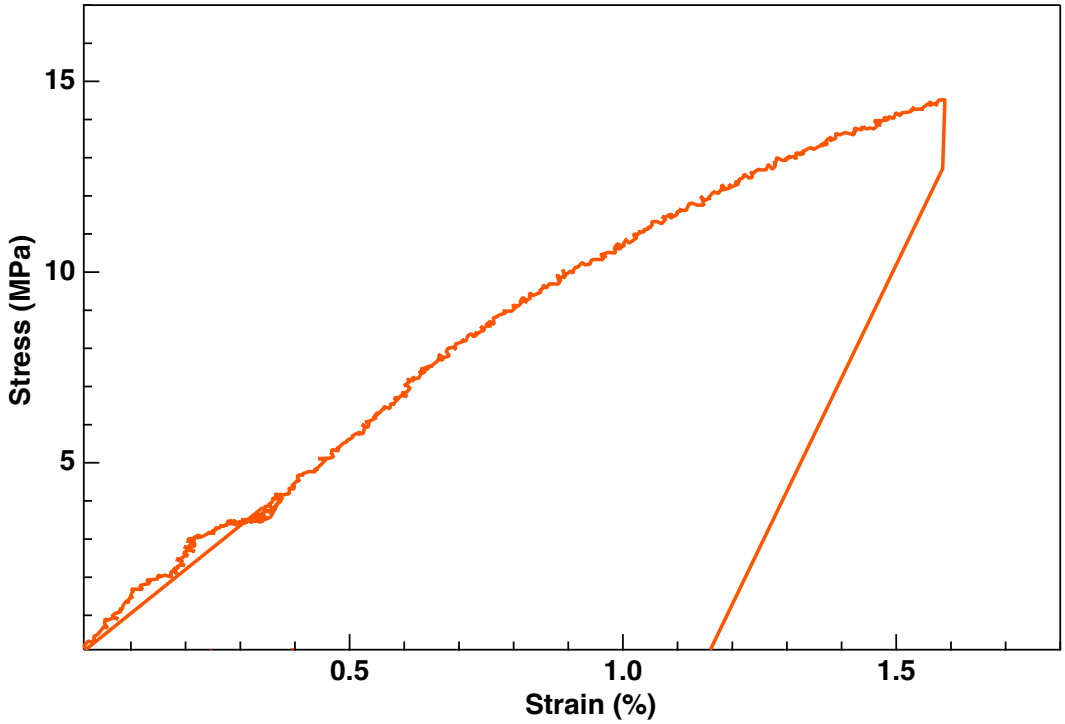


Figure S3.96. The tensile stress-strain curve of the crude large sample of **Pol 6** with the dimensions following the ASTM D638-14 standard.[60] The strain rate is 1 mm/min. From the curve, the Young's modulus is calculated to be 1.15 GPa based on the slope of the linear fitting line. The ultimate tensile strength is 14.53 MPa, and the elongation at break is 1.59%.

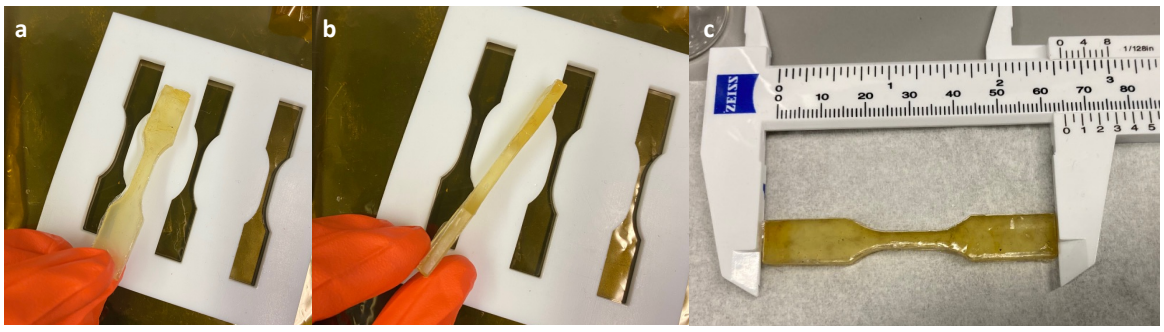


Figure S3.97. Pictures of the crude large sample of **Pol 6** with the dimensions following the ASTM standard in its (a) front view, (b) side view, and (c) size measurement with a caliper.

Table S3.7. Young's modulus, tensile strength, and elongation values were obtained from the stress-strain curves of the purified and crude samples of **Pol 6** (**Figures S96** and **S97**).

Pol 6	Sample #	Young's modulus (MPa)	Ultimate tensile strength (MPa)	Elongation at break (%)
Crude	1	413.4	22.54	5.93
	2	468.2	18.94	4.30
	3	464.4	17.82	4.42
	4	557.1	18.22	3.51
	5	551.6	18.12	3.47
	Average ± standard deviation	490.9±55.3	19.13±1.75	4.33±0.89
Purified	1	565.4	28.95	6.04
	2	469.5	20.00	4.56
	3	550.8	18.12	3.47
	Average ± standard deviation	528.6±42.2	22.36±4.72	4.69±1.05

Chain-end examination and polymerization monitor via SEC and NMR spectra:

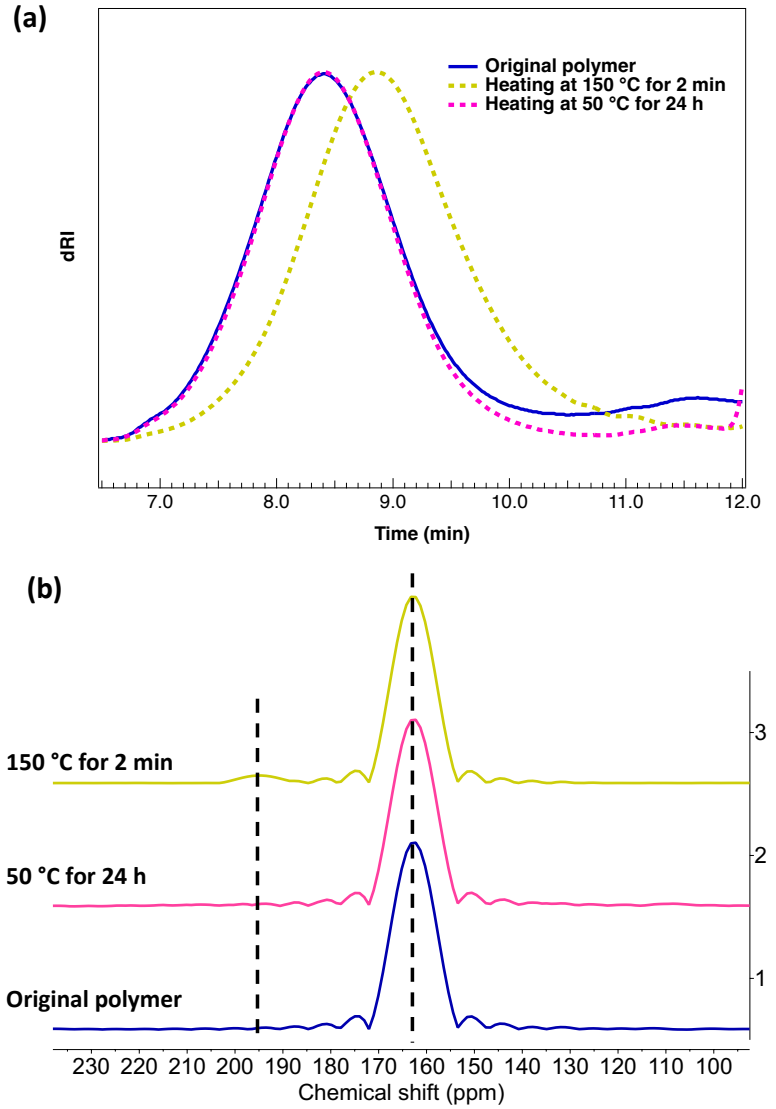


Figure S3.98. (a) The SEC curves of the **Pol 1** without any heat treatment and with heat treatment at 50 °C for 24 h versus at 150 °C for 2 min. The "capping" reagent, ^{15}N-phenyl maleimide, and the radical inhibitor, BHT, were both added. The lower MW was obtained with the sample that was heated at 150 °C or at the rDA temperature for Cp dimer. Of note, 1 mg of ^{15}N-phenyl maleimide was included in the 5 mg of the polymer sample, along with 1 wt% BHT for the sample that was heated at 150 °C, neat. For the samples at RT and 50 °C, 5 mg of ^{15}N-phneyl maleimide was added in 5 mg of polymer, along with 0.1 mL DCM and 1 wt% BHT. (b) The chain-ends were only detected when the polymer was depolymerized at

150 °C for 2 min (yellowish-green trace) that is indicative from the peak at 195 ppm. The Cp-maleimide adduct peak matches with the value that was reported in our previous publication.[39]

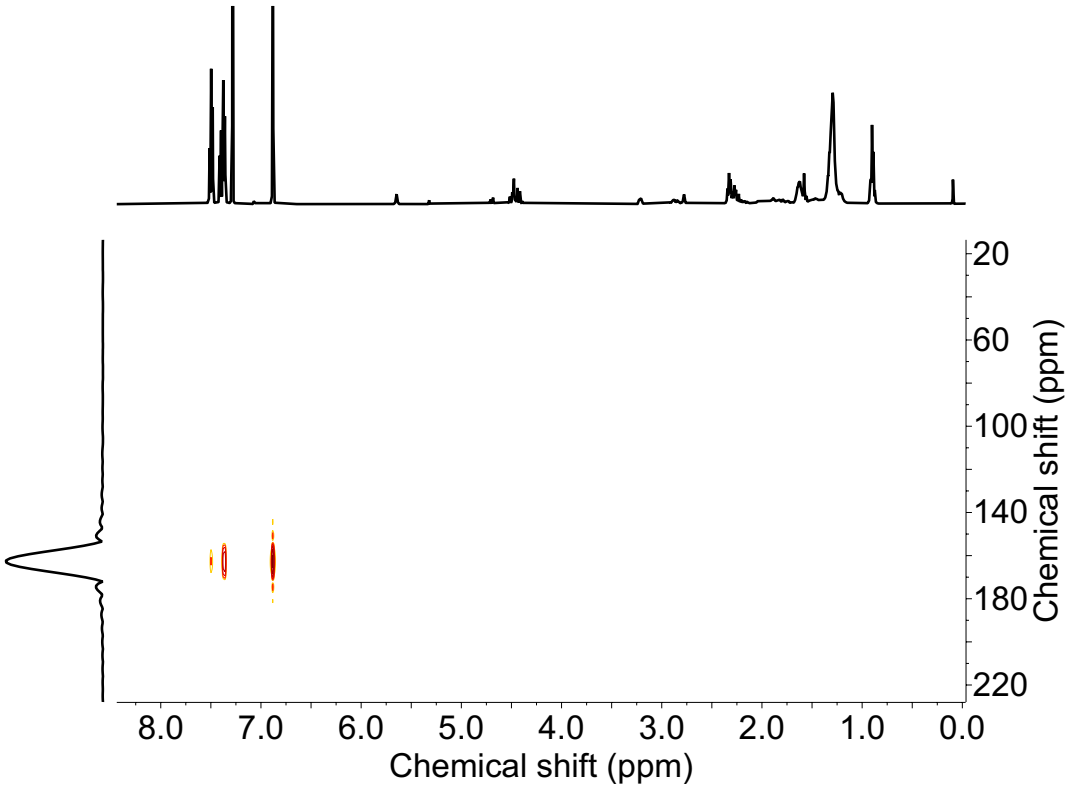


Figure S3.99. The full two-dimensional HMBC NMR spectrum of the polymer with the added ^{15}N-phenyl maleimide without any heat treatment. No chain-end was detected as shown by no observed peak at the 195-ppm region (y-axis). The peak from ^{15}N-phenyl maleimide is at 163 ppm, as shown.

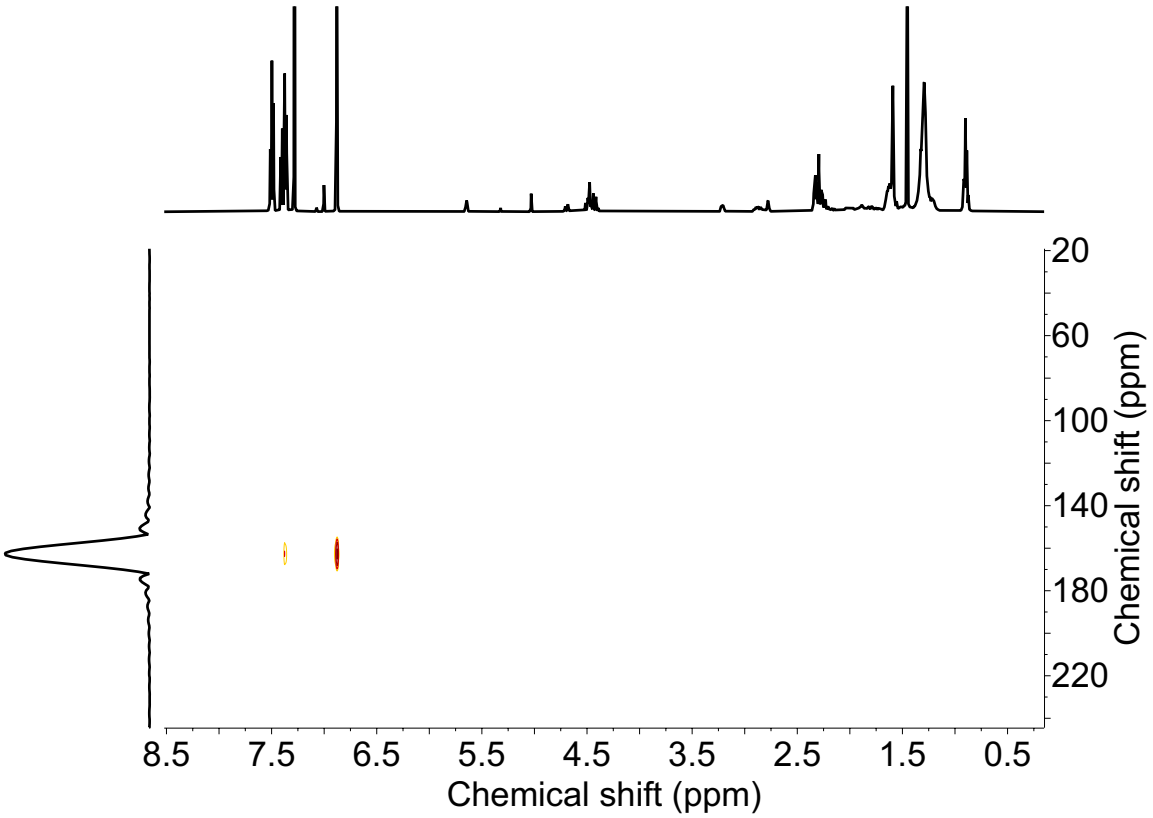


Figure S3.100. The full two-dimensional HMBC NMR spectrum of the polymer with the added ^{15}N-phenyl maleimide with heat treatment at 50 °C for 24 h. No chain-end was detected as shown by no observed peak at the 195-ppm region (y-axis). The peak from ^{15}N-phenyl maleimide is at 163 ppm, as shown.

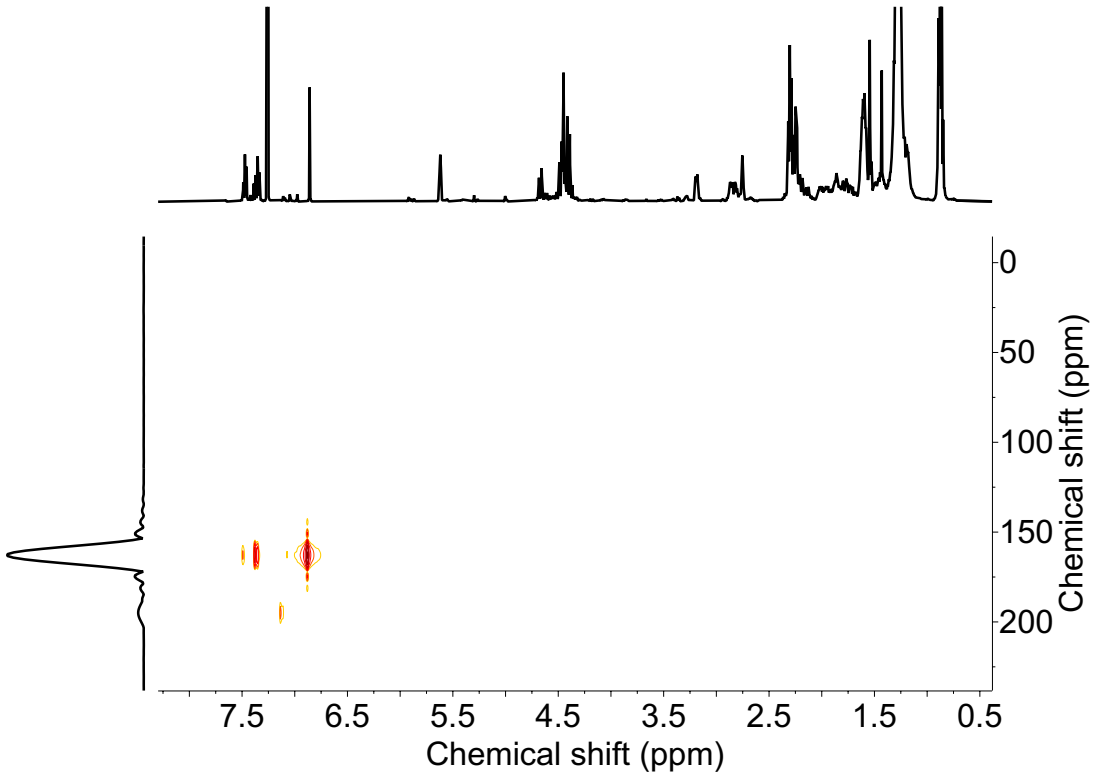


Figure S3.101. The full two-dimensional HMBC NMR spectrum of the polymer with the added ^{15}N-phenyl maleimide with heat treatment at 90 °C for 2 min. The chain-end was detected as shown by an observed peak at the 195-ppm region (y-axis), matching with the Cp-maleimide peak from literature.[5] The peak from remaining excess amount of ^{15}N-phenyl maleimide is at 163 ppm, as shown.

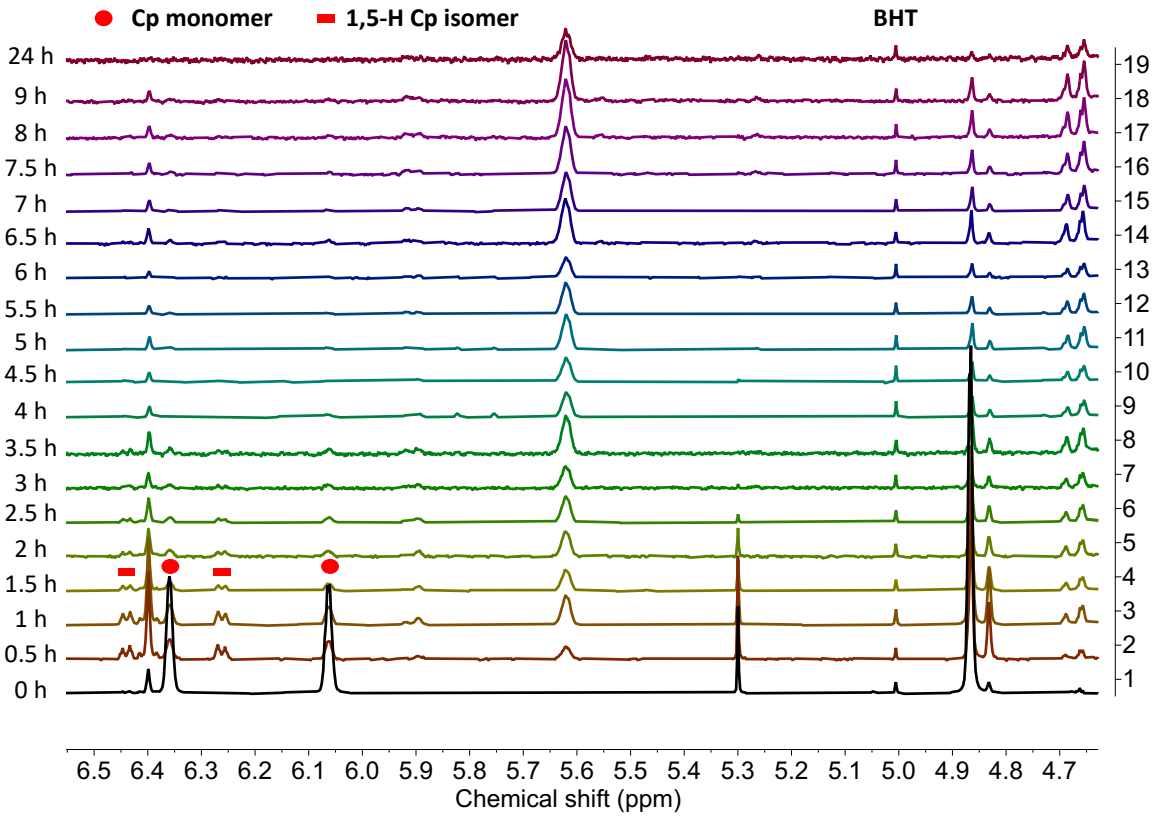


Figure S3.102. Stacked ^{1}H NMR spectra of the Cp monomer in $CDCl_3$ upon polymerization neat at 90 °C in the timescale from 0 to 8 h with 30-minute interval, then 9 and 24 h. The monomer consumption was based on the peaks from the Cp monomer and its 1,5-H shift isomers as labeled on the graph. The BHT peak is also indicated, which was used as the internal standard for ^{1}H NMR integral analysis.

Table S3.8. ^{1}H NMR integral analysis of the Cp monomer peaks, including the 1,5-H shift isomers, and the corresponding number-average molecular weight (M_n) are reported. The internal standard peak from BHT was referenced as 1.00. Percentage of monomer consumption was reported based on the total integration at the specific time divided by the integration at initial time (0 h).

Time (h)	Integration of the peak from the major Cp isomer	Integration of the peak from 1,5-H shift Cp isomer	Total integration	% Consumption of Cp monomer	Number-average molecular weight ($M_{n,}$ kDa)
0	33.1	0.90	34.0	0.0	0.511
0.5	6.84	5.53	12.37	63.6	1.508
1	4.00	3.22	7.22	78.8	2.362
1.5	2.44	2.00	4.44	86.9	3.174
2	1.87	1.93	3.80	88.8	3.989
2.5	1.5	1.3	2.80	91.8	4.671
3	1.00	0.77	1.77	94.8	5.742
3.5	0.67	0.67	1.34	96.1	6.438
4	0.72	0.79	1.51	95.6	6.924
4.5	0.75	0.83	1.58	95.4	7.409
5	0.8	0.82	1.62	95.2	8.003
5.5	0.77	0.87	1.64	95.2	8.539
6	0.76	0.87	1.63	95.2	10.593
6.5	0.85	0.95	1.80	94.7	10.971
7	0.82	0.9	1.72	94.9	11.528
7.5	0.82	0.93	1.75	94.9	12.953
8	0.88	0.97	1.85	94.6	15.017
9	0.85	1.03	1.88	94.5	15.131

Investigation of the Diels–Alder polymerization efficiency to achieve high MW range:

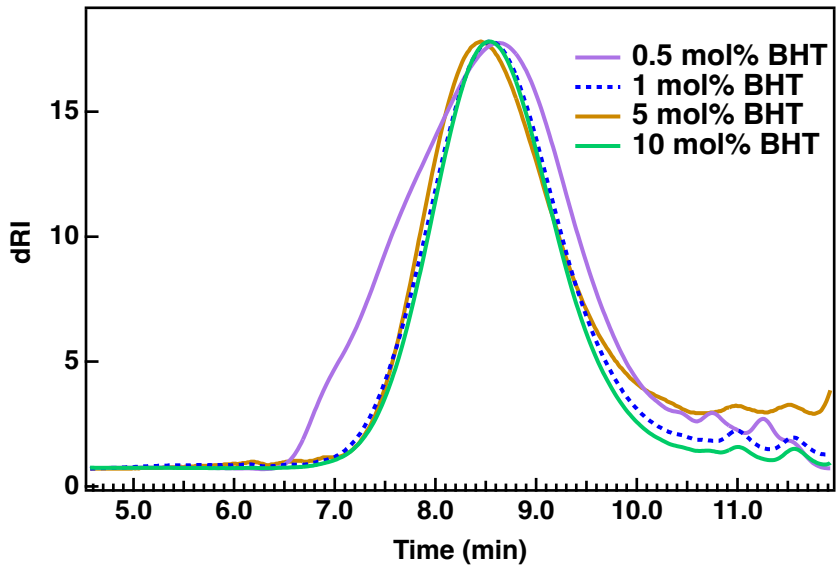


Figure S3.103. The effect of BHT inhibitor to the polymerization of **M1** monomer. As shown, 1 mol% BHT is adequate to inhibit the radical cross-linking process. The best polymerization behavior was observed with 5 mol% inhibitor. However, there was no big difference from 1 to 10 mol% BHT.

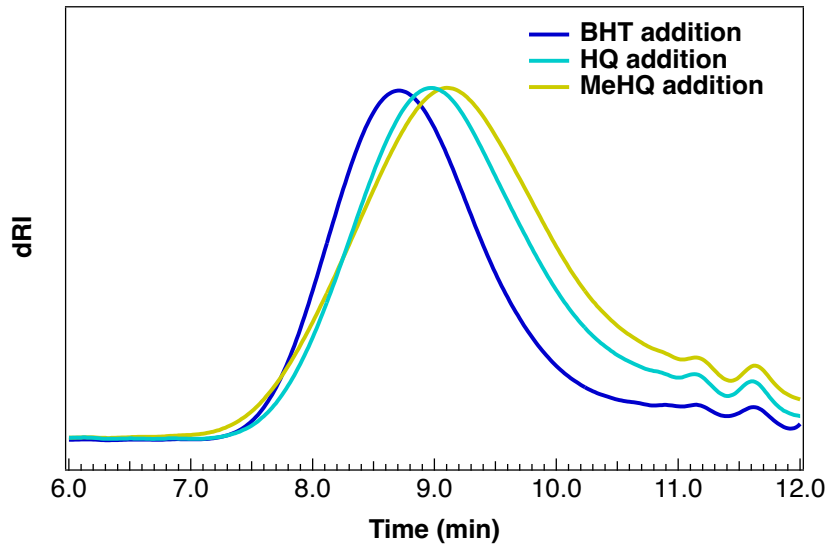


Figure S3.104. The effect of different radical inhibitors (5 mol%) to the polymerization of **M1** monomer, such as BHT, hydroquinone (HQ), and mequinol (MeHQ). As shown, the mixture with BHT displays the best polymerization behavior, compared to the those with HQ and MeHQ.

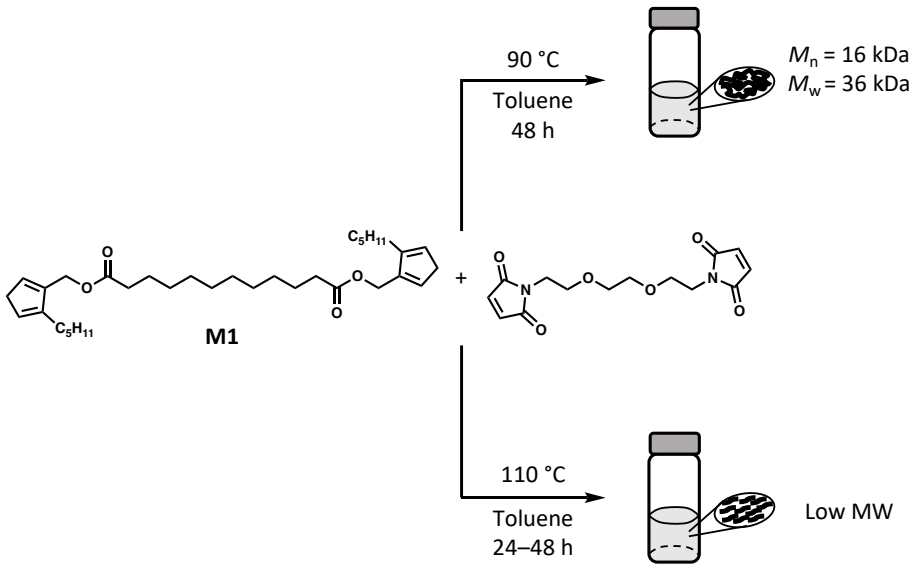


Figure S3.105. Initial trials of reacting **M1** monomer with 1,8-bis(maleimido)-3,6-dioxaoctane show the formation of low-MW polymer. Prolonged heating further decreased the molecular weight range, presumably due to the lower rDA temperature between Cp and maleimide than the Cp dimer. Low MWs were observed compared to those generated by the Cp homopolymerization. Since it is essential to maintain exact stoichiometry for the two-component system, the Cp dimerization hypothetically reduced the amount of available Cp chain-ends and thus, terminated the polymerization at low MW range. Furthermore, the addition of solvents might also reduce the efficiency of the polymerization. Of note, the 1,8-bis(maleimido)-3,6-dioxaoctane was synthesized based on the reported literature.[77]

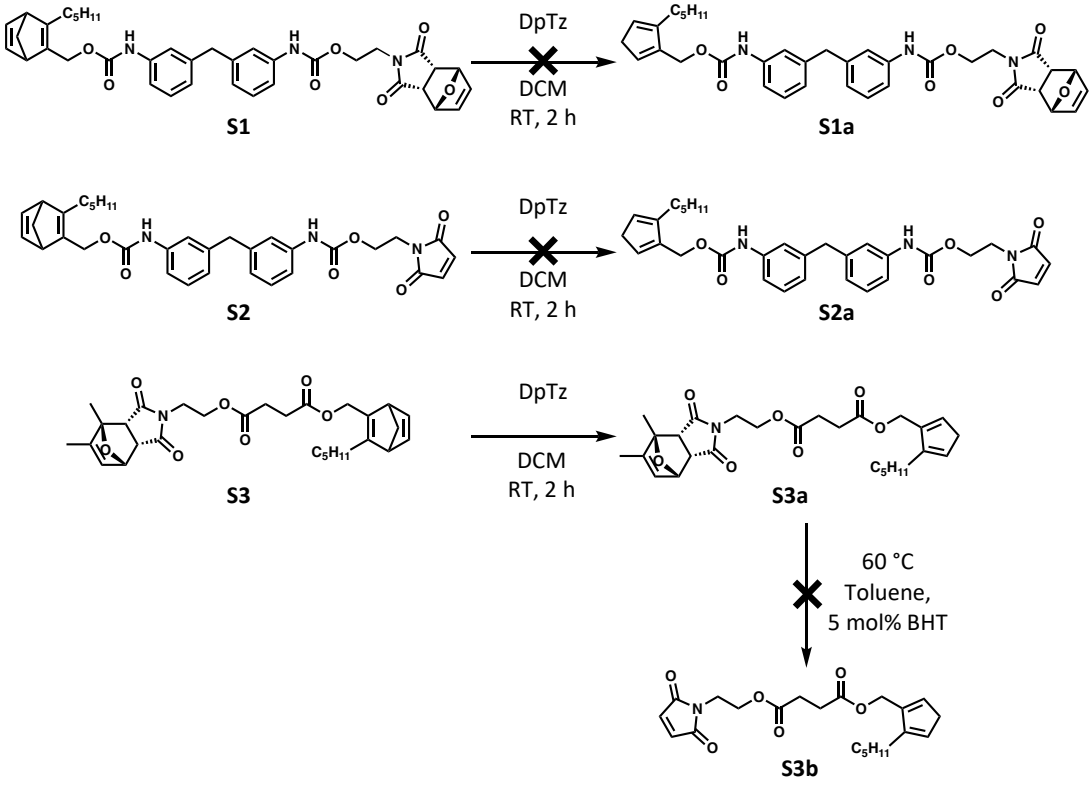


Figure S106. Proposed scheme to achieve single-component Cp-maleimide polymerization via the deprotection of the NBD and the *endo*-furan-maleimide adducts. Of note, the hydroxyethyl *endo*-furan-maleimide precursor was synthesized based on the previously reported procedure.[78] However, the initial synthetic attempts show incompatibility between these two routes. For example, furan-maleimide adduct can react with DpTz reagent.[79] Fast reaction between Cp and maleimide also interferes with isolation after tetrazine deprotection.

Furthermore, Cp dimerization affects the stoichiometry between Cp and maleimide chain-ends. Change in the substituent (pentyl to more bulk groups such as phenyl) to prevent Cp dimerization can lead to a more efficient route, as briefly studied in the thesis from the Deck group at Virginia University.[32]

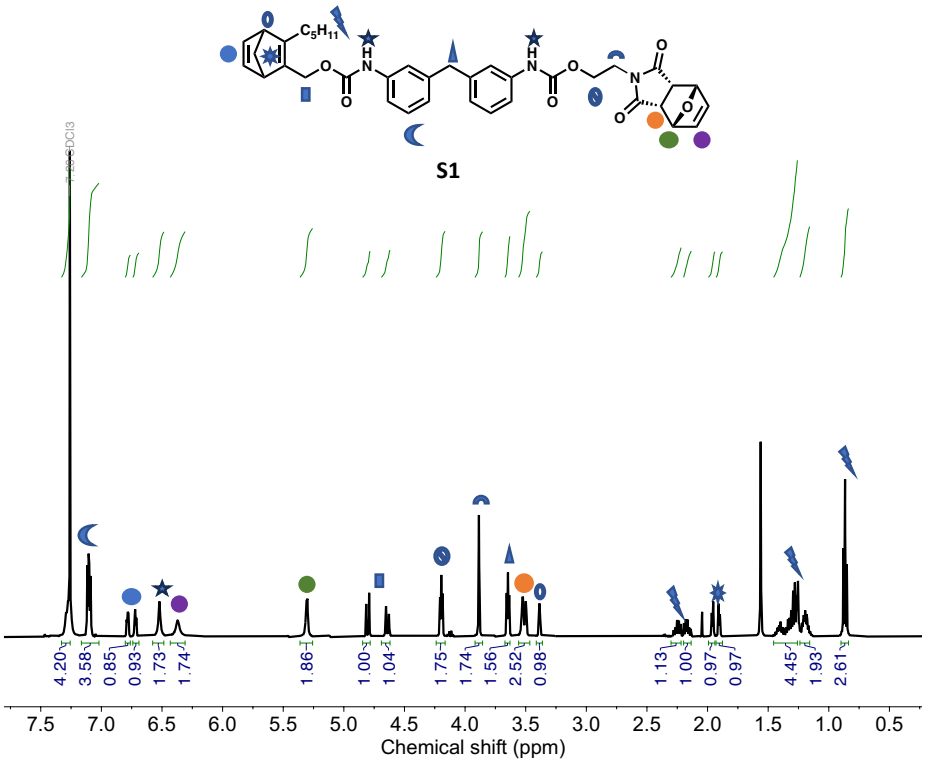


Figure S3.107. ^{1}H NMR spectrum of the **S1** analog in $CDCl_3$ with the assigned peaks.

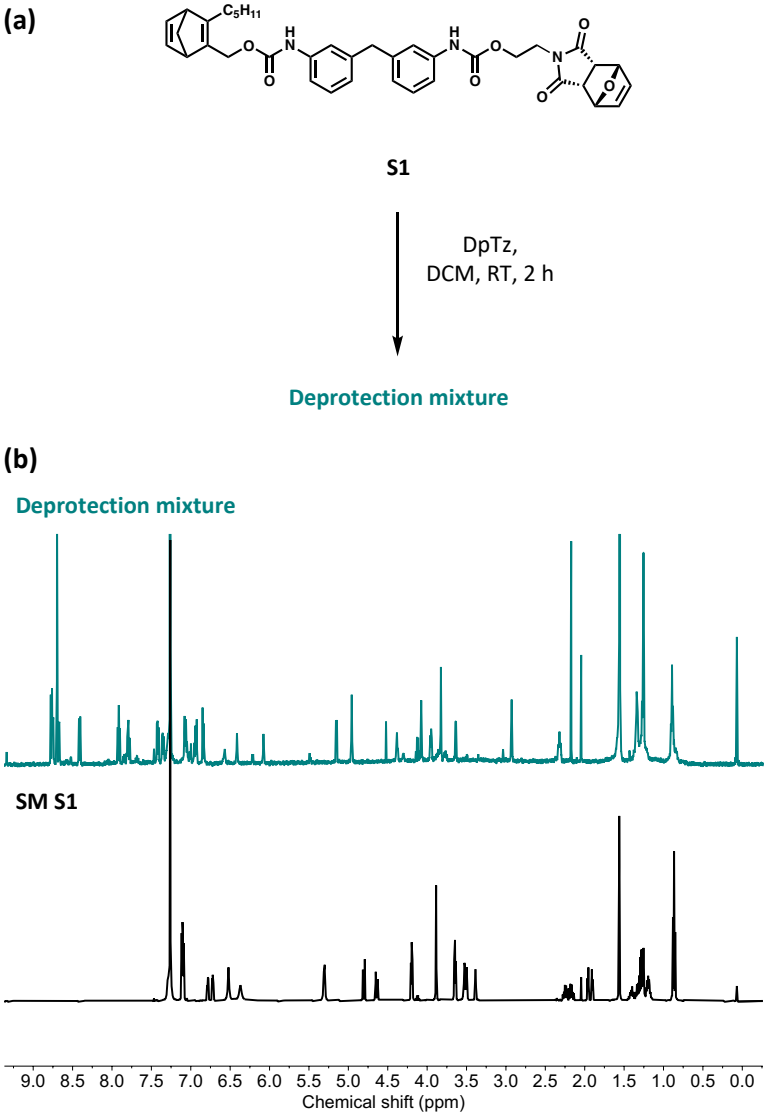


Figure S3.108. (a) Scheme of S1 deprotection using the tetrazine reagent. (b) Based on the ^{1}H NMR spectrum, deprotection of **S1** analog shows side reaction between the *endo* furan-maleimide moiety with the DpTz reagent, which was known in literature.[18,19]

Depolymerization experiments show efficient closed-loop chemical recycling:

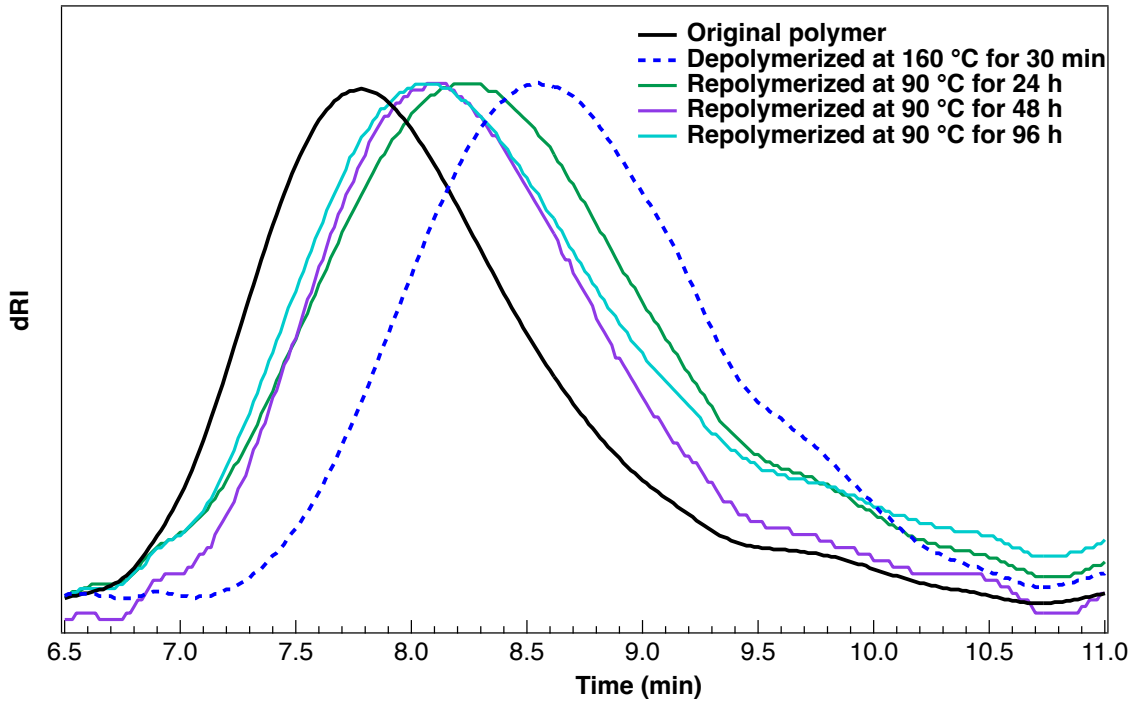


Figure S3.109. The SEC curves of the polymers as original, after depolymerization at 160 °C, and after repolymerization with different durations (24, 48, and 96 h). An initial depolymerization trial of hydrogenated polybutadiene-Cp polymer (**Pol 4**) at 160 °C shows partial degradation, and full recovery of MW is not achieved. Of note, the polymer processing includes 1 wt% BHT. No solvent was added, and no purification was performed in between the de- and re-polymerization.

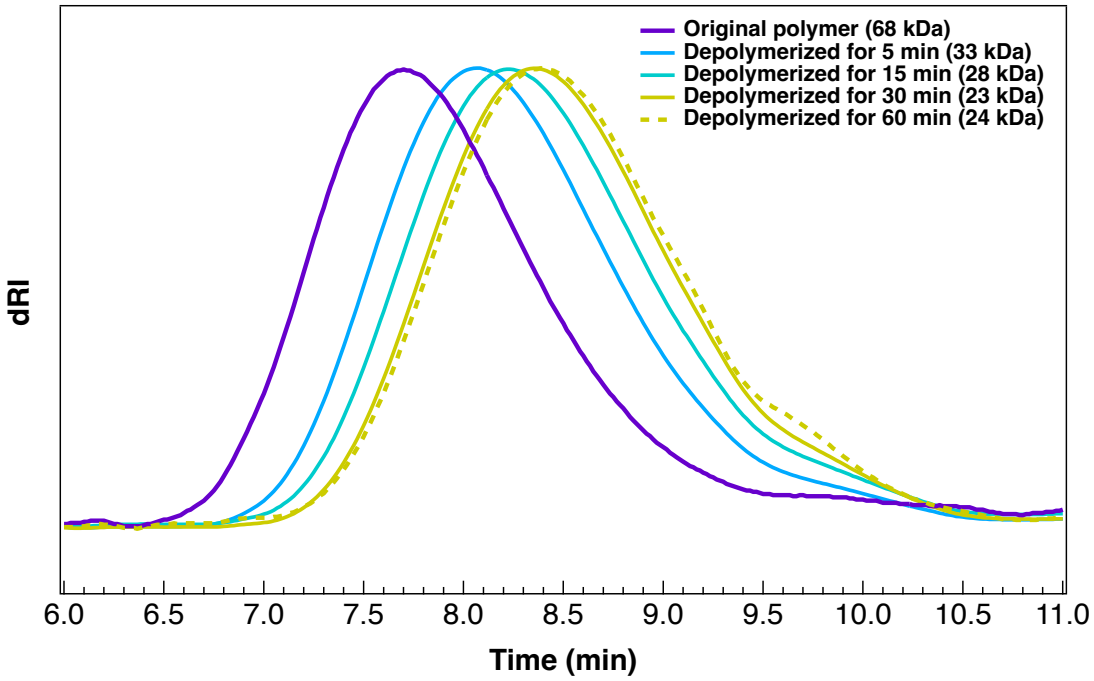


Figure S3.110. The SEC curves of the **Pol 4** as original (M_n = 68 kDa) and after depolymerization (heating at 150 °C for 15, 30 and 60 min). Further screening of depolymerization of **Pol 4** shows optimal condition is heating at 150 °C for 30 min. Prolonged heating shows partial degradation and no further decrease in MW. Of note, the polymer processing includes 1 wt% BHT. No solvent was added, and no purification was performed in between the de- and re-polymerization.

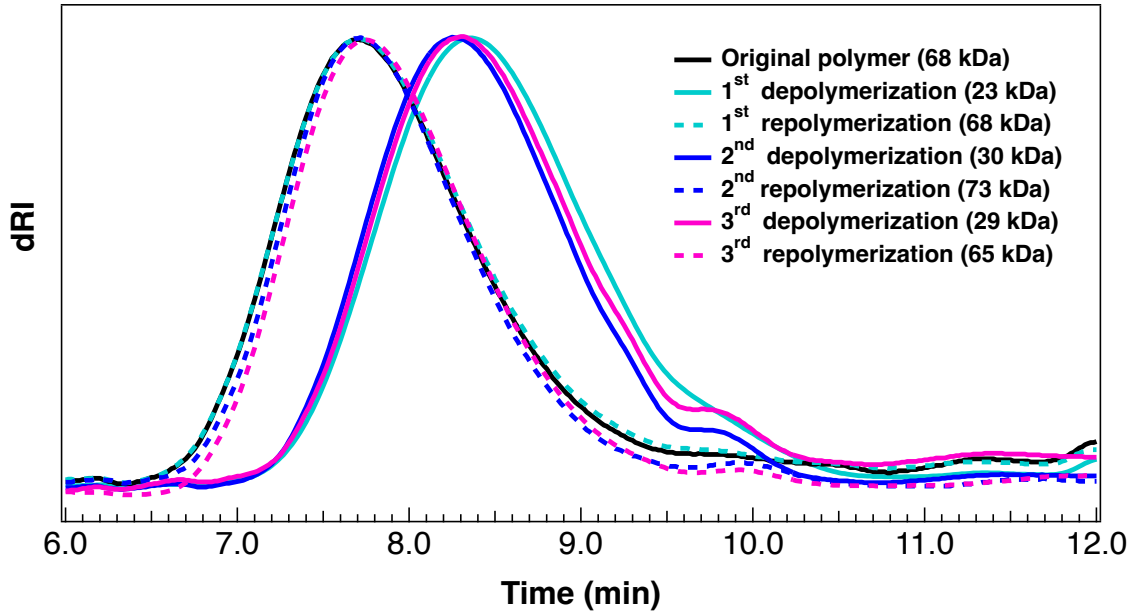


Figure S111. The SEC curves of the **Pol 4** as the original, after depolymerization, and repolymerization. The cycle was repeated 3 times. Depolymerization of **Pol 4** at 150 °C for 30 minutes and subsequent repolymerization at 90 °C for 96 hours. The process shows preservation of molecular weight throughout the 3 cycles, demonstrating an effective closed-loop recycling. Of note, the polymer processing includes 1 wt% BHT. The number-average molecular weight of the polymer (M_n) is reported, followed by the depolymerization and repolymerization annotation. No solvent was added, and no purification was performed in between the de- and re-polymerization.

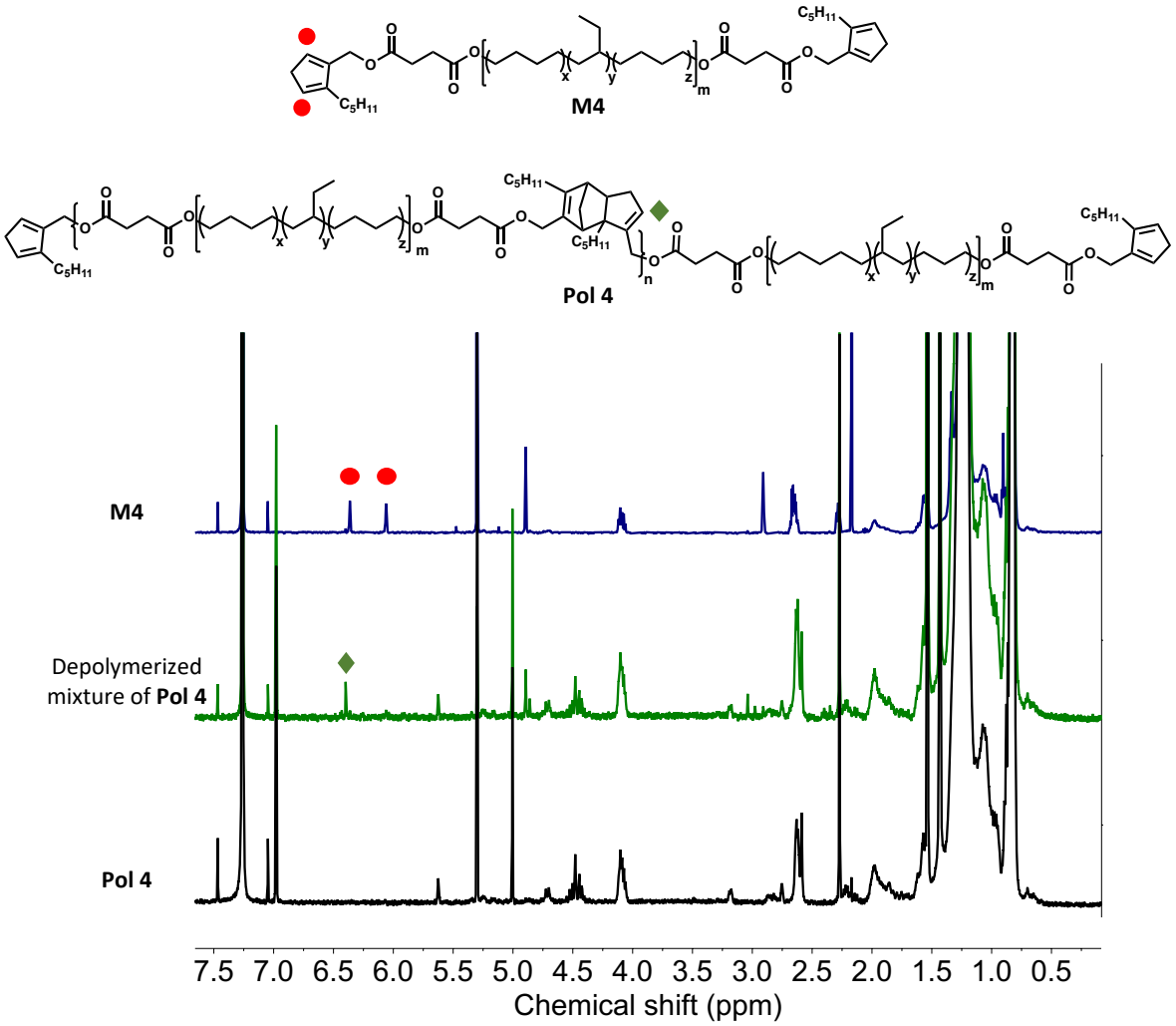


Figure S3.112. Overlay of ^{1}H NMR spectra from the hydrogenated butadiene-Cp **M4** monomer (top), depolymerized mixture of **Pol 4** after heating at 150 °C for 30 min (middle), and the original polymer **Pol 4** (bottom). The two proton signals from the Cp chain-ends were indicated as the red-circle symbols. The proton of the *endo*-Cp-dimer adduct was indicated as the green-diamond symbol. Based on the spectrum, the Cp chain-ends were revealed after depolymerization, along with the *endo*-Cp-dimer adduct.

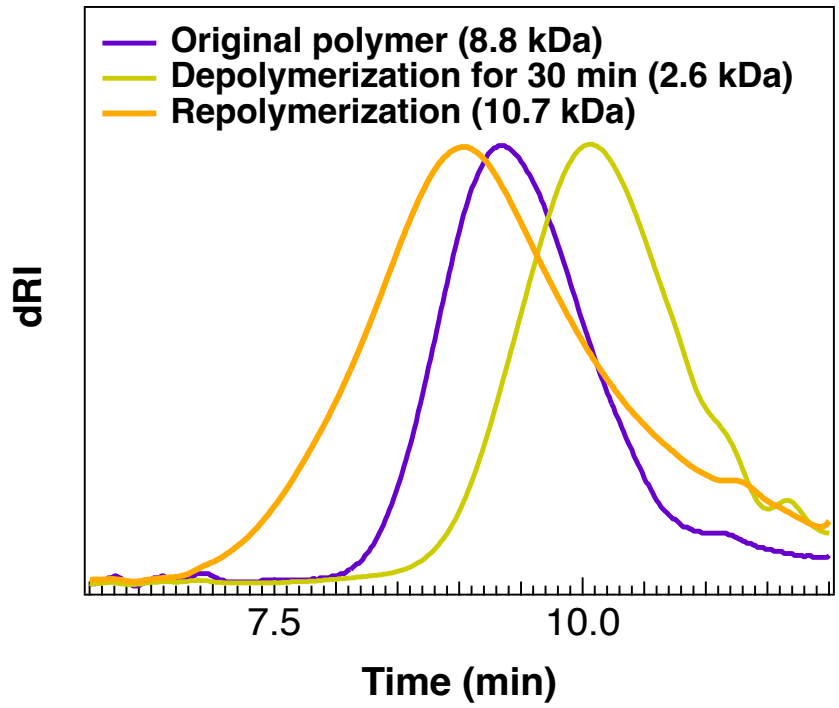


Figure S3.113. The SEC curves of the urethane-Cp polymer (**Pol 2**) as the original, after depolymerization at 150 °C for 30 min, and after repolymerization at 90 °C for 48 h. After repolymerization, the M_n was increased (from 8.8 kDa to 10.7 kDa). The observed increase in MW can be presumably based on the dynamic urethane linkages. Of note, the polymer processing includes 1 wt% BHT. No solvent was added, and no purification was performed in between the de- and re-polymerization.

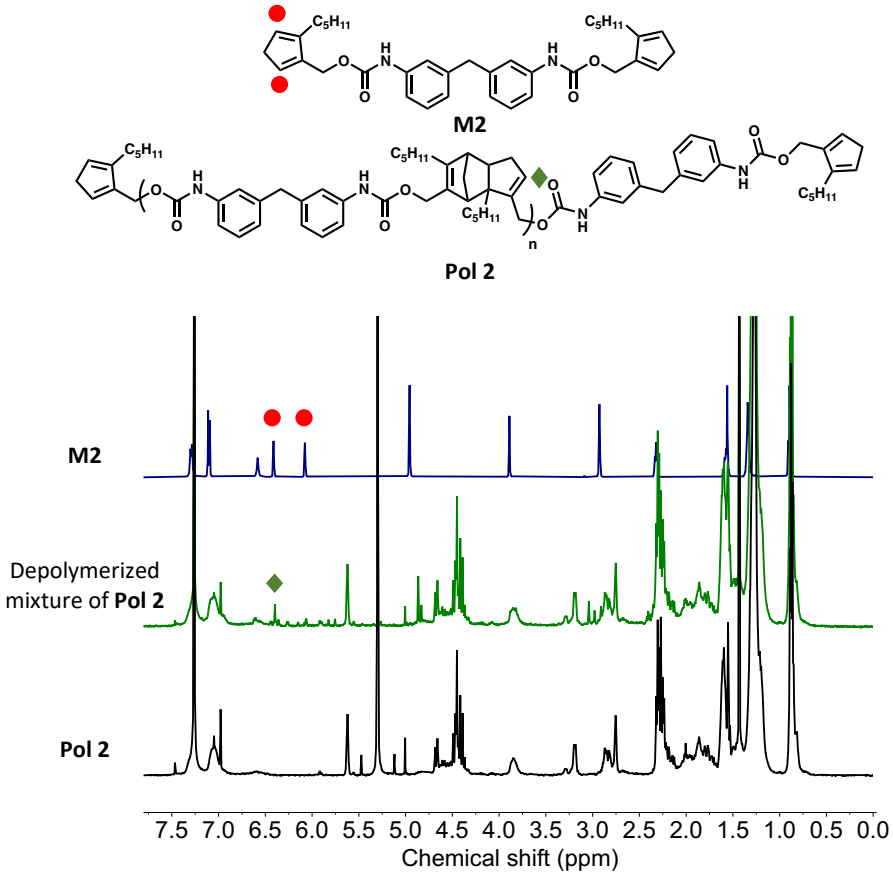


Figure S3.114. Overlay of ^{1}H NMR spectra from the urethane-Cp **M2** monomer (top), depolymerized mixture of **Pol 2** after heating at 150 °C for 30 min (middle), and the original polymer **Pol 2** (bottom). The two proton signals from the Cp chain-ends were indicated as the red-circle symbols. The proton of the *endo*-Cp-dimer adduct was indicated as the green-diamond symbol. Based on the spectrum, the Cp chain-ends were revealed after depolymerization, along with the *endo*-Cp-dimer adduct.

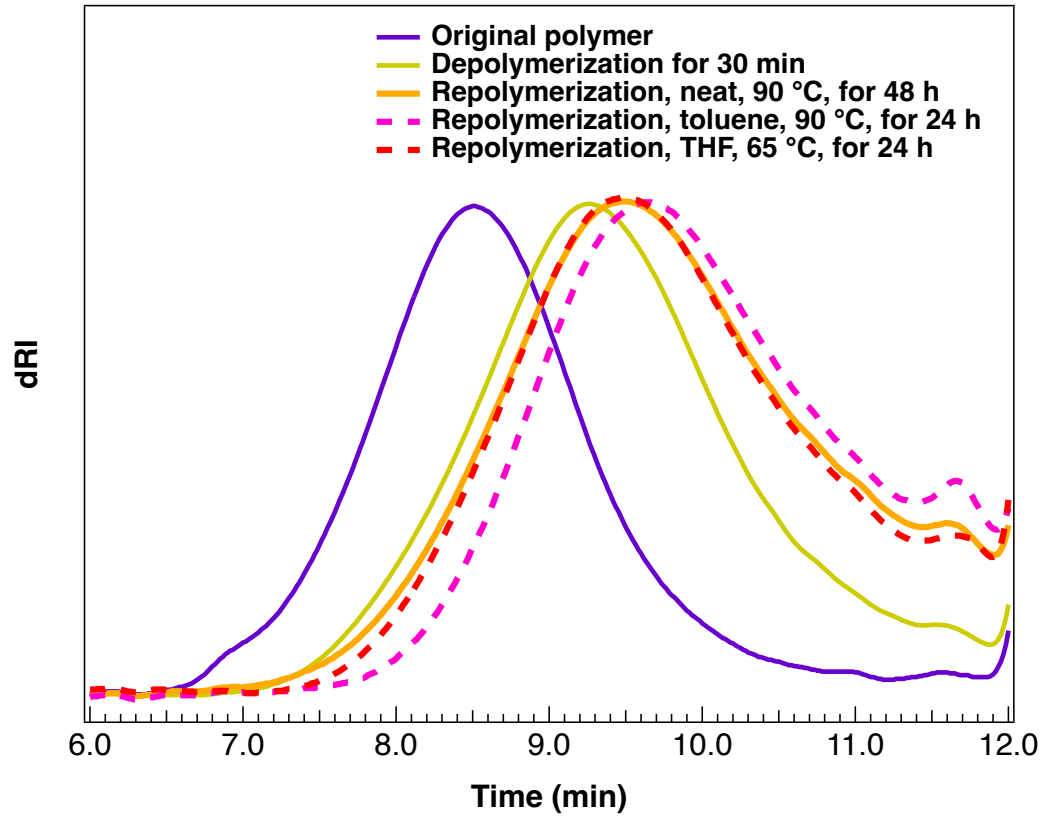


Figure S3.115. The SEC curves of the alkyl-Cp polymer (**Pol 1**) as the original, after depolymerization at 150 °C for 30 min, and repolymerization at different conditions. **Pol 1** was depolymerized from an M_n value of 26.2 kDa to 6.1 kDa. Heating the resulting oligomers under the optimized procedure (neat, 90 °C for 48 h), however, did not revert to the MW of **Pol 1**. Change of polymerization conditions, such as increasing the amount of BHT (from 1 to 6 wt%), for the de- and re-polymerization did not facilitate the process. Furthermore, changing the temperature and adding solvents (dotted traces) to the repolymerization did not provide higher-MW polymer.

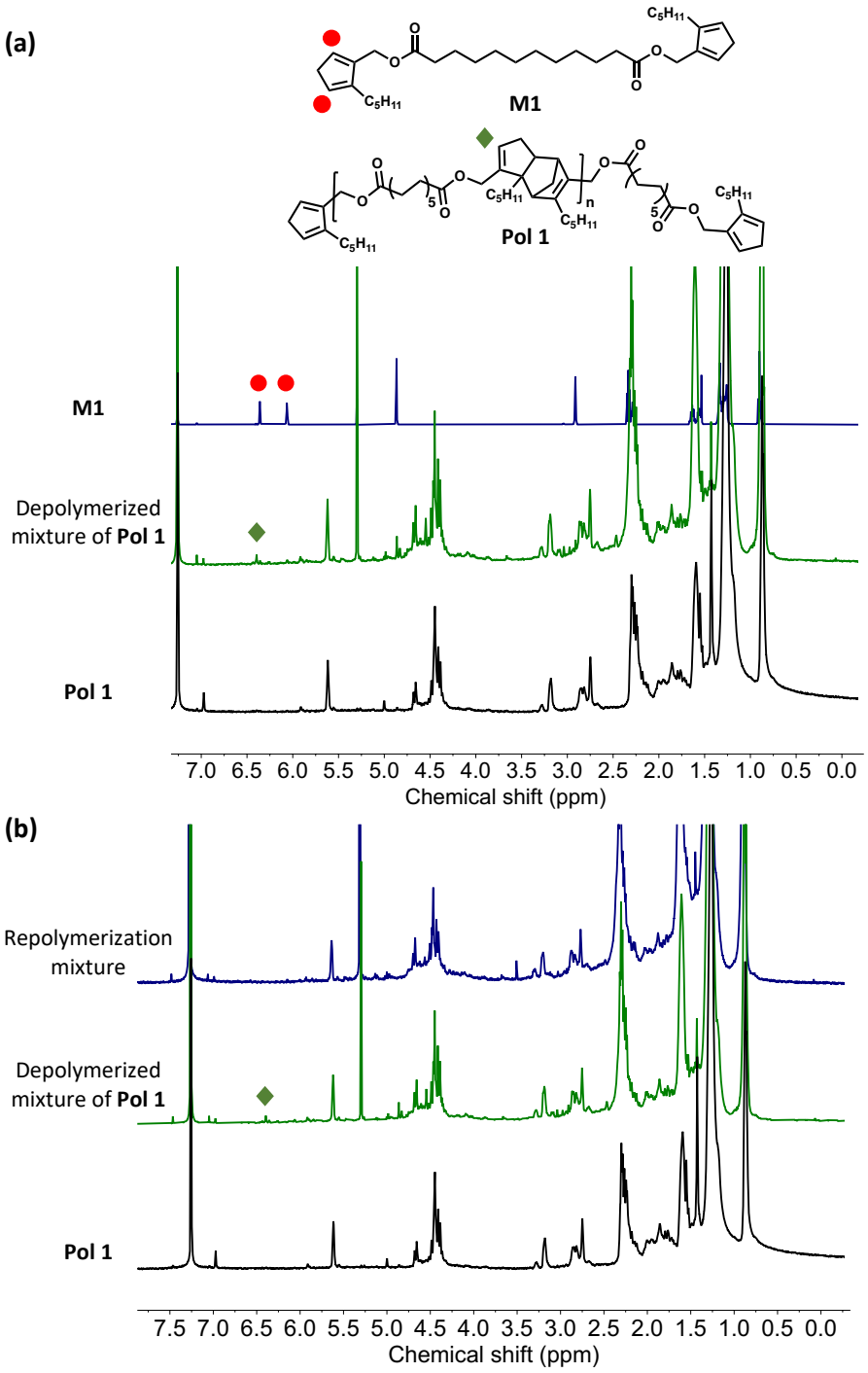

(a)
M1
Pol 1
M1
Depolymerized mixture of Pol 1
Pol 1
7.0 6.5 6.0 5.5 5.0 4.5 4.0 3.5 3.0 2.5 2.0 1.5 1.0 0.5 0.0
Chemical shift (ppm)
(b)
Repolymerization mixture
Depolymerized mixture of Pol 1
Pol 1
7.5 7.0 6.5 6.0 5.5 5.0 4.5 4.0 3.5 3.0 2.5 2.0 1.5 1.0 0.5 0.0
Chemical shift (ppm)

Figure S3.116. (a) Overlay of ^{1}H NMR spectra from the alkyl-Cp **M1** monomer (top), depolymerized mixture of **Pol 1** after heating at 150 °C for 30 min (middle), and the original polymer **Pol 1** (bottom). The two proton signals from the Cp chain-ends were indicated as the red-circle symbols. The proton of the *endo*-Cp-dimer adduct was indicated as the green-diamond symbol. Based on the spectrum, the Cp chain-ends were revealed after depolymerization, along with the *endo*-Cp-dimer adduct. (b) The ^{1}H NMR spectrum of repolymerization mixture was compared with the spectra of **Pol 1** and the depolymerized materials. After repolymerization, the signal from the *endo*-Cp-dimer adduct was consumed as well as the Cp chain-ends.

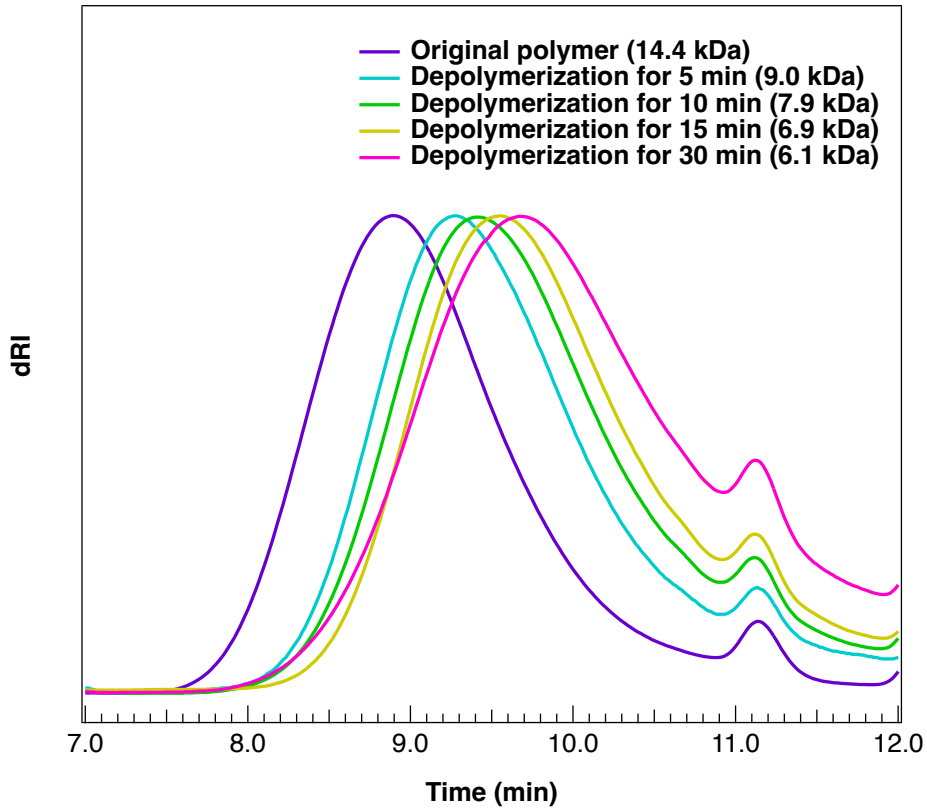


Figure S3.117. The SEC curves of **Pol 6** as the original, and after depolymerization at 150 °C with different durations (5, 10, 15, and 30 min). Of note, the polymer processing includes 1 wt% BHT. The number-average molecular weight of the polymer (M_n) is reported followed by the depolymerization and repolymerization annotation. No solvent was added, and no purification was performed in between the de- and re-polymerization.

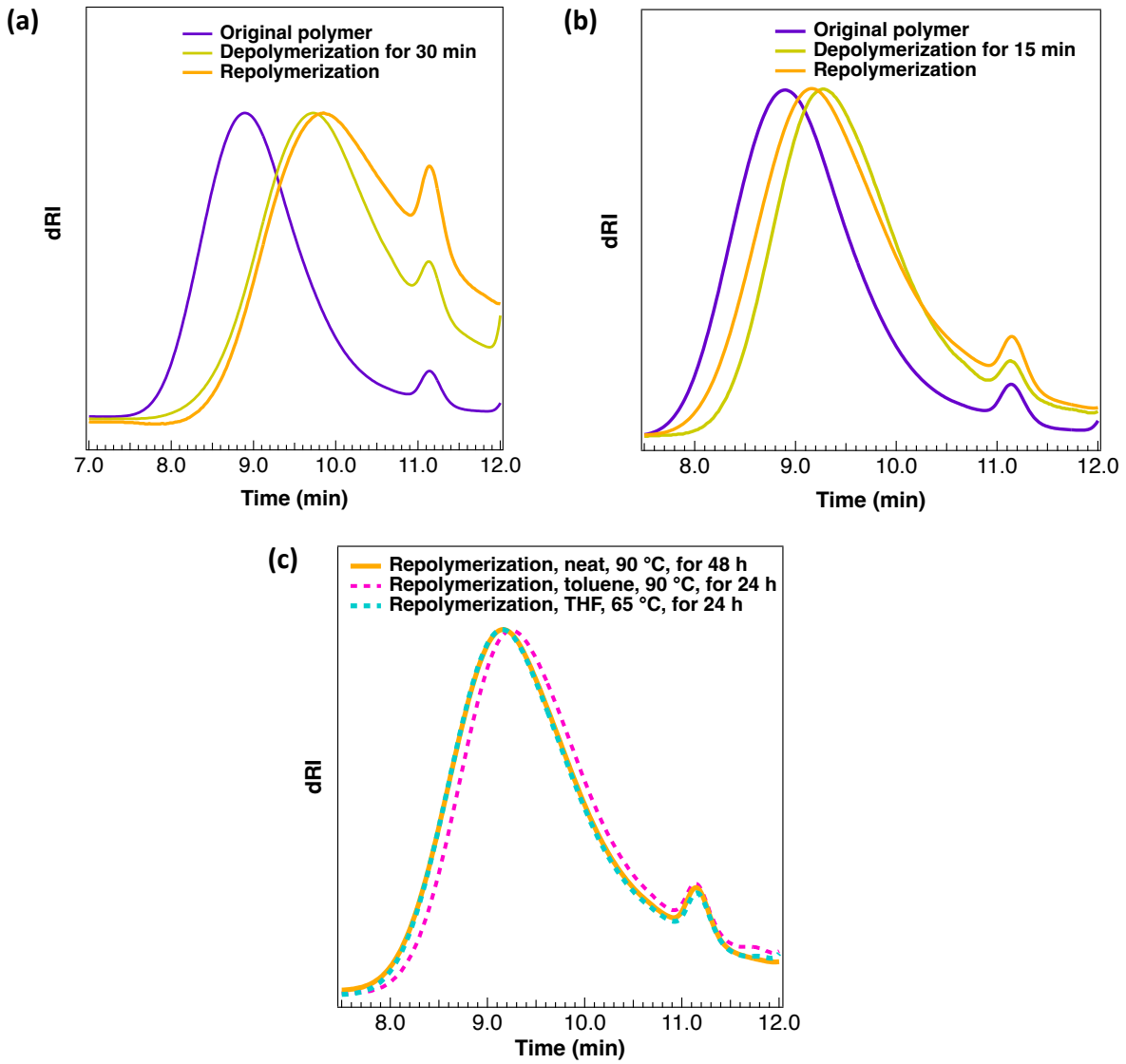


Figure S3.118. The SEC curves of **Pol 6** as (a) the original, after depolymerization at 150 °C for 30 min, and repolymerization at 90 °C for 48 h; (b) the original, after depolymerization at 150 °C for 15 min, and repolymerization at 90 °C for 48h; (c) the repolymerization of the 15-min depolymerized sample under different conditions (at 90 °C without solvent, at 90 °C with toluene for 24 h, and at 65 °C in THF for 24 h). Heating **Pol 6** at 150 °C for 15 min and repolymerization of the mixture show promising recovery of the MW, despite not fully to the original.

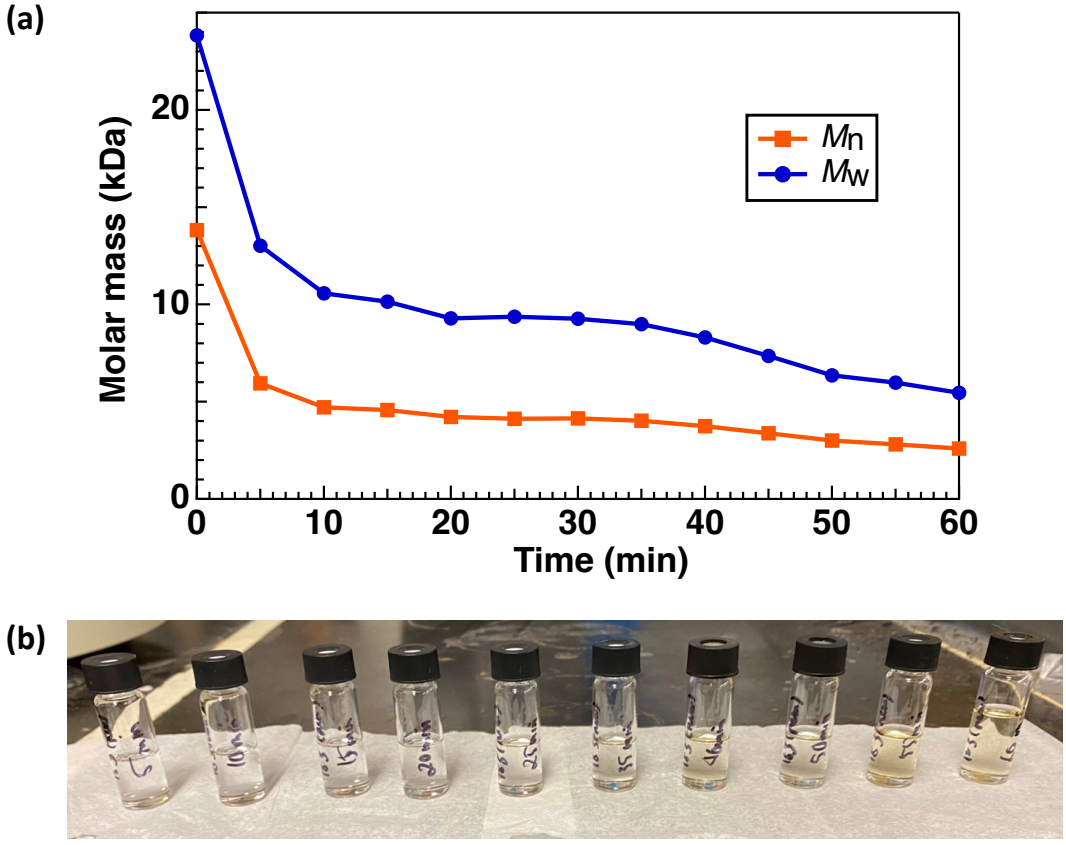


Figure S3.119. (a) The reported M_n and M_w values of the depolymerized mixture of **Pol 6** after different durations (5, 10, 15, 20, 25, 30, 35, 40, 45, 50, 55, and 60 min). The values were obtained from SEC. (b) The color of the polymer shows the gradual degradation (from transparent to slightly yellowish, solvent was added for clear visualization). Gelation or cross-linked materials were observed if the heating was performed for too long or at very high temperature (i.e., 110 °C or higher) or the amount of radical inhibitor was not enough to prevent the uncontrolled processes.

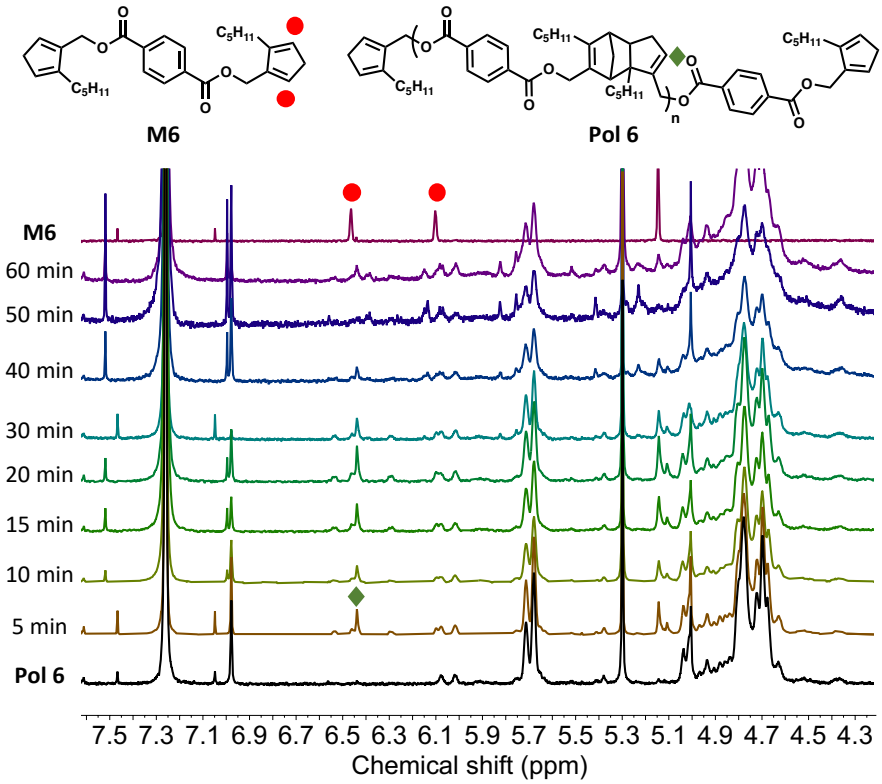


Figure S3.120. (a) Overlay of the ^{1}H NMR spectra from the ethyl terephthalate-Cp **M6** monomer (top); depolymerized mixture of **Pol 6** after heating at 150 °C for 60 min with 5, 10, 15, 20, 30, 40, 50, and 60-min interval; and the original polymer **Pol 6** (bottom). The two proton signals from the Cp chain-ends were indicated as the red-circle symbols. The peak that is assigned with the green diamond symbol indicates the proton from the *endo* Cp-dimer adduct. Based on the spectrum, the Cp chain-ends were revealed after depolymerization, along with the *endo*-Cp-dimer adduct.

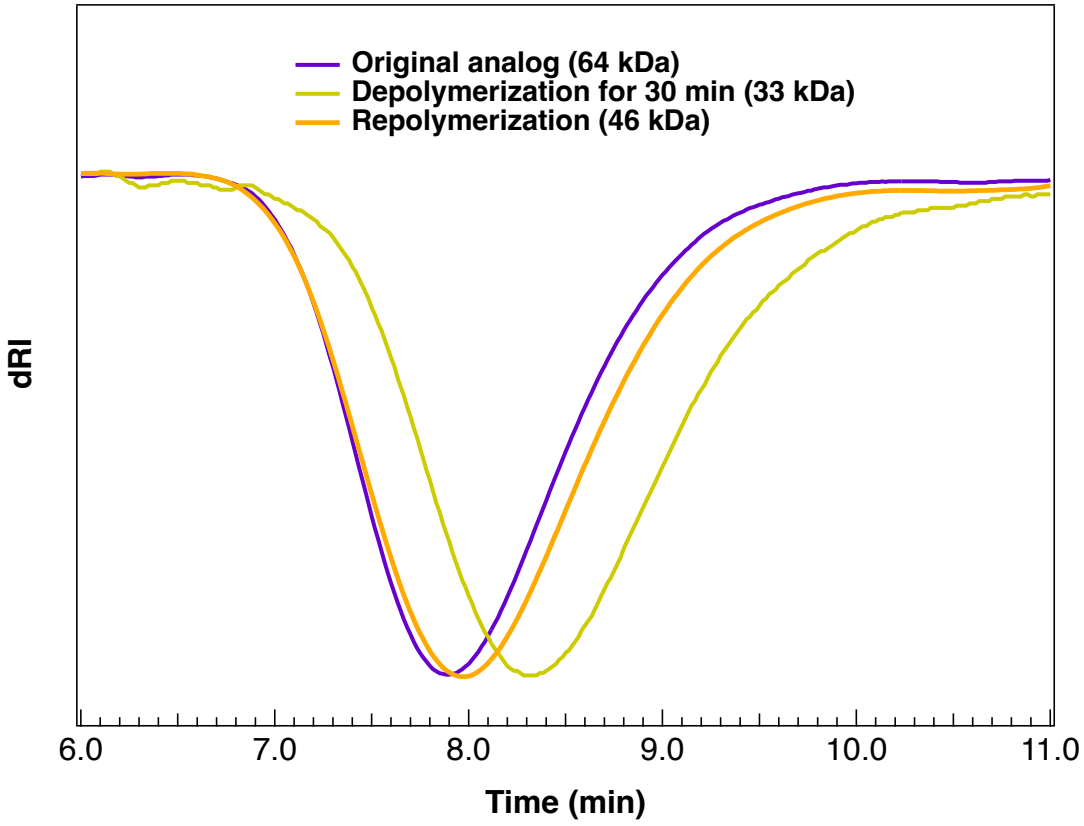


Figure S121. The SEC curves of the siloxane-Cp polymer (**Pol 3**) as the original, after depolymerization at 150 °C for 30 min, and repolymerization at different conditions. Depolymerization of the **Pol 3** (M_n = 64 kDa) affords the oligomer mixture with M_n of 33 kDa. The repolymerization (orange trace) results in the polymer with M_n = 46 kDa, which is close to the value of the original analog.

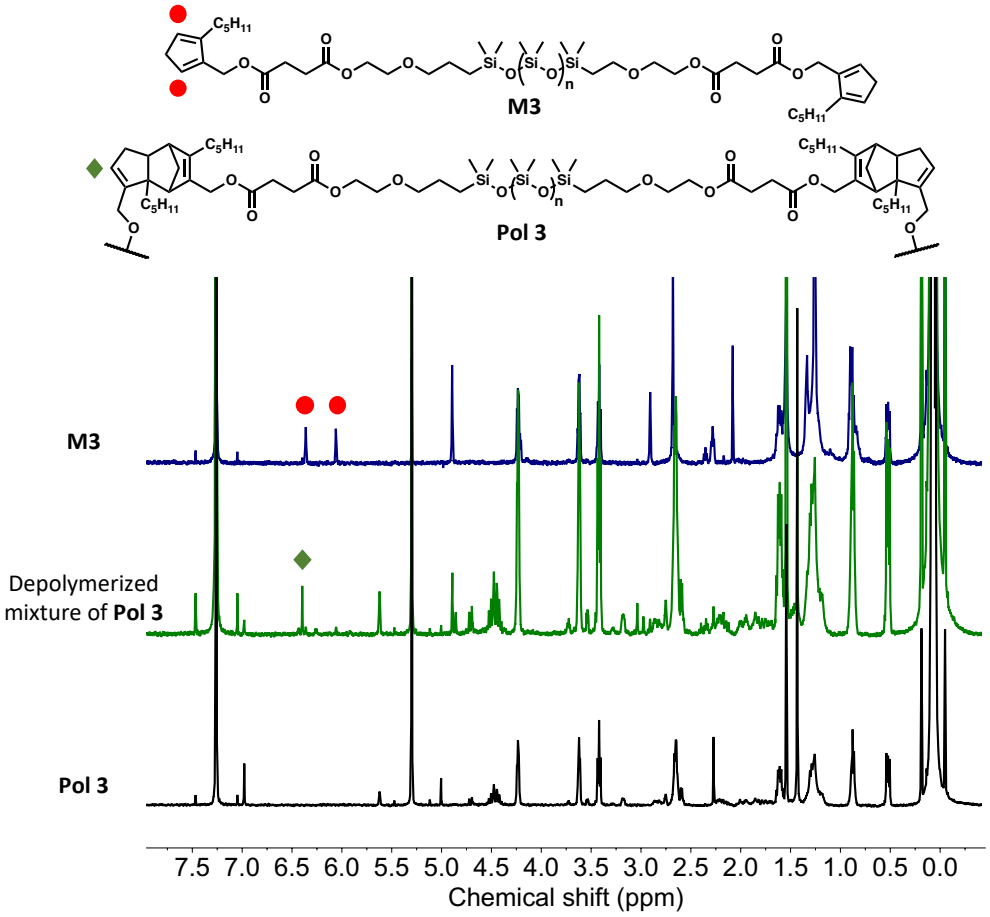


Figure S3.122. Overlay of ^{1}H NMR spectra from the polydimethylsiloxane-Cp **M3** monomer (top), depolymerized mixture of **Pol 3** after heating at 150 °C for 30 min (middle), and the original polymer **Pol 3** (bottom). The two proton signals from the Cp chain-ends were indicated as the red-circle symbols. The proton of the *endo*-Cp-dimer adduct was indicated as the green-diamond symbol. Based on the spectrum, the Cp chain-ends were revealed after depolymerization, along with the *endo*-Cp-dimer adduct.

3.8 References

(1) Geyer, R.; Jambeck, J. R.; Law, K. L. Production, Use, and Fate of All Plastics Ever Made. *Sci. Adv.* **2017**, *3*, e1700782. DOI: 10.1126/sciadv.1700782.

(2) Oladele, I. O.; Okoro, C. J.; Taiwo, A. S.; Onuh, L. N.; Agbeboh, N. I.; Balogun, O. P.; Olubambi, P. A.; Lephuthing, S. S. Modern Trends in Recycling Waste Thermoplastics and

Their Prospective Applications: A Review. *J. Compos. Sci.* **2023**, *7*, 198. DOI: 10.3390/jcs7050198.

(3) Billiet, S.; Trenor, S. R. 100th Anniversary of Macromolecular Science Viewpoint: Needs for Plastics Packaging Circularity. *ACS Macro Lett.* **2020**, *9*, 1376–1390. DOI: 10.1021/acsmacrolett.0c00437.

(4) Worch, J. C.; Dove, A. P. 100th Anniversary of Macromolecular Science Viewpoint: Toward Catalytic Chemical Recycling of Waste (and Future) Plastics. *ACS Macro Lett.* **2020**, *9*, 1494–1506. DOI: 10.1021/acsmacrolett.0c00582.

(5) Fagnani, D. E.; Tami, J. L.; Copley, G.; Clemons, M. N.; Getzler, Y. D. Y. L.; McNeil, A. J. 100th Anniversary of Macromolecular Science Viewpoint: Redefining Sustainable Polymers. *ACS Macro Lett.* **2021**, *10*, 41–53. DOI: 10.1021/acsmacrolett.0c00789.

(6) Uekert, T.; Singh, A.; DesVeaux, J. S.; Ghosh, T.; Bhatt, A.; Yadav, G.; Afzal, S.; Walzberg, J.; Knauer, K. M.; Nicholson, S. R.; Beckham, G. T.; Carpenter, A. C. Technical, Economic, and Environmental Comparison of Closed-Loop Recycling Technologies for Common Plastics. *ACS Sustain. Chem. Eng.* **2023**, *11*, 965–978. DOI: 10.1021/acssuschemeng.2c05497.

(7) Clark, R. A.; Shaver, M. P. Depolymerization within a Circular Plastics System. *Chem. Rev.* **2024**, *124*, 2617–2650. DOI: 10.1021/acs.chemrev.3c00739.

(8) Thiyagarajan, S.; Maaskant-Reilink, E.; Ewing, T. A.; Julsing, M. K.; Van Haveren, J. Back-to-Monomer Recycling of Polycondensation Polymers: Opportunities for Chemicals and Enzymes. *RSC Adv.* **2022**, *12*, 947–970. DOI: 10.1039/D1RA08217E.

(9) Chen, Z.; Sun, H.; Kong, W.; Chen, L.; Zuo, W. Closed-Loop Utilization of Polyester in the Textile Industry. *Green Chem.* **2023**, *25*, 4429–4437. DOI: 10.1039/D3GC00407D.

(10) Yang, W.; Liu, R.; Li, C.; Song, Y.; Hu, C. Hydrolysis of Waste Polyethylene Terephthalate Catalyzed by Easily Recyclable Terephthalic Acid. *Waste Manag.* **2021**, *135*, 267–274. DOI: 10.1016/j.wasman.2021.09.009.

(11) Häußler, M.; Eck, M.; Rothauer, D.; Mecking, S. Closed-Loop Recycling of Polyethylene-like Materials. *Nature* **2021**, *590*, 423–427. DOI: 10.1038/s41586-020-03149-9.

(12) Zhao, Y.; Rettner, E. M.; Harry, K. L.; Hu, Z.; Miscall, J.; Rorrer, N. A.; Miyake, G. M. Chemically Recyclable Polyolefin-like Multiblock Polymers. *Science* **2023**, *382*, 310–314. DOI: 10.1126/science.abh0626.

(13) Coates, G. W.; Getzler, Y. D. Y. L. Chemical Recycling to Monomer for an Ideal, Circular Polymer Economy. *Nat. Rev. Mater.* **2020**, *5*, 501–516. DOI: 10.1038/s41578-020-0190-4.

(14) Kiel, G. R.; Lundberg, D. J.; Prince, E.; Husted, K. E. L.; Johnson, A. M.; Lensch, V.; Li, S.; Shieh, P.; Johnson, J. A. Cleavable Comonomers for Chemically Recyclable Polystyrene: A General Approach to Vinyl Polymer Circularity. *J. Am. Chem. Soc.* **2022**, *144*, 12979–12988. DOI: 10.1021/jacs.2c05374.

(15) Abel, B. A.; Snyder, R. L.; Coates, G. W. Chemically Recyclable Thermoplastics from Reversible-Deactivation Polymerization of Cyclic Acetals. *Science* **2021**, *373*, 783–789. DOI: 10.1126/science.abh0626.

(16) Tanaka, J.; Archer, N. E.; Grant, M. J.; You, W. Reversible-Addition Fragmentation Chain Transfer Step-Growth Polymerization. *J. Am. Chem. Soc.* **2021**, *143*, 15918–15923. DOI: 10.1021/jacs.1c07553.

(17) Siragusa, F.; Demarteau, J.; Habets, T.; Olazabal, I.; Robeyns, K.; Evano, G.; Mereau, R.; Tassaing, T.; Grignard, B.; Sardon, H.; Detrembleur, C. Unifying Step-Growth Polymerization and On-Demand Cascade Ring-Closure Depolymerization via Polymer Skeletal Editing. *Macromolecules* **2022**, *55*, 4637–4646. DOI: 10.1021/acs.macromol.2c00696.

(18) Lu, X.; Liu, Y.; Zhou, H. Learning Nature: Recyclable Monomers and Polymers. *Chem. Eur. J.* **2018**, *24*, 11255–11266. DOI: 10.1002/chem.201704461.

(19) Leir, C. M.; Stark, J. E. Ionene Elastomers from Polytetramethylene Oxide Diamines and Reactive Dihalides. I. Effect of Dihalide Structure on Polymerization and Thermal Reversibility. *J. Appl. Pol. Sci.* **1989**, *38*, 1535–1547. DOI: 10.1002/app.1989.070380810.

(20) Wagener, K. B.; Engle, L. P. Thermally Reversible Polymer Linkages. II. Linear Addition Polymers. *J. Polym. Sci. A Polym. Chem.* **1993**, *31*, 865–875. DOI: https://doi.org/10.1002/pola.1993.080310404.

(21) Kawaguchi, A. W.; Sudo, A.; Endo, T. Polymerization–Depolymerization System Based on Reversible Addition-Dissociation Reaction of 1,3-Benzoxazine with Thiol. *ACS Macro Lett.* **2013**, *2*, 1–4. DOI: 10.1021/mz3005296.

(22) Motoki, S.; Nakano, T.; Tokiwa, Y.; Saruwatari, K.; Tomita, I.; Iwamura, T. Synthesis of Recyclable Molecular LEGO Block Polymers Utilizing the Diels-Alder Reaction. *Polymer* **2016**, *101*, 98–106. DOI: 10.1016/j.polymer.2016.08.024.

(23) Gandini, A. The Application of the Diels-Alder Reaction to Polymer Syntheses Based on Furan/Maleimide Reversible Couplings. *Polímeros* **2005**, *15*, 95–101. DOI: 10.1590/S0104-14282005000200007.

(24) Gandini, A. The Furan/Maleimide Diels–Alder Reaction: A Versatile Click–Unclick Tool in Macromolecular Synthesis. *Prog. Polym. Sci.* **2013**, *38*, 1–29. DOI: 10.1016/j.progpolymsci.2012.04.002.

(25) Gandini, A.; Coelho, D.; Silvestre, A. J. D. Reversible Click Chemistry at the Service of Macromolecular Materials. Part 1: Kinetics of the Diels–Alder Reaction Applied to Furan–Maleimide Model Compounds and Linear Polymerizations. *Eur. Polym. J.* **2008**, *44*, 4029–4036. DOI: 10.1016/j.eurpolymj.2008.09.026.

(26) Diels, O.; Alder, K. Synthesen in der hydroaromatischen Reihe. *Justus Liebigs Ann. Chem.* **1928**, *460*, 98–122.

(27) Stille, J. K. Step-Growth Polymerization. *J. Chem. Educ.* **1981**, *58*, 862. DOI: 10.1021/ed058p862.

(28) Yoshie, N. Diels-Alder Polymers. In *Encyclopedia of Polymer Science and Technology*; John Wiley & Sons, Inc., Ed.; John Wiley & Sons, Inc.: Hoboken, NJ, USA, **2013**; p pst607.

(29) Stille, J. K.; Plummer, L. Polymerization by the Diels-Alder Reaction. *J. Org. Chem.* **1961**, *26*, 4026–4029. DOI: 10.1021/jo01068a092.

(30) Kennedy, J. P.; Carlson, G. M. Synthesis, Characterization, and Diels–Alder Extension of Cyclopentadiene Telechelic Polyisobutylene. IV. α,ω-Di(3-cyclopentadienylpropyldimethylsilyl)Polyisobutylene. *J. Polym. Sci. Polym. Chem. Ed.* **1983**, *21*, 3551–3561. DOI: 10.1002/pol.1983.170211216.

(31) Staudinger, H.; Bruson, H. A. Hochpolymere Verbindungen. 7. Mitteilung. Über das Dicyclopentadien und weitere polymere Cyclopentadiene. *Justus Liebigs Ann. Chem.* **1926**, *447*, 97–110.

(32) Stegall, J. B. Cyclopentadiene-Maleimide Platform for Thermally Reversible Polymers; Virginia Tech: Blacksburg, VA, **2014**.

(33) Murphy, E. B.; Bolanos, E.; Schaffner-Hamann, C.; Wudl, F.; Nutt, S. R.; Auad, M. L. Synthesis and Characterization of a Single-Component Thermally Remendable Polymer Network: Staudinger and Stille Revisited. *Macromolecules* **2008**, *41*, 5203–5209. DOI: 10.1021/ma800432g.

(34) Levandowski, B. J.; Raines, R. T. Click Chemistry with Cyclopentadiene. *Chem. Rev.* **2021**, *121*, 6777–6801. DOI: 10.1021/acs.chemrev.0c01055.

(35) Tesoro, G. C.; Sastri, V. R. Synthesis of Siloxane-Containing Bis(Furans) and Polymerization with Bis(Maleimides). *Ind. Eng. Chem. Prod. Res. Dev.* **1986**, *25*, 444–448. DOI: 10.1021/i300023a013.

(36) Brand, T.; Klapper, M. Control of Viscosity through Reversible Addition of Telechelics via Repetitive Diels-Alder Reaction in Bulk. *Des. Monomers Polym.* **1999**, *2*, 287–309. DOI: 10.1163/156855599X00106.

(37) Briou, B.; Améduri, B.; Boutevin, B. Trends in the Diels–Alder Reaction in Polymer Chemistry. *Chem. Soc. Rev.* **2021**, *50*, 11055–11097. DOI: 10.1039/D0CS01382J.

(38) Kuramoto, N.; Hayashi, K.; Nagai, K. Thermoreversible Reaction of Diels—Alder Polymer Composed of Difurufuryladipate with Bismaleimidodiphenylmethane. *J. Polym. Sci., Part A: Polym. Chem.* **1994**, *32*, 2501–2504. DOI: 10.1002/pola.1994.080321312.

(39) Tran, T. M.; Read de Alaniz, J. Controlled Synthesis of a Homopolymer Network Using a Well-Defined Single-Component Diels–Alder Cyclopentadiene Monomer. *J. Am. Chem. Soc.* **2023**, *145*, 3462–3469. DOI: 10.1021/jacs.2c11416.

(40) St. Amant, A. H.; Discekici, E. H.; Bailey, S. J.; Zayas, M. S.; Song, J.-A.; Shankel, S. L.; Nguyen, S. N.; Bates, M. W.; Anastasaki, A.; Hawker, C. J.; Read de Alaniz, J. Norbornadienes: Robust and Scalable Building Blocks for Cascade "Click" Coupling of High Molecular Weight Polymers. *J. Am. Chem. Soc.* **2019**, *141*, 13619–13624. DOI: 10.1021/jacs.9b06328.

(41) Bailey, S. J.; Discekici, E. H.; Barbon, S. M.; Nguyen, S. N.; Hawker, C. J.; Read de Alaniz, J. Norbornadiene Chain-End Functional Polymers as Stable, Readily Available Precursors to Cyclopentadiene Derivatives. *Macromolecules* **2020**, *53*, 4917–4924. DOI: 10.1021/acs.macromol.0c00967.

(42) Cardellini, F.; Brinchi, L.; Germani, R.; Tiecco, M. Convenient Esterification of Carboxylic Acids by S_N2 Reaction Promoted by a Protic Ionic-Liquid System Formed in Situ

in Solvent-Free Conditions. *Synth. Commun.* **2014**, *44*, 3248–3256. DOI: 10.1080/00397911.2014.933353.

(43) Facinelli, J. V.; Gardner, S. L.; Dong, L.; Sensenich, C. L.; Davis, R. M.; Riffle, J. S. Controlled Molecular Weight Polyimides from Poly(Amic Acid) Salt Precursors. *Macromolecules* **1996**, *29*, 7342–7350. DOI: 10.1021/ma960885s.

(44) Liaw, D.-J.; Wang, K.-L.; Huang, Y.-C.; Lee, K.-R.; Lai, J.-Y.; Ha, C.-S. Advanced Polyimide Materials: Syntheses, Physical Properties and Applications. Prog. Polym. Sci. **2012**, *37*, 907–974. DOI: 10.1016/j.progpolymsci.2012.02.005.

(45) Wright, W. W.; Hallden-Abberton, M. Polyimides. In *Ullmann's Encyclopedia of Industrial Chemistry*; Wiley-VCH, Ed.; Wiley, 2000.

(46) Flory, P. J. *Principles of Polymer Chemistry*; Baker lectures 1948; Cornell University Press, **1953**.

(47) Tanford, C.; Huggins, M. L. Physical Chemistry of Macromolecules. *J. Electrochem. Soc.* **1962**, *109*, 98C. DOI: 10.1149/1.2425390.

(48) Ouano, A. C. Gel Permeation Chromatography. *J. of Chromatogr. A* **1976**, *118*, 303–312.

(49) Wang, K.; Huang, H.; Sheng, J. Determination of the Mark-Houwink Equation Parameters and Their Interrelationship. *J. Liq. Chromatogr. Relat. Technol.* **1998**, *21*, 1457–1470.

(50) Ito, K.; Ukai, T. Determination of Mark–Houwink–Sakurada Constants for Measurements of the Molecular Weights by Gel Permeation Chromatography I. On the Generalization of Mathematical Procedure. *Polym. J.* **1986**, *18*, 593–600. DOI: 10.1295/polymj.18.593.

(51) Giebel, L.; Borsali, R.; Fischer, E. W.; Benmouna, M. Dynamic Light Scattering from Poly(Dimethylsiloxane) (PDMS)/PMMA/Solvent: Effect of Optical Properties. *Macromolecules* **1992**, *25*, 4378–4381. DOI: 10.1021/ma00043a021.

(52) Podzimek, S.; Vlcek, T. Characterization of Branched Polymers by SEC Coupled with a Multiangle Light Scattering Detector. II. Data Processing and Interpretation. *J. Appl. Polym. Sci.* **2001**, *82*, 454–460. DOI: 10.1002/app.1871.

(53) Janardhan, R.; Ramamurthy, K.; Anand, J. S. Solution Properties of Polyurethane. *Polym. Test.* **1994**, *13*, 397–404. DOI: 10.1016/0142-9418(94)90049-3.

(54) Flory, P. J. Molecular Weights and Intrinsic Viscosities of Polyisobutylenes. *J. Am. Chem. Soc.* **1943**, *65*, 372–382. DOI: 10.1021/ja01243a022.

(55) Büyüktanir, E. A.; Küçükyavuz, Z. Solution Properties of Poly(Dimethyl Siloxane). *J. Polym. Sci., Part B: Polym. Phys.* **2000**, *38*, 2678–2686. DOI: 10.1002/1099-0488(20001015)38:20<2678::AID-POLB80>3.0.CO;2-H.

(56) Evans, J. M. Gel Permeation Chromatography: A Guide to Data Interpretation. *Polym. Eng. Sci.* **1973**, *13*, 401–408. DOI: 10.1002/pen.760130602.

(57) Borman, W. F. H. Molecular Weight–Viscosity Relationships for Poly(1,4-butylene Terephthalate). *J. Appl. Polym. Sci.* **1978**, *22*, 2119–2126. DOI: 10.1002/app.1978.070220804.

(58) Silvaspinace, M.; Lucato, M.; Ferrao, M.; Davanzo, C.; Depaoli, M. Determination of Intrinsic Viscosity of Poly(Ethylene Terephthalate) Using Infrared Spectroscopy and Multivariate Calibration Method. *Talanta* **2006**, *69*, 643–649. DOI: 10.1016/j.talanta.2005.10.035.

(59) J. E. Mark, *Polymer Data Handbook*, Oxford University Press, Oxford **2009**.

(60) International, A. ASTM D638-14, Standard Test Method for Tensile Properties of Plastics; ASTM International, **2015**.

(61) Tapia-Picazo, J. C.; Luna-Bárcenas, J. G.; García-Chávez, A.; Gonzalez-Nuñez, R.; Bonilla-Petriciolet, A.; Alvarez-Castillo, A. Polyester Fiber Production Using Virgin and Recycled PET. *Fibers Polym.* **2014**, *15*, 547–552. DOI: 10.1007/s12221-014-0547-7.

(62) Schyns, Z. O. G.; Patel, A. D.; Shaver, M. P. Understanding Poly(Ethylene Terephthalate) Degradation Using Gas-Mediated Simulated Recycling. *Resour. Conserv. Recycl.* **2023**, *198*, 107170. DOI: 10.1016/j.resconrec.2023.107170.

(63) Edwards, J. P.; Wolf, W. J.; Grubbs, R. H. The Synthesis of Cyclic Polymers by Olefin Metathesis: Achievements and Challenges. *J. Polym. Sci., Part A: Polym. Chem.* **2019**, *57*, 228–242. DOI: 10.1002/pola.29253.

(64) Olsén, P.; Odelius, K.; Albertsson, A.-C. Thermodynamic Presynthetic Considerations for Ring-Opening Polymerization. *Biomacromolecules* **2016**, *17*, 699–709. DOI: 10.1021/acs.biomac.5b01698.

(65) Bhat, G.; Kandagor, V. Synthetic Polymer Fibers and Their Processing Requirements. In *Advances in Filament Yarn Spinning of Textiles and Polymers*; Elsevier, **2014**; pp 3–30.

(66) Ibeh, C. C. Thermoplastic Materials: Properties, Manufacturing Methods, and Applications; CRC Press, **2011**.

(67) St. Amant, A. H.; Huang, F.; Lin, J.; Lemen, D.; Chakiath, C.; Mao, S.; Fazenbaker, C.; Zhong, H.; Harper, J.; Xu, W.; Patel, N.; Adams, L.; Vijayakrishnan, B.; Howard, P. W.; Marelli, M.; Wu, H.; Gao, C.; Read De Alaniz, J.; Christie, R. J. A Reactive Antibody Platform for One-Step Production of Antibody–Drug Conjugates through a Diels–Alder Reaction with Maleimide. *Bioconjugate Chem.* **2019**, *30*, 2340–2348. DOI: 10.1021/acs.bioconjchem.9b00436.

(68) Bailey, S. J.; Stricker, F.; Hopkins, E.; Wilson, M. Z.; Read De Alaniz, J. Shining Light on Cyclopentadienone–Norbornadiene Diels–Alder Adducts to Enable Photoinduced Click Chemistry with Cyclopentadiene. *ACS Appl. Mater. Interfaces* **2021**, *13*, 35422–35430. DOI: 10.1021/acsami.1c08670.

(69) Bailey, S. J.; Hopkins, E.; Rael, K. D.; Hashmi, A.; Urueña, J. M.; Wilson, M. Z.; Read De Alaniz, J. Design, Synthesis, and Application of a Water-soluble Photocage for Aqueous Cyclopentadiene-based Diels-Alder Photoclick Chemistry in Hydrogels. *Angew. Chem. Int. Ed.* **2023**, *62*, e202301157. DOI: 10.1002/anie.202301157.

(70) Bailey, S. J.; Hopkins, E.; Baxter, N. J.; Whitehead, I.; De Alaniz, J. R.; Wilson, M. Z. Diels–Alder Photoclick Patterning of Extracellular Matrix for Spatially Controlled Cell Behaviors. *Adv. Mater.* **2023**, *35*, 2303453. DOI: 10.1002/adma.202303453.

(71) Baudry, A.; Dufay, J.; Regnier, N.; Mortaigne, B. Thermal Degradation and Fire Behaviour of Unsaturated Polyester with Chain Ends Modified by Dicyclopentadiene. *Polym. Degrad. Stab.* **1998**, *61*, 441–452. DOI: 10.1016/S0141-3910(97)00230-9.

(72) Karad, S. N.; Chung, W.-K.; Liu, R.-S. Gold-Catalyzed Formal [4π+2π]-Cycloadditions of Tert-Butyl Propiolates with Aldehydes and Ketones to Form 4H-1,3-Dioxine Derivatives. *Chem. Commun.* **2015**, *51*, 13004–13007. DOI: 10.1039/C5CC04538J.

(73) O'Connor, T. J.; Toste, F. D. Gold-Catalyzed Hydrofluorination of Electron-Deficient Alkynes: Stereoselective Synthesis of β-Fluoro Michael Acceptors. *ACS Catal.* **2018**, *8*, 5947–5951. DOI: 10.1021/acscatal.8b01341.

(74) Ismail, Z. M.; Hoffmann, H. M. R. Endo Selectivity of Allenic Esters in Diels-Alder Additions to Cyclopentadiene. The Effect of Added Aluminum Trichloride and an Approach to Dehydrosantalene Analogs. *J. Org. Chem.* **1981**, *46*, 3549–3550. DOI: 10.1021/jo00330a036.

(75) Bohdaneckỳ, M.; Kovář, J. *Viscosity of Polymer Solutions*; Alsevier Scientific Publishing Company, **1982**. Print

(76) Billmeyer, F. W. *Textbook of Polymer Science*; John Wiley & Sons, **1984**.

(77) Chen, X.; Wudl, F.; Mal, A. K.; Shen, H.; Nutt, S. R. New Thermally Remendable Highly Cross-Linked Polymeric Materials. *Macromolecules* **2003**, *36*, 1802–1807. DOI: 10.1021/ma0210675.

(78) Discekici, E. H.; St. Amant, A. H.; Nguyen, S. N.; Lee, I.-H.; Hawker, C. J.; Read De Alaniz, J. *Endo* and *Exo* Diels–Alder Adducts: Temperature-Tunable Building Blocks for Selective Chemical Functionalization. *J. Am. Chem. Soc.* **2018**, *140*, 5009–5013. DOI: 10.1021/jacs.8b01544.

(79) Warrener, R. N.; Butler, D. N.; Margetic, D. Preparation of the First Isobenzofuran Containing Two Ring Nitrogens: A New Diels–Alder Diene for the Synthesis of Molecular Scaffolds Containing One or More End-Fused 3,6-Di(2-Pyridyl)Pyridazine Ligands. *Aust. J. Chem.* **2003**, *56*, 811. DOI: 10.1071/CH03045.

4. Chapter 4: *Controlled Degradation of Spandex Thermoplastic Polyurethanes through the Incorporation of Diels–Alder Cyclopentadiene Dimers*

4.1 Overview

In Chapter 2, the efficiency of thermal recycling of a unique class of Diels–Alder (DA) cyclopentadiene (Cp) based polymers was demonstrated in different types of thermoplastics. In this work, I explored the use of the retro-DA (rDA) reaction of Cp dimer to recycle one of the most challenging materials, thermoplastic polyurethane. Thermoplastic polyurethanes (TPUs) with their strong physical cross-links through hydrogen non-covalent bonding provides the robustness and elasticity in these materials. Spandex, derived from TPU, is the main component in stretchy clothes and has attributed to the adverse environmental impacts of these materials because they are mostly discarded immediately after use. To implement the Diels–Alder chemistry to degrade and recycle these materials, we are interested in incorporating the Cp dimers unit across the polyurethane backbones. Specifically, a Cp dimer with a diol functionality was synthesized that can react with a diisocyanate derivative along with the polytetrahydrofuran (PTHF) to form the desired polyurethane (PU), Spandex. A chain extender, butanediol (BDO) was also added to control the distribution of Cp dimers across the polyurethane backbone. The polyurethane synthesis was performed by our experienced collaborator, Dr. Livius Muff. The location of Cp dimers was shown to interfere with the

hydrogen bonding across the urethane units and possibly compromise the mechanical properties. Therefore, engineering the location of Cp units is crucial to achieve the desired elasticity for Spandex, which was proposed by Dr. Livius Muff. By manipulating the time of adding Cp dimers hydroxylated derivatives to the intermediate mixtures during the polyurethane synthesis, we were able to maintain the elasticity of polyurethane. The materials can also be degraded through the rDA reaction at 150 °C for 30 min.

4.2 Abstract

Spandex, also known as Elastane or Lycra, has been used extensively in the textile industry and contributes to the high elasticity in clothing. Most of these materials, which are derived from thermoplastic polyurethanes (TPUs), are not recycled because their physically stretchy nature is unfit for most industrial mechanical re-processing. Chemical degradation of TPUs using chemical reagents is also challenging due to the lack of intercalation of these reagents into the tight physical cross-links across the polymer chains. Herein, we propose that the strategic incorporation of reversible Diels–Alder cyclopentadiene dimer linkages across the polyurethane backbones will enable the chemical degradation and ideally, recycling of these materials. The degraded fragments can potentially become re-processable and suitable for other applications or can re-polymerized to the virgin-like materials. After synthetic optimization, polyurethane that is integrated with Cp dimers displays comparable mechanical properties to Spandex and can be de-polymerized at 150 °C after 5–30 min in the absence of solvents. Control materials (i.e., polyurethane without Cp units) show no degradation after

being treated under the same conditions. There are also certain aspects that will be addressed in this study to achieve the re-polymerization of the Cp-incorporated polyurethane oligomers and establish the efficient closed-loop recycling. Overall, this work demonstrates the design of degradable polyurethane with thermally reversible linkages. Faster decomposition of these materials under milder conditions was observed, compared to the conventional tough Spandex materials. The platform holds the potential as a new strategy to degrade and recycle tough and elastic step-growth thermoplastics, that are otherwise well-known for being challenging to be deconstructed.

4.3 Introduction

Stretchy clothing has served an indispensable role in our common activities, especially with a surge of interest in healthy pursuits and competitive sports. However, Spandex (also known as Elastane or Lycra), the main component that provides the elasticity to our clothes, is not recycled.[1–3] Therefore, even though only ~5% of these materials is embedded in the textile fibers, they pose a serious environmental threat because they are discarded into a landfill or incineration (i.e., energy recovery) even after their first use.[1–3] This factor, coupled with the fast-growing rate of the textile industry, is worsening the adverse environmental impact of these materials. The long-standing recycling challenge of these materials derives from the structure of Spandex that comprises of polyurethane thermoplastic backbones.[4]

Thermoplastic polyurethanes (TPUs) represent a family of versatile synthetic materials that are created by a polycondensation reaction between the diisocyanate derivatives (–NCOs

functionality) and the diols/polyols (–OH groups). These substances possess valuable mechanical performance (e.g., toughness, elasticity) due to their strong physical cross-links that are created by the hydrogen non-covalent bonding between the urethane (–HN–COO–) and urea (–HN–CO–NH–) units across the linear polymer chains (**Figure 4.1**).[4,5] In general, the materials is arranged of soft segments and hard segments. Soft segments are normally consisted of the long-chain polyols (e.g., polytetrahydrofuran or PTHF). Hard blocks are formed between the diisocyanates and the chain extender (e.g., 1,4-butanediol or BDO). The hard segments typically contribute to the efficiency of the hydrogen bonding that determines the physical connections along the polymer backbones. Depending on the selected diisocyanates, the resulting polymer chains can be tightly or loosely connected and be melt-processed under proper temperatures (e.g., 150–200 °C). Aliphatic groups are generally less rigid compared to aromatic diisocyanates and tend to form polyurethanes with lower processing temperatures.[5] With the diverse structural modification, TPUs can be designed to target a wide range of applications, mainly used as the additives to enhance the structure of industrial materials such as textiles (e.g., Spandex) or liquid coatings, adhesives, medical devices, and automotive parts.[5] However, the closely packed polymer chains, tight physical cross-links, and diverse functionality that provide TPUs with favorable properties also lead to a huge challenge in recycling these materials.[6]

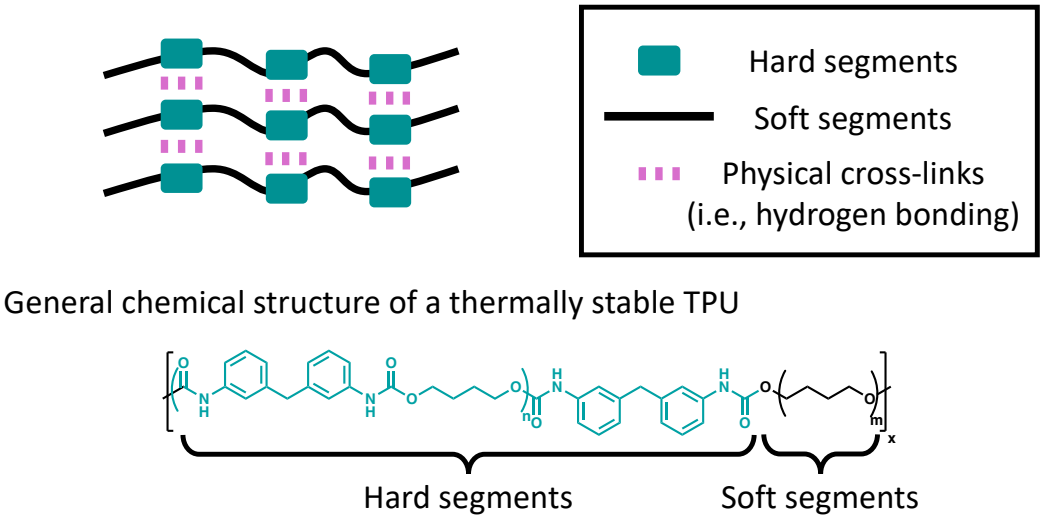


Figure 4.1. Spandex is derived from thermoset polyurethane (TPUs), which composes of hard segments and soft segments. The strong physical cross-links are created by the hydrogen non-covalent bonding between the urethane (–HN–COO–) and urea (–HN–CO–NH–) units across the linear polymer chains.

In industry, the straightforward pathways to recycle these materials include high shearing, hot compression, extrusion, and re-molding.[4] However, the elasticity and varied processing temperatures make these materials unfit for many types of industrial mechanical processes. Other recycling strategies should be considered. One of the most promising methods is the chemical degradation because it offers the recovery of feedstock starting materials by deconstructing the long-chain polymer into the low-molecular-weight (low-MW) oligomers.[6,7] Furthermore, the monomer resources can be maximized through the closed-loop recycling if these smaller fragments can re-polymerize into the virgin-like compounds.[7,8] This strategy has become popular to recycle some common thermoplastics. One of the classic examples is polyethylene terephthalate (PET), which can be depolymerized into the

monomers or similar derivatives under hydrolysis, glycolysis, or methanolysis. For example, in hydrolysis, the chemical reagents are added to water (e.g., strong bases, acids, or sometimes with catalysts) and the mixture is used to deconstruct the labile ester linkages in PETs.[9] In comparison, polyurethane also possesses labile bonds (e.g., urethane and urea) and hypothetically should be chemically degraded under similar conditions. However, the physical cross-links in TPUs are much stronger compared to PET. The chemical reagents and catalysts are not easily intercalated into the tight packing of the polymer chains to assist in the decomposition (**Figure 4.2**).[6] Therefore, utilizing chemical reagents to degrade certain types of TPUs is much more difficult, time- and cost-consuming. Nonetheless, current strategies are still limited to this strategy of chemical degradation (i.e., glycolysis or transesterification).[6,10,11] Fabrication of biodegradable materials has also been proposed as one of deconstruction pathway.[11] Though potential, biodegradable TPUs are generally less tough and elastic, compared to the materials that are used for a more durable setting, such as Spandex in the textile industry. Furthermore, longer time (i.e., more than 100–300 days) is generally observed for these materials to decompose.

We propose that heat can be a simple and wide-spread stimulus to deconstruct these robust structures without the issues associated with using chemical reagents. We hypothesize that the degradation properties of these tough TPU materials can be improved by incorporating a small quantity of reversible linkages during the polymer fabrication. These reversible bonds should be dissociated under mild heating (i.e., 150–180 °C) across the polyurethane backbone

(**Figure 4.2**) to facilitate and accelerate the chemical degradation of TPUs. Of note, a radical inhibitor, butylated hydroxytoluene (BHT), was used for the de-polymerization as it assists in preventing the uncontrolled side reactions at the investigated temperature for both Cp and polyurethane moieties.[12] Furthermore, it is important to realize a suitable component and synthetic methodology that does not compromise the elasticity of these materials (i.e., useful as Spandex).

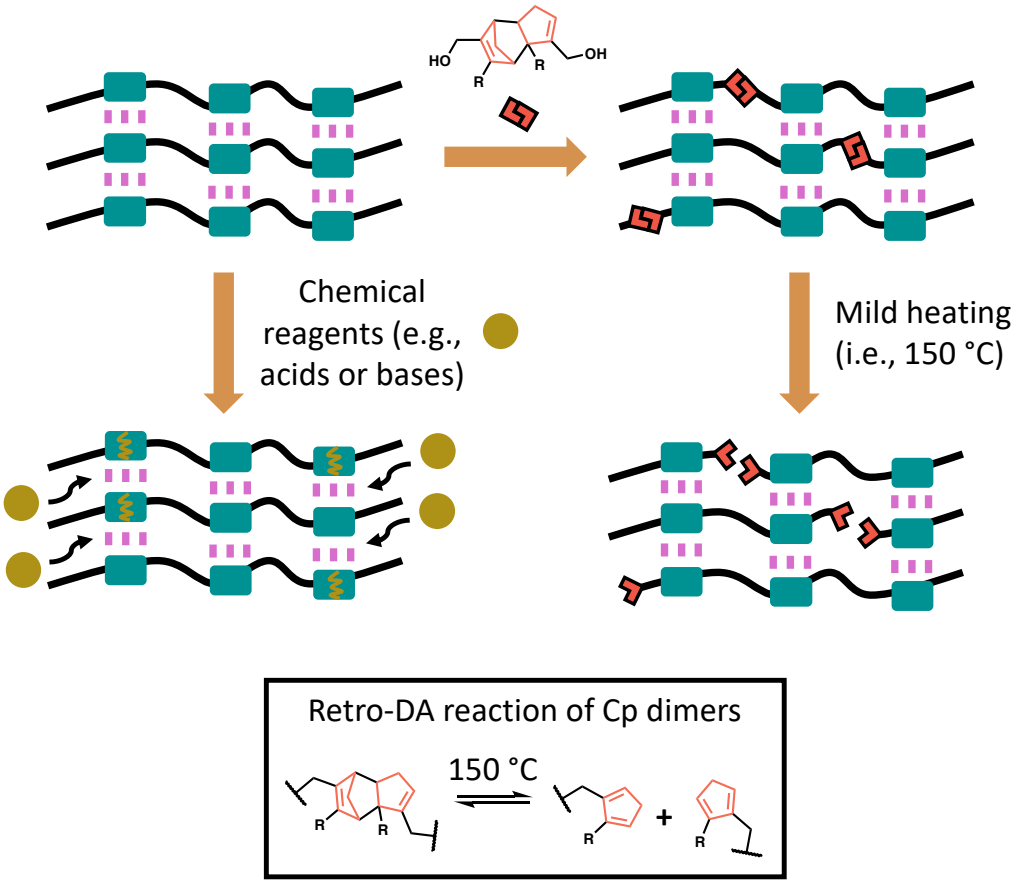


Figure 4.2. Chemical degradation using chemical reagents are challenging due to the strong physical cross-links across the polyurethane backbones. Incorporation of Cp dimers that can undergo rDA reaction at 150 °C can increase the efficiency of degradation.

In our previous work, we investigated a unique class of thermally reversible Diels–Alder cyclopentadiene (Cp) dimers in a variety of thermoplastics that display efficient closed-loop recycling. Cp can dimerize to form Cp dimers, which can undergo a retro-DA (rDA) reaction at 150–180 °C to recover the Cp monomeric unit. Exploiting Cp dimers as the reversible linkages can lead to a promising platform to recycle tough plastics. In this study, we strategically incorporate Cp dimers into different polyurethane backbones (**Figure 4.2**). To

ensure that Cp dimers do not compromise the physical cross-links and mechanical performance in TPUs, an optimal synthetic design is devised to obtain the desired elasticity for Spandex. After obtaining the target polyurethane analogs, we exploit the rDA reaction of Cp dimers. The units can be reverted to the monomeric moieties or Cp-chain-end oligomers at 150 °C for 5–30 min in the absence of solvents, leading the collapse of the polymer backbone into smaller fragments. Hypothetically, the Cp chain-ends of these oligomers should remain active and provide a promising handle for re-polymerization, potentially leading to the closed-loop recycling. However, considering the possible degradation of Cp or the tight physical cross-links, it can become particularly complicated for the oligomeric mixtures to re-polymerize. We will also discuss these aspects in our study and propose solutions to assist in resolving this complication. In this work, we focus on the tough materials that are not re-processable or degraded unless being treated with extremely high temperatures (i.e., ≥ 220 °C). To further generalize our approach, we also synthesize and compare the degradation and mechanical properties of the polyurethane backbone with a lower processing temperature.

Overall, this approach provides a straightforward and unique platform to degrade the otherwise challenging-to-deconstruct TPUs via a mild and short heating process. This gentle chemical degradation can become a promising strategy to selectively degrade and isolate Spandex from other recyclable polymers in the mixed fibers for potentially up-recycling of polyurethane to maximize the resources.[13] Furthermore, our work proposes a general

methodology that can be applicable for other tough thermoplastics to increase the recycling efficiency of these materials.

4.4 Results and Discussion

As noted, the properties of TPUs are highly dependent on the structures of the hard segments and the soft segments. We aim for the polymers with the high melt-processing temperatures due to the long-standing challenge in recycling these materials. Hypothetically, as we incorporated Cp-dimer units along the polymer backbones, the materials can become re-processable or degradable at a lower temperature range. Re-polymerization of these degraded fragments with the active Cp chain-ends, assuming no side reactions, should enable closed-loop recycling. The synthetic plans include the functionalization of Cp-dimer with two alcohol groups (**1**). Compound **1** will then react with the diisocyanate derivatives, along with the chain extender, 1,4-butanediol (BDO), and the soft building blocks, polytetrahydrofuran (PTHF) (**Figure 4.2a**). By tuning the amount of the starting materials (i.e., Cp-dimer diol derivatives, BDO, PTHF, diisocyantes) and controlling the time to add Cp-dimer diol, the formed polyurethanes can be synthesized in one pot that possess the target chain-length of the soft and the hard segments as well as the positions of the Cp-dimers along the backbone (**Figure 4.2a**).

Three important tasks need to be achieved to obtain the desired materials (**Figure 4.3**). First, the proper diisocynate analog is carefully selected to form the hard segments that will create the strong hydrogen bonding among the polyurethane backbones, aiming for the high

melt-processing temperatures. As shown in **Figure 4.3a**, within the scope of the investigation in this project, the R group in the diisocyanate starting materials is composed of either the cyclic aliphatic moiety (i.e., hydrogenated methylene diphenyl diisocyanate or HMDI) or the aromatic ring (i.e., methylene diphenyl diisocyanate or MDI). Second, the locations of the Cp-dimer units along the polymer backbone are crucial to achieve the desired mechanical performance (**Figure 4.3c**). Cp-dimer can be majorly incorporated into either the soft or hard segments depending on the time of adding the Cp-dimer diol derivative to the reaction mixture and/or if the chain extender BDO is used during the polymer fabrication. The bulky Cp-dimer potentially interferes with the chain packing of the polyurethane and thus, the material properties hypothetically will be less affected by the soft-segment incorporation. Lastly, different Cp-dimer diol derivatives should be investigated to probe the influence of the Cp-dimer structures on the mechanical performance of the modified polyurethanes. Two analogs are to be explored, **1** and **2**, each with a different alkyl chain length and functional group proximal to the Cp-dimer unit (i.e., alcohol versus ester) (**Figure 4.3b**). As learned from the previous chapters, Cp derivatives can undergo uncontrolled cross-linking or side reactions (e.g., Alder-ene rearrangement), which will also be considered while constructing polyurethanes with compounds **1** and **2**. Tuning the synthetic conditions and selecting the proper starting materials to achieve all the above criteria potentially enables access to the high-performance polyurethane materials with the promising thermo-selective degradation ability.

Our goal is to obtain materials with similar properties as elastane or Spandex and thus, it is important to quickly screen the elasticity of the synthesized materials to identify the optimal synthetic routes. The mechanical performance of Cp-incorporated materials was qualitatively checked by stretching them using a pair of tweezers and compared with the control that is without any Cp-modified backbones. The degradation tests were performed for all the materials at 150 °C (i.e., rDA temperature), including the Cp-integrated and the control polyurethanes to showcase the selective degradation with heat. Re-polymerization of the degraded fragments through Cp dimerization was also investigated to establish the closed-loop recycling of these materials, which remains challenging but within the scope of our interest. After qualitatively screening the elasticity and testing the degradation/recycling capability, optimal-performance materials will be fully characterized with differential scanning calorimetry (DSC), dynamical mechanical analysis (DMA), thermogravimetric analysis (TGA), and tensile testing.

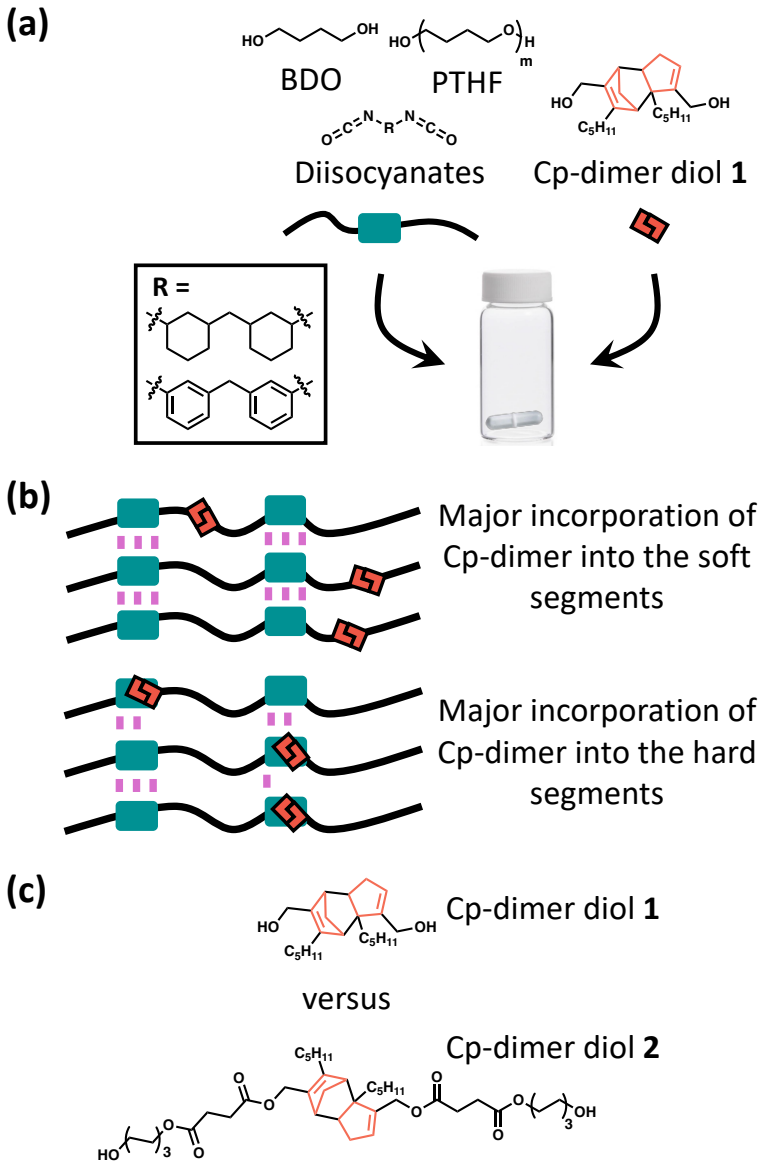
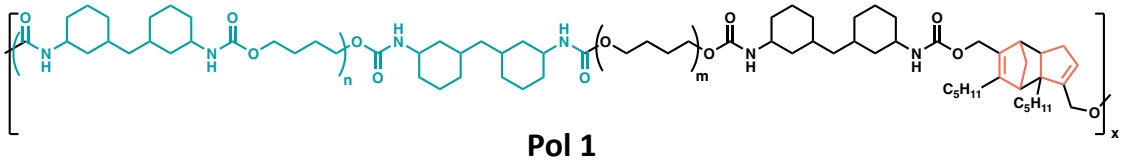


Figure 4.3. (a) One pot synthesis of the target Cp-integrated polyurethanes by tuning the amount of the starting materials and controlling the time to add them. The starting materials include the diisocyanate (i.e., HMDI or MDI), DBO, PTHF, and Cp-dimer diol derivative. The reaction is initiated by dibutyltin dilaurate (DBTDL) catalyst. The reaction is performed at 50 °C in tetrahydrofuran (THF). (b) The major incorporation of Cp-dimer into the soft segments (top drawing) is performed by adding the Cp-dimer diol derivative as the last reactant to the polyurethane reaction mixture. Lack of the chain extender BDO will potentially

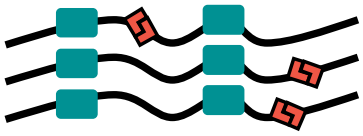
lead to the major incorporation of the Cp-dimer diol units into the hard segments (bottom drawing). (c) The structures of the two Cp-dimer diol derivatives **1** and **2**. The alcohol groups are proximal to the Cp-dimer unit in compound **1**, compared the ester groups in compound **2**. The alkyl chain in compound **2** is longer than that in compound **1**.

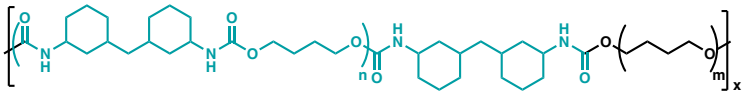
Initial Degradation Screening of Cp-Integrated Hydrogenated Methylene Diphenyl Polyurethanes. Cp-dimer diol **1** was incorporated into the hydrogenated methylene diphenyl polyurethane backbones (~50% of the Cp-dimer) to form **Pol 1** (**Scheme 4.1**) with a number-average molecular weight (M_n) value of 28 kDa. A control polymer was also synthesized, or **Pol 1C** (M_n = 31 kDa). Of note, the MW range of these materials are comparable, which is promising that Cp incorporation does not interfere much with the hydrogen bonding of polyurethane backbones. Both materials were subjected to the degradation and re-polymerization tests with the addition of 5 mol% BHT in the absence of solvents. **Pol 1** shows gradual degradation at 150 °C after 5–120 min with a 5-min interval (**Figure 4.4**). Based on the optimal polymerization condition from our previous studies in Chapter 3, re-polymerization of these smaller fragments (i.e., 30-,60-, and 90-min samples) was performed at 90 °C. However, there was no increase in the MW. We noticed that the control polymer **Pol 1C** also undergoes degradation at 150 °C overtime (Supporting Figure S4.6). This phenomenon could complicate our studies regarding both degradation and re-polymerization of the Cp-modified materials. As aforementioned, polyurethanes that are re-processable at low temperature (i.e., 150 °C) are not within the scope of our investigation and thus, IPDI is not an applicable component for our polymer synthesis platform.

Scheme 4.1. Polymer structures of hydrogenated methylene diphenyl polyurethane that is integrated with Cp-dimer (**Pol 1**) and the control analog without Cp-dimer-modified backbone (**Pol 1C**).

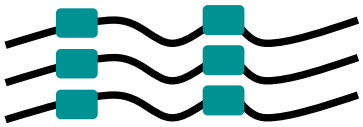


Pol 1





Pol 1C



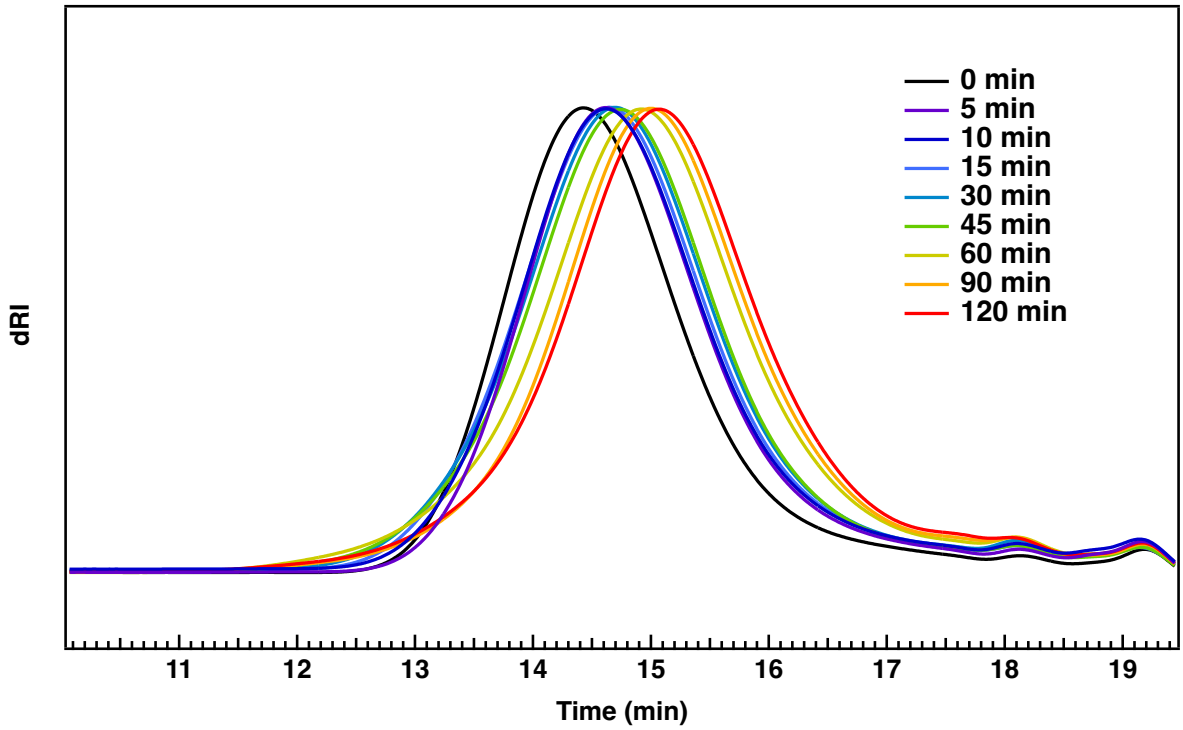
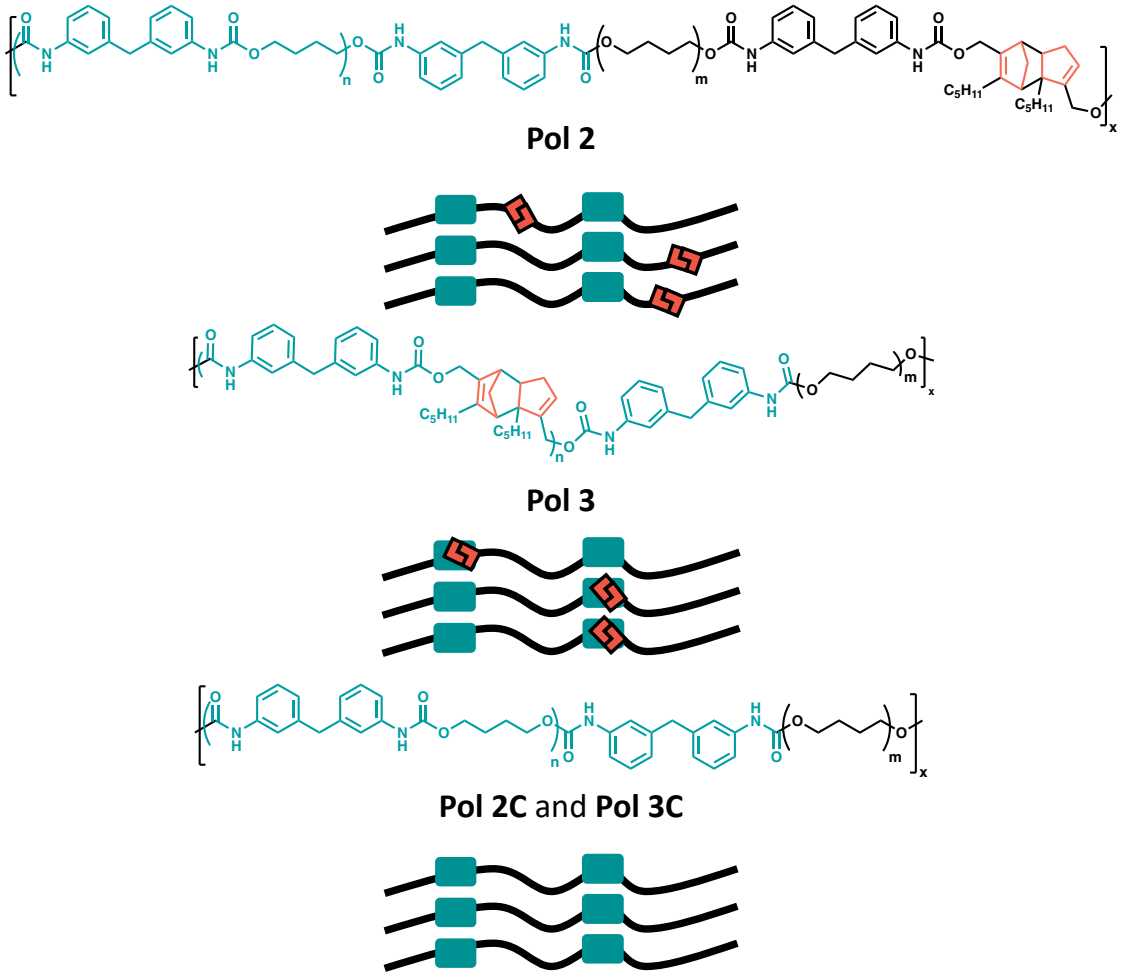


Figure 4.4. Thermal degradation of Cp-integrated hydrogenated methylene diphenyl polyurethanes at 150 °C for 5–120 min with a 5-min interval. M_n = 25 kDa (0 min), 21 kDa (30 min), 17 kDa (60 min), and 14 kDa (120 min).

Synthesis and Thermo-Selective Degradation of the Cp-Incorporated Methylene Diphenyl Polyurethanes. We target high-performance polyurethanes that are not re-processable at low temperature range. The MDI was used instead of IPDI as the diisocyanate for the polymer synthesis because methylene diphenyl urethane bonds are known to deliver stronger hydrogen bonding across the polyurethane backbones. **Pol 2** (M_n = 23 kDa) was synthesized along with the control polymer **Pol 2C** (M_n = 13 kDa) (**Scheme 4.2**). We are also intrigued by the effects of incorporating Cp-dimer into the soft segments (**Pol 2**) versus into the hard segments. We replaced BDO with Cp-dimer diol derivative **1** as the chain extender

for our polymer synthesis (**Pol 3**, M_n = 12 kDa, and the control analog **Pol 3C**, M_n = 14 kDa), as shown in **Scheme 4.2**. As aforementioned, it is crucial to minimize the bulky effect of the Cp-dimer to optimize the mechanical performance of the modified polyurethanes. Supposedly, the bulky effect from Cp-dimer is aggravated by the incorporation of the Cp-dimer into the hard segments, where most of the strong hydrogen bonding occur. The incorporation of Cp-dimer into the soft segments, in contrast, potentially minimizes the disruptive effect of the large Cp-dimer. **Figure 4.5** illustrates that the material is largely softened with the incorporation of Cp-dimer into the hard segments (**Pol 3**), while **Pol 2** maintains the mechanical integrity that is more similar to the control polymer (**Pol 3C**). Hence, **Pol 2** with the desired mechanical property is further explored for the degradation experiment.

Scheme 4.2. Polymer structures of methylene diphenyl polyurethane that is integrated with Cp-dimer, mostly into the soft segments (**Pol 2**) versus the hard segments (**Pol 3**). The control analog is without Cp-dimer-modified backbone (**Pol 2C**).



Heating **Pol 2** at 150 °C for 30 min in the presence of BHT inhibitor (2 wt%) shows de-polymerization of **Pol 2** (M_n = 23 to 8 kDa) (**Figure 4.6**). In contrast, the control polymer **Pol 2C** did not degrade (M_n stays at 13 kDa) under the same heating condition (i.e., 150 °C for 30 min) (**Figure 4.5**). As demonstrated, methylene diphenyl polyurethanes possess high-

temperature re-processing and degradation, which correlates with literature.[5,14] Through the incorporation of reversible Cp-dimer, we can de-polymerize/re-process the material at a lower temperature range, proposing a promising platform to control the degradation of high-performance polyurethane under milder conditions (i.e., 150 °C for 30 min). Re-polymerization of the degraded fragments was also investigated, though not successful, presuming due to the possible decomposition of the Cp chain-ends. Tight physical cross-links across the polyurethane backbones can also potentially prevent Cp chain-ends to react with each other. All these factors will be further discussed and investigated in the following sections.

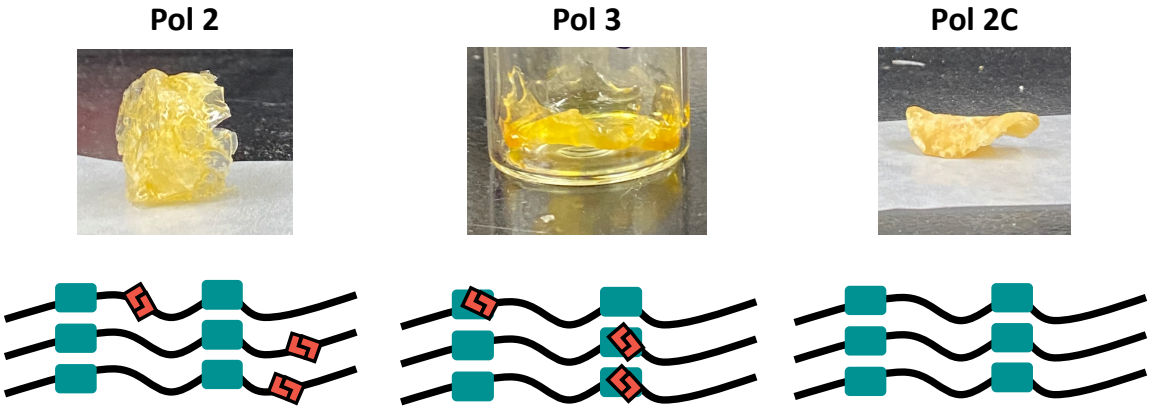


Figure 4.5. Visual illustration of the mechanical integrity of **Pol 2**, **Pol 3** and **Pol 2C**. **Pol 2** maintains the mechanical property more similar to the control polymer (**Pol 2C**), compared to **Pol 3**, which is elastic, sticky and softened.

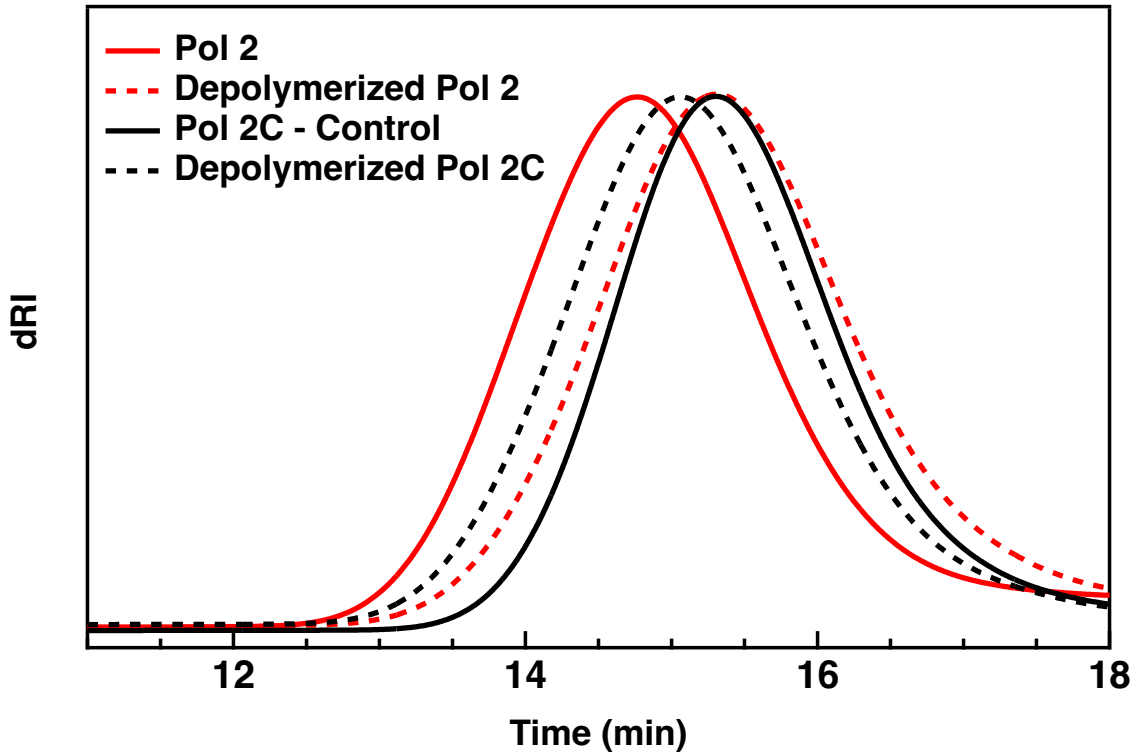


Figure 4.6. Depolymerization of **Pol 2** and the control **Pol 2C** shows the lower de-polymerization temperature of Cp-dimer-modified polyurethanes (i.e., 150 °C). After 30 min at 150 °C, **Pol 2** (M_n = 23) is de-polymerized to an M_n of 8 kDa. **Pol 2C** is robust and the MW did not change much under the same heating condition. The de-polymerization included 2 wt% BHT and no solvents were utilized.

Investigation of the Effects of Different Cp-Dimer Diol Derivatives to the Polyurethane Synthesis. As learned from the previous chapters, Cp-dimer diol derivative can undergo uncontrolled cross-linking or side reactions (e.g., Alder-ene rearrangement) during the polymer synthesis. Two different derivatives **1** and **2** with the structures are shown in **Figure 4.3b** were used for the polymer synthesis. Compound **2** is hypothetically more stable than **1**. The ester groups that are proximal to the Cp-dimer unit in compound **2** would possibly

block any uncontrolled side reactions (e.g., Alder-ene rearrangement). The long distance of the Cp-dimer from the alcohol groups in **2** also potentially contribute to the side-reaction elimination upon de-polymerization and re-polymerization. Of note, compound **2** with the longer alkyl chain might also affect the mechanical property of the formed polyurethane. These factors will be all considered when comparing the properties of the polyurethanes with their hard segments integrated with compounds **1** and **2** (**Pol 3** and **Pol 4**, respectively, as shown in **Scheme 4.3**). Of note, hard segments of **Pol 3** and **Pol 4** are modified with Cp-dimer to augment the disruptive effects of investigated Cp-dimer units and assist in the comparison. Through the stretching test, no apparent difference in properties of these materials was observed (Supporting Figure S4.8). The degradation of **Pol 4** shows a wider range of MW decrease, presumably because the longer alkyl chain of compound **2** leads to a higher MW of the formed polyurethane. However, no re-polymerization was observed for both **Pol 3** and **Pol 4** (Supporting Figure S4.7). Through the experiment, no clear evidence of the uncontrolled reactions of Cp derivatives was observed that would interfere with the polymer synthesis and degradation. Since compound **1** is more synthetically accessible, we settle with this derivative for further optimization of the polymerization.

Ongoing Optimization of the Degradation and Closed-loop Recycling of High-Performance Thermoplastic Polyurethanes. In Chapter 3, I have demonstrated that the increased concentration of Cp-dimer incorporation across the polymer backbone displays decreased recycling efficiency, presumably due to the higher chance of Cp decomposition.

Therefore, in this project, we re-designed our synthetic plans to target a lower quantity of Cp-dimer units along the polyurethane backbone. Combined with the above investigation, we use Cp-dimer diol derivative **1** and MDI as the starting materials. Incorporation of the Cp-dimer into the soft segments was also achieved by delaying the addition of **1** as the last component to the reaction mixture. New materials were synthesized along with the control polymers (**Pol 5** and **Pol 5C**, respectively). **Figure 4.7** indicates no apparent difference in the polymer properties. The degradation and re-polymerization are ongoing. Quantitative tests (e.g., TGA, DSC, DMA, tensile testing) will be demonstrated after we establish the efficient thermo-selective degradation and ideally, closed-loop recycling of the polyurethanes.

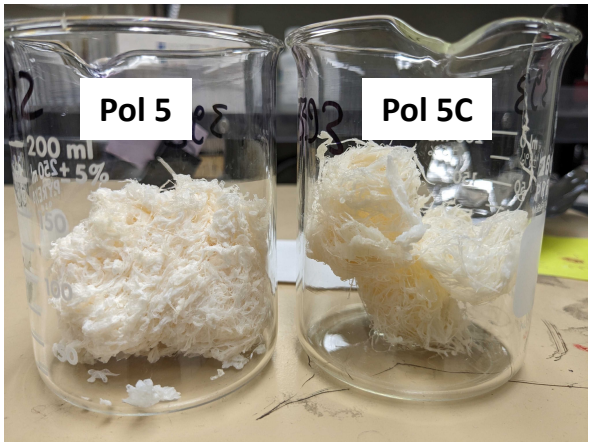


Figure 4.7. The methylene diphenyl polyurethane that is integrated with Cp-dimer diol derivative **1** (**Pol 5** in the left beaker) and the control polymer that is without Cp-dimer (**Pol 5C** in the right beaker) after the polymer synthesis.

4.5 Conclusion

A novel synthetic platform to synthesize high-performance polyurethanes that is integrated with Cp-dimer is explored. The materials show controlled degradation at 150 °C

(rDA temperature) for 30 min in the presence of BHT inhibitor without the use of solvents. A proposed optimization of the polymer synthesis is demonstrated to achieve tough materials with efficient thermo-selective degradation and closed-loop recycling. Further investigation is ongoing to investigate the recycling capability of **Pol 5**. When the degradation and re-polymerization of **Pol 5** are established, characterization of the material will be performed to showcase the promising thermal and mechanical properties that are comparable to Elastane or Spandex.

4.6 Acknowledgements

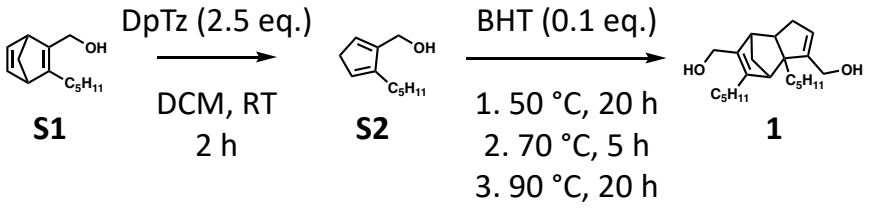
I would like to thank the organizers and speakers from the Tosoh conference 2022. The wide scientific communication and the informed recycling challenge of Spandex have inspired and initiated the original goals of this project. I am thankful for a collaboration with Dr. Livius Muff, an expert in the synthesis of polyurethane. I would like to also acknowledge my undergraduate research and mentee, Ashley Nowzari, who actively prepared the Cp-dimer diol derivative that is the critical part for the synthesis of polyurethane. I am also thankful to Komal who will push the project forward. The NMR instruments were supported by the National Science Foundation under award No. MRI-1920299. We used the MRL Shared Experimental Facilities that are supported by the MRSEC Program of the NSF under Award No. DMR 1720256; a member of the NSF-funded Materials Research Facilities Network. The research was funded by the National Science Foundation (CHE-2204077).

4.7 Supporting Information

Material Synthesis and ^{1}H NMR Spectra:

Cp-dimer diol monomer synthesis. Unless stated otherwise all reactions were carried out under ambient atmosphere with oven dried (100 °C) glassware and magnetic stir bars. Compounds **S1** and **S3** were prepared as reported in literature.[15,16] All commercially obtained reagents were bought from Sigma Aldrich, Fisher Scientific, Ambeed, VWR International and were used as received unless otherwise noted. Thin-layer chromatography (TLC) was conducted with E. Merck silica gel 60 F254 pre-coated plates (0.25 mm) and visualized by exposure to UV light (254 nm) or stained with p-anisaldehyde. Flash column chromatography was performed using normal phase silica gel (60 Å, 0.040 – 0.063 mm, Geduran).

Scheme S4.1. Synthetic scheme to access the Cp-dimer diol derivative **1**.



Synthesis of compound **S2**:

A solution of compound **S1** (1.0 g, 5.2 mmol, 1.0 eq.) and dipyridyl tetrazine (DpTz) (3.1 g, 13 mmol, 2.5 eq.) in 130 mL DCM was stirred at room temperature for 2 h. The crude solution was passed through a plug of silica with DCM as the eluent. After the silica plug, concentration of the filtrate afforded the pure product **S2** as transparent oil (700 mg, 81%

yield). ^{1}H NMR (500 MHz, $CDCl_3$) δ 6.33 – 6.28 (m, 1H), 6.07 (p, *J* = 1.8 Hz, 1H), 4.45 (dq, *J* = 5.8, 1.6 Hz, 2H), 2.90 (m, 2H), 2.37 – 2.29 (m, 2H), 1.61 – 1.55 (m, 2H), 1.40 – 1.30 (m, 5H), 0.94 – 0.84 (m, 3H).

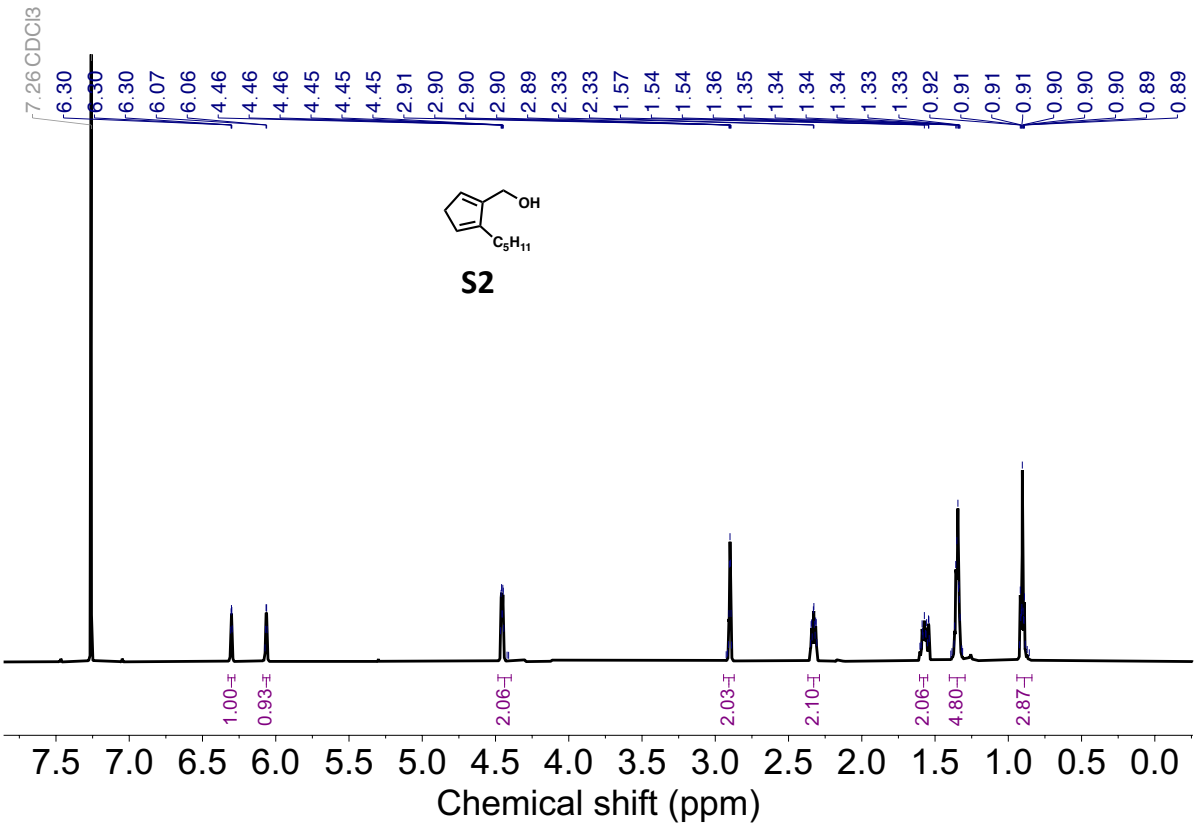


Figure S4.1. ^{1}H NMR spectrum of the hydroxylated Cp monomer in $CDCl_3$.

Synthesis of compound **1**:

To a 20-mL vial was added compound **S2** (480 mg, 3.0 mmol, 1.0 eq.) followed by 64 mg of BHT (0.30 mmol, 0.1 eq.). No other reagents or solvents were added for the dimerization. The vial with the mixture was heated at 50 °C for 20 h, followed by 70 °C for 5 h, and then

90 °C for 18 h. The mixture was then cooled to RT and dissolved in DCM. The solution was passed through a silica plug with the DCM as the eluent. Roughly 80 mL of DCM was used to remove the BHT from the silica plug. Then the plug was run through with 30% ethyl acetate (EtOAc)/DCM to collect the crude Cp-dimer diol product **1** as transparent oil (~400 mg). Of note, the material is stored in the freezer (i.e., -20 °C) if not used immediately for the next step.

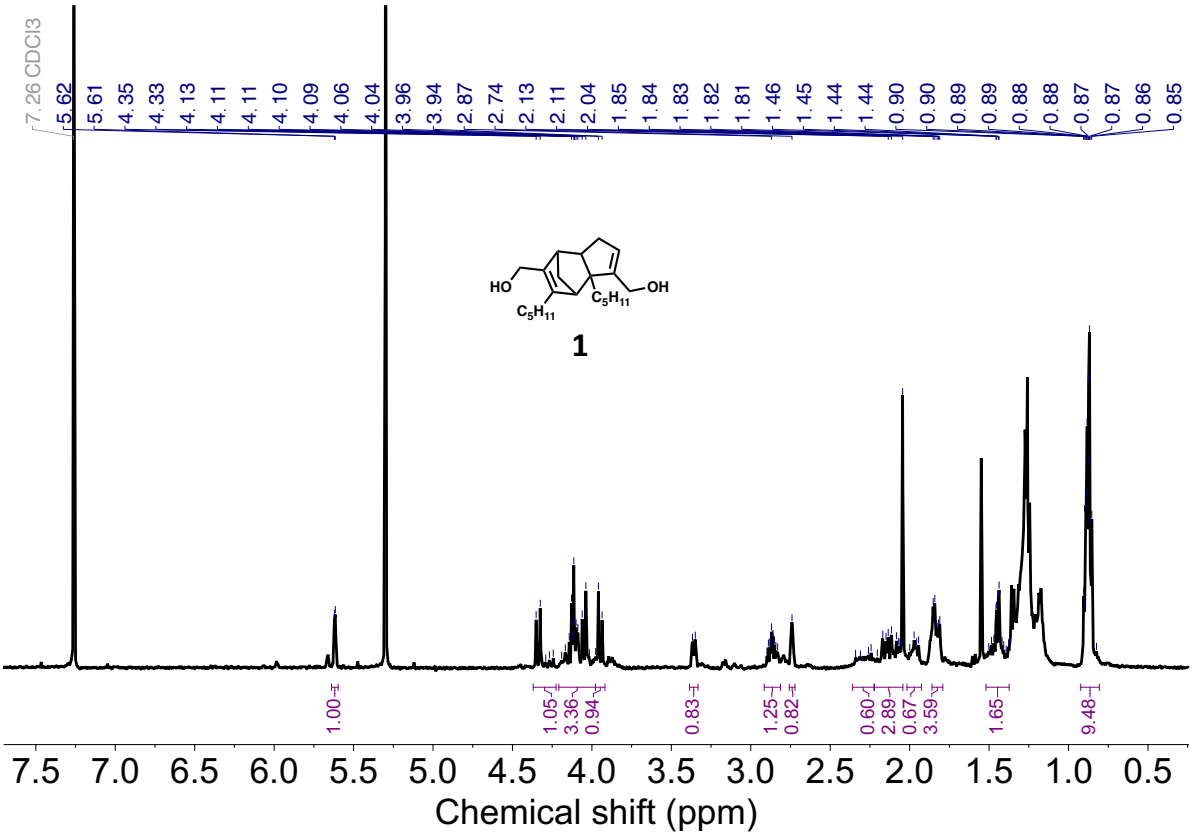
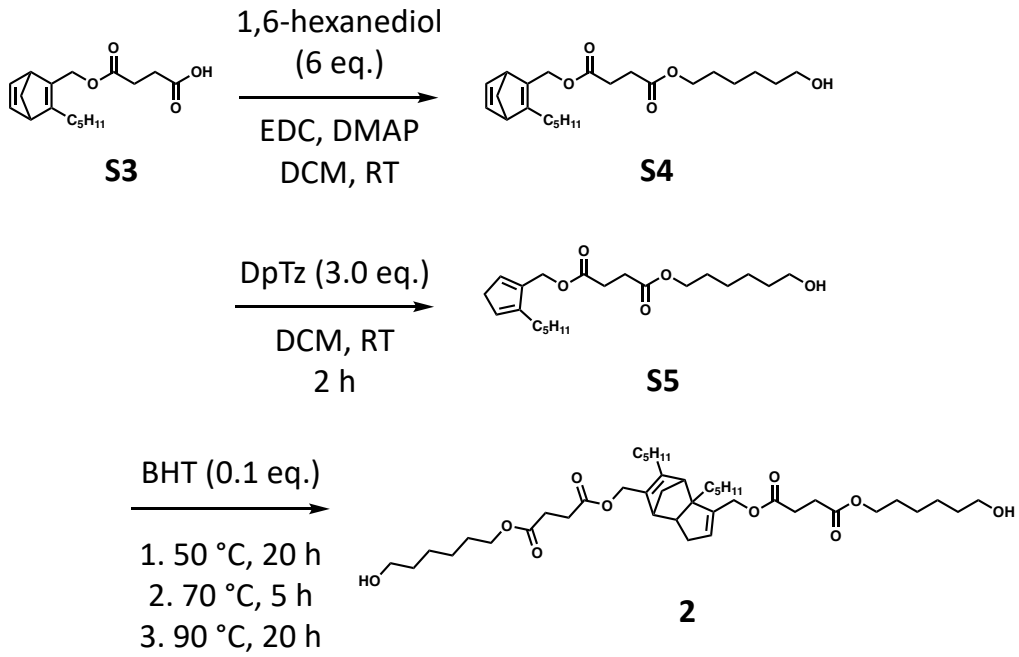


Figure S4.2. ^{1}H NMR spectrum of the Cp-dimer diol **1** in $CDCl_3$.

Scheme S4.2. Synthetic scheme to access the Cp-dimer diol derivative **2**.



Synthesis of compound **S4**:

To a dried 250 mL round-bottom flask were added compound **S3** (1.71 g, 6.0 mmol, 1.0 eq.), 1,6-hexanediol (4.2 g, 35 mmol, 6.0 eq.) and 150 mL DCM. To this solution were added EDC (2.8 g, 15 mmol, 2.5 eq.) and DMAP (140 mg, 0.1 mmol, 0.2 eq.). Once added, the solution was allowed to stir at room temperature for 24 h. The crude solution was concentrated and subjected to a silica plug using DCM as the eluent. The plug was run through with DCM and then 10% EtOAc/DCM to afford the pure product **S4** as a colorless oil (1.96 g, 85% yield). R_f of the product = 0.55 in 50% EtOAc/hexanes. ^{1}H NMR (500 MHz, $CDCl_3$) δ 6.76 (dd, J = 5.2, 3.0 Hz, 1H), 6.70 (dd, J = 5.2, 3.0 Hz, 1H), 4.74 (d, J = 12.3 Hz, 1H), 4.58 (d, J = 12.2

Hz, 1H), 4.15 – 4.05 (m, 2H), 3.65 (td, *J* = 6.5, 5.2 Hz, 2H), 3.44 (t, *J* = 2.3 Hz, 1H), 3.37 (q, *J* = 2.2 Hz, 1H), 2.62 (d, *J* = 2.0 Hz, 4H), 2.22 (ddd, *J* = 14.3, 8.4, 6.4 Hz, 1H), 2.13 (ddd, *J* = 14.0, 8.3, 6.6 Hz, 1H), 1.94 (dt, *J* = 6.0, 1.7 Hz, 1H), 1.89 (dt, *J* = 6.0, 1.7 Hz, 1H), 1.73 – 1.60 (m, 2H), 1.61 – 1.55 (m, 2H), 1.39 (m, 5H), 1.29 (m, 4H), 1.23 – 1.13 (m, 2H), 0.87 (t, *J* = 7.3 Hz, 3H).

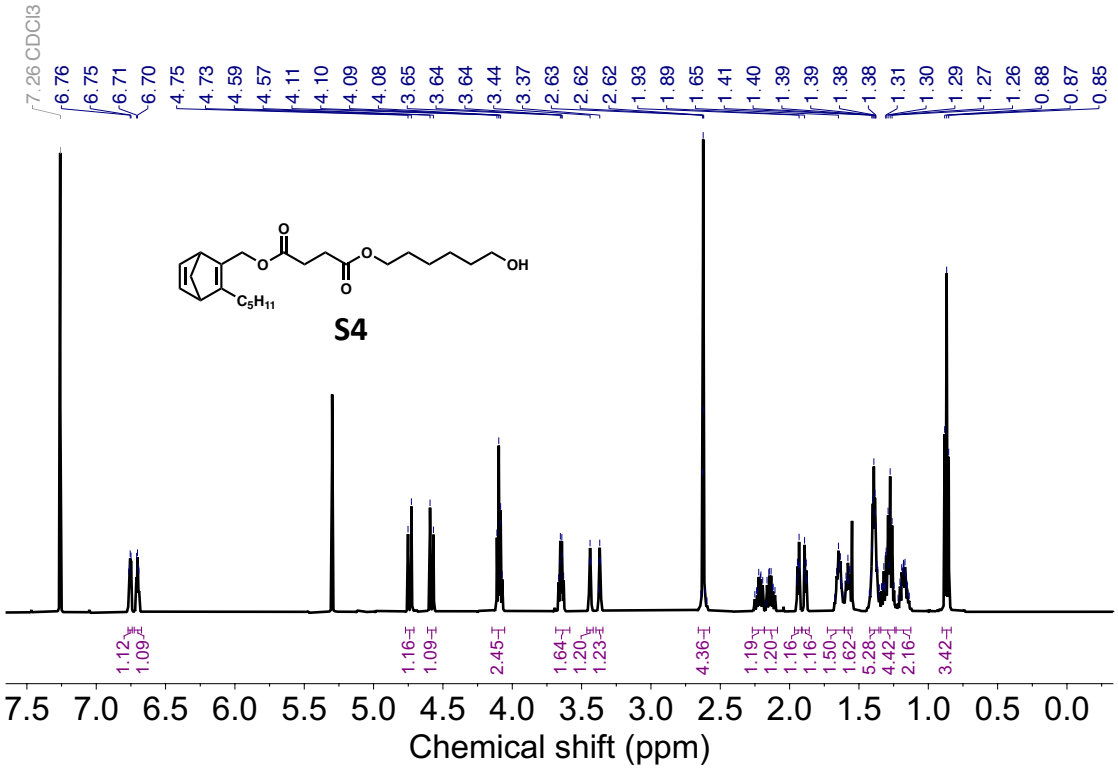


Figure S4.3. ^{1}H NMR spectrum of compound **S4** in $CDCl_3$.

Synthesis of compound **S5**:

S5 was prepared in a procedure similar to the one used to produce compound **S2**. A solution of compound **S4** (1.0 g, 2.6 mmol, 1.0 eq.) and DpTz (1.8 g, 7.6 mmol, 3.0 eq.) in 64

mL DCM was stirred at room temperature for 2 h. The crude solution was passed through a plug of silica with DCM as the eluent. After the silica plug, concentration of the filtrate afforded the pure product **S5** as transparent oil (590 mg, 62% yield). ^{1}H NMR (500 MHz, $CDCl_3$) δ 6.37 (dt, *J* = 2.6, 1.4 Hz, 1H), 6.06 (m, 1H), 4.89 (q, *J* = 1.4 Hz, 2H), 4.10 (m, 2H), 3.65 (td, *J* = 6.5, 5.4 Hz, 2H), 2.91 (p, *J* = 1.7 Hz, 2H), 2.71 – 2.59 (m, 4H), 2.32 – 2.24 (m, 2H), 1.67 – 1.60 (m, 2H), 1.60 – 1.55 (m, 4H), 1.42 – 1.29 (m, 7H), 1.29 – 1.23 (m, 1H), 0.93 – 0.85 (m, 3H).

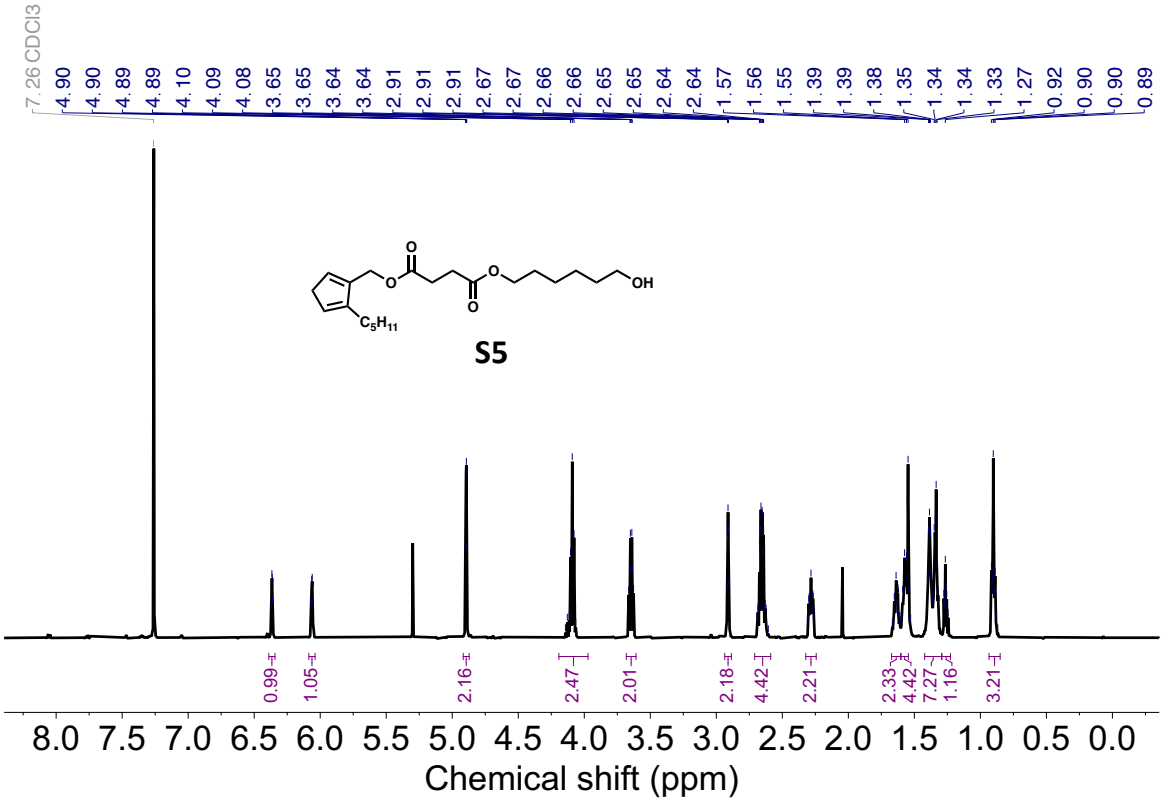


Figure S4.4. ^{1}H NMR spectrum of compound **S5** in $CDCl_3$.

Synthesis of compound **2**:

2 was prepared in a procedure similar to the one used to produce compound **2** using 590 mg of **S5** and 35 mg of BHT. ~450 mg of the Cp-dimer diol **2** was obtained.

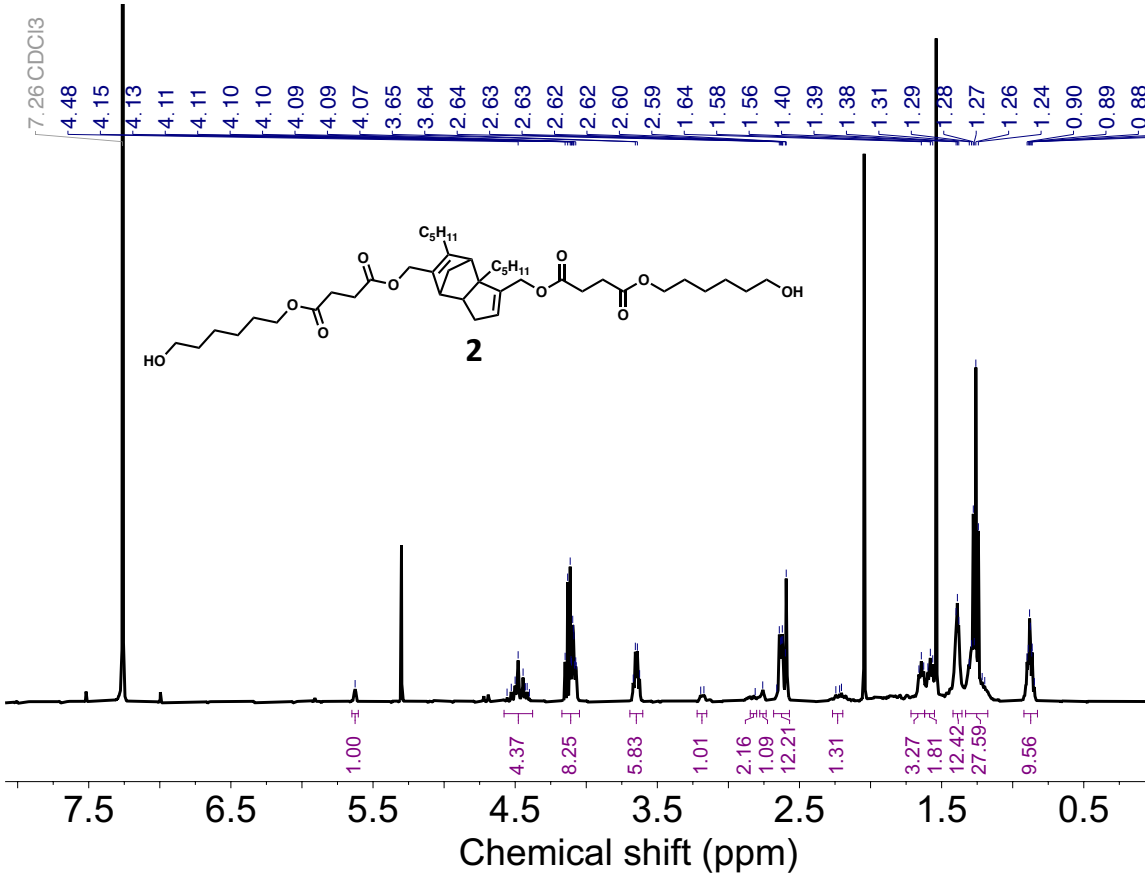


Figure S4.5. ^{1}H NMR spectrum of compound **2** in $CDCl_3$.

Polyurethane synthesis. Unless stated otherwise all reactions were carried out under inert atmosphere (argon) with oven dried (120 °C) glassware and magnetic stir. BDO (purchased from Sigma Aldrich), HMDI and MDI (purchased from Sigma Aldrich), and Cp-dimer diol derivatives **1** and **2** were dried under high vacuum for 24 h. PTHF (M_n = 2 kg mol^{-1} and 2.9 kg mol^{-1} purchased from Sigma Aldrich) was melted at 70 °C and dried under high

vacuum for 24 h. DBTDL (purchased from Sigma Aldrich) was stored over calcium sulfate (Drierite, Thermo Fisher Scientific) desiccant under vacuum before use. Dry THF was purchased from Sigma Aldrich.

Synthesis of **Pol 1** and **Pol 1C**: Melted PTHF (M_n = 2.9 kg mol^{-1}, 2.1 g, 1.3 mmol) in a Schlenk round bottom flask under argon was dissolved in 20 ml anhydrous THF and the temperature was adjusted to 40°C. To a 20-mL vial were added 8.5-mL of the prepared PTHF stock solution, HMDI (0.26 mL, 3.3 eq.), and for preparation of **Pol 1**, Cp-dimer diol compound **1** (0.1 g, 0.3 mmol) prepared 0.1 g ml^{-1} stock solution (in anhydrous THF). DBTDL (0.01 ml, 0.02 mmol) was added as catalyst to form a prepolymer at 40 °C for 2 h. BDO was added as chain extender to preparation of **Pol 1C** (0.06 ml, 0.62 mmol, 2.0 eq.) and **Pol 1** (0.03 ml, 0.31 mmol, 1.0 eq.). After 48 h the polymerization was quenched with methanol (1 ml) and stirred for an additional 30 min before the reaction mixture was precipitated into hexanes (~750 ml). The stringy elastic precipitate was collected and dried in a vacuum oven at 70 °C overnight and subsequently stored over calcium sulfate (Drierite, Thermo Fisher Scientific) desiccant under vacuum for further processing and characterization.

Synthesis of **Pol 2** and **Pol 2C**: Melted PTHF (M_n = 2.9 kg mol^{-1}, 2.0 g, 1.3 mmol) in a Schlenk round bottom flask under argon was dissolved in 20 ml anhydrous THF and the temperature was adjusted to 40°C. To this, MDI (0.33 g, 4.3 eq.) prepared as 0.075 g ml^{-1} stock solution (in anhydrous THF), and for **Pol 2**, Cp-dimer diol compound **1** (0.12 g, 0.3 mmol) prepared as 0.1 g ml^{-1} stock solution (in anhydrous THF) was added. Of note for

control **Pol 2C**, 3.3 eq. of MDI was used (0.26 g). DBTDL (0.01 ml, 0.02 mmol) was added as catalyst to form a prepolymer at 40 °C for 2 h followed by the addition of BDO (0.06 ml, 0.62 mmol) as chain extender. After 48 h the polymerization was quenched with methanol (1 ml) and stirred for an additional 30 min before the reaction mixture was precipitated into hexanes (~750 ml). The stringy elastic precipitate was collected and dried in a vacuum oven at 70 °C overnight and subsequently stored over calcium sulfate (Drierite, Thermo Fisher Scientific) desiccant under vacuum for further processing and characterization.

Synthesis of **Pol 3**, **Pol 4** and **Pol 3C**: Melted PTHF (M_n = 2.9 kg mol^{-1}, 2.0 g, 1.3 mmol) in a Schlenk round bottom flask under argon was dissolved in 20 ml anhydrous THF and the temperature was adjusted to 40°C. For **Pol 3**, to a 20-mL vial were added 0.6 g of PTHF, MDI (0.17 g, 3.3 eq.) prepared as 0.075 g ml^{-1} stock solution (in anhydrous THF), and Cp-dimer diol compound **1** (0.15 g, 0.5 mmol) prepared as 0.1 g ml^{-1} stock solution (in anhydrous THF). For preparation of **Pol 4**, 0.25 g of PTHF, 0.07 g of MDI and 0.14 g of compound **2** were added to another vial. For preparation of **Pol 3C**, 1 g of PTHF, 0.28 g of MDI, and 0.07 g of BDO were used. DBTDL (0.01 ml, 0.02 mmol) was added as the catalyst to each vial. After 48 h the polymerization was quenched with methanol (1 ml) and stirred for an additional 30 min before the reaction mixture was precipitated into hexanes (~750 ml). The stringy elastic precipitate was collected and dried in a vacuum oven at 70 °C overnight and subsequently stored over calcium sulfate (Drierite, Thermo Fisher Scientific) desiccant under vacuum for further processing and characterization.

Synthesis of **Pol 5** and **Pol 5C**: Melted PTHF (M_n = 2 kg mol^{-1}, 5 g, 2.5 mmol) in a Schlenk round bottom flask under argon was dissolved in 10 ml anhydrous THF and the temperature was adjusted to 40°C. To this, MDI (2.06 g, 8.25 mmol) prepared as 0.075 g ml^{-1} stock solution (in anhydrous THF), and for **Pol 5**, Cp-dimer diol compound **1** (0.1 g, 0.3 mmol) prepared as 0.1 g ml^{-1} stock solution (in anhydrous THF) was added. DBTDL (0.02 ml, 0.025 mmol) was added as catalyst to form a prepolymer at 40 °C for 2 h followed by the addition of BDO (0.48 ml, 5.44 mmol) as chain extender. After 48 h the polymerization was quenched with methanol (1 ml) and stirred for an additional 30 min before the reaction mixture was precipitated into hexanes (~750 ml). The stringy elastic precipitate was collected and dried in a vacuum oven at 70 °C overnight and subsequently stored over calcium sulfate (Drierite, Thermo Fisher Scientific) desiccant under vacuum for further processing and characterization.

Characterization methods. ^{1}H NMR spectra were recorded on Varian and Bruker spectrometers (400, 500, or 600 MHz) and are reported relative to the residual protio-signal in deuterated solvents. Data for ^{1}H NMR spectra are reported as follows: chemical shift (δ ppm), multiplicity, coupling constant (Hz) and integration. ^{13}C NMR spectra were recorded on Varian Spectrometers (500 MHz). Data for ^{13}C NMR spectra are reported in terms of chemical shift (δ ppm). M_n values were characterized using Size Exclusion Chromatography (SEC) eluting with dimethylformamide (DMF) and calibrated relative to polyethylene glycol (PEG) standards was performed on a Waters Alliance HPLC System, 2690 separation module,

equipped with Wyatt DAWN HELEOS-II light scattering and Waters 2410 Differential Refractometer (RI) and Waters 2998 Photodiode Array (PDA) detectors.

Degradation Tests:

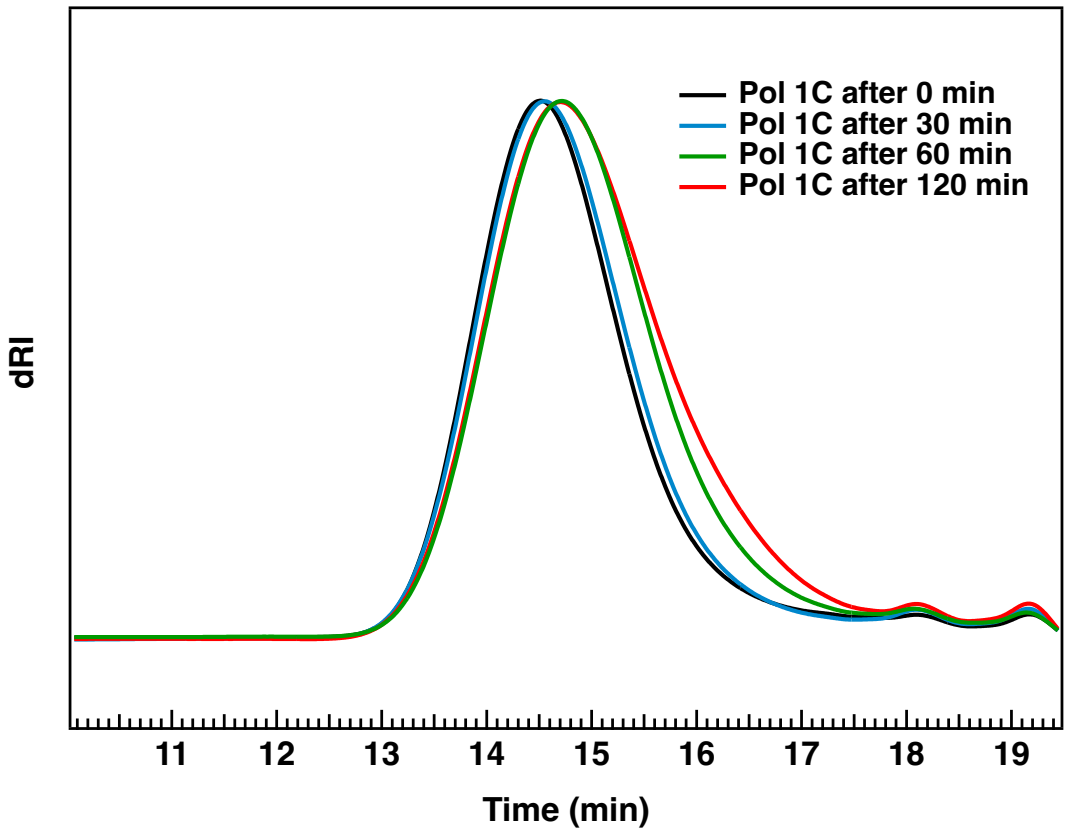


Figure S4.6. Thermal degradation of the control hydrogenated methylene diphenyl polyurethane **Pol 1C** with the addition of 5 mol% BHT after 0-, 30-, 60-, and 120-min heating at 150 °C. M_n = 25 kDa (0 min), 24 kDa (30 min), 19 kDa (60 min), and 13 kDa (120 min).

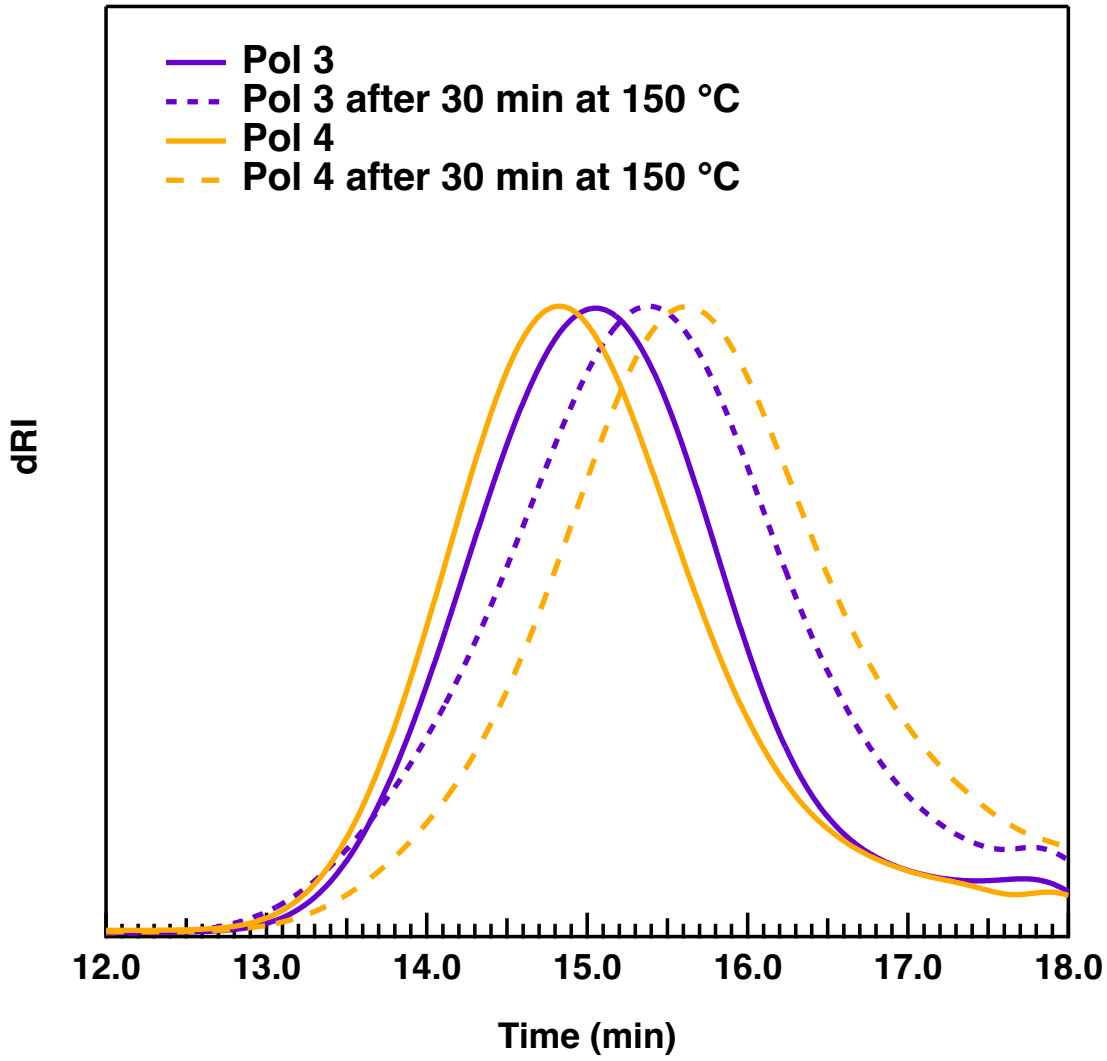


Figure S4.7. Thermo-selective degradation of **Pol 3** versus **Pol 4** with the addition of 2 wt% BHT after 30-min heating at 150 °C. M_n (**Pol 3**) = 14 kDa (0 min), 11 kDa (30 min). M_n (**Pol 3**) = 17 kDa (0 min), and 9 kDa (30 min).

Polymer Pictures:

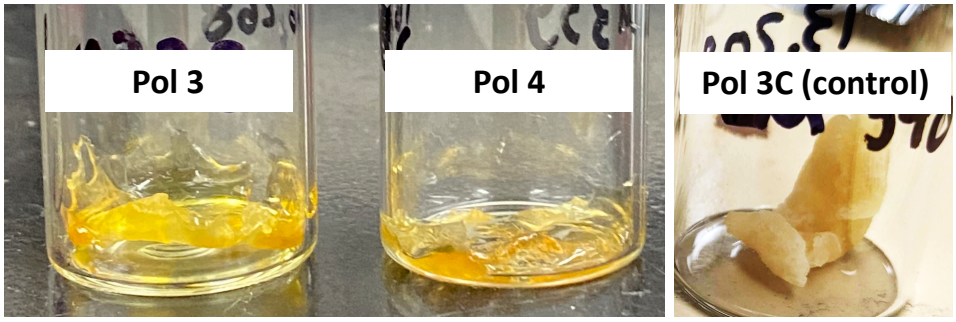


Figure S4.8. From left to right, pictures of **Pol 3**, **Pol 4**, and the control polymer **Pol 3C**.

4.8 References

(1) Pensupa, N.; Leu, S.-Y.; Hu, Y.; Du, C.; Liu, H.; Jing, H.; Wang, H.; Lin, C. S. K. Recent Trends in Sustainable Textile Waste Recycling Methods: Current Situation and Future Prospects. *Top. Curr. Chem.* **2017**, *375*, 76. DOI: 10.1007/s41061-017-0165-0.

(2) Wang, L.; Huang, S.; Wang, Y. Recycling of Waste Cotton Textile Containing Elastane Fibers through Dissolution and Regeneration. *Membranes* **2022**, *12*, 355. DOI: 10.3390/membranes12040355.

(3) Gong, C.; Zhang, K.; Yang, C.; Chen, J.; Zhang, S.; Yi, C. Simple Process for Separation and Recycling of Nylon 6 and Polyurethane Components from Waste Nylon 6/Polyurethane Debris. *Text. Res. J.* **2021**, *91*, 18–27. DOI: 10.1177/0040517520931893.
(4) Rossignolo, G.; Malucelli, G.; Lorenzetti, A. Recycling of Polyurethanes: Where We Are and Where We Are Going. *Green Chem.* **2024**, *26*, 1132–1152. DOI: 10.1039/D3GC02091F.

(5) Akindoyo, J. O.; Beg, M. D. H.; Ghazali, S.; Islam, M. R.; Jeyaratnam, N.; Yuvaraj, A. R. Polyurethane Types, Synthesis and Applications – a Review. *RSC Adv.* **2016**, *6*, 114453–114482. DOI: 10.1039/C6RA14525F.

(6) Howard, G. T. Biodegradation of Polyurethane: A Review. *Int. Biodeter. Biodegr.* **2002**, *49*, 245–252. DOI: 10.1016/S0964-8305(02)00051-3.

(7) Liu, B.; Westman, Z.; Richardson, K.; Lim, D.; Stottlemyer, A. L.; Farmer, T.; Gillis, P.; Vlcek, V.; Christopher, P.; Abu-Omar, M. M. Opportunities in Closed-Loop Molecular

Recycling of End-of-Life Polyurethane. *ACS Sustain. Chem. Eng.* **2023**, *11*, 6114–6128. DOI: 10.1021/acssuschemeng.2c07422.

(8) Uekert, T.; Singh, A.; DesVeaux, J. S.; Ghosh, T.; Bhatt, A.; Yadav, G.; Afzal, S.; Walzberg, J.; Knauer, K. M.; Nicholson, S. R.; Beckham, G. T.; Carpenter, A. C. Technical, Economic, and Environmental Comparison of Closed-Loop Recycling Technologies for Common Plastics. *ACS Sustain. Chem. Eng.* **2023**, *11*, 965–978. DOI: 10.1021/acssuschemeng.2c05497.

(9) Thiyagarajan, S.; Maaskant-Reilink, E.; Ewing, T. A.; Julsing, M. K.; Van Haveren, J. Back-to-Monomer Recycling of Polycondensation Polymers: Opportunities for Chemicals and Enzymes. *RSC Adv.* **2022**, *12*, 947–970. DOI: 10.1039/D1RA08217E.

(10) Xu, W.-H.; Chen, L.; Zhang, S.; Du, R.-C.; Liu, X.; Xu, S.; Wang, Y.-Z. New Insights into Urethane Alcoholysis Enable Chemical Full Recycling of Blended Fabric Waste. *Green Chem.* **2023**, *25*, 245–255. DOI: 10.1039/D2GC03663K.

(11) Charlon, M.; Heinrich, B.; Matter, Y.; Couzigné, E.; Donnio, B.; Avérous, L. Synthesis, Structure and Properties of Fully Biobased Thermoplastic Polyurethanes, Obtained from a Diisocyanate Based on Modified Dimer Fatty Acids, and Different Renewable Diols. *European Polymer Journal* **2014**, *61*, 197–205. DOI: 10.1016/j.eurpolymj.2014.10.012.

(12) Clauss, M.; Andrews, S. M.; Botkin, J. H.; Macena, L. Antioxidant Systems for Stabilization of Flexible Polyurethane Slabstock Foams. *Journal of Cellular Plastics* **1997**, *33*, 457–476. DOI: 10.1177/0021955X9703300503.

(13) Yin, Y.; Yao, D.; Wang, C.; Wang, Y. Removal of Spandex from Nylon/Spandex Blended Fabrics by Selective Polymer Degradation. *Text. Res. J.* **2014**, *84*, 16–27. DOI: 10.1177/0040517513487790.

(14) Kim, B.-H.; Yoon, K.; Moon, D. C. Thermal Degradation Behavior of Rigid and Soft Polyurethanes Based on Methylene Diphenyl Diisocyanate Using Evolved Gas Analysis-(Gas Chromatography)–Mass Spectrometry. *J. Analyt. Appl. Pyro.* **2012**, *98*, 236–241. DOI: 10.1016/j.jaap.2012.09.010.

(15) St. Amant, A. H.; Discekici, E. H.; Bailey, S. J.; Zayas, M. S.; Song, J.-A.; Shankel, S. L.; Nguyen, S. N.; Bates, M. W.; Anastasaki, A.; Hawker, C. J.; Read De Alaniz, J. Norbornadienes: Robust and Scalable Building Blocks for Cascade "Click" Coupling of High Molecular Weight Polymers. *J. Am. Chem. Soc.* **2019**, *141*, 13619–13624. DOI: 10.1021/jacs.9b06328.

(16) Bailey, S. J.; Discekici, E. H.; Barbon, S. M.; Nguyen, S. N.; Hawker, C. J.; Read De Alaniz, J. Norbornadiene Chain-End Functional Polymers as Stable, Readily Available Precursors to Cyclopentadiene Derivatives. *Macromolecules* **2020**, *53*, 4917–4924. DOI: 10.1021/acs.macromol.0c00967.

5. Chapter 5: *A Re-mendable and Degradable Thermoset Using Thermally Reversible Diels–Alder Cyclopentadiene-Maleimide Adducts*

5.1 Overview

As described in Chapter 2, re-mendable behavior was not efficient in the Cp homopolymer network, presumably due to the high cross-link density in these materials that limits polymer chain flow and interactions in the solid-state. Possible degradation of Cp units along the backbone upon treatment to rDA temperatures (i.e., 150–180 ºC) can also decrease the re-mending efficiency. While fabricating Cp homopolymers, I hypothesized that reacting Cp monomer with maleimide derivatives could form a new class of re-mendable polymer networks. The reported lower rDA temperature in Cp-maleimide adduct and the faster forward reaction between Cp and maleimide moieties compared to the Cp dimerization hold the potential to improve the self-healing property from the Cp cross-linked homopolymer. This chapter will disclose the attempts to synthesize a tough and re-mendable thermoset using Cp as the diene and maleimide as the dienophile. Specifically, the different synthetic routes explored to access a tough polymer network while also maintaining an efficient self-healing property will be discussed. With this goal in mind, we focused on the preparation of a

telechelic Cp and the tri-functional maleimide to fabricate an elastic and tough thermoset. Because solvent is used to solubilize the two components, we observed curling of the polymer samples after curing, presumably caused by the inhomogeneous cross-linking during the polymerization process. As such, optimization of the curing strategy was crucial to construct a uniformly cross-linked Cp-maleimide polymer to achieve samples enhanced properties for characterization and mechanical testing. Self-healing and degradation experiments for this thermoset will also be described.

5.2 Abstract

A new thermally reversible thermoset is developed based on a Diels–Alder (DA) reaction between cyclopentadiene as the diene and maleimide as the dienophile. The chemically cross-linked polymer is prepared by reacting a bis-pentacyclopentadienyl dodecanedioate with a tris-maleimide. The forward DA reaction is fast under ambient atmosphere, while the retro-DA reaction is induced at elevated temperature (i.e., 150 °C). An optimal curing condition was applied to achieve a uniformly cross-linked polymer for thermal and mechanical characterization. The polymer is tough and elastic with the tensile strength of ~12 MPa and the strain of ~200%, along with a glass transition temperature of 60 °C. The material is also thermally stable with the self-mendability enabled at a high temperature (i.e., 150 °C or the rDA temperature of Cp-maleimide adducts). We demonstrated that the broken pieces after tensile testing can be welded at 150 °C. Multiple self-healing tests were performed and discussed in detail to optimize the re-mending efficiency of the damaged samples. A

degradation experiment was also conducted by exploiting the reversibility of the DA bonds. Specifically, the polymer network was heated at 160 °C in the absence of solvent with an excess amount of dicyclopentadiene in a pressure vessel. The degraded materials were soluble and characterized by ^{1}H NMR spectroscopy. Further vacuum distillation is ongoing to investigate the degraded mixture.

5.3 Introduction

Thermosetting polymers represent one of the most useful materials that assist in the advancements of technology and industrial products with a wide range of applications ranging from rigid composites, tough automotive components, to high-performance adhesives.[1] The cross-linking in these materials provides their robust three-dimensional structures and desired mechanical properties (e.g., toughness, elasticity, chemical resistance, and thermal stability).[1] However, the affixation of the chemical bonding also significantly hinders their re-processing, and degrading capabilities. Once cured, the shapes of thermosets are permanent and cannot be re-molded.[1,2] Self-healing, where a material can heal on its own once it is damaged using different stimulus, has become one of the most promising strategies to "fix" the thermosets and prolong the service lifetimes of these materials.[3]

There are different routes to achieve self-healing in materials, such as the integration of capsules that contain healing reagents (i.e., new monomers or catalyst), control of the physical entanglement or interdiffusion of the polymer chains, and the implementation of reversible dynamic chemistry into the thermoset backbone.[3–5] Magnetic activation through

superparamagnetic embedded nanoparticles has also been developed.[6] Among the promising approaches, modifying the polymer structures with reversible covalent bonds during the fabrication of the cross-linked polymers offers several advantages. First, assuming the reversible bonds do not undergo degradation during healing, the materials can be repaired multiple times. Second, since the fabrication of the polymers relies mainly on the accessibility of the monomeric building blocks, it does not require additional synthetic steps to incorporate "healing reagents". For example, the design and incorporation of capsules or nanoparticles. Furthermore, compared to the non-covalent bonding (i.e., ionic, hydrogen bonding), covalent linkages are much stronger and can equip the materials with enhanced mechanical integrity and robust performance for applications that are normally encountered in harsh environments, such as structural and automotive components.[7,8]

Recently, the implementation of retro-Diels–Alder (rDA) reactions for the fabrication of crack-mending materials has become one of the most favorable chemical strategies. The fabrication and self-mending of the cross-linked polymer can be activated simply by orthogonal thermal treatments.[9] No catalysts or chemical reagents (i.e., bases, acids) are present throughout the preparation and self-healing process and thus, supplying the field with a self-contained platform. Furthermore, using heat as an external stimulus, the material can maintain their mechanical integrity until they are activated to self-heal upon damage.[9] Finally, the forward Diels–Alder (DA) and retro-Diels–Alder (rDA) are in equilibrium at elevated temperatures. This provides a pathway for the material to re-configure and heal without fully

dissociating all the chemical linkages. As such, the material can retain mechanical properties during the process. The first successful fabrication of a crack-mending material was established by Wudl and coworkers in 2002,[8] which has propelled the field forward with an exciting direction for reversible self-healing thermosets. Specifically, this work exploits the stable multi-functional building blocks, 4-arm furan as the diene and 3-arm maleimide (Mal) as the dienophile, to construct a densely cross-linked material. Incorporation of the DA adducts as cross-linkers facilitates the bond rearrangement upon heating.[8] When damaged (e.g., crack propagation), the desired mechanical property can be restored through the breakage and re-formation of the reversible linkages at the rDA temperature range (i.e., 100–120 °C).[8]

The facile handling and versatile substrate scope of furan and Mal starting materials have resulted in the synthesis of a diverse range of new re-mendable polymer networks.[9,10] Although this temperature is relevant for most applications, it is low enough that the reverse reaction could occur when it is not desirable and thus, limits its possible applications at high temperatures. Anthracene-Mal chemistry with a rDA temperature ≥ 200 °C was also reported.[5,10,11] A significant amount of energy is typically used to re-heal the polymer network at this temperature range. Moreover, 200 °C is around the decomposition realm of many organic compounds, which can lead to increased complication during the self-healing process.[10] As demonstrated, this temperature is challenging to execute and thus, the bonds can be considered nearly irreversible. Our group recently synthesized a novel reversible

homopolymer network based on a well-defined Cp analog (Chapter 2).[12] Cp is known to be unstable under ambient atmosphere and can dimerize at room temperature. By utilizing a mild deprotection pathway, we were able to isolate a pure tetra-functional Cp monomer and control the homopolymerization/cross-linking, which was previously known as challenging. A selective degradation of this material at a rDA temperature of 150 °C with *N*-phenyl maleimide was efficiently performed.[12] Despite a relevant rDA temperature range, the re-mending property in this cross-linked polymer, however, was not observed at 150 °C, presumably because of the degradation of Cp chain-ends during this process.[12]

Notably, a common trait of the stable DA dienes (i.e., furan and anthracene) and the Cp dimerization is the slow reactivity in the forward DA reaction.[13,14] As aforementioned, self-healing is based on the bond rearrangement upon heating where the linkages are actively broken and re-formed. Therefore, we hypothesized that the fast reactivity of a suitable diene and dienophile coupling could improve the bond rearrangement and thus, self-healing efficiency. Furthermore, by increasing the bond re-formation rate upon the heating and cooling cycles, the chance of the de-cross-linked chain-ends being decomposed at high temperatures is potentially lower. This concept has been employed to achieve the fast self-healing kinetics of a polymer network from Barner-Kowollik and coworkers, utilizing the rapid reaction between cyclopentadiene (Cp) and cyanodithioester.[15] The material experiences low degradation and free of hysteresis among self-healing cyclability in a temperature range of 40–120 °C under less than 5 minutes.[15] However, the rDA temperature of this polymer

network, which is lower than that of furan-maleimide material, is also not applicable for harsh environments.

We identify a different DA partner with the preferrable traits, composed of Cp and Mal. The reaction between Cp and Mal is much faster (up to 2000 times faster) compared to furan or anthracene with Mal and Cp dimerization.[13] Furthermore, the Cp-Mal adduct is known to undergo rDA temperature at relatively high temperature of ~150 °C,[16] which could be a Goldilocks option among the previously reported DA adducts (i.e., 100–120 °C from furan-Mal, 200 °C or higher from anthracene-Mal, or 150–180 °C from Cp dimers). To prepare the polymer network, we react a di-functional Cp derivative (was synthesized based on the synthetic procedure in Chapter 3) with a tris-maleimide compound to form a tough and pliable thermoset. The self-healing of the material was observed by welding the two damaged samples from the tensile testing together. Further improvement of the healing strategy will be investigated and discussed in detail. The selective degradation experiment with dicyclopentadiene at 160 °C displays soluble material after the de-cross-linking process in the absence of solvents. The degraded mixture was also analyzed via H^1 NMR spectroscopy. Further vacuum distillation is ongoing to investigate the degraded mixture.. Overall, this work exploits a new DA polymer network that is tough, can self-heal and be degraded selectively. Furthermore, the thermally stable covalent bonding between Cp and Mal would provide the field with a new strategy to fabricate promising self-healing and robust materials that can withstand harsh environments and can be repaired when activated.

5.4 Experimental Section

Monomer synthesis. Unless stated otherwise all reactions were carried out under nitrogen atmosphere with oven dried (100 °C) glassware and magnetic stir bars. All commercially obtained reagents were bought from Sigma Aldrich, Fisher Scientific, Ambeed, VWR International and were used as received unless otherwise noted. Thin-layer chromatography (TLC) was conducted with E. Merck silica gel 60 F254 pre-coated plates (0.25 mm) and visualized by exposure to UV light (254 nm) or stained with p-anisaldehyde. Flash column chromatography was performed using normal phase silica gel (60 Å, 0.040 – 0.063 mm, Geduran). The bis-pentacyclopentadienyl dodecanedioate monomer (**2C**) was synthesized as described in Supporting Information from Chapter 3 (**Section 3.7**). Tris(2-maleimidoethyl)amine (**3M**) was synthesized as in the procedure that is reported in literature.[8]

Synthesis of polymer (Pol 1). To a 20-mL vial was added **2C** (120 mg, 3.0 eq.) in 0.2 mL dichloroform (DCM), followed by 0.17 mL of butylated hydroxytoluene (BHT) solution in DCM (concentration of 10 mg/mL). 0.2 mL of **3M** (60.5 mg, 2.0 eq.) was then added to the mixture. The solution was mixed very quickly by pipetting up and down, which was subsequently poured into a mold for curing. The scheme and picture of the hand-made mold are shown in **Figures 5.1** and **5.2**, respectively. Of note, the material is cross-linked rapidly at room temperature upon the evaporation of the solvent. It is imperative that the mixture is poured into the mold right after mixing to ensure a homogeneous curing process. Moreover, the material is cured vertically (**Figure 5.1**) to prevent curling of the thermoset during the

solvent evaporation and polymerization. The mold that contains the mixture was tapped lightly to remove any bubbles. After that, the mold with the mixture was kept in a vacuum oven at 50 °C for 1 h to completely remove the solvent (i.e., DCM), followed by an optimal curing at 110 °C for 2 h under air (without vacuum). Depending on the characterization tests, the formed polymer network was then cut into a dumbbell-shape or rectangular sample.

Characterization methods. ATR FT-IR spectra were recorded on a Varian 640-IR FT-IR spectrometer equipped with an ATR (attenuated total reflection) accessory or a Thermo Nicolet iS10 FTIR Spectrometer with a Smart Diamond ATR; applied as neat samples or cured thermosets with smooth surfaces and absorbance bands reported as $1/\lambda$ in cm^{-1}. ^{1}H NMR spectra were recorded on Varian and Bruker spectrometers (400, 500, or 600 MHz) and are reported relative to the residual protio-signal in deuterated solvents. Data for ^{1}H NMR spectra are reported as follows: chemical shift (δ ppm), multiplicity, coupling constant (Hz) and integration. ^{13}C NMR spectra were recorded on Varian Spectrometers (500 MHz). Data for ^{13}C NMR spectra are reported in terms of chemical shift (δ ppm). Dynamic mechanical analysis (DMA) data were collected with a Discovery DMA 850. The film clamp geometry was used for the polymer films with dimensions of approximately 8 mm × 2 mm × 0.3 mm. Samples were loaded at room temperature with a 0.01 N preload, cooled to –20 °C, and equilibrated for a minimum of 5 minutes. Data were then collected by ramping temperature from –20 °C to 150 °C at the ramp rate of 3 °C/min to observe the glass transition temperature (at a constant strain of 0.04%, and frequency of 10 Hz).

Mechanical testing. Tensile testing was performed on a texture analyzer (TA) that combines a linear actuator with a load cell. The model is TA.XT Plus Connect that has a load cell with a maximum force of 50 N and an approximate resolution of ±1 mN and a distance resolution of 1 μm. Displacement is quantified via a stepper motor in conjunction with a known gear ratio. The materials were tested via uniaxial tension mode using mini tensile clamp fixtures. The speed of extension was 1.2 mm/min and the tests were performed at room temperature and ambient atmosphere. The samples were cut into dumbbell-shaped specimens with active region of 10.0 mm × 1.5 mm × 1 mm. Pictures were captured using iPhone 11 camera.

Self-healing test. The two broken pieces from the tensile testing were held together in a vertical mold (**Figure 5.3**) to ensure the healing surfaces of the two pieces are in contact with each other throughout the healing process. A piece of Kapton® sheet was covered over the soon-to-be-healed polymer and taped with a polyimide tape. The mold that contains the material was heated at 150 °C for 3 h under air (without vacuum).

Degradation experiment. Roughly 20 mg of **Pol 1** was added to a 50 mL of dicyclopentadiene (diCp) in a pressure vessel. The mixture was stirred at 160 °C for 8 h. The cross-linked polymer became soluble under the selective degradation conditions. Further vacuum distillation is ongoing to investigate the degraded mixture.

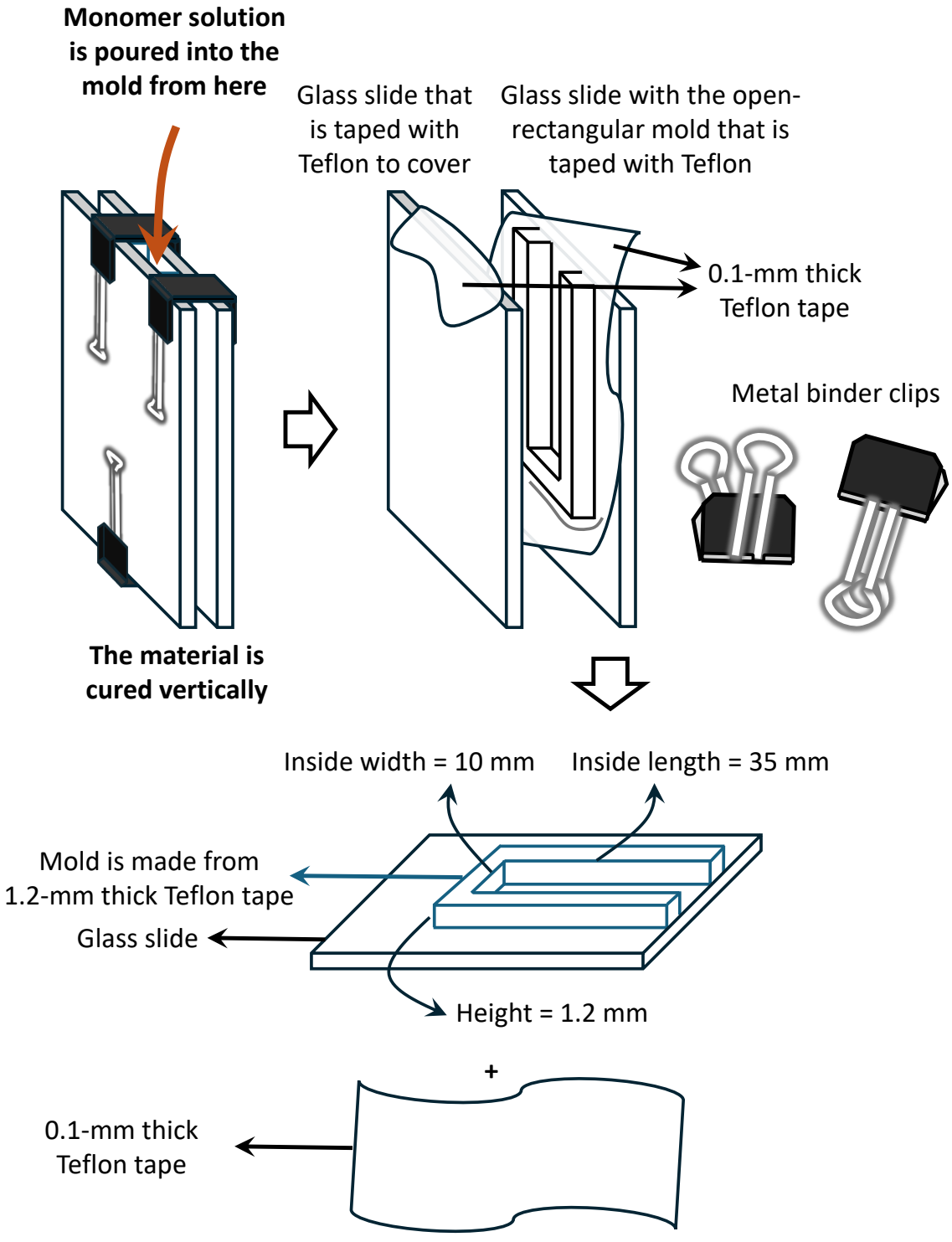

Monomer solution is poured into the mold from here
Glass slide that is taped with Teflon to cover
Glass slide with the open-rectangular mold that is taped with Teflon
0.1-mm thick Teflon tape
Metal binder clips
The material is cured vertically
Inside width = 10 mm
Inside length = 35 mm
Mold is made from 1.2-mm thick Teflon tape
Glass slide
Height = 1.2 mm
+
0.1-mm thick Teflon tape

Figure 5.1. The detailed hand-made mold design, including two parts. The first part entails the glass slide with the mold on one side, which is taped with 0.1-mm thick Teflon. The mold is made from a 1.2-mm thick Teflon tape to ensure the height of the mold is 1.2 mm. The second part is the other glass slide that is also taped with 0.1-mm thick Teflon to cover the mold. The two parts were clipped together tightly with metal binder clips. The clippers should be on top of the outside part of the mold to ensure that the solution does not drip out of the mold while curing.



Figure 5.2. Picture of the hand-made mold.

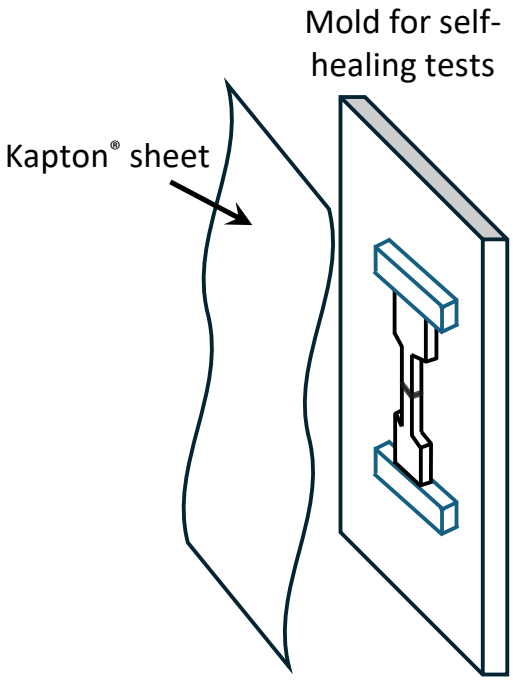


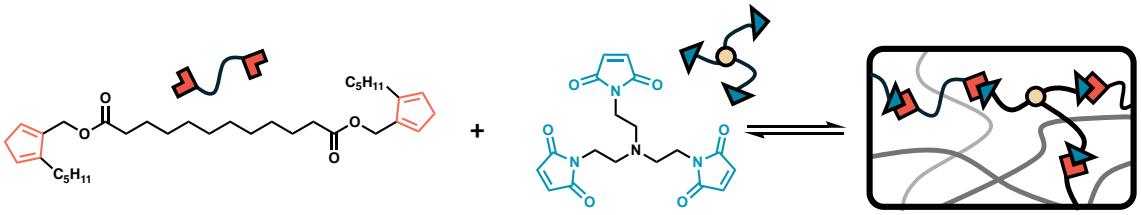
Figure 5.3. Mold designed for self-healing tests including the 1.2-mm thick Teflon tape to a metal block. After the two broken pieces of **Pol 1** were fitted to the mold, a Kapton® sheet was covered on top of the material. The sheet was affixed with a polyimide tape.

5.5 Results and Discussion

To fabricate a high-performance and re-mendable thermoset, we target the synthesis of a cross-linked polymer network using a di-functional Cp (i.e., bis-pentacyclopentadienyl dodecanedioate or **2C**) and a tri-functional maleimide (i.e., tris(2-maleimidoethyl)amine or **3M**) (**Scheme 5.1**). We have screened different synthetic routes (Supporting Scheme 5.1 in Section 5.7) and finalized with **2C** and **3M** monomers because they are synthetically accessible and provide a tough thermoset that is suitable for our goals of studies. We first investigated the feasibility of synthesizing a fast-curing polymer network (**Pol 1**) using **2C**

and **3M**. After the polymerization was established, optimal curing conditions were analyzed, followed by the self-healing tests. Of note, curling of the samples has been observed in these preliminary studies. Ongoing efforts are invested to form a tough and uniform thermoset with a straight shape that will assist in the mechanical property and self-healing capability enhancement.

Scheme 5.1. The synthesis of a thermo-reversible Cp-Mal cross-linked polymer using a di-functional Cp monomer and a tri-functional Mal cross-linker.



Preliminary Screening of the Curing Conditions to Form Pol 1. As aforementioned, maleimide and Cp derivatives reacts rapidly at room temperature. Therefore, the polymerization occurs immediately after we dissolved the two components, **2C** and **3M**, with DCM at room temperature. To prevent premature curing, each of the components (i.e., **2C** and **3M**) was dissolved in dichloromethane (DCM) separately. These solutions were only mixed when we were ready to pour the mixture into the appropriate molds to cure the material. Of note, as described in Chapters 3 and 4, Cp can undergo dimerization, though slowly, at room temperature. In this case, the fast reaction between Cp and Mal presumably competes with the Cp dimerization during the polymerization process. Hence, we assume the chemical bonding

of the polymer network is mainly composed of the Cp-Mal adducts. Furthermore, at 150 °C, if any Cp-dimers were formed during the polymerization, they also participate in the self-healing process because the Cp-dimer is reversible at the similar temperature range (i.e., 150–180 °C) compared to the Cp-Mal adduct. Therefore, the entirety of the polymer network is built upon the reversible DA chemistry to facilitate the self-healing.

Upon curing the material in the presence of the solvent (i.e., DCM) in a rectangular mold horizontally, we noticed the curling of the polymer network. It has been known in literature that while the solvent evaporates, an uneven surface can be formed due to the capillary effect along the edges of the mold (i.e., meniscus), leading to a gradient in the cross-link density and the curling of our thermoset after curing.[17] The shrinkage of cross-linked polymer (i.e., syneresis) is also one of the leading reasons for the curling phenomenon.[18] Rapid reaction between **C2** and **M3** at room temperature also augmented the inhomogeneous cross-linking and induced curling of the sample.[8,17,18] Therefore, a proper mold and polymerization technique are required to synthesize a uniform thermoset, which will be discussed in the following sections. Since the materials are flexible and can be re-shaped temporarily at RT, the curling of samples did not largely affect the thermal characterization of these materials via the dynamic mechanical analysis (DMA). To investigate the optimal curing condition, different samples were cured at varied temperatures, including 50, 90, and 110 °C and subsequently characterized via DMA. The preliminary analysis shows that the polymerization behaviors of **Pol 1** is consistent at different temperatures because these samples possess

relatively the same glass transition temperature (T_g) (**Figure 5.4a**). Fourier-transform infrared spectroscopy (FTIR) was also used to confirm the similarity among these polymer samples (**Figure 5.4b**). Of note, the diagnostic C=C stretching at 1628 cm^{-1} from the free Cp moiety was diminished in all samples, showing the complete consumption of Cp even at room temperature.

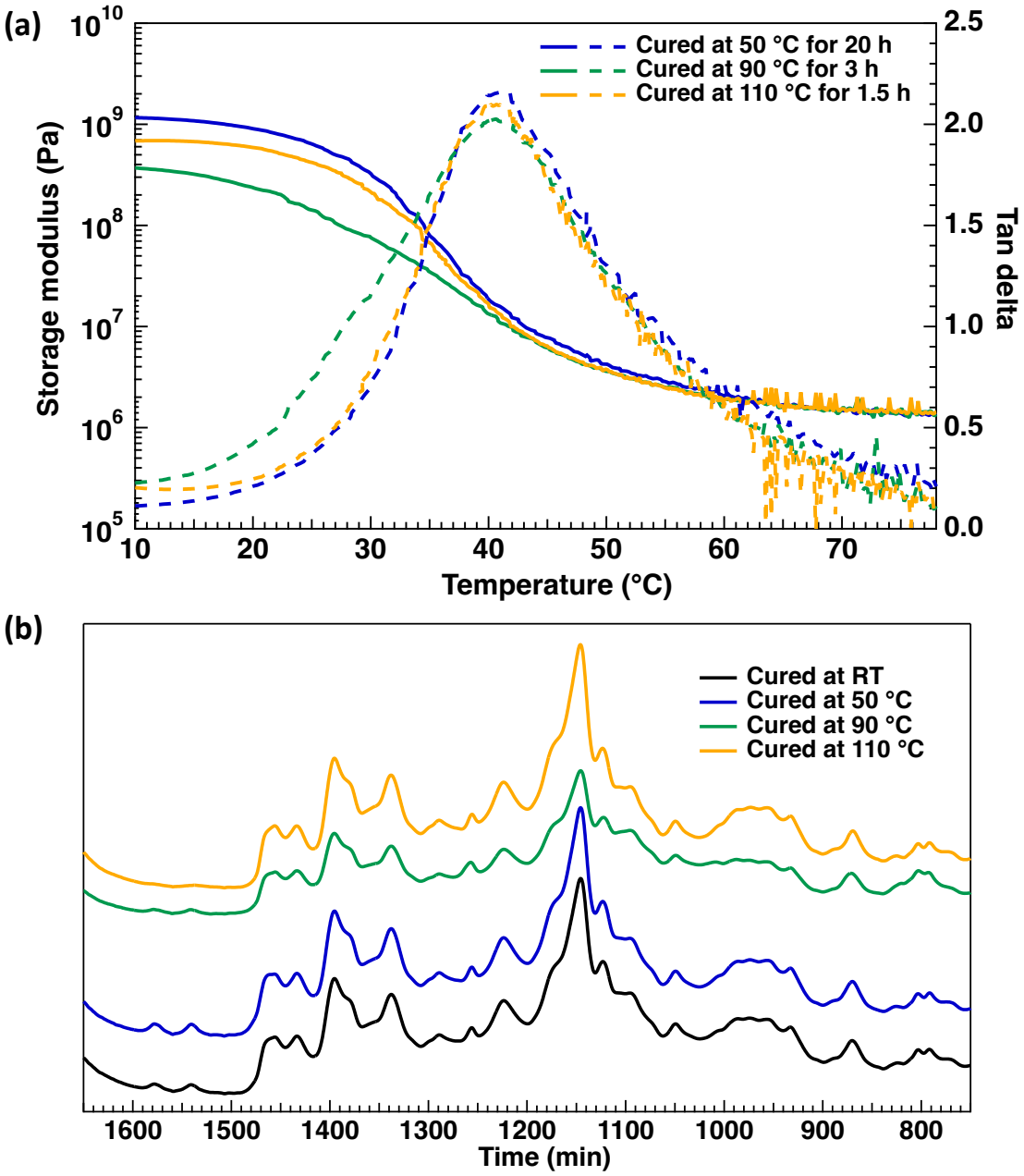
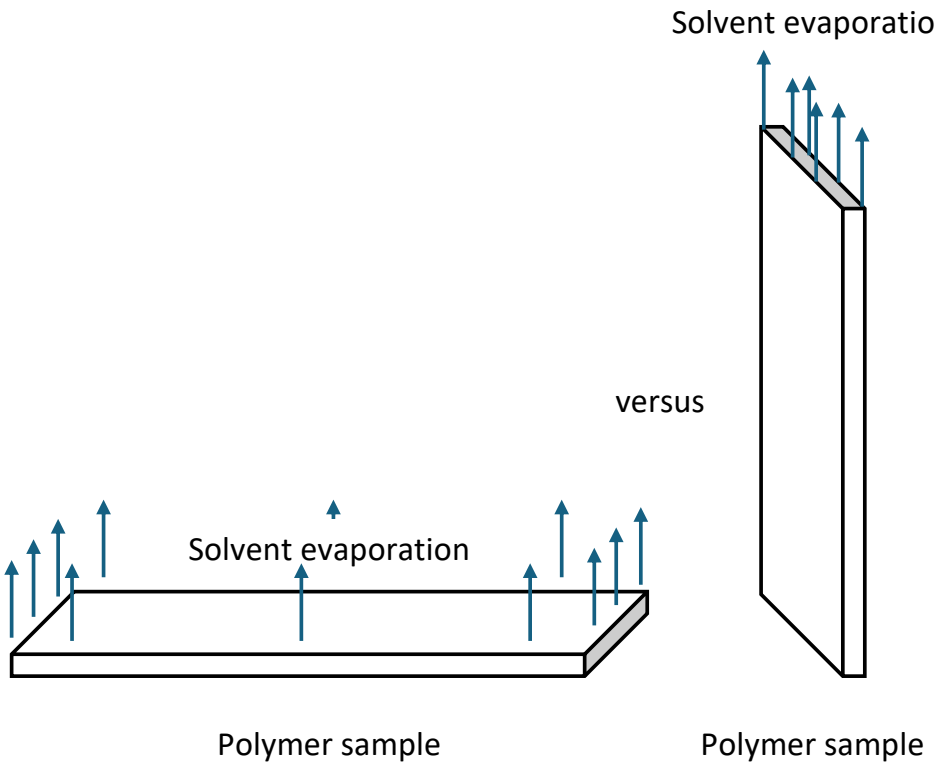


Figure 5.4. (a) Storage modulus (solid lines) and tan delta curves (dotted lines) of different samples that were cured at varied temperatures (i.e., 50 °C for 20 h, 90 °C for 3 h, and 110 °C

for 1.5 h). (b) Overlay of FTIR spectra of different cured samples shows no apparent difference.

Optimal Curing Conditions to Fabricate a Uniform and Tough Thermoset. Curling can affect the mechanical performance and the self-healing efficiency of the thermosets due to the uneven surfaces and cross-linking gradient that cause mechanical defects in the samples. Therefore, we re-designed our mold to prevent the curling of the material during the polymerization. A vertical mold was used with the setup schematically shown in **Figure 5.1**. The vertical curing of the thermoset supposedly minimizes the capillary effect from the solvent evaporation (**Scheme 5.2**). Furthermore, the sample is sandwiched between the two glass slides to ensure even surfaces of the sample during the curing process. Straight samples were successfully synthesized using this mold setup (Supporting Figure S5.1 in Section 5.7).

Scheme 5.2. Curing the polymer sample vertically versus horizontally to minimize the capillary effect from solvent evaporation.



Mechanical and Self-Healing Tests. Tensile testing was performed on both curled and straight samples to obtain and compare the mechanical performance of these materials (Supporting Figure S5.3). The materials are elastic and tough with a strain of 200% and the tensile strength of 12 MPa, respectively. An initial experiment of the self-healing was also demonstrated by welding the two broken pieces of a dumbbell-shape sample after the tensile testing. The two parts were welded and healed at 150 °C for 3 h (**Figure 5.7**). The joints between the two broken samples were not put together perfectly but the self-healing is

efficient to hold them together and the two pieces can be pulled and tugged. The tensile testing was also performed for the healed sample (Supporting Figure S5.2) but the samples did not show high tensile strength recovery. We observed that when the two samples were sandwiched in between the two metal blocks with force and healed horizontally, they did not align well and resulted in the uneven joints. To ensure an optimal healing, a vertical mold is set up as shown in **Figure 5.3**. The samples should be held perfectly in between the two Teflon pieces. The mold is vertical so that the surface areas of the broken parts remain in contact with each other due to gravity. A Kapton® sheet is used and secured with a heat-resistant tape to contain the sample in the mold but no force is induced horizontally. Using this setup, the materials can now be healed perfectly. Even though the healed samples are tightly joined, they tend to become brittle and discolored under the healing conditions (i.e., 150 °C for 3 h) and broken during the clamping for the tensile testing. As noted in Chapter 2 and 3 and in literature, Cp and maleimide can undergo radical side reactions at high temperatures (i.e., 150–200 °C).[19] Therefore, we repeat the polymer synthesis with the addition of a radical inhibitor, butylated hydroxytoluene (BHT, 10 mol%). Notably, BHT is volatile[20] and thus, vacuum is omitted throughout the curing and healing process.

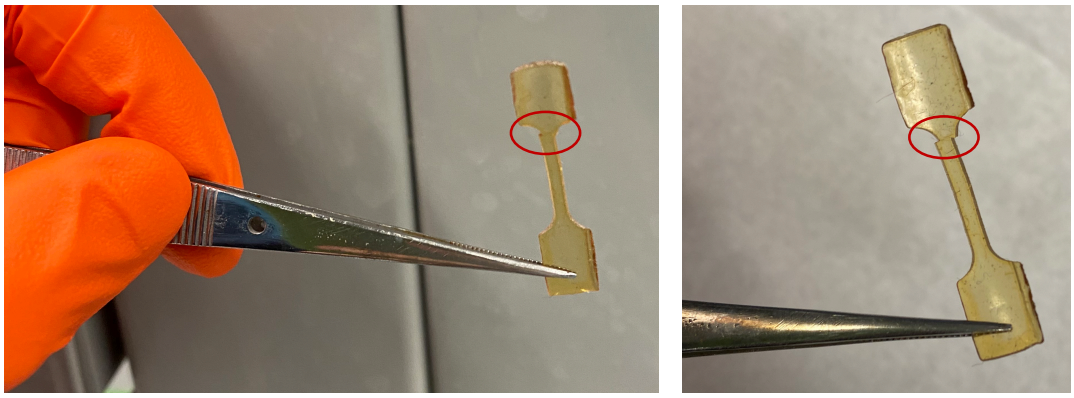


Figure 5.7. The healed samples that were welded at 150 °C for 3 h (left picture) and the zoomed-in picture to show the joints that were healed (right). The healed part was circled in red.

Selective Degradation Experiments. We first tested the thermos-selective degradation of **Pol 1** at 150 °C with the addition of excess amount of anthracene. Anthracene is known to react with Mal irreversibly[5] and thus, potentially serving as a "capping" reagent and pushing the reaction equilibrium to the starting materials at the rDA temperature. However, the material instead thermally decomposed and did not show solubility under the selective degradation conditions with anthracene. Presumably, the slow reaction between anthracene and Mal did not provide an efficient pathway to de-cross-link the polymer network. We changed our method to utilize Cp as the "capping" reagent because of the fast reaction between Cp and Mal. Furthermore, Cp can also dimerize with the Cp units of **C2** in the polymer network to form the Cp-dimer chain-ends. Combining all the above factors, Cp is a promising capping reagent to de-cross-link **Pol 1**. We then reacted **Pol 1** with diCp, which will convert to Cp at the investigated degradation temperature, in the pressure vessel at 160 °C. The

material is successfully degraded, and the crude mixture was analyzed by ^{1}H NMR spectroscopy (Supporting Figure S5.4). However, most peaks are from the diCp or Cp. Therefore, vacuum distillation is ongoing to further analyze the degraded mixture.

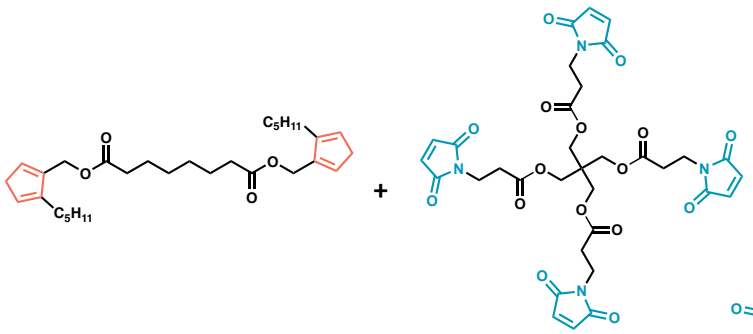
5.6 Conclusion

Herein, we presented a strategy to synthesize a novel fast-curing cross-linked polymer that is formed entirely by reversible DA linkages (i.e., Cp-Mal and possibly a small quantity of Cp-dimers). A radical inhibitor is used in the polymer synthesis to prevent radical side reactions that were known for both Cp and Mal at high temperatures to assist at the later stage, self-healing at high temperatures. Mechanical and self-healing tests were also performed. Current studies are ongoing to enhance and optimize the mechanical and self-mending properties of **Pol 1**. Degradation shows reversibility and solubility of the polymer network when reacting **Pol 1** with the diCp at 160 °C, compared to thermal decomposition and no solubility at the same temperature range with an excess amount of anthracene. Purification of the degraded mixture is ongoing to investigate the possibility of recovering the starting materials for re-polymerization. Overall, this work provides a novel synthetic platform to fabricate a self-mending and degradable thermoset with a fast curing kinetic and high mechanical performance, potentially expanding the access to new advanced functional thermosets.

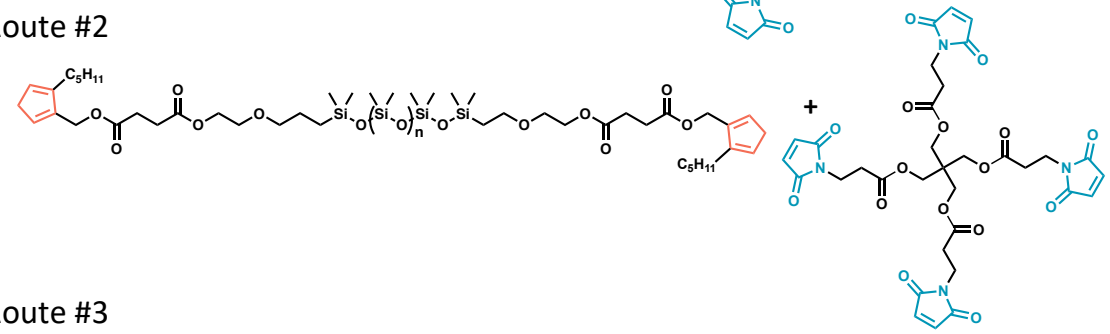
5.7 Supporting Information

Scheme S5.1. Different synthetic routes were explored to access a high-performance Cp-Mal polymer network. These routes are not applicable due to the low-yield access to the starting materials and/or the compromised mechanical properties (i.e., soft, brittle, loosely cross-linked).

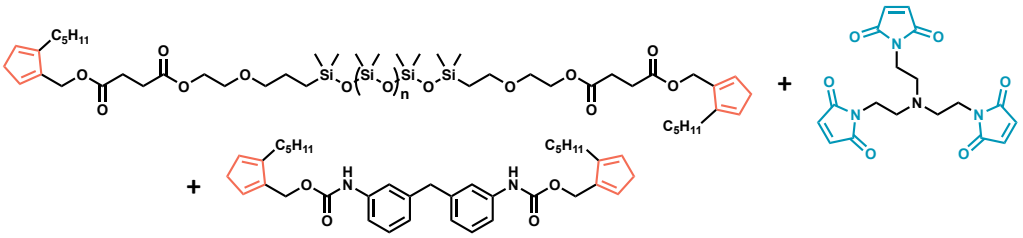
Route #1



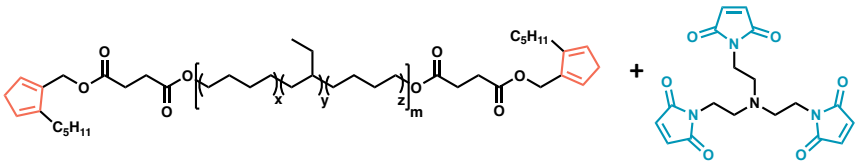
Route #2



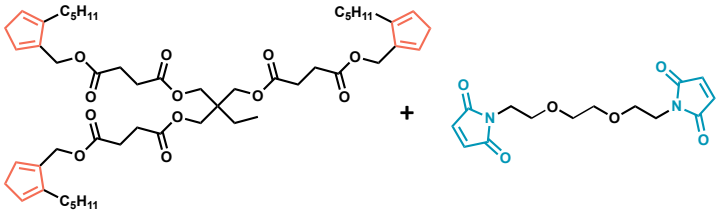
Route #3

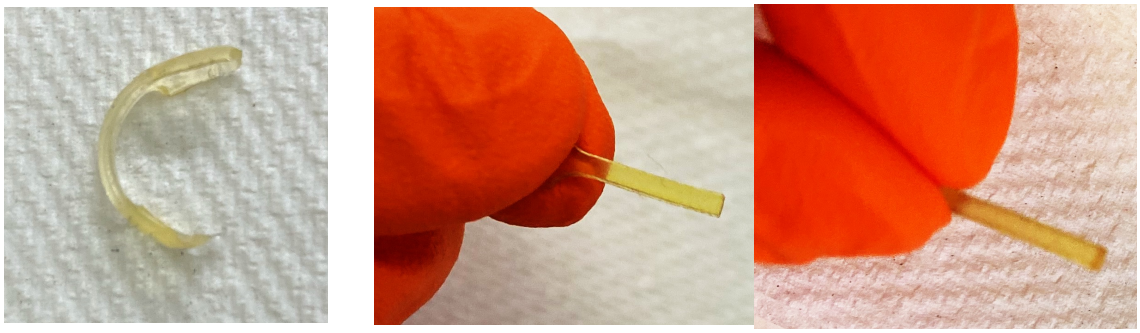


Route #4



Route #5





Sample curling observed with horizontal curing

Straight samples after vertical curing

Figure S5.1. Pictures of the samples when cured horizontally versus vertically. Curling occurs when the samples were cured horizontally while straight polymer network was obtained with the vertical curing.

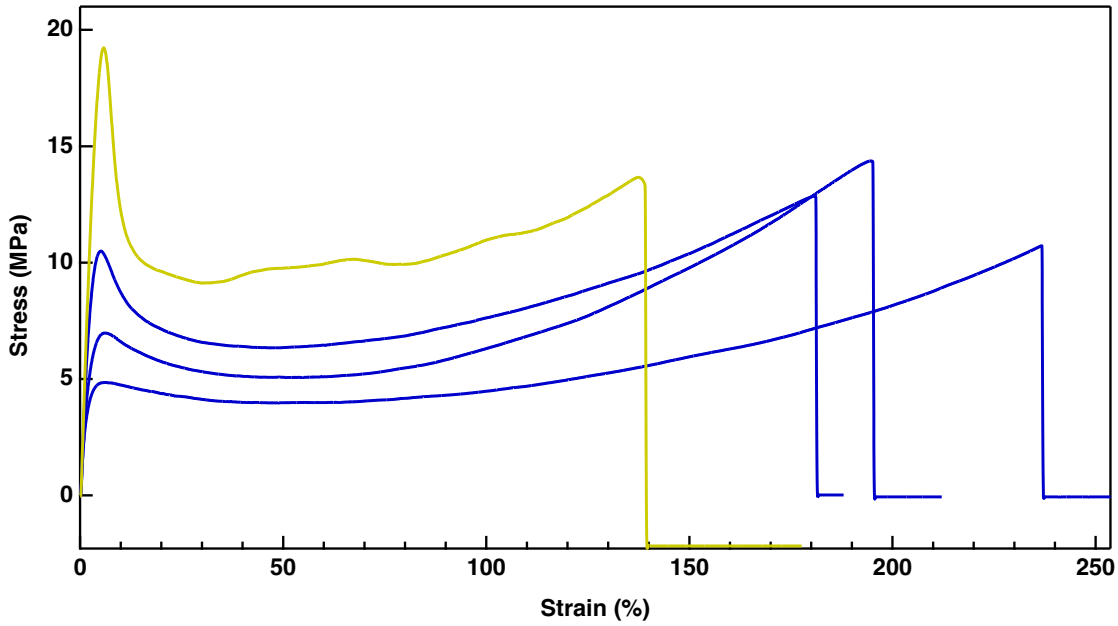


Figure S5.2. Tensile testing of three samples of **Pol 1** that are curled during horizontal curing at 50 °C for 20 h (blue traces) versus the one sample of **Pol 1** that was cured vertically at 110 °C for 3 h (yellowish green trace).

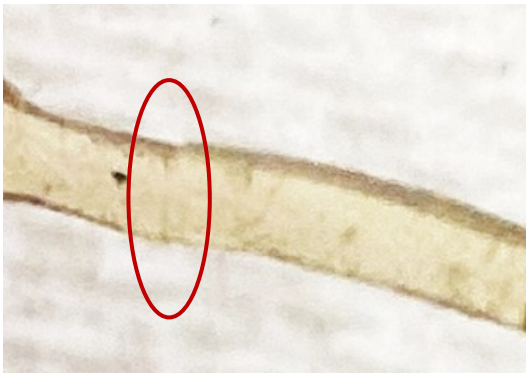


Figure S5.3. Close-up picture of a healed sample at the healing joints.

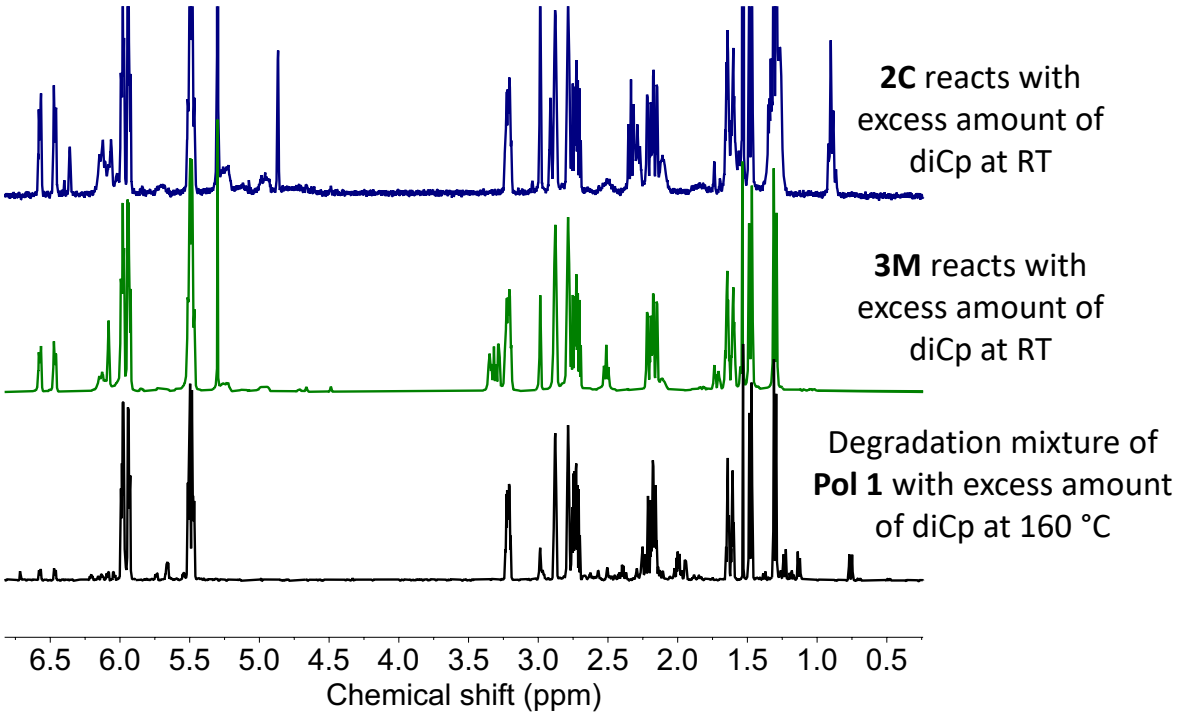


Figure S5.4. ^{1}H NMR spectrum of the crude degraded mixture of **Pol 1** after reacting with excess amount of diCp at 160 °C in the pressure vessel. The ^{1}H NMR spectra of the starting materials **2C** and **3M** that react with diCp at RT were overlaid to compare and identify the possible recovery of the starting material after thermo-selective degradation. However, most peaks are from diCp or free Cp that make it difficult to confirm the presence of recovered

starting materials. Therefore, further vacuum distillation is necessary to assist in the analysis of the degraded products.

5.8 Acknowledgements

The research was funded by the National Science Foundation (CHE-2204077). I would like to thank my two wonderful undergraduate researchers and mentees, Ashley Nowzari and Kaitlyn Talamantez, who contribute significantly to push this project to a promising direction. I am also thankful for the help from Munshi Sahid Hossain to bulk up the material to facilitate the completion of this project. I would like to also thank Juan Manuel Urueña for the helpful discussion about the polymer curing. The NMR instruments were supported by the National Science Foundation under award No. MRI-1920299. We used the MRL Shared Experimental Facilities that are supported by the MRSEC Program of the NSF under Award No. DMR 1720256; a member of the NSF-funded Materials Research Facilities Network.

5.9 References

(1) Guo, Q. *Thermosets: Structure, Properties, and Applications*; Woodhead Publishing, 2017.

(2) Ma, S.; Webster, D. C. Degradable Thermosets Based on Labile Bonds or Linkages: A Review. *Prog. Pol. Sci.* **2018**, *76*, 65–110. DOI: 10.1016/j.progpolymsci.2017.07.008.

(3) Wang, S.; Urban, M. W. Self-Healing Polymers. *Nat. Rev. Mater.* **2020**, *5*, 562–583. https://doi.org/10.1038/s41578-020-0202-4.

(4) Paladugu, S. R. M.; Sreekanth, P. S. R.; Sahu, S. K.; Naresh, K.; Karthick, S. A.; Venkateshwaran, N.; Ramoni, M.; Mensah, R. A.; Das, O.; Shanmugam, R. A Comprehensive Review of Self-Healing Polymer, Metal, and Ceramic Matrix Composites and Their Modeling Aspects for Aerospace Applications. *Materials* **2022**, *15*, 8521. DOI: 10.3390/ma15238521.

(5) Yoshie, N.; Saito, S.; Oya, N. A Thermally-Stable Self-Mending Polymer Networked by Diels–Alder Cycloaddition. *Polymer* **2011**, *52*, 6074–6079. DOI: 10.1016/j.polymer.2011.11.007.

(6) Corten, C. C.; Urban, M. W. Repairing Polymers Using Oscillating Magnetic Field. *Adv. Mater.* **2009**, *21*, 5011–5015. DOI: 10.1002/adma.200901940.

(7) Li, B.; Cao, P.-F.; Saito, T.; Sokolov, A. P. Intrinsically Self-Healing Polymers: From Mechanistic Insight to Current Challenges. *Chem. Rev.* **2023**, *123*, 701–735. DOI: 10.1021/acs.chemrev.2c00575.

(8) Chen, X.; Dam, M. A.; Ono, K.; Mal, A.; Shen, H.; Nutt, S. R.; Sheran, K.; Wudl, F. A Thermally Re-Mendable Cross-Linked Polymeric Material. *Science* **2002**, *295*, 1698–1702. DOI: 10.1126/science.1065879.

(9) Liu, Y.-L.; Chuo, T.-W. Self-Healing Polymers Based on Thermally Reversible Diels–Alder Chemistry. *Polym. Chem.* **2013**, *4*, 2194. DOI: 10.1039/c2py20957h.

(10) Ratwani, C. R.; Kamali, A. R.; Abdelkader, A. M. Self-Healing by Diels-Alder Cycloaddition in Advanced Functional Polymers: A Review. *Prog. Mater. Sci.* **2023**, *131*, 101001. DOI: 10.1016/j.pmatsci.2022.101001.

(11) Syrett, J. A.; Mantovani, G.; Barton, W. R. S.; Price, D.; Haddleton, D. M. Self-Healing Polymers Prepared via Living Radical Polymerisation. *Polym. Chem.* **2010**, *1*, 102. DOI: 10.1039/b9py00316a.

(12) Tran, T. M.; Read de Alaniz, J. Controlled Synthesis of a Homopolymer Network Using a Well-Defined Single-Component Diels–Alder Cyclopentadiene Monomer. *J. Am. Chem. Soc.* **2023**, *145*, 3462–3469. DOI: 10.1021/jacs.2c11416.

(13) St. Amant, A. H.; Discekici, E. H.; Bailey, S. J.; Zayas, M. S.; Song, J.-A.; Shankel, S. L.; Nguyen, S. N.; Bates, M. W.; Anastasaki, A.; Hawker, C. J.; Read De Alaniz, J. Norbornadienes: Robust and Scalable Building Blocks for Cascade "Click" Coupling of High Molecular Weight Polymers. *J. Am. Chem. Soc.* **2019**, *141*, 13619–13624. DOI: 10.1021/jacs.9b06328.

(14) Rideout, D. C.; Breslow, R. Hydrophobic Acceleration of Diels-Alder Reactions. *J. Am. Chem. Soc.* **1980**, *102*, 7816–7817. DOI: 10.1021/ja00546a048.

(15) Oehlenschlaeger, K. K.; Mueller, J. O.; Brandt, J.; Hilf, S.; Lederer, A.; Wilhelm, M.; Graf, R.; Coote, M. L.; Schmidt, F. G.; Barner-Kowollik, C. Adaptable Hetero Diels–Alder Networks for Fast Self-Healing under Mild Conditions. *Adv. Mater.* **2014**, *26*, 3561–3566. DOI: 10.1002/adma.201306258.

(16) Stegall, J. B. Cyclopentadiene-Maleimide Platform for Thermally Reversible Polymers; Virginia Tech: Blacksburg, VA, **2014**.

6. Chapter 6: *The Synthesis and Studies of Stereo- and Regio- Diels–Alder Homopolymer Networks Based on a Class of Azetidine-Cyclopentadiene Derivatives*

6.1 Overview

The deprotection and isolation of cyclopentadiene (Cp) derivatives propose not only an efficient pathway to access novel sustainable materials but also an appealing platform to investigate the structure-property relationship. One aspect that captured our attention while working with these materials is that controlling stoichiometry in single component step-growth polymerization is not required. Thermal curing of a single component (i.e., tetra-functional Cp cross-linker) led to the formation of a cross-linked Cp homopolymer. In fact, no solvents, catalysts, and/or chemical reagents were used during the polymerization process. The construction of the cross-linked homopolymers depends solely on the monomer features and the heating conditions. Hence, we hypothesize that the application of this strategy will hold potential for a direct way to correlate the structure property relationship between the monomer structures and the polymer properties, even in a complex context such as cross-linked polymers. Specifically, this chapter will present about the opportunities to construct and study a new class of azetidine-Cp homopolymer networks, each was synthesized from a different stereo- or regioisomer of the azetidine-Cp cross-linker (**Figures 6.3**). The relationship between the azetidine-Cp cross-linkers and the properties of the cross-linked

homopolymers will be explored. Moreover, as discussed in chapter 2, the structural diversity of the Cp linkages was demonstrated, which arises from the various diastereomers of the DA products that can form via the self-dimerization of Cp monomers, including its 1,5-H shift isomers. The varied conformation of these DA adducts, each with independent "bite angle," potentially contribute to the obtained mechanical performance of the tetra-Cp homopolymer network. This complexity creates a space to further investigate whether the diversity of the DA adduct linkages will be affected by the stereo- and regiochemistry of the cross-linking points and thus, expanding the studies of increasingly complex systems (i.e., diverse linkages in polymer networks).

6.2 Abstract

A novel class of stereo- and regiochemical homopolymer networks was synthesized by thermally curing a single component, a class of azetidine-cyclopentadiene compounds, neat through a step-growth homopolymerization. Azetidine-cyclopentadiene derivatives (i.e., two different stereoisomers and one regioisomer) are exploited as the multi-functional cross-linkers. The cyclopentadiene (Cp) chain-ends of these monomers can dimerize via a Diels–Alder cycloaddition to form the targeted homopolymer networks in absence of solvents. Using this system, we analyzed the correlation between the monomeric structures and the properties of resulting polymer networks to understand the influence of stereo- and regio-chemistry in cross-linked polymers. Though not significant, the synthesized polymers display a difference in their glass transition temperatures. Modification of functionality in the polymer chains of

the cross-linkers can assist in improving the structure-property relationship correlation, which will also be discussed. Furthermore, these materials are built upon a reversible dynamic chemistry and thus, is promising for degradation investigations. Overall, this work highlights a general strategy to synthesize and study stereo- and regio-chemical homopolymer networks, holding potential to expand the understanding of the three-dimensional effects to the cross-linking process.

6.3 Introduction

The spatial arrangement of bonds, also known as stereochemistry, is known to impact the properties of polymers and remains a research area with a long-standing interest.[1] For example, the *cis*- and *trans*- regioisomers of polyisoprene lead to the properties of natural rubber (i.e., soft and elastic) versus gutta-percha (i.e, a rubberlike gum, but tough and non-elastic), respectively.[1] The arrangement of the stereocenters along the main chains of polypropylene leads to isotactic, syndiotactic, and atactic stereochemistry, each with a different thermal and mechanical property.[1] Stereochemistry of the side chains in conjugated polymers (e.g., polyacetylenes, polythiophenes, and polypyrroles) leads to varied properties of these materials in sensing and conduction.[1] Hydrogen-bonding and tensile strength are also directly related to the stereochemistry of the isosorbide and isomannide that are incorporated along the backbone of biodegradable polyurethane thermoplastics.[2] Even though stereochemistry has been rigorously investigated for linear materials, it remains complicated to apply the stereochemical effects to synthesize and study chemically cross-linked analogs.[3]

Chemical cross-linking has long been performed since the eighteenth century to enhance the properties of polymers (i.e., rubber vulcanization).[4] Simplistically, the process affixes the linear polymer chains via the "cross-linking points" or "junctions" (**Figure 6.1**) that leads to the rigid three-dimensional (3D) structures of polymer networks and provides them with the desired mechanical performance (e.g., toughness, thermal stability, and chemical resistance).[4,5] The fast-growing technology and industrial modernization have demanded a vast array of research endeavors to synthesize and study high-performance cross-linked materials. Along with the rigorous synthetic efforts, structure-property relationship correlation has become fruitful to form and study advanced functional materials.[4–6] In fact, the investigation into network topology offers critical insights to design and construct materials with optimized mechanical performance (i.e., toughness, minimization of defects).[7–11]

The effects from structures and behaviors of the polymer chains to the property of the cross-linked polymers have been rigorously investigated.[12] For instance, loop formation, dangling chain-ends, and chain lengths between cross-links could alter the expected mechanical performance.[12,13] This recognition has guided the rapid discovery of novel synthetic strategies to remove defects and optimize the network homogeneity.[14–16] In contrast, the influence arising from cross-linking points on the properties of polymer networks are underexamined even though they are the key to the structural integrity of cross-linked polymers.[17] A recent report from Johnson and Olsen has proposed systematic theories and experimental data that establish the correlation between the odd and even numbers of junction

functionality (A_f) and the formation of loops in step-growth polymerization.[17] This work reinstates the importance of junction to network topology. However, apart from the prominent understanding in branch functionality and cross-link density, effects of cross-linking points are still a neglected subject in the investigation of mechanical integrity in polymer networks.[18] One of the main reasons derives from the limited synthetic modification of cross-linkers. In fact, variation in number of junctions is the most explored topic. Scope of research interest also includes the junction topology (e.g., zip-like versus point-like junctions), resulted from chain-growth polymerization.[18] Herein, we propose that by embedding a 3D factor (i.e., stereochemistry) to the network junctions, the synthetic toolbox to form diverse cross-linking points will be expanded and thus, network junctions will potentially capture more attention in ongoing structure-property relationship studies. Furthermore, most of the effects are more appropriate to investigate in a 2D space while the network topology is 3D. Therefore, the inclusion of 3D factors to study network formation is promising to extend the examination of structure-property relationship in the cross-linking process.

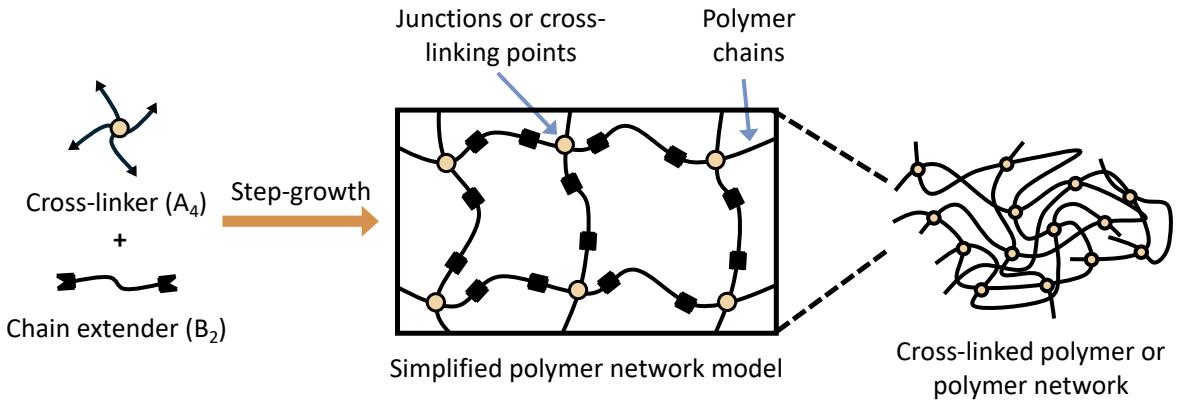


Figure 6.1. An example of step-growth polymerization utilizing a multi-functional cross-linker (A_4 monomer) and a di-functional chain-extender (B_2). Junctions or cross-linking points and polymer chains in a polymer network model are indicated (arrows).

The challenges in promoting 3D factors to polymer networks are associated with the lack of an appropriate synthetic platform. Most cross-linking process is heterogeneous.[4–6,12,13] In addition, batch-to-batch variation during curing or large experimental errors can be misleading for the structure-property relationship studies. Synthetic accessibility of stereochemical junctions also remains limited. In our previous work, we presented a unique step-growth homopolymerization strategy utilizing a multi-functional single component that can dimerize via Diels–Alder cycloaddition (i.e., a tetra-functional cyclopentadiene derivative) (**Figure 6.2**).[19] The construction of the cross-linked homopolymers depends solely on the features of the cyclopentadiene (Cp) monomer and the heating conditions. The lack of stoichiometry in this step-growth polymerization proposes an improved homogeneity in the cross-link density.[19] Furthermore, no solvents, catalysts, or chemical reagents are used during the curing process, potentially reducing the batch-to-batch variation. Hence, we hypothesize that the application of this strategy will hold potential for a direct and uncomplicated correlation between the monomer structures and the polymer properties in the complex context of cross-linking. To construct stereo- and regiochemical network junctions, the promising azetidine derivatives were utilized.[20,21] Azetidine possesses multi-functionality and has become an attractive synthetic target to construct stereo- and regio-chemical energetic materials with a remarkable difference in physical properties.[20,21] Moreover, the recent development to

increase the scalability and accessibility of azetidine holds potential for its incorporation into the cross-linked polymers (**Figure 6.3**).[21]

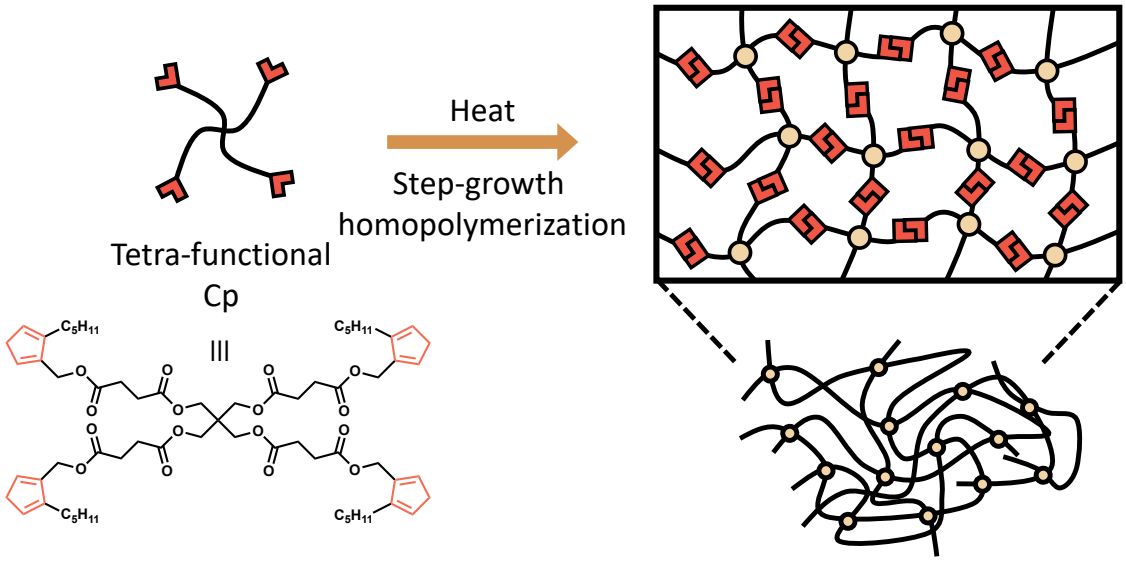


Figure 6.2. Our group designed a step-growth homopolymerization using a single component, a tetra-functional Cp derivative. The lack of stoichiometry and consistent curing conditions (i.e., only heat was used) will potentially lead to increased homogeneity in the cross-linking process.

Applying the proposed synthetic design, we successfully synthesize and study a new class of stereo- and regiochemical cross-linked polymers via the Diels–Alder dimerization of the cyclopentadiene-azetidine derivatives (**Figure 6.3**). The materials are characterized to obtain the glass transition temperatures. Though not significant, the cross-linked polymers display a difference in their glass transition temperatures. Modification of structures of the polymer chains can assist in improving the structure-property relationship correlation, which will also be discussed. Overall, this work highlights a general strategy to construct and study stereo-

and regio-chemical homopolymer networks, holding potential to expand the understanding of the three-dimensional factors to the cross-linking process.

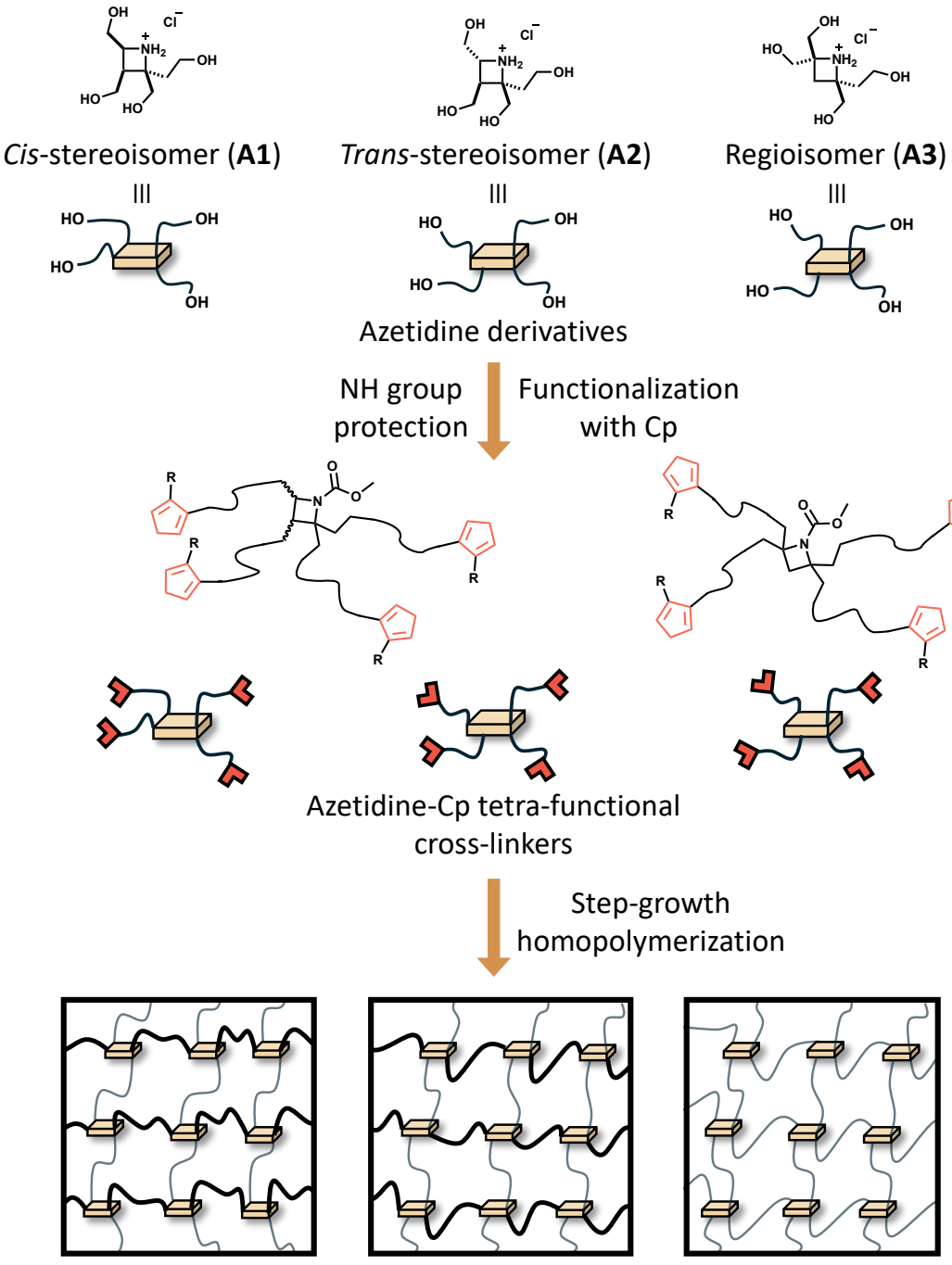

Cis-stereoisomer (**A1**)
Trans-stereoisomer (**A2**)
Regioisomer (**A3**)
Azetidine derivatives
NH group protection
Functionalization with Cp
Azetidine-Cp tetra-functional cross-linkers
Step-growth homopolymerization

Figure 6.3. The high scalability and synthetic accessibility of azetidine derivatives propose an appealing class of stereo- and regiochemical small molecules. The protection of the NH groups in azetidine and one-step esterification reaction lead to the formation of tetra-functional azetidine-Cp cross-linkers. The fabrication of novel stereochemical polymer networks results from the homopolymerization under an optimal heating condition in the absence of solvents.

6.4 Results and Discussion

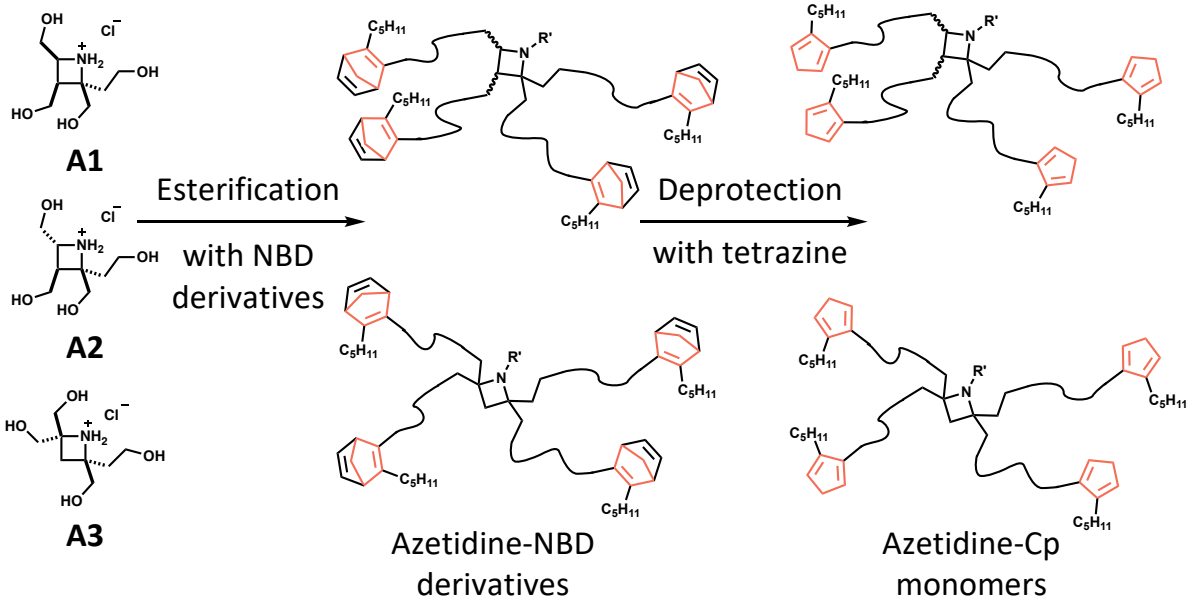
The key to achieve the stereo-chemical homopolymers includes the accessibility of the stereo-chemical Cp monomers and the possibility to polymerize these materials. To access the stereo-chemical Cp monomers in high yields for efficient polymerization and subsequent characterization, different synthetic routes were explored. The strategies include an esterification between the norbornadiene (NBD) derivatives functionalized with carboxylic acid and the alcohol groups of the azetidine compounds, followed by the deprotection of the formed azetidine-NBD with a tetrazine reagent (**Scheme 6.1**). Synthesis and deprotection of several NBD analogs to reveal free Cp moieties were shown in detail in Chapter 2 and Chapter 3. We chose long alkyl polymer chains in between the cross-linkers that are derived from the NBD derivative functionalized with carboxylic acid **1** to maximize the amount of the materials that we can work with by increasing the molecular weight of the monomer to ~2 kDa (**Scheme 6.2**). The synthetic screening was coupled with the analysis from the ^{1}H NMR spectroscopy and mass spectrometry. For the preliminary proof of concept, a shorter polymer chain was used to assist in the accurate mass spectrometry analysis. Therefore, the carboxylic norbornadiene (NBD) derivative **2** was used as the initial analog for esterification condition screening (Supporting Scheme S6.1a). We used **A3** to test different reaction conditions

because it is the most synthetically accessible compared to the other 2 azetidine stereoisomers (i.e., **A1** and **A2**).

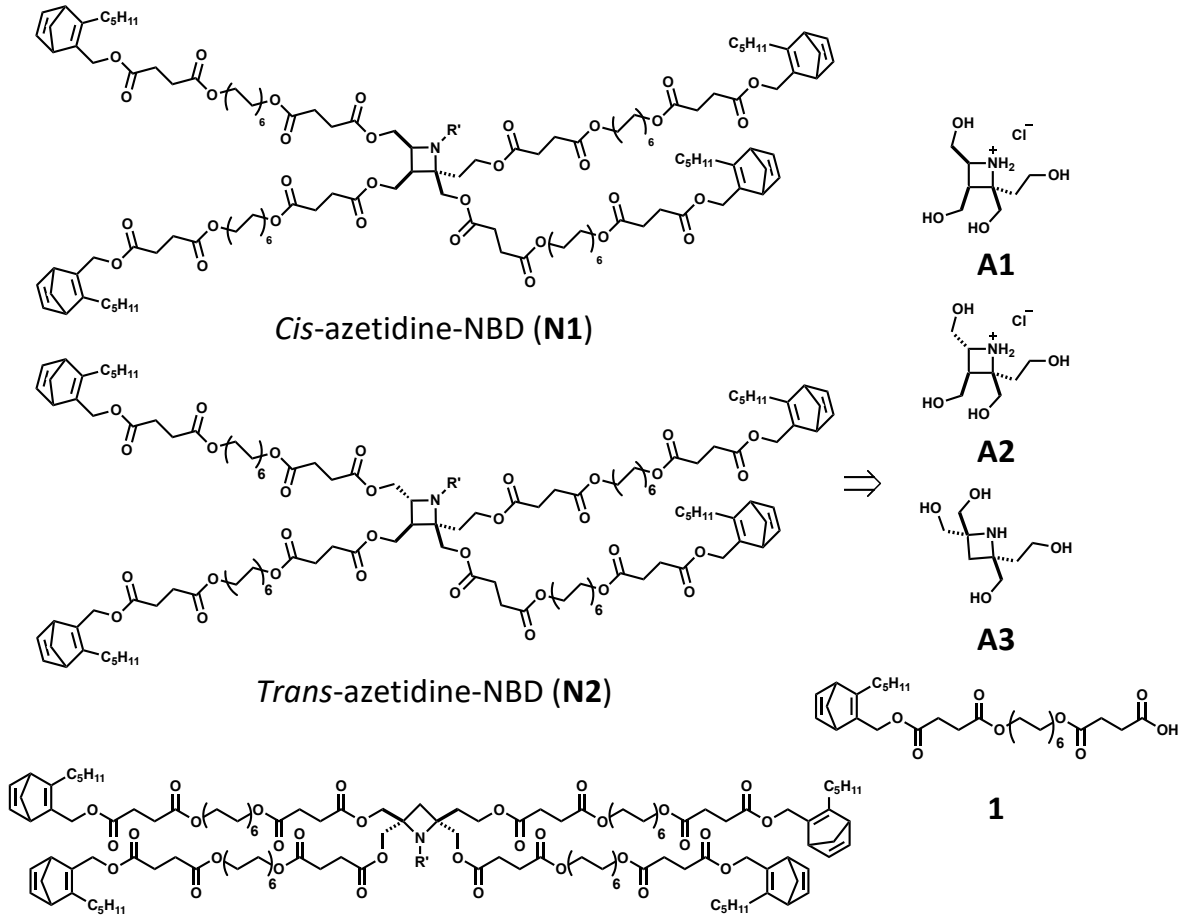
Screening of Reaction Conditions to Access the Azetidine-Cp Monomers. Esterification between **2** and the azetidine regioisomer **A3** did not work even with the addition of triethylamine (TEA) (Supporting Scheme S6.1a). Since it is possible that the salt-form of azetidine might cause complication during esterification, basification of **A3** was also attempted with sodium hydroxide solution (3M) or with TEA but the isolation was troublesome due to the polar compounds (Supporting Scheme S6.1b). We also hypothesize that the amine groups of the azetidine either in its neutral or salt form interfere with the esterification. Thus, several protection strategies were exploited, including the reductive amination, amine alkylation, and *N*-acetylation (Supporting Scheme S6.1c–f). Among these reactions, despite a low conversion (i.e., <30%), the *N*-acetylation of **A3** works well using a promising mild condition that is reported in literature[22] to produce the protected amine (Supporting Scheme S6.1f and Scheme S6.2). Mass spectrum confirms the presence of **AN3** in the crude mixture (Supporting Figure S6.2). No workup or purification were conducted to isolate the *N*-protected analog **AN3**. The crude product was subjected directly to the next-step reaction. The esterification between **2** and the crude *N*-protected **AN3** was successful (Supporting Scheme S6.2), as shown in the ^{1}H NMR and mass spectra (Supporting Figure S6.2–S6.4). Therefore, we finalized with this synthetic route. Acetylation of **A2** leads to the full conversion, followed by **A1** with 50–60% and then **A3** with < 30% conversion

(Supporting Scheme S6.2 and S6.3). The subsequent esterification of **AN1**–**AN3** with **1** works smoothly to produce the NBD derivatives of the three azetidine analogs (**N1**–**N3**) (Supporting Scheme S6.4). The ^{1}H NMR spectrum of **N3** with the assigned peaks is shown in **Figure 6.4**. The deprotection of **N1**–**N3** was performed using the optimized condition with the tetrazine reagent, dipyridyl tetrazine (DpTz) (**Scheme 6.3**), as described in Chapter 2. Successful revelation and isolation of single Cp isomers **C1**–**C3** was achieved (**Figure 6.5**). Of note, a very small amount of impurity (< 10%), presumably the pyridazine derivative, was observed among the three compounds and might interfere with the homopolymerization and the property of the formed cross-linked homopolymers.

Scheme 6.1. Synthetic scheme to access the azetidine-Cp derivatives through the esterification of azetidine compounds followed by the deprotection of the azetidine-NBD analogs with the tetrazine reagent.



Scheme 6.2. The target three stereo-chemical NBD precursors (i.e., *cis*-azetidine-NBD **N1**, *trans*-azetidine-NBD **N2**, and azetidine-NBD regioisomer **N3**) that are derived from the azetidine compounds (**A1**–**A3**) and the NBD derivative functionalized with carboxylic acid (**1**).



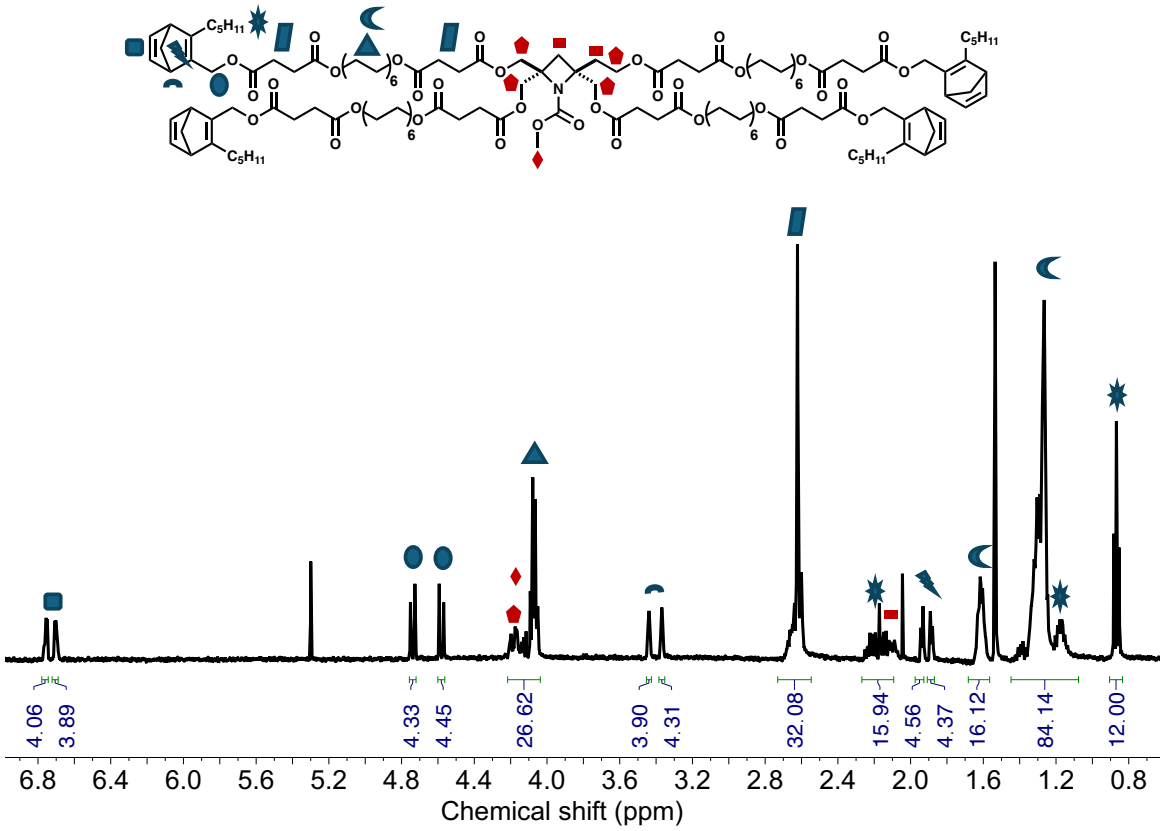
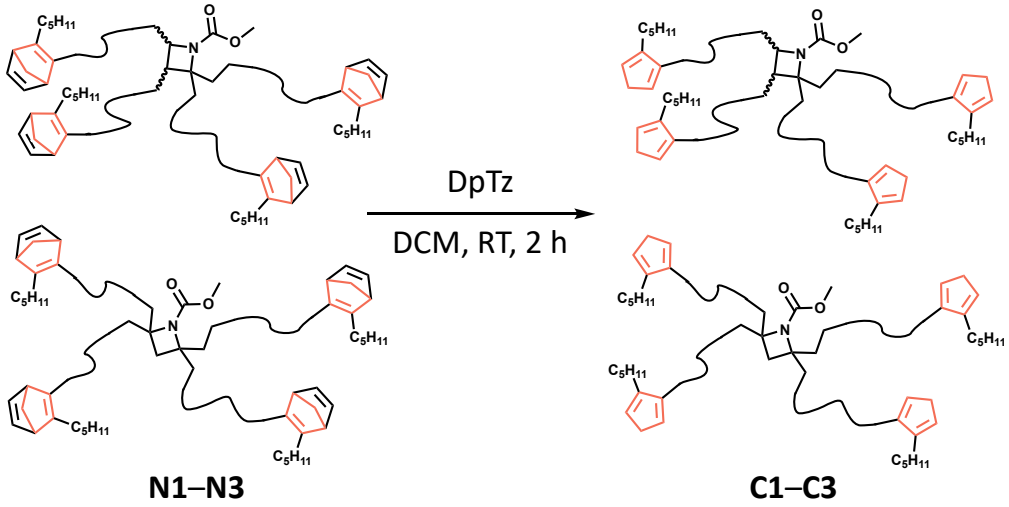


Figure 6.4. The ^{1}H NMR spectrum of diastereomer azetidine-NBD analog **N3** with the assigned peaks in $CDCl_3$.

Scheme 6.3. Revelation of free Cp (**C1**–**C3**) through the optimized deprotection of the azetidine-NBD analogs (**N1**–**N3**) with tetrazine reagent (DpTz).



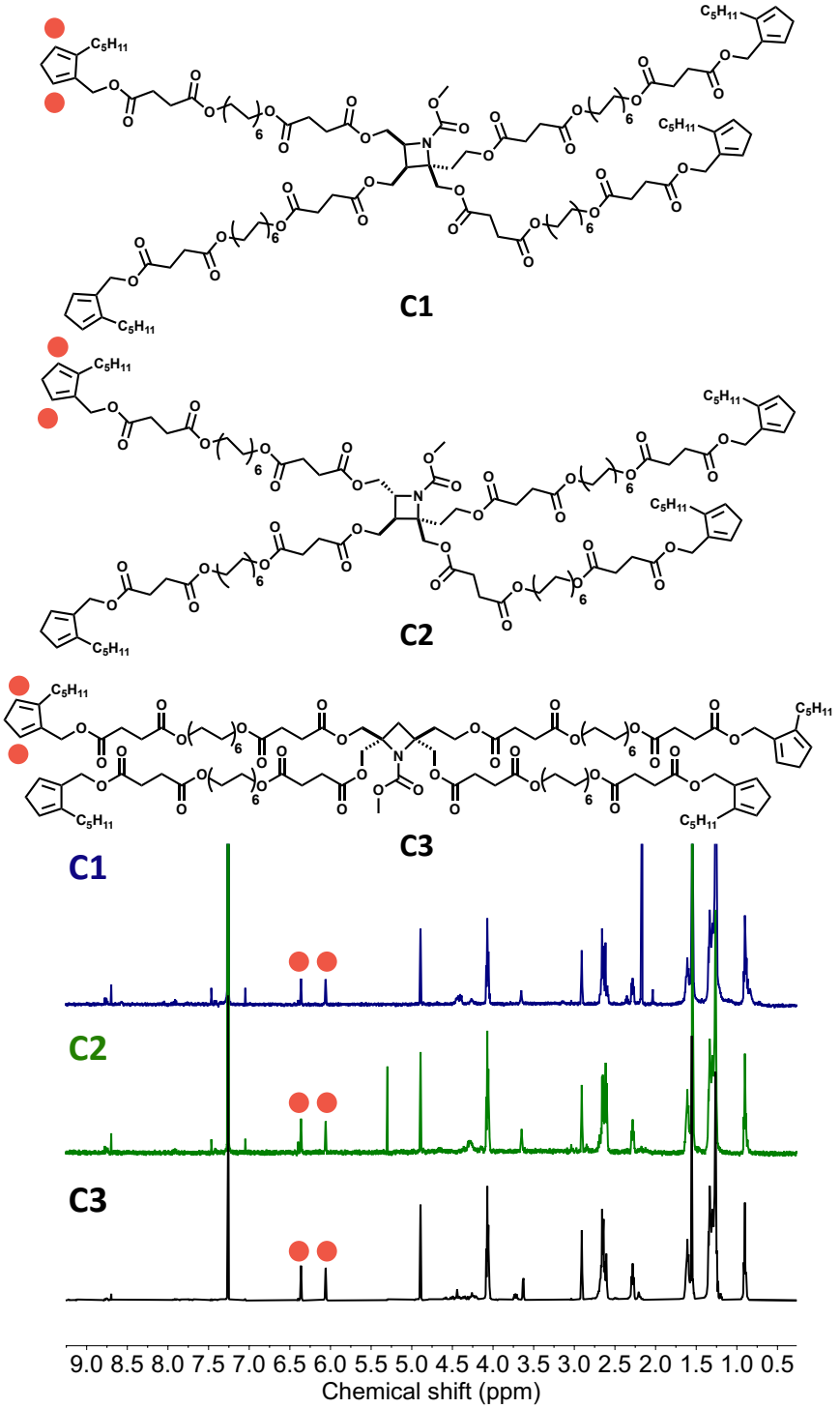

C1
C2
C3
C1
C2
C3
9.0 8.5 8.0 7.5 7.0 6.5 6.0 5.5 5.0 4.5 4.0 3.5 3.0 2.5 2.0 1.5 1.0 0.5
Chemical shift (ppm)

Figure 6.5. ^{1}H NMR spectra comparison among the 3 azetidine-Cp analogs (**C1**–**C3**). The clear signal of a single free Cp isomer was indicated by the red circle shape. There is a small amount of impurity that is visible in the 8.5–9.0 ppm region, presumably the pyridazine derivative that is known to be challenging to remove after the deprotection reaction, as noted in Chapter 3.

Cp Homopolymerization and the Characterization of the Azetidine-Cp Homopolymer Networks. After successful synthesis of the azetidine-Cp monomers, the homopolymerization of **C1**, **C2**, and **C3** was carried out individually at 110 °C for 3 h to obtain the three stereo-chemical homopolymer networks (**P1**–**P3**, respectively, as shown in **Figure 6.6**). The formed polymers were characterized using the differential scanning calorimetry (DSC) to obtain the values of glass transition temperature (T_g). **P1** possess a T_g of -26 °C, which is close to that of **P3** (i.e., -23 °C)**,** while **P2** displays a small difference with the T_g value of -17 °C (**Figure 6.6**). Though not significant, there is a difference in the T_g values of these materials that proposes an intriguing trend. The properties of the three stereo-chemical homopolymer networks might correlate with the three-dimensional arrangement of the stereo- and regio-chemical azetidine derivatives (**Figure 6.6**), with the small-molecule stick models presented in Supporting Figure S6.6. Further optimization of the synthetic routes to completely remove the small impurity after the deprotection of the NBD analogs will potentially lead to promising detailed studies of the structure-property relationship of these stereo-chemical materials.

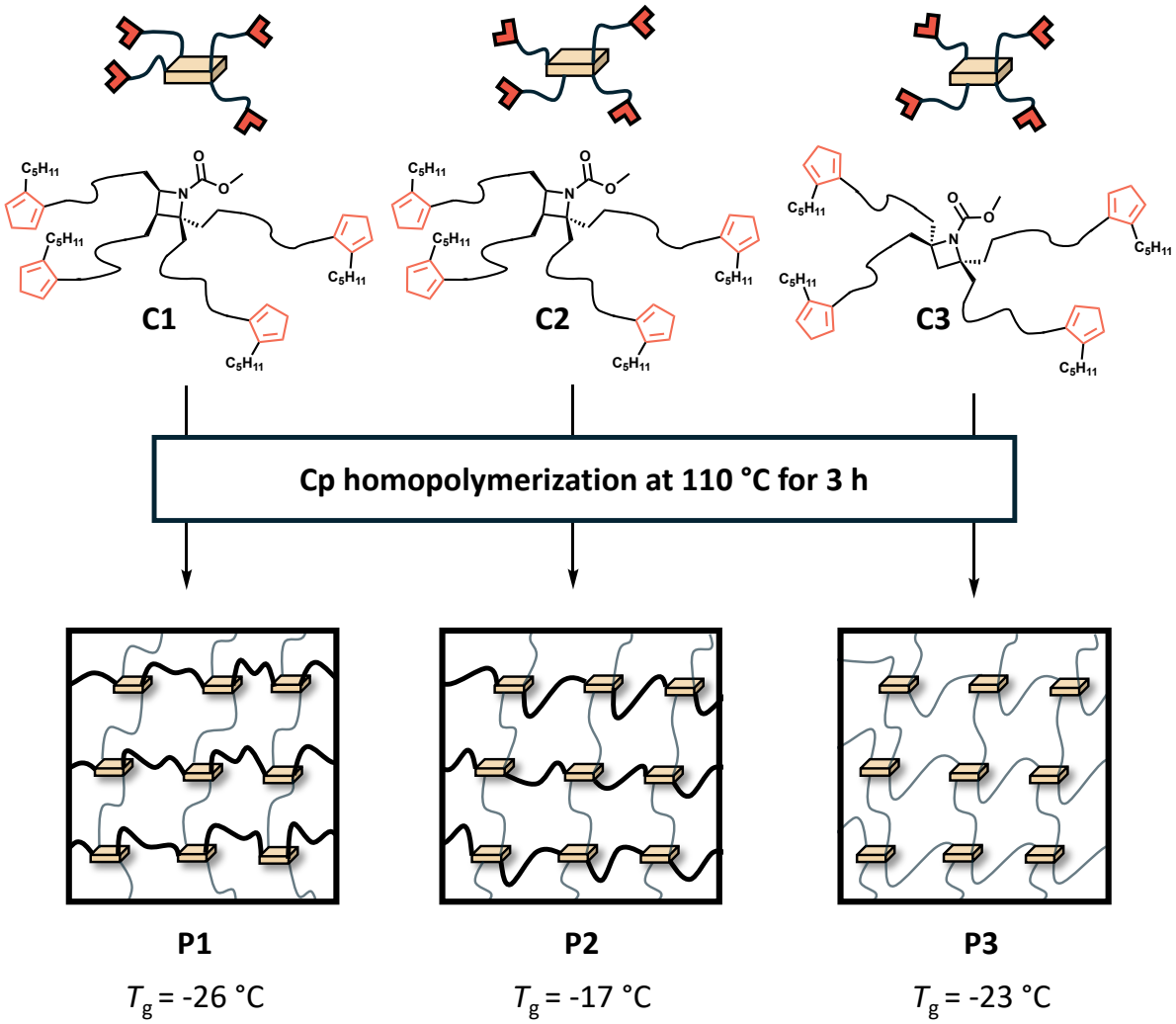
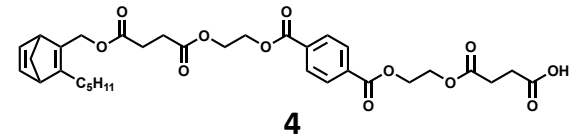


Figure 6.6. Cp homopolymerization of the 3 azetidine-Cp derivatives (**C1**–**C3**) provide the three stereo-chemical homopolymer networks. The T_g of **P1** and **P3** are in the similar range (-26 and -23 °C, respectively), while **P2** displays a lower T_g value of -17 °C. Of note, a small impurity after the isolation of the azetidine-Cp monomers might affect the accuracy of these values. Further optimization of the synthesis will allow a promising platform for the structure-property relationship studies.

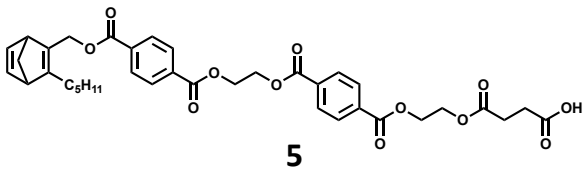
Exploration of Different Polymer Chains. The polymer chains between the cross-linkers are also crucial to determine the mechanical properties of the resulting homopolymer

networks. We explored the long-alkyl polymer chains initially to identify the optimal synthetic plans. The stereo-chemical materials did not possess a large difference in the T_g, which might result from the flexible alkyl chain and the low cross-link density. The polymer chains with increased crystallinity normally produce a difference in the polymer chain packing.[23] Combined with the lower molecular weight between the cross-linking points to increases the cross-linking density will create a large impact on the mechanical properties of the polymer networks.[24] Therefore, hypothetically, the stereo-chemical cross-linked polymers with higher cross-link density and more crystalline polymer chains will lead to the discrepancy in the thermal and mechanical properties. Current investigation is ongoing to understand the effect of the packing in the polymer chains and cross-link density to the cross-linking of the stereo-chemical polymers. The potential starting materials include the NBD analogs with the increased crystallinity (i.e., aromatic ring) and shorter alkyl chain to fabricate new stereo-chemical azetidine-Cp homopolymer networks (**Scheme 6.4**).

Scheme 6.4. Potential NBD starting materials with increased crystallinity and shorter alkyl chain to synthesize the new stereo-chemical azetidine-Cp homopolymer networks that can possess a difference in the thermal and mechanical properties.



4



5

6.5 Conclusion

A novel synthetic platform is proposed to achieve the fabrication of a new class of stereo-chemical homopolymer networks using Cp dimerization and the azetidine derivatives. The initial results display a promising structure-property relationship in these materials with a small difference in the glass transition temperature of **P2** compared to the values of the other two polymers (i.e., **P1** and **P3**). Further optimization of the synthesis and the modification of the polymer chains will assist in improving the structure-property relationship correlation. A general strategy to construct and study stereo- and regio-chemical homopolymer networks can be realized through the Cp homopolymerization, holding potential to expand the understanding of the three-dimensional factors to the cross-linking process.

6.6 Acknowledgements

I would like to thank my fantastic collaborator, Katie Rykaczewski, who synthesized the small molecule azetidine derivatives in large scale that facilitate the fabrication of stereo-chemical homopolymer networks. I am also grateful for the helpful insight and collaborative spirit from Prof. Corinna Schindler. The NMR instruments were supported by the National Science Foundation under award No. MRI-1920299. We used the MRL Shared Experimental Facilities that are supported by the MRSEC Program of the NSF under Award No. DMR 1720256; a member of the NSF-funded Materials Research Facilities Network. The research was funded by the National Science Foundation (CHE-2204077).

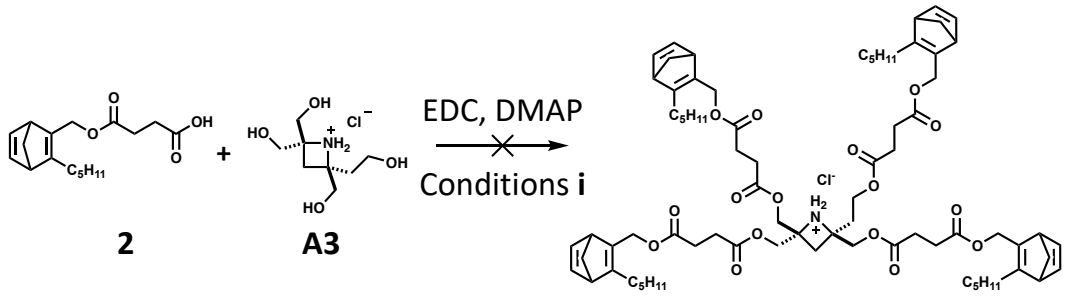
6.7 Supporting Information

Synthesis Procedures:

Unless stated otherwise all reactions were carried out under nitrogen atmosphere with oven dried (100 °C) glassware and magnetic stir bars. All commercially obtained reagents were bought from Sigma Aldrich, Fisher Scientific, Ambeed, VWR International and were used as received unless otherwise noted. Compound **2** was synthesized based on a previously reported procedure.[9] The O-alkyl S-(pyridin-2-yl)carbonothiolate reagent was synthesized based on literature.[22] Thin-layer chromatography (TLC) was conducted with E. Merck silica gel 60 F254 pre-coated plates (0.25 mm) and visualized by exposure to UV light (254 nm) or stained with p-anisaldehyde. Flash column chromatography was performed using normal phase silica gel (60 Å, 0.040 – 0.063 mm, Geduran).

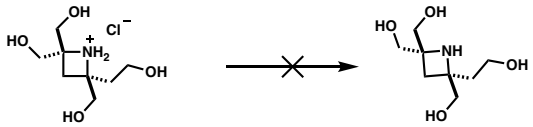
Scheme S6.1. (a) An initial esterification between the NBD functionalized with carboxylic acid **2** and the salt-form of the azetidine derivative **A3** did not work; condition **i**: DCM; DCM with TEA. (b) Basification of **A3** was also tried but was not successful to form the free amine form for further reactions. (c–f) Different synthetic routes were explored to protect the amine in the azetidine core of **A3**. Condition **ii**: THF, RT, 1.5 h; DCE, RT, 1.5 h; DCE, TEA, RT, 1.5 h.

(a)



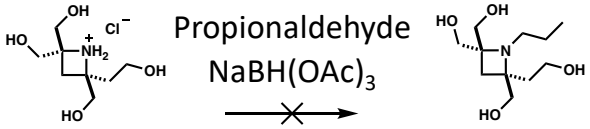
2 **A3**

(b)



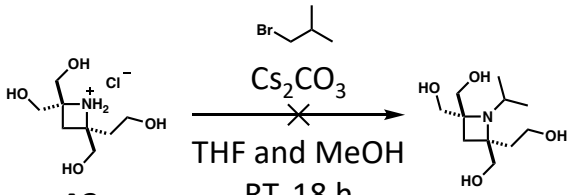
A3

(c)



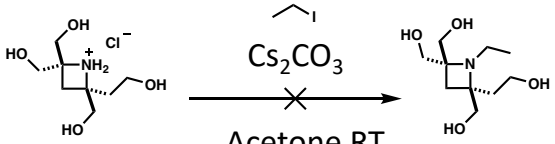
A3

(d)



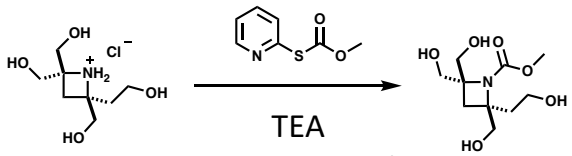
A3

(e)



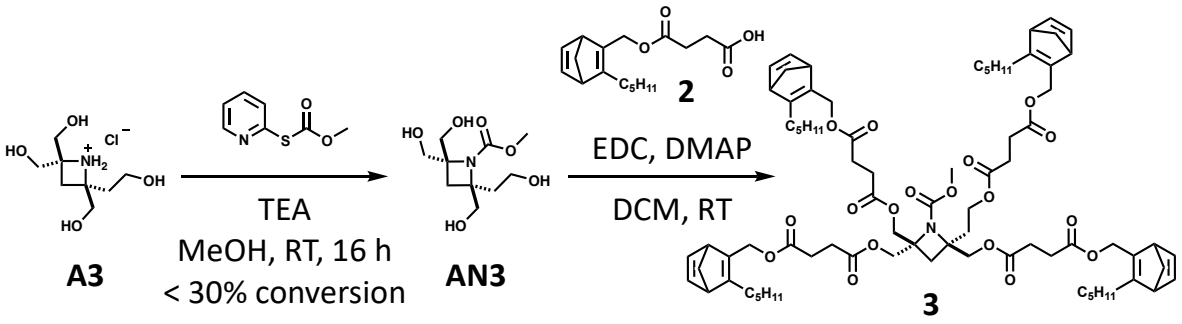
A3

(f)



A3

Scheme S6.2. Successful synthetic route to access an azetidine-NBD derivative **3** as the preliminary reaction condition screening.



Synthesis of compound **1**:

To a dried 150 mL round-bottom flask were added compound **2** (1.0 g, 3.4 mmol, 1.0 eq.), and 1,12-dodecanediol (3.5 g, 17 mmol, 5.0 eq.) in 80 mL DCM. To this solution were added EDC (1.6 g, 8.5 mmol, 2.5 eq.) and DMAP (120 mg, 1.0 mmol, 0.3 eq.). Once added, the solution was allowed to stir at room temperature for 24 h. The solution was concentrated and the crude mixture was subjected to a flash column chromatography with two solvent systems, 1:6 ethyl acetate (EtOAc):hexanes and 50% EtOAc/hexnes, to afford the pure intermediate alcohol product. The intermediate compound was re-subjected to the ring opening of succinic anhydride. To a 25-mL dried round-bottom flask was added the intermediate alcohol compound, succinic anhydride (420 mg, 4.2 mmol). DMAP (80 mg, 0.7 mmol) and TEA (0.5 mL) in 10 mL DCM. The reaction was stirred at RT for 1.5 h and additional DCM was added along with 1M HCl. The organic layer was extracted and washed 2 more times with water and dried over Na_2SO_4 and filtered. Concentration of the filtrate affords the pure product **1** as a colorless oil (1.2 g, 60% yield). ^{1}H NMR (500 MHz, $CDCl_3$) δ 6.76 (dd, J = 5.3, 2.9

Hz, 1H), 6.70 (dd, *J* = 5.2, 2.9 Hz, 1H), 4.74 (d, *J* = 12.2 Hz, 1H), 4.58 (d, *J* = 12.2 Hz, 1H), 4.08 (t, *J* = 6.8 Hz, 2H), 3.64 (td, *J* = 6.7, 5.4 Hz, 2H), 3.44 (s, 1H), 3.37 (s, 1H), 2.62 (d, *J* = 2.0 Hz, 4H), 2.22 (dt, *J* = 14.4, 7.0 Hz, 1H), 2.18 – 2.09 (m, 2H), 1.94 (dt, *J* = 5.8, 1.7 Hz, 1H), 1.91 – 1.86 (m, 1H), 1.66 – 1.55 (m, 4H), 1.44 – 1.24 (m, 26H), 1.22 – 1.14 (m, 3H), 0.87 (t, *J* = 7.3 Hz, 3H).

Synthesis of compound **AN3**:

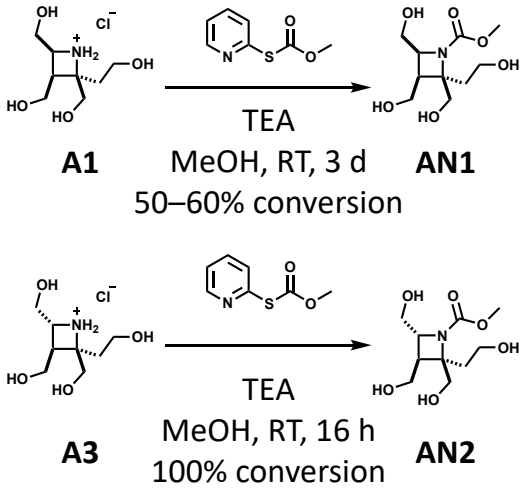
To a 20-mL vial were added 40 mg of **A3** (0.18 mmol, 1.0 eq.), the carbonothiolate reagent (45 mg, 0.26 mmol, 1.5 eq.) and triethylamine (TEA, 25 µL, 0.18 mmol, 1.0 eq.) in 2 mL dried methanol. The mixture was stirred at RT for 16 h. The reaction displays a 30% conversion to the product **AN3**. No workup or purification were performed, and the crude product was carried to the next-step reaction.

Synthesis of compound **3**:

To a 20-mL vial were added **AN3** (24 mg, 0.10 mmol, 1.0 eq.), compound **2** (120 mg, 0.40 mmol, 4.1 eq.), EDC reagent (150 mg, 0.78 mmol, 8.0 eq.), and 4-(dimethylamino)pyridine (DMAP, 5 mg, 0.04 mmol, 0.4 eq.) in 10 mL DCM. The solution was stirred at RT for 24 h. The reaction was worked up with water. Additional DCM was used to extract the product. The organic layer was dried over anhydrous Na_2SO_4 and concentrated. The crude residue was subjected to flash column chromatography with 30% ethyl acetate (EtOAc):Hexanes to afford the pure product **3**. Analysis of the structure of **3** was performed

using ^{1}H NMR, heteronuclear multiple bond correlation (HMBC) NMR spectroscopy and mass spectrometry with the spectra shown in Figure S6.3–S6.5.

Scheme S6.3. *N*-acetylation of **A1** and **A2** leads to varied conversion with full conversion of **A2** to **AN2** compared to 50–60% conversion of **A1** to **AN1**.



Synthesis of compound **AN1**:

AN1 was prepared in a procedure similar to the one used to produce compound **AN3**. A solution of **A1** (40 mg), carbonothiolate (45 mg), and TEA (25 µL) in 2 mL methanol was stirred for 3 days at RT to afford **AN1** with a 50–60% conversion. The crude product was subjected to the next step without workup or purification.

Synthesis of compound **AN2**:

AN2 was prepared in a procedure similar to the one used to produce compound **AN3**. A solution of **A2** (40 mg), carbonothiolate (45 mg), and TEA (25 µL) in 2 mL methanol was stirred for 16 h at RT to afford **AN2** with a 100% conversion. The crude product was subjected to the next step without workup or purification.

Synthesis of compound **N1**:

To a dried 250 mL round bottom were added compound **AN1** (44 mg, 0.18 mmol, 1.0 eq.), compound **1** (415 mg, 0.72 mmol, 4.1 eq.) and 4.4 mL DCM. To this solution were added EDC (270 mg, 1.4 mmol, 8.0 eq.) and DMAP (8.6 mg, 0.07 mmol, 0.4 eq.). Once added, the solution was allowed to stir at room temperature for 24 h. The crude solution was concentrated and subjected to flash column chromatography with a gradient solvent system from 1:6 EtOAc:Hexanes to 30% EtOAC/Hexanes to afford the product **N1** as a colorless oil (91 mg, 20% yield, two steps). R_f of the product is 0.75 in 30% EtOAc:Hexanes. Full ^{1}H NMR spectrum of **N1** in $CDCl_3$ is shown in Figure S6.7.

Synthesis of compound **N2**:

N2 was prepared in a procedure similar to the one used to produce compound **N1** with the same amount of reagents and solvent. After purification, product **N2** was obtained as a colorless oil (180 mg, 40% yield, two steps). Full ^{1}H NMR spectrum of **N2** in $CDCl_3$ is shown in Figure S6.8.

Synthesis of compound **N3**:

N3 was prepared in a procedure similar to the one used to produce compound **N1**. To a dried 250 mL round bottom were added compound **AN3** (20 mg, 0.08 mmol, 1.0 eq.), compound **1** (187 mg, 0.3 mmol, 4.1 eq.) and 2.0 mL DCM. To this solution were added EDC (123 mg, 0.6 mmol, 8.0 eq.) and DMAP (4.0 mg, 0.03 mmol, 0.4 eq.). Once added, the solution was allowed to stir at room temperature for 24 h. The crude solution was concentrated and

subjected to flash column chromatography with a gradient solvent system from 1:6 EtOAc:Hexanes to 30% EtOAC/Hexanes to afford the product **N3** as a colorless oil (30 mg, 15% yield, two steps). Full ^{1}H NMR spectrum of **N3** in $CDCl_3$ is shown in Figure S6.9.

Synthesis of compound **C1**:

A solution of compound **N1** (45 mg, 0.02 mmol, 1.0 eq.) and dipyridyl tetrazine (DpTz) (45 mg, 0.2 mmol, 10.5 eq.) in 2.0 mL DCM was stirred at room temperature for 2 h. The crude solution was passed through a plug of silica with DCM as the eluent. After the silica plug, concentration of the filtrate afforded the product **C1** as a transparent oil (6 mg) that is contaminated with a small amount of presumably pyridazine derivative impurity. ^{1}H NMR spectrum of **C1** in $CDCl_3$ is shown in Figure S6.10.

Synthesis of compound **C2**:

A solution of compound **N2** (88 mg, 0.04 mmol, 1.0 eq.) and DpTz (90 mg, 0.4 mmol, 10.5 eq.) in 4.0 mL DCM was stirred at room temperature for 2 h. The crude solution was passed through a plug of silica with DCM as the eluent. The yellowish band was collected. The crude mixture was concentrated and washed with cold ethanol x2 to remove the yellowish impurity. The product **C2** was collected as a transparent oil (10 mg) that is still contaminated with a small amount of presumably pyridazine derivative impurity. ^{1}H NMR spectrum of **C2** in $CDCl_3$ is shown in Figure S6.11.

Synthesis of compound **C3**:

C3 was prepared in a procedure similar to the one used to produce compound **C1**. A solution of compound **C3** (30 mg, 0.01 mmol, 1.0 eq.) and DpTz (30 mg, 0.1 mmol, 10.5 eq.) in 1.0 mL DCM was stirred at room temperature for 2 h. The crude solution was passed through a plug of silica with DCM as the eluent. After the silica plug, concentration of the filtrate afforded the product **C3** as a transparent oil (9 mg) that is contaminated with a small amount of presumably pyridazine derivative impurity. ^{1}H NMR spectrum of **C3** in $CDCl_3$ is shown in Figure S6.12.

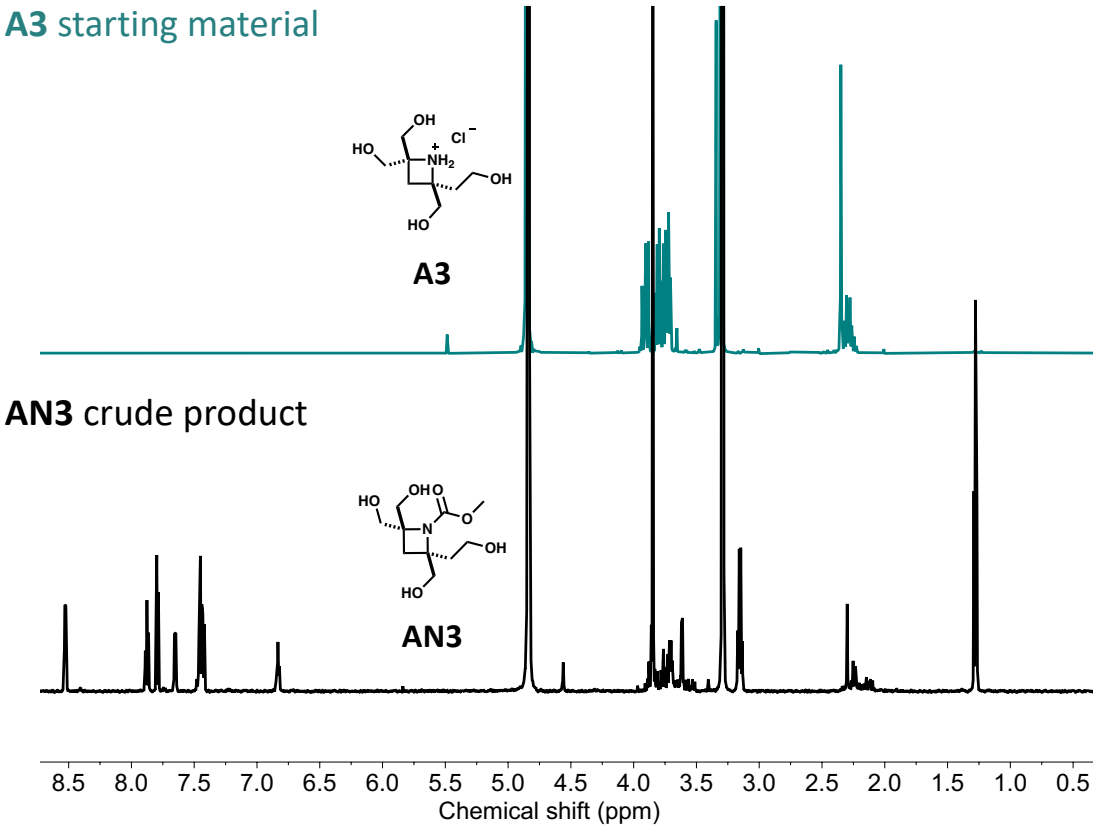


Figure S6.1. ^{1}H NMR spectrum of the **AN3** crude product compared to that of the **A3** starting material.

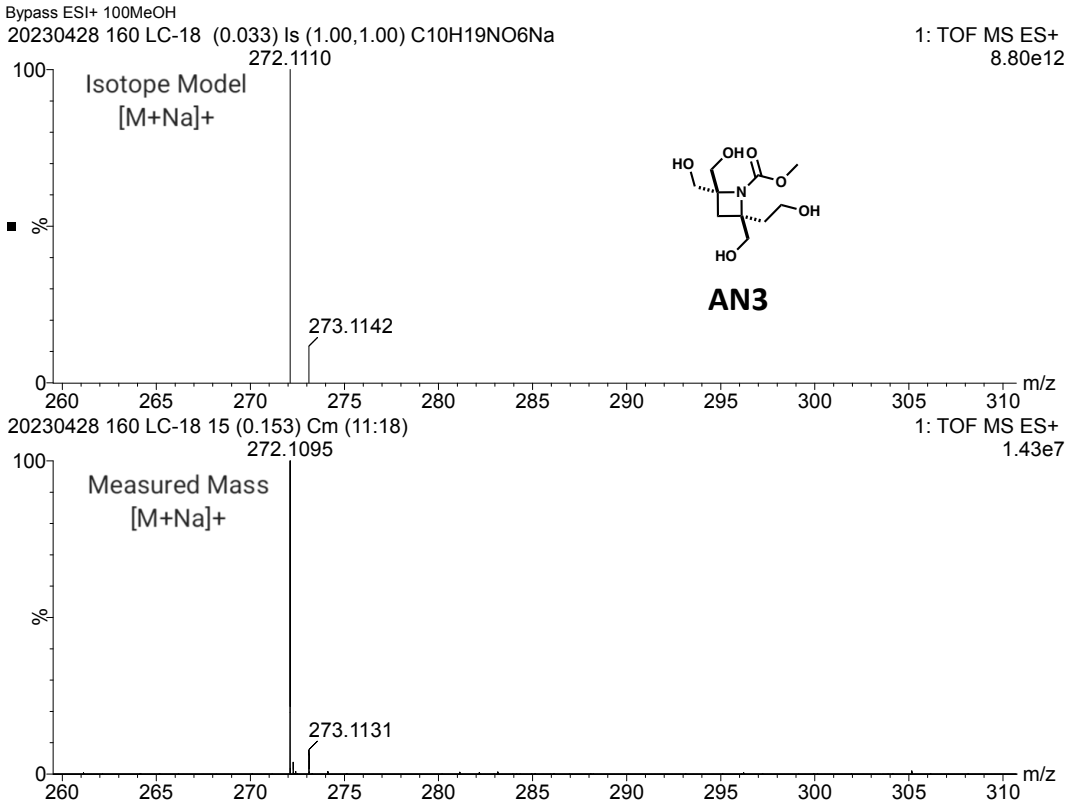


Figure S6.2. Mass spectrum of **AN3** shows the expected mass, $[M+Na]^{+}$ = 272.1095 that is comparable to the isotope model ($[M+Na]^{+}$ = 272.1110).

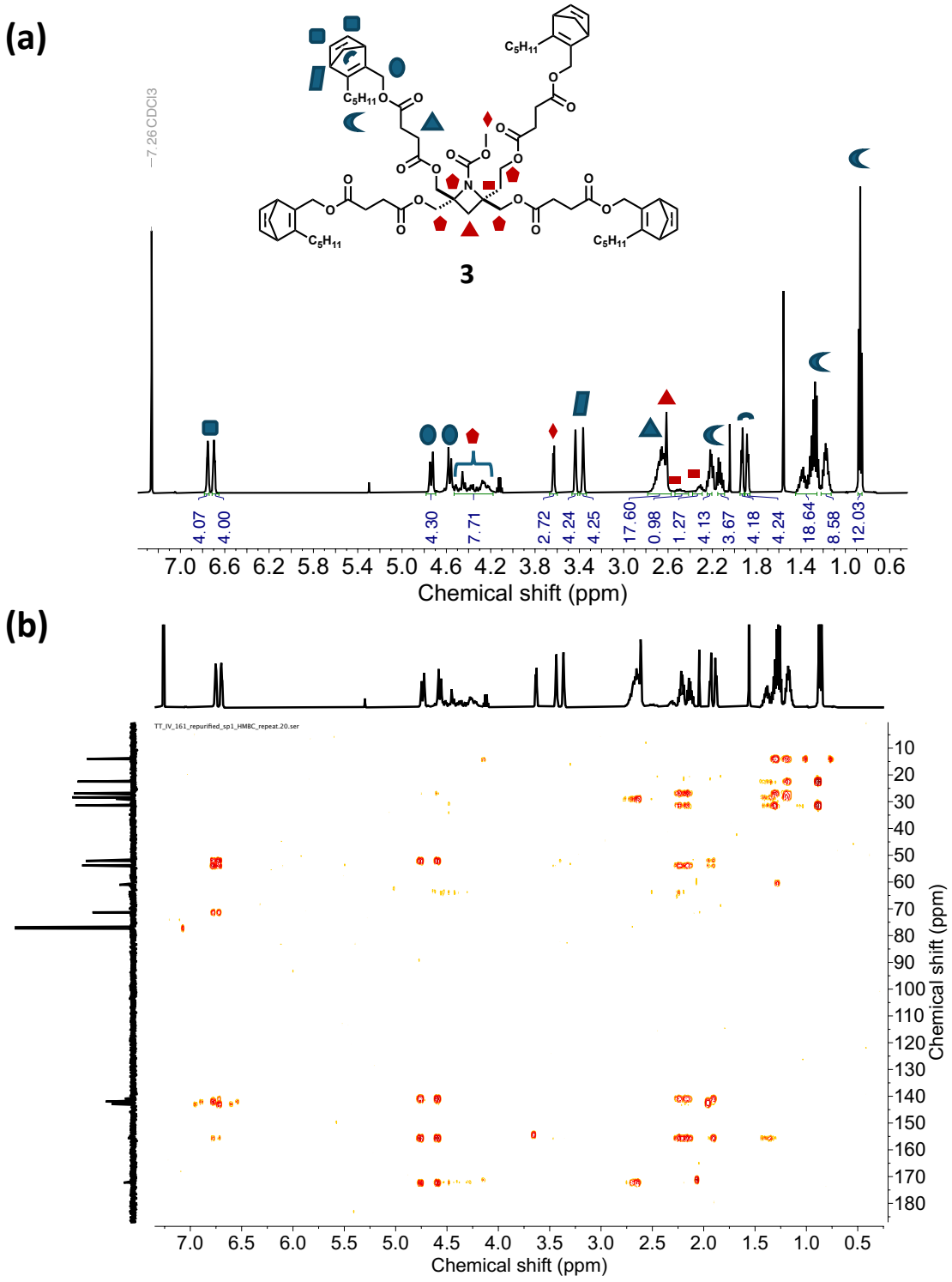

(a)
7.26 CDCl3
3
4.07
4.00
4.30
7.71
2.72
4.24
4.25
17.60
0.98
1.27
4.13
3.67
4.18
4.24
18.64
8.58
12.03
7.0 6.6 6.2 5.8 5.4 5.0 4.6 4.2 3.8 3.4 3.0 2.6 2.2 1.8 1.4 1.0 0.6
Chemical shift (ppm)
(b)
TT_IV_161_repurified_sp1_HMBC_repeat.20.ser
10 20 30 40 50 60 70 80 90 100 110 120 130 140 150 160 170 180
Chemical shift (ppm)
7.0 6.5 6.0 5.5 5.0 4.5 4.0 3.5 3.0 2.5 2.0 1.5 1.0 0.5
Chemical shift (ppm)

Figure S6.3. (a) ^{1}H NMR spectrum and (b) heteronuclear multiple bond correlation (HMBC) NMR of compound **3** in $CDCl_3$.

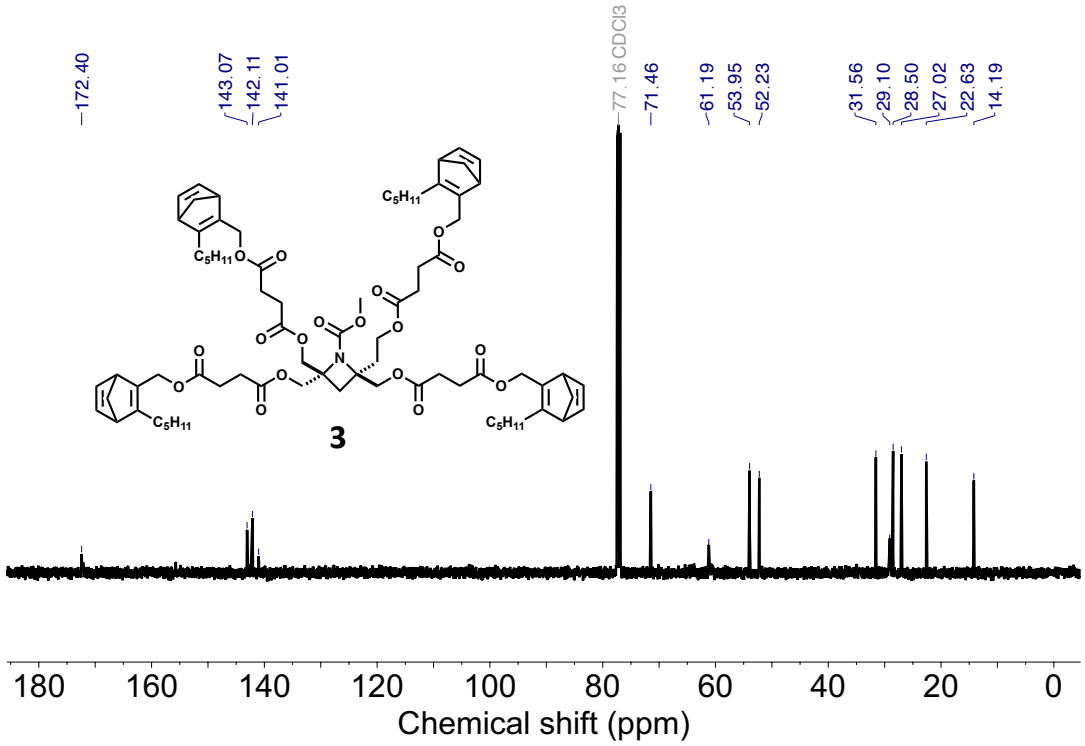


Figure S6.4. ^{13}C NMR spectrum of **3** in $CDCl_3$.

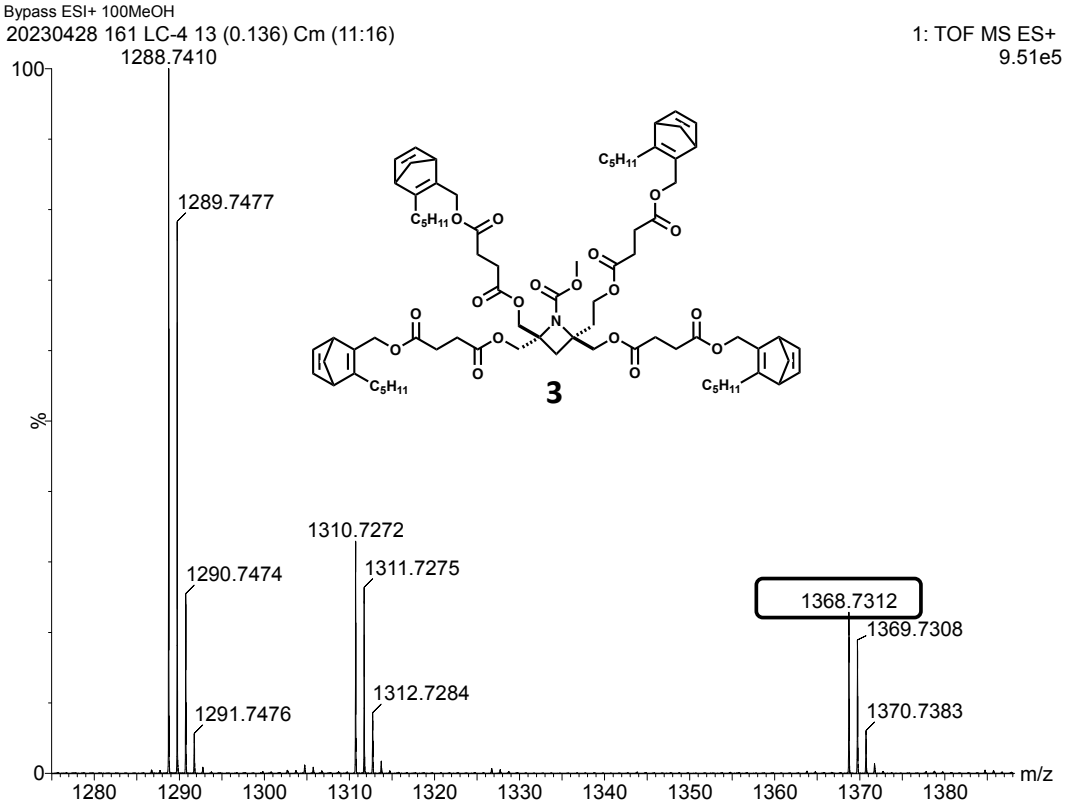


Figure S6.5. Mass spectrum of **3** shows the expected mass, $[M+Na]^+$ = 1368.7312 that is comparable to the calculated mass ($[M+Na]^+$ = 1368.7386).

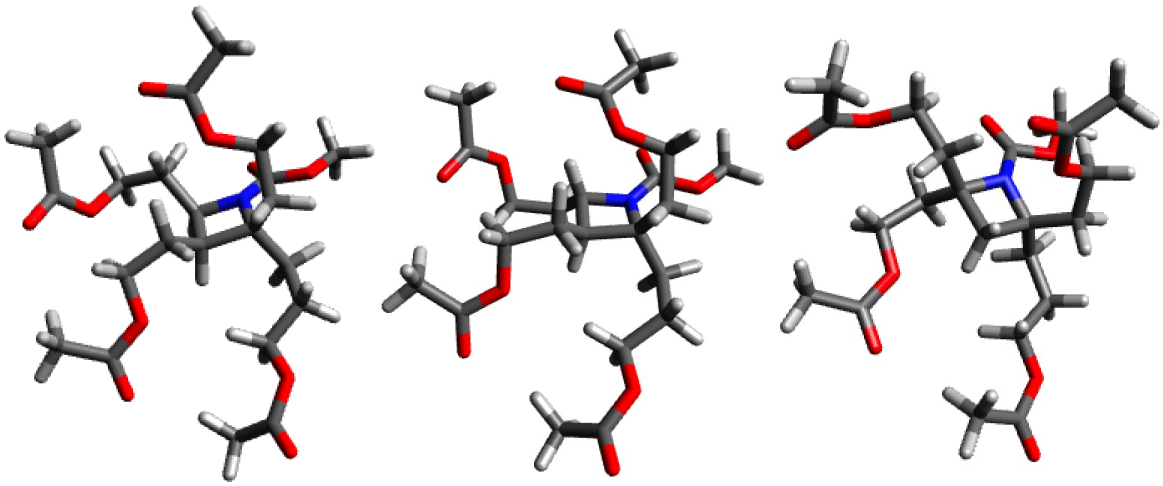


Figure S6.6. The 3D chemical structures (stick models) of the small molecules, azetidine (**A1**–**A3**).

^{1}H NMR Spectra:

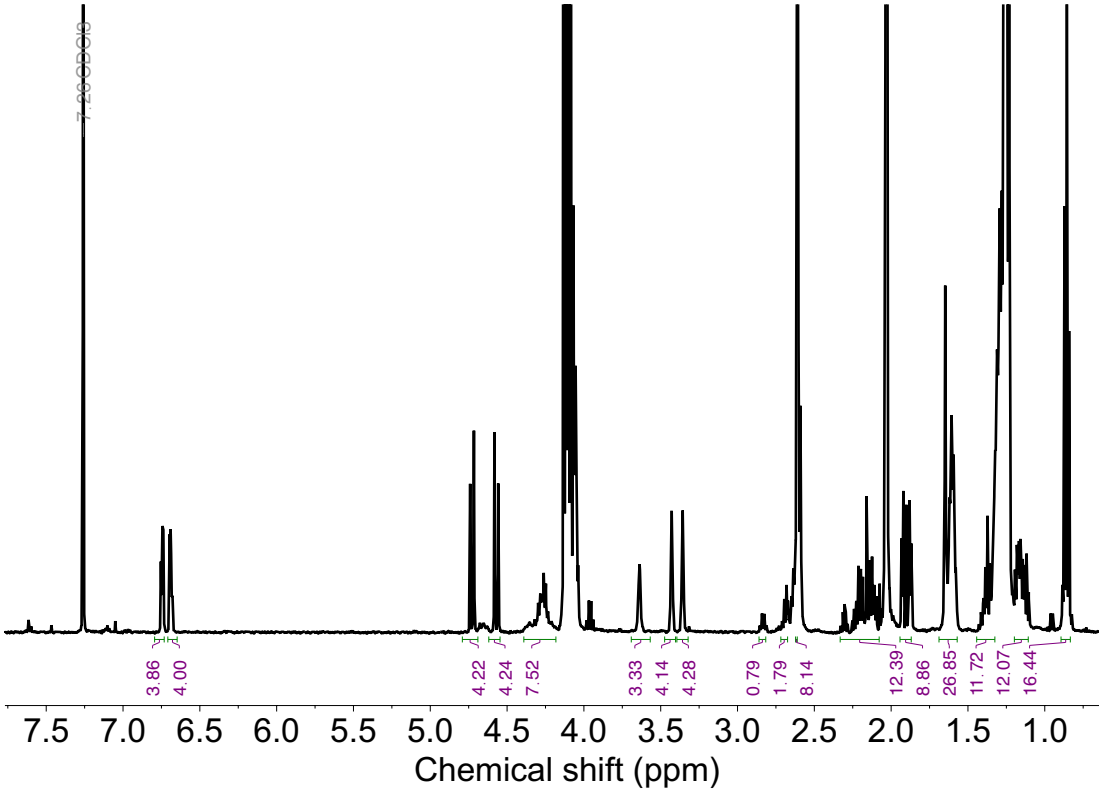


Figure S6.7. ^{1}H NMR spectrum of **N1** in $CDCl_3$.

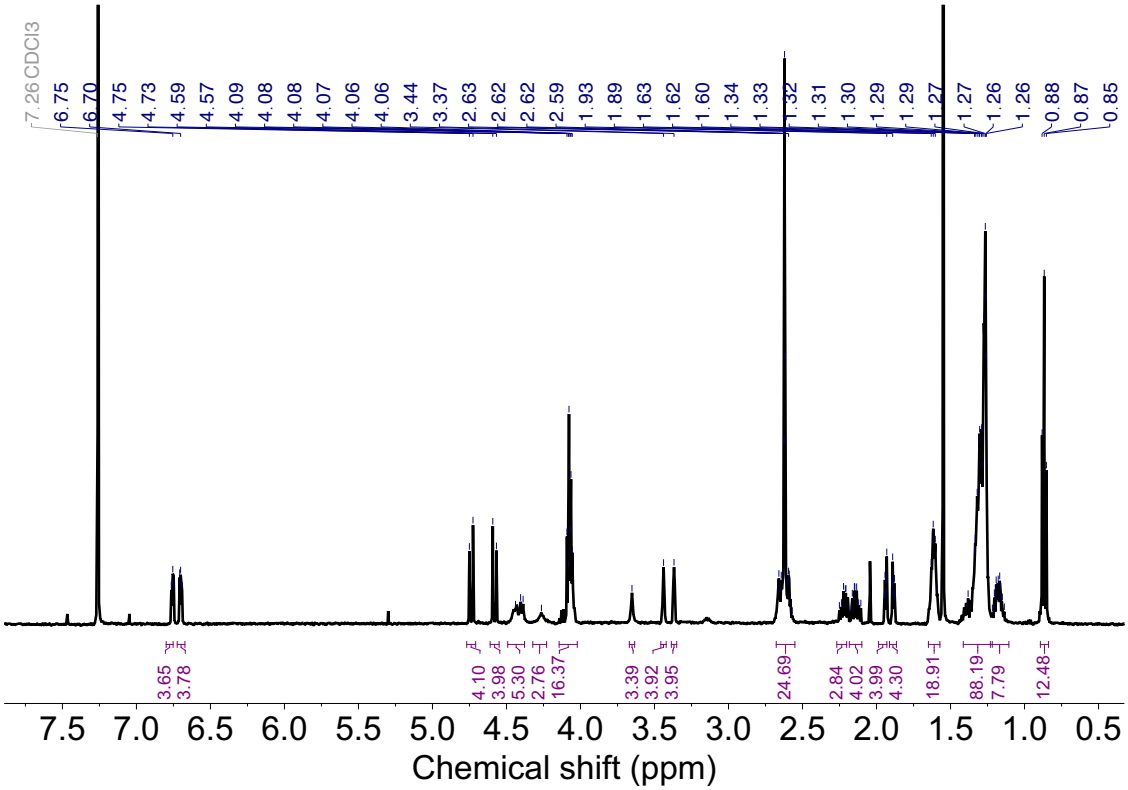


Figure S6.8. ^{1}H NMR spectrum of **N2** in $CDCl_3$.

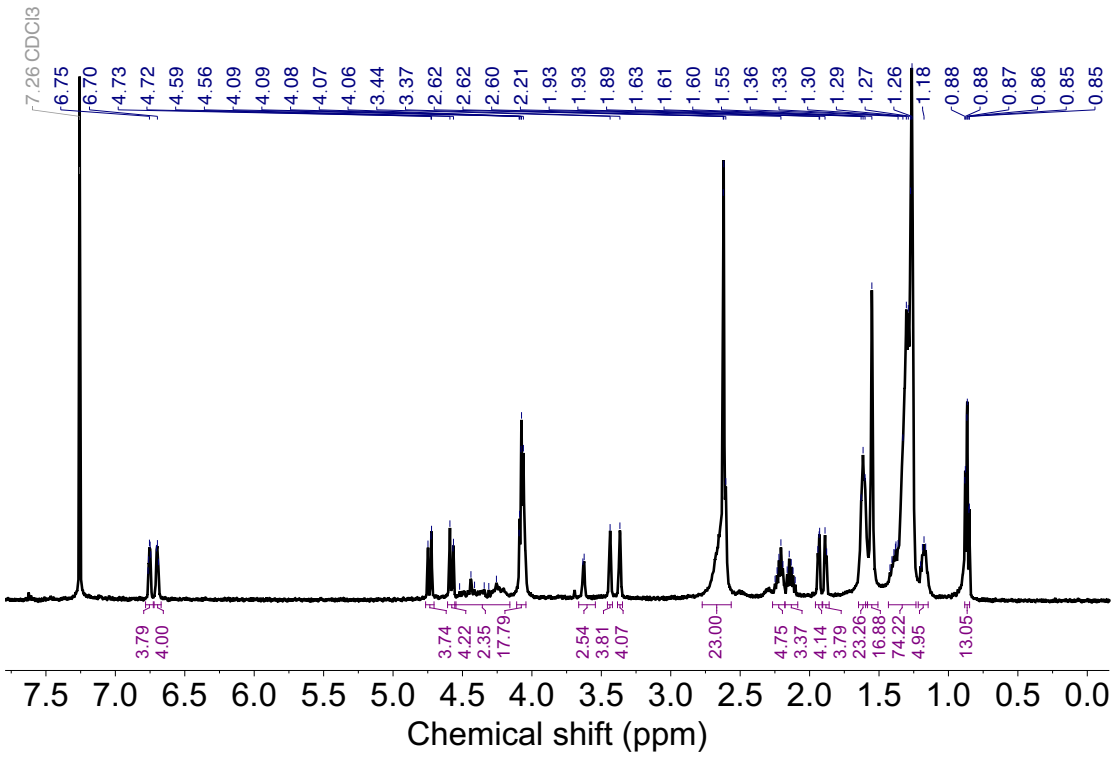


Figure S6.9. ^{1}H NMR spectrum of **N3** in $CDCl_3$.

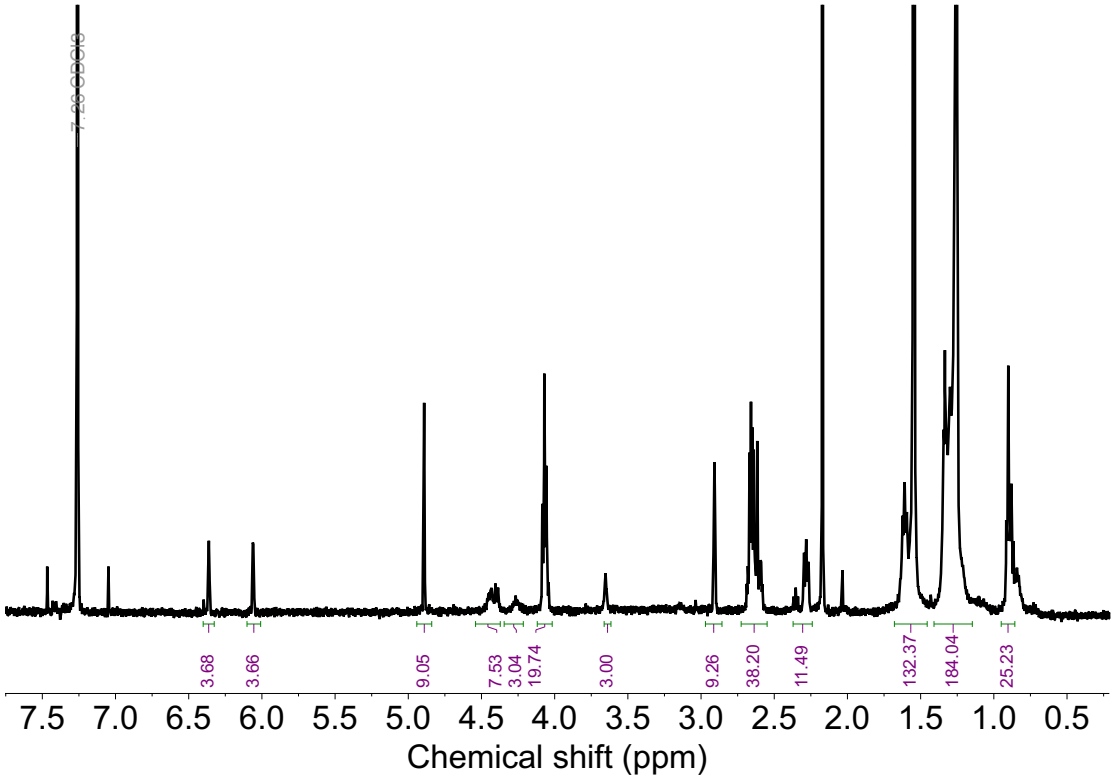


Figure S6.10. ^{1}H NMR spectrum of **C1** in $CDCl_3$.

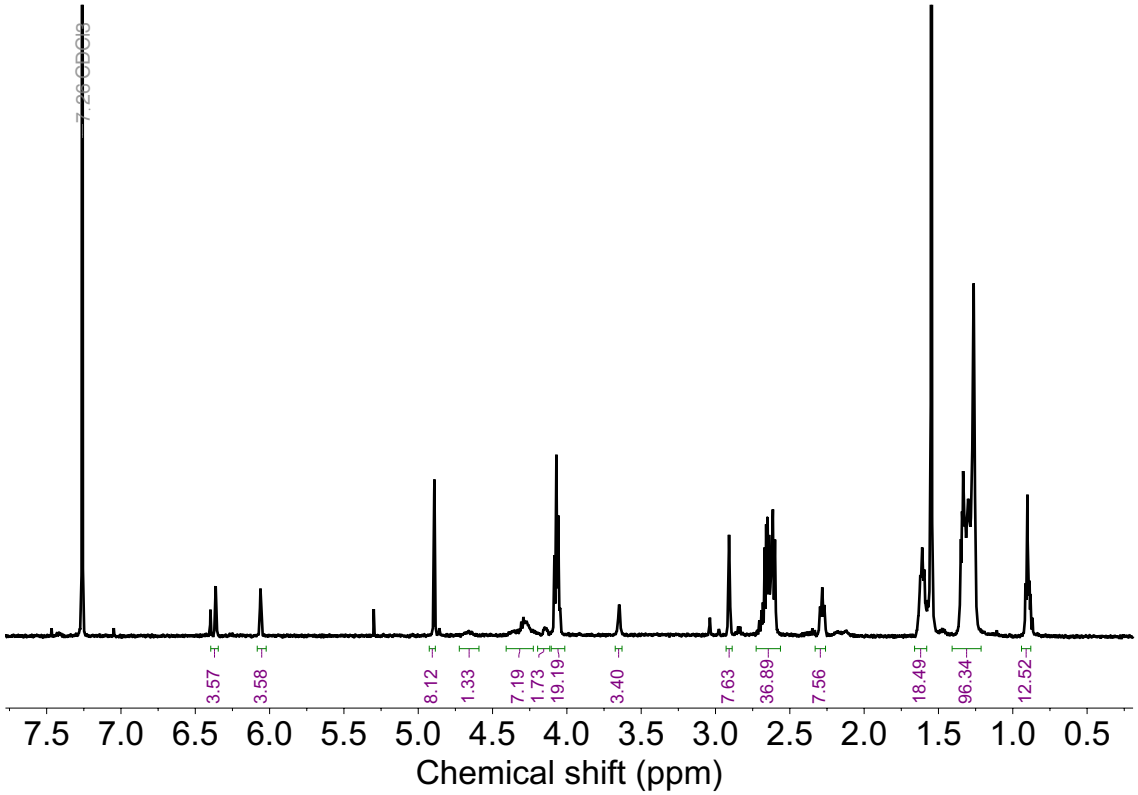


Figure S6.11. ^{1}H NMR spectrum of **C2** in $CDCl_3$.

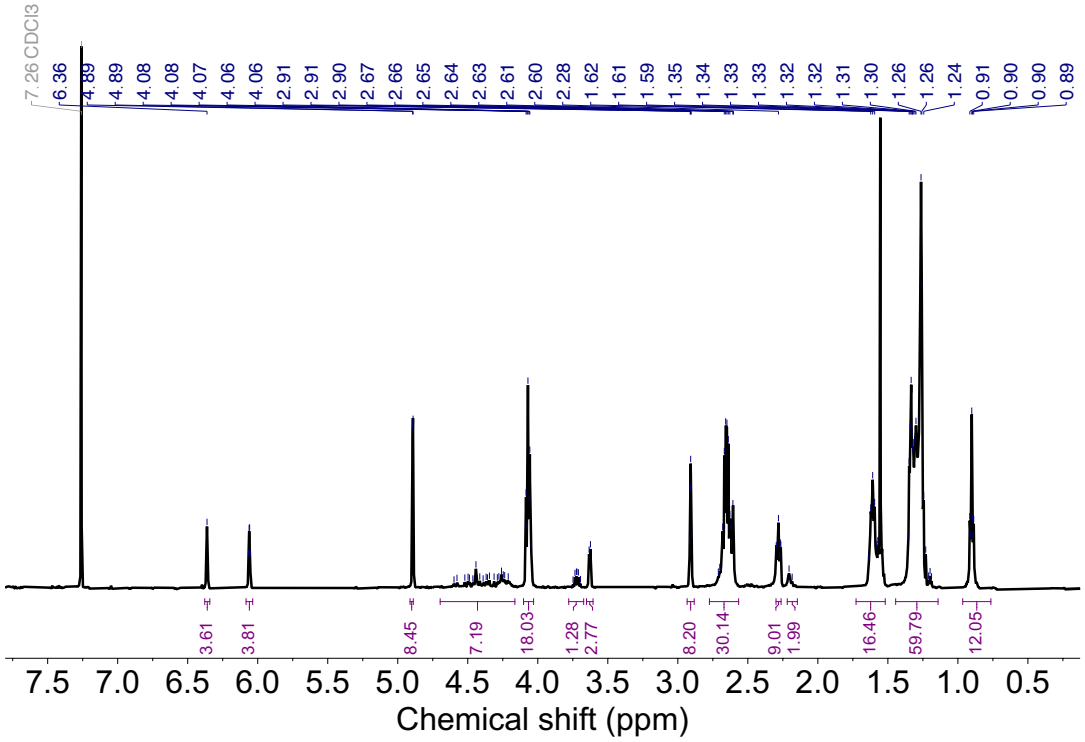


Figure S6.12. ^{1}H NMR spectrum of **C3** in $CDCl_3$.

Characterization methods. ^{1}H NMR spectra were recorded on Varian and Bruker spectrometers (400, 500, or 600 MHz) and are reported relative to the residual protio-signal in deuterated solvents. Data for ^{1}H NMR spectra are reported as follows: chemical shift (δ ppm), multiplicity, coupling constant (Hz) and integration. ^{13}C NMR spectra were recorded on Varian Spectrometers (500 MHz). Data for ^{13}C NMR spectra are reported in terms of chemical shift (δ ppm). Mass spectra were obtained using Waters Acquity H-class Ultra High Pressure Liquid Chromatography (UPLC) system coupled with a Waters Xevo G2-XS Time-of-Flight Mass Spectrometer with an ESI or ASAP source. Differential scanning calorimetry

(DSC) was performed on a liquid-nitrogen-cooled TA Instruments Q2000 DSC system at a heating rate of 10 °C/min under a nitrogen atmosphere with a sensitivity < 0.2 μW and a baseline drift < 10 μW. The amount of materials in the thermal pans is ~ 5–6 mg. The isothermal experiments were performed by heating the sample at a certain temperature and collect data for typically 100–120 min.

6.8 References

(1) Worch, J. C.; Prydderch, H.; Jimaja, S.; Bexis, P.; Becker, M. L.; Dove, A. P. Stereochemical Enhancement of Polymer Properties. *Nat. Rev. Chem.* **2019**, *3*, 514–535. DOI: 10.1038/s41570-019-0117-z.

(2) Petersen, S. R.; Prydderch, H.; Worch, J. C.; Stubbs, C. J.; Wang, Z.; Yu, J.; Arno, M. C.; Dobrynin, A. V.; Becker, M. L.; Dove, A. P. Ultra-Tough Elastomers from Stereochemistry-Directed Hydrogen Bonding in Isosorbide-Based Polymers. *Angew. Chem. Int. Ed.* **2022**, *61*, e202115904. DOI: 10.1002/anie.202115904.

(3) Macdougall, L. J.; Pérez-Madrigal, M. M.; Shaw, J. E.; Worch, J. C.; Sammon, C.; Richardson, S. M.; Dove, A. P. Using Stereochemistry to Control Mechanical Properties in Thiol–Yne Click-Hydrogels. *Angew. Chem. Int. Ed.* **2021**, *60*, 25856–25864. DOI: 10.1002/anie.202107161.

(4) Varnava, C. K.; Patrickios, C. S. Polymer Networks One Hundred Years after the Macromolecular Hypothesis: A Tutorial Review. *Polymer* **2021**, *215*, 123322. DOI: 10.1016/j.polymer.2020.123322.

(5) Whittaker, A. K. The Structure of Polymer Networks. In *Modern Magnetic Resonance*; Webb, G. A., Ed.; Springer Netherlands: Dordrecht, 2006; pp 583–589. DOI: 10.1007/1-4020-3910-7_74.

(6) *Cross-Linked Polymers: Chemistry, Properties, and Applications*; Dickie, R. A., Labana, S. S., Bauer, R. S., Eds.; ACS Symposium Series; American Chemical Society: Washington, DC, 1988; Vol. 367. DOI: 10.1021/bk-1988-0367.

(7) Parada, G. A.; Zhao, X. Ideal Reversible Polymer Networks. *Soft Matter* **2018**, *14*, 5186–5196. DOI: 10.1039/C8SM00646F.

(8) Sakai, T.; Akagi, Y.; Kondo, S.; Chung, U. Experimental Verification of Fracture Mechanism for Polymer Gels with Controlled Network Structure. *Soft Matter* **2014**, *10*, 6658–6665. DOI: 10.1039/C4SM00709C.

(9) Akagi, Y.; Katashima, T.; Katsumoto, Y.; Fujii, K.; Matsunaga, T.; Chung, U.; Shibayama, M.; Sakai, T. Examination of the Theories of Rubber Elasticity Using an Ideal Polymer Network. *Macromolecules* **2011**, *44*, 5817–5821. DOI: 10.1021/ma201088r.

(10) Marco-Dufort, B.; Iten, R.; Tibbitt, M. W. Linking Molecular Behavior to Macroscopic Properties in Ideal Dynamic Covalent Networks. *J. Am. Chem. Soc.* **2020,** *142*, 15371–15385. DOI: 10.1021/jacs.0c06192.

(11) Akagi, Y.; Gong, J. P.; Chung, U.; Sakai, T. Transition between Phantom and Affine Network Model Observed in Polymer Gels with Controlled Network Structure. *Macromolecules* **2013**, *46*, 1035–1040. DOI: 10.1021/ma302270a.

(12) Gu, Y.; Zhao, J.; Johnson, J. A. Polymer Networks: From Plastics and Gels to Porous Frameworks. *Angew. Chem. Int. Ed.* **2020**, *59*, 5022–5049. DOI: 10.1002/anie.201902900.

(13) Gu, Y.; Zhao, J.; Johnson, J. A. A (Macro)Molecular-Level Understanding of Polymer Network Topology. *Trends Chem.* **2019**, *1*, 318–334. DOI: 10.1016/j.trechm.2019.02.017.

(14) Hild, G. Model Networks Based on `endlinking' Processes: Synthesis, Structure and Properties. *Prog. Polym. Sci.* **1998**, *23*, 1019–1149. DOI: 10.1016/S0079-6700(97)00055-5.

(15) Matsunaga, T.; Sakai, T.; Akagi, Y.; Chung, U.; Shibayama, M. Structure Characterization of Tetra-PEG Gel by Small-Angle Neutron Scattering. *Macromolecules* **2009**, *42*, 1344–1351. DOI: 10.1021/ma802280n.

(16) Zhong, M.; Wang, R.; Kawamoto, K.; Olsen, B. D.; Johnson, J. A. Quantifying the Impact of Molecular Defects on Polymer Network Elasticity. *Science* **2016**, *353*, 1264–1268. DOI: 10.1126/science.aag0184.

(17) Wang, R.; Johnson, J. A.; Olsen, B. D. Odd–Even Effect of Junction Functionality on the Topology and Elasticity of Polymer Networks. *Macromolecules* **2017**, *50*, 2556–2564. DOI: 10.1021/acs.macromol.6b01912.

(18) Wu, B.; Chassé, W.; Peters, R.; Brooijmans, T.; Dias, A. A.; Heise, A.; Duxbury, C. J.; Kentgens, A. P. M.; Brougham, D. F.; Litvinov, V. M. Network Structure in Acrylate Systems: Effect of Junction Topology on Cross-Link Density and Macroscopic Gel Properties. *Macromolecules* **2016**, *49*, 6531–6540. DOI: 10.1021/acs.macromol.6b01070.

(19) Tran, T. M.; Read de Alaniz, J. Controlled Synthesis of a Homopolymer Network Using a Well-Defined Single-Component Diels–Alder Cyclopentadiene Monomer. *J. Am. Chem. Soc.* **2023**, *145*, 3462–3469. DOI: 10.1021/jacs.2c11416.

(20) Barton, L. M.; Edwards, J. T.; Johnson, E. C.; Bukowski, E. J.; Sausa, R. C.; Byrd, E. F. C.; Orlicki, J. A.; Sabatini, J. J.; Baran, P. S. Impact of Stereo- and Regiochemistry on Energetic Materials. *J. Am. Chem. Soc.* **2019**, *141*, 12531–12535. DOI: 10.1021/jacs.9b06961.

(21) Rykaczewski, K. A.; Becker, M. R.; Anantpur, M. J.; Sausa, R. C.; Johnson, E. C.; Orlicki, J. A.; Bukowski, E. J.; Sabatini, J. J.; Schindler, C. S. Photochemical Strategies Enable the Synthesis of Tunable Azetidine-Based Energetic Materials. *J. Am. Chem. Soc.* **2022**, *144*, 19089–19096. DOI: 10.1021/jacs.2c08191.

(22) Suzuki, T.; Tanaka, K.; Hashimoto, Y.; Morita, N.; Tamura, O. O-Alkyl S-(Pyridin-2-Yl)Carbonothiolates: Operationally Simple and Highly Nitrogen-Selective Reagents for Alkoxy Carbonylation of Amino Groups. *Synlett.* **2020**, *31*, 899–902. DOI: 10.1055/s-0039-1690856.

(23) Peterlin, A. Crystalline Character in Polymers. *J. polym. sci., C Polym. symp.* **1965**, *9*, 61–89. DOI: 10.1002/polc.5070090106.

(24) Sheng, X.; Lee, J. K.; Kessler, M. R. Influence of Cross-Link Density on the Properties of ROMP Thermosets. *Polymer* **2009**, *50*, 1264–1269. DOI: 10.1016/j.polymer.2009.01.021.

7. Chapter 7: *Future Directions and Outlook*

As demonstrated throughout the dissertation, the controlled Diels–Alder (DA) Cp polymerization has enabled the synthesis and studies of a variety of complex and reversible cross-linked polymer architectures. The potential applications of these materials encompass high-performance thermosets, textile products, re-mendable and tough elastomers. Remarkably, the understanding of the uncontrolled cross-linking of Cp derivatives has led to the first Cp homopolymerization and the fabrication of a new class of thermally recyclable thermoplastics. One important note that will expand the scope of the synthetic platforms is the investigation to completely impede the radical cross-linking in these materials. Butylated hydroxytoluene (BHT) was utilized as the most promising radical inhibitor to prevent uncontrolled cross-linking and degradation of the Cp polymers that were synthesized and studied in these projects. However, there are certain limitations of using BHT, such as its volatility at high temperature and under vacuum, which are the common conditions to fabricate and re-process most polymers. In industry, this phenomenon is well-established and multiple radical inhibitors have been developed to improve the properties and the re-processing of materials, such as TEMPO, 2,4-dinitrophenol (DNP), and 2,4-dinitro-6-sec-butyl phenol (DNBP).[1] Extensive exploration of different radical inhibitors will potentially reveal the enhanced synthetic platform to access advanced functional and tailored Cp materials.

The realization of Cp monomers for step-growth polymerization will deliver multiple exciting pathways for the polymer field due to the accessibility and wide scope of the chain-end building blocks. As discussed in Chapter 3, the backbones of the linear Cp polymer can be modified with a variety of common polymers through the alteration of the chain-end building blocks. We have explored polysiloxane, ethylene terephthalate, urethane, and hydroxylated polybutadiene. There are other types of polymers that will be intriguing to investigate, especially vinyl-type polymers. Notably, the reversible dimerization of Cp does not require the presence of heteroatoms as in other methods (i.e., polycondensation and disulfide bonding). Therefore, the unique approach can be realized using Cp homopolymerization platform to degrade and recycle the C–C based polymers without the presence of heteroatoms (**Figure 7.1**). Increasingly intricate starting materials can also be achieved with the same approach by introduction of complex architectures into the backbone of the building blocks. For example, the construction of cyclic Cp monomers proposes exciting synthetic routes to access new multi-cyclic architectures (i.e., spiro-multicyclic polymers) that are formed entirely by reversible covalent bonding (**Figure 7.1**).

The efficient utilization of Cp derivatives as the new building blocks for the construction of thermos-reversible DA polymers will potentially expand the chemical toolbox to fabricate multi-responsive advanced functional materials. For example, the high retro-DA (rDA) temperatures of Cp-dimer (i.e., 150–180 °C) or Cp-maleimide (i.e., ~150 °C) add to the library of re-mendable polymers with a wide range of usable temperatures. Therefore, combining Cp-

dimer or Cp-maleimide moieties with other known DA adducts, such as furan-maleimide (rDA temperature of 100–120 °C) or anthracene-maleimide (rDA temperature of 200–250 °C), will provide the field with tailored materials that possess diverse architectures and improved multi-responsiveness. One imminent approach is the fabrication of polymer networks that are composed of Cp-dimer and furan-maleimide adducts. The materials can be potentially de-polymerized at different temperature ranges, allowing for the selective post-functionalization or enhanced thermos-selective polymer recycling (**Figure 7.1**).

As demonstrated, Cp is highly promising as the dynamic handle to fabricate re-mendable and recycling thermosets and thermoplastics with increasingly intricate polymer architectures. Another aspect of Cp that holds great potential is its high reactivity as a diene and can react rapidly with a variety of different dienophiles and thus, will create a generous space for new types of materials and post-functionalization. In fact, Cp-Mal is qualified as a "click" reaction and has been utilized in our group for photopatterning[5–8] or polymer post-functionalization.[9,10] Moreover, the DA cyclic products of Cp derivatives are also favorable for a wide range of polymer post-functionalization. For instance, the ring-opening metathesis polymerization (ROMP) of dicyclopentadiene through the strained norbornene has been known to produce rubber-like materials.[11,12] Recently, ROMP has been applied to form exciting degradable[10] and mechanophore polymers.[13–15] Cp derivatives as the highly reactive dienes to form cyclic DA products are promising to be explored as starting materials for ROMP and other exciting

post-functionalized materials (e.g., hydrogenation,[16] vinyl-type polymerization[17–19]) (**Figure 7.1**).

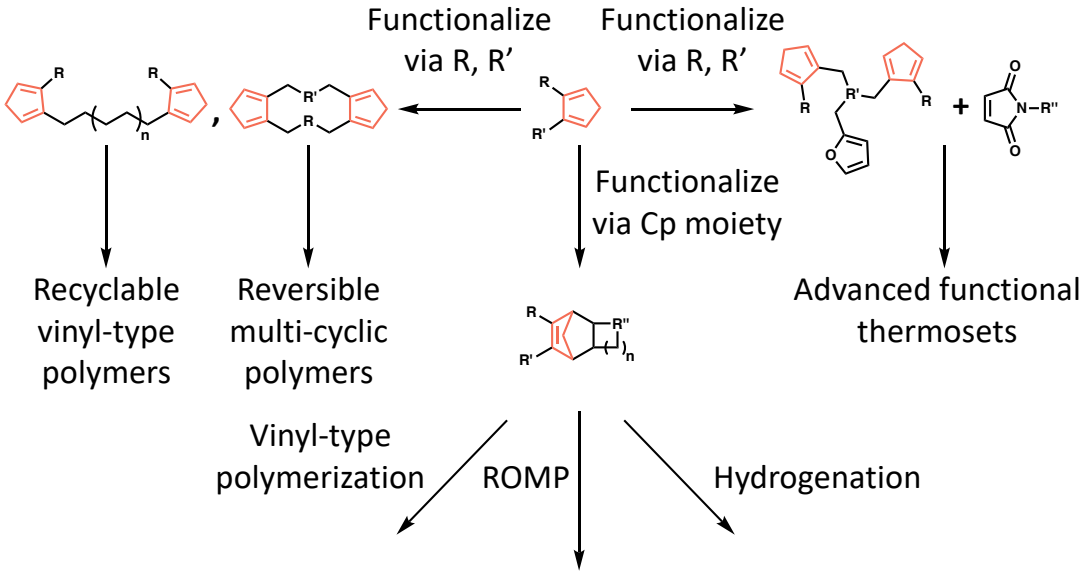


Figure 7.1. Future directions that are promising to promote the controlled Cp polymerization and reactivity. Cp derivatives can be functionalized via the R, R' group or via the Diels–Alder reaction between Cp as the diene and other dienophiles. The versatility of the group functionalization will potentially expand the chemical toolbox to synthesize and study a variety of increasingly intricate polymer architectures.

7.1 Concluding Remarks

As illustrated throughout the dissertation, the controlled Cp polymerization has enabled access to a variety of complicated and reversible polymer architectures that possess a wide range of applications from degradable elastomers, re-mendable tough thermosets, reversible physically cross-linked polymers, to thermally recyclable thermoplastics. Remarkable, Cp homopolymerization has provided the field with a new tool for reversible step-growth

polymerization, which potentially expanding the construction of increasingly complex polymeric materials. An array of future directions can be realized using these synthetic platforms, including the synthesis of multi-cyclic polymers, multi-responsive polymer networks, recyclable vinyl-type polymers, and mechanophore materials. Furthermore, the established methodology also assists in the structure-relationship correlation as the synergistic efforts to facilitate research across multi-disciplines (e.g., computational investigation, organic synthesis, polymer, and material sciences). The goals are to advance the polymer field to fabricate and study novel tailored-function and sustainable materials.

7.2 References

(1) Maafa, I. M. Inhibition of Free Radical Polymerization: A Review. *Polymers* **2023**, *15*, 488. DOI: 10.3390/polym15030488.

(2) Chen, C.; Weil, T. Cyclic Polymers: Synthesis, Characteristics, and Emerging Applications. *Nanoscale Horiz.* **2022**, *7*, 1121–1135. DOI: 10.1039/D2NH00242F.

(3) Li, B.; Cao, P.-F.; Saito, T.; Sokolov, A. P. Intrinsically Self-Healing Polymers: From Mechanistic Insight to Current Challenges. *Chem. Rev.* **2023**, *123*, 701–735. DOI: 10.1021/acs.chemrev.2c00575.

(4) St. Amant, A. H.; Huang, F.; Lin, J.; Lemen, D.; Chakiath, C.; Mao, S.; Fazenbaker, C.; Zhong, H.; Harper, J.; Xu, W.; Patel, N.; Adams, L.; Vijayakrishnan, B.; Howard, P. W.; Marelli, M.; Wu, H.; Gao, C.; Read De Alaniz, J.; Christie, R. J. A Reactive Antibody Platform for One-Step Production of Antibody–Drug Conjugates through a Diels–Alder Reaction with Maleimide. *Bioconjugate Chem.* **2019**, *30*, 2340–2348. DOI: 10.1021/acs.bioconjchem.9b00436.

(5) Bailey, S. J.; Stricker, F.; Hopkins, E.; Wilson, M. Z.; Read De Alaniz, J. Shining Light on Cyclopentadienone–Norbornadiene Diels–Alder Adducts to Enable Photoinduced Click Chemistry with Cyclopentadiene. *ACS Appl. Mater. Interfaces* **2021**, *13*, 35422–35430. DOI: 10.1021/acsami.1c08670.

(6) Bailey, S. J.; Hopkins, E.; Rael, K. D.; Hashmi, A.; Urueña, J. M.; Wilson, M. Z.; Read De Alaniz, J. Design, Synthesis, and Application of a Water-soluble Photocage for Aqueous Cyclopentadiene-based Diels-Alder Photoclick Chemistry in Hydrogels. *Angew. Chem. Int. Ed.* **2023**, *62*, e202301157. DOI: 10.1002/anie.202301157.

(7) Bailey, S. J.; Hopkins, E.; Baxter, N. J.; Whitehead, I.; De Alaniz, J. R.; Wilson, M. Z. Diels–Alder Photoclick Patterning of Extracellular Matrix for Spatially Controlled Cell Behaviors. *Adv. Mater.* **2023**, *35*, 2303453. DOI: 10.1002/adma.202303453.

(8) St. Amant, A. H.; Discekici, E. H.; Bailey, S. J.; Zayas, M. S.; Song, J.-A.; Shankel, S. L.; Nguyen, S. N.; Bates, M. W.; Anastasaki, A.; Hawker, C. J.; Read De Alaniz, J. Norbornadienes: Robust and Scalable Building Blocks for Cascade "Click" Coupling of High Molecular Weight Polymers. *J. Am. Chem. Soc.* **2019**, *141*, 13619–13624. DOI: 10.1021/jacs.9b06328.

(9) Bailey, S. J.; Discekici, E. H.; Barbon, S. M.; Nguyen, S. N.; Hawker, C. J.; Read De Alaniz, J. Norbornadiene Chain-End Functional Polymers as Stable, Readily Available Precursors to Cyclopentadiene Derivatives. *Macromolecules* **2020**, *53*, 4917–4924. DOI: 10.1021/acs.macromol.0c00967.

(10) Davidson, T. A.; Wagener, K. B.; Priddy, D. B. Polymerization of Dicyclopentadiene: A Tale of Two Mechanisms. *Macromolecules* **1996**, *29*, 786–788. DOI: 10.1021/ma950852x.

(11) Kovačič, S.; Slugovc, C. Ring-Opening Metathesis Polymerisation Derived Poly(Dicyclopentadiene) Based Materials. *Mater. Chem. Front.* **2020**, *4*, 2235–2255. DOI: 10.1039/D0QM00296H.

(12) Fishman, J. M.; Kiessling, L. L. Synthesis of Functionalizable and Degradable Polymers by Ring-Opening Metathesis Polymerization. *Angew. Chem. Int. Ed.* **2013**, *52*, 5061–5064. DOI: 10.1002/anie.201300293.

(13) Yang, J.; Horst, M.; Romaniuk, J. A. H.; Jin, Z.; Cegelski, L.; Xia, Y. Benzoladderene Mechanophores: Synthesis, Polymerization, and Mechanochemical Transformation. *J. Am. Chem. Soc.* **2019**, *141*, 6479–6483. DOI: 10.1021/jacs.9b01736.

(14) Bowser, B. H.; Craig, S. L. Empowering Mechanochemistry with Multi-Mechanophore Polymer Architectures. *Polym. Chem.* **2018**, *9*, 3583–3593. DOI: 10.1039/C8PY00720A.

(15) Chen, Z.; Zhu, X.; Yang, J.; Mercer, J. A. M.; Burns, N. Z.; Martinez, T. J.; Xia, Y. The Cascade Unzipping of Ladderane Reveals Dynamic Effects in Mechanochemistry. *Nat. Chem.* **2020**, *12*, 302–309. DOI: 10.1038/s41557-019-0396-5.

(16) Hirai, H.; Komatsuzaki, S.; Toshima, N. Selective Hydrogenation of Cyclopentadiene to Cyclopentene Using Colloidal Palladium Supported on Chelate Resin. *Bulletin of the Chemical Society of Japan* **1984**, *57*, 488–494. DOI: 10.1246/bcsj.57.488.

(17) Rapallo, A.; Ricci, G.; Porzio, W.; Arrighetti, G.; Leone, G. A Crystalline 2,3- *Exo* - Disyndiotactic Dicyclopentadiene Tetramer. *Crystal Growth & Design* **2014**, *14* (11), 5767–5772. DOI: 10.1021/cg501033f.

(18) Müller, K.; Jung, Y.; Yoon, D. Y.; Agarwal, S.; Greiner, A. Vinyl-Type Polymerization of Alkylester-Substituted Norbornenes Without Endo/Exo Separation. *Macro Chemistry & Physics* **2010**, *211*, 1595–1601. DOI: 10.1002/macp.200900647.

(19) Dall'Asta, G.; Motroni, G.; Manetti, R.; Tosi, C. Homopolymerization of Dicyclopentadiene Induced by Ziegler-Natta Catalysts and by Other Transition Metal Systems. *Makromol. Chem.* **1969**, *130*, 153–165. DOI: 10.1002/macp.1969.021300108.

8. Appendix

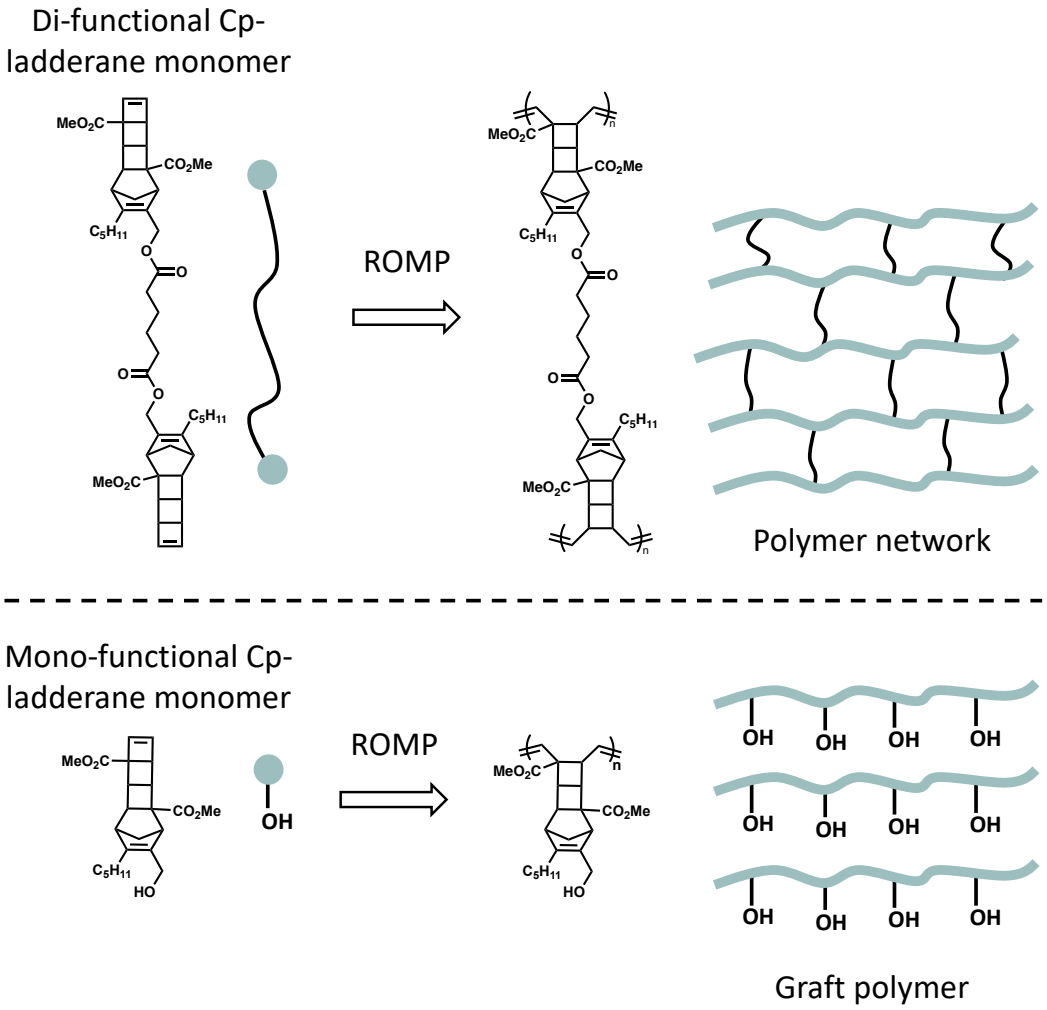


Figure 8.1. The potential exploration of a new class of cyclopentadiene (Cp)-ladderane compounds that possess promising properties of a mechanophore. Di-functional and mono-functional monomers can lead to the fabrication of polymer networks and graft polymers, respectively, through the ring opening metathesis polymerization (ROMP).

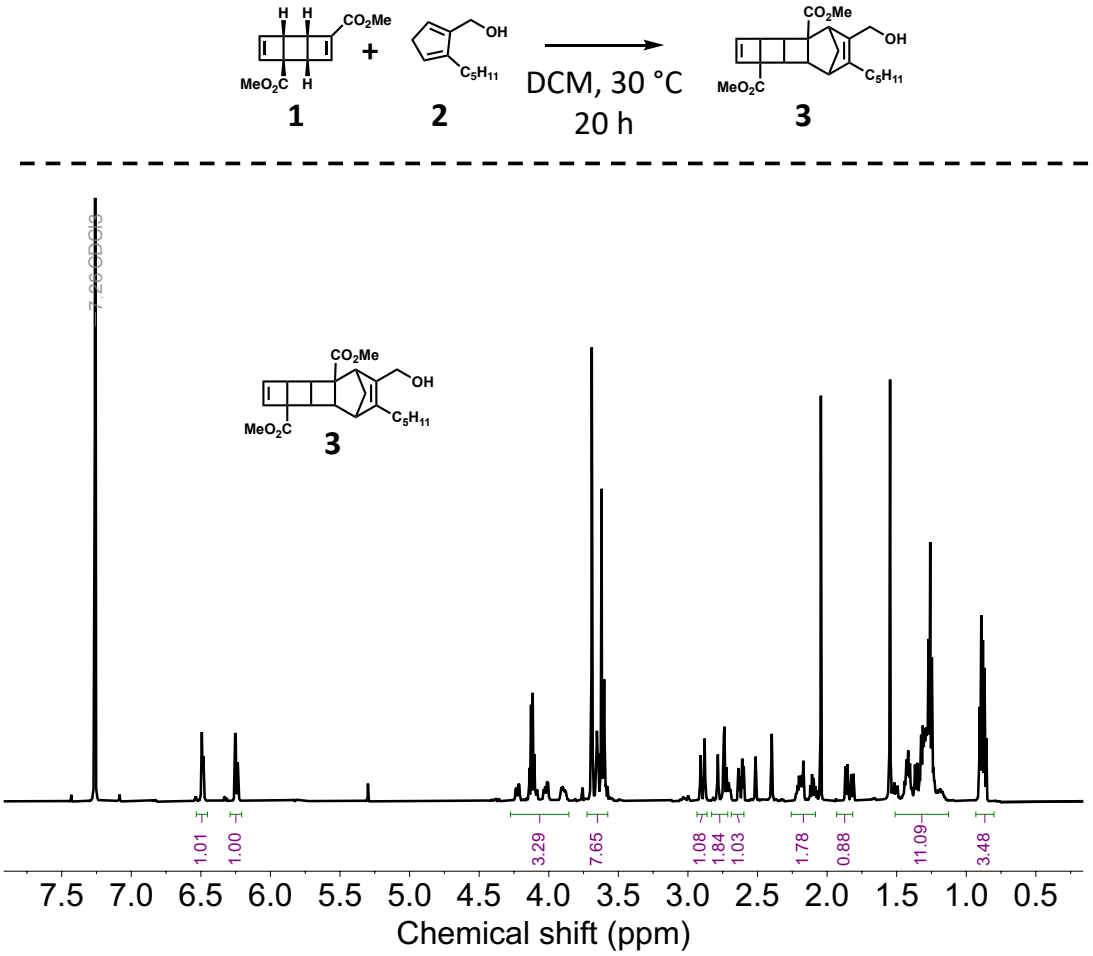


Figure 8.2. Synthetic route to access Cp-ladderane alcohol (compound **3**) from the reaction Diels–Alder reaction between Cp and ladderane (selectively at the double bond with the electron withdrawing substituent). ^{1}H NMR of compound **3** is shown in $CDCl_3$. The presence of product is also confirmed by mass spectrometry.

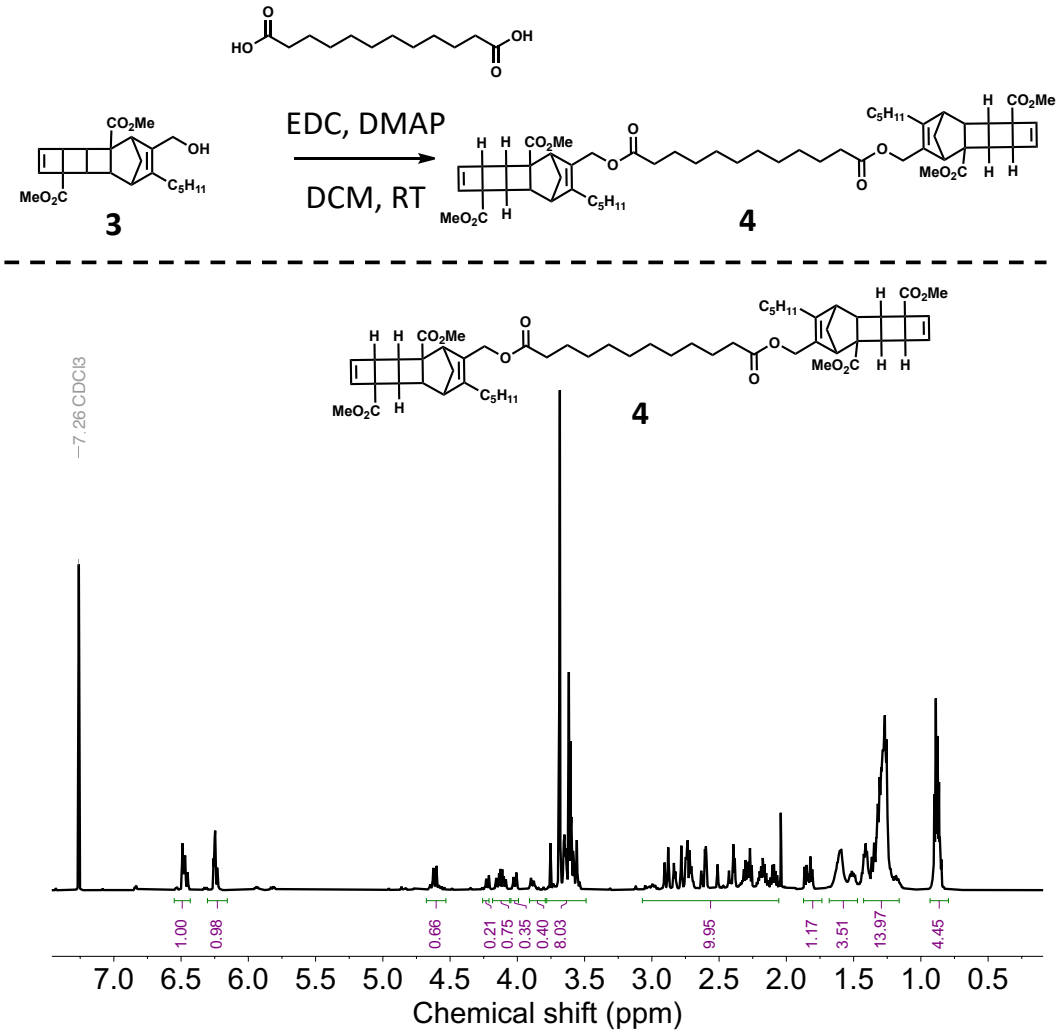


Figure 8.3. Synthetic route to access di-functional Cp-ladderane (compound **4**) via an esterification reaction with EDC reagent. ^{1}H NMR of compound **4** is shown in $CDCl_3$. The presence of product is also confirmed by mass spectrometry.

Utilizing the high reactivity of cyclopentadiene (Cp) as the diene to react with ladderane as the dienophile, a new class of Cp-ladderane compounds can be realized. Cp can react with the ladderane via the Diels–Alder reaction, selectively at the double bond with the electron

withdrawing substituent. Di-functional and mono-functional monomers can lead to the fabrication of polymer networks and graft polymers, respectively, through the ring opening metathesis polymerization (ROMP). Since ladderane is known to possess mechanophore properties,[1,2] these polymers hold potential as mechanical-labile materials that can be applied in a wide range of advanced functions (e.g., tools for structure-relationship studies).[3]

Monomer synthesis procedures. Unless stated otherwise all reactions were carried out under nitrogen atmosphere with oven dried (100 °C) glassware and magnetic stir bars. The ladderane compound **1** was synthesized by our collaborator, Alan Wortman from University of Michigan (Corey Stephens group). Compound **2** was synthesized based on the procedure reported in Chapter 4.

Synthesis of compound **3**:

Compound **1** (100 mg, 0.45 mmol, 1.0 eq.) and **2** (150 mg, 0.91 mmol, 2.0 eq.) in 2 mL dried DCM were added to a 20-mL vial equipped with a stir bar. The mixture was stirred at RT for 20 h. After that, the solution was concentrated. The crude residue was subjected to flash column chromatography with two solvent systems, 1:6 ethyl acetate (EtOAc):hexanes and 50% EtOAc/hexnes, to afford the pure product **3** (81 mg, 50% yield). ^{1}H NMR of the product is shown in **Figure 8.2**.

Synthesis of compound **4**:

To a dried 150 mL round-bottom flask were added compound **3** (60 mg, 0.16 mmol, 2.1 eq.), and 1,12-dodecanedioic acid (17.4 mg, 0.08 mmol, 1.0 eq.) in 2 mL DCM. To this

solution were added EDC (87 mg, 0.46 mmol, 6.0 eq.) and DMAP (3.0 mg, 0.03 mmol, 0.3 eq.). Once added, the solution was allowed to stir at room temperature for 24 h. The solution was concentrated, and the crude mixture was subjected to a silica plug with two solvent systems, DCM and EtOAc. The plug was first wash with DCM to remove any by-products and then EtOAc to collect the solution of product. Concentration of the filtrate affords the pure product **4**.

Polymer synthesis discussion. The initial small-scale polymerization of these compounds (i.e., **3** and **4**) did not show the presence of formed polymeric materials. Future investigation might include the protection of the alcohol in compound **3**, which might interfere with the ROMP step, to study the feasibility of the ROMP to form linear polymer. When the ROMP of these compounds is realized, polymerization of the di-functional to fabricate the cross-linked polymer will be the next step to form new intriguing materials. Other routes to polymerize/functionalize these materials can also be promising, such as vinyl-type polymerization, and thiol-ene reaction.

References:

(1) Chen, Z.; Zhu, X.; Yang, J.; Mercer, J. A. M.; Burns, N. Z.; Martinez, T. J.; Xia, Y. The Cascade Unzipping of Ladderane Reveals Dynamic Effects in Mechanochemistry. *Nat. Chem.* **2020**, *12*, 302–309. DOI: 10.1038/s41557-019-0396-5.

(2) Yang, J.; Horst, M.; Romaniuk, J. A. H.; Jin, Z.; Cegelski, L.; Xia, Y. Benzoladderene Mechanophores: Synthesis, Polymerization, and Mechanochemical Transformation. *J. Am. Chem. Soc.* **2019**, *141*, 6479–6483. DOI: 10.1021/jacs.9b01736.

(3) Chen, Y.; Mellot, G.; Van Luijk, D.; Creton, C.; Sijbesma, R. P. Mechanochemical Tools for Polymer Materials. *Chem. Soc. Rev.* **2021**, *50*, 4100–4140. DOI: 10.1039/D0CS00940G.